



HAL
open science

Supramolecular Redox Transduction: Macrocyclic Receptors for Organic Guests

Sébastien Goeb, David Canevet, Marc Sallé

► **To cite this version:**

Sébastien Goeb, David Canevet, Marc Sallé. Supramolecular Redox Transduction: Macrocyclic Receptors for Organic Guests. Organic Synthesis and Molecular Engineering, Wiley, pp.213-256, 2014, 978-1-118-15092-4. 10.1002/9781118736449.ch8 . hal-03344813

HAL Id: hal-03344813

<https://univ-angers.hal.science/hal-03344813>

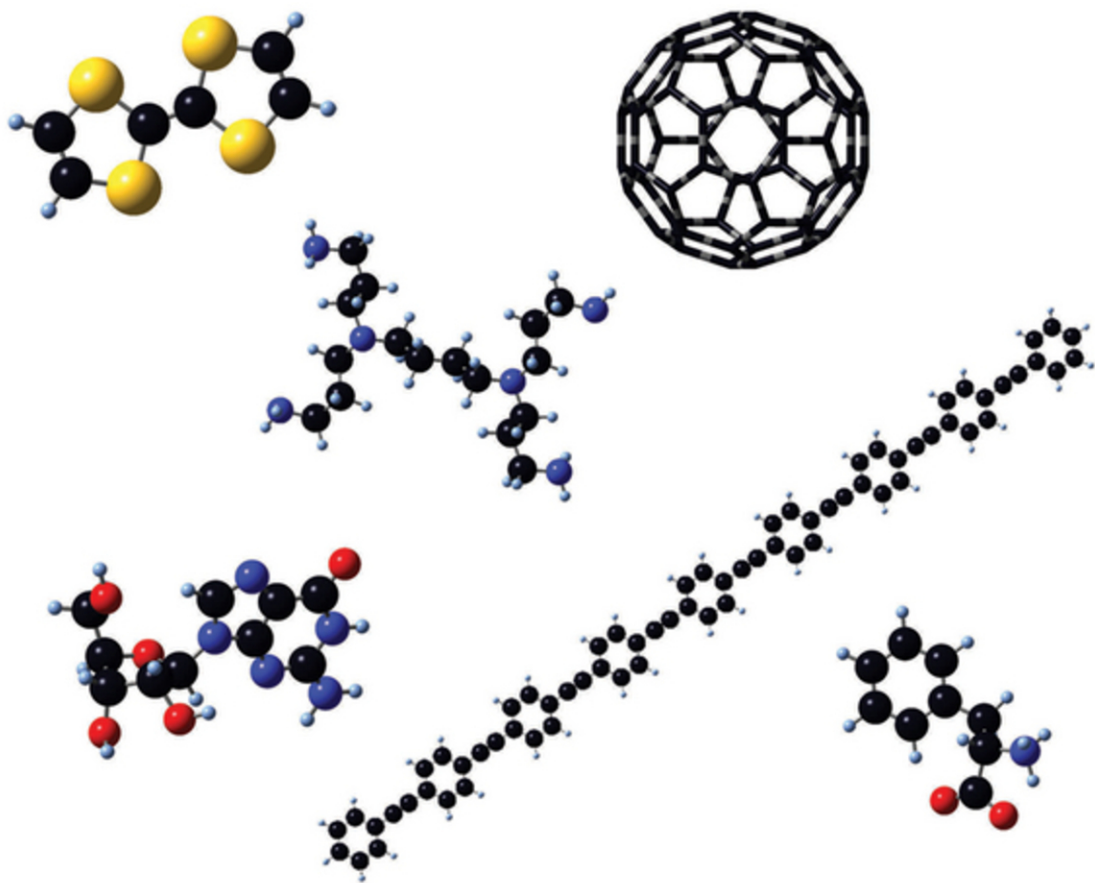
Submitted on 15 Sep 2021

HAL is a multi-disciplinary open access archive for the deposit and dissemination of scientific research documents, whether they are published or not. The documents may come from teaching and research institutions in France or abroad, or from public or private research centers.

L'archive ouverte pluridisciplinaire **HAL**, est destinée au dépôt et à la diffusion de documents scientifiques de niveau recherche, publiés ou non, émanant des établissements d'enseignement et de recherche français ou étrangers, des laboratoires publics ou privés.

Organic Synthesis and Molecular Engineering

Edited by
Mogens Brøndsted Nielsen



WILEY

ORGANIC SYNTHESIS
AND MOLECULAR
ENGINEERING

ORGANIC SYNTHESIS AND MOLECULAR ENGINEERING

Edited by

MOGENS BRØNSTED NIELSEN

Department of Chemistry
University of Copenhagen
Copenhagen, Denmark

WILEY

Copyright © 2014 by John Wiley & Sons, Inc. All rights reserved

Published by John Wiley & Sons, Inc., Hoboken, New Jersey
Published simultaneously in Canada

No part of this publication may be reproduced, stored in a retrieval system, or transmitted in any form or by any means, electronic, mechanical, photocopying, recording, scanning, or otherwise, except as permitted under Section 107 or 108 of the 1976 United States Copyright Act, without either the prior written permission of the Publisher, or authorization through payment of the appropriate per-copy fee to the Copyright Clearance Center, Inc., 222 Rosewood Drive, Danvers, MA 01923, (978) 750-8400, fax (978) 750-4470, or on the web at www.copyright.com. Requests to the Publisher for permission should be addressed to the Permissions Department, John Wiley & Sons, Inc., 111 River Street, Hoboken, NJ 07030, (201) 748-6011, fax (201) 748-6008, or online at <http://www.wiley.com/go/permissions>.

Limit of Liability/Disclaimer of Warranty: While the publisher and author have used their best efforts in preparing this book, they make no representations or warranties with respect to the accuracy or completeness of the contents of this book and specifically disclaim any implied warranties of merchantability or fitness for a particular purpose. No warranty may be created or extended by sales representatives or written sales materials. The advice and strategies contained herein may not be suitable for your situation. You should consult with a professional where appropriate. Neither the publisher nor author shall be liable for any loss of profit or any other commercial damages, including but not limited to special, incidental, consequential, or other damages.

For general information on our other products and services or for technical support, please contact our Customer Care Department within the United States at (800) 762-2974, outside the United States at (317) 572-3993 or fax (317) 572-4002.

Wiley also publishes its books in a variety of electronic formats. Some content that appears in print may not be available in electronic formats. For more information about Wiley products, visit our web site at www.wiley.com.

Library of Congress Cataloging-in-Publication Data:

Nielsen, Mogens Brøndsted.

Organic synthesis and molecular engineering / Mogens Brøndsted Nielsen.

pages cm

Includes bibliographical references and index.

ISBN 978-1-118-15092-4 (hardback)

1. Physical organic chemistry.
2. Organic compounds--Synthesis.
3. Molecular structure.
4. Biomolecules. I. Title.

QD476.N54 2013

547'.13--dc23

2013019098

Printed in the United States of America

ISBN: 9781118150924

10 9 8 7 6 5 4 3 2 1

CONTENTS

ACKNOWLEDGMENTS	vii
CONTRIBUTORS	ix
1 INTRODUCTION	1
<i>Mogens Brøndsted Nielsen</i>	
2 ORGANIC BUILDING BLOCKS FOR MOLECULAR ENGINEERING	4
<i>Kasper Lincke and Mogens Brøndsted Nielsen</i>	
3 DESIGN AND SYNTHESIS OF ORGANIC MOLECULES FOR MOLECULAR ELECTRONICS	46
<i>Karsten Jennum and Mogens Brøndsted Nielsen</i>	
4 CARBON NANOTUBES AND GRAPHENE	76
<i>Helena Grennberg</i>	
5 H-BOND-BASED NANOSTRUCTURATION OF SUPRAMOLECULAR ORGANIC MATERIALS	128
<i>Tomas Marangoni and Davide Bonifazi</i>	
6 MOLECULAR SYSTEMS FOR SOLAR THERMAL ENERGY STORAGE AND CONVERSION	179
<i>Kasper Moth-Poulsen</i>	
7 STRATEGIES TO SWITCH FLUORESCENCE WITH PHOTOCHROMIC OXAZINES	197
<i>Erhan Deniz, Janet Cusido, Massimiliano Tomasulo, Mutlu Battal, Ibrahim Yildiz, Marco Petriella, Mariano L. Bossi, Salvatore Sortino, and Francisco M. Raymo</i>	
8 SUPRAMOLECULAR REDOX TRANSDUCTION: MACROCYCLIC RECEPTORS FOR ORGANIC GUESTS	213
<i>Sébastien Goeb, David Canevet, and Marc Sallé</i>	

9	DETECTION OF NITROAROMATIC EXPLOSIVES USING TETRATHIAFULVALENE-CALIX[4]PYRROLES	257
	<i>Karina R. Larsen, Kent A. Nielsen, Jonathan L. Sessler, and Jan O. Jeppesen</i>	
10	RECOGNITION OF CARBOHYDRATES	284
	<i>Martina Cacciarini</i>	
11	CYCLODEXTRIN-BASED ARTIFICIAL ENZYMES: SYNTHESIS AND FUNCTION	305
	<i>Christian Marcus Pedersen and Mikael Bols</i>	
12	ORGANOZYMES: MOLECULAR ENGINEERING AND COMBINATORIAL SELECTION OF PEPTIDIC ORGANO- AND TRANSITION-METAL CATALYSTS	333
	<i>Morten Meldal</i>	
13	DENDRIMERS IN BIOLOGY AND NANOMEDICINE	361
	<i>Jørn Bolstad Christensen</i>	
14	DYNAMIC COMBINATORIAL CHEMISTRY	393
	<i>Brian Rasmussen, Anne Sørensen, Sophie R. Beeren, and Michael Pittelkow</i>	
	INDEX	437

ACKNOWLEDGMENTS

I sincerely thank all the authors who have contributed their chapters to this book. These contributions have allowed a wide coverage of fields within organic molecular engineering, hopefully of interest to both experts and nonexperts in the field.

I would also like to thank valuable feedback from students who have read some parts of the book, in particular, the students who have followed my course in supramolecular chemistry. With its wide coverage, it is indeed my hope that this book will be useful as a textbook for courses in organic, supramolecular, and macromolecular chemistry.

M.B.N.

CONTRIBUTORS

MUTLU BATTAL, Department of Chemistry, University of Miami, Coral Gables, FL

SOPHIE R. BEEREN, Carlsberg Laboratory, Copenhagen V, Denmark

MIKAEL BOLS, Department of Chemistry, University of Copenhagen, Copenhagen Ø, Denmark

DAVIDE BONIFAZI, Department of Chemistry, University of Namur, rue de Bruxelles, Namur, Belgium

MARIANO L. BOSSI, INQUIMAE, Facultad de Ciencias Exactas y Naturales, Universidad de Buenos Aires, Buenos Aires, Argentina

MARTINA CACCIARINI, Department of Chemistry, University of Florence, Sesto Fiorentino, Italy

DAVID CANEVET, Laboratoire MOLTECH-Anjou, UMR CNRS 6200 UFR Sciences, Université d'Angers, Angers, France

JØRN BOLSTAD CHRISTENSEN, Department of Chemistry, University of Copenhagen, Copenhagen Ø, Denmark

JANET CUSIDO, Department of Chemistry, University of Miami, Coral Gables, FL

ERHAN DENIZ, Department of Chemistry, University of Miami, Coral Gables, FL

SÉBASTIEN GOEB, Laboratoire MOLTECH-Anjou, UMR CNRS 6200 UFR Sciences, Université d'Angers, Angers, France

HELENA GRENNBERG, Department of Chemistry – BMC, Uppsala Universitet, Uppsala, Sweden

KARSTEN JENNUM, Department of Chemistry, University of Copenhagen, Copenhagen Ø, Denmark

JAN O. JEPPESEN, Department of Physics, Chemistry and Pharmacy, University of Southern Denmark, Odense M, Denmark

KARINA R. LARSEN, Department of Physics, Chemistry and Pharmacy, University of Southern Denmark, Odense M, Denmark

KASPER LINCKE, Department of Chemistry, University of Copenhagen, Copenhagen Ø, Denmark

TOMAS MARANGONI, Department of Chemistry, University of Namur, rue de Bruxelles, Namur, Belgium

MORTEN MELDAL, Department of Chemistry, University of Copenhagen, Copenhagen Ø, Denmark

KASPER MOTH-POULSEN, Department of Chemical and Biological Engineering, Chalmers University of Technology, Gothenburg, Sweden

KENT A. NIELSEN, Department of Physics, Chemistry and Pharmacy, University of Southern Denmark, Odense M, Denmark

MOGENS BRØNDSTED NIELSEN, Department of Chemistry, University of Copenhagen, Copenhagen Ø, Denmark

CHRISTIAN MARCUS PEDERSEN, Department of Chemistry, University of Copenhagen, Copenhagen Ø, Denmark

MARCO PETRIELLA, INQUIMAE, Facultad de Ciencias Exactas y Naturales, Universidad de Buenos Aires, Buenos Aires, Argentina

MICHAEL PITTELKOW, Department of Chemistry, University of Copenhagen, Copenhagen Ø, Denmark

BRIAN RASMUSSEN, Department of Chemistry, University of Copenhagen, Copenhagen Ø, Denmark

FRANÇOIS M. RAYMO, Department of Chemistry, University of Miami, Coral Gables, FL

MARC SALLÉ, Laboratoire MOLTECH-Anjou, UMR CNRS 6200 UFR Sciences, Université d'Angers, Angers, France

JONATHAN L. SESSLER, Department of Chemistry and Biochemistry, The University of Texas at Austin, Austin, TX

ANNE SØRENSEN, Department of Chemistry, University of Copenhagen, Copenhagen Ø, Denmark

SALVATORE SORTINO, Department of Drug Sciences, University of Catania, Catania, Italy

MASSIMILIANO TOMASULO, Department of Chemistry, University of Miami, Coral Gables, FL

IBRAHIM YILDIZ, Department of Chemistry, University of Miami, Coral Gables, FL

CHAPTER 1

INTRODUCTION

MOGENS BRØNDSTED NIELSEN

Molecular engineering is an interdisciplinary research field, where design, synthesis, and manipulation of molecules and molecular assemblies are used to create advanced functions. Molecular engineering is an inherent part of nanotechnology and often involves manipulation of molecules at the nanoscale. The synthesis of organic molecules is usually the first experimental step to take whether the overall aim is to develop a nanomachine or molecular motor, a memory device, or an artificial enzyme that can catalyze specific transformations. Organic synthesis is therefore an integral part of this book, and several chapters have a special emphasis on synthetic protocols. With respect to the molecular and supramolecular function, the field of molecular engineering is relevant to a broad range of disciplines, from materials science, molecular electronics, environmental chemistry, chemical biology to pharmaceutical science. Some important targets are molecule-based computers (faster and smaller than silicon-based ones), intelligent drug delivery systems, organic molecules that are as efficient as enzymes for performing catalytic reactions but structurally much simpler (by being much smaller), peptide engineering of new catalysts, molecular sensors, materials for optical data storage, new electrically conducting materials, and new energy-storage materials. This book attempts to cover broadly these fields via chapters of which some are very general and some more specific. The chosen topics described in the chapters present a selection of important scientific contributions that have been made. Many other important contributions could have been covered in a book with such a broad title, but at least I hope that the reader will get an impression of the rich possibilities that exist to create molecules and supramolecular systems with unique properties and functions from those examples covered in this book.

The book is organized as follows. Chapter 2 gives an overview of useful molecular building blocks, covering, for example, different chromophores, redox-active molecules, photoswitches, peptide building blocks, macrocyclic receptors, and examples of how they can be integrated in advanced systems with specific functions. Some of these units are particularly useful in the design of molecular electronics components, which is the

Organic Synthesis and Molecular Engineering, First Edition.

Edited by Mogens Brøndsted Nielsen.

© 2014 John Wiley & Sons, Inc. Published 2014 by John Wiley & Sons, Inc.

focus of Chapter 3. According to *Moore's law* [1], the number of components on integrated circuits doubles approximately every 2 years. Nobel Laureate Richard P. Feynman stated in his famous talk in 1959 at an American Physical Society meeting at Caltech that "There is plenty of room at the bottom," which can be considered the start of nanotechnology and the idea of using a "bottom-up" manufacturing technique by self-assembly of suitable molecules. Thus, development of molecules as components for molecular electronics may provide a way to extend Moore's law beyond the limits of small-scale conventional silicon-integrated circuits. Carbon allotropes are also successfully exploited in this field as well as in organic photovoltaics, and production and functionalization of carbon nanotubes and graphene (single sheets of graphite) are covered in Chapter 4. For achieving functional devices and nanomachines, self-assembly of the molecular components in a desired manner is crucial. Chapter 5 describes how hydrogen bonding interactions can be employed for obtaining self-organizing nanostructures. By rational design of the structural parameters of the single molecular modules and by a strict control of the solvent and temperature conditions, it is possible to produce supramolecular polymeric materials possessing different geometrical structures such as nanofibers, two-dimensional organic networks, vesicles, or toroids.

Exploitation of solar energy is the focus of Chapter 6 and in particular how to store energy in chemical bonds by light-induced isomerization reactions. As described in this chapter, some of several challenges are to harvest light at the right wavelengths and to release the stored energy as heat in an efficient way when needed. Photoswitchable compounds are also central to Chapter 7, which describes strategies to switch fluorescence of photochromic oxazines. Such photoswitchable fluorophores have potential for the visualization of biological samples with subdiffraction resolution.

Supramolecular chemists have, over the last decades, developed a wide variety of macrocyclic receptors for binding of ionic or neutral guests. Specific efforts have focused on transducing the host-guest recognition process in a redox event, targeting sensors, smart materials, or devices for molecular electronics. Such redox-responsive systems are the focus of Chapter 8. The subsequent chapter shows how a chemosensor for nitroaromatic explosives, based on color changes, is designed, improved by systematic variation of the chemical structure, and how this molecule can be integrated into different solid-state devices.

Development of artificial receptors for substrates in water is particularly challenging, but central for engineering of biomimetic systems. In Chapter 10, the focus is recognition of carbohydrates in water and the different techniques used to evaluate this process. Carbohydrates are involved in the metabolic pathways of living organisms and play a crucial function in the first step of cell-cell, cell-virus and cell-bacteria interactions. Chapter 11 describes the development and synthesis of artificial enzymes based on cyclic oligosaccharide receptors, so-called cyclodextrins, which can bind substrates in a hydrophobic cavity and catalyze their conversion to specific products via suitably located catalytically active groups. The subsequent chapter covers another class of catalysts, organozymes, based on rationally designed peptides. Peptide-based catalysts that display some of the qualities of enzyme conversions have been developed in an approach partly based on the application of combinatorial methods. While natural enzymes have evolved to be efficient and selective through millions of years, combinatorial evolution in the laboratory can be performed rapidly within a few years. Catalysis and/or transport can also occur inside so-called dendrimers, which are classes of highly branched "tree-shaped" nanosized molecules. Exploitation of these molecules in biology and nanomedicine and the synthetic strategies to achieve them are covered

in Chapter 13. Chapter 14 describes how reversible formation of host molecules can be used to identify the most suitable receptors for substrates in water, a field which is termed dynamic combinatorial chemistry. In this approach, the most suitable molecule is selected—“survival of the fittest” at the molecular level.

REFERENCE

- [1] Moore, G. E. (1965). Cramming more components onto integrated circuits. *Electronics*, 38, 114–117.

CHAPTER 2

ORGANIC BUILDING BLOCKS FOR MOLECULAR ENGINEERING

KASPER LINCKE and MOGENS BRØNDSTED NIELSEN

2.1 MOLECULAR FUNCTION

Organic engineering of advanced molecules and supramolecular assemblies requires a variety of molecular modules with specific functions and properties, as shown schematically in Figure 2.1. Redox activity is an example of an important function, which allows charging of the organic molecule, either by removal or by donation of electrons. π -Conjugated molecules are often redox active and are usually also conveniently used as wires for electron transport (conductance). We also need building blocks that can absorb and emit light at specific wavelengths (chromophores and fluorophores) or that can undergo light or thermally induced structural changes (photo/thermoswitches) to form molecules with new properties. We need structural motifs that allow complexation of specific guest molecules or ions in various media via noncovalent interactions. Such molecular hosts may concomitantly act as catalysts for the chemical conversion of the guest molecules, substrates, into new products, thereby mimicking enzymes, or they could act as carriers for transporting the guest molecules from one phase to another, for example, through a cell membrane. Host–guest complexation may also alter properties such as fluorescence, which can be employed in the design of molecular sensors. Other important molecular properties include Brønsted and Lewis acidity and basicity, chirality, dipole moment, magnetic properties, nonlinear optical (NLO) and two-photon absorption properties, liquid crystallinity, solubility in polar (in particular, water) or nonpolar solvents, and not least, chemical stability and photostability.

Altered properties of the functional unit by virtue of interactions with its surroundings should also be taken into account. For example, chromophores can exhibit solvatochromism and hence exhibit different absorption maxima in different solvents. Absorption tuning is particularly important for the action of many proteins, such as opsin proteins present in the eye. These proteins are involved in the process of vision. The entire visible region is covered by three different cone pigment cells, each containing photoactive transmembrane proteins. While the chromophore is identical in these

Organic Synthesis and Molecular Engineering, First Edition.

Edited by Mogens Brøndsted Nielsen.

© 2014 John Wiley & Sons, Inc. Published 2014 by John Wiley & Sons, Inc.

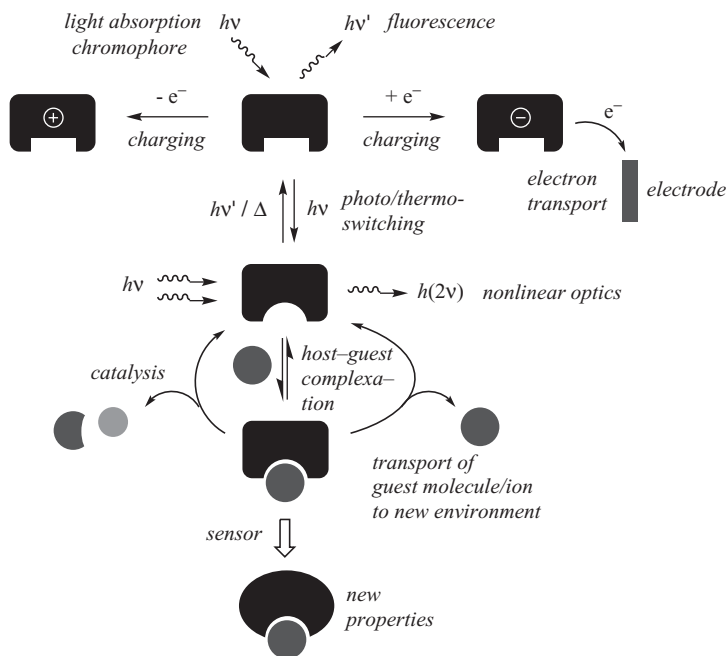


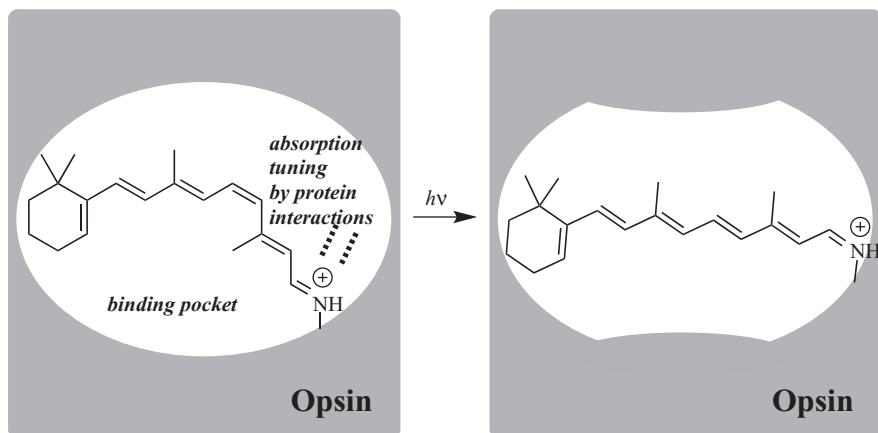
Figure 2.1. Schematic overview of different molecular functions.

proteins, namely, a protonated retinal Schiff base linked to a specific lysine residue, the protein-binding pockets differ slightly in the three types of cones. By subtle protein-chromophore interactions, one protein tunes the chromophore absorption maximum to blue, one to green, and one to red light [1–3]. As shown in Scheme 2.1, the absorption of light induces a *cis* to *trans* isomerization of a double bond in retinal; this is the primary event in visual excitation and alters the geometry of the retinal in the protein-binding pocket, which triggers a cascade of processes [1]. Along the same line, the green fluorescent protein (GFP), which absorbs blue light and emits green light, provides a rigid environment for its chromophore (a 4-hydroxybenzylideneimidazolinone, Figure 2.2), which is only very weakly fluorescent in solution, but inside the binding pocket, fluorescence is turned on. On account of its fluorescent properties, GFP is widely used as a marker protein in molecular and cell biology [4–6].

Systems can be cleverly engineered that couple together individual functions, such as light absorption, energy transfer, and electron transfer, which is of importance when constructing, for example, photovoltaic cells or artificial photosynthesis systems. A selection of specific molecular building blocks will be provided in this chapter, and a few advanced systems will be discussed. Some reaction types useful in synthesis will also be presented, of which several will be encountered in the following chapters.

2.2 REDOX-ACTIVE UNITS

Organic molecules with alternating single and double or triple bonds, that is, π -conjugated molecules, are as mentioned earlier, often redox active and can either



Scheme 2.1. Schematic illustration of the protonated retinal Schiff base in the opsin-binding pocket. The absorption maximum of the chromophore is tuned by protein interactions. Absorption of light is followed by a *cis-trans* isomerization of the chromophore, which leads to geometrical changes of the protein.

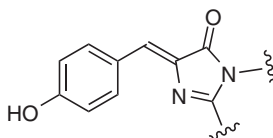
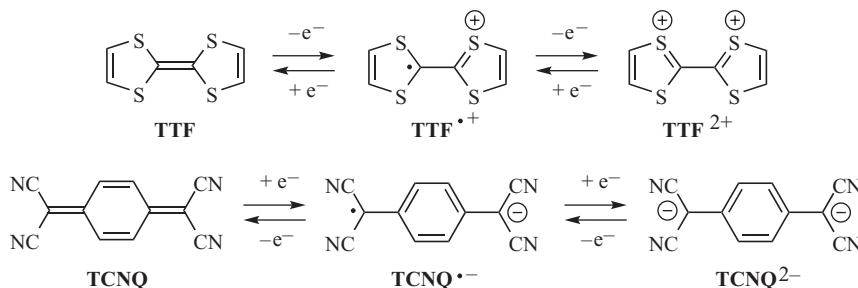


Figure 2.2. The GFP chromophore. It is covalently linked at two positions (indicated by wavy lines) to the protein and is present either as neutral phenol or as phenolate.

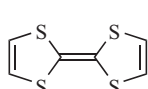


Scheme 2.2. Reversible oxidations of tetrathiafulvalene (TTF) and reversible reductions of tetracyano-*p*-quinodimethane (TCNQ).

donate or receive electrons resulting in stable cations or anions. Such redox-active organic molecules are particularly useful in supramolecular and materials chemistry. For example, the first conducting organic metals were based on a charge-transfer salt between tetrathiafulvalene (TTF) and tetracyano-*p*-quinodimethane (TCNQ) [7, 8]. TTF is a so-called Weitz-type redox system (end groups are cyclic π -systems that exhibit aromatic character in the oxidized form), which is oxidized in two one-electron steps to generate two aromatic 1,3-dithiolium rings (Scheme 2.2) [9]. TCNQ is instead a

Wurster-type redox system (end groups located outside a cyclic π -system that exhibits aromatic character in the reduced form), which, like *N,N,N',N'*-tetramethyl-*p*-phenylenediamine (Wurster's blue), is aromatic in its reduced form (Scheme 2.2). Its acceptor strength can be further enhanced by functionalization with electron-withdrawing fluoro substituents. Buckminsterfullerene (C_{60}) can undergo up to six reversible one-electron reductions in solution [10], but usually three to four reductions are observed depending on the solvent [11]. C_{60} and its derivatives are widely explored as electron-acceptor moieties for photovoltaic devices such as solar cells [12]. Large carbon-rich acetylenic scaffolds have also achieved recognition as good electron acceptors [13, 14]. The expanded [6]radialene shown in Figure 2.3 presents one such example [15]; interestingly, its perethynylated core comprises a total of 60 carbon atoms. Figure 2.3 shows a variety of other electron-donor and acceptor molecules, including ferrocene

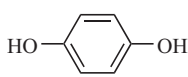
Electron donors



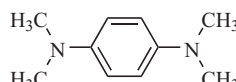
TTF



Fc

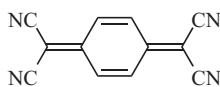


Hydroquinone

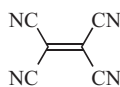


Wurster's blue

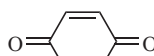
Electron acceptors



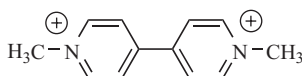
TCNQ



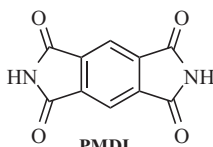
TCNE



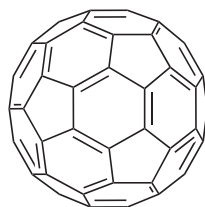
Benzoquinone



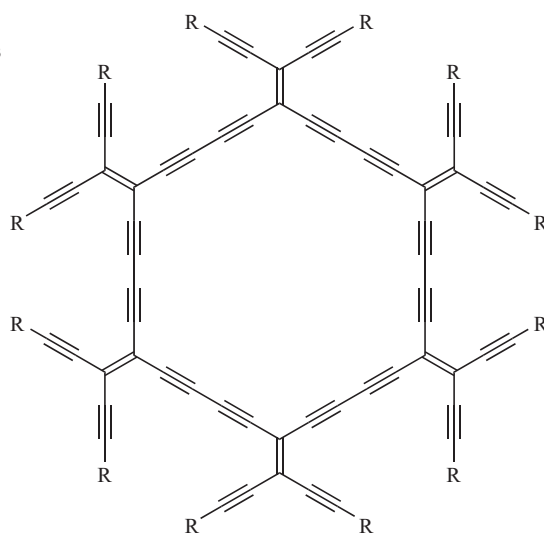
Paraquat



PMDI



Buckminsterfullerene, C_{60}



Expanded [6]radialene: $C_{60}R_{12}$

Figure 2.3. Redox-active organic electron donors and acceptors.

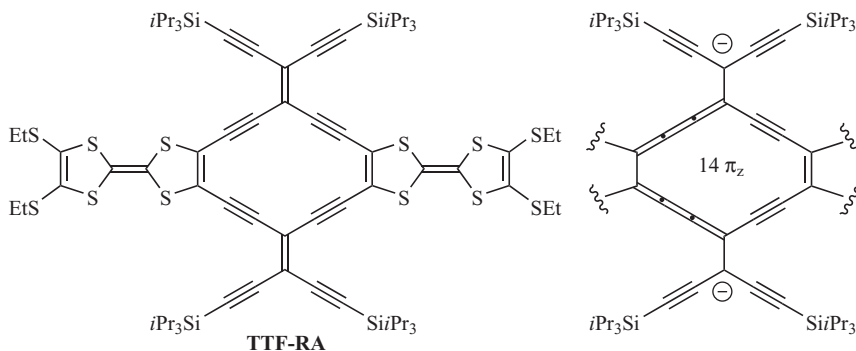


Figure 2.4. TTF-Radiaannulene (TTF-RA), a combined Weitz–Wurster-type redox system. Upon two-electron reduction, the central core formally becomes 14π -aromatic.

(Fc), hydroquinone/benzoquinone, tetracyanoethylene (TCNE), paraquat, and pyromellitic diimide (PMDI).

Fusing together redox-active systems can result in molecules with multiple redox states furnished by either oxidation or reduction. For example, a so-called expanded radiaannulene core (containing both endo- and exocyclic double bonds) was recently fused together with two TTF units to afford a molecule (TTF-radiaannulene [TTF-RA], Figure 2.4), which was found to reversibly exist in six redox states: -2 , -1 , 0 , $+1$, $+2$, $+4$ [16]. The cyclic core of the dianion contains 14π -electrons, and it thereby satisfies the Hückel $4n + 2$ aromaticity rule for planar cycles with $n = 3$ (in general, n should be zero or a positive integer). The TTF-RA molecule can accordingly be considered as a Wurster-type redox system (the cyclic core) combined with Weitz-type redox systems (the TTFs). Thus, it formally gains aromaticity by either reduction or oxidation. The resonance formula drawn for the dianionic core in Figure 2.4 resembles an annulene structure. Annulenes are completely conjugated monocyclic hydrocarbons with endocyclic double bonds, of which the simplest are cyclobutadiene, benzene, and cyclooctatetraene. Instead, radialenes are alicyclic organic compounds with exocyclic double bonds, of which trimethylenecyclopropane is the simplest. By fusing together two perethynylated radiaannulenes in a bicyclic structure as shown in Figure 2.5 [17], a particularly strong electron acceptor is obtained, even stronger than C_{60} . Thus, this compound shows a first reduction at -0.83 V versus Fc^+/Fc (in THF + $0.1 \text{ M Bu}_4\text{NPF}_6$), while that of C_{60} is at -1.02 V under comparable conditions. Such large two-dimensional, carbon-rich scaffolds, resembling all-carbon graphene sheets, are particularly interesting in the quest for optoelectronic and conducting materials.

2.2.1 Case Study: TTF Building Blocks

TTF has, in particular, found use as a redox-active building block. Its successful incorporation into macromolecular and supramolecular systems takes advantage of ready access to useful building blocks, which can be converted into nucleophiles by treatment with suitable bases, as shown in Scheme 2.3. Direct lithiation can be accomplished with lithium diisopropylamide (LDA), and the resulting lithiated species can be treated with, for example, 1,2-diiodoethane to provide an iodo-substituted TTF for further

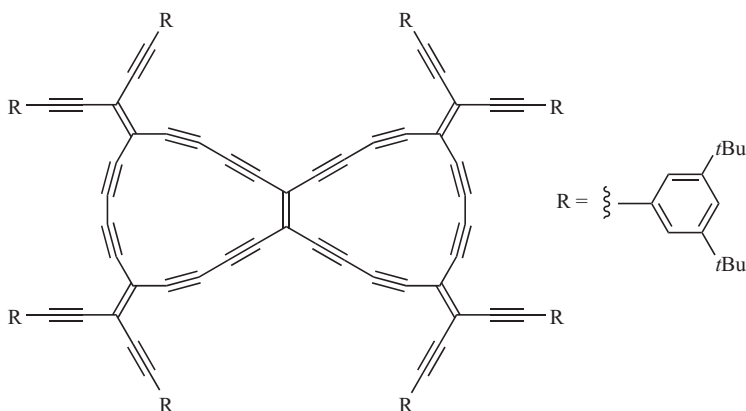
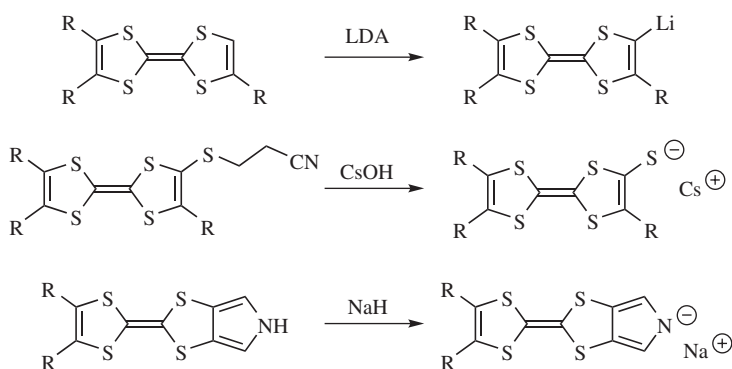


Figure 2.5. Bicyclic radiannulene.



Scheme 2.3. Preparation of nucleophilic TTF building blocks.

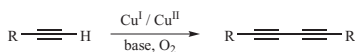
functionalization by, for example, Sonogashira cross-coupling reactions [18–20] (see Box 2.1). Cyanoethyl-protected TTF thiolates have been used extensively for construction of macrocyclic structures; the cyanoethyl group is usually removed by either cesium hydroxide or sodium methoxide, and the resulting thiolate is an excellent nucleophile for S_N2 substitution reactions [21, 22]. Pyrrole-annulated TTFs are also attractive building blocks and are readily converted to nucleophilic species after removal of the pyrrole N–H proton by sodium hydride [23].

2.3 PHOTO/THERMOSWITCHES

Photoswitches (or photochromic molecules) that upon irradiation undergo conversion to an isomeric structure are employed for a variety of applications, ranging from molecular switches for data storage, molecular electronics, light-controllable liquid

BOX 2.1 METAL-CATALYZED CARBON-CARBON COUPLING REACTIONS

Glaser–Eglinton–Hay

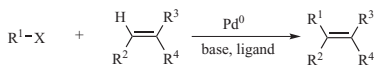


R = alkyl, alkenyl, alkynyl, aryl
Base = pyridine or TMEDA (Me₂NCH₂CH₂NMe₂)

Review:

Siemsen, P., Livingston, R. C., Diederich, F. (2000). *Angewandte Chemie—International Edition*, 39, 2632–2657.

Heck



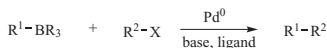
R¹ = aryl, benzyl, alkenyl, alkyl
R² = R³ = R⁴ = alkyl, aryl, alkenyl
X = Cl and Br
Base = 2° or 3° amine, KOAc, NaOAc, NaHCO₃
Ligand = trialkyl phosphines, triaryl phosphines, chiral phosphines

Review:

(a) De Meijere, A., Meyer, F. E. (1994). *Angewandte Chemie—International Edition*, 33, 2379–2411;

(b) Beletskaya, I. P., Cheprakov, A. V. (2000). *Chemical Reviews*, 100, 3009–3066.

Suzuki



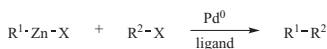
R¹ = alkyl, allyl, alkenyl, aryl
R² = alkyl, alkenyl, aryl
R = alkyl, OH or O-alkyl
X = Cl, Br, I, OTf
Base = CO₃²⁻, Ba(OH)₂, K₃PO₄, KF, CsF, Bu₄F, NaOH, RO⁻
Ligand = trialkyl phosphines, triaryl phosphines, chiral phosphines

Reviews:

(a) Suzuki, A. (1999). *Journal of Organometallic Chemistry*, 576, 147–168;

(b) Beilina, F., Carpita, A., Rossi, R. (2004). *Synthesis*, 2419–2440.

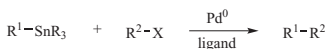
Negishi



R¹ = aryl, alkenyl, benzyl, allyl
R² = alkenyl, alkynyl, aryl, acyl
R = alkyl, OH or O-alkyl
X = Cl, Br, I
Ligand = trialkyl phosphines, triaryl phosphines, chiral phosphines

Reviews:

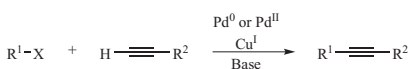
(a) Negishi, E. I. (1982). *Accounts of Chemical Research*, 15, 340–348; (b) Erdik, E. (1992). *Tetrahedron*, 48, 9577–9648.

Stille

R¹ = alkyl, allyl, alkenyl, aryl
 R² = alkyl, alkenyl, aryl
 R = alkyl, OH or O-alkyl
 X = Cl, Br, I, OTf
 Ligand = trialkyl phosphines, triaryl phosphines, chiral phosphines

Reviews:

(a) Stille, J. K. (1986). *Angewandte Chemie—International Edition*, 25, 508–523; (b) Mitchell, T. N. (1992). *Synthesis*, 803–815.

Sonogashira

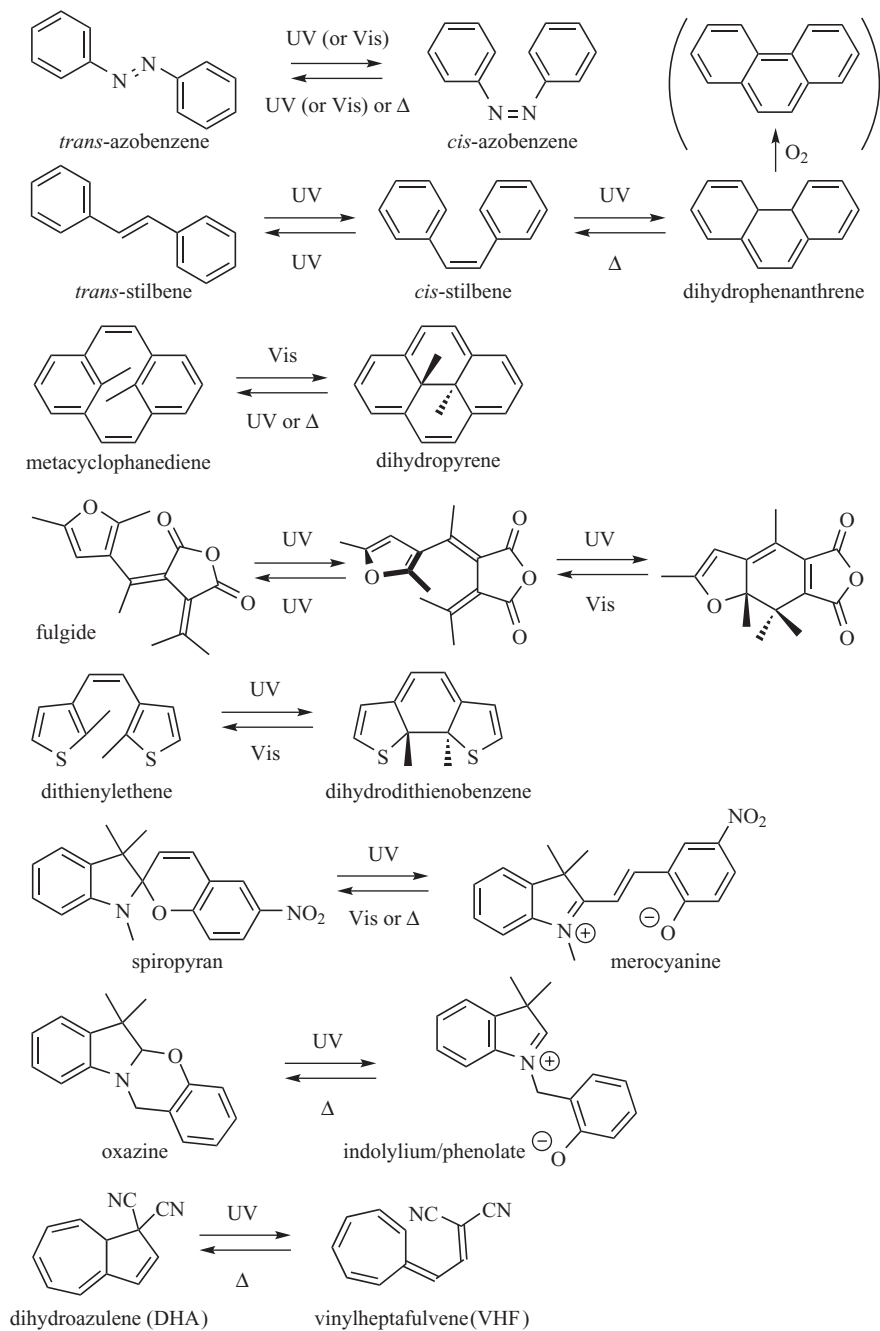
R¹ = aryl, heteroaryl, alkenyl
 R² = H, alkyl, aryl, alkenyl, SiR₃
 X = Cl, Br, I, OTf
 Base = Et₂NH, Et₃N, (*i*-Pr)₂NH

Review: Chinchilla, R., Najera, C. (2007). *Chemical Reviews*, 107, 874–922.

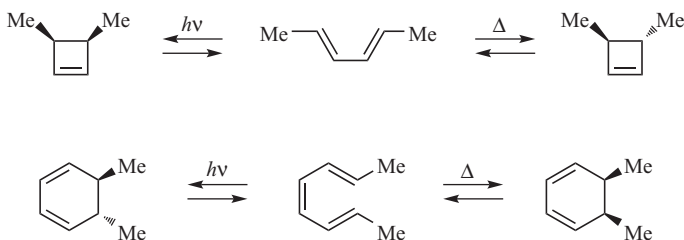
crystals, light-controllable membrane proteins, and nanomachines [24]. In some cases, return to the original isomer is promoted by light; in others, it is promoted thermally. A variety of molecular photoswitches is shown in Scheme 2.4. The use of UV or visible light is indicated at the arrows, but the exact wavelength for each conversion will, in general, depend somewhat on the further functionalization of the system. The switching process is either a *cis*–*trans* isomerization about a double bond, like the isomerization of retinal in the process of visual excitation (Scheme 1.1), or an electrocyclic reaction (see Box 2.2). Conversions of azobenzenes [25] and dithienylethenes [26] present examples of these two processes, and these molecules are some of the most extensively used photoswitches. The presence of methyl substituents in the dihydrodithienobenzene isomer is important for avoiding oxidation to the fully unsaturated compound (as shown for dihydrophenanthrene [27] in Scheme 2.4).

The use of oxazines in relation to fluorescence switching will be covered in Chapter 7. For examples of suitably functionalized photoswitches used to control liquid crystallinity and for holographic optical data storage, the reader is referred to the literature, for example, References 28 and 29. In brief, liquid crystallinity is usually obtained by functionalization with unpolar alkyl chains and cyano or other polar end groups.

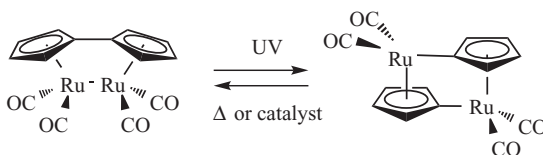
The fulvalene diruthenium system is another interesting photo/thermoswitch, which isomerizes by a rather unusual chemical rearrangement (Scheme 2.5). This system is interesting for development of molecular solar thermal energy storage devices, as discussed in Chapter 6.



Scheme 2.4. Examples of molecular photo/thermoswitches.

BOX 2.2 ELECTROCYCLIC REACTIONS

Review: Pindur, U., Schneider, G. H. (1994). *Chemical Society Reviews*, 23, 409–415.



Scheme 2.5. Switching via chemical rearrangement.

2.3.1 Case Study: Azobenzenes

As azobenzenes are easy to prepare and have found so wide interest, a few details on their optical properties shall be provided here; for a more extensive coverage, see, for example, Reference 25. *trans*-Azobenzene exhibits $\pi \rightarrow \pi^*$ and $n \rightarrow \pi^*$ absorptions at 320 nm ($\epsilon \sim 22,000 \text{ M}^{-1} \text{ cm}^{-1}$) and 450 nm ($\epsilon \sim 400 \text{ M}^{-1} \text{ cm}^{-1}$), respectively, while *cis*-azobenzene exhibits $\pi \rightarrow \pi^*$ absorptions at 270 nm ($\epsilon \sim 5000 \text{ M}^{-1} \text{ cm}^{-1}$)/250 nm ($\epsilon \sim 11,000 \text{ M}^{-1} \text{ cm}^{-1}$) and a $n \rightarrow \pi^*$ absorption at 450 nm ($\epsilon \sim 1500 \text{ M}^{-1} \text{ cm}^{-1}$). The quantum yield for *trans* to *cis* isomerization after $\pi \rightarrow \pi^*$ excitation is around 0.1–0.2 (depending on solvent polarity), while it is 0.2–0.4 after $n \rightarrow \pi^*$ excitation. The quantum yield of *cis* to *trans* isomerization varies between 0.1 and 0.5 in different solvents after $\pi \rightarrow \pi^*$ excitation and 0.4–0.6 after $n \rightarrow \pi^*$ excitation. Continuous irradiation of *trans*-azobenzene at wavelengths of either 313 or 436 nm results in photostationary states with contents of the *trans* isomer of ca. 20% and 90%, respectively. The *cis* isomer can undergo spontaneous isomerization in the dark to the more stable *trans* isomer with an activation energy of 90–100 kJ mol⁻¹. The next chapter will provide examples of how this photoswitch, as well as the dithienylethene/dihydrodithienobenzene and dihydroazulene/vinylheptafulvene switches, can be used for light-controlled conductance switching in molecular electronics.

2.4 FLUOROPHORES, LIGHT HARVESTERS, AND DYES

Fluorescent molecules have several different applications, ranging from fluorescent labeling, fluorescence imaging, optical sensors, biological detectors, and light harvesters for photoinduced processes. Some examples of fluorophores are shown in Figure 2.6.

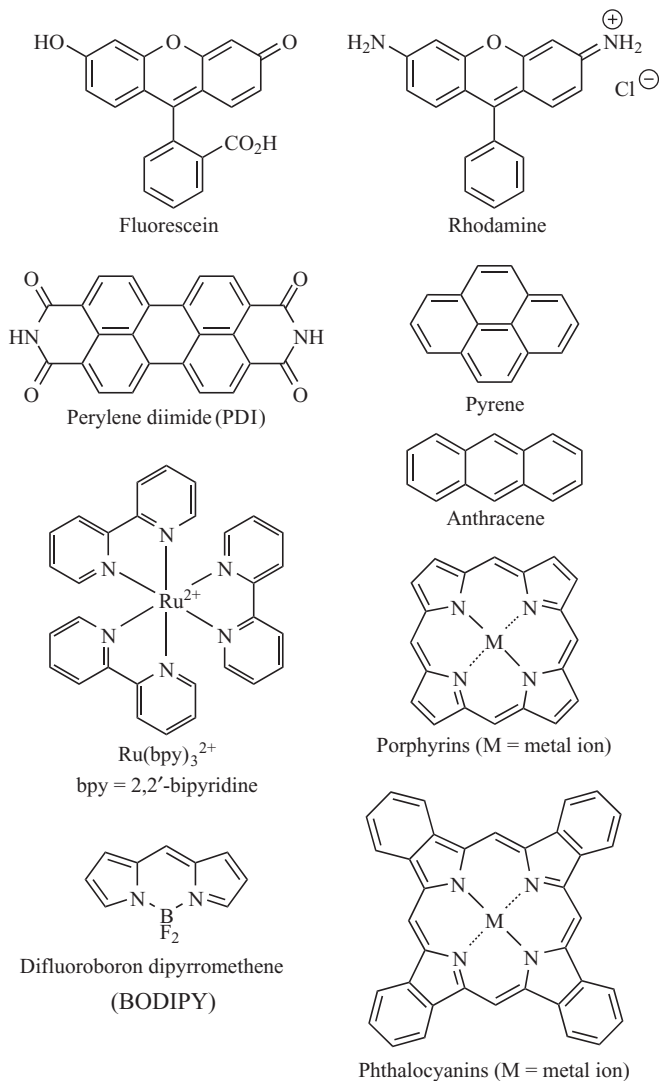


Figure 2.6. Fluorophores.

Porphyrins structurally resemble chlorophyll molecules, which harvest light in natural photosynthesis, and several cyclic porphyrin antenna systems have been designed as efficient light harvesters [30]. Porphyrins are also of interest in photodynamic cancer therapy as photosensitizers for generation of singlet oxygen [31]. Ruthenium(II) complexes of didentate ligands, such as 2,2'-bipyridine (bpy), have long-lived phosphorescent states and have also been used extensively as light harvesters in supramolecular light-induced charge-transfer devices [32, 33]. As mentioned earlier, the GFP chromophore is only weakly fluorescent outside the protein-binding pocket. However, several derivatives have in recent years been prepared to enhance its fluorescence, for example,

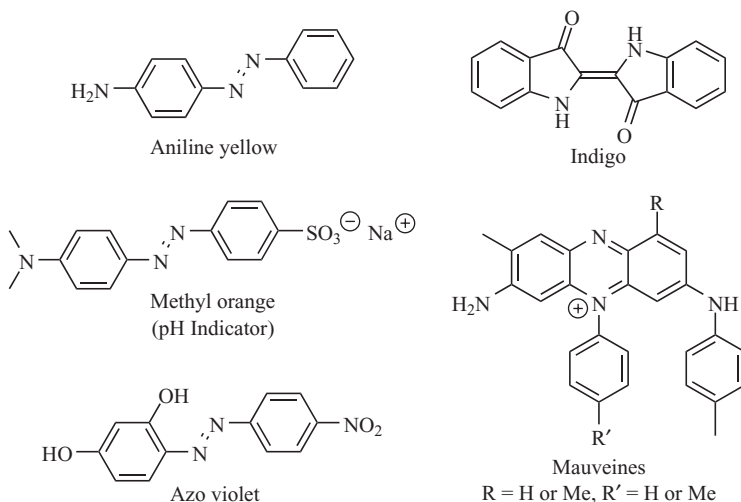


Figure 2.7. Organic dyes.

by locking the two rings in a fixed conformation [34]. Exploitation of fluorophores for monitoring and screening reactions on a solid support is described in Chapter 12. Three other uses of fluorophores will be exemplified in the three case studies discussed later.

Phthalocyanins are strongly blue-green colored compounds and are also widely used as dyes. Figure 2.7 shows some other important dyes, namely, examples of azo compounds ($\text{R}-\text{N}=\text{N}-\text{R}'$), indigo (blue color, used to color jeans), and mauveine, which is also known as aniline purple and was the first synthetic organic chemical dye.

2.4.1 Case Study: Fluorescent Probe for Carbohydrates

Fluorescent boron-dipyrromethene (BODIPY) derivatives have been employed as indicators for a variety of species, such as metal ions and biomolecules [35]. The BODIPY/phenylboronic acid derivative shown in Figure 2.8 [36] is able to bind monosaccharides, owing to the Lewis acidity of boron. The probe itself exhibits narrow absorption and emission bands with maxima at 495 and 510 nm (fluorescence quantum yield of 0.41), respectively, in a phosphate buffer at pH 7.5. A blueshift and increase in both the molar absorption and the emission were observed in the presence of increasing amounts of D-fructose due to its binding to the boron. The affinity for three different sugars decreased in the sequence D-fructose > D-galactose > D-glucose, with the following dissociation constants determined from emission data: 1.0, 24, and 73 mM (dissociation constants are the inverse of association constants). Examples of carbohydrate binding based instead on hydrogen bonding interactions are provided in Chapter 10.

2.4.2 Case Study: Logic Gate

Quenching of fluorescence by either energy or electron transfer (reductive or oxidative quenching) has been employed for construction of both optical sensors and logic gates. Thus, by attaching both a crown ether and a tertiary amine group in proximity to a central anthracene, its fluorescence is almost quenched by photoinduced electron

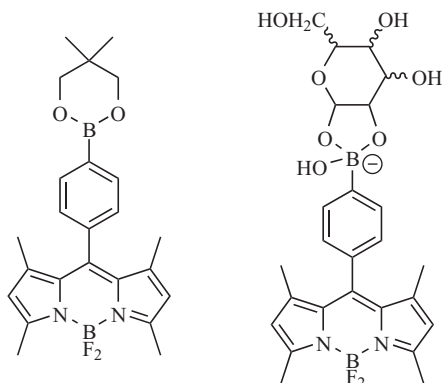


Figure 2.8. Left: BODIPY indicator for D-fructose, D-glucose, and D-galactose. Right: Monosaccharide bound to the boronic acid.

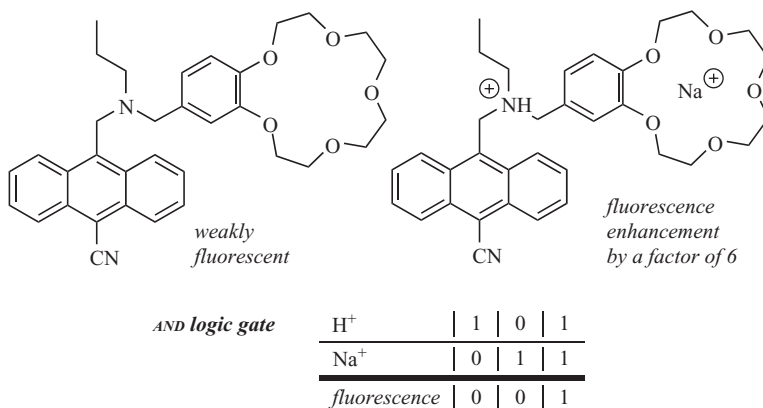


Figure 2.9. AND logic gate based on the fluorescence output of anthracene.

transfer from either of these two units (Figure 2.9) [37]. By both protonation of the amine group and complexation of a sodium ion in the crown ether (this event is covered in more detail later), the fluorescence of the anthracene is enhanced by a factor of 6. The fluorescence output only increases by a factor of 1.1 in the presence of sodium ions alone and by a factor of 1.7 in the presence of protons alone. The system thus functions as an AND logic gate as it requires both inputs (H^+ and Na^+) to show a fluorescence output.

2.4.3 Case Study: Combining Chromophores and Redox-Active Units in an Artificial Photosynthesis Device

Adenosine triphosphate (ATP) is used as an energy source in metabolic processes in cells. A light-driven transmembrane proton pump has been used to generate ATP from adenosine diphosphate (ADP) and phosphate [38]. First, a liposome (i.e., a vesicle composed of a lipid bilayer) was prepared and then a covalently linked triad system composed of carotene (C), porphyrin (P), and quinone (Q), C–P–Q (Figure 2.10), was

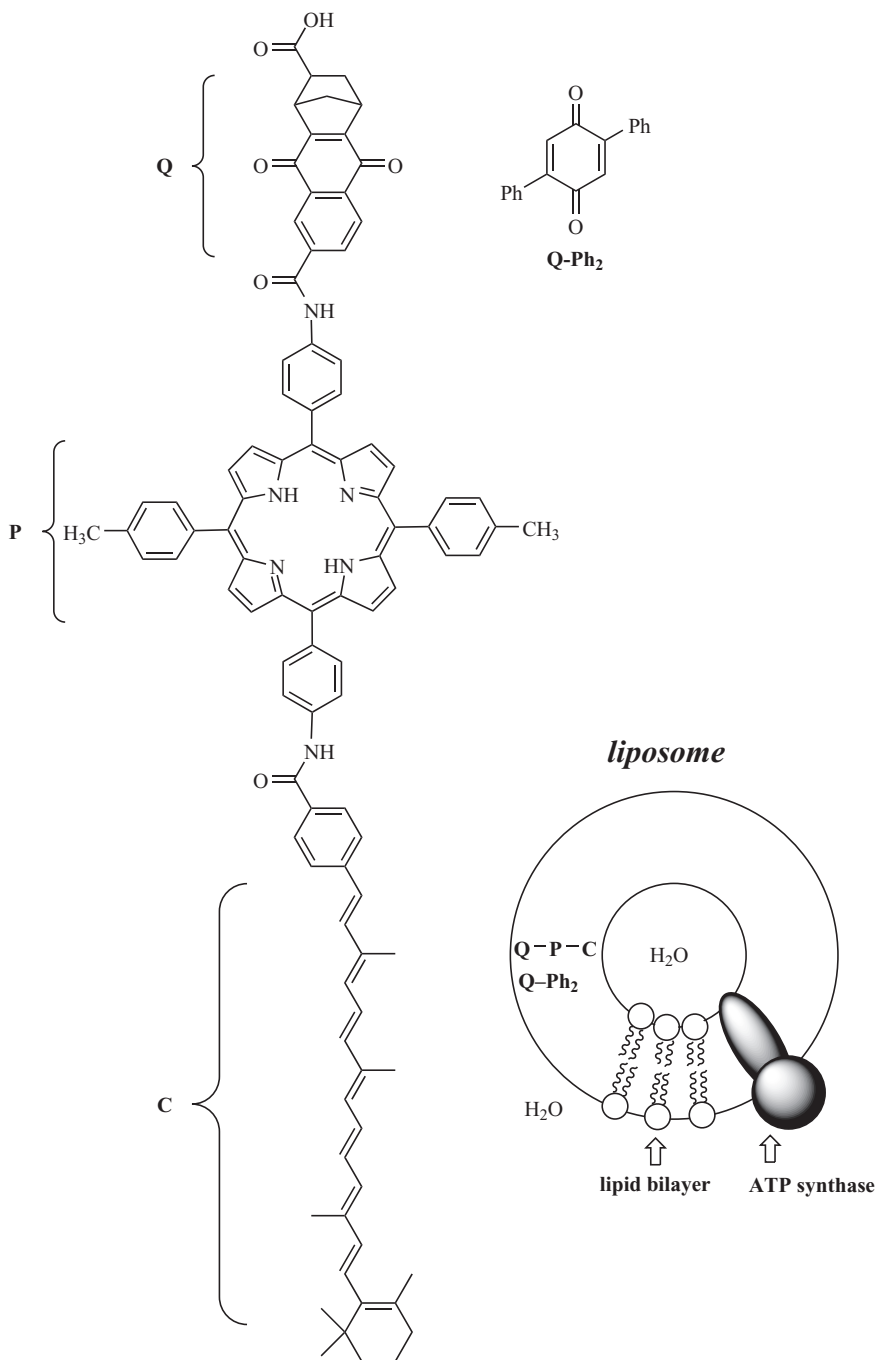
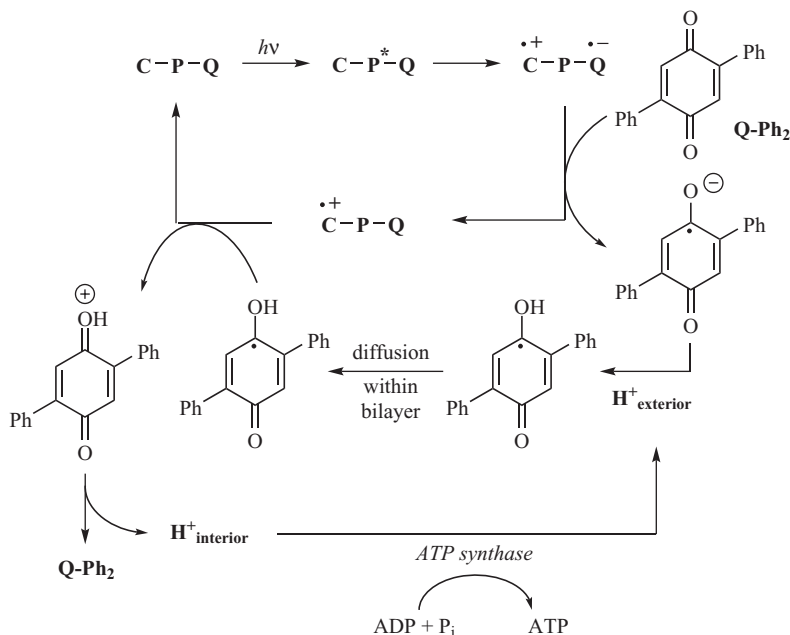


Figure 2.10. Triad system composed of carotene (C), porphyrin (P), and quinone (Q) was inserted in a liposome (vesicle composed of lipid bilayer), which also contains an ATP synthase transmembrane protein (schematically shown at the lower right corner).



Scheme 2.6. Excitation of the porphyrin unit P in the C-P-Q triad ultimately leads to transfer of a proton from the aqueous exterior of the liposome to its aqueous interior, resulting in a proton motive force. Flow of protons out of the liposome is coupled to conversion of ADP and phosphate (P_i) to ATP via the ATP synthase.

inserted into the bilayer membrane of the liposome. As the quinone end of the triad has a carboxylate group attached while the carotenoid end is hydrophobic, the carotenoid end first enters the membrane, hence allowing for insertion of the triad in a directional manner. Thus, the quinone end is pointing toward the external surface, while the carotene end is pointing toward the interior of the liposome. In addition, another unpolar quinone (Q- Ph_2) having stronger acceptor strength than that present in the triad is incorporated into the bilayer. Light excitation of the porphyrin induces a charge separation by which the carotene is oxidized to a radical cation, while the quinone is reduced to a radical anion (Scheme 2.6). The reduced quinone then transfers an electron to a Q- Ph_2 in its proximity, which hereby becomes basic enough to accept a proton from the exterior aqueous environment. The neutral semiquinone radical can diffuse in the bilayer, and when it meets the carotene radical cation near the inner membrane, it transfers an electron, thereby regenerating the neutral C-P-Q triad and forming a protonated quinone. This protonated quinone will subsequently deliver a proton to the interior aqueous environment. This net proton transfer from the exterior to the interior generates a proton motive force. In the membrane, an ATP synthase is also vectorially inserted, and the flow of protons out of the liposome through this enzyme is coupled with its production of ATP. Thus, the system functions as an artificial photosynthesis device, which converts light energy into chemical energy.

2.4.4 Case Study: “Clicking” Together Functional Units by the CuAAC Reaction

Two functional units containing a terminal alkyne and an azide, respectively, as reactive handles can be conveniently linked together via the Cu(I)-catalyzed azide-alkyne cycloaddition (CuAAC, Box 2.3), generating a 1,4-disubstituted triazole [39, 40]. In contrast to the uncatalyzed 1,3-dipolar cycloaddition between such functional groups (the Huisgen reaction [41]), this reaction is regioselective (generating only, or mainly, one regioisomer) and can be performed under mild conditions (at room temperature and in water if solubilities of substrates allow for this). Cu(I) is usually generated *in situ* by reduction of Cu(II) by ascorbic acid, and an example of this reaction is shown in Scheme 2.7 for linking together the perylene diimide (PDI) fluorophore with the TTF redox-active unit [42], here using *N,N*-dimethylformamide (DMF) as solvent as the reactants lack water solubility.

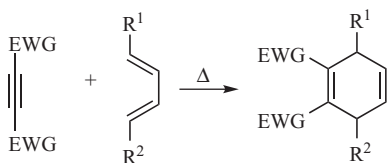
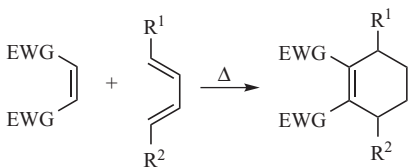
CuAAC reactions often satisfy requirements of “click chemistry,” a term that was coined by Sharpless and coworkers [43]. Click reactions should be modular, wide in scope, high yielding, generate readily removable inoffensive by-products, and stereospecific. The reaction conditions should be simple, involving either no solvents or benign solvents such as water, include simple, easily obtainable starting materials and reagents, and the product should be simple to isolate by nonchromatographic methods, such as crystallization or distillation. In addition, the product should be stable under physiological conditions. The reaction shown in Scheme 2.7 violates many of these requirements, but it is still a good example of how the CuAAC reaction is conveniently used to link together functional building blocks.

2.5 MACROCYCLIC HOST MOLECULES

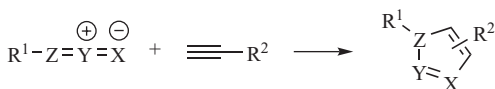
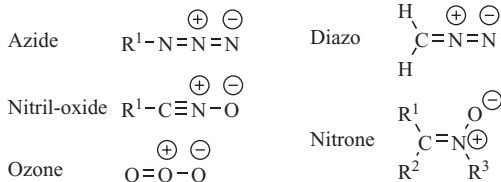
A molecular host for a specific guest molecule or ion must have complementary binding sites to those of the guest, and these binding sites should be placed in the right spatial orientation. Macrocycles are particularly useful host molecules as their binding sites can be preorganized for guest complexation, meaning that if designed properly, the macrocycle does not need to undergo significant conformational changes upon binding. Thus, in comparison to an acyclic structure that has to wrap around a guest, thereby losing degrees of freedom, guest complexation by a preorganized macrocycle will not be as entropically unfavorable. Enthalpy can also play a key role for the preorganization as is the case for the complexation of alkali metal cations by crown ethers.

2.5.1 Cation and Anion Complexation

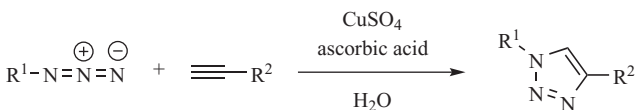
Figure 2.11 shows a variety of macrocyclic molecules that can encapsulate either cations or anions. Crown ethers are some of the most commonly employed macrocycles for encapsulation of alkali metal cations by ion–dipole interactions and were discovered by Pedersen in the mid-1960s [44]. They are cyclic ethers with ethylene bridges between the oxygen-binding sites. In particular, crown ethers are preorganized for cation complexation in a solvent such as dichloromethane in which the oxygen lone pairs are directed inward (while the opposite is the case in a hydrophilic medium). The preorganization is in this case mainly of enthalpic origin as the macrocycle exhibits

BOX 2.3 CYCLOADDITIONS**Diels–Alder [4+2] Cycloaddition**

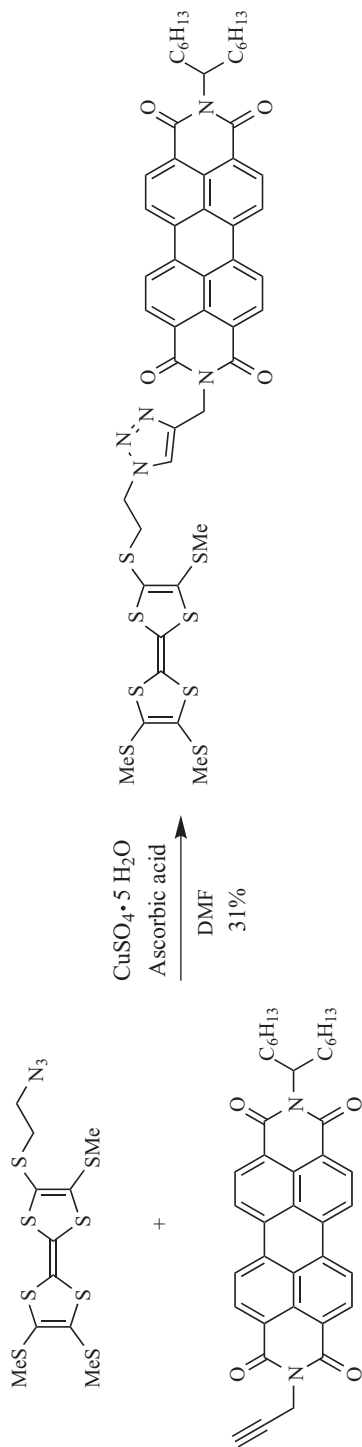
Reviews: (a) Brieger, G., Bennett, J. N. (1980). *Chemical Reviews*, 80, 63–97; (b) Mehta, G., Uma, R. (2000). *Accounts of Chemical Research*, 33, 278–286; (c) Corey, E. J. (2002). *Angewandte Chemie—International Edition*, 41, 1650–1667; (d) Nicolaou, K. C., Snyder, S. A., Montagnon, T., Vassilikogiannakis, G. (2002). *Angewandte Chemie—International Edition*, 41, 1668–1698.

1,3-Dipolar Cycloaddition**1,3-dipoles**

Reviews: (a) Gothelf, K. V., Jørgensen, K. A. (1998). *Chemical Reviews*, 98, 863–909; (b) Meldal, M., Tornøe, C. W. (2008). *Chemical Reviews*, 108, 2952–3015.

CuAAC Reaction

Review: Meldal, M., Tornøe, C. W. (2008). *Chemical Reviews*, 108, 2952–3015.



Scheme 2.7. Synthesis of TTF-PDI conjugate by the CuAAC reaction.

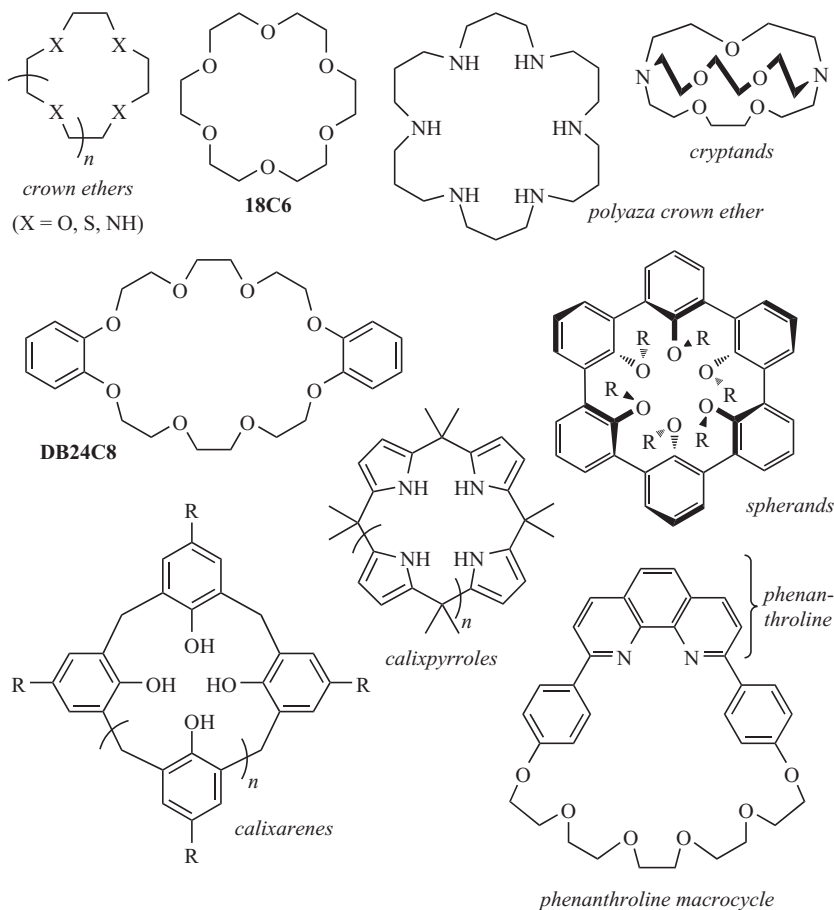
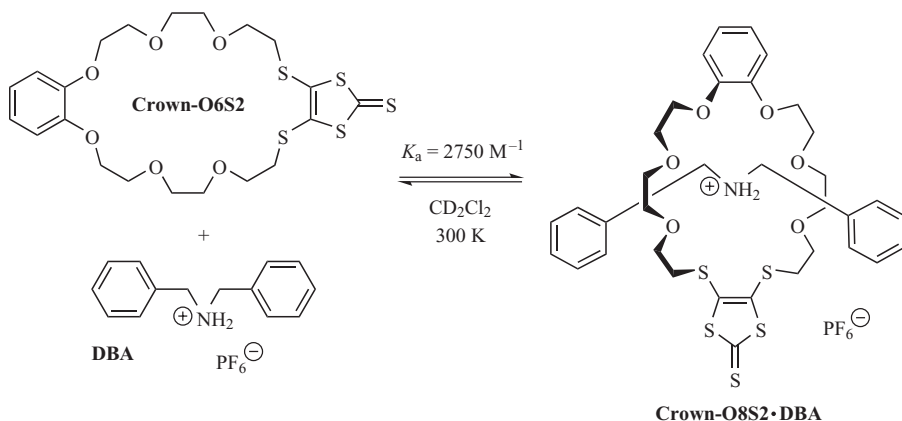


Figure 2.11. Macrocyclic host molecules for cations and anions.

unfavorable lone-pair–lone-pair repulsions already in its uncomplexed form, while an acyclic polydentate ligand (also termed “podand”) has to change conformation from an elongated form (with as little lone-pair–lone-pair repulsions as possible) to a form in which the oxygen atoms wrap around the cation upon complexation. The crown ether [18]crown-6 (18C6; 6 oxygen atoms bridged by 6 ethylene groups; i.e., 18 atoms in ring) has, in particular, found wide use in cation sensors, and several binding studies have been undertaken [45, 46]. It forms 1 : 1 complexes with Na^+ , K^+ , and Cs^+ , with association constants determined by calorimetry of $\log K_a = 4.32$ (Na^+), 6.07–6.29 (K^+), and 4.14 (Cs^+) in methanol. Moreover, 18C6 has an ideal geometry for complexation of alkyl ammonium cations by hydrogen-bonding interactions. Thus, complexation of RNH_3^+ involves three hydrogen bonds as every second oxygen atom in the ring can make a hydrogen bond to one of the three ammonium protons. The cavity of dibenzo[24]crown-8 (DB24C8) is large enough to allow for threading of dibenzylammonium (DBA), forming the so-called pseudorotaxane complexes with an association constant



Scheme 2.8. Formation of pseudorotaxane complex between the crown ether crown-O6S2 and dibenzylammonium (DBA). The association constant K_a was determined from the $^1\text{H-NMR}$ spectrum recorded in CD_2Cl_2 ; see Figure 2.12.

of $2.7 \times 10^4 \text{ M}^{-1}$ in CDCl_3 [47]. A rotaxane has one or more macrocycles threaded along a molecular axle with bulky end groups preventing dethreading; when these stopper groups are absent, the word pseudorotaxane is used (threading or dethreading can occur freely). Pseudorotaxane DB24C8•DBA is stabilized for the most part by hydrogen bonds between the oxygen atoms of DB24C8 and (i) the NH_2^+ protons of DBA and (ii) the benzylic methylene protons of DBA. Replacing two oxygen atoms in DB24C8 with two sulfur atoms as in the macrocycle crown-O6S2 (containing a 1,3-dithiol-2-thione unit instead of the one *o*-phenylene) presented in Scheme 2.8 reduces the association constant by one order of magnitude ($K_a = 2.75 \times 10^3 \text{ M}^{-1}$ in CD_2Cl_2 at 300 K) [48]. As the exchange is slow on the 400 MHz NMR chemical shift timescale at 300 K, the association constant is readily determined from the $^1\text{H-NMR}$ spectrum using the integrals of complexed and uncomplexed species (Figure 2.12), when knowing the total concentrations of each species (the so-called single-point method). In general, if $I(A_u)$ denotes the integral of a proton resonance belonging to a species A in its uncomplexed form and $I(A_c)$ denotes the integral of the corresponding proton resonance belonging to A in its 1:1 complex with a species B, then the association constant for the A•B complex is given by

$$K_a = (I(A_c))/(I(A_u) \times [c(B) - (I(A_c) \times c(A))/(I(A_u) + I(A_c))]),$$

where $c(A)$ and $c(B)$ are the initial concentrations of the species A and B (i.e., their total concentrations whether complexed or uncomplexed).

Substitution of the oxygen atoms of crown ethers with sulfur or nitrogen atoms (thia- and aza-crown ethers) can provide suitable host molecules for softer metal ions, such as Ag^+ or Hg^{2+} . Cryptands and spherands (Figure 2.11) exhibit a higher degree of rigidity and are hence more preorganized receptors for specific metal cations, resulting in higher association constants [45, 46]. Calixarenes composed of phenol units (usually 4, 6, or 8) linked together by methylene bridges can include cations either via electrostatic interactions with the oxygen atoms or via cation- π interactions to the aromatic

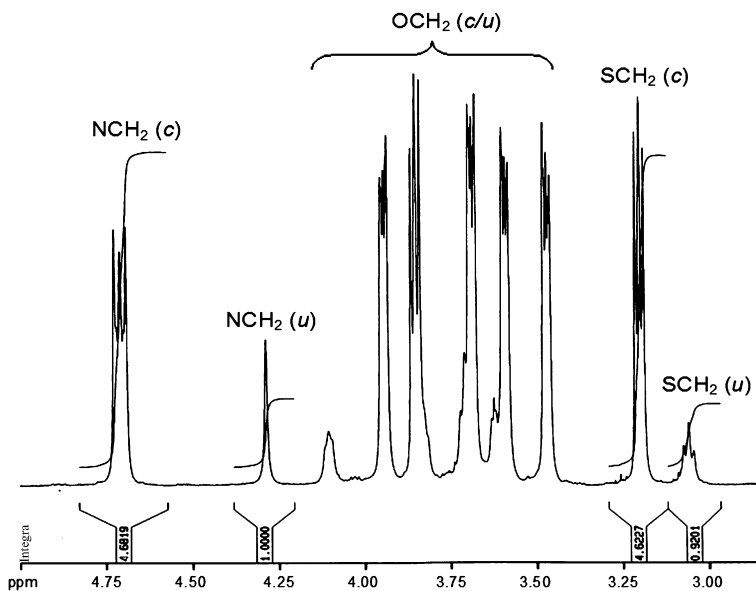


Figure 2.12. Part of the $^1\text{H-NMR}$ spectrum (400 MHz, CD_2Cl_2) of a mixture of crown-O6S2 and DBA in 10^{-2}M concentrations; c = complexed species (pseudorotaxane crown-O6S2•DBA); u = uncomplexed species (either crown-O6S2 or DBA).

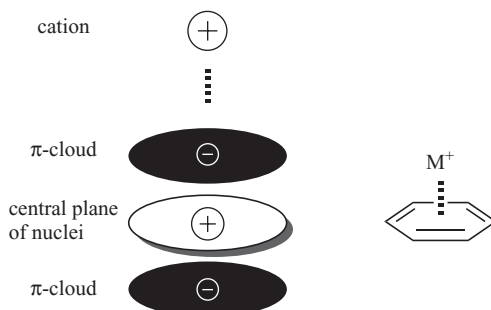


Figure 2.13. Schematic illustration of the cation- π -interaction, which originates from the quadrupole moment of benzene.

units [45]. This latter interaction is a result of the quadrupole moment of benzene (Figure 2.13). Based on this interaction, a variety of ammonium cations have been employed as templates for formation of cyclophanes of different sizes, as described in Chapter 14 (cyclophane = macrocycle containing at least one aromatic unit). Calixpyrroles contain instead bridged pyrrole units (Figure 2.11) and are some of the strongest known anion receptors [49]; thus, calix[4]pyrrole binds fluoride (as tetrabutyl ammonium salt) via its four pyrrole NH groups by an association constant of $1.7 \times 10^4 \text{M}^{-1}$ in CD_2Cl_2 [50]. Protonated or alkylated azacrown ethers also act as host molecules for anions. For example, at low pH, such crown ethers can bind biologically important

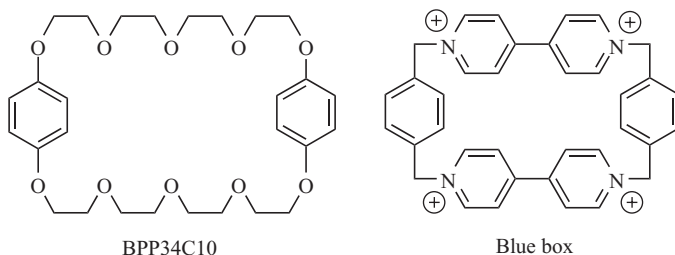


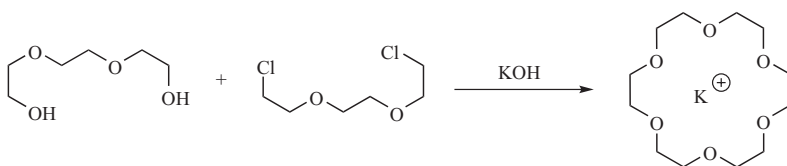
Figure 2.14. Host molecule for electron-deficient aromatics (left) and for electron-rich aromatics (right).

anions such as ATP^+ in water and catalyze the hydrolysis of this nucleotide [51]. Amides, such as cyclic peptides, can also be employed for anion complexation (see Chapter 14).

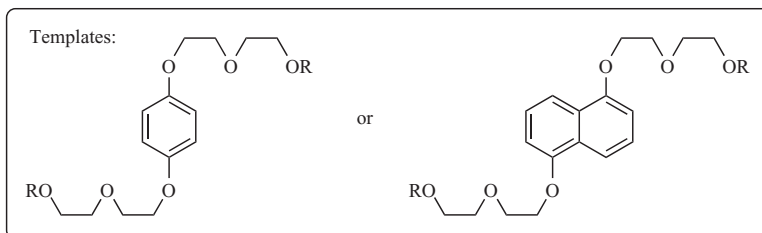
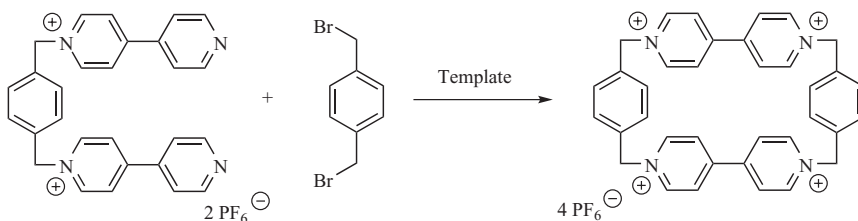
Crown ethers containing a phenanthroline unit (Figure 2.11) can bind Cu^+ , and by metal-directed assembly, a variety of rotaxanes, catenanes (two or more interpenetrating rings), and molecular knots have been prepared from such scaffolds [52, 53]. When coordinating Cu^+ , the catenane is called a catenate, while the uncomplexed catenane with free ligand units is termed a catenand.

2.5.2 π -Donor-Acceptor Complexation

Crown ethers containing electron-rich aromatics such as hydroquinones are excellent receptors for π -electron-deficient guests [54–57]. Thus, bisparaphenylene[34]crown-10 (BPP34C10 Figure 2.14) forms a donor-acceptor complex with paraquat (*N,N'*-dimethyl-4,4'-bipyridinium), a pseudorotaxane. On the other hand, the cyclophane cyclobis(paraquat-*p*-phenylene), also termed *blue box* (Figure 2.14), is able to accommodate electron-rich aromatics, such as hydroquinone, 1,5-dihydroxynaphthalene, and TTF, in its cavity [54–57]. This cyclophane is prepared by a so-called template-directed synthesis (as is the synthesis of crown ethers, see Box 2.4). The dependence on donor strength of the encapsulated molecule is reflected by the fact that the association constant of encapsulation in MeCN is three orders of magnitude higher for the parent TTF ($K_a = 1 \times 10^4 \text{ M}^{-1}$) than for tetramethylthio-TTF (TMT-TTF, $K_a = 180 \text{ M}^{-1}$) [57]. The complexations are somewhat weaker in acetone, but again, a reduced binding of TMT-TTF relative to TTF is observed (Figure 2.15). TTF is indeed a stronger electron donor than TMT-TTF, as reflected by the half-wave potentials of their first oxidation listed in Figure 2.15. A linear correlation between the Gibbs free energy of association and $1/(E_{\text{TTF}}^{\text{ox1}} - E_{\text{blue box}}^{\text{red1}})$ was established, where $E_{\text{blue box}}^{\text{red1}}$ is the first reduction potential of blue box. Deviations from this correlation can be explained by differences in overlap integrals; thus, the bispyrrolo-TTF BP-TTF has a significantly stronger association than the parent TTF despite it being a weaker electron donor (higher redox potential). Additional stabilization of the complex can be obtained by functionalizing the donor with polyether chains, thereby introducing hydrogen-bonding interactions between the polyether oxygens and the pyridinium α -H protons. Thus, the association constant for the monopyrrolo-TTF MP-TTF-PEG and blue box is about double as that between MP-TTF and blue box (Figure 2.15) [58]. The complexation between blue box and electron donors has successfully been employed to construct a variety of

BOX 2.4 TEMPLATE-DIRECTED SYNTHESIS**Synthesis of 18C6**

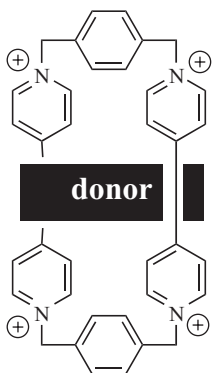
References: (a) Pedersen, C. J. (1967). *Journal of the American Chemical Society*, 89, 7017–7036; (b) Pedersen, C. J. (1967). *Journal of the American Chemical Society*, 89, 2495–2496; (c) Gokel, G. W., Cram, D. J., Liotta, C. L., Harris, H. P., Cook, F. L. (1977). *Organic Syntheses*, 57, 30.

Synthesis of cyclobis(paraquat-*p*-phenylene) or “blue box”

Reference: Asakawa, M., Dehaen, W., L’abbé, G., Menzer, S., Nouwen, J., Raymo, F. M., Stoddart, J. F., Williams, D. J. (1996). *The Journal of Organic Chemistry*, 61, 9591–9595.

interlocked molecules such as rotaxanes and catenanes [54]. Examples hereof shall be covered in Chapters 3 and 8.

When complexation of one guest species enhances binding of a second, the binding is called cooperative. An example hereof is shown in Figure 2.16. The calix[4]pyrrole can, like calix[4]arenes, take four different conformations (cone, partial cone, 1,3-alternate, 1,2-alternate). Upon binding a chloride anion, it is forced into the cone conformation. For calixpyrroles in which each pyrrole is fused to a TTF, this allows complexation of the electron-poor C₆₀ via donor–acceptor interactions [59]. Further examples of donor–acceptor complexes are provided in Chapters 8 and 9.





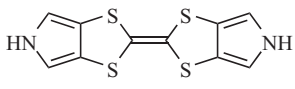
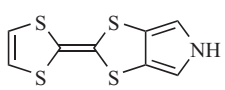
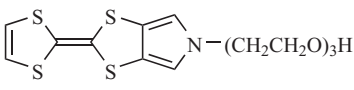
Donor	K_a / M^{-1}	$E_{1/2}^1 / V$
 TTF	2,600	+0.34
 TMT-TTF	40	+0.51
 BP-TTF	12,000	+0.38
 MP-TTF	5,800	+0.37
 MP-TTF-PEG	13,000	+0.38

Figure 2.15. Association constants (K_a) between blue box and different TTF derivatives in acetone and the first half-wave oxidation potential (vs. Ag/AgCl) of TTFs in MeCN + 0.1M Bu₄NPF₆.

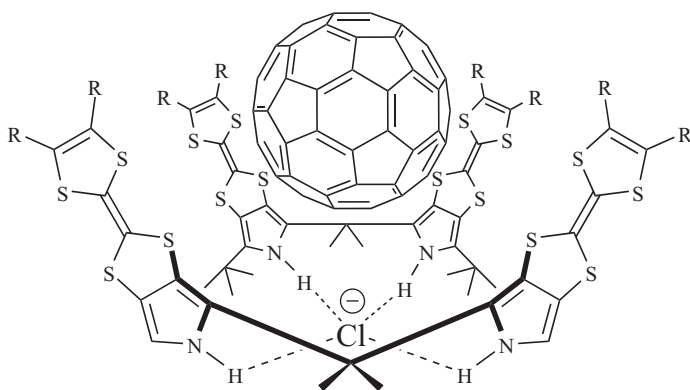


Figure 2.16. Chloride-triggered binding of C₆₀ by a TTF-calixpyrrole.

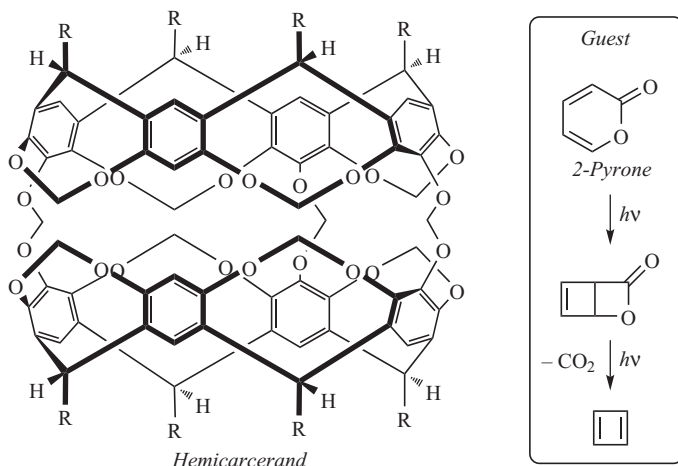


Figure 2.17. Trapping of cyclobutadiene in a hemicarcerand.

2.5.3 Encapsulation of Instable Compounds

Permanent trapping of molecules has been accomplished in the so-called carcerands, which consist of two bowl-like units connected by bridges [60]. The guest molecule becomes trapped during the synthesis of the carcerand. If the guest can escape at high temperature, the term hemicarcerand is used. The complexes are termed carciplexes and hemicarceplexes, respectively. Instable molecules such as cyclobutadiene and benzyne have been studied in such systems by entrapping more stable precursors [61, 62]. Thus, 2-pyrone was trapped in a hemicarcerand and converted inside the cavity by irradiation to cyclobutadiene and CO_2 , the latter being expelled from the cavity (Figure 2.17) [61]. This encapsulation allowed for $^1\text{H-NMR}$ spectroscopic measurements, from which a singlet ground-state configuration of cyclobutadiene was deduced.

2.5.4 Encapsulation of Organic Molecules in Water

Cyclodextrins (CDs) [63] and cucurbiturils (CBs) [64] (Figure 2.18) contain hydrophobic cavities and are hence excellent receptors for unpolar organic molecules in water. Both classes of macrocycles can exist in different ring sizes. The cavity diameters of α -, β -, and γ -CD are 4.7–5.3, 6.0–6.5, and 7.5–8.3 Å, respectively. By incorporation of suitable functional groups at the rim of the CD, artificial enzymes can be obtained that catalyze specific reactions, as described in Chapter 11. CBs are composed of glycoluril units linked by methylene bridges. CB[6] with 6 glycolurils has a cavity diameter of ca. 5.7 Å, which is similar to that of α -CD. In contrast to CDs, CBs have two identical openings. In addition to a hydrophobic cavity, CBs have polar carbonyl groups that allow binding of ions and molecules through charge–dipole and hydrogen-bonding interactions. Thus, CB[7] has a cavity size similar to that of β -CD and forms, in contrast to β -CD, a very stable 1:1 inclusion complex with paraquat in water characterized by an association constant of $\log K_a = 5.30$ [65]. Very recently, it was shown that also acyclic CBs, containing four sodium sulfonate groups to enhance water solubility, are

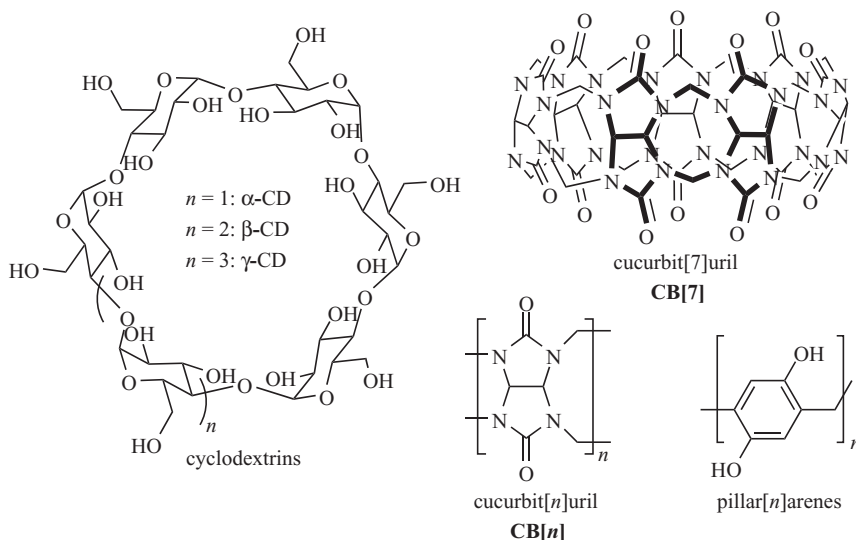


Figure 2.18. Macrocycles with hydrophobic cavities.

interesting host molecules, which were employed to enhance the solubility and bioactivity of several poorly soluble pharmaceuticals [66].

Calixarenes functionalized with water-solubilizing groups can also be employed for encapsulation of organic molecules in water. A related class of molecules is the pillararenes composed of hydroquinone units connected by methylene bridges (Figure 2.18) [67]. The rigidity of these macrocycles enhances selectivity in binding in comparison to, for example, calixarenes. On account of the electron-rich hydroquinones, pillararenes can encapsulate viologens such as paraquat in organic solution. By incorporation of water-solubilizing groups (such as carboxylate or ammonium groups), complexation of viologens can also take place in water as can complexation of unipolar alkyl chains in the hydrophobic cavity [67].

2.6 DNA AND HYDROGEN-BONDED DIMERS

Hydrogen bonding is the most important of all weak interactions and is, for example, responsible for folding of peptides and proteins and the double helix formation of two deoxyribonucleic acid (DNA) strands. A DNA strand (Figure 2.19) contains the purine and pyrimidine bases thymine (T), adenine (A), cytosine (C), and guanine (G) linked to a backbone of phosphorylated sugars. Thymine and adenine have complementary hydrogen donor and acceptor sites as do cytosine and guanine, and the helix formation between two strands is formed via pairing of these complementary bases, as shown in Figure 2.20. Due to the phosphate backbone, DNA is a polyanion, which can bind to polycations, such as protonated polyamines (see Chapter 14).

In general, hydrogen-bonded dimer complexes depend on the number of hydrogen bonds (primary interactions) and on how the donor and acceptor groups are situated relative to each other (secondary interactions, *Jorgensen model*), as illustrated in

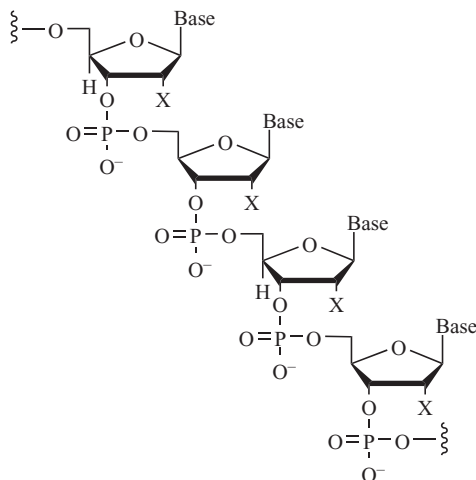


Figure 2.19. Portion of polynucleotide (X = H: DNA; X = OH: RNA, ribonucleic acid).

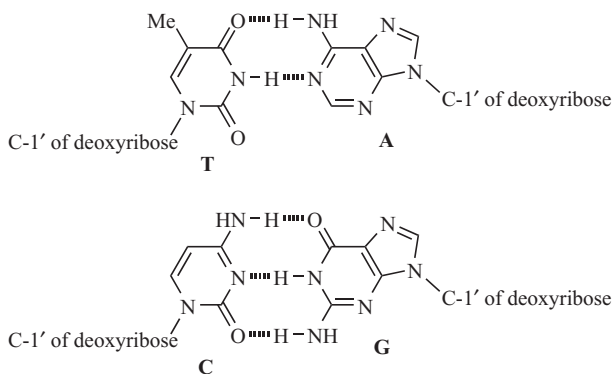


Figure 2.20. Base pairing in double-stranded DNA.

Figure 2.21 [68]. When designing the most stable dimer complexes, one should seek to have as many hydrogen donor sites (D) in one molecule and the corresponding acceptor sites (A) in the other rather than having the sites mixed in the two molecules. Thus, a DD-AA complex is more stable than an AD-DA complex. This will be of further focus in Chapter 4.

Owing to their Y-shaped, planar orientations, ureas and guanidiniums are useful as bidentate receptors for anions such as carboxylates or phosphates via hydrogen-bonding interactions (Figure 2.22) [69]. Using this recognition motif for design of oxanion acceptors has strong inspiration from nature. Thus, it plays an important role in enzyme active sites as the guanidinium group is part of the side chain of the amino acid arginine, and it also contributes to the stabilization of protein tertiary structures via internal salt bridges.

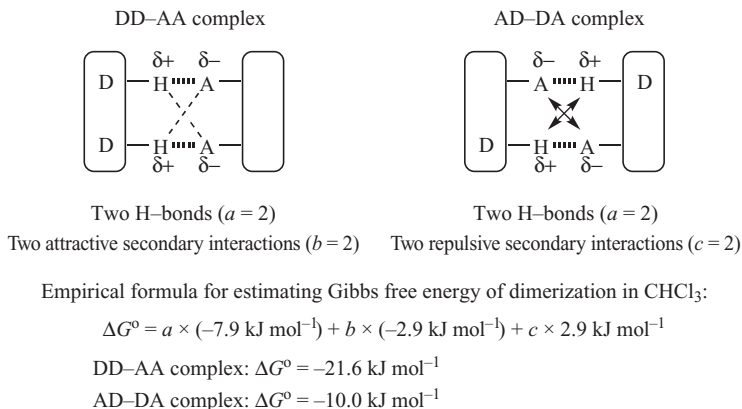


Figure 2.21. Hydrogen-bonded dimer complexes and empirical formula for estimating Gibbs free energy of dimerization [68].

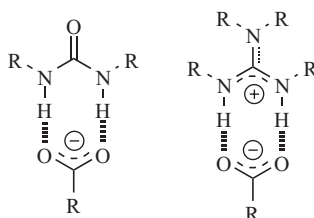


Figure 2.22. Ureas (left) and guanidiniums (right) are receptors for carboxylate and phosphate anions.

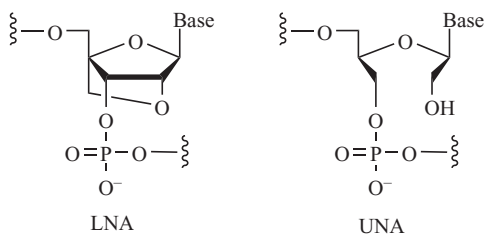


Figure 2.23. Structures of LNA and UNA nucleotides.

2.7 MODIFIED OLIGONUCLEOTIDES

Oligonucleotides can be changed by either modifying the nucleobases, sugars, and/or the phosphate backbone, which can have a strong influence on their ability to form duplexes. Short, modified oligonucleotides have found use in biotechnology, diagnostics, therapeutics, and nanotechnology. Here, two chemical modifications of the sugar part shall be briefly covered: the locked nucleic acid (LNA) and unlocked nucleic acid (UNA) (Figure 2.23) [70]. The LNA has a methylene bridge between the 2'-oxygen

and 4'-carbon of the ribose sugar. Gradual heating of a DNA duplex will cause separation of the two strands, and the temperature at which half of the duplex is denatured is termed the melting temperature. By including LNA monomers into a strand of DNA or RNA, an increase in the melting temperature by 2–10°C per LNA can be observed. The LNA has, for this reason, found use in antisense oligonucleotide technology by protecting target RNA from cellular nucleases [70]. In UNA, which is synthetically easier to accomplish than LNA, the ribose ring is cleaved between the 2'- and 3'-carbons, which leads to a more flexible structure. Indeed, incorporation of UNA in oligonucleotides not only decreases the stability of duplex formation, but also increases or decreases specificity of oligonucleotide binding, and applications are under development.

2.8 AMINO ACIDS: PEPTIDE BUILDING BLOCKS

Natural proteins are constructed, via amide bonds (in this context also termed peptide bonds), from 20 different α -amino acids in which the “ α -carbon” bears a CO_2H , NH_2 , H, and a side chain (Figure 2.24 and Figure 2.25). Based on the side chain, a classification into three groups is usually done: polar (serine, threonine, lysine, arginine, histidine, asparagine, aspartic acid, glutamine, glutamic acid), hydrophobic (alanine, valine, leucine, isoleucine, methionine, tyrosine, tryptophan, phenylalanine), or “special” (glycine, proline, cysteine). Except for glycine, the amino acids are chiral and can exist as two enantiomers (L- and D-amino acids). The L-amino acids are the components of most proteins, but D-amino acids are, however, found in the peptidoglycan cell walls of bacteria. The specific choice and sequence of amino acids in peptides are responsible for both the secondary structure (folding of peptide chain) and the tertiary structure

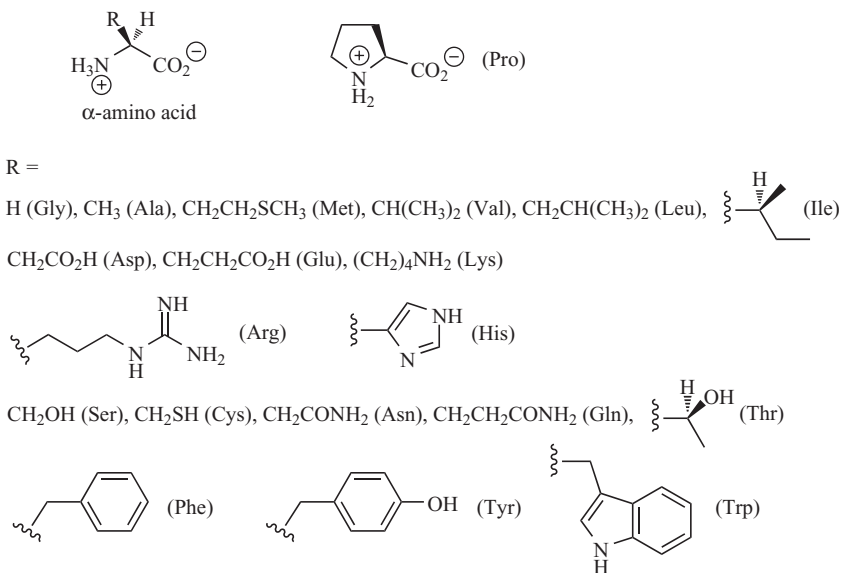


Figure 2.24. Naturally occurring amino acids.

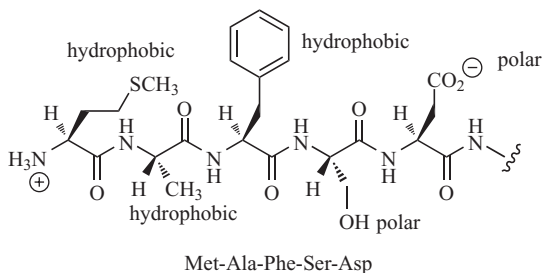


Figure 2.25. An example of a pentapeptide with hydrophobic and polar residues.

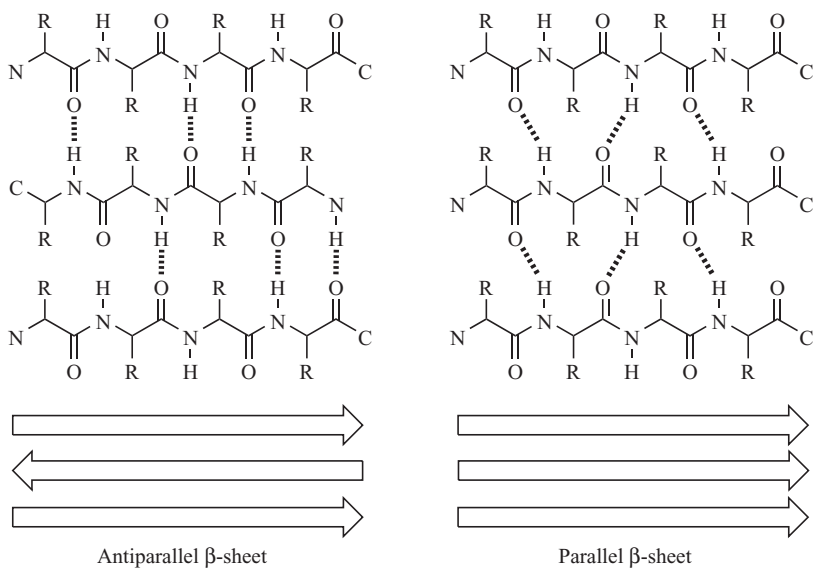
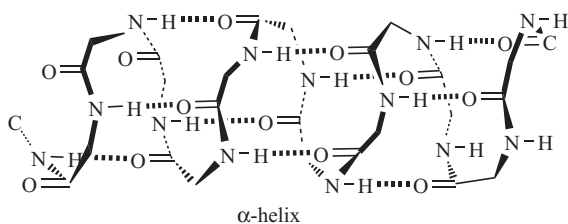


Figure 2.26. Secondary structures in peptides: α -helices and β -sheets.

(three-dimensional global structure of the folded subunits) and hence for the overall function of the polypeptide, for example, as catalyst (enzyme), membrane channel, or for energy transduction. The most important secondary structures in peptides are α -helices and β -sheets (Figure 2.26) [71]. α -Helices are formed via hydrogen bonding between C=O and NH groups four residues apart in the polypeptide chain. β -Sheets

are formed by hydrogen bonds between stretched polypeptide chains (β -strands) typically 3 to 10 amino acids long. While reasonable sequence-to-structure relationships exist for protein folding into these secondary structures, it is more challenging to predict folding into tertiary structures in which hydrophobic surfaces are shielded from water. β -Sheets are often formed from peptides containing amino acids with alternating polar and hydrophobic residues. These sheets can associate further into structures such as β -sandwiches in which hydrophobic faces are buried. One key design principle for the higher-order assembly of α -helices is that side chains of hydrophobic residues being three or four units apart will be close together in space, and the helices will then assemble in water to bury these hydrophobic faces.

By “peptide engineering,” efforts are focused on designing new, unnatural peptides with specific enzyme functions or biological activity [71]. In general, computer models are used extensively in the field to design peptides that fold to the desired structure. One approach is to make the amino acids more conformationally restricted to enforce biological activity of the peptide. Another approach is to use more flexible amino acid building blocks such as β -amino acids, which contain one additional methylene group, resulting in peptides with new properties and biological activity. For example, the β -hexapeptide shown in Figure 2.27 was found to be stable to cleavage by pepsin at pH 2 in water for at least 60 h at 37°C, while the related α -peptide was cleaved instantaneously under these conditions [72]. Solid-support synthesis, together with a variety of peptide coupling reagents (see Box 2.5), has been developed to facilitate peptide synthesis.

Cyclic peptides can be employed to form self-assembled nanotubes, as shown in Figure 2.28 [73]. These peptides are composed of alternating L- and D-amino acids, which adopt a conformation so that the N–H hydrogen-bond donor and C=O hydrogen-bond acceptor are situated perpendicular to the plane of the macrocycle. By changing the number of amino acids in the cycle, nanotubes of different sizes can be obtained. Such nanotubes have potential as transport channels for molecules across lipid bilayer membranes.

Instead of modifying the sugar unit (LNA and UNA described earlier), another successful approach to DNA mimics and biotechnological applications has been to replace the entire phosphodiester backbone by a pseudopeptide backbone, resulting in the so-called peptide nucleic acid (PNA) (Figure 2.29) [74]. The backbone of PNA is composed of aminoethylglycine units, and a nucleobase is attached to the central

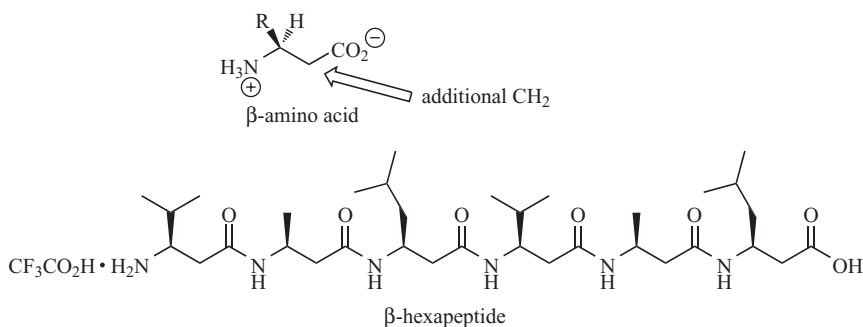
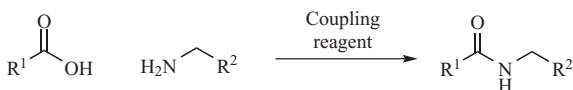
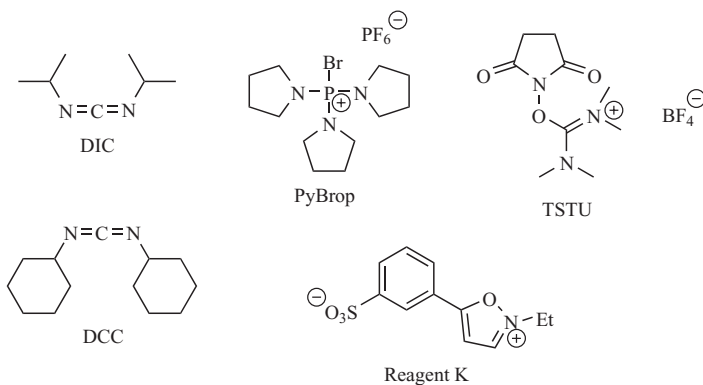


Figure 2.27. General structure of a β -amino acid and an example of a β -hexapeptide.

BOX 2.5 PEPTIDE COUPLING REACTIONS**Examples of coupling reagents****Reviews:**

- (a) Montalbetti, C. A. G. N., Falque, V. (2005). *Tetrahedron*, 61, 10827–10852;
 (b) Valeur, E., Bradley, M. (2009). *Chemical Society Reviews*, 38, 606–631.

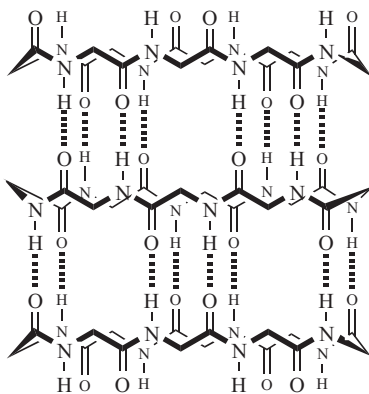


Figure 2.28. Nanotube formed from self-assembled cyclic peptides. The side chains have been removed in the drawing for clarity.

amine of each of these units via an acetyl linker. PNA is thus a hybrid between an oligonucleotide (the nucleobases) and a peptide (the backbone) and shows properties relating to both these oligomers. While phosphodiester oligomers are anionic, the PNA backbone is neutral and, in consequence, the stabilities of PNA hybrids are fairly independent of the ionic strength of the medium. PNA oligomers form strong complexes

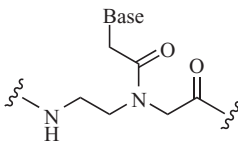


Figure 2.29. Chemical structure of PNA (base = adenine, cytosine, guanine, or thymine).

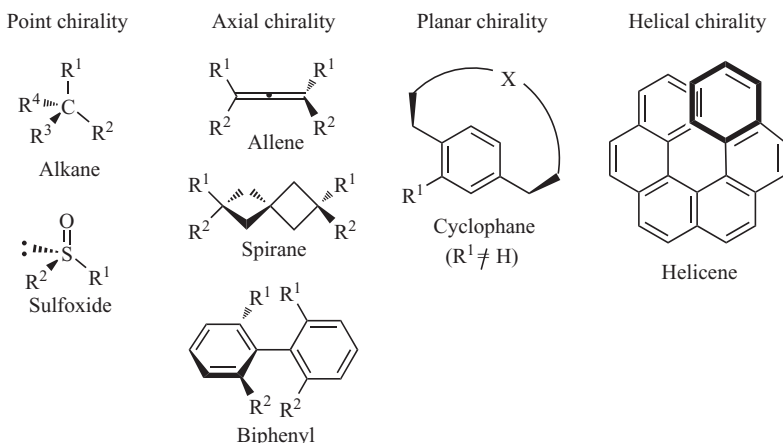


Figure 2.30. Different kinds of chirality.

with high sequence discrimination to complementary oligomers of DNA, RNA, or another PNA. In general, the thermal stabilities for identical sequences follow the order PNA-PNA > PNA-RNA > PNA-DNA [74]. As PNAs are not easily recognized by nucleases or proteases, they are resistant to enzyme degradation.

2.9 CHIRALITY

The chirality of amino acids is important for the fundamental processes of life. The chirality originates in this case from the presence of four different groups at a stereogenic carbon atom. Sulfoxides with different substituent groups present another example of this so-called point chirality as the lone pair on sulfur constitutes the fourth substituent. Other types of chirality are axial chirality (displayed by suitably substituted allenes, spiranes, and biphenyls), planar chirality (displayed by suitably functionalized cyclophanes), and helical chirality (displayed by helicenes), as shown in Figure 2.30. The chirality of substituted biphenyls and cyclophanes originates from hindered rotation about single bonds and is termed atropisomerism; if the temperature is high enough, racemization may occur by rotation about the single bond(s). For a planar chiral cyclophane, such racemization will depend on the size of substituent groups and the length and bulkiness of the bridge X. As a guideline, monosubstituted paracyclophanes with a bridge length shorter than 11 atoms are stable to racemization at room temperature [75].

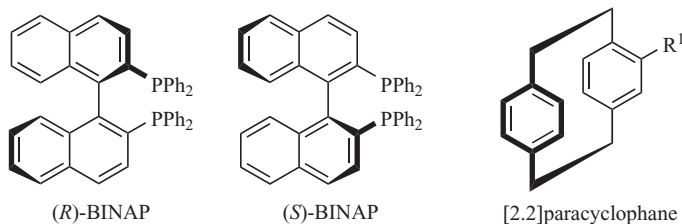
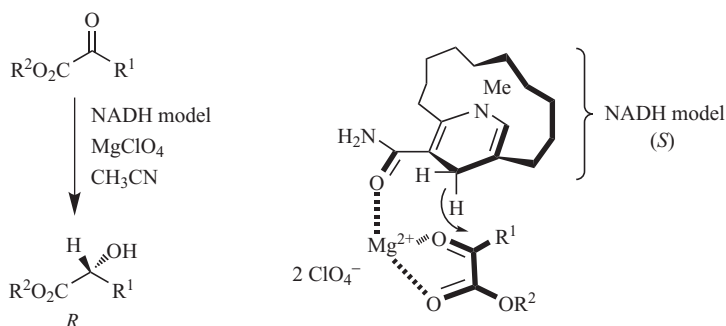


Figure 2.31. The two enantiomers of BINAP and a substituted [2.2]paracyclophane.



Scheme 2.9. The parapyridinophane NADH model, exhibiting planar chirality, reduces pyruvate substrates by stereospecific hydride transfer.

The organophosphorus compound 2,2'-bis(diphenylphosphino)-1,1'-binaphthyl (BINAP, Figure 2.31) presents an example of a molecule displaying axial chirality. (*R*)-BINAP and (*S*)-BINAP are widely used as bidentate ligands in metal-catalyzed asymmetric synthesis, for example, in asymmetric hydrogenation of alkenes and ketones [76]. Several examples of using differently substituted [2.2]paracyclophane catalysts (Figure 2.31) in this field have also been reported [77]. Several heteroaromatics showing planar chirality are known as well. Thus, a parapyridinophane was designed for stereospecific hydride transfer to a pyruvate substrate (Scheme 2.9) [78], hence mimicking the enzyme L-lactate dehydrogenase which, together with its nicotinamide adenine dinucleotide (NADH) coenzyme, catalyzes the enantioselective reduction of pyruvate to L-lactate. In the presence of magnesium ions, a variety of pyruvate analogs were stereospecifically reduced by the model system into chiral lactate analogs in high enantioselectivities. The magnesium ion is expected to coordinate both the amide carbonyl oxygen atom of the cyclophane and the two carbonyl oxygen atoms of the substrate. The specificity is explained by the fact that the bridge only allows approach of the substrate from its opposite side; that is, only one side of the NADH ring is the active face.

2.10 CONJUGATED OLIGOMERS AND POLYMERS

As described earlier, oligonucleotides and peptides are examples of oligomers/polymers with saturated or partly saturated backbones. Polystyrene (used for plastic

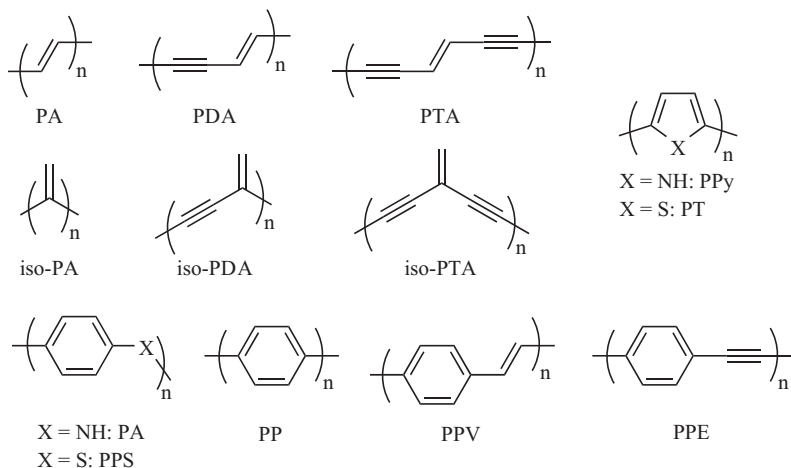


Figure 2.32. Conjugated polymers.



Figure 2.33. Linear and cross-conjugated pathways in the same molecule indicated by thick bonds. The cross-conjugated pathway involves two consecutive single bonds, while the linear one has alternating double and single bonds.

model kits) and polyamides (nylon, synthetic fibers) are other examples hereof. π -Conjugated oligomers and polymers comprise another class and are extensively employed for the construction of advanced materials such as conductive polymers, field-effect transistors, photovoltaic devices, organic light-emitting diodes (OLEDs), electrochromic materials, sensors, fluorescent materials, NLO materials, and molecular wires for molecular electronics (see Chapters 3 and 4) [79–86]. Most engineering of conjugated oligomers is focused on modifying the “parent structures” shown in Figure 2.32 in regard to solubility, processability, stability, highest occupied molecular orbital–lowest unoccupied molecular orbital (HOMO–LUMO) gap, and second- and third-order NLO properties. These structures constitute polyacetylenes (PAs), poly(diacetylene)s (PDAs), poly(triacetylene)s (PTAs), their cross-conjugated counterparts (*iso*-PAs/PDAs/PTAs), as well as polypyrroles (PPys), polythiophenes (PTs), polyanilines (PAs), poly(phenylenesulfide)s (PPSs), polyphenylenes (PPs), poly(phenylenevinylene)s (PPVs), and poly(phenyleneethynylene)s (PPEs).

The difference between linearly and cross-conjugated molecules (Figure 2.33) is an important design criterion [85, 86]. Thus, *iso*-PAs, also termed dendralenes, are, in fact, best characterized structurally as isolated butadiene units in regard to electronic properties. Thus, a series of derivatives ([4]-[8]dendralenes) of the parent structure exhibits almost the same longest-wavelength absorption maximum of around 220 nm (5.6 eV) [87], which is similar to that of butadiene (217 nm). In contrast, the longest-wavelength absorption energy of linearly conjugated PA is around 1.8 eV [88]. The

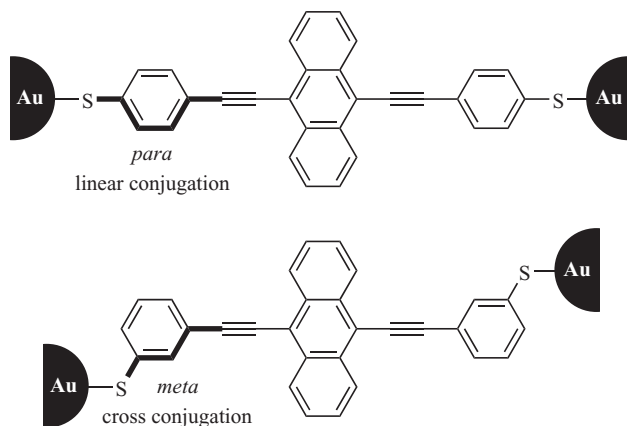


Figure 2.34. Anchoring of a single molecule between two gold electrodes via *para* or *meta* configurations.

longest-wavelength absorption maximum of (*E*)-PTA has been determined to 2.8 eV [89], while a value of 3.5 eV is extrapolated for the cross-conjugated *iso*-PTA from systematic studies on monodisperse oligomers [90]. The less efficient electron delocalization via cross conjugation relative to linear conjugation is also reflected in molecular electronics conductivity studies on single molecules. Thus, the molecular wire shown in Figure 2.34 was anchored between two gold electrodes via either *para*-phenylene (linear conjugation) or *meta*-phenylene (cross-conjugation) groups [91]. The currents recorded for the *meta*-anchoring were almost two orders of magnitudes smaller than those measured for the *para*-anchoring.

Supramolecular polymers based on host–guest complexation between monomer units are covered in Chapter 4; in contrast to covalent polymers, these supramolecular polymers can be formed reversibly. Another important class is the branched “tree-shaped” nanosized molecules called dendrimers. These molecules can have molecular sizes and molecular weights similar to proteins and are covered in Chapter 13.

2.11 NONLINEAR OPTICAL CHROMOPHORES

Nonlinear optical (NLO) materials change the frequency of incident laser light. Thus, a second-order material results in frequency doubling, while a third-order material results in frequency tripling. Design of organic materials with this property is attractive due to fast responses and high-speed applications, large nonresonant nonlinearities, and potentially low costs [92, 93]. Moreover, there are unlimited design possibilities for tailoring the NLO properties of organic molecules, and suitable oligomers and polymers can be made soluble by proper functionalizations to allow them to be processed into devices. NLO phores can also be incorporated in crystals or self-assembled films. A drawback of organic materials in comparison to inorganic NLO crystals is, however, often a reduced photochemical stability.

In general, design of organic molecules exhibiting second- or third-order NLO properties is based on molecules with donor and acceptor moieties separated by a



Figure 2.35. Schematic drawing of organic NLO phore.

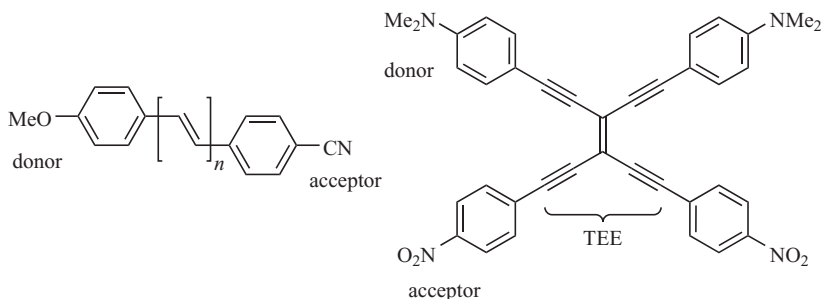


Figure 2.36. Examples of organic NLO phores.

π -conjugated bridge (Figure 2.35) [92, 93]. For second-order NLO properties, one seeks a structure that will provide (i) large change in dipole moment on excitation, (ii) large transition dipole moment, and (iii) small-energy difference between the excited and ground states. Often the NLO properties are enhanced by expanding the conjugated bridge. For example, for the donor–acceptor OPVs shown in Figure 2.35, the first hyperpolarizability (second-order NLO) increases with the length of the conjugated spacer, proceeding from $n = 1$ to 3 [94]. For this series of molecules, the second hyperpolarizability (third-order NLO) was also found to increase with the conjugation length. Donor–acceptor substituted tetraethynylethenes (TEEs), like the one shown in Figure 2.36, have been found to be strong third-order NLO phores [93]. It is more difficult to generalize the optimum structural design for gaining third-order NLO properties, but from systematic studies on arylated TEEs, it seems that two-dimensional conjugation and low symmetry are the most powerful tools for optimizing the second hyperpolarizability in small molecules [93]. The advantage of the TEE core is that it allows coplanarity of the aryl groups and hence two-dimensional conjugation.

REFERENCES

- [1] Wald, G. (1968). Molecular basis of visual excitation. *Science*, *162*, 230–239.
- [2] Kochendoerfer, G. G., Lin, S. W., Sakmar, T. P., Mathies, R. A. (1999). How color visual pigments are tuned. *Trends in Biochemical Sciences*, *24*, 300–305.
- [3] Nielsen, M. B. (2009). Model systems for understanding absorption tuning by opsin proteins. *Chemical Society Reviews*, *38*, 913–914.
- [4] Tsien, R. Y. (1989). Fluorescent probes of cell signaling. *Annual Review of Neuroscience*, *12*, 227–253.
- [5] Chalfie, M., Tu, Y., Euskirchen, G., Bard, W. W., Prasher, D. C. (1994). Green fluorescent protein as a marker for gene expression. *Science*, *263*, 802–805.

- [6] Sanders, J. K. M., Jackson, S. E. (Guest Eds.) (2009). Highlights in chemical biology (issue 10). *Chemical Society Reviews*, 38, 2813–2968.
- [7] Ferraris, J., Cowan, D. O., Walatka, V., Jr., Peirlstein, J. H. (1973). Electron transfer in a new highly conducting donor-acceptor complex. *Journal of the American Chemical Society*, 95, 948–949.
- [8] Batail, P. (Ed.). (2004). Molecular conductors (special issue). *Chemical Reviews*, 104, 4487–5782.
- [9] For a treatment of Weitz- and Wurster-type redox systems, see Deuchert, K., Hünig, S. (1978). Multistage organic redox systems—A general structural principle. *Angewandte Chemie (International ed. in English)*, 17, 875–886.
- [10] Xie, Q., Ptrez-Cordero, E., Echegoyen, L. (1992). Electrochemical detection of C_{60}^{6-} and C_{70}^{6-} : Enhanced stability of fullerides in solution. *Journal of the American Chemical Society*, 114, 3978–3980.
- [11] Noviadri, I., Bolskar, R. D., Lay, P. A., Reed, C. A. (1997). Solvent effects on the electrochemistry of C_{60} . Thermodynamics of solvation of C_{60} and fullerides. *The Journal of Physical Chemistry B*, 101, 6350–6358.
- [12] (a) Sariciftci, N. S., Braun, D., Zhang, C. (1993). Semiconducting polymer-buckminsterfullerene heterojunctions: Diodes, photodiodes, and photovoltaic cells. *Applied Physics Letters*, 62, 585–587; (b) Chan, S.-H., Lai, C.-S., Chen, H.-L., Ting, C., Chen, C.-P. (2011). Highly efficient P3HT: C_{60} solar cell free of annealing process. *Macromolecules*, 44, 8886–8891.
- [13] Gisselbrecht, J.-P., Moonen, N. N. P., Boudon, C., Nielsen, M. B., Diederich, F., Gross, M. (2004). Redox properties of linear and cyclic scaffolds based on di- and tetraethynylethene. *European Journal of Organic Chemistry*, 2959–2972.
- [14] Diederich, F., Kivala, M. (2010). All-carbon scaffolds by rational design. *Advanced Materials*, 22, 803–812.
- [15] Nielsen, M. B., Schreiber, M., Baek, Y. G., Seiler, P., Lecomte, S., Boudon, C., Tykwinski, R. R., Gisselbrecht, J.-P., Gramlich, V., Skinner, P. J., Bosshard, C., Günter, P., Gross, M., Diederich, F. (2001). Highly functionalized dimeric tetraethynylethenes and expanded radialenes: Strong evidence for macrocyclic cross-conjugation. *Chemistry—A European Journal*, 7, 3263–3280.
- [16] Lincke, K., Frellsen, A. F., Parker, C. R., Bond, A. D., Hammerich, O., Nielsen, M. B. (2012). A tetrathiafulvalene-functionalized radiannulene with multiple redox states. *Angewandte Chemie (International ed. in English)*, 51, 6099–6102.
- [17] Mitzel, F., Boudon, C., Gisselbrecht, J.-P., Seiler, P., Gross, M., Diederich, F. (2004). Donor-substituted perethynylated dehydroannulenes and radiannulenes: Acetylenic carbon sheets featuring intense intramolecular charge transfer. *Helvetica Chimica Acta*, 87, 1130–1157.
- [18] Bryce, M. R., Cooke, G. (1991). Halogenation of tetrathiafulvalene. *Synthesis*, 263–265.
- [19] Iyoda, M., Kuwatani, K. H., Ogura, E., Suzuki, H., Ito, H., Mori, T. (1997). Halogenated bis(methylthio)tetrathiafulvalenes as a unique donor system. *Chemistry Letters*, 26, 599–600.
- [20] Lincke, K., Christensen, M. A., Diederich, F. (2011). Acetylenic tetrathiafulvalene scaffolds—Intramolecular charge-transfer molecules. *Helvetica Chimica Acta*, 94, 1743–1753.
- [21] Simonsen, K. B., Svenstrup, N., Lau, J., Simonsen, O., Mørk, P., Kristensen, G. J., Becher, J. (1996). Sequential functionalization of bis-protected tetrathiafulvalene-dithiolates. *Synthesis*, 407–418.
- [22] Simonsen, K. B., Becher, J. (1997). Tetrathiafulvalene thiolates: Important synthetic building blocks for macrocyclic and supramolecular chemistry. *Synlett: Accounts and Rapid Communications in Synthetic Organic Chemistry*, 1211–1220.
- [23] Jeppesen, J. O., Becher, J. (2003). Pyrrolo-tetrathiafulvalenes and their applications in molecular and supramolecular chemistry. *European Journal of Organic Chemistry*, 3245–3266.

- [24] Feringa, B. L., Browne, W. R. (Eds.). *Molecular Switches*, Vols. 1 and 2, Wiley-VCH, Weinheim, 2011.
- [25] Bandara, H. M. D., Burdette, S. C. (2012). Photoisomerization in different classes of azobenzene. *Chemical Society Reviews*, *41*, 1809–1825.
- [26] Tian, H., Yang, S. (2004). Recent progresses on diarylethene based photochromic switches. *Chemical Society Reviews*, *33*, 85–97.
- [27] Mitchell, R. H. (1999). The metacyclophanediene-dihydropyrene photochromic π switch. *European Journal of Organic Chemistry*, 2695–2703.
- [28] Matharu, A. S., Jeeva, S., Ramanujam, P. S. (2007). Liquid crystals for holographic optical data storage. *Chemical Society Reviews*, *36*, 1868–1880.
- [29] van Leeuwen, T., Pijper, T. C., Areephong, J., Feringa, B. L., Browne, W. R., Katsonis, N. (2011). Reversible photochemical control of cholesteric liquid crystals with a diamine-based diarylethene chiroptical switch. *Journal of Materials Chemistry*, *21*, 3142–3146.
- [30] Nakamura, Y., Aratani, N., Osuka, A. (2007). Cyclic porphyrin arrays as artificial photosynthetic antenna: Synthesis and excitation energy transfer. *Chemical Society Reviews*, *36*, 831–845.
- [31] Sternberg, E. D., Dolphin, D., Brückner, C. (1998). Porphyrin-based photosensitizers for use in photodynamic therapy. *Tetrahedron*, *54*, 4151–4202.
- [32] Ward, M. D. (1997). Photo-induced electron and energy transfer in non-covalently bonded supramolecular assemblies. *Chemical Society Reviews*, *26*, 365–375.
- [33] Sun, L., Hammarström, L., Åkermark, B., Styring, S. (2001). Towards artificial photosynthesis: Ruthenium–manganese chemistry for energy production. *Chemical Society Reviews*, *30*, 36–49.
- [34] Baranov, M. S., Lukyanov, K. A., Borissova, A. O., Shamir, J., Kosenkov, D., Slipchenko, L. V., Tolbert, L. M., Yampolsky, I. V., Solntsev, K. M. (2012). Conformationally locked chromophores as models of excited-state proton transfer in fluorescent proteins. *Journal of the American Chemical Society*, *134*, 6025–6032.
- [35] Boens, N., Leen, V., Dehaen, W. (2012). Fluorescent indicators based on BODIPY. *Chemical Society Reviews*, *41*, 1130–1172.
- [36] DiCesare, N., Lakowicz, J. R. (2001). Fluorescent probe for monosaccharides based on a functionalized boron-dipyrromethene with a boronic acid group. *Tetrahedron Letters*, *42*, 9105–9108.
- [37] de Silva, A. P., Gunaratne, H. Q. N., McCoy, C. P. (1993). A molecular photoionic AND gate based on fluorescent signaling. *Nature*, *364*, 42–44.
- [38] Steinberg-Yfrach, G., Rigaud, J.-L., Durantini, E. N., Moore, A. L., Gust, D., Moore, T. A. (1998). Light-driven production of ATP catalyzed by F_0F_1 -ATP synthase in an artificial photosynthetic membrane. *Nature*, *392*, 479–482.
- [39] Tornøe, C. W., Christensen, C., Meldal, M. (2002). Peptidotriazoles on solid phase: [1,2,3]-triazoles by regioselective copper(I)-catalyzed 1,3-dipolar cycloadditions of terminal alkynes to azides. *The Journal of Organic Chemistry*, *67*, 3057–3064.
- [40] Rostovtsev, V. V., Green, L. G., Fokin, V. V., Sharpless, K. B. (2002). A stepwise Huisgen cycloaddition process: Copper(I)-catalyzed regioselective “ligation” of azides and terminal alkynes. *Angewandte Chemie (International ed. in English)*, *41*, 2596–2599.
- [41] Huisgen, R., Szeimies, G., Möbius, L. (1967). 1,3-Dipolare Cycloadditione, XXXII. Kinetik der Addition organischer Azide an CC-Mehrfachbindungen. *Chemische Berichte*, *100*, 2494–2507.
- [42] Qvortrup, K., Petersen, M. Å., Hassenkam, T., Nielsen, M. B. (2009). A tetrathiafulvalene-peryrene diimide conjugate prepared via click chemistry. *Tetrahedron Letters*, *50*, 5613–5616.

- [43] Kolb, H. C., Finn, M. G., Sharpless, K. B. (2001). Click chemistry: Diverse chemical function from a few good reactions. *Angewandte Chemie (International ed. in English)*, *40*, 2004–2021.
- [44] Pedersen, C. J. (1967). Cyclic polyethers and their complexes with metal salts. *Journal of the American Chemical Society*, *89*, 2495–2496.
- [45] Izatt, R. M., Pawlak, K., Bradshaw, J. S. (1991). Thermodynamic and kinetic data for macrocycle interaction with cations and anions. *Chemical Reviews*, *91*, 1721–2085.
- [46] Gokel, G. W., Leevy, W. M., Weber, M. E. (2004). Crown ethers: Sensors for ions and molecular scaffolds for materials and biological models. *Chemical Reviews*, *104*, 2723–2750.
- [47] Ashton, P. R., Campbell, P. J., Chrystal, E. J. T., Glink, P. T., Menzer, S., Philp, D., Spencer, N., Stoddart, J. F., Tasker, P. A., Williams, D. J. (1995). Dialkylammonium ion/crown ether complexes: The forerunners of a new family of interlocked molecules. *Angewandte Chemie (International ed. in English)*, *34*, 1865–1869.
- [48] Ashton, P. R., Becher, J., Fyfe, M. C. T., Nielsen, M. B., Stoddart, J. F., White, A. J. P., Williams, D. J. (2001). Tetrathiafulvalene-containing pseudorotaxanes formed between dibenzylammonium salts and crown ethers. *Tetrahedron*, *57*, 947–956.
- [49] Gale, P. A., Anzenbacher, P., Jr., Sessler, J. L. (2001). Calixpyrroles II. *Coordination Chemistry Reviews*, *222*, 57–102.
- [50] Gale, P. A., Sessler, J. L., Král, V., Lynch, V. (1996). Calix[4]pyrroles: Old yet new anion-binding agents. *Journal of the American Chemical Society*, *118*, 5140–5141.
- [51] Lu, Q., Martell, A. E., Motekaitis, R. J. (1996). Complexation of nucleotides and molecular catalysis of ATP-hydrolysis by a protonated hexaaza macrocyclic ligand. *Inorganica Chimica Acta*, *251*, 365–370.
- [52] Dietrick-Buchecker, C. O., Sauvage, J.-P. (1987). Interlocking of molecular threads: From statistical approach to the templated synthesis of catenands. *Chemical Reviews*, *87*, 795–810.
- [53] Forgan, R. S., Sauvage, J.-P., Stoddart, J. F. (2011). Chemical topology: Complex molecular knots, links, and entanglements. *Chemical Reviews*, *111*, 5434–5464.
- [54] Raymo, F. M., Stoddart, J. F. (1999). Interlocked macromolecules. *Chemical Reviews*, *99*, 1643–1663.
- [55] Asakwa, M., Ashton, P. R., Boyd, S. E., Brown, C. L., Gillard, R. E., Kocian, O., Raymo, F. M., Stoddart, J. F., Tolley, M. S., White, A. J. P., Williams, D. J. (1997). Recognition of bipyridinium-based derivatives by hydroquinone- and/or dioxynaphthalene-based macrocyclic polyethers: From inclusion complexes to the self-assembly of [2]catenanes. *The Journal of Organic Chemistry*, *62*, 26–37.
- [56] Allwood, B. L., Spencer, N., Shahriarizavareh, H., Stoddart, J. F., Williams, D. J. (1987). Complexation of paraquat by a bisparaphenylene-34-crown-10 derivative. *Journal of the Chemical Society. Chemical Communications*, 1064–1066.
- [57] Nielsen, M. B., Jeppesen, J. O., Lau, J., Lomholt, C., Damgaard, D., Jacobsen, J. P., Becher, J., Stoddart, J. F. (2001). Binding studies between tetrathiafulvalene derivatives and cyclobis(paraquat-*p*-phenylene). *The Journal of Organic Chemistry*, *66*, 3559–3563.
- [58] Nygaard, S., Hansen, C. N., Jeppesen, J. O. (2007). Binding studies between triethylene glycol-substituted monopyrrolotetrathiafulvalene derivatives and cyclobis(paraquat-*p*-phenylene). *The Journal of Organic Chemistry*, *72*, 1617–1626.
- [59] Nielsen, K. A., Cho, W.-S., Sarova, G. H., Petersen, B. M., Bond, A. D., Becher, J., Jensen, F., Guldi, D. M., Sessler, J. L., Jeppesen, J. O. (2006). Supramolecular receptor design: Anion-triggered binding of C₆₀. *Angewandte Chemie (International ed. in English)*, *45*, 6848–6853.
- [60] Jasat, A., Sherman, J. C. (1999). Carceplexes and hemicarceplexes. *Chemical Reviews*, *99*, 931–967.

- [61] Cram, D. J., Tanner, M. E., Thomas, R. (1991). The taming of cyclobutadiene. *Angewandte Chemie (International ed. in English)*, *30*, 1024–1027.
- [62] Warmuth, R. (1997). *o*-Benzyne: Strained alkyne or cumulene?—NMR characterization in a molecular container. *Angewandte Chemie (International ed. in English)*, *36*, 1347–1350.
- [63] Szejtli, J. (1998). Introduction and general overview of cyclodextrin chemistry. *Chemical Reviews*, *98*, 1743–1753.
- [64] Kim, K. (2002). Mechanically interlocked molecules incorporating cucurbituril and their supramolecular assemblies. *Chemical Society Reviews*, *31*, 96–107.
- [65] Kim, H.-J., Jeon, W. S., Ko, Y. H., Kim, K. (2002). Inclusion of methylviologen in cucurbit[7]uril. *Proceedings of the National Academy of Sciences of the United States of America*, *99*, 5007–5011.
- [66] Ma, D., Hettiarachchi, G., Nguyen, D., Zhang, B., Wittenberg, J. B., Zavalij, P. Y., Briken, V., Isaacs, L. (2012). Acyclic cucurbit[*n*]uril molecular containers enhance the solubility and bioactivity of poorly soluble pharmaceuticals. *Nature Chemistry*, *4*, 503–510.
- [67] Xue, M., Yang, Y., Chi, X., Zhang, Z., Huang, F. (2012). Pillararenes, a new class of macrocycles for supramolecular chemistry. *Accounts of Chemical Research*, *45*, 1294–1308.
- [68] Sartorius, J., Schneider, H.-J. (1996). A general scheme based on empirical increments for the prediction of hydrogen-bond associations of nucleobases and of synthetic host-guest complexes. *Chemistry—A European Journal*, *2*, 1446–1452.
- [69] Blondeau, P., Segura, M., Pérez-Fernández, R., de Mendoza, J. (2007). Molecular recognition of oxanions based on guanidinium receptors. *Chemical Society Reviews*, *36*, 198–210.
- [70] Campbell, M. A. (2011). Locked vs. unlocked nucleic acids (LNA vs. UNA): Contrasting structures work towards common therapeutic goals. *Chemical Society Reviews*, *40*, 5680–5689.
- [71] Boyle, A. L., Woolfson, D. N. (2011). *De novo* designed peptides for biological applications. *Chemical Society Reviews*, *40*, 4295–4306.
- [72] Seebach, D., Overhand, M., Kühnle, F. N. M., Martinoni, B., Oberer, L., Hommel, U., Widmer, H. (1996). β -Peptides: Synthesis by Arndt-Eistert homologation with concomitant peptide coupling. Structure determination by NMR and CD spectroscopy and by X-ray crystallography. Helical secondary structure of a β -hexapeptide in solution and its stability towards pepsin. *Helvetica Chimica Acta*, *79*, 913–941.
- [73] Ghadiri, M. R., Granja, J. R., Milligan, R. A., McRee, D. E., Khazanovich, N. (1993). Self-assembling organic nanotubes based on a cyclic peptide architecture. *Nature*, *366*, 324–327.
- [74] Nielsen, P. E., Haaima, G. (1997). Peptide nucleic acid (PNA). A DNA mimic with a pseudo-peptide backbone. *Chemical Society Reviews*, *26*, 73–78.
- [75] Wolf, C. (Ed.) *Dynamic Stereochemistry of Chiral Compounds: Principles and Applications*, RSC Publishing, Cambridge, 2008.
- [76] Noyori, R., Takaya, H. (1990). BINAP: An efficient chiral element for asymmetric catalysis. *Accounts of Chemical Research*, *23*, 345–350.
- [77] Rozenberg, V., Sergeeva, E., Hopf, H. Cyclophanes as templates in stereoselective synthesis. In *Modern Cyclophane Chemistry*, Gleiter, R., Hopf, H. (Eds.), Wiley-VCH, Weinheim, 2004; pp. 435–462.
- [78] Kanomata, N., Nakata, T. (2000). A compact chemical miniature of a holoenzyme, coenzyme NADH linked dehydrogenase. Design and synthesis of bridged NADH models and their highly enantioselective reduction. *Journal of the American Chemical Society*, *122*, 4563–4568.
- [79] Müllen, K., Wegner, G. (Eds.). *Electronic Materials: The Oligomer Approach*, Wiley-VCH, Weinheim, 1998.
- [80] Martin, R. E., Gubler, U., Cornil, J., Balakina, M., Boudon, C., Bosshard, C., Gisselbrecht, J.-P., Diederich, F., Günter, P., Gross, M., Brédas, J.-L. (2000). Monodisperse poly(triacetylene)

- oligomers extending from monomer to hexadecamer: Joint experimental and theoretical investigation of physical properties. *Chemistry—A European Journal*, 6, 3622–3635.
- [81] Cheng, Y.-J., Yang, S.-H., Hsu, C.-S. (2009). Synthesis of conjugated polymers for organic solar cell applications. *Chemical Reviews*, 109, 5868–5923.
- [82] Heeger, A. J. (2010). Semiconducting polymers: The third generation. *Chemical Society Reviews*, 39, 2354–2371.
- [83] Maggini, L., Bonifazi, D. (2012). Hierarchised luminescent organic architectures: Design, synthesis, self-assembly, self-organisation and functions. *Chemical Society Reviews*, 41, 211–241.
- [84] Wang, C., Dong, H., Hu, W., Liu, Y., Zhu, D. (2012). Semiconducting π -conjugated systems in field-effect transistors: A material odyssey of organic electronics. *Chemical Reviews*, 112, 2208–2267.
- [85] Nielsen, M. B., Diederich, F. (2005). Conjugated oligoenynes based on the diethynylethene unit. *Chemical Reviews*, 105, 1837–1867.
- [86] Gholami, M., Tykwinski, R. R. (2006). Oligomeric and polymeric systems with a cross-conjugated π -framework. *Chemical Reviews*, 106, 4997–5027.
- [87] Fielder, S., Rowan, D. D., Sherburn, M. S. (2000). First synthesis of the dendralene family of fundamental hydrocarbons. *Angewandte Chemie (International ed. in English)*, 39, 4331–4333.
- [88] Skotheim, T. A., Elsenbaumer, R. L., Reynolds, J. R. (Eds.). *Handbook of Conducting Polymers*, 2nd ed., Marcel Dekker, New York, 1998.
- [89] Xiao, J., Yang, M., Lauher, J. W., Fowler, F. W. (2000). A supramolecular solution to a long-standing problem: The 1,6-polymerization of a triacetylene. *Angewandte Chemie (International ed. in English)*, 39, 2132–2135.
- [90] Zhao, Y., Campbell, K., Tykwinski, R. R. (2002). Iterative synthesis and characterization of cross-conjugated iso-polydiacetylenes. *The Journal of Organic Chemistry*, 67, 336–344.
- [91] Mayor, M., Weber, H. B., Reichert, J., Elbing, M., von Hänisch, C., Beckmann, D., Fischer, M. (2003). Electric current through a molecular rod—Relevance of the position of the anchor groups. *Angewandte Chemie (International ed. in English)*, 42, 5834–5838.
- [92] Verbiest, T., Houbrechts, S., Kauranen, M., Clays, K., Persoons, A. (1997). Second-order nonlinear optical materials: Recent advances in chromophore design. *Journal of Materials Chemistry*, 7, 2175–2189.
- [93] Tykwinski, R. R., Gubler, U., Martin, R. E., Diederich, F., Bosshard, C., Günter, C. (1998). Structure-property relationships in third-order nonlinear optical chromophores. *The Journal of Physical Chemistry B*, 102, 4451–4465.
- [94] Cheng, L.-T., Tam, W., Marder, S. R., Stiegman, A. E., Rikken, G., Spangler, C. W. (1991). Experimental investigations of organic molecular nonlinear optical polarizabilities. 2. A study of conjugation dependences. *The Journal of Physical Chemistry*, 95, 10643–10652.

CHAPTER 3

DESIGN AND SYNTHESIS OF ORGANIC MOLECULES FOR MOLECULAR ELECTRONICS

KARSTEN JENNUM and MOGENS BRØNDSTED NIELSEN

3.1 INTRODUCTION

Innovative developments within electronic device fabrication have turned millimeter transistors into micrometer-integrated circuit systems throughout the last half of the former century. This technological advance has given us faster, smaller, and more advanced computer systems. If this miniaturization trend continues to push the size boundaries for integrated circuits to meet the growing demands of society, some limitations in the classical silicon-based devices will occur. The present technology might encounter some inherent limitations that would lead to a dead end within the next few years because of some major challenges: for example, the micropatterning techniques to produce circuitry on the silicon wafers in the nanometer regime or the fact that, when silicon layers are just a few atoms thick, the band structure disappears [1]. To secure further advances within this field, it is crucial to develop novel manufacturing procedures for future nanoscale electronics. For this purpose, organic materials could be the right alternative to obtain the desired electronic capabilities for a given molecular-based device. π -Conjugated molecules are particularly attractive as wires and electronic components, with their size in the range of nanometers, delocalized electrons, and small highest occupied molecular orbital and lowest unoccupied molecular orbital (HOMO–LUMO) gaps, which can be tuned by suitable functionalization. The aim of this multidisciplinary research field is to mimic key electronic components such as wires, rectifiers, switches, and memory devices [2].

Device fabrication on the molecular scale and controlled assembly of molecules are still major issues to overcome if computers are to be equipped with “molecular” circuits. Nevertheless, much knowledge has been added to this field in the last decades, and several new techniques have been developed. For instance, today’s microscope techniques allow measurements on single molecules both in solid state and in solution [3],

Organic Synthesis and Molecular Engineering, First Edition.

Edited by Mogens Brøndsted Nielsen.

© 2014 John Wiley & Sons, Inc. Published 2014 by John Wiley & Sons, Inc.

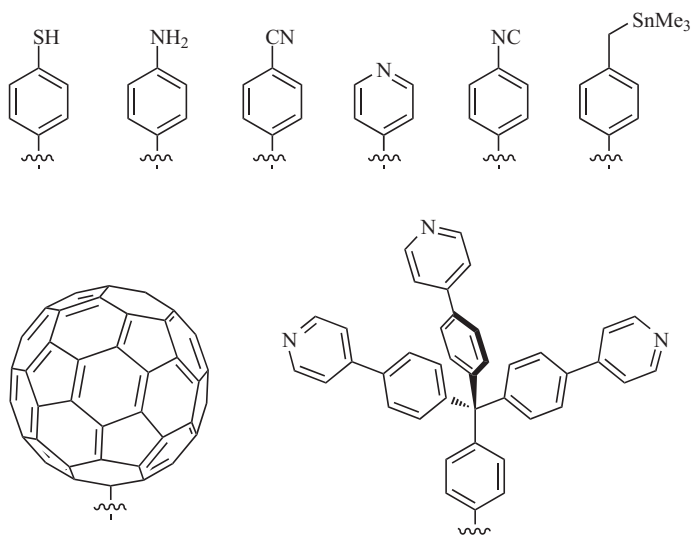


Figure 3.1. Anchoring groups that can act as connecting link between the molecular wire and the metal electrodes.

and this provides a golden opportunity to test and measure the intrinsic properties of molecular systems. This chapter, however, will instead focus on the actual design of organic molecules as components for molecular electronics and, in particular, on their synthesis.

3.2 ORGANIC MOLECULAR WIRES

3.2.1 Terminal Connectivity: The “Alligator Clip Principle”

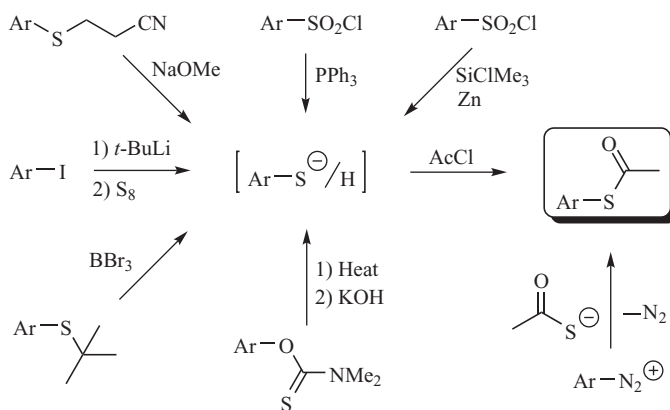
A molecular wire has to be bound to metal-based electrodes via suitable anchoring groups. Considering these anchoring groups in a macro perspective, one could imagine them as being alligator clips on metal wires used for simple test circuits. Figure 3.1 shows a selection of such molecular anchoring groups [2–17]. The thiol (SH) anchoring group was the first to be exploited in charge transport experiments through single organic wires, and it is still the most widely used anchoring group. This is due to the strong binding of sulfur to metals such as silver, copper, and gold [4]. In a recent study by Wandlowski and coworkers [5], four toluene derivatives with $-\text{SH}$ (thiol), $-\text{NH}_2$ (amino), $-\text{CN}$ (cyano), and $-\text{PY}$ (pyridine) end groups were compared in regard to anchoring to gold electrodes in single-molecular conductance experiments using mechanically controlled microscopy break junctions (MCBJs) and scanning tunneling microscopy break junctions (STM-BJs). The following sequence for junction formation probability and stability was obtained: $\text{PY} > \text{SH} > \text{NH}_2 > \text{CN}$. Charge transport through SH/ NH_2 -bound molecular junctions is dominated by hole transport via the HOMO, since the HOMO energy levels are here closest to the metal Fermi level [6]. On the other hand, charge transport through a nitrile (CN) or a pyridine (PY) linker is

expected to go through the LUMO [7]. In addition to the above-mentioned anchoring groups, the isonitrile (NC) group has also been used as a linker in single-molecular junction measurements [8] and is among a group of alternative alligator clips counting carboxylic acid (COOH) [9], nitro (NO₂) [10], dimethylphosphine (PMe₂) [11], and methylsulfide (SMe) [11]. Recently, Venkataraman and coworkers [12] investigated molecules (Me₃Sn-CH₂-π-system-CH₂-SnMe₃) terminated with trimethyltin end groups that were cleaved off *in situ*. This gave rise to a direct σ-bond between the carbon backbone (methylene unit) and the gold metal electrodes and, in consequence, a direct coupling between the neighboring π-system and the electrodes, which resulted in a 100-fold enhancement in the conductivity compared with junctions with conventional linkers.

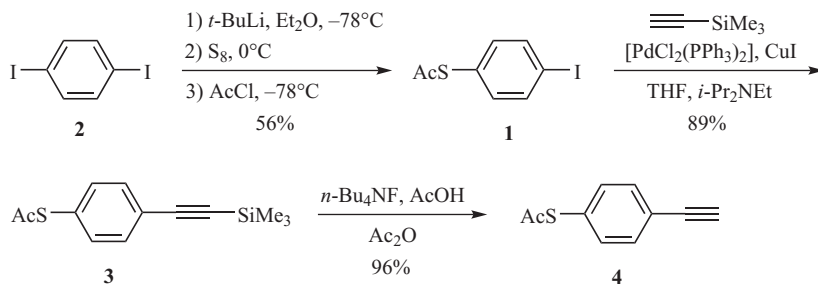
It is essential for reliable molecular junctions that the anchoring group is either covalently bound or well adsorbed to the electrode surface. A study of the adsorption of Buckminsterfullerene (C₆₀) on gold surfaces has revealed that C₆₀ hybridizes strongly with gold [13], leading to a high single-molecular conductance [14]. In the case of 1,4-dithiobenzene, 1,4-diaminobenzene, and a fullerene diaminobenzene dumbbell molecule, MCBJ experiments showed that the C₆₀ dumbbell exhibited an increasing stretching length before breaking compared with the others, indicating that fullerenes form stable molecular junctions and are suitable as anchoring groups [15]. Yao and Tour [16] have also reported a tripod structure containing three protected thiolate groups, which when standing on its three legs should create a more well-defined wire-to-metal surface interface. In a recent example, three pyridine units were also arranged in a tripod structure (Figure 3.1) that was found to be very suitable as an anchoring group in single-molecular junctions [17].

The thiophenol anchoring group has found the most widespread usage. A toolbox for synthesizing thiophenols is presented in Scheme 3.1. The thiophenols are normally converted into the *S*-acetyl-protected derivatives because of their air instability. Nevertheless, this *S*-acetyl-protecting group is very labile and can easily be cleaved under various conditions [18].

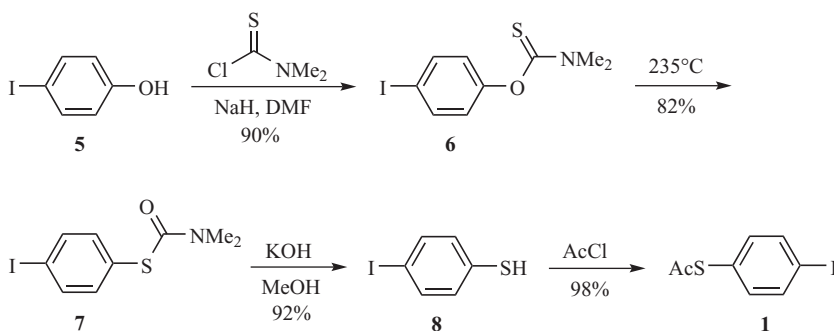
Alternatively, it can be an advantage to protect the thiophenols with more persistent groups. This could be either the *tert*-butyl protecting group, which is resistant to both



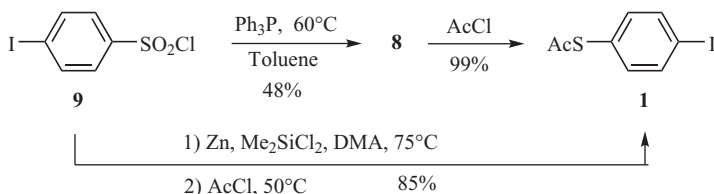
Scheme 3.1. Synthesis of thiophenols.



Scheme 3.2. Synthesis of acetyl-protected thiol end-capped building block.



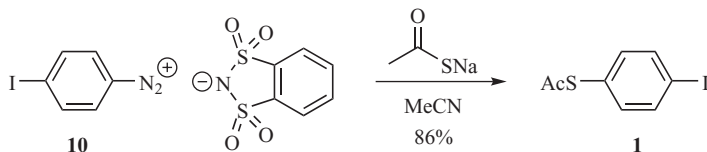
Scheme 3.3. Alternative synthesis of building block **1**.



Scheme 3.4. Alternative synthesis of building block **1**.

strongly basic and acidic conditions but is easily removed with BBr_3 [19], or the cyanoethyl group, which is suitable when nonalkaline conditions are used; NaOMe/HOME removes this protecting group readily [20].

A particularly interesting compound is the *S*-acetyl-4-iodothiophenole **1**, which is a key compound for thiol end-capped molecular wires, since the iodine functionality is a precursor for C–C bond formations to aromatics [21], double [22], and triple [23] bonds in various metal-mediated coupling reactions. The synthetic approach toward compound **1** has evolved into a handful of different pathways, which are shown in Scheme 3.2, Scheme 3.3, Scheme 3.4, and Scheme 3.5. Pearson and Tour [24] synthesized alligator clip **1** from diiodide **2**, which was treated with *t*-BuLi to form the monolithiated phenyliodide that was then treated with elemental sulfur, and SAc was finally formed upon quenching with AcCl. Subjecting compound **1** to a Sonogashira



Scheme 3.5. Alternative synthesis of building block **1**.

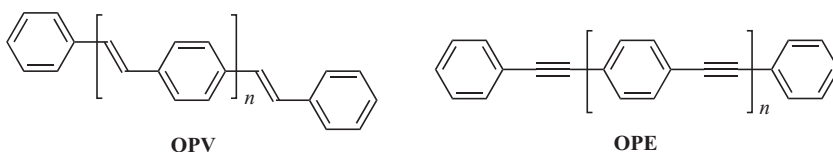


Figure 3.2. Two commonly used wire scaffolds in molecular electronics.

palladium-catalyzed cross-coupling reaction with trimethylsilylacetylene gave compound **3**, which ultimately was converted into ethynylbenzene **4** after removal of the trimethylsilyl group. Compound **4** can subsequently be coupled with other halide scaffolds for further expansions of the π -conjugated wire.

In the route toward compound **1**, it is crucial to form only the monolithiated iodobenzene, a reaction that is not always easy to reproduce. To solve this problem, Bryce and coworkers [25] developed a four-step high-yielding synthetic procedure shown in Scheme 3.3. *N,N*-Dimethylthiocarbamoyl chloride was treated with 4-iodophenol **5** forming compound **6**, which at high temperatures underwent a Newman–Kwart rearrangement affording product **7**. Hydrolysis of **7** yielded iodothiophenol **8** that finally was converted into **1** by treatment with AcCl.

A shorter pathway to **1** is by reduction of commercially available pipsyl chloride (4-iodobenzenesulfonyl chloride) **9** with triphenylphosphine (Scheme 3.4), giving in one step iodothiophenol **8**, which was then subjected to *S*-acylation [26]. Alternatively, pipsyl chloride **9** can be reduced by zinc powder and dichlorodimethylsilane in *N,N*-dimethylacetamide (DMA) and 1,2-dichloroethane, followed by the addition of acetyl chloride to form **1** in a one-pot reaction (Scheme 3.4) [27].

Reaction between sodium thioacetate and stable iodo-diazonium salt **10** in a nucleophilic aromatic substitution gave **1** in high yield (Scheme 3.5). This procedure could also be extended to a variety of substituted diazonium salts [28].

3.2.2 Synthesis and Properties of Organic Wires

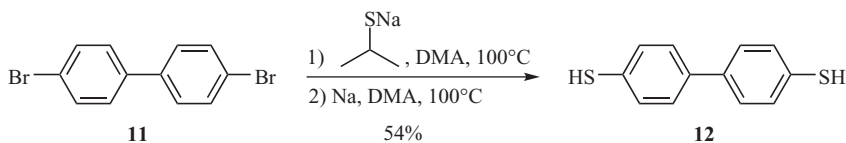
Fundamental investigations of the relationship between molecular and electronic properties at the single-molecule level are crucial for the development of molecular wires. Different types of organic wire scaffolds have been synthesized throughout the years. In particular, focus has been on derivatives of oligo(phenylenevinylene) (OPV) and oligo(phenyleneethynylene) (OPE) (Figure 3.2) [19, 29]. Comparison of the conducting properties of these two wires reveals that OPV conducts current slightly better than OPE [30]. Studies also state that the OPV scaffold conducts better than oligothiophenes and aliphatic wires [31]. In an electron transport study on self-assembled monolayers (SAMs) of nitro-substituted oligophenylene (OP) and OPE molecules, it

was shown that OPE SAMs perform better than OPs [32]. This is explained by the steric-induced inter-ring twisting being greater in OPs than in OPEs. Elegant single-molecule junction studies have revealed how conductance through biphenyldithiol wires depends on the torsion angle [3f, 33]. It was observed that an angle-fixed biphenyl with a torsion angle of 89° has ~ 24 times lower conductance than one with an angle of 16.8° [33]. Electron transport through a single molecule is therefore greatly facilitated by orbital overlap between the individual components of the wire. In summary, the following relative conductance order has been established: OPV > OPE > OP > aliphatics.

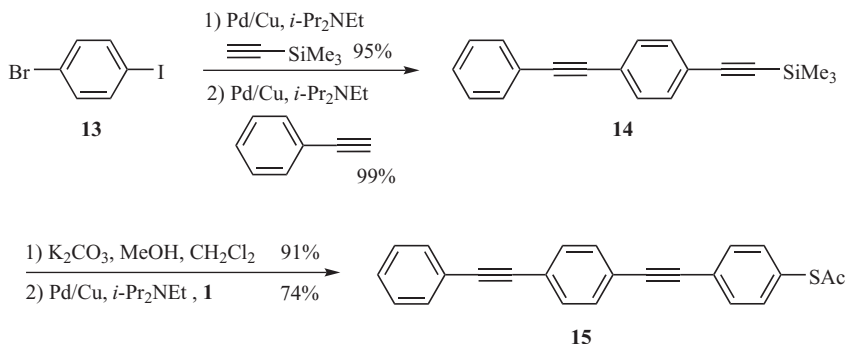
Another important parameter is the length of the wire, since electron transport through organic molecules is retarded when the pathway is increased. In a recent single-junction conductance study of OPEs, it was stated that an increased molecular length and/or increased HOMO–LUMO gap leads to a decrease in the conductance of linear conjugated acenes [34]. Besides that, insertion of a cross-conjugated anthraquinone or a dihydroanthracene as the central unit also results in a lower conductance, which is attributed to a cross-conjugated pathway for the former and a broken π -conjugation for the latter. A decrease in the current flow through a single molecule is also observed when the conjugation pathway includes a *meta*-benzene system, which can be seen as a cross-conjugated pathway [35]. These findings are in perfect agreement with measurements on cross-conjugated/broken π -conjugated OPV wires [31]. On the other hand, increasing the conjugated system along the conducting pathway, and thereby decreasing the HOMO–LUMO gap, can also enhance the conductance of the wire [34, 36]. In addition to this, it is found that solubilizing side chains, such as alkoxy substituents, do not noticeably influence the conductance value [30].

Thiol end-capped biphenylenes and selected oligomer derivatives have been used in different molecular junction experiments. For instance, in a single-molecule STM-BJ measurement, it was shown that dithiobiphenylene wires can produce thermoelectricity when placed between a cold and a hot electrode [37]. Scheme 3.6 depicts the synthesis to form end-capped thiols on the biphenylene systems, by converting the commercially available dibromobiphenylene **11** into dithiobiphenylene **12** via a nucleophilic aromatic substitution followed by removal of the isopropyl groups [38].

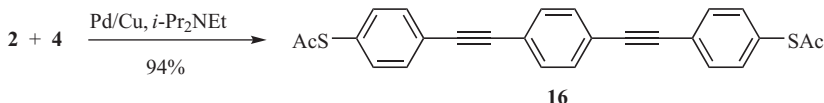
The biggest disadvantage of biphenylenes is their poor ability to move electrons in a junction, due to their twisted nature, and hence lack of overlap between the π -systems. This problem is eliminated in the OPE and OPV systems, since the H–H collision in the α -positions of the benzene rings is diminished by the triple- or double-bond spacer. The route to an OPE3 with only one anchoring group is shown in Scheme 3.7. Bromiodobenzene **13** is a particularly attractive starting material for asymmetric OPE synthesis. The chemoselectivity for aryl–iodine bonds in Sonogashira cross-coupling reactions makes it possible to attach one alkyne substituent before the other one to furnish OPE2 **14** in high yield [29a]. This was followed by a mild carbonate/methanol



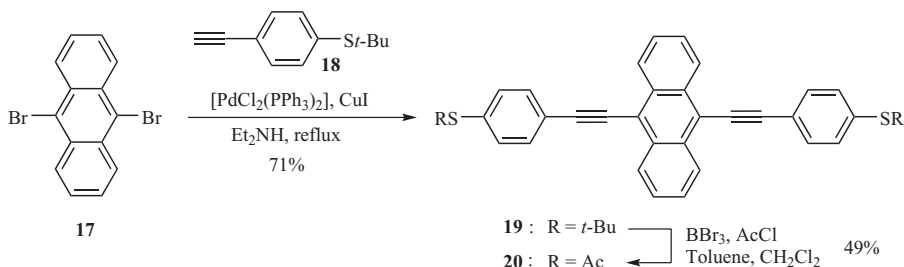
Scheme 3.6. Synthesis of OP2 molecular wire with two anchoring groups.



Scheme 3.7. Synthesis of OPE3 molecular wire with one anchoring group.



Scheme 3.8. Synthesis of OPE3 molecular wire with two anchoring groups.



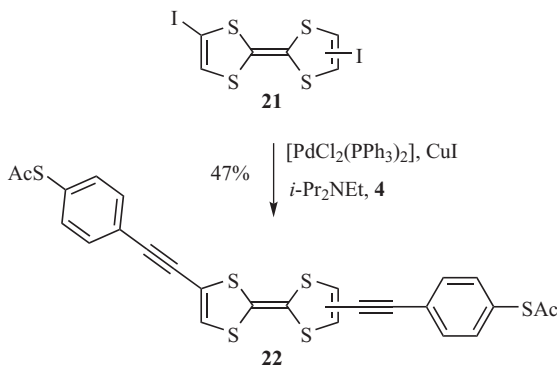
Scheme 3.9. Synthesis of OPE3 molecular wire with a central anthracene unit.

removal of the trimethylsilyl protecting group, which provided a terminal alkyne functionality that could be coupled with compound **1**, resulting in OPE3 **15**.

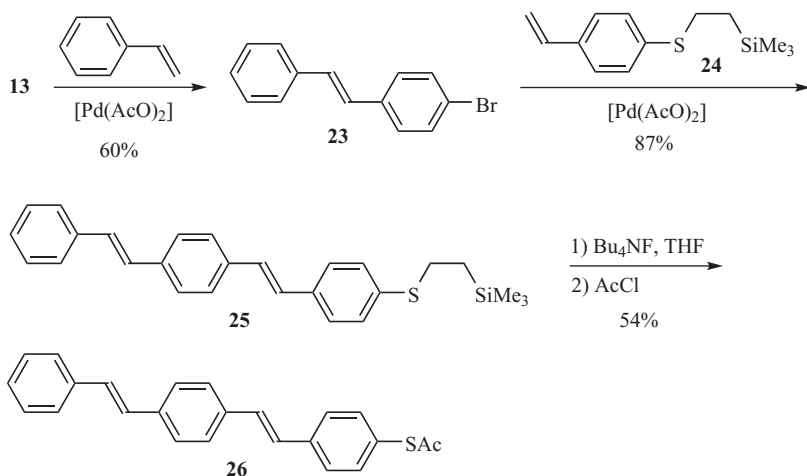
The synthesis of two-terminal OPE3 wire **16** presented in Scheme 3.8 can readily be carried out from 1,4-diodobenzene **2** and alkyne **4** [29a]. The OPE3 scaffold has been widely used in a variety of wires; properties are tuned by substituents such as cyano (CN), nitro (NO₂), or redox-active moieties [29d, 39].

Another way to tune the properties of the wire is to expand the π -conjugated system along the core by insertion of an anthracene moiety, as revealed in Scheme 3.9. Combining the commercially available 9,10-dibromoanthracene **17** with ethynylbenzene **18** in a metal-catalyzed double cross-coupling reaction gave *tert*-butyl protected OPE3 wire **19** [35]. To activate the alligator clips on the wire, it is necessary to turn the *tert*-butyl moiety into an acetyl group, which can be done in a one-pot reaction with BBr₃ and AcCl, thereby generating wire **20**.

Also strong donor molecules, such as tetrathiafulvalene (TTF), have been employed in combination with an OPE scaffold to enhance electron transport and to lower the



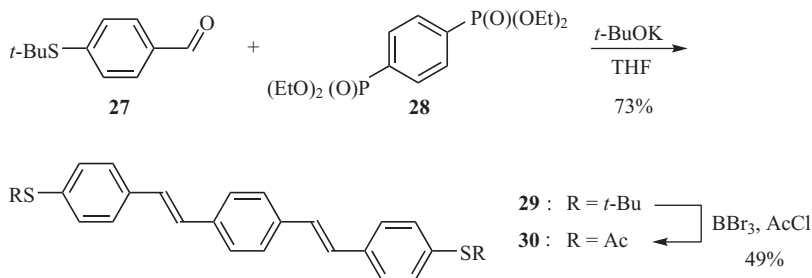
Scheme 3.10. Synthesis of TTF-based molecular wire with two anchoring groups.



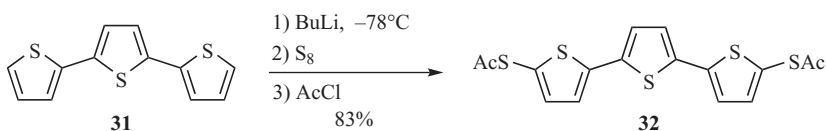
Scheme 3.11. Synthesis of OPV3 molecular wire with one anchoring group.

resistance in the wire [40]. TTF can be iodinated under strong basic conditions, leading to a mixture of regioisomers of diiodoTTF **21** presented in Scheme 3.10. This TTF can then undergo a twofold Sonogashira cross-coupling reaction with alkyne **4**, thereby generating molecular wire **22**.

While the synthesis of the OPE scaffold is based on Sonogashira metal-catalyzed cross-coupling reactions, it is common to employ the Horner–Wadsworth–Emmons (HWE) olefination reaction to form OPV wires, or alternatively Heck Pd-catalyzed reactions. Scheme 3.11 shows the synthesis of a one-terminal OPV, which is assembled in a two-step Heck metal-catalyzed fashion from unsymmetrically dihalide **13** [29d]. Monocoupling of dihalide **13** with styrene yielded OPV2 **23**, which subsequently was coupled with thioether derivative **24**, resulting in OPV3 **25**. Treatment of this compound with fluoride ions gave a thiolate, which ultimately was subjected to acetylation, forming OPV3 wire **26**.



Scheme 3.12. Synthesis of OPV3 molecular wire with two anchoring groups.



Scheme 3.13. Synthesis of OT3 molecular wire with two anchoring groups.

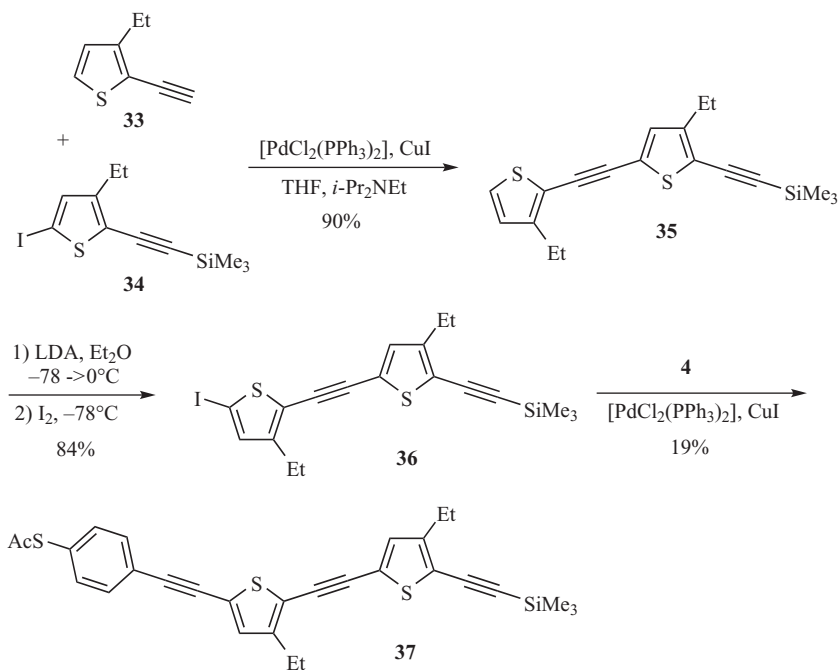
Two-terminal OPV wires can readily be assembled via HWE reactions between benzaldehydes and suitable phosphonates, as in the case presented in Scheme 3.12, where the reaction between aldehyde **27** and diphosphonate **28** under alkaline conditions gave OPV3 **29** [19a]. Finally, replacement of the *S*-*t*-butyl group for the more labile *S*-acetyl moiety was carried out under standard conditions to result in compound **30**.

Oligothiophenes (OTs) are alternatives to OPE and OPV wires. Thiophene units have, for instance, been used as either the single π -conjugated component or in a combination with, for example, alkynes in wire motifs, as illustrated in Scheme 3.13 and Scheme 3.14 [24, 41]. By utilizing the reactivity of thiophene toward strong bases, it is possible to lithiate thiophene trimer **31** twice and hence to add sulfur in each ends of the wire. The dithiolate, which is formed under these conditions, can then be treated with acetyl chloride to form the acetyl end-capped thiophene wire **32**.

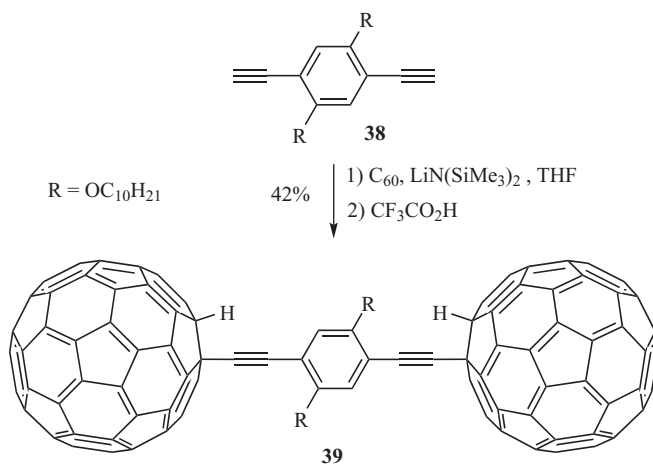
Synthesis of oligo(thiopheneethynylene)s (OTEs) is similar to that of the OPEs, since the backbones of these systems are assembled via the Sonogashira cross-coupling reaction [24]. Reaction between ethynylthiophene **33** and iodothiophene **34** furnished OTE2 **35**, which was iodinated with lithium diisopropyl amine (LDA) and iodine to allow further expansion of the wire. OTE **36** was then treated with alkyne **4** to affix an anchoring group upon one end of wire **37**. Removing the trimethylsilyl protecting group on OTE wire **37** enables further expansion of the scaffold.

Buckminsterfullerene (C_{60}) not only has, as previously described, good binding affinity to metal surfaces but can also exist in multiple redox states, and for that reason, it has been employed in various wire scaffolds [42]. Dialkyne **38** can, in the presence of C_{60} and strong base in THF, be converted to dumbbell molecule **39** shown in Scheme 3.15 [43].

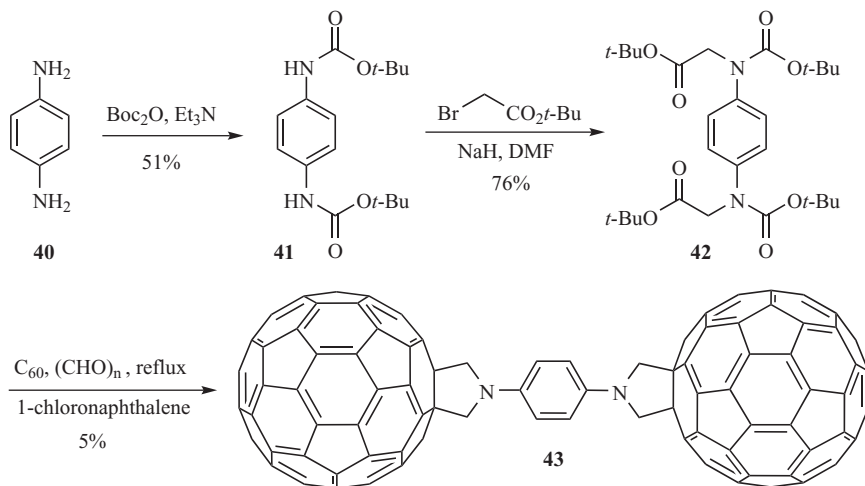
Fullerene dumbbell molecules can also be prepared by a variant of the Prato 1,3-dipolar cycloaddition reaction. Starting from phenylenediamine **40** (Scheme 3.16) it is possible to first generate dicarbamate **41** after reaction with di-*tert*-butyl-dicarbonate



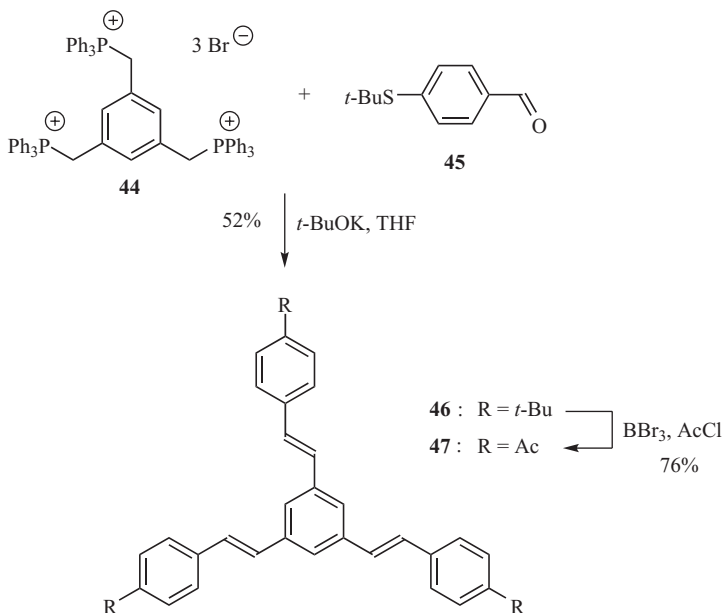
Scheme 3.14. Synthesis of OTE3 molecular wire/building block with one anchoring group and a trimethylsilyl-protected terminal alkyne (position for further scaffolding).



Scheme 3.15. Synthesis of dumbbell-like molecule with two C_{60} end-groups.



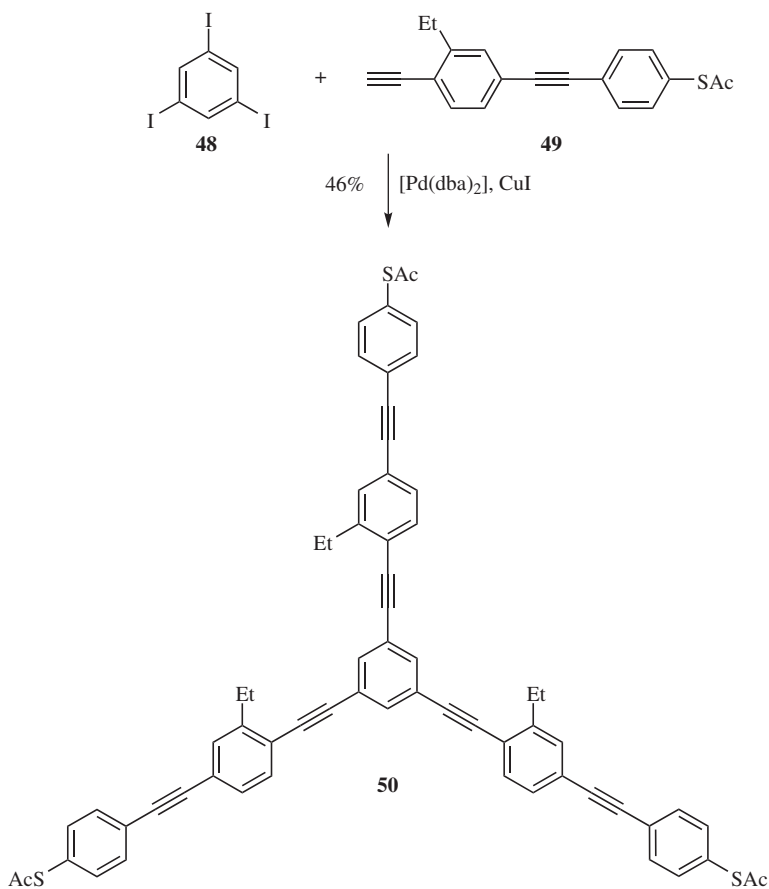
Scheme 3.16. Synthesis of dumbbell-like molecule containing a central phenylenediamine unit and two C_{60} end groups.



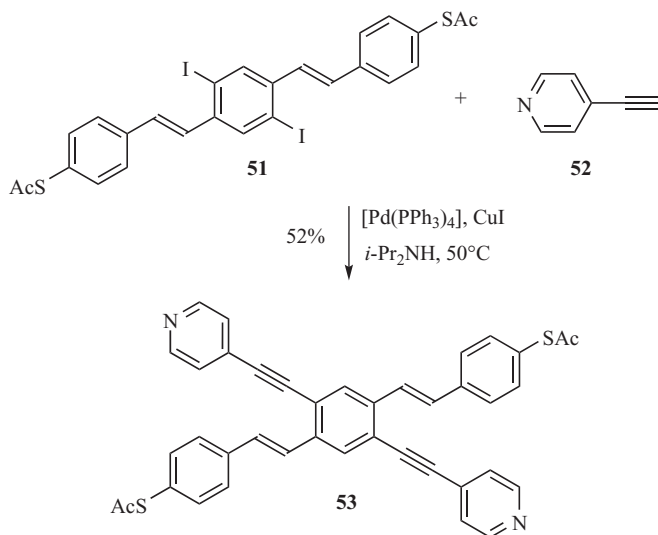
Scheme 3.17. Synthesis of three-terminal OPV molecular wire.

(Boc_2O) and then subsequently to form 1,3-dipolar-precursor **42** by alkylation with *tert*-butyl bromoacetate. Refluxing compound **42** with paraformaldehyde and C_{60} in 1-chloronaphthalene gave dumbbell **43** [44].

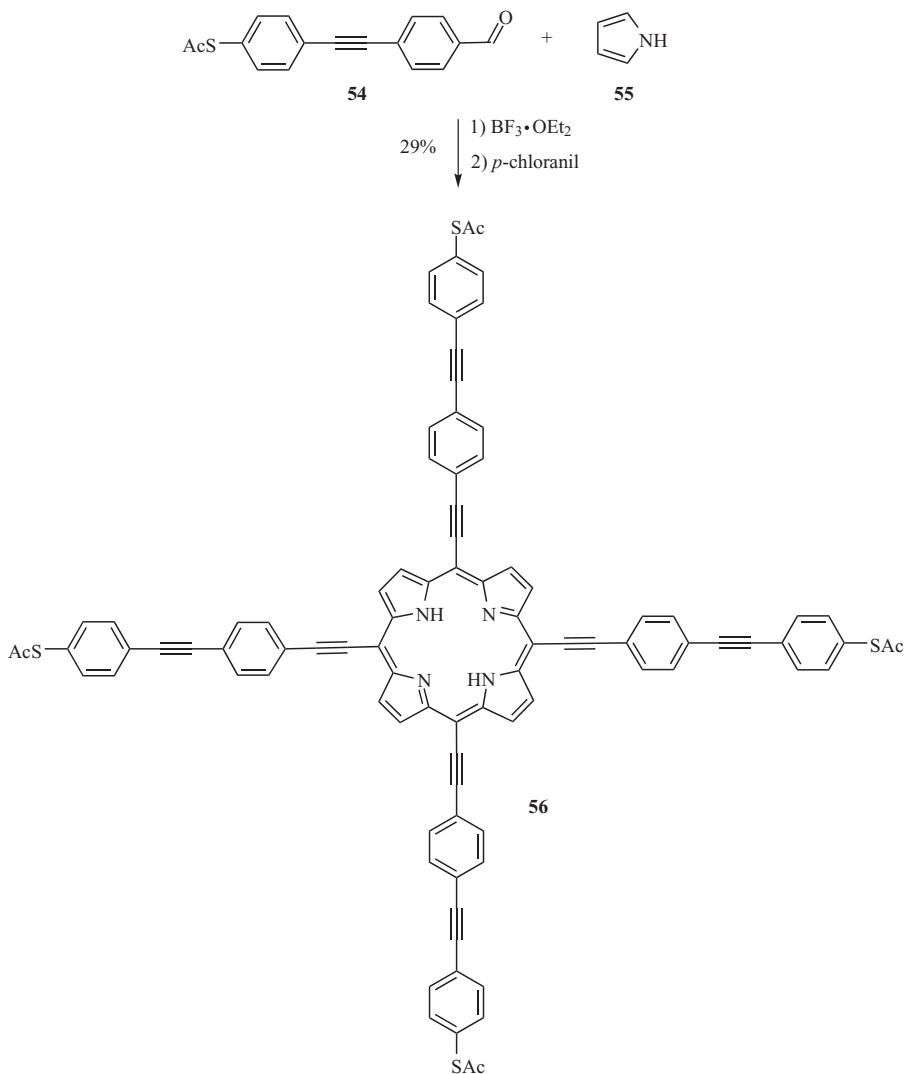
Three- and four-terminal wires, such as those presented in Scheme 3.17, Scheme 3.18, Scheme 3.19, and Scheme 3.20, have successfully been synthesized, with the design



Scheme 3.18. Synthesis of three-terminal OPE molecular wire.



Scheme 3.19. Synthesis of cruciform-like four-terminal molecular wire.



Scheme 3.20. Synthesis of four-terminal molecular wire with a central porphyrin unit.

purpose of having multiple pathways to pass current through. A threefold Wittig reaction of trisphosphonium salt **44** with aldehyde **45** represents an efficient route to three-terminal OPV **46**, which afterward is readily converted into *S*-acetyl compound **47** (Scheme 3.17) [19a]. Three-terminal OPE wires can be assembled via Sonogashira reaction from 1,3,5-triiodobenzene **48** and OPE2 **49** to give triangle-shaped wire **50** (Scheme 3.18) [29a].

A four-terminal wire as the one illustrated in Scheme 3.19 combines OPV and OPE motifs as well as two different anchoring groups [45]. The OPE wire is in this case formed in the last step using a double Sonogashira reaction between diiodo-OPV wire

51 and 4-ethynylpyridine **52** to yield a combined OPV/OPE four-terminal wire **53**. The potential of this cruciformlike wire is to control binding/unbinding of the pyridine rod to electrodes and hence to alternate between a situation in which both wires can bind and one in which only the sulfur end-capped wire binds.

A perpendicular four-terminal system can be constructed by combining the OPE scaffold with the porphyrin motif, as depicted in Scheme 3.20. This was done by a fourfold condensation between OPE aldehyde **54** and pyrrole **55** in the presence of a Lewis acid, followed by oxidation with *p*-chloranil to form the aromatic porphyrin core of cruciform structure **56** [29a].

3.3 ORGANIC MOLECULAR RECTIFIERS

For the development of molecular electronics, we need, in addition to molecular wires, also more advanced devices such as rectifiers, switches, and transistors, which play key roles in the present technology. For instance, rectification of current by rectifiers or diodes is a simple and common property present in almost every device produced today. Aviram and Ratner [46] proposed in 1974 that such a simple device property could be possible for a single organic molecule (**57**) based on TTF and tetracyanoquinodimethane (TCNQ) (Figure 3.3). Their concept was to incorporate the rectification ability into a single molecule by linking together a donor π -system (TTF), a σ -spacer (tunneling bridge), and an acceptor π -system (TCNQ). In this way, it was expected that the current would pass in only one direction when the molecule is immobilized between two electrodes. So far, several attempts to realize this idea have been carried out, some with greater success than others [47].

Scheme 3.21 presents a dyad containing similar organic parts as those present in the proposed molecular rectifier **57**. Anthraquinone-derived TCNQ compound **58** can, in combination with TTF-carbonyl chloride compound **59**, form dyad **60** in an esterification reaction [48]. Dyad **60** revealed a very weak intramolecular TTF to TCNQ charge-transfer property, and electrical conductivity experiments showed that the compound acted more like an insulator than a rectifier.

The synthetic route to another donor–acceptor molecule is presented in Scheme 3.22. It was assembled by reacting *N*-cetyllepudininium tosylate **61** with the lithium salt of TCNQ radical anion **62** [49]. The resulting zwitterionic compound **63** exhibited a rectification ratio of up to 26:1 when Langmuir–Blodgett grown films hereof were placed between two aluminum electrodes [50].

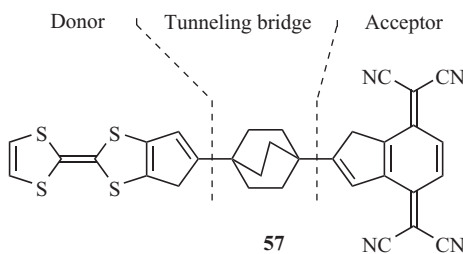
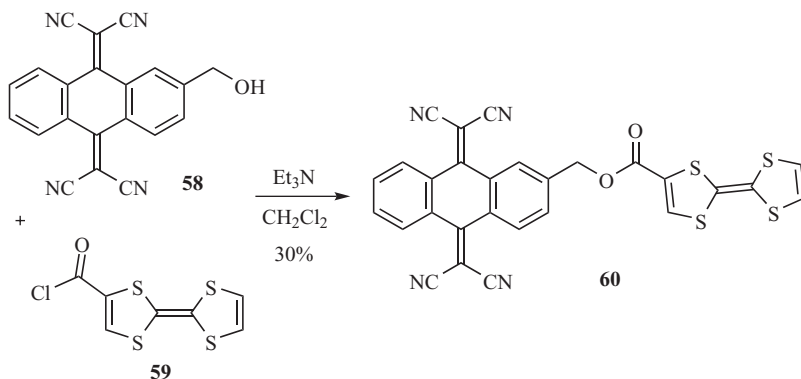
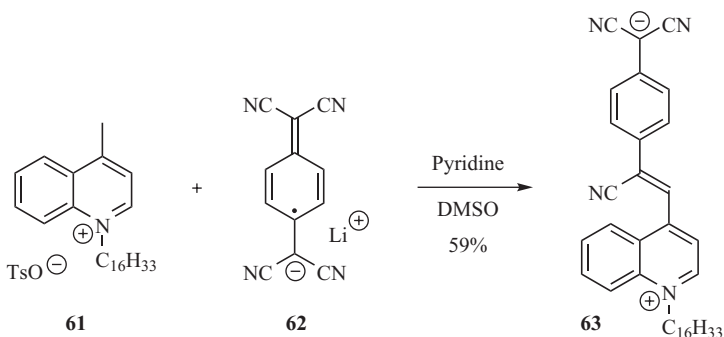


Figure 3.3. Design of molecular rectifier.



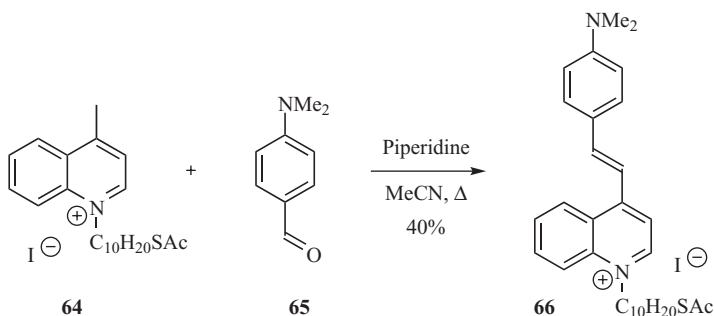
Scheme 3.21. Synthesis of donor-acceptor dyad (TTF—anthraquinone-derived TCNQ).



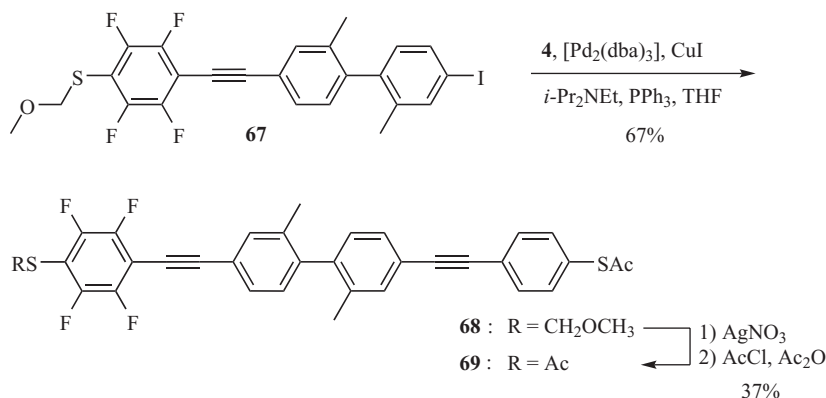
Scheme 3.22. Synthesis of zwitterionic donor-acceptor dyad.

Another similar donor–acceptor dyad system was designed to form SAMs on gold surfaces. Compound **64** was subjected to a condensation reaction at the methyl moiety with benzaldehyde **65** to furnish dyad salt **66** (Scheme 3.23) [51]. SAMs of compound **66** displayed rectification ratios of up to approximately 18:1.

Instead of using the Aviram and Ratner model (**57**), which utilizes sp^3 -hybridized carbon atoms as a barrier between the donor and acceptor π -systems, it is possible to insert an α,α' -dimethylbiphenylene unit between the two moieties in the molecule. The biphenylene unit twists the molecule out of plane and thereby dampens the π -electron delocalization, providing an overall effect similar to that of a tunneling bridge. Such a molecular tool was applied when the OPE-like rectifier **69** was designed (Scheme 3.24) [52]. The synthesis starts from the iodo-compound **67** that was treated with compound **4** using the Sonogashira reaction to give asymmetrically OPE wire **68**, which finally was converted into molecular rectifier **69**. Unlike the two previous examples of organic rectifiers (**63** and **66**), which were measured as a bundle of molecules (LB film or SAM), this molecule (**69**) showed current rectification as a single molecule with a ratio of up to ~10:1 when measured in an MCBJ experiment.



Scheme 3.23. Synthesis of donor-acceptor dyad salt.



Scheme 3.24. Synthesis of OPE-like molecular rectifier based on a nonplanar biphenylene core.

3.4 ORGANIC MOLECULAR SWITCHES

To imitate, for instance, a transistor on the molecular level, the molecule is usually designed to have two alligator clips to anchor the molecule between source and drain electrodes, plus an additional third linker to control the switching event (the gate). Theoretical studies done on thiol-substituted benzene **70** (Figure 3.4) has predicted effective switching in the current transmission between the *source* (In) and the *drain* (Out) when a potential on the *gate* is alternated [53]. In this case, the source and the drain electrodes are placed *meta* to each other, which gives the lowest transmission probability through the molecule when the gate is inactive. Upon gate activation (a potential applied), the energies of the molecular orbitals move toward the Fermi level, and the current from the source to the drain electrode can pass with a lower resistance [53].

Gate-modulated studies performed on perylene diimide compound **71** (Figure 3.5) showed response to an electrochemical gate potential when the molecule was captured between a gold substrate and an STM tip [54]. The compound showed around 500 times

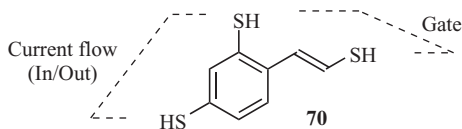


Figure 3.4. Design of a molecular transistor.

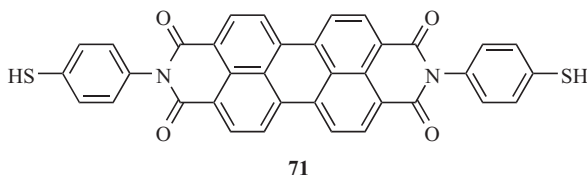
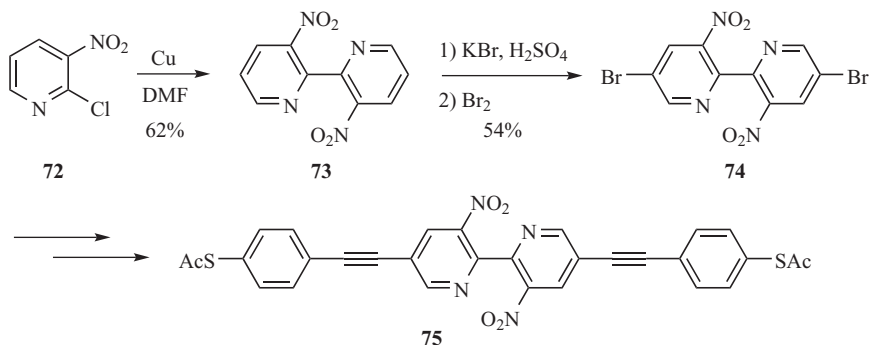


Figure 3.5. Perylene diimide compound.

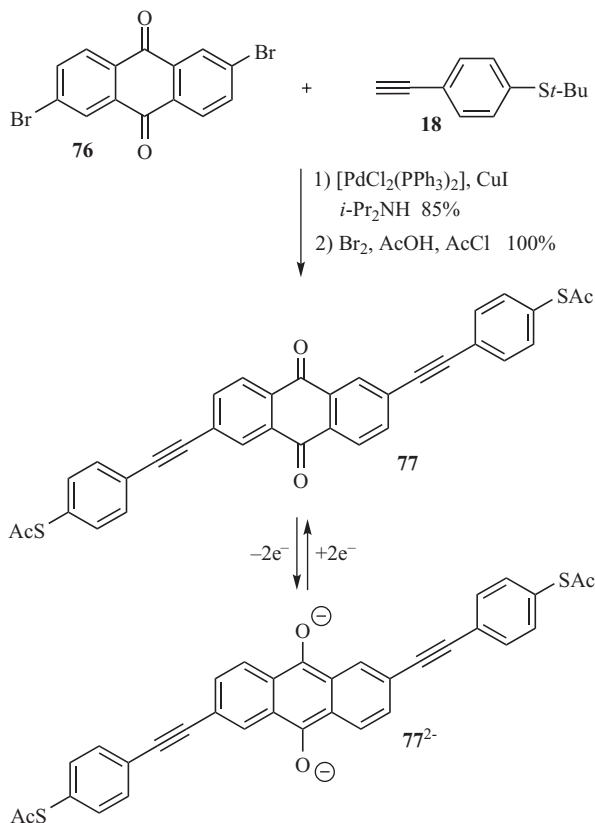


Scheme 3.25. Synthesis of molecular switch based on a dinitro-bipyridyl core.

enhanced conductivity at the peak gate potential compared with when the gate potential was zero.

In contrast to the setup described earlier, it is possible to switch dinitro-bipyridyl systems in a metal–single-molecule–metal setup between stable states only triggered by voltage pulses passed through the molecule [55]. It was shown that a single molecule was able to respond to write, read, and erase pulses, which makes this system potentially suitable for molecular memory elements. The dinitro-bipyridyl core of this switch can be assembled via an Ullmann-type dimerization of chloropyridine **72**, which at elevated temperatures and in the presence of copper(0) forms bipyridine **73** (Scheme 3.25) [29d]. This was followed by a bromination, giving functionalized dibromo-bipyridyl **74** which, after two subsequent steps, was converted to thioacetate terminated switch **75**.

Switching in a single molecule can also be facilitated by changes in molecular topology, which can be done by affecting the molecule with either light or electrochemical potentials. Scheme 3.26 presents an electrochemical redox-active switch based on an anthraquinone core which, upon a two-electron reduction, switches into an anthracene core with a linearly conjugated pathway between the two sulfur moieties [56]. Subjecting anthraquinone **76** to alkyne **18** in a metal-mediated cross-coupling reaction

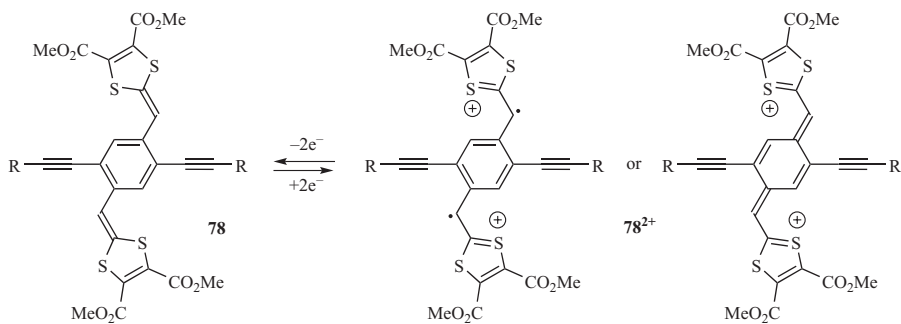


Scheme 3.26. Synthesis of redox-active switch based on an anthraquinone core.

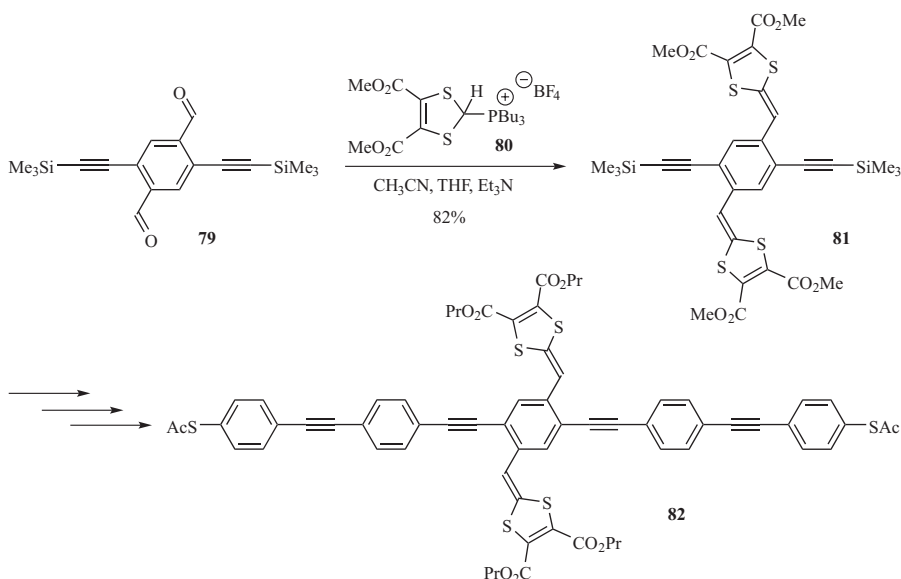
followed by a conversion of the *S*-*tert*-butyl group into an *S*-acetate provided redox-active switch **77** in high yield. It has been shown that compound **77** has a lower conductance compared with an anthracene analog [34], although switching experiments of compound **77** in a metal–single-molecule–metal junction have not yet been reported. Other studies on an OPV incorporating a hydroquinone end group have, however, shown that a hydroquinone does indeed result in a higher conductance than its oxidized quinone form [57].

Another redox-active molecule is the benzene-extended TTF **78** that under oxidation may form either a diradical or a quinoid structure, as revealed in Scheme 3.27 [58].

Formation of the benzene-extended TTF structure was accomplished via a Wittig-type reaction between terephthalaldehyde derivative **79** and phosphonium salt **80** in the presence of base to give compound **81** (Scheme 3.28) [26]. Compound **81** was subsequently in a series of synthetic steps, involving desilylation and palladium-catalyzed cross-coupling reactions, converted into redox-active molecular wire **82**. Three-terminal studies at low temperatures on this compound provided access to three charge states (-1 , 0 , and $+1$) by changing the gate voltage (Scheme 3.29) [59]. All these three charge states contained unpaired spins; for example, the radical anion exhibited



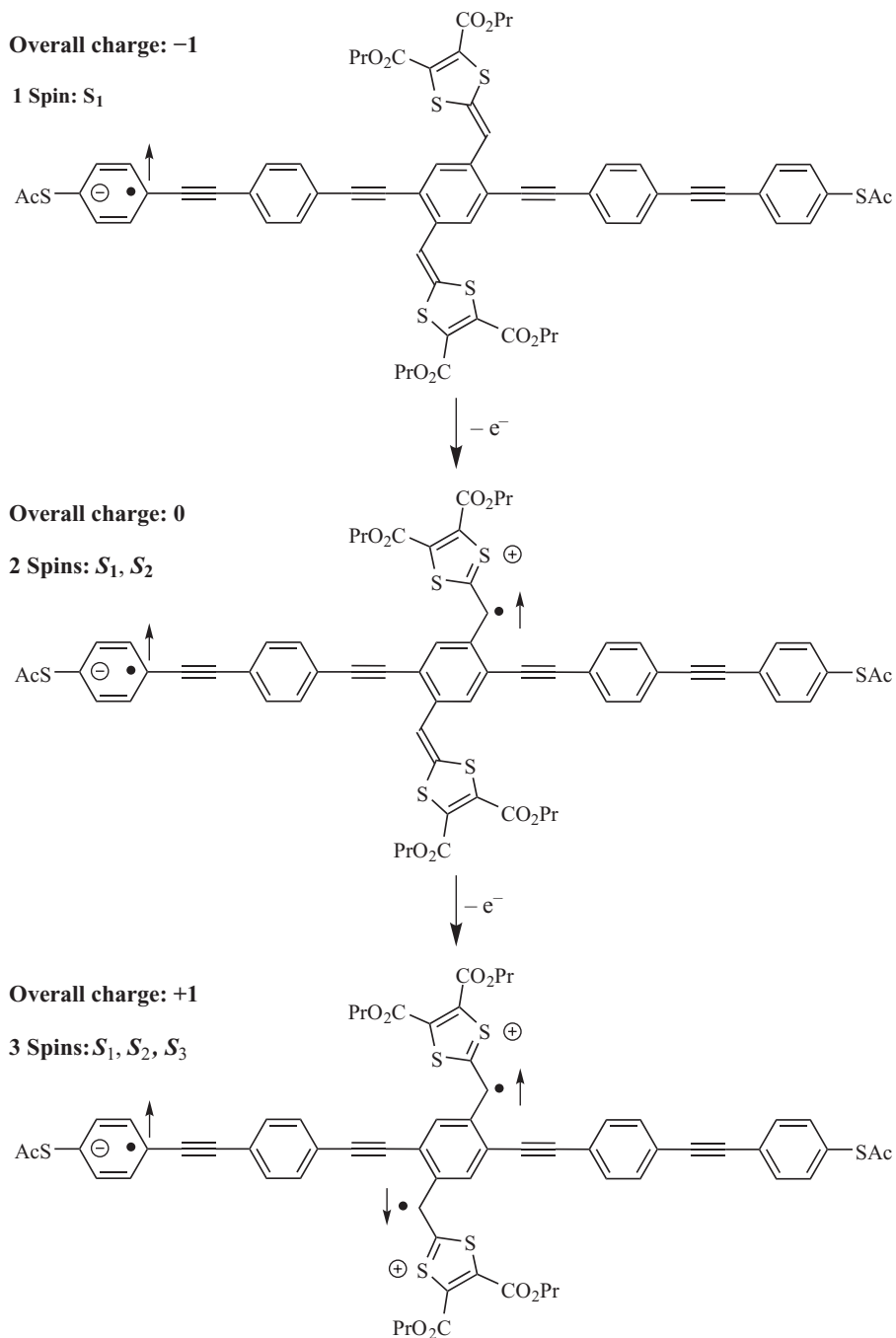
Scheme 3.27. Two-electron oxidation of benzene-extended TTF.



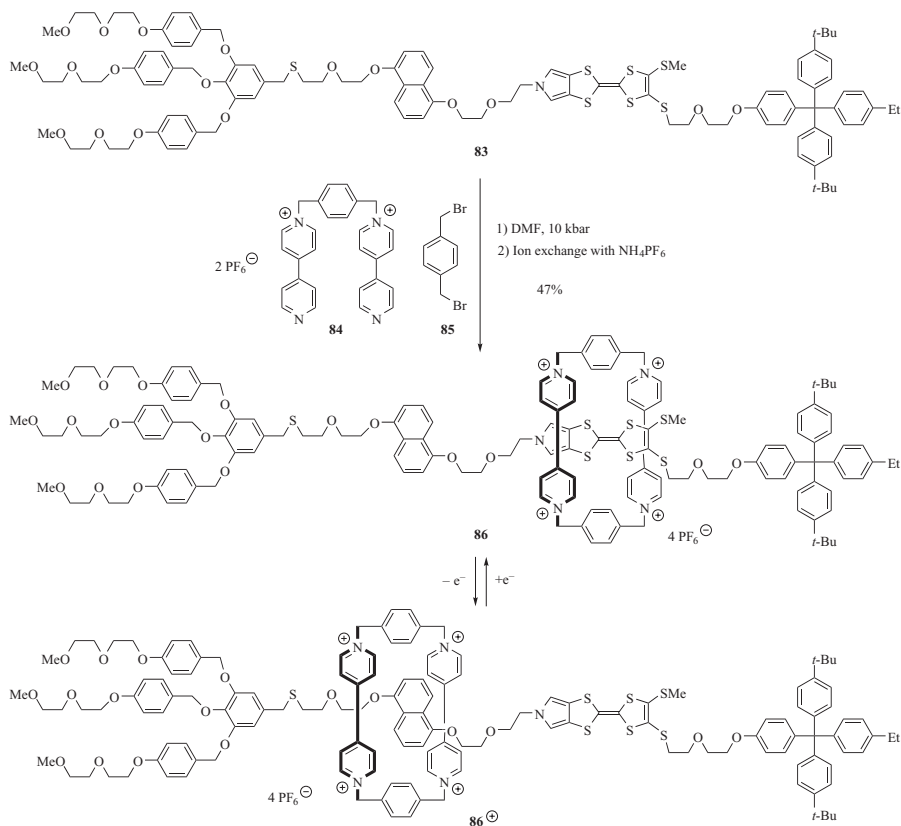
Scheme 3.28. Synthesis of OPE5-TTF cruciform-like molecular switch.

a strong zero-bias Kondo effect, which was split in the presence of a magnetic field. For the neutral species, a zero-bias Kondo effect still implies a spin-degenerate ground state; the removal of one electron must therefore generate an additional spin, which couples ferromagnetically to the first one (triplet ground state). Removal of one more electron generates a singly charged species with two ferromagnetically coupled spins, which are both antiferromagnetically coupled to the third spin. Thus, the molecule could be reversibly switched between polyradical states by changing the gate potential and the further manipulation by an external magnetic field-enabled advanced control of quantum spin in a single organic molecule.

It has been demonstrated that it is possible to create a two-dimensional logic memory molecular circuit based on bistable [2]rotaxanes containing a redox-active



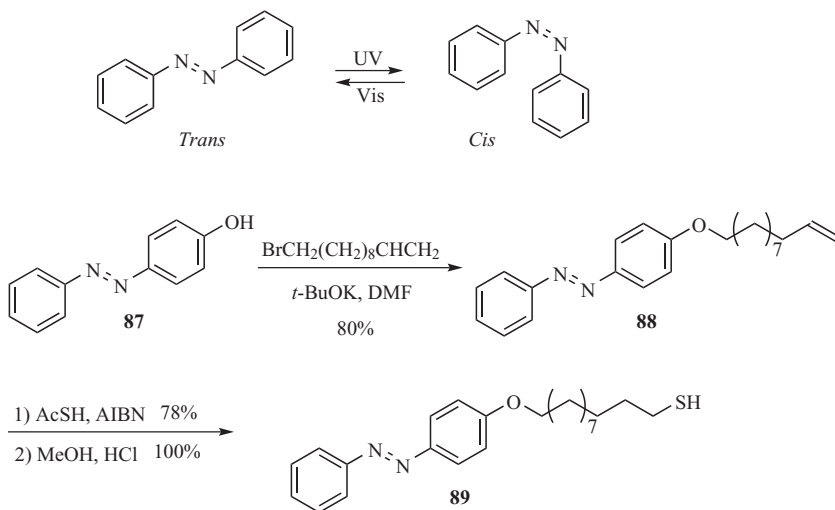
Scheme 3.29. Charge states of OPE5-TTF cruciform in a three-terminal device.



Scheme 3.30. Synthesis of redox-active bistable [2]rotaxane.

TTF unit and a dioxynaphthalene unit [60]. Scheme 3.30 shows how a rotaxane can be assembled by the *clipping* method [60]. The rodlike molecule **83** acts as template in the ring closing reaction, leading to cyclobis(paraquat-*p*-phenylene) (CBPQT⁴⁺) unit from dicationic precursor **84** and dibromide **85**, which eventually leads to [2]rotaxane **86** [60]. The redox-active TTF moiety in the [2]rotaxane can then be oxidized to the radical cation, which repels the positively charged CBPQT⁴⁺ unit and thereby forces it to move to the naphthalene donor station. The CBPQT⁴⁺ unit will slowly fluctuate back to the TTF part again when it is reduced to its neutral state. The hydrophobic and hydrophilic end groups do not only prevent dethreading of the cyclophane but also allows the molecule to be assembled in a Langmuir–Blodgett film. This film was sandwiched between electrodes in crossbar devices. Movement of the cyclophane from the TTF unit to the naphthalene unit when applying a potential resulted in conductance switching to a higher conducting state. A hysteresis effect was seen, which makes the system useful for the construction of memory devices. The switch could be recycled several times.

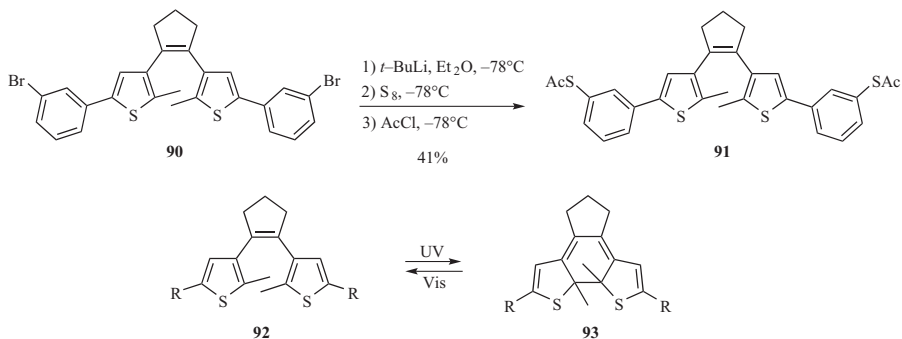
A different way to switch molecules is to use light [61], which in some cases can be an advantage, since photoactive molecules can switch without necessitating the use of



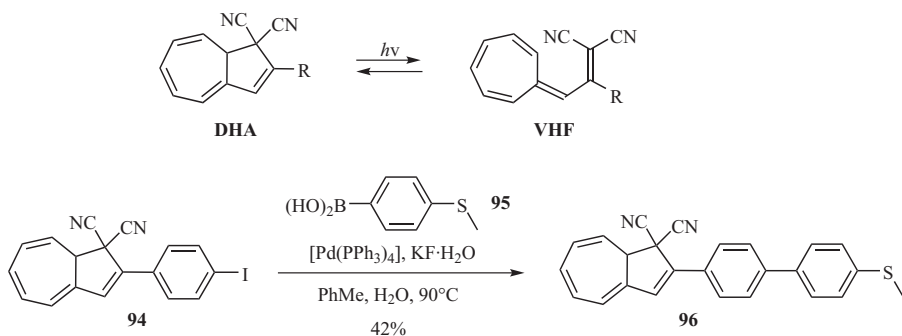
Scheme 3.31. Synthesis of azobenzene photoswitch with one anchoring group.

a third electrode (gate). Azobenzene is a simple photoswitch which, upon irradiation with UV light, switches from the N=N *trans* isomer into the *cis* isomer that can be isomerized back to the *trans* isomer by irradiation with visible light (Scheme 3.31) [62]. Although the change in the molecular topology in the switching of azobenzenes is small, it has been reported that an SAM of azobenzene on a gold substrate shows a conductance difference between the two isomers, the *cis* isomer being the high-conducting state. This was assigned to a reduced tunneling distance through the *cis* isomer [63]. Scheme 3.30 shows the procedure for synthesizing an azobenzene derivative with a thiol end-capped linker. Azobenzene derivative **87** was converted by a nucleophilic substitution reaction into alkene **88**, which then was converted to free thiol compound **89** [64]. Photoresponsive switch **89** was applied to gold nanoparticles and placed into a gel matrix film, in which it was possible to print images with UV light and to erase them again with visible light [64].

Photoresponsive switches are often greatly affected by interactions with metal surfaces or metal nanoparticles, since a strong coupling between the metal surface and the photoactive switch can lead to quenching of the excited state and hence lowering of the quantum yield of the photoisomerization [65]. One way to overcome this problem in π -conjugated molecules is to place the thiol anchoring group at a *meta* position on the aryl linking unit, as in the dithienylethene system shown in Scheme 3.32 [66, 67]. Dibromide **90** was subjected to a halide–lithium exchange followed by the addition of sulfur and finally acetylchloride to furnish product **91**. The two photoisomers of the photoactive system are represented by molecules **92** and **93**. In compound **92** there is a cross-conjugated connection between the two *R*-groups, which is changed into a linear conjugation pathway upon photoisomerization into compound **93**. This feature was demonstrated in reversible light-controlled conductance switching experiments of compound **91** in metal–molecule–metal devices; the open form corresponded to the *off* state, while the closed form corresponded to the *on* state [66, 68].



Scheme 3.32. Synthesis of dithienylethene photoswitch with two anchoring groups.



Scheme 3.33. Synthesis of dihydroazulene photoswitch with one anchoring group.

The dihydroazulene (DHA)/vinylheptafulvene (VHF) system presents another switch, which has recently been employed in molecular electronics. DHA is converted into the VHF by irradiation, while the VHF reverts back to DHA thermally (Scheme 3.33) [69]. A model system that could be evaporated into a silver nanogap junction was designed [70]. One *S*-methyl group was used as a linker and was attached by a Suzuki cross-coupling reaction between iodo-DHA **94** and boronic acid **95**, furnishing *S*-methyl DHA **96**. This compound was then captured in a silver nanogap at 4K, and light-controlled conductance switching was observed between DHA (off) and VHF (on) states at certain gate and bias potentials (Figure 3.6) [70]. Due to the weak anchoring via the SMe group, the single-molecule device was found to be operating in the Coulomb blockade regime, in which electron transport is proceeding via sequential tunneling, that is, an electron jumps from one electrode to the molecule, resides there for a time, before jumping to the second electrode.

3.5 CONCLUSIONS AND OUTLOOK

A wide variety of molecular components have, in the last years, become available as anchoring groups, wires, rectifiers, switches, and transistors, and immense research

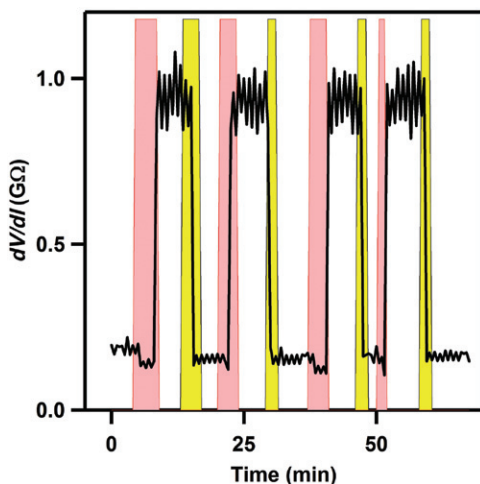


Figure 3.6. A series of *on–off* switchings of SMe end-capped DHA **96** at a gate potential of 2.7V. The highlighted background indicates the time intervals when the sample was subjected to light (yellow) or the temperature was increased from 4 to 25K (rose). The differential resistance dV/dI was taken at a bias voltage of 25 mV for both *on* (VHF) and *off* (DHA) states. Source: [70]. Reproduced with permission of Wiley-VCH Verlag GmbH & Co. KGaA. See color insert.

focuses on improving these components and on developing new functional molecules. Reliable contacting and self-assembly of billions of these molecular components present important challenges for the further development of molecular electronic devices. An important step has been taken, however, by the successful construction of crossbar architectures based on monolayers of rotaxane molecules trapped between wires in two-dimensional arrays. DNA-programmed assembly of nanostructures should also be mentioned as a particularly promising tool for the controlled construction of electronic devices [71]. Thus, DNA can be used as a template for the growth of nanowires and addressable nanostructures in one, two, and three dimensions. In Chapter 5, different routes to the self-organization of nanostructures via hydrogen-bonding interactions are in focus. But before that, we shall look at all-carbon conjugated materials, namely, carbon nanotubes and graphene, which have also found promising use in organic electronics.

REFERENCES

- [1] Robertson, N., McGowan, C. A. (2003). A comparison of potential molecular wires as components for molecular electronics. *Chemical Society Reviews*, 32, 96–103.
- [2] (a) Reinerth, W. A., Jones, L., II, Burgin, T. P., Zhou, C., Muller, C. J., Deshpande, M. R., Reed, M. A., Tour, J. M. (1998). Molecular scale electronics: Syntheses and testing. *Nanotechnology*, 9, 246–250; (b) Tour, J. M. (2000). Molecular electronics: Synthesis and testing of components. *Accounts of Chemical Research*, 33, 791–804; (c) Pease, A. R., Jeppesen, J. O., Stoddart, J. F., Luo, Y., Collier, C. P., Heath, J. R. (2001). Switching devices based on interlocked molecules.

- Accounts of Chemical Research*, 24, 433–444; (d) Nørgaard, K., Bjørnholm, T. (2005). Supramolecular chemistry on water—Towards self-assembling molecular electronic circuitry. *Chemical Communications*, 1812–1823; (e) Weibel, N., Grunder, S., Mayor, M. (2007). Functional molecules in electronic circuits. *Organic & Biomolecular Chemistry*, 5, 2343–2353; (f) McCreery, R. L., Bergen, A. J. (2009). Progress with molecular electronic junctions: Meeting experimental challenges in design and fabrication. *Advanced Materials*, 21, 4303–4322; (g) Moth-Poulsen, K., Bjørnholm, T. (2009). Molecular electronics with single molecules in solid-state devices. *Nature Nanotechnology*, 4, 551–556; (h) Guldi, D. M., Illescas, B. M., Atienza, C. M., Wielopolski, M., Martín, N. (2009). Fullerene for organic electronics. *Chemical Society Reviews*, 38, 1587–1597.
- [3] (a) Cui, X. D., Primak, A., Zarate, X., Tomfohr, J., Sankey, O. F., Moore, A. L., Moore, T. A., Gust, D., Harris, G., Lindsay, S. M. (2001). Reproducible measurement of single-molecule conductivity. *Science*, 294, 571–574; (b) Kushmerick, J. G., Holt, D. B., Pollack, S. K., Ratner, M. A., Yang, J. C., Schull, T. L., Naciri, J., Moore, M. H., Shashidhar, R. (2002). Effect of bond-length alternation in molecular wires. *Journal of the American Chemical Society*, 124, 10654–10655; (c) Park, J., Pasupathy, A. N., Goldsmith, J. I., Chang, C., Yaish, Y., Petta, J. R., Rinkoski, M., Sethna, J. P., Abruna, H. D., McEuen, P. L., Ralph, D. C. (2002). Coulomb blockade and the Kondo effect in single-atom transistors. *Nature*, 417, 722–725; (d) Smit, R. H. M., Noat, Y., Untiedt, C., Lang, N. D., van Hemert, M. C., van Ruitenbeek, J. M. (2002). Measurement of the conductance of a hydrogen molecule. *Nature*, 419, 906–909; (e) Dadosh, T., Gordin, Y., Krahne, R., Khivrich, I., Mahalu, D., Frydman, V., Sperling, J., Yacoby, A., Bar-Joseph, I. (2005). Measurement of the conductance of single conjugated molecules. *Nature*, 436, 677–680; (f) Venkataraman, L., Klare, J. E., Nockolls, C., Hybertsen, M. S., Steigerwald, M. L. (2006). Dependence of single-molecule junction conductance on molecular conformation. *Nature*, 442, 904–907; (g) Reep, J., Meyer, G., Paavilainen, S., Olsson, F. E., Persson, M. (2006). Imaging bond formation between a gold atom and pentacene on an insulating surface. *Science*, 312, 1196–1199.
- [4] (a) Reed, M. A., Zhou, C., Muller, C. J., Burgin, T. P., Tour, J. M. (1997). Conductance of a molecular junction. *Science*, 278, 252–254; (b) Xu, B., Tao, N. J. (2003). Measurement of single-molecule resistance by repeated formation of molecular junctions. *Science*, 301, 1221–1223; (c) Ulrich, J., Esrail, D., Pontius, W., Venkataraman, L., Millar, D., Doerr, L. H. (2006). Variability of conductance in molecular junctions. *The Journal of Physical Chemistry B*, 110, 2462–2466.
- [5] Hong, W., Manrique, D. Z., Moreno-García, P., Gulcur, M., Mishchenko, A., Lambert, C. J., Bryce, M. R., Wandlowski, T. (2012). Single molecular conductance of tolanes: Experimental and theoretical study on the junction evolution dependent on the anchoring group. *Journal of the American Chemical Society*, 134, 2292–2304.
- [6] (a) Jones, D. R., Troisi, A. (2007). Single molecule conductance of linear dithioalkanes in the liquid phase: Apparently activated transport due to conformational flexibility. *The Journal of Physical Chemistry*, 111, 14567–14573; (b) Pauly, F., Viljas, J. K., Cuevas, J. C., Schön, G. (2008). Density-functional study of tilt-angle and temperature-dependent conductance in biphenyl dithiol single-molecule junctions. *Physical Review B*, 77, 155312; (c) Dell'Angela, M., Kladnik, G., Cossaro, A., Verdini, A., Kamenetska, M., Tamblyn, I., Quek, S. Y., Neaton, J. B., Cvetko, D., Morgante, A., Venkataraman, L. (2010). Relating energy level alignment and amine-linked single molecule junction conductance. *Nano Letters*, 10, 2470–2474.
- [7] (a) Bagrets, A., Arnold, A., Evers, F. (2008). Conduction properties of bipyridinium-functionalized molecular wires. *Journal of the American Chemical Society*, 130, 9013–9018; (b) Mishchenko, A., Zotti, L. A., Vonlanthen, D., Burkle, M., Pauly, F., Cuevas, J. C., Mayor, M., Wandlowski, T. (2011). Single-molecule junctions based on nitrile-terminated biphenyls: A promising new anchoring group. *Journal of the American Chemical Society*, 133, 184–187.

- [8] Kim, B., Beebe, J. M., Jun, Y., Zhu, X. Y., Frisbie, C. D. (2006). Correlation between HOMO alignment and contact resistance in molecular junctions: Aromatic thiols versus aromatic isocyanides. *Journal of the American Chemical Society*, *128*, 4970–4971.
- [9] Chen, F., Li, X., Hihath, J., Huang, Z., Tao, N. (2006). Effect of anchoring groups on single-molecule conductance: Comparative study of thiol-, amine-, and carboxylic-acid-terminated molecules. *Journal of the American Chemical Society*, *128*, 15874–15881.
- [10] Zotti, L. A., Kirchner, T., Cuevas, J.-C., Pauly, F., Huhn, T., Scheer, E., Erbe, A. (2010). Revealing the role of anchoring groups in the electrical conduction through single-molecule junctions. *Small*, *6*, 1529–1535.
- [11] (a) Park, Y. S., Whalley, A. C., Kamenetska, M., Steigerwald, M. L., Hybertsen, M. S., Nuckolls, C., Venkataraman, L. (2007). Contact chemistry and single-molecule conductance: A comparison of phosphines, methyl sulfides, and amines. *Journal of the American Chemical Society*, *129*, 15768–15769; (b) Kamenetska, M., Koentopp, M., Whalley, A. C., Park, Y. S., Steigerwald, M. L., Nuckolls, C., Hybertsen, M. S., Venkataraman, L. (2009). Formation and evolution of single-molecule junctions. *Physical Review Letters*, *102*, 126803.
- [12] Chen, W., Widawsky, J. R., Vásquez, H. V., Schneebeli, S. T., Hybertsen, M. S., Breslow, R., Venkataraman, L. (2011). Highly conducting π -conjugated molecular junctions covalently bonded to gold electrodes. *Journal of the American Chemical Society*, *133*, 17160–17163.
- [13] Rogero, C., Pascual, J. I., Gómez-Herrero, J., Baró, A. M. (2002). Resolution of site-specific bonding properties of C_{60} adsorbed on Au(111). *Journal of Chemical Physics*, *116*, 832–836.
- [14] Böhler, T., Edtbauer, A., Scheer, E. (2007). Conductance of individual C_{60} molecules measured with controllable gold electrodes. *Physical Review B*, *76*, 125432.
- [15] Martin, C. A., Ding, D., Sørensen, J. K., Bjørnholm, T., van Ruitenbeek, J. M., van der Zant, H. S. J. (2008). Fullerene-based anchoring groups for molecular electronics. *Journal of the American Chemical Society*, *130*, 13198–13199.
- [16] Yao, Y., Tour, J. M. (1999). Facile convergent route to molecular caltrops. *The Journal of Organic Chemistry*, *64*, 1968–1971.
- [17] Ie, Y., Hirose, T., Nakamura, H., Kiguchi, M., Takagi, N., Kawai, M., Aso, Y. (2011). Nature of electron transport by pyridine-based tripodal anchors: Potential for robust and conductive single-molecule junctions with gold electrodes. *Journal of the American Chemical Society*, *133*, 3014–3022.
- [18] (a) Hsung, R. P., Babcock, J. R., Chidsey, C. E. D., Rita, L. R. (1995). Thiophenol protecting groups for the palladium-catalyzed heck reaction: Efficient syntheses of conjugated arylthiols. *Tetrahedron Letters*, *36*, 4525–4528; (b) Donhauser, Z. J., Mantooth, B. A., Kelly, K. K., Bumm, L. A., Monnell, J. D., Stapleton, J. J., Price, D. W., Jr., Rawlett, A. M., Allara, D. L., Tour, J. M., Weiss, P. S. (2001). Conductance switching in single molecules through conformational changes. *Science*, *292*, 2303–2307; (c) Valkenier, H., Huisman, E. H., van Hal, P. A., de Leeuw, D. M., Chiechi, R. C., Hummelen, J. C. (2011). Formation of high-quality self-assembled monolayers of conjugated dithiols on gold: Base matters. *Journal of the American Chemical Society*, *133*, 4930–4939.
- [19] (a) Stühr-Hansen, N., Christensen, J. B., Harrit, N., Bjørnholm, T. (2003). Novel synthesis of protected thiol end-capped stilbenes and oligo(phenylenevinylene)s (OPVs). *The Journal of Organic Chemistry*, *68*, 1275–1282; (b) Stühr-Hansen, N. (2003). The *tert*-butyl moiety—A base resistant thiol protecting group smoothly replaced by the labile acetyl moiety. *Synthetic Communications*, *33*, 641–646.
- [20] Wang, C., Batsanov, A. S., Bryce, M. R., Sage, I. (2004). Nanoscale aryleneethynylene molecular wires with reversible fluorenone electrochemistry for self-assembly onto metal surfaces. *Organic Letters*, *6*, 2181–2184.
- [21] Hassan, J., Sévignon, M., Gozzi, C., Schulz, E., Lemaire, M. (2002). Aryl-aryl bond formation one century after the discovery of the Ullmann reaction. *Chemical Reviews*, *102*, 1359–1460.

- [22] Beletskaya, I. P., Sheprakov, A. W. (2000). The Heck reaction as a sharpening stone of palladium catalysis. *Chemical Reviews*, 100, 3009–3066.
- [23] (a) Chinchilla, R., Nájera, C. (2007). The Sonogashira reaction: A booming methodology in synthetic organic chemistry. *Chemical Reviews*, 107, 874–922; (b) Chinchilla, R., Nájera, C. (2011). Recent advances in Sonogashira reactions. *Chemical Society Reviews*, 40, 5084–5121.
- [24] Pearson, D. L., Tour, J. M. (1997). Rapid synthesis of oligo(2,5-thiophene ethynylene)s with thioester termini: Potential molecular scale wires with alligator clips. *The Journal of Organic Chemistry*, 62, 1376–1387.
- [25] Wang, C., Batsanov, A. S., Bryce, M. R., Sage, I. (2003). An improved synthesis and structural characterisation of 2-(4-acetylthiophenylethynyl)-4-nitro-5-phenylethynylaniline: The molecule showing high negative differential resistance (NDR). *Synthesis*, 2089–2095.
- [26] Jennum, K., Vestergaard, M., Pedersen, A. H., Fock, J., Jensen, J., Santella, M., Led, J. J., Kilså, K., Bjørnholm, T., Nielsen, M. B. (2011). Synthesis of oligo(phenyleneethynylene)s with vertically disposed tetrathiafulvalene units. *Synthesis*, 539–548.
- [27] Gryko, D. T., Clausen, C., Roth, K. M., Dontha, N., Bocian, D. F., Kuhr, W. G., Lindsay, J. S. (2000). Synthesis of “porphyrin-linker-thiol” molecules with diverse linkers for studies of molecular-based information storage. *The Journal of Organic Chemistry*, 65, 7345–7355.
- [28] Barbero, M., Degani, I., Dughera, S., Fochi, R. (2003). An improved, general procedure to *S*-Aryl thioesters: A new synthetic application of dry arene diazonium *o*-benzenedisulfonimides. *Synthesis*, 1225–1230.
- [29] (a) Tour, J. M., Rawlett, A. M., Kozaki, M., Yao, Y., Jagessar, R. C., Dirk, S. M., Price, D. W., Reed, M. A., Zhou, C.-W., Chen, J., Wang, W., Campbell, I. (2001). Synthesis and preliminary testing of molecular wires and devices. *Chemistry—A European Journal*, 7, 5118–5134; (b) Kushmerick, J. G., Holt, D. B., Yang, J. C., Naciri, J., Moore, M. H., Scashidhar, R. (2002). Metal-molecule contacts and charge transport across monomolecular layers: Measurement and theory. *Physical Review Letters*, 89, 086802; (c) Kubatkin, S., Danilov, A., Hjort, M., Cornil, J., Brédas, J.-L., Stuhr-Hansen, N., Hedegård, P., Bjørnholm, T. (2003). Single-electron transistor of a single organic molecule with access to several redox states. *Nature*, 425, 698–701; (d) Flatt, A. K., Dirk, S. M., Henderson, J. C., Shen, D. E., Su, J., Reed, M. A., Tour, J. M. (2003). Synthesis and testing of new end-functionalized oligomers for molecular electronics. *Tetrahedron*, 59, 8555–8570; (e) Long, D. P., Patterson, C. H., Moore, M. H., Seferos, D. S., Bazan, G. C., Kushmerick, J. G. (2005). Magnetic directed assembly of molecular junctions. *Applied Physics Letters*, 86, 153105.
- [30] Huber, R., González, M. T., Wu, S., Langer, M., Grunder, S., Horhoiu, V., Mayor, M., Bryce, M. R., Wang, C., Jichati, R., Schönenberger, C., Calame, M. (2008). Electrical conductance of conjugated oligomers at the single molecule level. *Journal of the American Chemical Society*, 130, 1080–1084.
- [31] Moth-Poulsen, K., Patrone, L., Stuhr-Hansen, N., Christensen, J. B., Bourgoin, J.-P., Bjørnholm, T. (2005). Probing the effect of conjugated path on the electronic transmission through single molecules using scanning tunneling microscopy. *Nano Letters*, 5, 783–785.
- [32] Fan, F.-R. F., Yang, J., Cai, L., Price, D. W., Dirk, S. M., Kosynkin, D. V., Yao, Y., Rawlett, A. M., Tour, J. M., Bard, A. J. (2002). Charge transport through self-assembled monolayers of compounds of interest in molecular electronics. *Journal of the American Chemical Society*, 124, 5550–5560.
- [33] Vonlanthen, D., Mishchenko, A., Elbing, M., Neuburger, M., Wandlowski, T., Mayor, M. (2009). Chemically controlled conductivity: Torsion-angle dependence in a single-molecule biphenyldithiol junction. *Angewandte Chemie (International ed. in English)*, 48, 8886–8890.
- [34] Kaliginedi, V., Moreno-García, P., Valkenier, H., Hong, W., García-Suárez, V. M., Buitert, P., Otten, J. L. H., Hummelen, J. C., Lambert, C. J., Wandlowski, T. (2012). Correlations between molecular structure and single-junction conductance: A case with oligo(phenyleneethynylene)-type wires. *Journal of the American Chemical Society*, 134, 5262–5275.

- [35] Mayor, M., Weber, H. B., Reichert, J., Elbing, M., von Hänisch, C., Beckmann, D., Fischer, M. (2003). Electric current through a molecular rod—relevance of the position of the anchor groups. *Angewandte Chemie (International ed. in English)*, 42, 5834–5838.
- [36] Wei, Z., Li, T., Jennum, K., Santella, M., Bovet, N., Hu, W., Nielsen, M. B., Bjørnholm, T., Solomon, G. C., Laursen, B. W., Nørgaard, K. (2012). Molecular junctions based on SAMs of cruciform oligo(phenyleneethynylene)s. *Langmuir: The ACS Journal of Surfaces and Colloids*, 28, 4016–4023.
- [37] (a) Reddy, P., Jang, S.-Y., Segalman, R. A., Majumdar, A. (2007). Thermoelectricity in molecular junctions. *Science*, 315, 1568–1571; (b) Tan, A., Balachandran, J., Sadat, S., Gavini, V., Dunietz, B. D., Jang, S.-Y., Reddy, P. (2011). Effect of length and contact chemistry on the electronic structure and thermoelectric properties of molecular junctions. *Journal of the American Chemical Society*, 133, 8838–8841.
- [38] Muesmann, T. W. T., Wickleder, M. S., Christoffers, J. (2011). Preparation of linear aromatic disulfonic acids: New linker molecules for metal-organic framework. *Synthesis*, 2775–2780.
- [39] Price, D. W., Dirk, S. M., Jr., Maya, F., Tour, J. M. (2003). Improved and new synthesis of potential molecular electronic devices. *Tetrahedron*, 59, 2497–2518.
- [40] Giacalone, F., Herranz, M. Á., Grüter, L., González, M. T., Calame, M., Schönenberger, C., Arroyo, C. R., Rubio-Bollinger, G., Vélez, M., Agraït, N., Martín, N. (2007). Tetrathiafulvalene-based molecular nanowires. *Chemical Communications*, 4854–4856.
- [41] Taniguchi, S.-I., Minamoto, M., Matsushita, M. M., Sugawara, T., Kawada, Y., Bethell, D. (2006). Electron transport in networks of gold nanoparticles connected by oligothiophene molecular wires. *Journal of Materials Chemistry*, 16, 3459–3465.
- [42] (a) Otsubo, T., Aso, Y., Takimiya, K. (2002). Functional oligothiophenes as advanced molecular electronic materials. *Journal of Materials Chemistry*, 12, 2565–2575; (b) Guldi, D. M., Ill-escas, B. M., Atienza, C. M., Wielopolski, M., Martín, N. (2009). Fullerene for organic electronics. *Chemical Society Reviews*, 38, 1587–1597.
- [43] Shirai, Y., Zhao, Y., Cheng, L., Tour, J. M. (2004). Facile synthesis of multifullerene-OPE hybrids via in situ ethynylation. *Organic Letters*, 6, 2129–2132.
- [44] Sørensen, J. K., Fock, J., Pedersen, A. H., Petersen, A. B., Jennum, K., Bechgaard, K., Kilså, K., Geskin, V., Cornil, J., Bjørnholm, T., Nielsen, M. B. (2011). Fulleropyrrolidine end-capped molecular wires for molecular electronics—Synthesis, spectroscopic, electrochemical and theoretical characterization. *The Journal of Organic Chemistry*, 76, 245–263.
- [45] Grunder, S., Huber, R., Horhoiu, V., González, M. T., Schönenberger, C., Calame, M., Mayor, M. (2007). New cruciform structures: Toward coordination induced single molecule switches. *The Journal of Organic Chemistry*, 72, 8337–8344.
- [46] Aviram, A., Ratner, M. A. (1974). Molecular rectifiers. *Chemical Physics Letters*, 29, 277–283.
- [47] Metzger, R. M. (2003). Unimolecular electrical rectifiers. *Chemical Reviews*, 103, 3803–3834.
- [48] de Miguel, P., Bryce, M. R., Goldenberg, L. M., Beeby, A., Khodorkovsky, V., Shapiro, L., Niemz, A., Cuello, A. O., Rotello, V. (1998). Synthesis and intramolecular charge-transfer properties of new tetrathiafulvalene- σ -tetracyanoanthraquinodimethane diad (TTF- σ -TCNAQ) and triad (TTF- σ -TCNAQ- σ -TTF) molecules. *Journal of Materials Chemistry*, 8, 71–76.
- [49] Metzger, R. M., Chen, B., Höpfner, U., Lakshmikantham, M. V., Vuillaume, D., Kawai, T., Wu, X., Tachibana, H., Hughes, T. V., Sakurai, H., Baldwin, J. W., Hosch, C., Cava, M. P., Brehmer, L., Ashwell, G. J. (1997). Unimolecular electrical rectification in hexadecylquinolinium tricyanoquinodimethanide. *Journal of the American Chemical Society*, 119, 10455–10466.
- [50] Metzger, R. M. (1999). Electrical rectification by a molecule: The advent of unimolecular electronic devices. *Accounts of Chemical Research*, 32, 950–957.

- [51] Ashwell, G. J., Tyrrell, W. D., Whittam, A. J. (2004). Molecular rectification: Self-assembled monolayers in which donor-(π -bridge)-acceptor moieties are centrally located and symmetrically coupled to both gold electrodes. *Journal of the American Chemical Society*, 126, 7102–7110.
- [52] Elbing, M., Ochs, R., Koentopp, M., Fischer, M., von Hänisch, C., Weigend, F., Evers, F., Weber, H. B., Mayor, M. (2005). A single-molecule diode. *Proceedings of the National Academy of Sciences of the United States of America*, 102, 8815–8820.
- [53] Cardamone, D. M., Stafford, C. A., Mazumdar, S. (2006). Controlling quantum transport through a single molecule. *Nano Letters*, 6, 2422–2426.
- [54] Xu, B., Xiao, X., Yang, X., Zang, L., Tao, N. (2005). Large gate modulation in the current of a room temperature single molecule transistor. *Journal of the American Chemical Society*, 127, 2386–2387.
- [55] (a) Lörtscher, E., Cizek, J. W., Tour, J. M., Riel, H. (2006). Reversible and controllable switching of a single-molecule junction. *Small*, 2, 973–977; (b) He, J., Fu, Q., Landsay, S., Cizek, J. W., Tour, J. M. (2006). Electrochemical origin of voltage-controlled molecular conductance switching. *Journal of the American Chemical Society*, 128, 14828–14835.
- [56] van Dijk, E. H., Myles, D. J. T., van der Veen, M. H., Hummelen, J. C. (2006). Synthesis and properties of an anthraquinone-based redox switch for molecular electronics. *Organic Letters*, 8, 2333–2336.
- [57] Tsoi, S., Griva, I., Trammell, S. A., Blum, A. S., Schnur, J. M., Lebedev, N. (2008). Electrochemically controlled conductance switching in a single molecule: Quinone-modified oligo(phenylene vinylene). *ACS Nano*, 2, 1289–1295.
- [58] Vestergaard, M., Jennum, K., Sørensen, J. K., Kilså, K., Nielsen, M. B. (2008). Synthesis and characterization of cruciform-conjugated molecules based on tetrathiafulvalene. *The Journal of Organic Chemistry*, 73, 3175–3183.
- [59] Fock, J., Leijnse, M., Jennum, K., Zyazin, A. S., Paaske, J., Hedegård, P., Nielsen, M. B., van der Zant, H. S. J. (2012). Manipulation of organic polyradicals in a single-molecule transistor. *Physical Review B*, 86, 235403.
- [60] Lou, Y., Collier, P., Jeppesen, J. O., Nielsen, K. A., Delonno, E., Ho, G., Perkins, J., Tseng, H.-R., Yamamoto, T., Stoddart, J. F., Heath, J. R. (2002). Two-dimensional molecular electronic circuits. *Chemphyschem: A European Journal of Chemical Physics and Physical Chemistry*, 3, 519–525.
- [61] Browne, W. R., Feringa, B. L. (2009). Light switching of molecules on surfaces. *Annual Review of Physical Chemistry*, 60, 407–428.
- [62] Klajn, R., Stoddart, J. F., Grzybowski, B. A. (2010). Nanoparticles functionalised with reversible molecular and supramolecular switches. *Chemical Society Reviews*, 39, 2203–2237.
- [63] Kim, Y., Wang, G., Choe, M., Kim, J., Lee, S., Park, S., Kim, D.-Y., Lee, B. H., Lee, T. (2011). Electronic properties associated with conformational changes in azobenzene-derivative molecular junctions. *Organic Electronics*, 12, 2144–2150.
- [64] Klajn, R., Wesson, P. J., Bishop, K. J. M., Grzybowski, B. A. (2009). Writing self-erasing images using metastable nanoparticle “inks”. *Angewandte Chemie (International ed. in English)*, 48, 7035–7039.
- [65] Zhang, J., Whitesell, J. K., Fox, M. A. (2001). Photoreactivity of self-assembled monolayers of azobenzene or stilbene derivatives capped on colloidal gold clusters. *Chemistry of Materials*, 13, 2323–2331.
- [66] van der Molen, S. J., Liao, J., Kudernac, T., Agustsson, J. S., Bernard, L., Calame, M., van Wees, B. J., Feringa, B. L., Schönenberger, C. (2009). Light-controlled conductance switching of ordered metal-molecule-metal device. *Nano Letters*, 9, 76–80.
- [67] Kudernac, T., de Jong, J. J., van Esch, J., Feringa, B. L., Duli, D., van der Molen, S. J., van Wees, B. J. (2005). Molecular switches get wired: Synthesis of diarylethenes containing one or two sulphurs. *Molecular Crystals and Liquid Crystals*, 430, 205–210.

- [68] Kronemeijer, A. J., Akkerman, H. B., Kudernac, T., van Wees, B. J., Feringa, B. L., Blom, P. W. M., de Boer, B. (2008). Reversible conductance switching in molecular devices. *Advanced Materials*, 20, 1467–1473.
- [69] (a) Daub, J., Knöchel, T., Mannschreck, A. (1984). Photosensitive dihydroazulenes with chromogenic properties. *Angewandte Chemie (International ed. in English)*, 23, 960–961; (b) Broman, S. L., Petersen, M. Å., Tortzen, C. G., Kadziola, A., Kilså, K., Nielsen, M. B. (2010). Arylethynyl derivatives of the dihydroazulene/vinylheptafulvene photo/thermoswitch—Tuning the switching event. *Journal of the American Chemical Society*, 132, 9165–9174.
- [70] Broman, S. L., Lara-Avila, S., Thisted, C. L., Bond, A. D., Kubatkin, S., Danilov, A., Nielsen, M. B. (2012). Dihydroazulene photoswitch operating in sequential tunneling regime: Synthesis and single-molecule junction studies. *Advanced Functional Materials*, 22, 4249–4258.
- [71] (a) Gothelf, K. V., LaBean, T. H. (2005). DNA-programmed assembly of nanostructures. *Organic and Biomolecular Chemistry*, 3, 4023–4037; (b) Aldaye, F. A., Palmer, A. L., Sleiman, H. F. (2008). Assembling materials with DNA as the guide. *Science*, 321, 1795–1799.

CHAPTER 4

CARBON NANOTUBES AND GRAPHENE

HELENA GRENNBERG

4.1 INTRODUCTION

Elemental carbon exists in three main forms: graphite, consisting of pi-stacked planar graphene layers, and diamond, where the carbon atoms are tetrahedrally bonded to each other, forming a 3D giant structure and the fullerenes, a large and diverse group of hollow spheres, ellipsoids, and tubes of (formally) sp^2 hybridized carbon atoms [1, 2]. The first reports of fullerenes [3] and carbon nanotubes (CNTs) [4] opened a new research area in which the knowledge of physics, chemistry, and the applications technology potential has increasingly grown [5, 6]. With the experimental verification of individual graphene layers in 2004 [7], the area has expanded even further. Each of the discoveries, in particular the latter two, has given rise to predictions of revolutions in materials science and electronics [8, 9].

The worldwide research investments in CNT and graphene research over the past two decades have considerably increased the level of knowledge, whereas applications utilizing in particular the electronic properties, beyond the demonstrator devices, are still to appear at the consumer side. One reason is the difficulties associated with, in particular, CNT synthesis; for any application, scalable reproducible synthetic methods and practical transfer of the product from the synthetic environment to a solid substrate suitable for characterization or device fabrication are primary requirements. The graphene area is benefiting from the knowledge gained in CNT research, hence initial progress has been considerably faster.

In the present chapter, synthesis of CNTs and graphene is discussed, in the former case including a discussion on purification and in the latter case with focus on the main synthetic routes for graphene fulfilling both the requirement of being scalable and yielding a product that can be deposited on any substrate. Examples of functionalization and other secondary processing toward devices are given with (far from comprehensive) literature coverage ending 2012. Fullerene chemistry, related to the chemistry

Organic Synthesis and Molecular Engineering, First Edition.

Edited by Mogens Brøndsted Nielsen.

© 2014 John Wiley & Sons, Inc. Published 2014 by John Wiley & Sons, Inc.

of CNTs, is touched upon, whereas synthesis, modification chemistry, and uses of diamond is an area of its own [10] and is not covered in this chapter.

4.1.1 Terms and Nomenclature

Graphene. According to an early definition developed for graphite intercalation compounds [11], graphene is a one-atom-thick sheet of hexagonally arranged sp^2 hybridized carbon atoms. Despite the strict definition, it has become established practice to use the term “graphene” also for flakes of more than one layer, of any sheet size from around a square micrometer and up and also for carbon sheets with significant deviations from the all-carbon and all- sp^2 criteria, such as graphite oxide (GO) and reduced graphite oxide (RGO). In this chapter, we have used “graphene” and “graphene flakes” for materials prepared via nonoxidative routes. Depending on the synthetic method, the product can be single layer or with a distribution of thicknesses. In the case of oxidation-reduction routes, the resulting material, a derivative of graphene, is denoted “RGO”; “RGO flakes” is used for unspecified RGO entities. Graphene flakes and sheets are often irregular in shape and with ragged edges (Figure 4.1) [12]. At the atomic level, the edges can be “armchair” or “zigzag,” depending on the direction of the carbon hexagons in the interior “basal plane” of the sheet. The edge carbon atoms can be saturated or unsaturated, and edge termination is most often considered to be by hydrogen or oxygen.

Carbon nanotubes (CNTs) belong to the same group of carbon allotropes as fullerene C_{60} . Whereas the latter is a spherical molecule, a CNT may be viewed as a fullerene that has been cut in two halves and combined with a graphene cylinder. CNTs are primarily categorized based on the number of tubes inside each other: single, double, or multiple, the latter being all CNTs with more than two “walls.” Multiple-wall carbon nanotubes (MWCNTs) have significantly larger diameters than single-wall carbon nanotubes (SWCNTs) (Figure 4.2). Although CNTs are very narrow in diameter, the smallest tubes have diameters approximately equal to the length of anthracene; the aspect ratio can be very high. As a result, CNTs are considered quasi-one-dimensional materials [13].

The cylinder part of a CNT may exhibit all orientations of the hexagonal lattice, from “armchair” to “zigzag.” Orientations between the two are chiral. The diameter of a CNT as well as the angle of the hexagonal lattice versus the axis of the CNT is defined by two integers (n, m) [14]. The first denotes the number of hexagons in a row that, in a hypothetical “unwrapped” cylinder, are parallel to a zigzag edge that is required to complete one turn around the circumference. The second integer describes the offset of one turn along the tube axis, that is, to which zigzag hexagon row the last hexagon of the first turn (in row 0) connects to for the second turn. For a zigzag tube, $m = 0$, whereas for armchair tubes $m = n$. Although it is possible to construct very narrow 4, 0 and 2, 2 tubes using ball-and-stick models, the smallest diameters experimentally observed in postsynthesis processed SWCNT samples are typically from 0.8 nm, which is achieved for (6, 6) armchair (12, 0) zigzag, and the five chiral combinations in between.

While perfect graphene is a semiconductor with zero bandgap [15], single-walled CNTs can have either zero or nonzero bandgap [16]. The bandgap of CNTs depends on the diameter as well as the chirality of the tubes. For MWCNTs, the individual tube layers may have different properties. Theoretically, one-third of the possible (n, m) CNTs belongs to the zero bandgap “metallic” category, but the structural differences

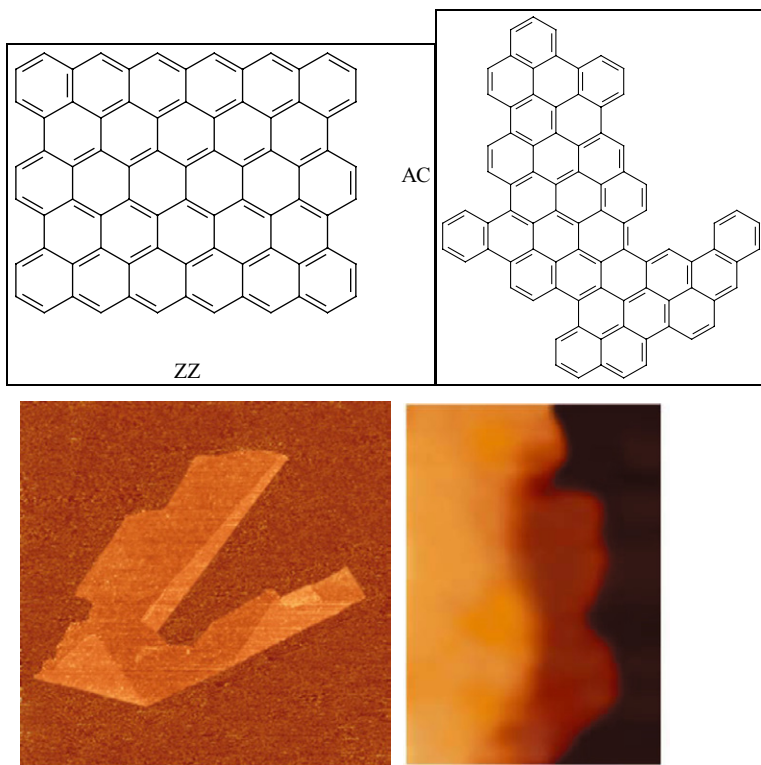


Figure 4.1. Upper row: (left) A rectangular nanographene with two of the armchair (AC) and zigzag (ZZ) edges marked. (right) A nanographene with irregular shape and the randomly mixed AC and ZZ edge areas, as observed for exfoliated graphene flakes. Lower row: AFM (atom force microscopy) of a slightly folded exfoliated graphene flake, approximately 10 μm long, on SiO_2 . AFM image from <http://www.condmat.physics.manchester.ac.uk/imagelibrary/>.

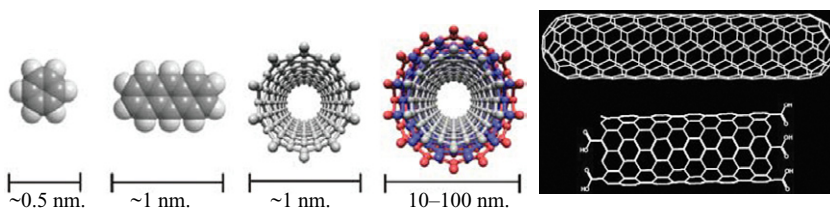


Figure 4.2. Left: Size comparison: Benzene, anthracene, and view along the CNT axis for a typical single- and multiwalled carbon nanotubes. Right: Side view of short, idealized SWCNTs. Upper: Armchair tube with closed ends. Lower: Zigzag tube with open ends.

between the two categories can be very small: an (n, m) CNT can be metallic, whereas an $(n + 1, m)$ can be semiconducting.

4.1.2 Handling of Carbon Nanoforms

Are nanoforms of carbon safe? Neither CNTs nor graphenes are water-soluble, but many derivatives are, including entities dispersed by surfactants. Nanoforms intended for biological applications are extensively tested for unwanted acute or chronic effects [17]. The risk associated with synthesis equipment and handling of reagents is minimized by proper precautions, for example, concerning handling of the carbon “soot,” be it graphite, RGO, or CNTs. To minimize spread of dust, handling should be in a confined space with proper ventilation, as inhalation exposure may lead to lung deposits [18]. In a later life cycle stage, lower quantities may leak into aquatic environments. In soil models, surfactant-dispersed CNTs were found to be mobile [19]. In general, the safety of processes and products needs to be part of the process and product design, and the design responsibility is with the scientists regardless of intended application [20].

4.2 CHARACTERIZATION METHODS

The standard solution-based tools of organic chemistry, such as NMR and mass spectrometry, can be readily applied for the characterization of C_{60} and its derivatives. For characterization of CNTs, graphenes, and graphene derivatives, these are less appropriate due to the low solubility and inhomogeneous nature of the materials. For derivatives with a high proportion of polar bonds, infrared spectroscopy (IR) can be useful, but Raman spectroscopy, X-ray absorption spectroscopy (XAS) and X-ray photoelectron spectroscopy (XPS), microscopy methods, and thermogravimetric analysis (TGA) are more common. The most accessible are Raman spectroscopy, TGA, and, for detection of graphene, optical microscopy, briefly described later. Methods for characterization of graphene with regard to flake thickness and presence of defects have been reviewed by, for example, Allen et al. [21].

4.2.1 Raman Spectroscopy

Raman spectroscopy employs electromagnetic radiation in the same wavelength region as IR, and the two are complementary in the information they give about a functionalized carbon material. Raman spectroscopy draws on inelastically scattered photons: when light is scattered by a molecule, most scattered photons have the same energy as the incident photons, but a small fraction will have lower or higher energy than the incident photons (inelastic scattering). This is due to the Raman effect; some of the energy of the incident photon is absorbed by the molecule and transformed to vibrational and/or rotational energy [22]. In crystals and in well-ordered materials, these vibrations (phonons) can have only certain distinct frequencies, while amorphous materials can absorb over a wider range, producing broader signals.

The Raman active vibration modes that are of particular importance for characterization of single-walled carbon nanotubes are the ones that give rise to the *G-band* (G from graphite), the *D-band* (disorder-induced band), and the *radial breathing modes* (*RBM*) [23, 24], exemplified in Figure 4.3. The G-band is characteristic for graphite

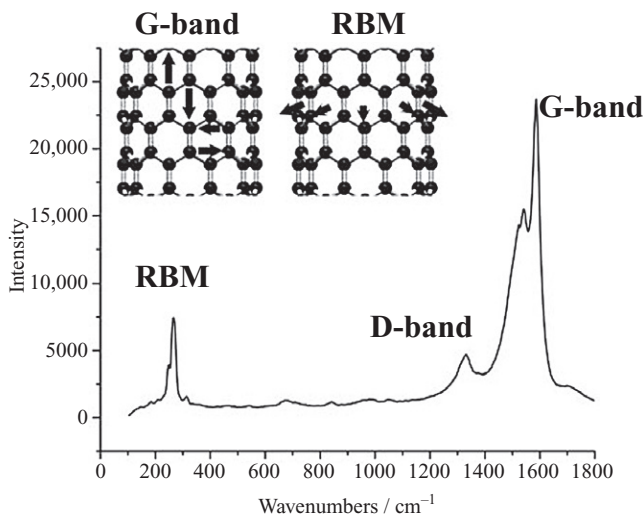


Figure 4.3. Raman spectrum of a commercial sample of single-walled carbon nanotubes (HiPCo). Inset: vibrations giving rise to the G-band and radial breathing modes (RBM).

materials and arises as a result of the vibrations, as shown in the figure inset. In SWCNTs, the G-band is a characteristic multipeak high-intensity band around 1580 cm^{-1} , whereas in graphite and graphene, it is a single-peak band [25]. The G-band provides a signature of SWCNTs in a sample and can furthermore be used to determine the relative distribution of semiconducting and metallic tubes. The RBM is the lowest-frequency band in the Raman spectrum of SWCNTs and originates from the atomic vibrations in the radial direction. Aside from providing direct evidence of SWCNTs in a sample, the position of the RBM gives information about the tube diameter. The intensity of the RBM is lower than the G-band and can sometimes be difficult to detect, as it may be buried in baseline noise from the sample or from the substrate.

The D-band appears around 1330 cm^{-1} and reflects defects such as sp^3 -hybridized carbons in the lattice. Such defects are always present to an extent, but their density can be significantly increased by chemical processes such as acid-oxidation treatments. However, amorphous carbon also has a prominent D-band, which can complicate the interpretation. Raman spectroscopy of MWCNTs is less informative than for SWCNTs. The G-band in MWCNTs generally appears as one broad peak without any visible fine structure, similar to the one found in graphite or graphene. For graphene and derivatives thereof, the D, G, and 2D bands (the latter also denoted D^* or G') are the most interesting, with the position, shape, and relative intensity of the 2D band around 2650 cm^{-1} (Figure 4.4) being a tool for fast determination of the number of layers in a flake (Figure 4.4) [26–28].

4.2.2 Thermogravimetric Analysis

Thermogravimetric analysis (TGA) can be used for purity assessment and can further provide quantitative information regarding derivatization outcome. The sample, on a

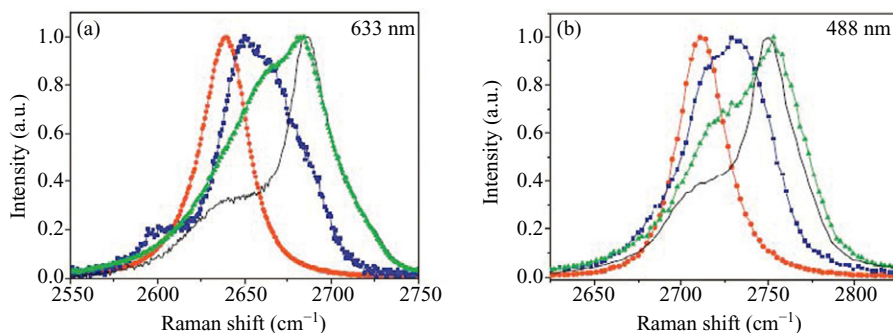


Figure 4.4. (a and b) Raman spectra of the 2G region for samples of monolayer graphene (bullets), bilayer (squares), few-layer (triangles), and highly ordered pyrolytic graphite (HOPG), for two excitation laser wavelengths. Source: [27]. Reproduced with permission of Wiley-VCH Verlag GmbH & Co. KGaA.

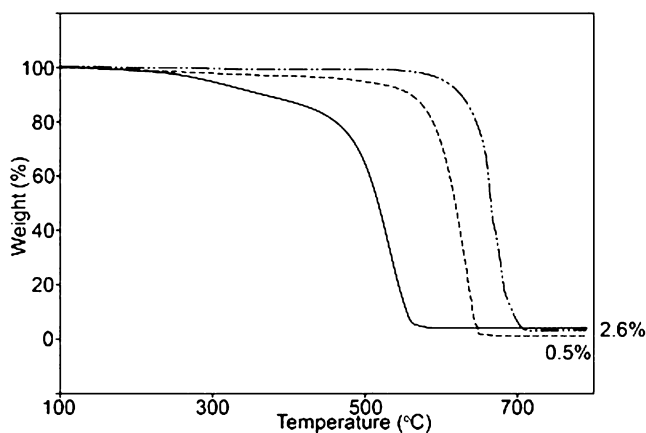


Figure 4.5. TGA profiles for two MWCNTs samples (dashed and dash-dot) and a sample of amorphous carbon material (solid) obtained for heating the samples in air. The residual mass that remains at 750°C is related to metal impurities.

highly sensitive balance inside a ceramic chamber, is heated in a controlled atmosphere (usually in N_2 or air) while the weight loss of the sample is monitored. Figure 4.5 shows TGA profiles for MWCNT samples, one of an amorphous carbon material. The thermal stability of the amorphous material is lower than for the CNTs, reflected by a lower degradation temperature. The residual mass after heating in air gives a measure of the amounts of inorganic impurities, whereas the residue after heating under inert atmosphere may leave also CNTs or graphene on the balance.

4.2.3 Microscopic Methods

Graphene on Si-SiO₂ substrates can be detected by (light) optical microscopy (LOM). Due to interference phenomena, single layers appear blue, whereas thicker flakes appear yellow-orange. Scanning electron microscopy (SEM) and transmission electron microscopy (TEM) are more powerful microscopy techniques. In particular, TEM can give very detailed information, even on atomic positions in individual nanotubes and graphene flakes [29–31]. In addition, atomic force microscopy (AFM) and scanning tunneling microscopy (STM) are techniques that can be used to visualize carbon materials at the atomic level [32].

4.3 PRODUCTION AND PURIFICATION OF CARBON NANOTUBES

4.3.1 Synthesis of Carbon Nanotubes

All CNT materials are produced from vaporized carbon at high temperatures [33]. The processes are nonselective; in addition to mixtures of CNTs, deposits of amorphous and graphitic carbon form in the reactor. Most methods can be adapted to produce either MWCNTs or SWCNTs, but only a few processes—chemical vapor deposition (CVD) and the closely related high pressure carbon monoxide (HiPco)—are suitable for large-scale production of materials with a high proportion of CNTs. In the CVD methods, a carbon-containing gas reacts on a solid substrate on which particles of metal catalyst have been predeposited. Tuning of the catalyst composition improves the SWCNT/MWCNT selectivity [34]; tuning of the gas composition to a specific catalyst system may allow a decrease of the growth temperature [35], all of which are crucial steps toward more selective CNT formation processes.

Although molecular total synthesis of fullerenes and CNTs aiming at certain diameters or chiralities has been attempted and, for C₆₀, accomplished [36–38], it is not likely that such routes will outcompete the CVD methods, despite the drawbacks of these methods in terms of formation of impurities.

4.3.2 Primary Purification of Carbon Nanotubes

A major drawback of all gas-phase production techniques is the impurities such as amorphous carbon, fullerenes, and encapsulated metal particles in the produced material [39, 40]. The removal of such species is of great importance, and purification of CNTs has therefore been an area of extensive research. Numerous protocols for increasing the CNT content by gas-phase [41, 42] and liquid-phase oxidations, most commonly using oxidizing acids such as HNO₃ and/or H₂SO₄ on CNT powders, have been developed [43–45]. The oxidative methods are the most commonly used, as these are technically simple and remove most unwanted material. In the oxidative processes, the encapsulated metal catalysts are transformed to metal oxides. As oxides occupy a larger volume of space than the parent metal, the volume expansions may break the surrounding carbon cage. However, for any reagents to access the interior, the CNTs need to be open. Under the conditions employed, the CNTs are also susceptible to oxidation. At regions with fullerene-like curvature, the carbon lattice is cleaved, rendering the tube interior accessible to the reagents. Metal removal from MWCNT material is more demanding, as the metal particles within the tubes are protected by several carbon layers. Edwards et al. found that sonication in concentrated HCl preserved the

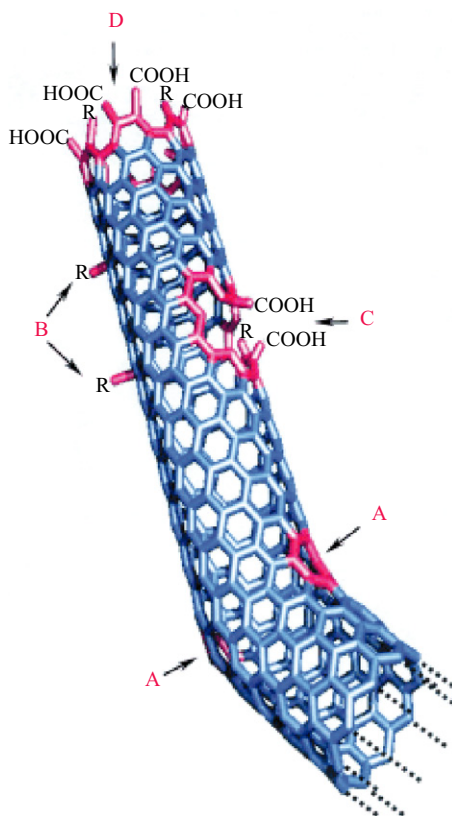


Figure 4.6. Typical defects in a SWNT: (A) five- or seven-membered rings in the C framework, instead of the normal six-membered ring, leads to a bend in the tube, (B) sp^3 -hybridized defects (R_H and OH), (C) C framework damaged by oxidative conditions, which leaves a hole lined with $-COOH$ groups, and (D) open end of the SWNT, terminated with $-COOH$ groups. Besides carboxy termini, the existence of which has been unambiguously demonstrated, other terminal groups such as $-NO_2$, OH, H, and $-O$ are possible. Source: [50]. Reproduced with permission of Wiley-VCH Verlag GmbH & Co. KGaA.

CNTs better than treatment with oxidizing acids while still giving a material with a very low residual metal content [46].

Treatment with strong acids will introduce oxygen-containing functional groups such as hydroxyl, carbonyl, and carboxyl at opened sites (Figure 4.6) [47–50]. These groups may increase dispersability of the CNTs [51, 52] and can be subsequently utilized for further derivatization (Section 4.6).

Although the liquid-phase oxidative purifications are scalable, most require several days at reflux temperature. This is generally followed by tedious workup and annealing procedures in order to restore many of the properties of pristine CNTs [53, 54]. Microwave heating has been used as a faster alternative to conventional heating, with the same workup protocols and very similar results concerning the quality of the purified

CNTs. In contrast, microwave heating of CNTs in a nonpolar organic solvent without any added reagents very rapidly (<5 minutes heating + a filtration step) removes amorphous carbon and metal particles from the nanotubes with considerably less sidewall damage than purification by aqueous oxidizing acid [55].

For purification of materials “on chip,” methods compatible with the growth substrate are necessary in order to preserve both the substrate and the desired carbon structure, for example, sulfidation of non-CNT carbon at elevated temperatures [56].

4.3.3 Fractionation of Carbon Nanotubes

To some extent, the diameter of CNTs can be predetermined by tuning of the catalyst particles, but none of the current methods for CNT synthesis is fully selective with respect to the helicity of the formed tubes. The as-produced diameter distribution and the ratio of metallic to semiconducting tubes is, to a limited extent, changed in the oxidative purification of the as-produced material [49, 57, 58]. A typical sample of SWNTs produced by the HiPco method contains about 50 different types of nanotubes, each with different (n, m) [39]. This is a major problem for potential applications that require CNTs with specific (n, m) values or at least either metallic or semiconducting tubes. Development of efficient techniques to fractionate the SWNT material has thus been a very active area [59–62], intimately linked to the issue of achieving reasonably individualized CNTs in solution or dispersion. For oxidized CNTs, this can be achieved by covalent or noncovalent strategies (Section 4.6).

Size-exclusion chromatography [63, 64] as well as flow field-flow fractionation [65, 66] has been used for separation according to CNT length. For covalently functionalized SWCNTs, separation of metallic from semiconducting CNTs was achieved by column chromatography on silica [67]. Electrophoresis with [68] and without [69] a gel has been employed for separation of metallic from semiconducting CNTs, with the one without a gel being more efficient. Centrifugation of aqueous suspensions of oxidatively purified CNTs has been used to separate bundles from individualized tubes [51]. Using surfactants in combination with bromine, it was possible to separate metallic from semiconducting tubes [70]. Centrifugation-assisted fractionation can also be achieved for noncovalent assemblies of CNTs with polymers, for example, regioregular poly(3-alkylthiophene) [71] or fluorene polymers, with the additional benefit of some helicity discrimination by carrying out the centrifugation in the presence of the density-gradient forming additive tribromotoluene [72]. Single-stranded (SS) DNA is another group of polymers that have been used for SWCNT fractionation; chiral discrimination was obtained from ion-exchange chromatography of SS-DNA-wrapped SWCNTs [73, 74].

The composition of a SWCNT fraction with respect to (n, m) values can be elucidated from the Raman RBM band [75]. However, purity assessment should ideally be by several independent methods [76], since the aggregation state of the CNT material at the analysis stage strongly influences the intensities in the RBM band [67, 77].

4.4 PRODUCTION OF GRAPHENE AND REDUCED GRAPHENE OXIDE (RGO)

4.4.1 Graphene Synthesis: Top-Down or Bottom-Up

In contrast to CNTs, graphene is available to everyone owning a pencil. The flakes that can be obtained from pencil exfoliation are small and of very poor quality compared

with those flakes prepared by sticky tape exfoliation from highly ordered pyrolytic graphite (HOPG), as first reported in 2004 [7]. Graphene prepared by such top-down micromechanical exfoliation is still the experimental benchmark, and the method is widely used despite being of low-yield and time-consuming. In contrast, routes where flakes upon exfoliation are dispersed in a solvent can be fast, readily scalable, and hence with the potential of being both high-yielding and cost-efficient. The materials prepared by exfoliation are less homogenous regarding flake size and thickness, edge structure, and termination, as well as incidence of process-induced defects than graphene prepared by the “bottom-up” methods: molecular synthesis and CVD. The decision of which general route to choose should depend on the requirements of the intended application.

4.4.2 RGO by Oxidative Exfoliation Followed by Reduction

Due to the high sheet-to-sheet contact area, the intermolecular forces to overcome in order to exfoliate sheets or flakes are larger than for solvation of smaller PAH congeners or unbundling of CNTs, and therefore more forceful and potentially damaging reaction conditions are necessary. The most commonly employed large-scale exfoliation routes have been those via GO, using combinations of oxidizing agents in strongly acidic media followed by a reductive treatment, as pioneered by Stankowich et al. [78] and extensively reviewed by Ruoff et al. [79–81]. In the oxidation step, oxygen-containing functional groups such as hydroxyl, ether, carbonyl, and carboxyl units are introduced, which can be subsequently utilized for further functionalization. Most oxidation-exfoliation protocols to form GO are adaptations of the method by Hummers [82], where the graphite is treated with potassium permanganate in concentrated sulfuric acid or the much older Brodie [83] or Staudenmaier [84] methods, which use mixtures of potassium chlorate and nitric acid. GO can also be prepared using nitric, sulfuric, or perchloric acid without additional co-oxidants [85]. It is of importance to ensure safe working practices to avoid accidents in the exothermic oxidation-expansion stage, during workup of the reaction mixtures, and while drying the GO.

In the oxidation process, oxygen-containing functional groups are introduced at reactive edge sites as well as in the layers. As the reaction proceeds, the interlayer forces are weakened, eventually leading to exfoliation of highly oxidized sheets of hydrophilic nonconductive GO easily processible in water. Although hydrophilic, GO can be transferred to organic solvents by the use of cationic surfactants [86].

The size and thickness of the exfoliated graphene flakes strongly depend on the source of graphite. In a comparative study by Wu et al., different kinds of graphite were subjected to identical reaction conditions [87]. Artificial graphite, with small grains and low crystallinity, gave a significantly higher proportion of flakes with one to three layers than was the case for HOPG, with larger grains. The reagent-graphite interactions ultimately leading to exfoliation take place at the edges of the graphite layers and in the interlayer space. For a starting material with lower crystallinity, the proportion of edges is higher and the diffusion routes for intercalation of reagents are shorter, and thus, the efficiency of exfoliation of few-layer flakes becomes higher.

Several structural hypotheses for GO have been put forward, and the one proposed by Szabo et al. [88] (Figure 4.7) correlates with most of the experimental evidence available at that time. A later solid-state ^{13}C NMR analysis of GO prepared from ^{13}C -graphite by the group of Ruoff supports the model [89]: The NMR information is always averaged, thus neither the identity nor exact position of the introduced

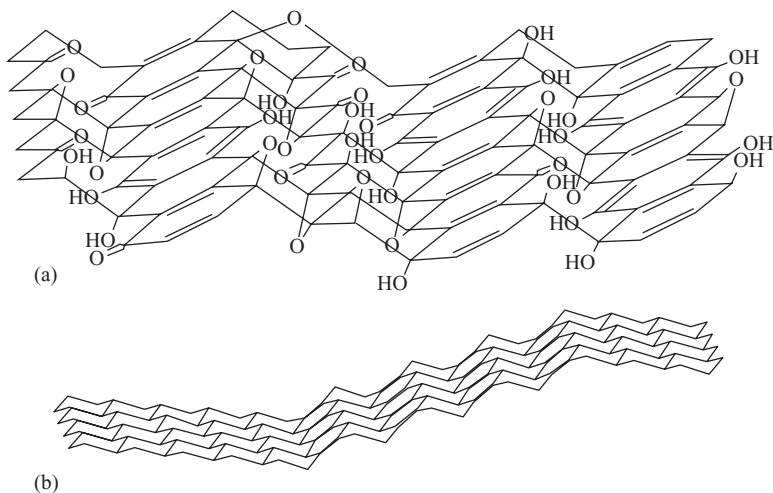


Figure 4.7. The structural model of graphite oxide proposed by Szabó et al. [88] (a) Structure including the possible functional groups. (b) Carbon skeleton view. Source: [88]. Reproduced with permission of the American Chemical Society.

oxygen-containing functional groups can be determined. The proportion of acidic groups can be determined by titration, however, as demonstrated by Yang et al. in a study that indicated about 8 mol% of acidic groups in a GO sample prepared by a modified Hummers oxidation [90].

By reductive treatment of GO, a material with the appearance and properties resembling that of pristine graphene can be obtained. Reduced GO (RGO) is black, hydrophobic, conducting, and has a significantly lower relative content of oxygen than GO. Most established protocols utilize versions of the original protocol with hydrazine [78]. No such reduction of GO has yet produced oxygen-free fully sp^2 -hybridized graphene; nevertheless, RGO materials with conductivities in the same range as micromechanically exfoliated graphene have been reported [79–81, 91].

For an RGO graphene material prepared via Hummers oxidation to GO followed by a thermal expansion, dispersion in the amide solvent NMP and reduced using H_2 , Wu et al. [87] obtained linear current–voltage characteristics and conductivities in individual flakes similar to what was reported by Novoselov et al. [7] and in the same range as reported by Wang et al. for graphene flakes prepared by a less oxidizing first step followed by solvothermal reduction with hydrazine in DMF [92].

Due to toxic and explosive properties, the use of hydrazine is restricted or forbidden in many parts of the world. The hazards are the same everywhere, and although studies employing hydrazine are among the referenced examples, use of alternatives is strongly recommended regardless of the local situation concerning restrictions. Less harmful yet efficient alternatives to hydrazine have been reported, such as H_2 [87], ascorbic acid [93], $NaBH_4$ [94], hydroquinone [95], ammonia vapor [96, 97], metallic iron [98], and tetrathiafulvalene [99]. The oxidized functional groups are thermally labile; hence,

annealing also reduces the O/C ratio [100–102], as does solvothermal treatment of GO with oleyl amine [103] or the amide solvent NMP [104]. Each combination of graphite oxidation and reduction conditions will produce an RGO of its own.

4.4.3 Graphene by Direct Exfoliation

Direct nonoxidative exfoliation processes that employ ultrasonication or supercritical extraction are highly practical alternatives to the expansion-exfoliation caused by exothermic chemical reactions of intercalated oxidants, with sonication-assisted exfoliation as the dominant method [105]. During sonication, formation and collapse of bubbles (acoustic cavitation) result in very high local pressures and temperatures [106–108]. The energy, if transferred to graphite, can be sufficient to cause exfoliation of graphene flakes. The solvent properties are important: The acoustic cavitation in a high-boiling solvent will give fewer cavities that collapse with larger temperature/pressure pulses than in a solvent with a lower boiling point. A high-boiling solvent may thus give a more efficient exfoliation. Also of importance is the stability of the resulting suspensions, which relies on the nature of the intermolecular bond between the exfoliated graphene flake and the solvent (or surfactant) molecules.

In a survey of sonication of graphite powder in a range of organic solvents followed by fractionation by centrifugation, Hernandez et al. found that the high-boiling amide solvents DMF and NMP gave excellent results concerning yield and quality of few-layer and monolayer graphene [109], similar to the findings of Bourlinos et al. [110] and Hamilton et al. [111] from sonication of graphite in perfluorinated solvents or *o*-dichlorobenzene, respectively.

Sonication of graphite powder in the presence of water-soluble surfactants, such as sodium dodecylphenylsulphonate [112], sodium cholate [113, 114], pyrenetetrasulfonic acid [115], or tetrapotassium coronene tetracarboxylate [116] gives, after centrifugation, aqueous dispersions of graphene with a high proportion of few-layer flakes covered with ionic surfactant molecules. If starting from graphite powder, the centrifugation step is essential in order to separate the monolayer and few-layer graphene from the starting material.

Not all solvents are stable under sonication conditions. In particular, amide solvents such as DMF and NMP may undergo sonication-induced decomposition into radical species [117, 118] with ability to add covalently with introduction of defects to the graphene. Sonication of CNTs in a chlorinated aromatic solvent has been reported to result in doping of the tubes by chlorine [119], and chloroform may decompose to various compounds, including HCl and dichlorocarbene [120]. The latter has been reported to react with soluble CNTs, forming cyclopropanes at the sidewalls [121]. Moreover, extended random sonication enhances aggregation of suspended graphene [122]. The sonication time and power, and hence the risk of process-induced damage, can be significantly decreased if the graphite is pretreated by intercalation of ICl [123] or Br₂ [124], for example.

Use of supercritical conditions constitutes a promising further development toward facile large-scale preparation of high-quality graphene. Rangappa et al. employed supercritical extraction with amide solvents (DMF and NMP) to prepare dispersions with high graphene content (Figure 4.8). About 90–95% of the exfoliated sheets were less than eight layers, and the characterized flakes exhibited very good conduction and electron-carrier capacity [125]. Supercritical CO₂ was used by Pu et al. to intercalate graphite powder [126]. On depressurizing, the volume of the confined gas molecules

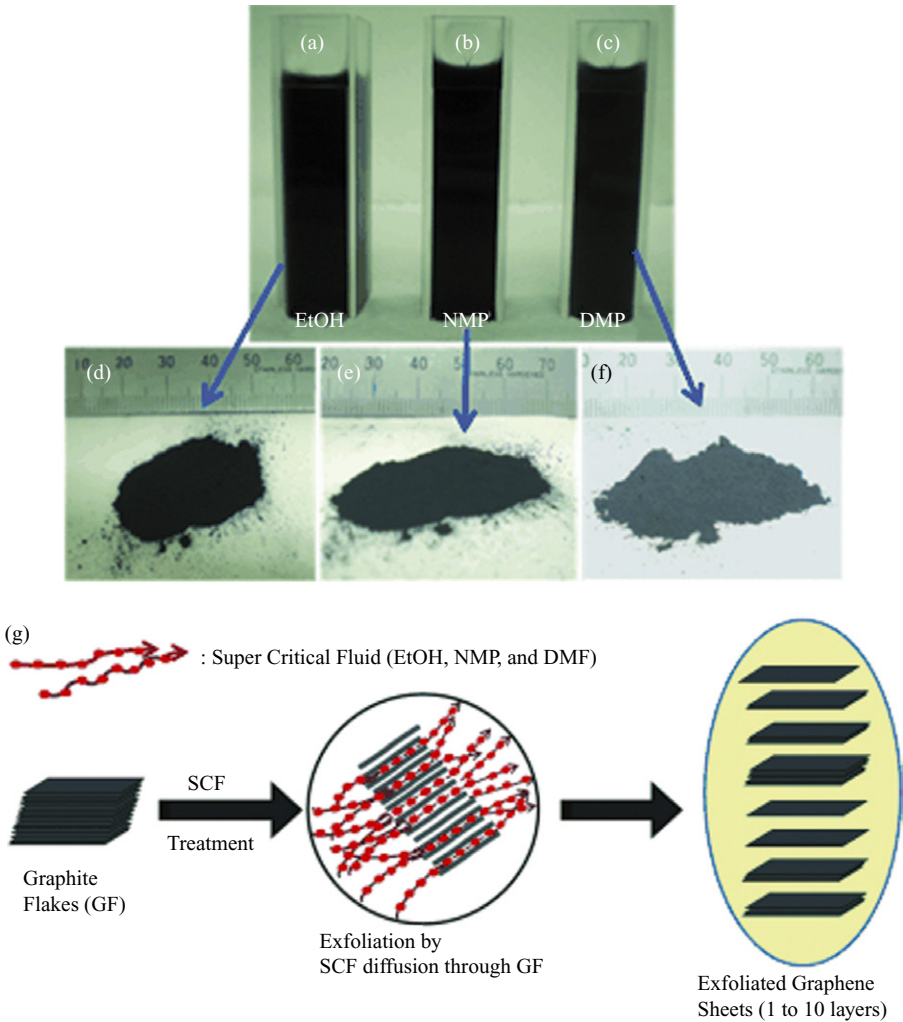


Figure 4.8. Photographs of exfoliated graphene sheets dispersed in (a) ethanol, (b) NMP, and (c) DMF, and approximately 1 g of their respective dried graphene powders (d–f); (g) scheme showing the SCF exfoliation of graphite crystals to graphene. Source: [125]. Reproduced with permission of Wiley-VCH Verlag GmbH & Co. KGaA. See color insert.

increases, leading to graphite expansion and exfoliation of high-quality graphene flakes into aqueous sodium dodecylsulfate.

4.4.4 Large-Area Graphene by CVD

For large-area graphene, CVD methods [127] or epitaxial growth from SiC [128, 129] are the most appropriate routes; however, they produce only a few entities per

experiment. For the SiC routes, the graphene is strongly coupled to the growth substrate and transfer to other solid substrates is still not possible, whereas graphene preparation on a metal surface by CVD allows control of composition (isotopes as well as dopant elements) as well as transfer from the growth substrate. Graphene can be grown on nickel [130–132] or, with more control, on copper using various carbon precursors [133–140]. The CVD processes can be adjusted for growth of nanosheets protruding from a graphite basal plane [141–143], for the formation of graphene on CNT “pillars” [144], or for growth of ribbons [145].

The transfer of CVD-grown graphene to other substrates more appropriate for intended applications is a stepwise process. Prior to removal of the metal by etching, the as-grown graphene is covered by a polymer, polydimethylsiloxane (PDMS) or polymethyl methacrylate (PMMA), which will act as a support layer to the resulting free-floating polymer/graphene film. Etching of Ni has been achieved using HCl [131], and of Cu using, for example, solutions of iron nitrate [136] or ammonium persulfate [146, 147]. With micropatterning of the graphene-PMMA support film prior to etching of the metal layer, cut graphene-PMMA entities of identical shape could be transferred from a metal grid to any substrate using a glass tip under the microscope (Figure 4.9) [148].

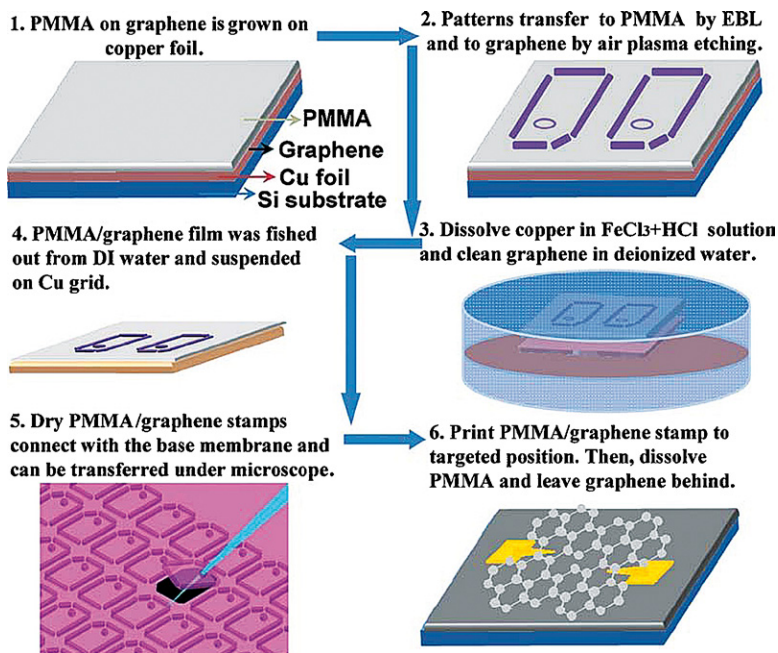


Figure 4.9. Transfer-print processes for graphene microsheets [148]. Panels 1–4 illustrate how to produce arrays of suspended and patterned PMMA/graphene microstamps. Panels 5 and 6 show the deployment of the prepared graphene sheets to construct a device. Source: [148]. Reproduced with permission of Wiley-VCH Verlag GmbH & Co. KGaA. See color insert.

For large-scale applications, high-throughput methods for transfer of very large area graphene to suitable substrates are required, such as the roll-to-roll process reported by Bae et al. [149]: Graphene grown on rolled Cu foil is covered by the polymer support, and the support/graphene/Cu sheet, while rolled out, is pulled through an etching bath removing the Cu. The remaining graphene/support can then be rolled onto a target substrate. This process, which can be repeated in order to obtain the desired number of graphene layers, has been used to produce as large as 30-inch graphene layers on a PET substrate.

A very important issue in all transfer processes is the influence of contaminants on the properties of the graphene. The etching, not surprisingly, can lead to damage as well as a chemical doping of the graphene [149, 150], and unless cleaning processes are applied, polymer residues can also dope the graphene [146].

4.4.5 Graphene Nanoribbons

In-plane lattice defects [151, 152], that is, pentagon-heptagon Stone–Wales defects joining patches of graphene with different orientation, can be regions with not only chemically more reactive bonds but also physically weaker regions, before or after functionalization of the defects [153]. A theoretical study suggests the curvature strain induced by the defects results in decreased tear resistance for such Stone–Wales seams between graphene areas with very similar orientation, whereas seams joining areas with larger mismatch angles would be stronger than the surrounding hexagons [154]. The presence of weak bonds has been experimentally confirmed: Micromechanically exfoliated graphene sheets can be torn in the process of removing graphene layers by adhesives, forming ribbon structures as reported by Sen et al. [155]. Tearing can also be a result of sonication, as was reported by Li et al. in a study where graphite intercalated with nitric and sulfuric acid was heated at 1000°C in an Ar–H₂ atmosphere, followed by sonication in dichloroethane containing a polymer that attaches noncovalently to the graphene fragments. Narrow graphene ribbons were obtained after centrifugation-assisted fractionation; other fractions contained fragments of different sizes and shapes [156].

Higher yields of graphene ribbons were achieved by longitudinal opening of CNTs (Figure 4.10), reported back-to-back by the groups of Dai [157] and Tour [158]. Starting from CNTs allows a higher level of control, as the starting material already is pseudo 1D. CVD methods are even better considering control and scalability: the overall shape of the graphene is predetermined by the shape of the accessible catalyst film, which can be prepatterned to yield large numbers of entities [145]. The CVD methods are more efficient than the top-down routes but cannot yet compete with molecular synthesis (below) if very large quantities of identical ribbons with control over edge structure are required.

4.4.6 Nanographenes by Organic Synthesis

In contrast to the efforts toward CNTs by organic synthesis methods [36–38], planar giant molecular nanographenes are accessible from structurally well-defined carbon-rich precursors [159–161]. A range of monodisperse soluble molecular nanographenes,

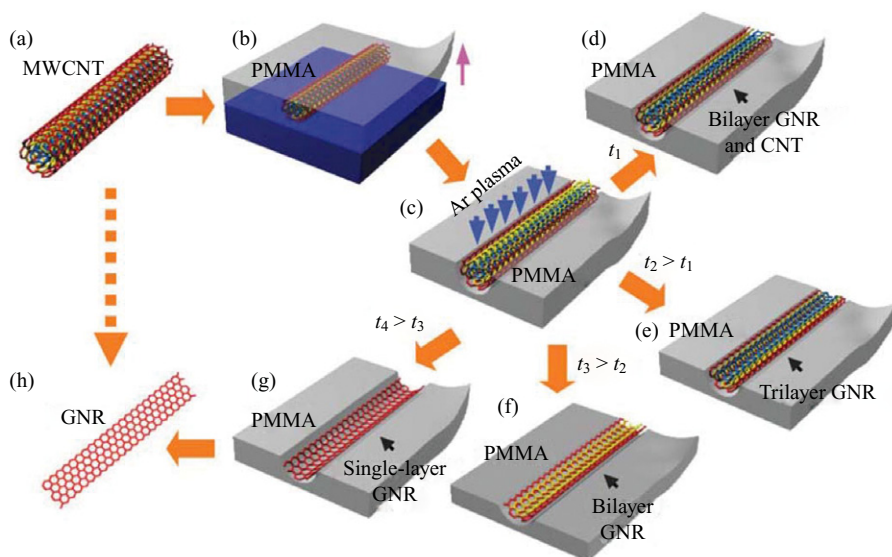


Figure 4.10. Production of graphene nanoribbons (GNR) from MWCNTs [157]. (a) A pristine MWCNT was used as the starting raw material. (b) The MWCNT was deposited on a Si substrate and then coated with a PMMA film. (c) The PMMA–MWCNT film was peeled from the Si substrate, turned over, and then exposed to an Ar plasma. (d–g) Several possible products were generated after etching for different times: GNRs with CNT cores were obtained after etching for a short time t_1 (d); tri-, bi-, and single-layer GNRs were produced after etching for times t_2 , t_3 , and t_4 , respectively ($t_4 > t_3 > t_2 > t_1$; e–g). (h) The PMMA was removed to release the GNR. Source: [157]. Reproduced with permission of the Nature Publishing Group.

up to a C₆-symmetric C₂₂₂H₄₂, have been obtained from cyclodehydrogenation of dendritic polyphenylenes (Figure 4.11), in turn accessible in several steps from di(4-bromophenyl)ethyne [162].

Nanographene propellers and nanographite discs have been obtained from a C₄₇₄ precursor, as a mixture, however [163]. Poor solubility of the products limits further size extension of monodisperse all-sp² systems. With solubility-enhancing branched alkane edge groups as part of the design, more than 10 nm long, soluble molecular nanoribbons with well-defined edge structures and masses of 20,000 μ were possible to prepare in good to excellent yields [164–166]. These achievements compare well to the top-down strategies for creation of nanoribbons by tearing of graphene or etching of CNTs (Section 4.4.5), the top-down routes suffering from poor predictability on edge structure or “cut angle” and limitations in the number of entities generated in each set of experiments. With these drawbacks in mind, molecular synthesis, although still challenging and time-consuming, could become the preferred route for preparation of large quantities of identical nanoribbons and other nanographene entities since the general shape, structure of edges, as well as position and identity of any desired functional groups can be decided at the synthesis design stage.

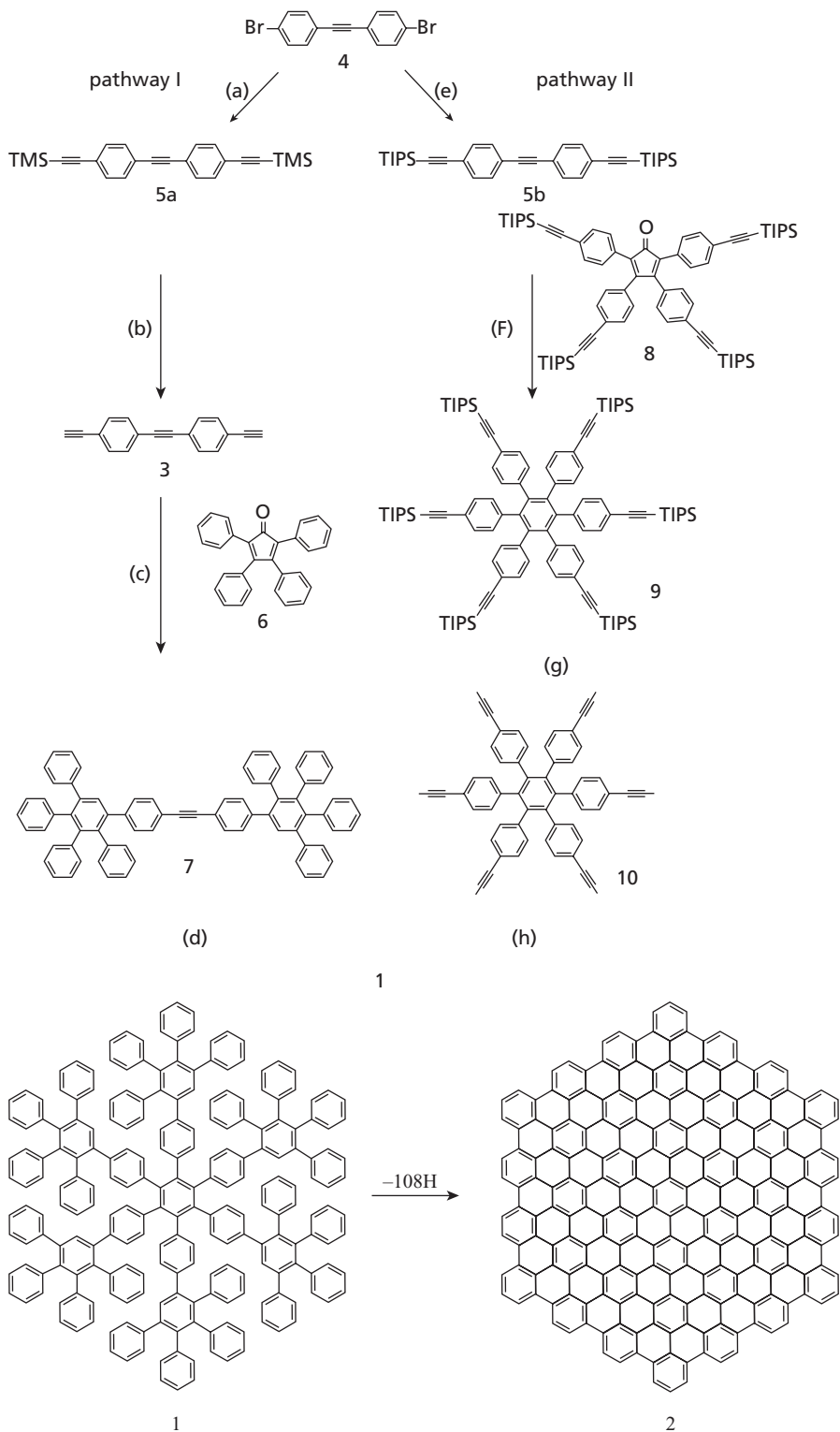


Figure 4.11. Synthesis of nanographene from well-defined building blocks. Oxidative cyclodehydrogenation of the precursor molecule **1** give the PAH **2** and two routes to **1** via well-defined intermediates. Source: [162]. Reproduced with permission of Wiley-VCH Verlag GmbH & Co. KGaA.

4.5 FUNCTIONALIZATION OF GRAPHENE AND CARBON NANOTUBES

4.5.1 Knowing Your Starting Material

In organic synthesis, a molecular species is transformed to a product, most often of greater complexity. For success, sufficiently pure starting materials and reagents are among the prerequisites, as are workup and purification protocols. Functionalization of the most commonly available fullerenes (C₆₀ and C₇₀, carbon-only molecules available as chromatographically pure compounds) clearly belongs to the “organic synthesis” category, but not to CNTs or graphene. None of the available methods for production of CNT (Section 4.3), graphene, or RGO (Section 4.4) gives what the synthetic organic chemistry would consider a pure material, considering neither the structural homogeneity of the nanotube (or graphene) entities nor the proportion of carbon or noncarbon impurities. Any graphene sample consisting of more than one flake will exhibit a distribution of thicknesses, area, defect density, and edge terminations [21]. Even within a flake, domains with properties differing from the surroundings can be present [27].

CNTs are less homogenous; in addition to various non-CNT impurities, SWCNT samples generally contain many different types of tubes in terms of length, diameter, helicity, and defects [76]. Postsynthesis processing (Section 4.3.2) not only decreases the proportion of non-CNT components but also increases the proportion of various lattice defects and potentially useful functional groups in the CNTs.

RGO materials are likely the least homogenous, not surprising given the wide range of conditions for transformation of graphite to GO and of GO to RGO (Section 4.4.2), where each combination may result in a different RGO material regarding, for example, C/O/N ratio, defect density, and functional groups available for further modification [91]. It is likely that the batch-to-batch differences are at least in the same range as observed for SWCNT oxidations [167].

For reactions using CNTs or graphene/GO/RGO starting materials, it is hence essential to know both the general method by which the carbon material was produced and which postsynthesis treatments have been carried out, since both factors strongly influence the physical and chemical properties of CNT and graphene materials. By applying conditions appropriate to the material in hand and accepting that neither the starting material nor the product is “pure” by the small molecule definition of the word, successful molecular engineering of these materials is possible.

4.5.2 Solubility

A common property of CNTs, graphene, and RGO is the very low solubility. Fullerene C₆₀ is reasonably soluble in aromatic solvents such as toluene and *o*-dichlorobenzene as well as in carbon disulfide [168]; functionalized fullerenes are more soluble. CNTs tend to aggregate due to van der Waals interactions (π -CNT stacking). This leads to the formation of large bundles that do not easily dissociate. As a result, CNTs are insoluble in most solvents before postsynthesis processing and only slightly soluble after purification (Section 4.3.2) [52, 169]. By attaching various solubilizing groups to the CNTs, covalently or noncovalently, it is possible to overcome the van der Waals forces and exfoliate individual tubes from CNT bundles. This is highly related to the exfoliation of graphene from graphite, only that the forces to overcome are larger in graphite and the tendency to reaggregate in a disordered fashion higher. True solutions

of graphene or RGO are generally of very low concentration, but fortunately, graphene and RGOs can be dispersed in toluene and *o*-dichlorobenzene, as well as in amide solvents such as NMP or DMF (Section 4.4.3). In addition, for these materials, functionalization increases the solubility.

4.5.3 Reactivity

Graphene and derivatives thereof, including CNTs, chemically belong to the diverse group of polycyclic aromatic hydrocarbons, in which naphthalene, anthracene, and benzopyrenes are the smallest planar members. The chemical properties of a series of progressively larger aromatic hydrocarbon compounds are similar, but due to the significantly higher bulk:edge ratio, graphene reactivity per carbon is considerably lower than for the smaller planar members of the group. The edges are reactive toward electrophiles and toward oxidation, whereas the bulk, if composed of a perfectly planar hexagonal lattice, is practically nonreactive. Most graphene, however, contains lattice defects [152]. All deviations from perfect graphene such as vacancies, pentagon-heptagon pairs (Stone–Wales defects), or 5–7 seams in grain boundaries between armchair and zigzag areas constitute regions of increased chemical reactivity. This is also true for CNTs [50].

Wrinkles and folds in graphene sheets, with local curvature resembling that of CNTs and fullerenes, are also regions with a substantially higher chemical reactivity and thus serve as initiation points for covalent functionalization reactions that may modify local as well as bulk properties [170, 171]. The reactivity of graphene, however, is much lower than for CNTs and fullerenes. Fullerenes are permanently curved in two dimensions, and the “cylinder” part of a perfect CNT is curved in one. Neither fullerenes nor CNTs are hence, by the strict definition, aromatic. The σ – π angle for a carbon atom in C_{60} is 101.6° , closer to the sp^3 tetrahedral σ – σ angle of 109° than to the 90° of a sp^2 arene system, and C_{60} reacts as an electron-poor polyolefin rather than a fully conjugated superarene [172]. The reactivity of fullerenes toward electrophiles, enophiles, and dienophiles is driven by release of strain energy [173], and all 30 double bonds, positioned at the junctions between the six-membered rings, are of equal reactivity.

The cylinder part of a perfect CNT is curved in one direction only, which leads to a less distorted π system and a lower reactivity at the sidewalls than at half-fullerene endcaps. The extent of pyramidalization depends on the diameter of the tube; CNTs with smaller diameters (smaller curvature radius) are generally more reactive. The pyramidalization is not identical in all directions: the strain parallel to the tube axis is lower than in any direction between parallel and perpendicular, and the CC bonds of an arbitrary “benzene” unit will possess nonidentical reactivity. Moreover, the local curvature radius is higher for bonds in a zigzag than for bonds in armchair CNTs [174]. This explains to some extent the observed chirality-dependent reactivity differences, with near-zigzag tubes being considerably less susceptible to oxidative degradation than near-armchair ones of the same diameter [175–177].

The reactivity of CNTs also depends on whether the tube (or tube area) is “metallic” or “semiconducting.” Metallic tubes are more reactive toward oxidation [178] than semiconducting tubes of the same diameter. Using solid-state terminology, a zero bandgap means that there is no energy difference between the valence band and conduction band, and hence, the electron density at the Fermi level (the boundary between occupied and unoccupied levels) is higher than for a material with a bandgap. The valence and conduction band of a material is analogous to the HOMO and LUMO

of a molecule; a low-lying HOMO is generally less reactive than a HOMO higher in energy.

The reactivity differences can also be rationalized using the concept of aromaticity and antiaromaticity. Treating the virtual transformation of a graphene sheet into an SWCNT cylinder as an electrocyclic reaction, “metallic” tubes are analogous to antiaromatic $[4n]$ annulenes, whereas the “semiconducting” tubes are analogous to aromatic $[4n + 2]$ annulenes, where lower reactivity is to be expected [15]. Although the “bandgap” is of importance for the reactivity, curvature effects are even more important; graphene has zero bandgap (as has a metallic CNT), but since addition at the interior of a planar sheet would induce pyramidalization strain and curvature, it is highly unfavorable and hence requires very much more forceful conditions than the corresponding transformation of a CNT, where the reaction instead releases strain.

4.5.4 The Functionalization Toolbox

The CNT functionalization area is well established [6, 179–182], and the younger graphene/RGO area is in rapid development [183, 184]. The transformations generalized in Figure 4.12 and exemplified in the next two paragraphs are chosen to illustrate the most common and versatile groups of reactions employed on CNTs and graphene.

Primary functionalization can be oxidative, reductive, or with no overall change of oxidation state of the carbon atoms. The reagents target areas of high reactivity such as endcaps, bends, wrinkles, edges, or other imperfections. Noncovalent adsorption of molecules to the π systems of CNTs, graphene, or RGO is another primary

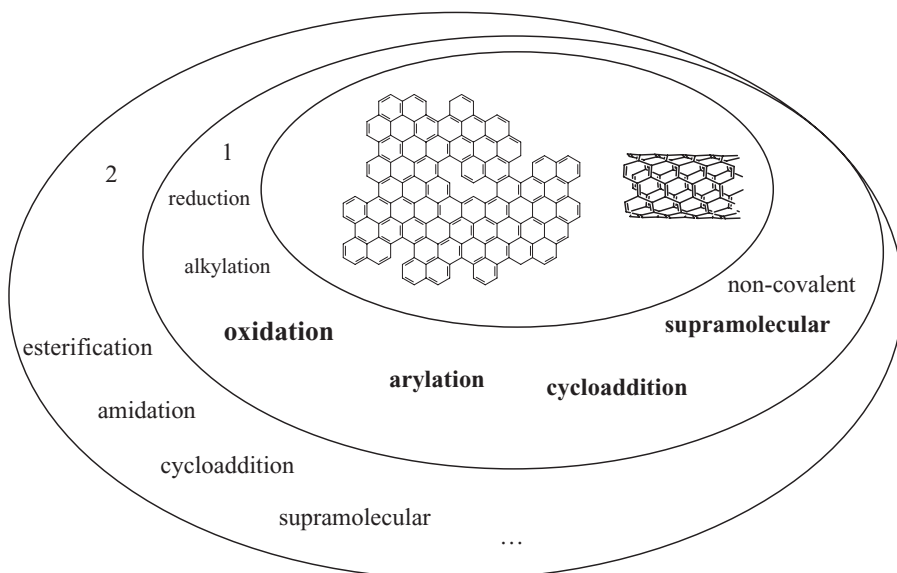


Figure 4.12. Some of the major primary and secondary functionalization options for carbon nanotubes and graphene.

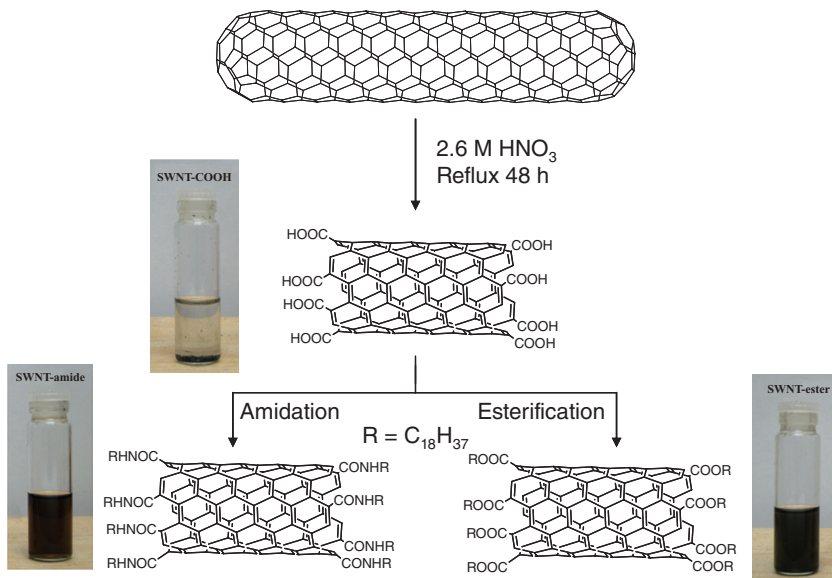


Figure 4.13. Oxidative primary treatment with aq HNO₃ gives open-ended CNTs with –COOH units possible to convert to ester or amides in a secondary functionalization step. CNT-COOH is not soluble in nonpolar organic solvents, whereas CNT amides and esters with long-chain substituents (>10C) can be soluble in, for example, toluene. See color insert.

functionalization strategy that does not cause permanent changes. Primary functionalizations that introduce reactive functional groups allow for secondary functionalizations, a linear approach to molecularly engineered CNTs and graphenes.

4.6 FUNCTIONALIZATION OF CARBON NANOTUBES

4.6.1 Defect-Group Generation and Functionalization

Most of the protocols for postsynthesis purification (Section 4.3.2) introduce carbonyl, hydroxyl, and carboxyl functional groups at ends and bends (Figure 4.6). Secondary functionalization of these groups is an important route to achieve soluble CNTs without further introduction of sp³ sites (Figure 4.13). Amide formation by treatment of CNT-COOH with SOCl₂ [185, 186] or dicyclohexylcarbodiimide [187], followed by an excess of octadecyl amine to give SWCNT amides soluble in nonpolar solvents, was introduced by the group of Haddon et al. in the late 1990s. Using amines with polyethylene glycol chains, Sun et al. prepared individualized CNTs with solubility high enough for solution-phase NMR characterization in CS₂ [188, 189], whereas PEG chains induce dispersability in water as well [190]. In a systematic comparison of published protocols for amidation via an SWCNT-acid chloride or direct amidation of CNT-COOH using peptide coupling agents, the acid chloride route was the only one that resulted in amide formation [167]. Esterification can be achieved not only by the same general acyl sub-

stitution routes, but also by alkylation of CNT-COO⁻ in a two-phase system [191], a route that, in addition to the one via the SWCNT-acyl chloride, is robust and high-yielding [167].

Octadecyl-esterified MWCNTs prepared by the alkylation method were found to be very soluble in toluene, and dip-deposition on a patterned Si-SiO₂ substrate resulted in a selective deposition of individual MWCNTs at the nonpolar Si areas, leaving the more polar SiO₂ patches essentially bare [192]. Using bifunctional functionalization components, such as aminoalkylmercaptane [193] or iodoarene-tagged carbohydrate derivatives [194], solubility as well as additional function, affinity to gold surfaces, and high-resolution TEM “visibility,” respectively, are introduced in only one synthetic transformation.

4.6.2 Sidewall Alkylation and Arylation

With the use of radicals *in situ* generated from alkyl iodides by treatment with benzoyl peroxide [195] or directly from benzoyl or lauryl peroxide [196], highly alkylated SWCNTs with excellent solubility in organic solvents can be obtained. By treating CNTs at Birch reduction conditions (alkali metal in liquid ammonia) and subsequently adding an organic halide to the reduced CNTs, the organic component becomes grafted to the CNT [197, 198]. The reductive route has some functional group tolerance; for example, quenching with a carboxyl-substituted primary alkyl bromide gave a CNT-R-COOH material that in a later step was transformed to a polyethylene glycol amide with excellent water solubility [199]. “CNT-COOH” is thus accessible from both oxidative and reductive treatments.

Pioneered by Tour et al., aryl diazonium salts have been used for preparation of arylated CNTs [200–202]. The treatment results in very soluble CNTs [203], which are possible to fractionate by silica gel chromatography [67]. The functional group tolerance of the process is excellent, which sets the stage for interesting secondary functionalizations. One example is the study by Strano et al. in which layered amide-cross-linked SWCNT membrane structures (Figure 4.14) were obtained from reacting SWCNT-[ArCOOH]_n with diamines of varying flexibility and interamine distance. The porosity of the membrane depends on the diamine used [204].

With 4-(prop-2-ynoxy)aniline as diazonium salt precursor, Andronov et al. obtained CNTs with terminal alkynyl groups that were subsequently coupled to azide-terminated polystyrene via a copper-catalyzed [3+2] Huisgen cycloaddition [205]. Giambastiani et al., aiming for the same secondary functionalization reaction, instead started from 4-azideaniline. The resulting SWCNT-[Ar-N₃]_n was successfully coupled to a range of functional alkynes in a convergent modular fashion (Figure 4.15) [206].

4.6.3 Cycloadditions

Among the cycloaddition reactions initially developed for functionalization of C₆₀ [207, 208], a few have been translated to CNT systems, and of these, the [3+2] cycloaddition using an azomethine ylide, also called the Prato reaction, is the dominant one (Figure 4.16) [209]. The azomethine ylide is formed *in situ* from the reaction between an aldehyde or ketone and an (alpha) amino acid. The highly versatile reaction theoretically allows up to 5 R groups to be introduced in a one-pot transformation, but 3 R units, not counting H as an R group, are likely a practical limit due to the accessibility

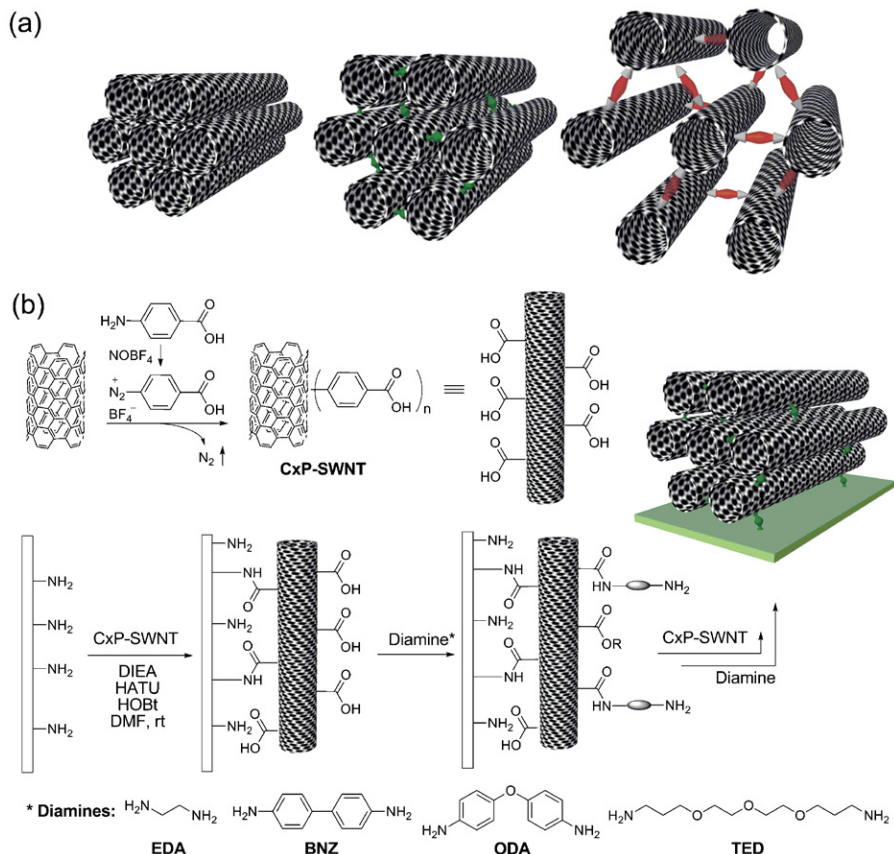


Figure 4.14. Synthesis of diamine-cross-linked SWNT frameworks [204]. (a) Schematic representation of pore size control by linker approach through covalent layer-by-layer assembly. (b) Alternate depositions of CxP-SWNT and diamine linkers on an amine-functionalized substrate. CxP-SWNT was prepared by diazonium-assisted functionalization and further activated by a uranium-based peptide coupling reagent (HATU). The linker molecules are EDA, BNZ, ODA, and TED. Source: [204]. Reproduced with permission of the American Chemical Society.

and reactivity of the components [210]. In contrast to the stepwise nature of defect group functionalization or functionalizations starting from alkylated or arylated CNTs, strategies using azomethine ylides can be highly convergent. The desired function can reside in the aldehyde or the amino acid component, the main restriction being compatibility with the ylide-formation step.

The reactions with CNTs, compared with those with the much more soluble fullerenes, are very slow. Using CNTs made soluble by esterification prior to the cycloaddition step increased the efficiency of the cycloaddition step, in reaction heated both by conventional means and by microwaves. The latter heating method was more than 50 times faster, with even sidewall distribution of added pyrrolidine groups both at high and low degree of functionalization [211].

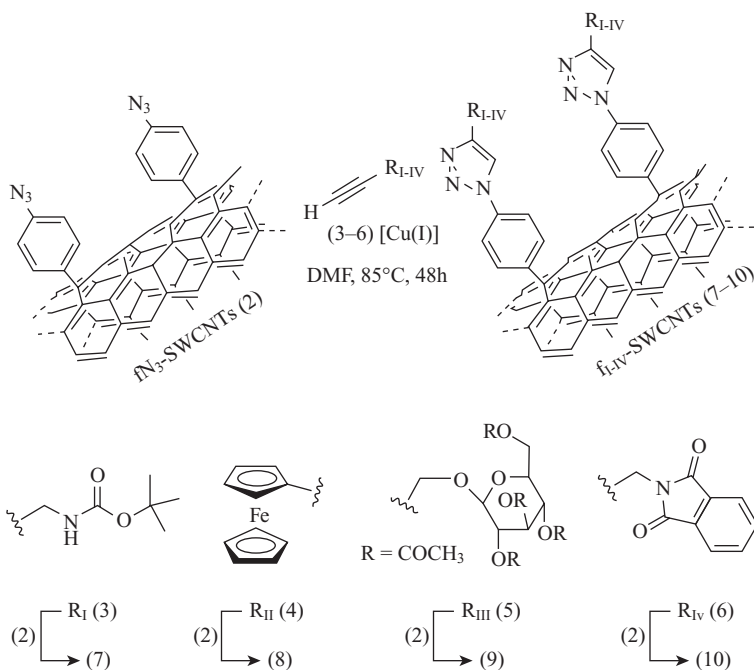


Figure 4.15. Secondary functionalization of arylated CNTs using a CuI-mediated azide-alkyne cycloaddition protocol to couple alkyne-terminated organic/organometallic compounds to arylazido-decorated SWCNTs. Source: [206]. Reproduced with permission of Wiley-VCH Verlag GmbH & Co. KGaA.

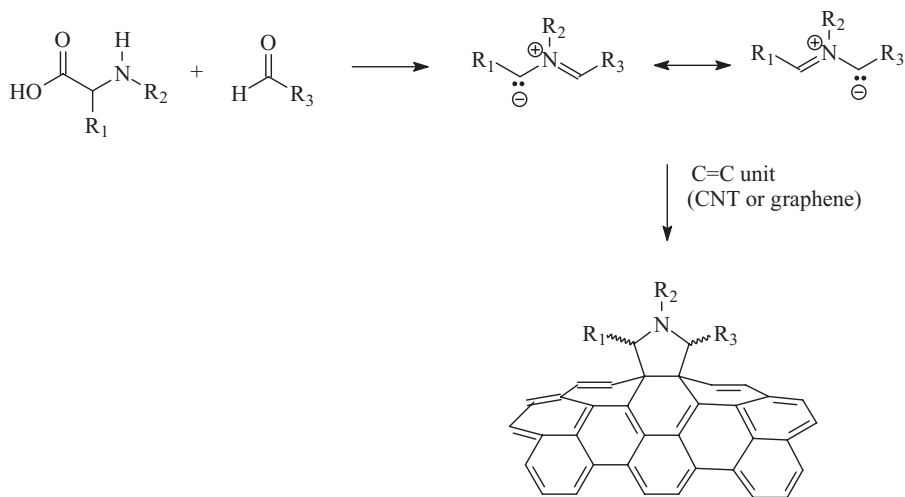


Figure 4.16. Pyrrolidine formation by [3+2] cycloaddition of and *in situ*-formed azomethine ylide to a reactive C=C of a CNT or graphene allows for facile one-pot introduction of three R functional substituents. Use of a 2,2-disubstituted N-substituted amino acid and a ketone could introduce five units.

Cyclopentenones can be formed by reaction between CNTs and zwitterionic addition products of 4-dimethylaminopyridine (DMAP) and disubstituted acetylenedicarboxylates (Figure 4.17). Quenching of the reactive pyridinium unit with alcohols gives enol ethers, with the R chain introduced in the last step at the tip of the five-membered ring. In a study toward selective CNT sensors, Wang and Swager utilized the two-step one-pot protocol for preparation of a set of MWCNTs carrying a wide range of units [212].

4.6.4 Noncovalent Functionalization

All covalent additions to CNTs transform the near- sp^2 hybridized carbons to sp^3 , which affects the electronic and mechanical properties of the material. For applications where an sp^2 lattice as intact as possible is desired, linking of the active components, including those that induce solubility, should instead be by noncovalent strategies such as salt formation between a suitable amine and acidic units introduced in oxidative purification [167] or, more common for introduction of “additional function,” by noncovalent π - π stacking interactions. The latter functionalization strategy, even more convergent than the covalent cycloadditions, has been reviewed by Herranz and Martín [213]. The component providing the π - π stacking interactions to CNTs is often a pyrene derivative, and depending on the properties of the derivative, solubility in organic or aqueous media is induced.

Many groups have reported efficient noncovalent derivatization of SWNTs with immobilization of small organic molecules as well as polymer biomacromolecules including enzymes, opening up to sensor applications [214–217]. The functionalization can be made reversible using ambipolar pyrenes [218] or essentially irreversible by using pyrenes with a polymer [219] or polymerizable [220] tail (Figure 4.18).

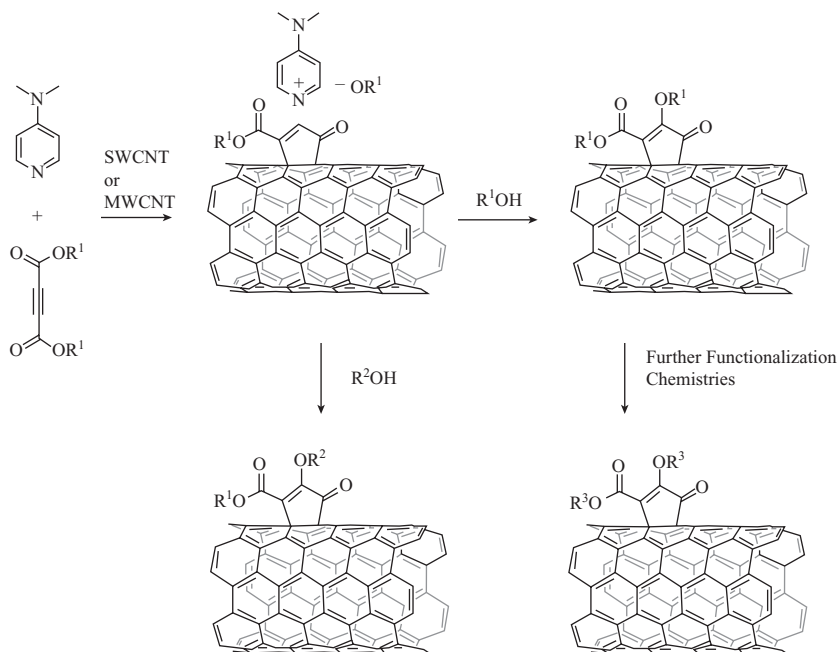
Supramolecular CNT-pyrene assemblies where the electrochemical and photophysical properties are significantly influenced by the added units have been extensively studied [221], as have assemblies between CNTs and porphyrins [222], and with tetra-thiafulvalene derivatives [223]. With two π - π stacking units in a tweezer arrangement, the interaction with the CNTs becomes even more efficient, and hence, the property changes induced are more prominent [224, 225].

4.7 FUNCTIONALIZATION OF GRAPHENE

4.7.1 Oxidation and Covalent Secondary Functionalization

Oxidation of graphene flakes will, as with the oxidative treatment of graphite with oxidants to form GO (Section 4.4.2), introduce oxygen-containing and, to some extent, thermally labile functional groups—hydroxyl, ether, carboxyl, carbonyl, and so on—at particularly reactive sites. The more forced the conditions, the more GO-like, that is, insulating and hydrophilic, the resulting material will become when the interior of the graphene lattice (the bulk) also becomes oxidized. Aqueous dispersions of oxidized graphene are brown, orange, or yellow depending on the degree of reaction.

In contrast to the reagent combinations that transform graphite to GO, a hypothetical structure of which is given in Figure 4.7, ozone treatment of HOPG mainly oxidizes the edges of the uppermost graphene layer (Figure 4.19). After annealing, the XPS and XAS analyses indicated complete removal of the functional groups, leaving “perfect



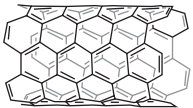
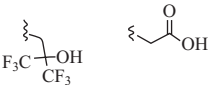
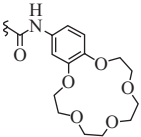
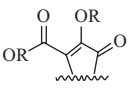
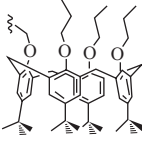
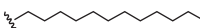
<p>MWCNT</p> 	<p>H-bond Acidity</p>  <p>Targeted Analytes: H-bond Acceptors such as Ethers, Ketones</p>	<p>H-bond Basicity</p>  <p>Targeted Analytes: H-bond Donors such as Acids, Alcohols</p>
<p>Polarity</p>  <p>R = allyl or propargyl</p> <p>Targeted Analytes: Vapors with High Polarity Such as Ketones, Ethers</p>	<p>Polarizability</p>  <p>Targeted Analytes: Aromatic and Chlorinated Hydrocarbons</p>	<p>Nonpolar Adsorption</p>  <p>Targeted Analytes: Aliphatic Hydrocarbons</p>

Figure 4.17. Upper box: Schematic representation of the reaction schemes for modular functionalization of CNTs, only one addend/CNT shown for clarity. Lower box: Selected recognition groups for differential interactions with targeted analytes added to the CNTs in the second step. Source: [212]. Reproduced with permission of the American Chemical Society.

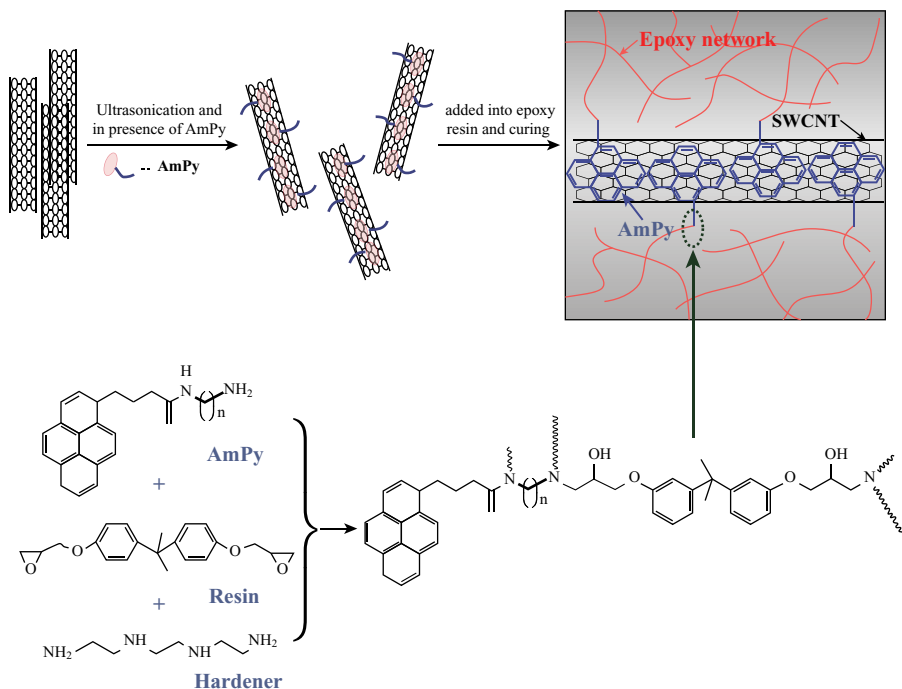


Figure 4.18. Noncovalent functionalization of CNTs with a pyrene derivative reactive toward epoxy resin followed by polymerization forms stable composites. Source: [220]. Reproduced with permission of the Royal Society of Chemistry.

graphene” [226]. Ozone treatment of nanographenes in solution gives rise to mixtures of edge-oxidized products that can be separated and analyzed by NMR in solution. Edges with “*cis*-diphenylethene” structure react faster with ozonolysis of C–C bonds than “phenyl” edges [227], which would indicate a higher reactivity for armchair edges than for zigzag ones.

Treatment with aqueous HCl, a strong acid with net nonoxidizing properties, adds water to lattice defects with localized C=C sites (both C sp^2). The initial H–C–C–OH (both C sp^3), in which formally one carbon has been reduced and one oxidized, may rearrange with formation of a cyclic ether if the initial addition reaction takes place at an internal lattice defect [228] or to a carbonyl if at an edge position [229]. Nanosheets of graphene were found to react with incorporation of oxygen into the carbon sheet plane [230], and the acid-treated material exhibited a lower resistivity than the controls [150].

Partially oxidized graphene, as well as activated carbon [231]—essentially belonging to the graphene group—and GO have been further modified by secondary functionalization, where, in particular, reactions targeting carboxyl units (amidation, esterification) using conditions highly similar to the corresponding transformations of oxidized CNTs (Figure 4.13) have been employed. The products are still insulating, but other

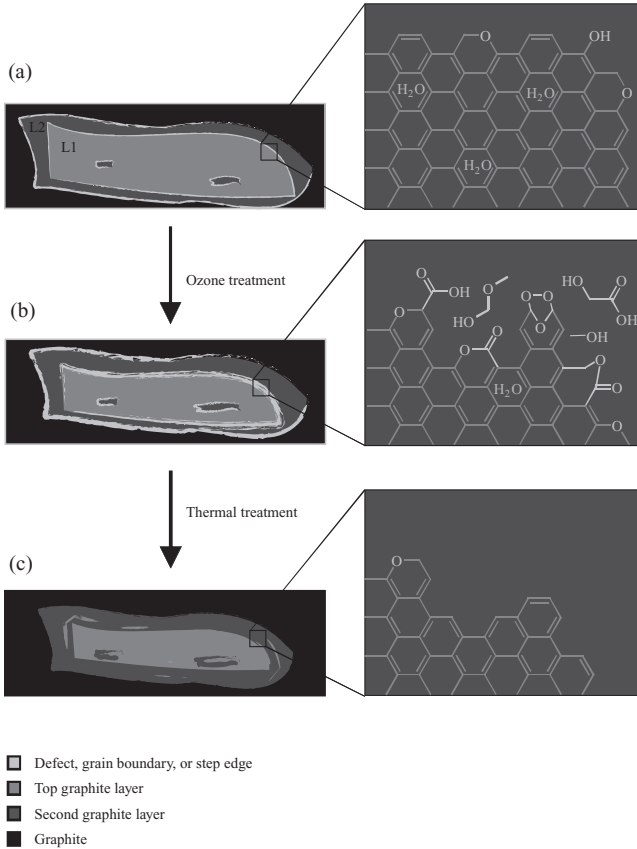


Figure 4.19. Proposed chemical etching of a graphite surface by ozone. (a) untreated HOPG surface, (b) surface after ozone treatment, and (c) surface after ozone and thermal treatment. Source: [226]. Reproduced with permission of Elsevier.

physical and chemical properties depend on the structure and functionalities of the esterification or amidation component [79–81, 232–235].

4.7.2 Reduction: Formation of Graphane

When exposed to cold hydrogen plasma, graphene undergoes a reversible transformation from conductor to insulator [236]. Graphene on SiO_2 , with only one side exposed to the reagent, was less reduced than graphene mounted on a holey membrane, where access to both sides allows the formation of “graphane,” with a relatively larger D:G ratio than for the partially reduced graphene on SiO_2 where only one side is available for the reagent. The graphene Raman signatures were almost completely recovered after annealing, an observation supporting the general reversibility of the applied

reduction process. The one-side reactivity and addition pattern may be different for graphene on substrates other than SiO₂ [237].

Significant quantities of reduced graphene were prepared by Billups et al. by Birch reduction of graphite powder. The reaction results in exfoliation of a highly reduced material with a bandgap of 4 eV. Elemental analysis gave a H:C atomic ratio of 1:1.3. Solid-state ¹³C NMR analysis confirmed saturated methylene at the edges, but the large number of different interior environments could not be resolved [238]. In contrast to the hydrogen plasma treatment, the Birch reduction appears to be nonreversible and could hence be a useful route to stable graphane.

4.7.3 Additions Using Nonoxidizing Reagents

Grafting of organic units is more easily controlled and hence less damaging to the π system than the processes giving the highly oxidized GO and the highly reduced graphane [170]. Use of aryl diazonium routes previously demonstrated for graphite [239] and CNT functionalizations (Section 4.6.2) have been proven successful also for graphenes. Hence, arylated graphene derivatives can be obtained from micromechanically cleaved graphene [240], GO [241], and RGO [242–244], as well as from ribbons derived from oxidative longitudinal opening of MWCNTs [245]. Alternatives to the diazonium route are the Friedel–Crafts acylation of RGO using 4-aminobenzoic acid, which introduces arylamine units [246], and radical addition of *in situ*-generated Bergman cyclization products to NMP-exfoliated graphene flakes, which produced a naphthyl-functionalized graphene derivative [247].

Cycloaddition reagents such as aryl azides and azomethine ylides, well established for convergent functionalization of CNTs, are reactive toward graphene as well. The structurally versatile reagents result in aziridination [248] (Figure 4.20) and pyrrolidination [249–251], respectively.

4.7.4 Supramolecular Noncovalent Functionalization

Noncovalent interactions between graphene and smaller molecules are of fundamental importance for the formation of stable dispersions in a solvent, either via direct graphene–solvent interactions or via graphene–surfactant + surfactant–solvent interactions. Although solvation depends on noncovalent interactions, it is normally not categorized as functionalization. At the other end of the scale are the noncovalent yet stable assemblies. According to a theoretical study by Kozlov et al. [252], the π – π stacking adsorption interaction between arenes and graphene is stronger than 10 kJ mol⁻¹ per carbon atom of the molecule. The material–molecule interaction can, depending on the structure of the molecule as well as the amount and functional group identity of defects in the graphene/GO/RGO, also involve dipole–dipole and ionic interactions.

If the properties of the assembly are significantly different from those of the individual components, the functionalization is categorized as being supramolecular, well established for CNT systems (Section 4.6.4) and demonstrated also for graphene and RGO on substrates. Both electron-donating and electron-withdrawing arenes such as quinones and tetrathiafulvalenes [253–256] and larger entities such as porphyrins [257] and polynucleotides [258] may attach and influence the electronic properties of the graphene π system. The effects are small compared with the often prominent changes of the electronic properties observed for covalently functionalized graphene.

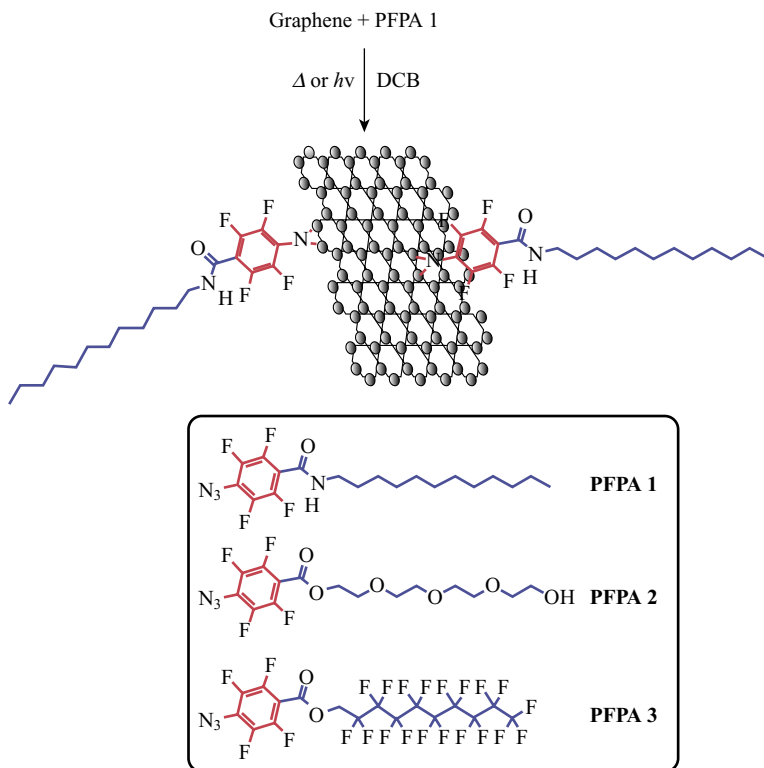


Figure 4.20. Aziridination of few-layer graphene exfoliated into *o*-dichlorobenzene using perfluorophenylnitrenes. Source: [248]. Reproduced with permission of the American Chemical Society.

Supramolecular functionalization can be achieved also for graphene suspensions, which may result in stable suspensions or solutions. An electron-poor carboxycoronene with characteristic optical properties was employed as a surfactant in a direct exfoliation of graphene into water. The long-term dispersability of the nonpolar graphene in a polar phase and the differences in absorption and emission indicative of significant charge–transfer interactions are proof of successful functionalization [116].

Noncovalent functionalization may provide a handle for secondary modifications, such as formation of composites, as was demonstrated by the group of Dai [259]. A carboxyperylene was found to adhere to micromechanically exfoliated graphene on a SiO₂ substrate, leaving the SiO₂ largely uncovered. The noncovalently attached molecules provided nucleation sites for atomic layer deposition (ALD) growth of Al₂O₃, rendering possible a mild route toward layered graphene-containing composite structures where the properties of the graphene layer remain intact.

The adsorption outcome depends on the graphene system's properties. In contrast to the homogenous distribution of perylenes on exfoliated graphene on SiO₂, Pollard

et al. observed formation of band patterns for perylene derivatives adsorbed onto as-prepared graphene on a Rh substrate [260].

4.8 FUNCTIONALIZATION OF GRAPHENE AND CARBON NANOTUBES BY METAL NANOPARTICLES

For the synthetic organic chemist, “Pd/C” has an established place in the stock of standard reagents, as has other carbon-supported metal catalysts where activated carbons or graphite powders constitute a large-area support to nanosized clusters of metal or metal compounds [231]. It is hence not surprising that CNTs and graphenes can also be “decorated.” Conditions developed for the less well-defined supports, however, are not straightforwardly translated to and between CNTs and graphenes.

For CNTs, preprocessing influences the outcome of the metal-loading step. A general observation is that oxidized CNTs carry nucleation sites for *in situ* formation of nanoparticles. Examples such as Pt and Pt–Rh clusters on MWCNTs, intended for fuel cell applications [261, 262], and magnetic Fe–Ni alloy particles [263] are abundant. Quantum dot-decoration of CNTs has been reported as well, for example, CdTe on acid-oxidized MWCNTs by Banerjee et al. [264] and CdS, Ag₂S, and HgS formation on surfactant-dispersed MWCNTs by Wei et al. [265].

An alternative stepwise covalent convergent approach to this class of hybrids was taken by Haremza et al. [266] in a study in which preformed CdSe nanoparticles with terminal alkylamine surface groups were reacted with MWCNT-COCl, a route with better control of the size distribution of the nanoparticles than the *in situ* formation one [264]. Such strategies, employing secondary functionalization to introduce groups with affinity for preformed nanoparticles or complexes, have been extensively utilized, either using the functional groups introduced in oxidative purification or direct sidewall functionalizations such as 1,3-dipolar additions to form pyrrolidines. A covalent molecular approach to a carbon-supported monometallic Rh hydrogenation catalyst was demonstrated by Lemus-Yegres et al. [267] In contrast to the amide route above, hydrocarbon chains with suitable metal-coordinating end groups were covalently bonded to an oxidized carbon material by siloxane bonds. The metal complex was formed from a precursor complex by ligand exchange. For applications where the carbon component does not provide suitable attachment functionalities or nucleation sites, noncovalently adsorbed derivatives of pyrene, perylene, or other small arenes can serve as interlinkers between the carbon material and the metal component [259]. In such noncovalent routes to oxides on graphenes, the control over the graphene quality in the final composite product is much easier to attain than in routes starting from GO dispersions [183, 184]. However, as is the case for oxidized CNTs, points of attachment for oxide, sulfide, or selenide precursors are significantly more abundant in GO than in RGO or graphene; a reduction step subsequent to the “decoration” step is far from ideal, yet more common than both the noncovalent or overall nonoxidative covalent [268] pretreatments.

The interaction between thiols and colloidal silver or gold has been of particular interest. For CNTs, both covalent [211, 269, 270] and noncovalent strategies with pyrene derivatives as interlinkers [271] efficiently bind to metal nanoparticles. Functionalization of graphene or RGO with gold nanoparticles appears to be both more straightforward and less easy to control. Gold evaporated onto micromechanically cleaved graphene flakes on Si–SiO₂ was found to aggregate to nanoparticles evenly distributed

over the surface, with larger particle sizes at thick flakes than at thinner ones [272]. In addition, preformed gold nanoparticles were found to adsorb to pristine graphene and graphites; hence, the assemblies can be formed without the need for any interlinking molecules or preoxidation [273, 274], which is a major difference from what has been observed for CNT systems [270].

4.9 APPLICATIONS OF MOLECULARLY ENGINEERED CARBON NANOTUBES AND GRAPHENES

4.9.1 Introduction

The initial focus in device-oriented CNT and graphene research has been applications in electronic devices such as transistors, transparent conductors, nanosized sensors, and photovoltaic systems, further detailed later (Sections 4.9.2–4.9.4). In such applications, the electronic properties of the sp^2 systems are important. Lightweight composites [275, 276] are another application area where the level of perfection of the sp^2 is of importance; defects such as pentagons, heptagons, and sp^3 -hybridized carbons alter not only the electronic but also the mechanical properties [277]. For both groups of applications, the inherently low solubility (Section 4.5.2) makes effective use of pristine CNTs or graphene complicated, and hence, functionalization is a primary requirement. The synthesis, purification, and functionalization options of CNTs and graphene outlined above can be tuned to add function while inflicting minimal damage to inherent properties needed in the intended application.

For many biomedical applications, a robust scaffold is of greater importance than a fully intact sp^2 -conjugated system, and use of moderately oxidized CNTs and GOs would be preferred over the more conjugated and less polar materials. The functional groups introduced in the oxidation step increase water solubility by providing sites for hydrogen bonding. The water solubility can be further enhanced by covalent attachment of polyethyleneglycol (PEG) chains using esterification [278] or amidation [279] conditions, whereas the less oxidized regions can be further functionalized using covalent or noncovalent routes. The noncovalent routes are of particular interest for drug delivery, for example References 17, 90, 280, and 281.

4.9.2 Toward Carbon Nanoelectronics

SWCNTs and graphene are, in theory, perfect candidates for a “next generation” of light and flexible nanoelectronic devices such as CNT transistors [13, 16, 160, 282]. Purity and homogeneity of the carbon material are factors of fundamental importance; devices made from as-grown SWCNTs were less efficient than those made from oxidatively purified SWCNTs, as demonstrated by Johnston et al. [283].

Wang et al. [284] have explored the homogenization effect of functionalization using aryl diazonium reagents, reactions in which metallic CNTs are more reactive than semiconducting ones. Functionalization may thus increase the proportion of semiconducting CNTs. Thin-film transistors (TFTs) with CVD-grown SWCNTs were treated on-chip with a solution of 4-bromobenzene diazonium tetrafluoroborate. After the reaction, the Raman D band intensity had increased, as expected from a covalent functionalization introducing sp^3 “defects” in the CNT sidewall. Analysis of individual

CNTs before and after functionalization revealed that semiconducting tubes were unaffected by the treatment, whereas the conductance of metallic tubes decreased significantly upon functionalization. The metallic character was never completely lost, however.

Inkjet printing is a further step toward scalable manufacturing of CNT or graphene devices [285]. Similar to the mixtures used for centrifugation-assisted fractionation (Section 4.3.3), the CNT inks are composite solutions or suspensions of purified CNTs and a polymer. The move from single-CNT to more robust network devices in combination with more selective CNT synthesis, improved purifications, and scalable fractionations of noncovalently functionalized CNTs has resulted in demonstrator TFTs with good carrier mobility and high on/off current ratio, as exemplified by Liu et al. for a composite of commercial prepurified CNTs and a fluorene-bithiophene copolymer [286]. When the SWCNT-polymer mixture was fractionated by centrifugation prior to preparation of the TFT, the device performance substantially improved [287]. Use of SWCNTs purified by a nonoxidative route [55] gave a slight further improvement [288]. In contrast to the TFTs, requiring semiconducting SWCNTs, the devices with graphene or graphene derivatives draw on the conducting properties of graphene (or RGO).

Utilizing general process knowledge from the CNT area, synthesis methods for large-area-few-flakes or large-scale-small-flakes, and efficient transfer-deposition routes, demonstrator devices are already less than a decade after the first graphene report of sizes and with performances closer to the requirements of components for consumer products than was the case for any CNT device even after twice the time. Examples such as the 30-inch transparent electrode prepared from CVD-grown large-area graphene by Bae et al. [149] or the thin-film RGO-polyvinylidene fluoride (PVDF) loudspeaker prepared by Shin et al. [289] by printing an aqueous GO-containing ink onto oxygen-plasma treated PVDF substrates, followed by annealing to form a conducting RGO layer (Figure 4.21), are only the beginning.

4.9.3 Sensor Applications of CNT and Graphene Electronics

The interaction between small molecules, typically arenes, and CNTs or graphenes is the foundation for noncovalent and supramolecular functionalization (Sections 4.6.4 and 4.7.4) and is one of the noncovalent interactions drawn on in the activated carbon “decolorization” during recrystallization purification of small molecules, as well as in various carbon-based filter materials for air or water purification [290, 291]. The adsorption interaction leads to slight changes in the π system of the CNT, graphene, or RGO [252, 292], changes that influence the current–voltage characteristics of the devices. If large enough, the changes can be used to electrochemically detect the presence of compounds adsorbed to the carbon component. This has been explored for gaseous analytes: Liu et al. have demonstrated that SWCNT network electrodes exhibit resistivity changes in the presence of methanol, decane, or trimethyl benzene [293]. Fowler et al. found that the presence of ammonia, NO_2 , or dinitrotoluene resulted in changes of the current–voltage characteristics of RGO films prepared from spin-coated GO films using anhydrous hydrazine as reducing agent [294].

The electrochemical response of monolayer pristine graphene is not significantly different from that of thicker flakes [295], hence the number of layers of the graphene used will thus likely be of less importance than the presence of defects inherent from the preparation method and of functional groups with affinity for the analytes.

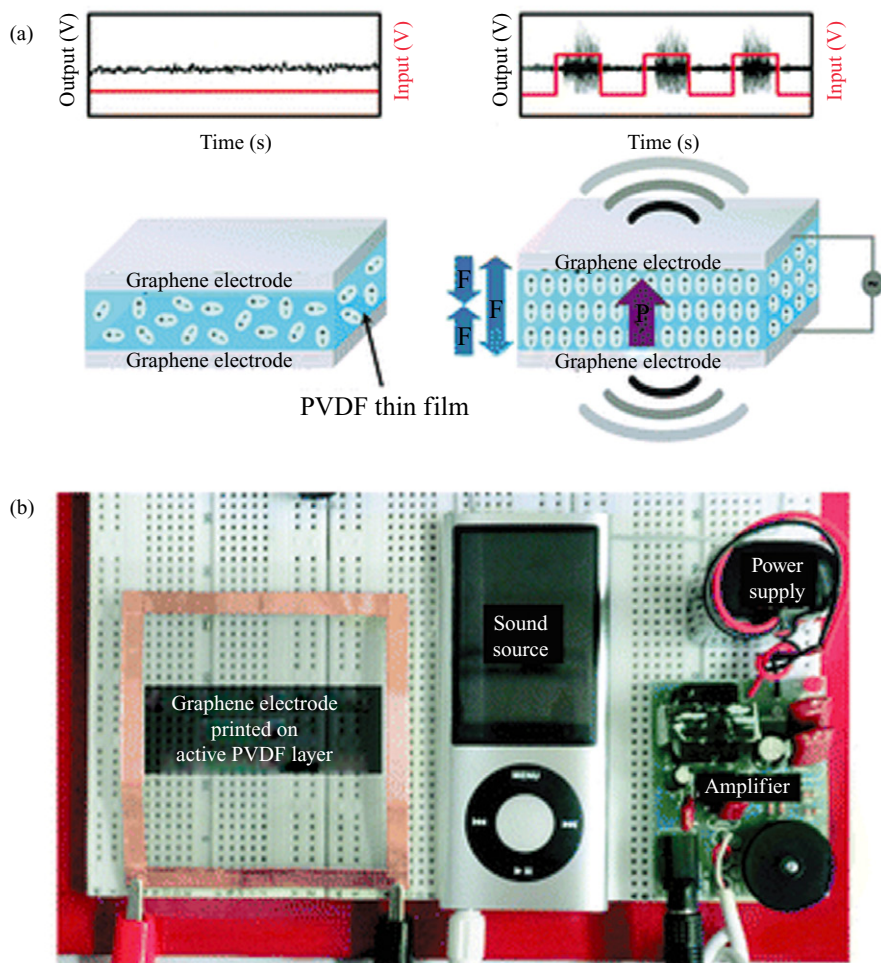


Figure 4.21. (a) Schematic illustration and (b) photograph of a PVDF-based thin film acoustic actuator using flexible and transparent graphene electrodes. The P and F mean polarization and force of the acoustic actuator, respectively. Source: [289]. Reproduced with permission of the Royal Society of Chemistry. See color insert.

Functionalization that introduces binding sites tailored toward certain classes of analytes increases sensitivity and selectivity [296]. RGO with adsorbed picket-fence iron porphyrins was explored by Tu et al. for amperometric detection of chlorite, a by-product from disinfection of drinking water [257]. Kong et al. used aryl diazonium precursors to attach cyclodextrin moieties to SWCNTs. The devices prepared from the functionalized CNTs responded to host-guest interaction between the cyclodextrin and chlorinated arenes belonging to the group of persistent organic pollutants [297]. CNT scaffolds have also found use as biosensor components [298–303].

Devices that give not only a general “yes/no” response to the presence of any analyte but also an indication of the identity will be more useful. Wang and Swager have constructed array devices from MWCNTs carrying a range of functionalities (Figure 4.17). Each functionalized MWCNT may interact with several classes of analytes but not in the same mode for each class, giving a signature response over the array that, after statistical treatment of the data, allows identification of the general class to which an analyte belongs [212].

4.9.4 Photovoltaic Applications

Purified CNTs, as well as graphene derivatives, show promise for use in photovoltaic applications, both as electron acceptors in bulk heterojunction cells and for transparent electrodes [304, 305]. With an RGO-poly(3,4-ethylenedioxythiophene-poly(styrenesulfonate) polymer-heterojunction anode, Valentini et al. obtained an overall power conversion efficiency of about 0.75% upon excitation with 100 mW cm⁻² AM 1.5 white light [306], in the same range as the 1% obtained by Wang et al. for heterojunction composites consisting of perylene and *in situ* reduced GO or SWCNTs [307]. Compared with the efficiencies around 5% obtained for bulk heterojunction solar cells with C₆₀ or C₆₀ derivatives as electron acceptors in combination with a range of donor compounds [308, 309], the CNT and graphene systems are still inferior, even more if compared with organic solar cells where efficiencies around 8% have been obtained, the >10% of dye-sensitized solar cells (DSSC), or the 15% of nanocrystalline silicon [310].

CNTs and graphene derivatives, in particular GO and RGO, have shown more promise in transparent electrode setups [311, 312]. For a DSSC system, Zhang et al. demonstrated that counter electrodes constructed of an ethyl cellulose composite with acid-oxidized CNTs were only slightly less efficient than the control ones with Pt as the top layer, and hence would be an alternative to Pt in this application system [313]. Interestingly, counter electrodes with carbon black or RGO were considerably less efficient than the CNT ones.

With increased control of synthetic procedures, purification, and functionalization, as well as deposition schemes, the performance of CNTs and, in particular, graphene derivatives in photovoltaic applications, will improve.

REFERENCES

- [1] Delgado, J. L., Herranz, M. A., Martín, N. (2008). The nano-forms of carbon. *Journal of Materials Chemistry*, 18, 1417–1426.
- [2] Mostofizadeh, A., Li, Y., Song, B., Huang, Y. (2011). Synthesis, properties and applications of low-dimensional carbon-related nanomaterials. *Journal of Nanomaterials*, article ID 685081.
- [3] Kroto, H. W., Heath, J. R., O'Brien, S. C., Curl, R. F., Smalley, R. E. (1985). C₆₀: Buckminsterfullerene. *Nature*, 318, 162–163.
- [4] Iijima, S. (1991). Helical microtubules of graphitic carbon. *Nature*, 354, 56–58.
- [5] Dresselhaus, M. S., Dresselhaus, G. F., Eklund, P. C. (Eds.). *Science of Fullerenes and Carbon Nanotubes*, Academic Press, San Diego, CA, 1996.
- [6] Guldi, D. M., Martín, N. (Eds.). *Carbon Nanotubes and Related Structures*, Wiley-VCH, Weinheim, 2010.

- [7] Novoselov, K. S., Geim, A. K., Morozov, S. V., Jiang, D., Zhang, Y., Dubonos, S. V., Grigorieva, I. V., Firsov, A. A. (2004). Electric field effect in atomically thin carbon films. *Science*, *306*, 666–669.
- [8] Terrones, M., Hsu, W. K., Kroto, H. W., Walton, D. R. M. (1999). Nanotubes: A revolution in materials science and electronics. *Topics in Current Chemistry*, *199*, 189–234.
- [9] Pati, S. K., Enoki, T., Rao, C. N. R. (Eds.). *Graphene and Its Fascinating Attributes*, World Scientific, Hackensack, NJ, 2011.
- [10] Kreuger, A. (2008). The structure and reactivity of nanoscale diamond. *Journal of Materials Chemistry*, *18*, 1485–1492.
- [11] Boehm, H. P., Setton R., Stumpp, E. (1986). Nomenclature and terminology of graphite intercalation compounds. *Carbon*, *24*, 241–245.
- [12] Singh, A. K., Penev, E. S., Yakobson, B. I. (2011). Armchair or zigzag? A tool for characterizing graphene edge. *Computer Physics Communications*, *182*, 804–807.
- [13] Trauzettel, B., Loss, D. (2009). Nanotubes: Carbon surprises again. *Nature Physics*, *5*, 317–318.
- [14] Dresselhaus, M. S. (1998). Nanotechnology: New tricks with nanotubes. *Nature*, *391*, 19–20.
- [15] Joselevich, E. (2004). Electronic structure and chemical reactivity of carbon nanotubes: A chemist's view. *Chemphyschem*, *5*, 619–624.
- [16] McEuen, P. L. (2000). Single-wall carbon nanotubes. *Physics World*, 31–36.
- [17] Singh, P., Da Ros, T., Kostarelos, K., Prato, M., Bianco, A. Carbon-based nanomaterial applications in biomedicine. In *Carbon Nanotubes and Related Structures*, Guldi, D. M., Martín, N. (Eds.), Wiley-VCH, Weinheim, 2010; pp. 199–232, and references therein.
- [18] Stella, G. M. (2011). Carbon nanotubes and pleural damage: Perspectives of nanosafety in the light of asbestosis experience. *Biointerphases*, *6*, 1–17, and references therein.
- [19] Chowdhury, I., Duch, M. C., Gits, C. G., Hersham, M. C., Walker, S. L. (2012). Impact of synthesis methods on the transport of single walled carbon nanotubes in the aquatic environment. *Environmental Science and Technology*, *46*, 11752–11760.
- [20] Maynard, A. D., Aitken, R. J., Butz, T., Colvin, V., Donaldson, K., Obersdörster, G., Philbert, M. A., Ryan, J., Seaton, A., Stone, V., Tinkle, S. S., Tran, L., Walker, N. J., Warheit, D. B. (2006). Safe handling of nanotechnology. *Nature*, *444*, 267–269.
- [21] Allen, M. J., Tung, V. C., Kaner, R. B. (2010). Honeycomb carbon: A review of graphene. *Chemical Reviews*, *110*, 132–145.
- [22] Gardiner, D. J. *Practical Raman Spectroscopy*, Springer-Verlag, New York, 1989.
- [23] Graupner, R. (2007). Raman spectroscopy of covalently functionalized single-wall carbon nanotubes. *Journal of Raman Spectroscopy*, *38*, 673–683.
- [24] Jorio, A., Dresselhaus, M. S., Saito, R., Dresselhaus, G. F. *Raman Spectroscopy in Graphene Related Systems*, Wiley-VCH, Weinheim, 2011.
- [25] Jorio, A., Pimenta, M. A., Souza Filho, A. G., Saito, R., Dresselhaus, G., Dresselhaus, M. S. (2003). Characterizing nanotube samples with resonance Raman scattering. *New Journal of Physics*, *5*, 139.1–139.17.
- [26] Ferrari, A. C. (2007). Raman spectroscopy of graphene and graphite: Disorder, electron–phonon coupling, doping and nonadiabatic effects. *Solid State Communications*, *143*, 47–57.
- [27] Haluška, M., Obergfell, D., Meyer, J. C., Scalia, G., Ulbricht, G., Krauss, B., Chae, D. H., Lohmann, T., Lebert, M., Kaempgen, M., Hulman, M., Smet, J., Roth, S., von Klitzing, K. (2007). Investigation of the shift of Raman modes of graphene flakes. *Physica Status Solidi (B)*, *244*, 4143–4146.
- [28] Ferrari, A. C., Meyer, J. C., Scardaci, V., Casiraghi, C., Lazzeri, M., Mauri, F., Piscanec, S., Jiang, D., Novoselov, K. V., Roth, S., Geim, A. K. (2006). Raman spectrum of graphene and graphene layers. *Physical Review Letters*, *97*, 187401.1–187401.4.

- [29] Goldberg, D., Bando, Y., Bourgeois, L., Kurashima, K. (1999). Atomic resolution of single-walled carbon nanotubes using a field emission high-resolution transmission electron microscope. *Carbon*, 37, 1858–1860.
- [30] Zhu, H., Suenaga, K., Hashimoto, A., Urita, K., Ijima, S. (2005). Structural identification of single- and double-walled carbon nanotubes by high-resolution transmission electron microscopy. *Chemical Physics Letters*, 412, 116–120.
- [31] Hashimoto, A., Suenaga, K., Gloter, A., Urita, K., Ijima, S. (2004). Direct evidence for atomic defects in graphene layers. *Nature*, 430, 870–872.
- [32] Venema, L. C., Wildöer, J. W. G., Dekker, C., Rinzler, G. A., Smalley, R. E. (1998). STM atomic resolution images of single-wall carbon nanotubes. *Applied Physics A*, 66, 153–155.
- [33] Popov, V. N., Lambin, P. (Eds.). *Carbon Nanotubes, from Basic Research to Nanotechnology*, NATO Science series II. Mathematics, physics and chemistry, Vol. 222, Springer, Dordrecht, The Netherlands, 2005.
- [34] Resasco, D. E., Herrera, J. E., Balzano, L. (2004). Decomposition of carbon-containing compounds on solid catalysts for single-walled carbon nanotube production. *Journal of Nanoscience and Nanotechnology*, 4, 1–10.
- [35] Plata, D. L., Meshot, E. R., Reddy, C. M., Hart, A. J., Gschwend, P. M. (2010). Multiple alkynes react with ethylene to enhance carbon nanotube synthesis, suggesting a polymerization-like formation mechanism. *ACS Nano*, 4, 7185–7192.
- [36] Scott, L. T. (2010). Polycyclic aromatic hydrocarbon bowls, baskets, balls and tubes: Challenging targets for chemical synthesis. *Polycyclic Aromatic Compounds*, 30, 247–259.
- [37] Wen, B., Wang, K. K. (2012). Solution-phase synthesis of bowl- and basket-shaped fullerene fragments via benzannulated enyne-allenes. *Pure and Applied Chemistry*, 84, 893–905.
- [38] Mueller, A., Yu, K., Jansen, M. (2010). Synthesis of end-cap precursor molecules for (6,6) armchair and (9,0) zig-zag single-walled carbon nanotubes. *Tetrahedron Letters*, 51, 3221–3225.
- [39] Chiang, I. W., Brinson, B. E., Huang, A. Y., Willis, P. A., Bronikowski, M. I., Margrave, J. L., Smalley, R. E., Hauge, R. H. (2001). Purification and characterization of single-wall carbon nanotubes. *The Journal of Physical Chemistry B*, 105, 8297–8301.
- [40] Park, T.-J., Banerjee, S., Hemraj-Benny, T., Wong, S. S. (2006). Purification strategies and purity visualization techniques for single-walled carbon nanotubes. *Journal of Materials Chemistry*, 16, 141–154.
- [41] Zimmerman, J. L., Bradley, R. K., Huffman, C. B., Hauge, R. H., Margrave, J. L. (2000). Gas-phase purification of single-walled carbon nanotubes. *Chemistry of Materials*, 12, 1361–1366.
- [42] Huang, S., Dai, L. (2002). Plasma etching for purification and controlled opening of aligned carbon nanotubes. *The Journal of Physical Chemistry B*, 106, 3543–3545.
- [43] Rinzler, A. G., Liu, J., Dai, H., Nikolaev, P., Huffman, C. B., Rodriguez-Macias, F. J., Boul, P. J., Lu, A. H., Heymann, D., Colbert, D. T., Lee, R. S., Fischer, J. E., Rao, A. M., Eklund, P. C., Smalley, R. E. (1998). Large-scale purification of single-wall carbon nanotubes: Process, product, and characterization. *Applied Physics A*, 67, 29–37.
- [44] Monthieux, M., Smith, B. W., Burtiaux, B., Claye, A., Fischer, J. E., Luzzi, D. E. (2001). Sensitivity of carbon nanotubes to chemical processing: An electron microscopy investigation. *Carbon*, 39, 1251–1272.
- [45] Kim, U. J., Furtado, C. A., Liu, X., Chen, G., Eklund, P. C. (2005). Raman and IR spectroscopy of chemically processed single-walled carbon nanotubes. *Journal of the American Chemical Society*, 127, 15437–15445.
- [46] Edwards, E. R., Antunes, E. F., Bothelho, E. C., Baldan, M. R., Corat, E. J. (2011). Evaluation of residual iron in carbon nanotubes purified by acid treatments. *Applied Surface Science*, 258, 641–648.

- [47] Wiltshire, J. G., Khlobystov, A. N., Li, L. J., Lyapin, S. G., Briggs, G. A. D., Nicholas, R. J. (2004). Comparative studies on acid and thermal based selective purification of HiPCO produced single-walled carbon nanotubes. *Chemical Physics Letters*, 386, 239–243.
- [48] Kukovecz, A., Kramberger, C., Holzinger, M., Kuzmany, H., Schalko, J., Mannsberger, M., Hirsch, A. (2002). On the stacking behaviour of functionalized single-wall carbon nanotubes. *The Journal of Physical Chemistry B*, 106, 6347–6380.
- [49] Li, J., Chajara, K., Lindgren, J., Grennberg, H. (2007). Rapid acid-mediated purification of single-walled carbon nanotubes with homogenization of bulk properties. *Journal of Nanoscience and Nanotechnology*, 7, 1525–1528.
- [50] Hirsch, A. (2002). Functionalization of single-walled carbon nanotubes. *Angewandte Chemie—International Edition*, 41, 1853–1859.
- [51] Hu, H., Yu, A., Kim, E., Zhao, B., Itkis, M. I., Bekyarova, E., Haddon, R. C. (2005). Influence of the zeta potential on the dispersability and purification of single-walled carbon nanotubes. *The Journal of Physical Chemistry B*, 109, 11520–11524.
- [52] Furtado, C. A., Kim, U. J., Gutierrez, H. R., Pan, L., Dickey, E. C., Eklund, P. C. (2004). Debundling and dissolution of single-walled carbon nanotubes in amide solvents. *Journal of the American Chemical Society*, 126, 6095–6105.
- [53] Guldi, D. M., Holzinger, M., Hirsch, A., Georgakilas, V., Prato, M. (2003). First comparative emission assay of single-walled carbon nanotubes-solutions and dispersions. *Chemical Communications*, 1130–1131.
- [54] Zhang, X., Sreekumar, T. V., Liu, T., Kumar, S. (2004). Properties and structure of nitric acid oxidized single walled carbon nanotube films. *The Journal of Physical Chemistry B*, 108, 16435–16440.
- [55] Chajara, K., Andersson, C.-H., Lu, J., Widenkvist, E., Grennberg, H. (2010). Reagent-free microwave-assisted purification of carbon nanotubes. *New Journal of Chemistry*, 34, 2275–2280.
- [56] Min, Y.-S., Bae, E. J., Park, W. (2005). Sulfidative purification of carbon nanotubes integrated in transistors. *Journal of the American Chemical Society*, 127, 8300–8301.
- [57] Yudasaka, M., Zhang, M., Ijima, S. (2003). Diameter-selective removal of single-walled carbon nanotubes through light-assisted oxidation. *Chemical Physics Letters*, 374, 132–136.
- [58] Hassanien, A., Tokumoto, M., Umek, P., Vrbanic, D., Mozetic, M., Mihailovic, D., Venturini, P., Pejovnik, S. (2005). Selective etching of metallic single-walled carbon nanotubes with hydrogen plasma. *Nanotechnology*, 16, 278–281.
- [59] Krupke, R., Hennrich, F. (2006). Separation techniques for carbon nanotubes. *Advanced Engineering Materials*, 7, 111–116.
- [60] Hershman, M. C. (2008). Progress towards monodisperse single-walled carbon nanotubes. *Nature Nanotechnology*, 3, 387–394.
- [61] Péres, E. M., Martín, N. (2012). Chiral recognition of carbon nanoforms. *Organic and Biomolecular Chemistry*, 10, 3577–3583.
- [62] Liu, J., Hershman, M. C. (2010). Recent developments in carbon nanotube sorting and selective growth. *MRS Bulletin*, 35, 315–321.
- [63] Farkas, E., Anderson, M. E., Chen, Z., Rinzler, A. G. (2002). Length sorting of cut single wall carbon nanotubes by high performance liquid chromatography. *Chemical Physics Letters*, 363, 111–116.
- [64] Yang, Y., Xie, L., Chen, Z., Liu, M., Zhu, T., Liu, Z. (2005). Purification and length separation of single-walled carbon nanotubes using chromatographic method. *Synthetic Metals*, 155, 455–460.
- [65] Moon, M. H., Kang, D., Jung, J., Kim, J. (2004). Separation of carbon nanotubes by frit inlet asymmetrical flow field-flow fractionation. *Journal of Separation Science*, 27, 710–717.

- [66] Tagmatarchis, N., Zattoni, A., Reschiglian, P., Prato, M. (2005). Separation and purification of functionalized water-soluble multi-walled carbon nanotubes by flow field-flow fractionation. *Carbon*, 43, 1984–1989.
- [67] Dyke, C. A., Stewart, M. P., Tour, J. M. (2005). Separation of single-walled carbon nanotubes on silica gel. Materials morphology and Raman excitation wavelength affect data interpretation. *Journal of the American Chemical Society*, 127, 4497–4509.
- [68] Umek, P., Mihailovic, D. (2001). Separation of SWNTs by diffusion. *Synthetic Metals*, 121, 1211–1212.
- [69] Krupke, R., Hennrich, F., von Lohneysen, H., Kappes, M. (2003). Separation of metallic from semiconducting single-walled carbon nanotubes. *Science*, 301, 344–347.
- [70] Chen, Z., Du, X., Du, M.-H., Rancken, D., Cheng, H.-P., Rintzler, A. G. (2003). Bulk separative enrichment in metallic or semiconducting single-walled carbon nanotubes. *Nano Letters*, 3, 1245–1249.
- [71] Lee, H. W., Yoon, Y., Park, S., Oh, J. H., Hong, S., Liyanage, L. S., Wang, H., Morishita, S., Patil, N., Park, Y. J., Park, J. J., Spakowitz, A., Galli, G., Gygi, F., Wong, P. H.-S., Tok, J. B.-H., Kim, J. M., Bao, Z. (2011). Selective dispersion of high-purity semiconducting single-walled carbon nanotubes with regioregular poly(3-alkylthiophene)s. *Nature Communications*, 2, 1–8.
- [72] Stürzl, N., Hennrich, F., Lebedkin, S., Kappes, M. F. (2009). Near monochiral single-walled carbon nanotube dispersions in organic solvents. *The Journal of Physical Chemistry C*, 113, 14628–14632.
- [73] Zheng, M., Jagota, A., Semke, E. D., Diner, B. A., McLean, R. S., Lustig, S. R., Richardson, R. E., Tassi, N. G. (2003). DNA-assisted dispersion and separation of carbon nanotubes. *Nature Materials*, 2, 338–342.
- [74] Zheng, M., Jagota, A., Strano, M. S., Santos, A. P., Barone, P., Chou, S. G., Diner, B. A., Dresselhaus, M. S., McLean, R. S., Onoa, G. B., Samsonidze, G. G., Semke, E. D., Usrey, M., Walls, D. J. (2003). Structure-based carbon nanotube sorting by sequence-dependent DNA assembly. *Science*, 302, 1545–1548.
- [75] Strano, M. S. (2003). Probing chiral selective reactions using a revised Katahura plot for the interpretation of single-walled carbon nanotube spectroscopy. *Journal of the American Chemical Society*, 125, 16148–16153.
- [76] Itkis, M. E., Perea, D. E., Jung, R., Niyogi, S., Haddon, R. C. (2004). Comparison of analytical techniques for purity evaluation of single-walled carbon nanotubes. *Journal of the American Chemical Society*, 127, 3439–3448.
- [77] Heller, D. A., Barone, P. W., Swanson, J. P., Mayrhofer, R. M., Strano, M. S. (2004). Using Raman spectroscopy to elucidate the aggregation state of single-walled carbon nanotubes. *The Journal of Physical Chemistry B*, 108, 6905–6909.
- [78] Stankovich, S., Dikin, D. A., Piner, R. D., Kohlhaas, K. A., Kleinhammes, A., Jia, Y., Wu, Y., Nguyen, S. T., Ruoff, R. S. (2007). Synthesis of graphene-based nanosheets via chemical reduction of exfoliated graphite oxide. *Carbon*, 45, 1558–1565.
- [79] Park, S., Ruoff, R. S. (2009). Chemical methods for the production of graphenes. *Nature Nanotechnology*, 4, 217–224.
- [80] Zhu, Y., Murali, S., Cai, W., Li, X., Won Suk, J., Potts, J. R., Ruoff, R. S. (2010). Graphene and graphene oxide: Synthesis, properties, and applications. *Advanced Materials*, 22, 3906–3924.
- [81] Dreyer, D. R., Park, S., Bielawski, C. W., Ruoff, R. S. (2010). The chemistry of graphene oxide. *Chemical Society Reviews*, 39, 228–240.
- [82] Hummers, W. S., Offeman, R. E. J. (1958). Preparation of graphitic oxide. *Journal of the American Chemical Society*, 80, 1339–1339.
- [83] Brodie, B. C. (1860). Sur le poids atomique du graphite. *Annales de Chimie et de Physique*, 59, 466–472.

- [84] Staudenmaier, L. (1898). Untersuchungen über den Graphit. *Berichte der Deutschen Chemischen Gesellschaft*, 32, 2824–2834.
- [85] Boehm, H. P., Eckel, W., Scholz, Z. (1967). Über den bildungsmechanismus des graphitoxid. *Zeitschrift für anorganische und allgemeine Chemie*, 353, 236–242.
- [86] Liang, Y., Wu, D., Feng, X., Müllen, K. (2009). Dispersion of graphene sheets in organic solvent supported by ionic interactions. *Advanced Materials*, 21, 1679–1683.
- [87] Wu, Z.-S., Ren, W., Gao, L., Liu, B., Jiang, C., Cheng, H.-M. (2009). Field emission of single-layer graphene films prepared by electrophoretic deposition. *Carbon*, 47, 493–499.
- [88] Szabo, T., Berkesi, O., Forgo, P., Josepovits, K., Sanakis, Y., Petridis, D., Dekany, I. (2006). Evolution of surface functional groups in a series of progressively oxidized graphite oxides. *Chemistry of Materials*, 18, 2740–2749.
- [89] Cai, W., Piner, R. D., Stadermann, F. J., Park, S., Shaibat, M. A., Ishii, Y., Yang, D., Velamakanni, A., An, S. J., Stoller, M., An, J., Chen, D., Ruoff, R. S. (2008). Synthesis and solid-state NMR structural characterization of ^{13}C -labeled graphite oxide. *Science*, 321, 1815–1817.
- [90] Yang, X., Zhang, X., Ma, Y., Huang, Y., Wang, Y., Chen, Y. (2009). Superparamagnetic graphene oxide- Fe_3O_4 nanoparticles hybrid for controlled targeted drug carriers. *Journal of Materials Chemistry*, 19, 2710–2714.
- [91] Inagaki, M., Kima, Y. A., Endo, M. (2011). Graphene: Preparation and structural perfection. *Journal of Materials Chemistry*, 21, 3280–3294.
- [92] Wang, H., Robinson, J. T., Li, X., Dai, H. (2009). Solvothermal reduction of chemically exfoliated graphene sheets. *Journal of the American Chemical Society*, 131, 9910–9911.
- [93] Dua, V., Surwade, S. P., Ammu, S., Agnihotra, S. R., Jain, S., Roberts, K. E., Park, S., Ruoff, R. S., Manohar, S. K. (2010). All-organic sensor using inkjet-printed reduced graphene oxide. *Angewandte Chemie—International Edition*, 49, 2154–2157.
- [94] Shin, H.-J., Kim, K. K., Benayad, A., Yoon, S.-M., Park, H. K., Jung, I.-S., Jin, M. H., Jeong, H.-K., Kim, J. M., Choi, J.-Y., Lee, Y. H. (2009). Efficient reduction of graphite oxide by sodium borohydride and its effect on electrical conductance. *Advanced Functional Materials*, 19, 1987–1992.
- [95] Wang, G. X., Yang, J., Park, J., Gou, X. L., Wang, B., Liu, H., Yao, J. (2008). Facile synthesis and characterization of graphene nanosheets. *The Journal of Physical Chemistry C*, 112, 8192–8195.
- [96] Li, X., Wang, H., Robinson, J. T., Sanchez, H., Diankov, G., Dai, H. (2009). Simultaneous nitrogen doping and reduction of graphene oxide. *Journal of the American Chemical Society*, 131, 15939–15944.
- [97] Long, J., Xie, X., Xu, J., Gu, Q., Chen, L., Wang, X. (2012). Nitrogen-doped graphene nanosheets as metal-free catalysts for aerobic selective oxidation of benzylic alcohols. *ACS Catalysis*, 2, 622–631.
- [98] Fan, Z.-J., Kai, W., Yan, J., Wei, T., Zhi, L.-J., Feng, J., Ren, Y.-M., Song, L.-P., Wei, F. (2011). Facile synthesis of graphene nanosheets via Fe reduction of exfoliated graphite oxide. *ACS Nano*, 5, 191–198.
- [99] Kaminska, I., Das, M. R., Coffiner, Y., Niedziolka-Jonsson, J., Woisel, P., Opallo, M., Szunerits, S., Boukherroub, R. (2009). Preparation of graphene/tetrathiafulfavene nanocomposite switchable surfaces. *Chemical Communications*, 48, 1221–1223.
- [100] McAllister, M. J., Li, J. L., Adamson, D. H., Schniepp, H. C., Abdala, A. A., Liu, J., Herrera-Alonso, M., Milius, D. L., Car, R., Prudhomme, R. K., Aksay, I. A. (2007). Single sheet functionalized graphene by oxidation and thermal expansion of graphite. *Chemistry of Materials*, 19, 4396–4404.
- [101] Haubner, K., Murawski, J., Olk, P., Eng, L. M., Ziegler, C., Adolphi, B., Jaehne, E. (2010). The route to functional graphene oxide. *Chemphyschem*, 11, 2131–2139.

- [102] Zhang, M., Liu, S., Yin, X. M., Du, Z. F., Hao, Q. Y., Lei, D. N., Li, Q. H., Wang, T. H. (2011). Fast synthesis of graphene sheets with good thermal stability by microwave irradiation. *Chemistry – An Asian Journal*, 6, 1151–1154.
- [103] Zhang, J., Di, C., Liu, Y., Liu, H., Guo, Y., Du, C., Wu, T., Yu, G., Zhu, D. (2010). High quality graphene with large flakes exfoliated by oleyl amine. *Chemical Communications*, 46, 5728–5730.
- [104] Dubin, S., Gilje, S., Wang, K., Tung, V. C., Cha, K., Hall, A. S., Farrar, J., Varshneya, R., Yang, Y., Kaner, R. B. (2010). A one-step solvothermal reduction method for producing reduced graphene oxide dispersions in organic solvents. *ACS Nano*, 4, 3845–3852.
- [105] Cravotto, G., Cintas, P. (2010). Sonication-assisted fabrication and post-synthetic modifications of graphene-like materials. *Chemistry—A European Journal*, 16, 5246–5259.
- [106] Suslick, K. S., Didenko, Y., Fang, M. M., Hyeon, T., Kolbeck, K. J., McNamara, W. B., Mdleleni, M. M., Wong, M. (1999). Acoustic cavitation and its chemical consequences. *Philosophical Transactions of the Royal Society A*, 357, 335–353.
- [107] Suslick, K. S., Price, G. J. (1999). Applications of ultrasound to materials chemistry. *Annual Review of Materials Science*, 29, 295–326.
- [108] Vichare, N. P., Senthikumar, P., Moholkar, V. S., Gogate, P. R., Pandit, A. B. (2000). Energy analysis in acoustic cavitation. *Industrial and Engineering Chemistry Research*, 39, 1480–1486.
- [109] Hernandez, Y., Nicolosi, V., Lotya, M., Blighe, F. M., Sun, Z., De, S., McGovern, I. T., Holland, B., Byrne, M., Gunko, Y. K., Boland, J. J., Niraj, P., Duesberg, G., Satheesh, K., Goodhue, R., Hutchison, J., Scardaci, V., Ferrari, A. C., Coleman, N. J. (2008). High-yield production of graphene by liquid-phase exfoliation of graphite. *Nature Nanotechnology*, 3, 563–567.
- [110] Bourlinos, A. B., Georgakilas, V., Zboril, R., Steriotis, T. A., Stubos, A. K. (2009). Liquid-phase exfoliation of graphite towards solubilized graphenes. *Small*, 5, 1841–1845.
- [111] Hamilton, C. E., Lomeda, J. R., Sun, Z., Tour, J. M., Barron, A. R. (2009). High-yield organic dispersions of unfunctionalized graphene. *Nano Letters*, 9, 3460–3462.
- [112] Lotya, M., Hernandez, Y., King, P. J., Smith, R. J., Nicolosi, V., Karlsson, L. S., Blighe, F. M., De, S., Wang, Z., McGovern, I. T., Duesberg, G. S., Coleman, J. N. (2009). Liquid phase production of graphene by exfoliation of graphite in surfactant/water solutions. *Journal of the American Chemical Society*, 131, 3611–3620.
- [113] Green, A. A., Hersam, M. C. (2009). Solution phase production of graphene with controlled thickness via density differentiation. *Nano Letters*, 9, 4031–4036.
- [114] Lin, S., Shih, C.-J., Strano, M., Blankschtein, D. (2011). Molecular insights into the surface morphology, layering structure and aggregation kinetics of surfactant-stabilized graphene dispersions. *Journal of the American Chemical Society*, 133, 12810–12823.
- [115] Zhang, M., Parajuli, R. R., Mastrogianni, D., Dai, B., Lo, P., Cheung, W., Brukh, R., Chiu, P. L., Zhou, T., Liu, Z., Garfunkel, E., He, H. (2010). Production of graphene sheets by direct dispersion with aromatic healing agents. *Small*, 6, 1100–1107.
- [116] Ghosh, A., Rao, K. V., George, S. J., Rao, C. N. R. (2010). Noncovalent functionalization, exfoliation and solubilization of graphene in water by employing a fluorescent coronene carboxylate. *Chemistry—A European Journal*, 16, 2700–2704.
- [117] Misik, V., Riesz, P. (1994). Free radical formation by ultrasound in organic liquids: A spin trapping and EPR study. *The Journal of Physical Chemistry*, 98, 1634–1640.
- [118] Misik, V., Kirschenbaum, L. J., Riesz, P. (1995). Free radical production by sonolysis of aqueous mixtures of N,N-dimethylformamide: An EPR spin trapping study. *The Journal of Physical Chemistry*, 99, 5970–5976.
- [119] Moonosawmy, K. R., Kruse, R. (2008). To dope or not to dope: The effect of sonicating single-wall carbon nanotubes in common laboratory solvents on their electronic structure. *Journal of the American Chemical Society*, 130, 13417–13424.

- [120] Semeluk, G. P., Bernstein, R. B. (1957). The thermal decomposition of chloroform. II. Kinetics. *Journal of the American Chemical Society*, *79*, 46–49.
- [121] Hu, H., Zhao, B., Hamon, M. A., Kamaras, K., Itkis, M. E., Haddon, R. C. (2003). Sidewall functionalization of single-walled carbon nanotubes by addition of dichlorocarbene. *Journal of the American Chemical Society*, *125*, 14893–14900.
- [122] Zhang, J., Xiao, J., Meng, X., Monroe, C., Huang, Y., Zuo, J.-M. (2010). Free folding of suspended graphene by random mechanical stimulation. *Physical Review Letters*, *104*, 166805.
- [123] Shih, C.-J., Vijayaraghavan, A., Krishnan, R., Sharma, R., Han, J.-H., Ham, M.-H., Jin, Z., Lin, S., Paulus, G. L. C., Reuel, N. F., Wang, Q. H., Blankschtein, D., Strano, M. S. (2011). Bi- and trilayer graphene solutions. *Nature Nanotechnology*, *6*, 439–445.
- [124] Widenkvist, E., Boukhalov, D. W., Rubino, S., Akhtar, S., Lu, J., Quinlan, R. A., Katsnelson, M. I., Leifer, K., Grennberg, H., Jansson, U. (2009). Mild sonochemical exfoliation of bromine-intercalated graphite: A new route towards graphene synthesis. *Journal of Physics D: Applied Physics*, *42*, 112003.
- [125] Rangappa, D., Sone, K., Wang, M., Gautam, U. K., Golberg, D., Itoh, H., Ichihara, M., Honma, I. (2010). Rapid and direct conversion of graphite crystals into high-yielding, good-quality graphene by supercritical fluid extraction. *Chemistry—A European Journal*, *16*, 6488–6494.
- [126] Pu, N. W., Wang, C. A., Sung, Y., Liu, Y. M., Ger, M. D. (2009). Production of few-layer graphene by supercritical CO₂ exfoliation of graphite. *Materials Letters*, *63*, 1987–1989.
- [127] Regmi, M., Chrisholm, M. F., Eres, G. (2012). The effect of growth parameters on the intrinsic properties of large-area single layer graphene grown by chemical vapour deposition. *Carbon*, *50*, 134–141.
- [128] Tzalenchuk, A., Lara-Avila, S., Cedergren, K., Syvaajaervi, M., Yakimova, R., Kazakova, O., Janssen, T. J. B. M., Moth-Poulsen, K., Bjornholm, T., Kopylov, S., Falko, V., Kubatkin, S. (2011). Engineering and metrology of epitaxial graphene. *Solid State Communications*, *151*, 1094–1099.
- [129] Riedl, C., Coletti, C., Starke, U. (2010). Structural and electronic properties of epitaxial graphene on SiC (0001): A review of growth, characterization, transfer doping and hydrogen intercalation. *Journal of Physics D: Applied Physics*, *43*, 374009.
- [130] Reina, A., Jia, X., Ho, J., Nezich, D., Son, H., Bulovic, V., Dresselhaus, M. S., Kong, J. (2009). Large area few-layer graphene films on arbitrary substrates by chemical vapour deposition. *Nano Letters*, *9*, 30–35.
- [131] Kim, K. S., Zhao, Y., Jang, H., Lee, S. Y., Kim, J. M., Kim, K. S., Ahn, J.-H., Kim, P., Choi, J.-Y., Hong, B. H. (2009). Large-scale pattern growth of graphene films for stretchable transparent electrodes. *Nature*, *457*, 706–710.
- [132] Huang, L., Chang, Q. H., Guo, G. L., Liu, Y., Xie, Y. Q., Wang, T., Ling, B., Yang, H. F. (2012). Synthesis of high-quality graphene films on nickel foils by rapid thermal chemical vapour deposition. *Carbon*, *50*, 551–556.
- [133] Liu, W., Li, H., Xu, C., Khatami, Y., Banerjee, K. (2011). Synthesis of high-quality monolayer and bilayer graphene on copper using chemical vapour deposition. *Carbon*, *49*, 4122–4130.
- [134] Bhaviripudi, S., Jia, X., Dresselhaus, M. S., Kong, J. (2010). Role of kinetic factors in chemical vapour deposition synthesis of uniform large area graphene using copper catalyst. *Nano Letters*, *10*, 4128–4133.
- [135] Li, X., Cai, W., An, J., Kim, S., Nah, J., Yang, D., Piner, R., Velamakanni, A., Jung, I., Tutuc, E., Banerjee, S. K., Colombo, L., Ruoff, R. S. (2009). Large-area synthesis of high-quality and uniform graphene films on copper foils. *Science*, *324*, 1312–1314.
- [136] Wood, J. D., Schmucker, S. W., Lyons, A. S., Pop, E., Lyding, J. W. (2011). Effects of polycrystalline Cu substrate on graphene growth by chemical vapor deposition. *Nano Letters*, *11*, 4547–4554.

- [137] Guermoune, A., Chari, T., Popescu, F., Sabri, S. S., Guillemette, J., Skulason, H. S., Szkopek, T., Sjaaj, M. (2011). Chemical vapour deposition synthesis of graphene on copper with methanol, ethanol and propanol precursors. *Carbon*, *49*, 4204–4210.
- [138] Ruan, G., Sun, Z., Peng, Z., Tour, J. M. (2011). Growth of graphene from food, insects, and waste. *ACS Nano*, *5*, 7601–7607.
- [139] Dong, X., Wang, P., Fang, W., Su, C.-Y., Chen, Y.-H., Li, L.-J., Huang, W., Chen, P. (2011). Growth of large-sized graphene thin films by liquid precursor-based chemical vapour deposition under atmospheric pressure. *Carbon*, *49*, 3672–3678.
- [140] Ishihara, M., Koga, Y., Kim, J., Tsugawa, K., Hasegawa, M. (2011). Direct evidence of advantage of Cu(111) for graphene synthesis by using Raman mapping and electron backscatter diffraction. *Materials Letters*, *65*, 2864–2867.
- [141] Zhu, M., Wang, J., Holloway, B. C., Outlaw, R. A., Zhao, X., Hou, K. V., Shutthanandan, V., Manos, D. M. (2007). A mechanism for carbon nanosheet formation. *Carbon*, *45*, 2229–2234.
- [142] French, B. L., Wang, J. J., Zhu, M. Y., Holloway, B. C. (2005). Structural characterization of carbon nanosheets via X-ray scattering. *Journal of Applied Physics*, *97*, 114317.
- [143] French, B. L., Wang, J. J., Zhu, M. Y., Holloway, B. C. (2006). Evolution of structure and morphology during plasma-enhanced chemical vapor deposition of carbon nanosheets. *Thin Solid Films*, *494*, 105–109.
- [144] Das, S., Seelaboyina, R., Verma, V., Lahiri, I., Hwang, J. Y., Banerjee, R., Choi, W. (2011). Synthesis and characterization of self-organized multilayered graphene-carbon nanotube hybrid films. *Journal of Materials Chemistry*, *21*, 7289–7295.
- [145] Campos-Delgado, J., Romo-Herrera, J. M., Jia, X., Cullen, D. A., Muramatsu, H., Kim, Y. A., Hayashi, T., Ren, Z., Smith, D. J., Okuno, Y., Ohba, T., Kanoh, H., Kaneko, K., Endo, M., Terrones, H., Dresselhaus, M. S., Terrones, M. (2008). Bulk production of a new form of sp^2 carbon: Crystalline graphene nanoribbons. *Nano Letters*, *8*, 2773–2778.
- [146] Pirkle, A., Chan, J., Venugopal, A., Hinojos, D., Magnuson, C. W., McDonnell, S., Columbo, L., Vogel, E. M., Ruoff, R. S., Wallace, R. M. (2011). The effect of chemical residues on the physical and electrical properties of chemical vapor deposited graphene transferred to SiO_2 . *Applied Physics Letters*, *99*, 122108 (3 pp).
- [147] Kim, B.-J., Lee, C., Jung, Y., Baik, K. H., Mastro, M. A., Hite, J. K., Eddy, C. R., Jr., Kim, J. (2011). Large-area transparent conductive few-layer graphene electrode in GaN-based ultra-violet light-emitting diodes. *Applied Physics Letters*, *99*, 143101 (3 pp).
- [148] Bie, Y.-Q., Zhou, Y.-B., Liao, Z.-M., Yan, K., Liu, S., Zhao, Q., Kumar, S., Wu, H.-C., Duesberg, G. S., Cross, G. L. W., Xu, J., Peng, H., Liu, Z., Yu, D.-P. (2011). Site-specific transfer-printing of individual graphene microscale patterns to arbitrary surfaces. *Advanced Materials*, *23*, 3938–3943.
- [149] Bae, S., Kim, H., Lee, Y., Xu, X., Park, J. S., Zheng, Y., Balakrishnan, J., Lei, T., Kim, H. R., Song, Y. I., Kim, Y. J., Kim, K. S., Özyilmaz, B., Ahn, J. H., Hong, B. H., Iijima, S. (2010). Roll-to-roll production of 30-inch graphene films for transparent electrodes. *Nature Nanotechnology*, *5*, 574–578.
- [150] Jafri, S. H. M., Carva, K., Widenkvist, E., Blom, T., Sanyal, B., Fransson, J., Eriksson, O., Jansson, U., Grennberg, H., Karis, O. C., Quinlan, R. A., Holloway, B. C., Leifer, K. (2010). Conductivity engineering of graphene by defect formation. *Journal of Physics D: Applied Physics*, *43*, 045404.
- [151] Meyer, J. C., Kisilowski, C., Erni, R., Rossell, M. D., Crommie, M. F., Zettl, A. (2008). Direct imaging of lattice atoms and topological defects in graphene membranes. *Nano Letters*, *8*, 3582–3586.
- [152] Banhart, F., Kotakoski, J., Krashenninikov, A. V. (2011). Structural defects in graphene. *ACS Nano*, *5*, 26–41.

- [153] Zheng, Q., Geng, Y., Wang, S., Li, Z., Kim, J.-K. (2010). Effects of functional groups on the mechanical and wrinkling properties of graphene sheets. *Carbon*, 48, 4315–4322.
- [154] Grantab, R., Shenoy, V. B., Ruoff, R. S. (2010). Anomalous strength characteristics of tilt grain boundaries in graphene. *Science*, 330, 946–948.
- [155] Sen, D., Novoselov, K. S., Reis, P. M., Buehler, M. J. (2010). Tearing graphene sheets from adhesive substrates produces tapered nanoribbons. *Small*, 6, 1108–1110.
- [156] Li, X., Wang, X., Zhang, L., Lee, S., Dai, H. (2008). Chemically derived, ultrasoft graphene nanoribbon semiconductors. *Science*, 319, 1229–1232.
- [157] Jiao, L., Zhang, L., Wang, X., Diankov, G., Dai, H. (2009). Narrow graphene nanoribbons from carbon nanotubes. *Nature*, 458, 877–880.
- [158] Kosynkin, D. V., Higginbotham, A. L., Sinitskii, A., Lomeda, J., Dimiev, A., Price, B. K., Tour, J. M. (2009). Longitudinal unzipping of carbon nanotubes to form graphene nanoribbons. *Nature*, 458, 872–876.
- [159] Clar, E., Ironside, C. T. (1958). Hexabenzocoronene. *Proceedings of the Chemical Society*, 150.
- [160] Wu, J. S., Pisula, W., Müllen, K. (2007). Graphene as potential material for electronics. *Chemical Reviews*, 107, 718–747.
- [161] Zhi, Z., Müllen, K. (2008). A bottom-up approach from molecular nanographenes to unconventional carbon materials. *Journal of Materials Chemistry*, 18, 1447–1484.
- [162] Simpson, C. D., Brand, J. D., Berresheim, A. J., Przybilla, L., Räder, H. J., Müllen, K. (2002). Synthesis of a giant 222 carbon graphite sheet. *Chemistry – A European Journal*, 8, 1424–1429.
- [163] Wu, J., Grimdale, A. C., Müllen, K. (2005). Combining one-, two- and three-dimensional polyphenylene nanostructures. *Journal of Materials Chemistry*, 15, 41–52.
- [164] Wu, J., Gherghel, L., Watson, M. D., Li, J., Wang, Z., Simpson, C. D., Kolb, U., Müllen, K. (2003). From branched polyphenylenes to graphite ribbons. *Macromolecules*, 36, 7082–7089.
- [165] Yang, X. Y., Dou, X., Rouhanipour, A., Zhi, L. J., Räder, H. J., Müllen, K. (2008). Two-dimensional graphene nanoribbons. *Journal of the American Chemical Society*, 130, 4216–4217.
- [166] Englert, J. M., Hirsch, A., Feng, X., Müllen, K. (2011). Chemical methods for the generation of graphenes and graphene nanoribbons. *Angewandte Chemie—International Edition*, DFG special edition, A17–A24, DOI: 10.002/anie.201105813.
- [167] Andersson, C.-H., Grennberg, H. (2009). Reproducibility and efficiency of carbon nanotube end-group generation and functionalization. *European Journal of Organic Chemistry*, 4421–4428.
- [168] Ruoff, R. S., Tse, D. S., Malhotra, R., Lorents, D. C. (1993). Solubility of fullerene (C₆₀) in a variety of solvents. *The Journal of Physical Chemistry*, 97, 3379–3383.
- [169] Bergin, S. D., Nicolosi, V., Streich, P. V., Giordani, S., Sun, Z., Windle, A. H., Ryan, P., Niraj, N. P. P., Wang, Z.-T. T., Carpenter, L., Blau, W. J., Boland, J. J., Hamilton, J. P., Coleman, J. N. (2008). Towards solutions of single-walled carbon nanotubes in common solvents. *Advanced Materials*, 20, 1876–1881.
- [170] Boukhvalov, D. W., Katsnelson, M. I. (2009). Chemical functionalization of graphene. *Journal of Physics: Condensed Matter*, 21, 344205 (12 pp).
- [171] Zheng, Q., Geng, Y., Wang, S., Li, Z., Kim, J.-K. (2010). Fabrication of highly conducting and transparent graphene films. *Carbon*, 48, 1815–1823.
- [172] Fowler, P. W., Ceulemans, A. (1995). Electron deficiency of the fullerenes. *The Journal of Physical Chemistry*, 99, 508–510.
- [173] Lu, X., Chen, Z. (2005). Curved pi-conjugation, aromaticity and the related chemistry of small fullerenes (<C₆₀) and single-walled carbon nanotubes. *Chemical Reviews*, 105, 3643–3696.

- [174] Li, J., Zhang, G., Chen, Y. (2006). Bond-curvature effect of sidewall [2+1] cycloadditions of single-walled carbon nanotubes: A new criterion to the adduct structures. *Journal of the American Chemical Society*, *127*, 1541–1547.
- [175] Miyata, Y., Kawai, T., Miyamoto, Y., Yanagi, K., Maniwa, Y., Katahura, H. (2007). Chirality-dependent combustion of single-walled carbon nanotubes. *The Journal of Physical Chemistry C*, *111*, 9671–9677.
- [176] Miyata, Y., Kawai, T., Miyamoto, Y., Yanagi, K., Maniwa, Y., Katahura, H. (2007). Bond-curvature effect on burning of single-wall nanotubes. *Physica Status Solidi (B)*, *244*, 4035–4039.
- [177] Kawai, T., Miyamoto, Y. (2008). Chirality-dependent C-C bond breaking of carbon nanotubes by cyclo-addition of oxygen molecule. *Chemical Physics Letters*, *453*, 256–261.
- [178] Kim, S. N., Rusling, J. F., Papadimitrakopoulos, F. (2007). Carbon nanotubes for electronic and electrochemical detection of biomolecules. *Advanced Materials*, *19*, 3214–3228.
- [179] Zhang, J., Zhou, H., Qing, Q., Yng, Y., Li, Q., Liu, Z., Guo, X., Du, Z. (2003). Effect of chemical oxidation on the structure of single-walled carbon nanotubes. *The Journal of Physical Chemistry B*, *107*, 3712–3718.
- [180] Banerjee, S., Kahn, M. G. C., Wong, S. S. (2003). Rational strategies for carbon nanotube functionalization. *Chemistry—A European Journal*, *9*, 1898–1908.
- [181] Balasubramanian, K., Burghard, M. (2005). Chemically functionalized carbon nanotubes. *Small*, *1*, 180–192.
- [182] Banerjee, S., Hemraj-Benny, T., Wong, S. S. (2005). Covalent surface chemistry of single-walled carbon nanotubes. *Advanced Materials*, *17*, 17–29.
- [183] Georgakilas, V., Otyepka, M., Bourlinos, A. B., Chandra, V., Kim, N., Kemp, K. C., Hobza, P., Zboril, R., Kim, K. S. (2012). Functionalization of graphene: Covalent and non-covalent approaches, derivatives and applications. *Chemical Reviews*, *112*, 6156–6214.
- [184] Guo, S., Dong, S. (2011). Graphene nanosheet: Synthesis, molecular engineering, thin film, hybrids, and energy and analytical applications. *Chemical Society Reviews*, *40*, 2644–2672.
- [185] Chen, J., Hamon, M. A., Hu, H., Chen, Y., Rao, A. M., Eklund, P. C., Haddon, R. C. (1998). Solution properties of single-walled carbon nanotubes. *Science*, *282*, 95–98.
- [186] Hamon, M. A., Chen, J., Hu, H., Chen, Y., Itkis, M. E., Rao, A. M., Eklund, P. C., Haddon, R. C. (1999). Dissolution of single-walled carbon nanotubes. *Advanced Materials*, *11*, 834–840.
- [187] Worsley, K. A., Kalinia, I., Bekyarova, E., Haddon, R. C. (2009). Functionalization and dissolution of nitric acid treated single-walled carbon nanotubes. *Journal of the American Chemical Society*, *131*, 18153–18158.
- [188] Huang, W., Fernando, S., Allard, L. F., Sun, Y.-P. (2003). Solubilization of single-walled carbon nanotubes with diamine-terminated oligomeric poly(ethylene glycol) in different functionalization reactions. *Nano Letters*, *3*, 565–568.
- [189] Zhou, B., Lin, Y., Li, H., Huang, W., Connell, J. W., Allard, L. F., Sun, Y.-P. (2003). Absorptivity of functionalized single-walled carbon nanotubes in solution. *The Journal of Physical Chemistry B*, *107*, 13588–13592.
- [190] Stephenson, J. J., Hudson, J. L., Leonard, A. D., Price, B. K., Tour, J. M. (2007). Repetitive functionalization of water-soluble single-walled carbon nanotubes. Addition of acid-sensitive addends. *Chemistry of Materials*, *19*, 3491–3498.
- [191] Qin, Y., Shi, J., Wu, W., Li, X., Guo, Z.-X., Zhu, D. (2003). Concise route to functionalized carbon nanotubes. *The Journal of Physical Chemistry B*, *107*, 12899–12901.
- [192] Widenkvist, E., Li, J., Jansson, U., Grennberg, H. (2007). Selected area deposition of multi-walled carbon nanotubes from solution. *Carbon*, *45*, 2732–2736.
- [193] Liu, J., Rinzler, A. G., Dai, H., Hafner, J. H., Bradley, R. K., Boul, P. J., Lu, A., Iverson, T., Shelimov, K., Huffman, C. B., Rodrigues-Macias, F., Shon, Y.-S., Lee, T. R., Colbert, D. T., Smalley, R. E. (1998). Fullerene pipes. *Science*, *280*, 1253–1256.

- [194] Hong, S. Y., Tobias, G., Ballesteros, B., El Oualid, F., Errey, J. C., Doores, K. J., Kirkland, A. I., Nellist, P. D., Green, M. L. H., Davis, B. G. (2007). Atom-scale detection of organic molecules coupled to single-walled carbon nanotubes. *Journal of the American Chemical Society*, *129*, 10966–10967.
- [195] Yang, Y., Saini, R. K., Sadana, A. K., Billups, W. E. (2003). Functionalization of carbon nanotubes by free radicals. *Organic Letters*, *5*, 1471–1473.
- [196] Peng, H., Reverdy, P., Khabashesku, V. N., Margrave, J. L. (2003). Sidewall functionalization of single-walled carbon nanotubes with organic peroxides. *Chemical Communications*, 362–363.
- [197] Linang, F., Sadana, A. K., Peera, A., Chattopadhyaya, J., Gu, Z., Hague, R. H., Billups, W. E. (2004). A convenient route to functionalized carbon nanotubes. *Nano Letters*, *4*, 1257–1260.
- [198] Wunderlich, D., Hauke, F., Hirsch, A. (2008). Preferred functionalization of metallic and small-diameter single-walled carbon nanotubes via reductive alkylation. *Journal of Materials Chemistry*, *18*, 1493–1497.
- [199] Chattopadhyaya, J., de Cortez, F., Chakaborty, S., Slater, N. K. H., Billups, W. E. (2006). Synthesis of water-soluble PEGylated single-walled carbon nanotubes. *Chemistry of Materials*, *18*, 5864–5868.
- [200] Bahr, J. L., Tour, J. M. (2001). Highly functionalized carbon nanotubes using *in situ* generated diazonium compounds. *Chemistry of Materials*, *13*, 3823–3824.
- [201] Dyke, C. A., Stewart, M. P., Maya, F., Tour, J. M. (2004). Diazonium-based functionalization of carbon nanotubes: XPS and GC-MS analysis and mechanistic implications. *Synlett*, 155–160.
- [202] Dyke, C. A., Tour, J. M. (2004). Covalent functionalization of single-walled carbon nanotubes for materials applications. *The Journal of Physical Chemistry A*, *108*, 11151–11159.
- [203] Dyke, C. A., Tour, J. M. (2004). Overcoming the insolubility of carbon nanotubes through high degrees of sidewall functionalization. *Chemistry—A European Journal*, *10*, 812–817.
- [204] Song, C., Kwon, T., Han, J.-H., Shandell, M., Strano, M. S. (2009). Controllable synthesis of single-walled carbon nanotube framework membranes and capsules. *Nano Letters*, *9*, 4279–4284.
- [205] Li, H., Cheng, F., Duft, A. M., Adronov, A. (2005). Functionalization of single-walled carbon nanotubes with well-defined polystyrene by “click” coupling. *Journal of the American Chemical Society*, *127*, 14518–14521.
- [206] Tuci, G., Vinattieri, C., Luconi, L., Ceppatelli, M., Cicci, S., Brandi, A., Filippi, J., Melucci, M., Giambastini, G. (2012). “Click” on tubes: A versatile approach towards multimodal functionalization of SWCNTs. *Chemistry—A European Journal*, *18*, 8454–8463.
- [207] Hirsch, A., Brettreich, M. *Fullerenes: Chemistry and Reactions*, Wiley-VCH, Weinheim, 2005.
- [208] Yurovskaya, M. A., Trushkov, I. V. (2002). Cycloadditions to buckminsterfullerene C₆₀: Advancements and future prospects. *Russian Chemical Bulletin International Edition*, *51*, 367–443.
- [209] Tasis, D., Tagmatarchis, N., Bianco, A., Prato, M. (2006). Chemistry of carbon nanotubes. *Chemical Reviews*, *106*, 1105–1136.
- [210] Prato, M., Maggini, M. (1998). Fulleropyrrolidines: A family of full-fledged fullerene derivatives. *Accounts of Chemical Research*, *31*, 519–526.
- [211] Li, J., Grennberg, H. (2006). Microwave-assisted covalent sidewall functionalization of multiwalled carbon nanotubes. *Chemistry—A European Journal*, *12*, 3869–3875.
- [212] Wang, F., Swager, T. M. (2011). Diverse chemiresistors based upon covalently modified multiwalled carbon nanotubes. *Journal of the American Chemical Society*, *133*, 11181–11193.

- [213] Herranz, M. A., Martín, N. Noncovalent functionalization of carbon nanotubes. In *Carbon Nanotubes and Related Structures*, Guldi, D. M., Martín, N. (Eds.), Wiley-VCH, Weinheim, 2010; pp. 103–134.
- [214] Chen, R. J., Zhang, Y., Wang, D., Dai, H. (2001). Noncovalent sidewall functionalization of single-walled carbon nanotubes for protein immobilization. *Journal of the American Chemical Society*, *123*, 3838–3839.
- [215] Guldi, D. M., Aminur Rahman, G. M., Jux, N., Balbinot, D., Hartnagel, U., Tagmatarchis, N., Prato, M. (2005). Functional single-wall carbon nanotube nanohybrids associating SWNTs with water-soluble enzyme model systems. *Journal of the American Chemical Society*, *127*, 9830–9838.
- [216] Wang, H., Gu, L., Lin, Y., Lu, F., Mezziani, M. J., Luo, P. G., Wang, W., Cao, L., Sun, Y.-P. (2006). Unique aggregation of Anthrax (*Bacillus anthracis*) spores by sugar-coated single-walled carbon nanotubes. *Journal of the American Chemical Society*, *128*, 13364–13365.
- [217] Zhao, Y.-L., Hu, L., Stoddart, J. F., Grüner, G. (2008). Pyrenecyclodextrin-decorated single-walled carbon nanotube field-effect transistors as chemical sensors. *Advanced Materials*, *20*, 1910–1915.
- [218] Andersson, C.-H., Lahmann, M., Oscarson, S., Grennberg, H. (2009). Reversible non-covalent derivatisation of carbon nanotubes with glycosides. *Soft Matter*, *5*, 2713–2716.
- [219] Xue, C.-H., Zhou, R.-J., Shi, M.-M., Gao, Y., Wu, G., Zhang, X.-B., Chen, H.-Z., Wang, M. (2008). The preparation of highly water-soluble multi-walled carbon nanotubes by irreversible noncovalent functionalization with a pyrene-carrying polymer. *Nanotechnology*, *19*, 215604 (7 pp).
- [220] Yan, Y., Cui, J., Zhao, S., Zhang, J., Liu, J., Cheng, J. (2012). Interface molecular engineering of single-walled carbon nanotube/epoxy composites. *Journal of Materials Chemistry*, *22*, 1928–1936.
- [221] Guldi, D. M., Menna, F., Maggini, M., Maraccio, M., Paolucci, D., Paolucci, F., Campidelli, S., Prato, M., Rahman, G. M. A., Schergna, S. (2006). Supramolecular hybrids of [60]fullerene and single-wall carbon nanotubes. *Chemistry—A European Journal*, *12*, 3975–3983.
- [222] Ehli, C., Rahman, G. M. A., Jux, N., Balbinot, D., Guldi, D. M., Paolucci, F., Maraccio, M., Paolucci, D., Melle-Franco, M., Zerbetto, F., Campidelli, S., Prato, M. (2006). Interactions in single wall carbon nanotubes/pyrene/porphyrin nanohybrids. *Journal of the American Chemical Society*, *128*, 11222–11231.
- [223] Ehli, C., Guldi, D. M., Herranz, M. A., Martín, N., Campidelli, S., Prato, M. (2008). Pyrene-tetrathiafulvalene supramolecular assembly with different types of carbon nanotubes. *Journal of Materials Chemistry*, *18*, 1498–1503.
- [224] Wurl, A., Goossen, S., Canevet, D., Sallé, M., Péres, E. M., Martín, N., Klinke, C. (2012). Supramolecular interaction of single-walled carbon nanotubes with a functional TTF-based mediator probed by field-effect transistor devices. *The Journal of Physical Chemistry C*, *116*, 20062–20066.
- [225] Romero-Nieto, C., García, R., Herranz, M. A., Ehli, C., Ruppert, M., Hirsch, A., Guldi, D. M., Martín, N. (2012). Tetrathiafulvalene-based nanotweezers—noncovalent binding of carbon nanotubes in aqueous media with charge transfer implications. *Journal of the American Chemical Society*, *134*, 9183–9192.
- [226] Webb, M. J., Palmgren, P., Pal, P., Karis, O., Grennberg, H. (2011). A simple method to produce almost perfect graphene on highly ordered pyrolytic graphite. *Carbon*, *49*, 3242–3249.
- [227] Lundstedt, A., Webb, M. J., Grennberg, H. Manuscript.
- [228] Sanyal, B., Eriksson, O., Jansson, U., Grennberg, H. (2009). Molecular adsorption in defected graphene. *Physical Review B*, *79*, 113409.
- [229] Bergson, G., Lundstedt, A., Palmkvist, P., Widenkvist, E., Jansson, U., Grennberg, H. Manuscript.

- [230] Colman, V. A., Knut, R., Karis, O., Grennberg, H., Jansson, U., Quinlan, R., Holloway, B. C., Sanyal, B., Eriksson, O. (2008). Defect formation in graphene nano-sheets by acid treatment: An X-ray absorption and density functional study. *Journal of Physics D: Applied Physics*, *41*, 062001.
- [231] López de la Torre, M. D., Guijarro, M. M. (2012). Covalent bonds on activated carbons. *European Journal of Organic Chemistry*, 5147–5154.
- [232] An, S. J., Zhu, Y., Lee, S. H., Stoller, M. D., Emilsson, T., Park, S., Velamakanni, A., Ho, J., Ruoff, R. S. (2010). Thin film fabrication and simultaneous anodic reduction of deposited graphene oxide platelets by electrophoretic deposition. *Journal of Physical Chemistry Letters*, *1*, 1259–1262.
- [233] Compton, O. C., Nguyen, S. T. (2010). Graphene oxide, highly reduced graphene oxide and graphene: Versatile building blocks for carbon-based materials. *Small*, *6*, 711–723.
- [234] Swager, T. M. (2012). Functional graphene: Top-down chemistry of the pi-surface. *ACS Macro Letters*, *1*, 3–5.
- [235] Špitalsky, Z., Danko, M., Mosnaček, J. (2011). Preparation of functionalized graphene sheets. *Current Organic Chemistry*, *15*, 1133–1150.
- [236] Elias, D. C., Nair, R. R., Mohiuddin, T. M. G., Morozov, S. V., Blake, P., Halsall, M. P., Ferrari, A., Boukhvalov, D. W., Katsnelson, M. I., Geim, A. K., Novoselov, K. S. (2009). Control of graphene's properties by reversible hydrogenation: Evidence for graphane. *Science*, *323*, 610–613.
- [237] Boukhvalov, D. W. (2011). Modelling of epitaxial graphene functionalization. *Nanotechnology*, *22*, 055708 (5 pp).
- [238] Yang, Z., Sun, Y., Alemany, L. B., Narayanan, T. N., Billups, W. E. (2012). Birch reduction of graphite. Edge and interior functionalization by hydrogen. *Journal of the American Chemical Society*, *134*, 18689–18694.
- [239] Kariuki, J. K., McDermott, M. T. (1999). Nucleation and growth of functionalized aryl films on graphite electrodes. *Langmuir*, *15*, 6534–6540.
- [240] Sharma, R., Bail, J. H., Perera, C. J., Strano, M. S. (2010). Anomalously large reactivity of single graphene layers and edges towards electron transfer chemistries. *Nano Letters*, *10*, 398–405.
- [241] Lomeda, J. R., Doyle, C. D., Kosynkin, D. V., Hwang, W.-F., Tour, J. M. (2008). Diazonium functionalization of surfactant-wrapped chemically converted graphene sheets. *Journal of the American Chemical Society*, *130*, 16201–16206.
- [242] Lim, H., Lee, J. S., Shin, H. J., Shin, H. S., Choi, H. C. (2010). Spatially resolved spontaneous reactivity of diazonium salt on edge and basal plane of graphene without surfactant and its doping effect. *Langmuir*, *26*, 12278–12284.
- [243] Bekyarova, E., Itkis, M. E., Ramesh, P., Berger, C., Sprinkle, M., de Heer, W. A., Haddon, R. C. (2009). Chemical modification of epitaxial graphene: Spontaneous grafting of aryl groups. *Journal of the American Chemical Society*, *131*, 1336–1337.
- [244] Sun, S., Kohama, S., Zhang, Z., Lomeda, J. R., Tour, J. M. (2010). Soluble graphene through edge-selective functionalization. *Nano Research*, *3*, 117–125.
- [245] Zhu, Y., Higginbotham, A. L., Tour, J. M. (2009). Covalent functionalization of surfactant-wrapped graphene nanoribbons. *Chemistry of Materials*, *21*, 5284–5291.
- [246] Chua, C. K., Pumera, M. (2012). Friedel–Crafts acylation of graphene. *Chemistry—An Asian Journal*, *7*, 1009–1012.
- [247] Ma, X., Li, F., Wang, Y., Hu, A. (2012). Functionalization of pristine graphene with conjugated polymers through diradical addition and propagation. *Chemistry—An Asian Journal*, *7*, 2527–2550.
- [248] Liu, L.-H., Lerner, M. M., Yan, M. (2010). Derivatization of pristine graphene with well-defined chemical functionalities. *Nano Letters*, *10*, 3754–3756.

- [249] Quintana, M., Spyrou, K., Grzelczak, M., Browne, W. R., Rudolf, P., Prato, M. (2010). Functionalization of graphene *via* 1,3-dipolar cycloaddition. *ACS Nano*, 4, 3527–3533.
- [250] Zhang, X., Hou, L., Cnossen, A., Coleman, A. C., Ivashenko, O., Rudolf, P., van Wees, B. J., Browne, W. R., Feringa, B. L. (2011). One-pot functionalization of graphene with porphyrin through cycloaddition reactions. *Chemistry—A European Journal*, 17, 8957–8964.
- [251] Georgakilas, V., Bourlinos, A. B., Zboril, R., Steriotis, T. A., Dallas, P., Stubos, A. K., Trapalis, C. (2010). Organic functionalization of graphene. *Chemical Communications*, 46, 1766–1768.
- [252] Kozlov, S. M., Vines, F., Görling, A. (2012). On the interaction of polycyclic aromatic compounds with graphene. *Carbon*, 50, 2482–2492.
- [253] Gosh, A., Rao, K. V., Voggu, R., George, S. J. (2010). Non-covalent functionalization, solubilization of graphene and single-walled carbon nanotubes with aromatic donor and acceptor molecules. *Chemical Physics Letters*, 488, 198–201.
- [254] Subrahmanyam, K. S., Ghosh, A., Gomathi, A., Govindaraj, A., Rao, C. N. R. (2009). Covalent and noncovalent functionalization and solubilization of graphene. *Nanoscience and Nanotechnology Letters*, 1, 28–31.
- [255] Manna, A. K., Pati, S. K. (2009). Tuning the electronic structure of graphene by molecular charge transfer: A computational study. *Chemistry—An Asian Journal*, 4, 855–860.
- [256] Zhang, Y.-H., Zhou, K.-G., Xie, K.-F., Zeng, J., Zhang, H.-L., Peng, Y. (2010). Tuning the electronic structure and transport of graphene by noncovalent functionalization: Effects of organic donor, acceptor and metal atoms. *Nanotechnology*, 21, 065201 (7 pp).
- [257] Tu, W., Lei, J., Zhang, S., Ju, H. (2010). Characterization, direct electrochemistry, and amperometric biosensing of graphene by non-covalent functionalization with picket-fence porphyrin. *Chemistry—A European Journal*, 16, 10771–10777.
- [258] Lin, J., Teweldebrhan, D., Ashraf, K., Liu, G., Jing, X., Yan, Z., Li, R., Ozkan, M., Lake, R. K., Balandin, A. A., Ozkan, C. S. (2010). Gating of single-layer graphene with single-stranded deoxyribonucleic acids. *Small*, 6, 1150–1155.
- [259] Wang, X., Tabakman, S. M., Dai, H. (2008). Atomic layer deposition of metal oxides on pristine and functionalized graphene. *Journal of the American Chemical Society*, 130, 8152–8153.
- [260] Pollard, A. J., Perkins, E. W., Smith, N. A., Saywell, A., Goretzki, G., Phillips, A. G., Argent, S. P., Sachdev, H., Müller, F., Hüfner, S., Gsell, S., Fischer, M., Schreck, M., Osterwalder, J., Greber, T., Berner, S., Champness, N. R., Beton, P. H. (2010). Supramolecular assemblies on an epitaxial graphene superstructure. *Angewandte Chemie—International Edition*, 49, 1794–1799.
- [261] Naidoo, Q.-L., Naidoo, S., Petrik, L., Nechaev, A., Ndungu, P. (2010). The influence of carbon-based supports and the role of synthetic procedures on the formation of platinum and platinum-ruthenium clusters and nanoparticles for the development of highly active fuel cell catalysts. *International Journal of Hydrogen Energy*, 37, 9459–9469.
- [262] Figueiredo, J. L., Pereira, M. F. R., Serp, P., Kalck, P., Samant, P. M., Fernandes, J. B. (2006). Development of carbon nanotube and carbon xerogel supported catalysts for the electro-oxidation of methanol in fuel cells. *Carbon*, 44, 2516–2522.
- [263] Wu, H.-Q., Cao, Y.-J., Yuan, P.-S., Xu, H.-Y., Wei, X.-W. (2005). Controlled synthesis, structure and magnetic properties of $\text{Fe}_{1-x}\text{Ni}_x$ alloy nanoparticles attached on carbon nanotubes. *Chemical Physics Letters*, 406, 148–153.
- [264] Banerjee, S., Wong, S. S. (2004). In-situ growth of “fused” ozonized single-walled carbon nanotube—CdTe quantum dot junctions. *Advanced Materials*, 16, 34–37.
- [265] Wei, X.-W., Song, X.-J., Xu, J., Ni, Y.-H., Zhang, P. (2005). Coating multi-walled carbon nanotubes with metal sulphides. *Materials Chemistry and Physics*, 92, 159–163.

- [266] Haremza, J. M., Hahn, M. A., Krauss, T. D., Chen, S., Calcines, J. (2002). Attachment of single CdSe nanocrystals to individual single-walled carbon nanotubes. *Nano Letters*, 2, 1253–1258.
- [267] Lemus-Yegres, L., Such-Basáñez, I., Salinas-Martínez de Lecea, C., Serp, P., Román-Martínez, M. C. (2006). Exploiting the surface –OH groups on activated carbons and carbon nanotubes for the immobilization of a Rh complex. *Carbon*, 44, 605–608.
- [268] Rooth, M., Quinlan, R., Widenkvist, E., Lu, J., Grennberg, H., Holloway, B. C., Hårsta, A., Jansson, U. (2009). Atomic layer deposition of titanium dioxide nanostructures using carbon nanosheets as a template. *Journal of Crystal Growth*, 311, 373–377.
- [269] Azamian, B. R., Coleman, K. S., Davis, J. J., Hanson, N., Green, M. L. H. (2002). Directly observed covalent coupling of quantum dots to single-walled carbon nanotubes. *Chemical Communications*, 366–367.
- [270] Sainsbury, T., Stolarczyk, J., Fitzmaurice, D. (2005). An experimental and theoretical study of the self-assembly of gold nanoparticles at the surface of functionalized multiwalled carbon nanotubes. *The Journal of Physical Chemistry B*, 109, 16310–16325.
- [271] Liu, L., Wang, T., Li, J., Guo, Z.-X., Dai, L., Zhang, D., Zhu, D. (2003). Self-assembly of gold nanoparticles to carbon nanotubes using a thiol-terminated pyrene as interlinker. *Chemical Physics Letters*, 367, 747–752.
- [272] Zhou, H., Qiu, C., Liu, Z., Yang, H., Hu, L., Liu, J., Yang, H., Gu, C., Sun, L. (2009). Thickness-dependent morphologies of gold on n-layer graphene. *Journal of the American Chemical Society*, 132, 944–946.
- [273] Yang, W., Widenkvist, E., Lu, J., Jansson, U., Grennberg, H. Manuscript.
- [274] Grumelli, D., Vericat, C., Benitez, G., Vela, M. E., Salvarezza, R. C., Giovanetti, L. J., Ramallo-López, J. M., Requejo, F. G., Craievich, A. F., Shon, Y. S. (2007). Thiol-capped gold nanoparticles on graphite: Spontaneous adsorption and electrochemically induced release. *The Journal of Physical Chemistry C*, 111, 7179–7184.
- [275] Hadjiev, V. G., Iliev, M. N., Arepalli, S., Nikolaev, P., Files, B. S. (2001). Raman scattering test of single-wall carbon nanotube composites. *Applied Physics Letters*, 78, 3193–3195.
- [276] Ramanathan, T., Abdala, A. A., Stankovich, S., Dikin, D. A., Herrera-Alonso, M., Piner, R. D., Adamson, D. H., Schniepp, H. C., Chen, X., Ruoff, R. S., Nguyen, S. T., Aksay, I. A., Prud'homme, R. K., Brinson, L. C. (2008). Functional graphene sheets for polymer nanocomposites. *Nature Nanotechnology*, 5, 327–331.
- [277] Charlier, J.-C. (2002). Defects in carbon nanotubes. *Accounts of Chemical Research*, 35, 1063–1069.
- [278] Sun, X., Liu, Z., Welscher, K., Robinson, J. T., Goodwin, A., Zaric, S., Dai, H. (2008). Nanographene oxide for cellular imaging and drug delivery. *Nano Research*, 1, 203–212.
- [279] Liu, Z., Robinson, J. T., Sun, X., Dai, H. (2008). PEGylated nanographene oxide for delivery of water-insoluble cancer drugs. *Journal of the American Chemical Society*, 130, 10876–10877.
- [280] Prato, M., Kostarelos, K., Bianco, A. (2007). Functionalized carbon nanotubes in drug design and discovery. *Accounts of Chemical Research*, 41, 60–68.
- [281] Do Nascimento, G. M., de Oliveira, R. C., Pradie, N. A., Gessolo Lins, P. R., Worfe, P. R., Martinez, G. R., Di Mascio, P., Dresselhaus, M. S., Corio, P. (2010). Single-wall carbon nanotubes modified with organic dyes: Synthesis, characterization and potential cytotoxic effects. *Journal of Photochemistry and Photobiology A: Chemistry*, 211, 99–117.
- [282] Ciraci, S., Dag, S., Yildrin, T., Gulseren, O., Senger, R. T. (2004). Functionalized carbon nanotubes and device applications. *Journal of Physics. Condensed Matter*, 16, R901–R960.
- [283] Johnston, D. E., Islam, M. F., Yodh, A. G., Johnston, A. T. (2005). Electronic devices based on purified carbon nanotubes grown by high-pressure decomposition of carbon monoxide. *Nature Materials*, 4, 589–592.

- [284] Wang, C., Cao, Q., Gaur, A., Rogers, J. A., Shim, M. (2005). Electronically selective functionalization of carbon nanotubes: Correlation between Raman spectral and electrical responses. *Journal of the American Chemical Society*, *127*, 11460–11468.
- [285] Rouhi, N., Jain, D., Burke, P. J. (2011). High-performance semiconducting nanotube inks: Progress and prospects. *ACS Nano*, *5*, 8471–8487.
- [286] Liu, Z., Zhang, Z.-B., Chen, Q., Zheng, L.-R., Zhang, S.-L. (2011). Solution-processable nanotube/polymer composite for high-performance TFTs. *IEEE Electron Device Letters*, *32*, 1299–1301.
- [287] Liu, Z., Li, H., Qiu, Z., Zhang, S.-L., Zhang, Z.-B. (2012). SMALL-hysteresis thin film transistors achieved by facile dip-coating of nanotube/polymer composite. *Advanced Materials*, *24*, 3633–3638.
- [288] De Catelle, A. (2012). Purified single walled carbon nanotubes for application in field-effect thin-film transistors. BSc thesis in Chemistry, Uppsala University UPKEM-24.
- [289] Shin, K.-Y., Hong, J.-Y., Jang, J. (2011). Flexible and transparent graphene films as acoustic actuator electrodes using inkjet printing. *Chemical Communications*, *47*, 8527–8529.
- [290] Brooks, A. J., Lim, H., Kilduff, J. E. (2012). Adsorption uptake of synthetic organic chemicals by carbon nanotubes and activated carbons. *Nanotechnology*, *23*, 294008 (13 pp).
- [291] Li, X., Chen, G. (2009). Surface modified graphite nanosheets used as adsorbent to remove 1,2-dichlorobenzene from water. *Materials Letters*, *63*, 930–932.
- [292] Wehling, T. O., Novoselov, K. S., Morozov, S. V., Vdovin, E. E., Katsnelson, M. I., Geim, A. K., Lichtenstein, A. I. (2008). Molecular doping of graphene. *Nano Letters*, *8*, 173–177.
- [293] Liu, F. L., Xiao, H. L., Fang, H. L., Dai, H. F., Quiao, L., Zhang, Y. H. (2011). Single-walled carbon nanotube-based biosensors for detection of volatile organic compounds of lung cancer. *Physica E*, *44*, 367–372.
- [294] Fowler, J. D., Allen, M. J., Tung, V. C., Yang, Y., Kaner, R. B., Weiller, B. H. (2009). Practical chemical sensors from chemically derived graphene. *ACS Nano*, *3*, 301–306.
- [295] Goh, M. S., Pumera, M. (2010). The electrochemical response of graphene sheets is independent of the number of layers from a single graphene sheet to multilayer stacked graphene platelets. *Chemistry—An Asian Journal*, *5*, 2355–2357.
- [296] Ahmed, M. U., Hossain, M. M., Tamiya, E. (2007). Electrochemical biosensors for medical and food applications. *Electroanalysis*, *20*, 616–626.
- [297] Kong, L., Wang, J., Meng, F., Chen, X., Jin, Z., Li, M., Liu, J., Huang, X.-J. (2011). Novel hybridized SWCNT-PCD: Synthesis and host-guest inclusion for electrical sensing recognition of persistent organic pollutants. *Journal of Materials Chemistry*, *21*, 11109–11115.
- [298] Anantram, M. P., Léonard, F. (2006). Physics of carbon nanotube electronic devices. *Reports on Progress in Physics*, *69*, 507–561.
- [299] Frank, S., Poncharal, P., Wang, Z. L., De Heer, W. A. (1998). Carbon nanotube quantum resistors. *Science*, *280*, 1744–1746.
- [300] Ouyang, M., Huang, J., Leiber, C. M. (2002). Fundamental electronic properties and applications of single-walled carbon nanotubes. *Accounts of Chemical Research*, *35*, 1018–1025.
- [301] Chen, R. J., Bangsaruntip, S., Drouvalkis, K. A., Kam, N. W. S., Shim, M., Li, Y., Kim, W., Utz, P. J., Dai, H. (2003). Noncovalent functionalization of carbon nanotubes for highly specific biosensors. *Proceedings of the National Academy of Sciences of the United States of America*, *100*, 4984–4989.
- [302] Byon, H. R., Choi, H. C. (2006). Network single-walled carbon nanotube-field effect transistors (SWNT-FETs) with increased Schottky contact area for highly sensitive biosensor applications. *Journal of the American Chemical Society*, *128*, 2188–2189.
- [303] Star, A., Tu, E., Niemann, J., Gabriel, J.-C. P., Joiner, C. S., Valcke, C. (2006). Label-free detection of DNA hybridization using carbon nanotube network field-effect transistors. *Proceedings of the National Academy of Sciences of the United States of America*, *103*, 921–926.

- [304] Kymakis, E. Photovoltaic devices based on carbon nanotubes and related structures. In *Carbon Nanotubes and Related Structures*, Guldi, D. M., Martín, N. (Eds.), Wiley-VCH, Weinheim, 2010; pp. 291–303.
- [305] Sgobba, V., Guldi, D. M. (2009). Carbon nanotubes—Electronic/electrochemical properties and application for nanoelectronics and photonics. *Chemical Society Reviews*, 38, 165–184.
- [306] Valentini, L., Cardinali, M., Bittolo Bon, S., Bagnis, D., Verdejo, R., Lopez-Manchado, M. A., Kenny, J. M. (2010). Use of butylamine modified graphene sheets in polymer solar cell. *Journal of Materials Chemistry*, 20, 995–1000.
- [307] Wang, S., Goh, B. M., Manga, K. K., Bao, Q., Yang, P., Loh, K. P. (2010). Graphene as atomic template and structural scaffold in the synthesis of graphene-organic hybrid wire with photovoltaic properties. *ACS Nano*, 4, 6180–6186.
- [308] Lin, C.-F., Zhang, M., Liu, S.-W., Chiu, T.-L., Lee, J.-H. (2011). High photoelectric conversion efficiency of metal phthalocyanine/fullerene heterojunction photovoltaic device. *International Journal of Molecular Sciences*, 12, 476–505.
- [309] Imahori, H., Fukuzumi, F. (2004). Porphyrin- and fullerene-based molecular photovoltaic devices. *Advanced Functional Materials*, 14, 525–536.
- [310] Brabec, C. J., Gowrisanker, S., Halls, J. J. M., Laird, D., Jia, S., Williams, S. P. (2010). Polymer-fullerene bulk-heterojunction solar cells. *Advanced Materials*, 22, 3839–3856.
- [311] Becerril, H. A., Mao, J., Liu, Z., Stoltenberg, R. M., Bao, Z., Chen, Y. (2008). Evaluation of solution-processed reduced graphene oxide films as transparent conductors. *ACS Nano*, 2, 463–470.
- [312] Weber, C. M., Eisele, D. M., Rabe, J. P., Liang, Y., Feng, X., Zhi, L., Müllen, K., Lyon, J. L., Williams, R., Vanden Bout, D. A., Stevenson, K. J. (2010). Graphene-based optically transparent electrodes for spectroelectrochemistry in the UV-vis region. *Small*, 6, 184–189.
- [313] Zhang, D., Li, X., Chen, S., Sun, Z., Yin, X. J., Huang, S. (2011). Performance of dye-sensitized solar cells with various carbon nanotube counter electrodes. *Microchimica Acta*, 174, 73–79.

CHAPTER 5

H-BOND-BASED NANOSTRUCTURATION OF SUPRAMOLECULAR ORGANIC MATERIALS

TOMAS MARANGONI and DAVIDE BONIFAZI

5.1 INTRODUCTION

Nowadays, with the term “nanomaterials,” the scientific community intends a class of functional materials characterized at least by one dimension below 100 nm [1]. Such objects can possess a wide variety of shapes, ranging from the more simple spherical shape, characteristic of nanoparticles and nanovesicles, to more complicated architectures such as helices or rosettes [2]. The great interest in this kind of molecular system is mainly centered on the fact that the material properties at the nanoscale can be substantially different from the bulk analogs [3]. Indeed the electronic [4], pharmaceutical [5], and medicinal [6] properties of many materials have proven to be significantly enhanced if opportune and reproducible nanostructuring processes are used. For this purpose, the key concepts proper [7] of supramolecular chemistry [8] have been revealed to be an extremely promising route for the preparation of nanoaggregates providing reproducible structural and functional properties. In this context, strong hope is now deriving from the possibility to control, in a defined way, the assembly of opportunely functionalized molecules exploiting noncovalent interactions such as H-bonds, Van der Waals, or electrostatic interactions [9]. Despite the great efforts undertaken by the scientific community to precisely control soft matter at the macroscopic scale, the precise control and transmission of the molecular properties at the nanoscale or microscale level still remain a difficult and partially unresolved task. Among all the different types of noncovalent interactions, H-bonds have been probably more exhaustively studied and understood. In this context, molecular recognition sites based on multiple H-bonds are one of the most exploited approaches to prepare organic nanostructured materials provided with highly controlled geometric and spatial features,

Organic Synthesis and Molecular Engineering, First Edition.

Edited by Mogens Brøndsted Nielsen.

© 2014 John Wiley & Sons, Inc. Published 2014 by John Wiley & Sons, Inc.

thanks to the high directionality, selectivity, and reversibility characteristics of such multiple interactions. To date, the exploitation of H-bonds as a supramolecular tool for the production of nanostructured materials has led to a wide range of nanostructures possessing different kinds of geometry and properties [10]. This chapter will focus on the most significant developments obtained in the field of H-bond-based supramolecular materials, giving a particular emphasis on the structural relationship between the molecular characteristics and the final self-organized nanostructures.

5.2 GENERAL PRINCIPLES IN H-BONDED SOFT MATTERS

When the bonds that hold together the monomeric units in a polymeric system are constituted by highly directional noncovalent interactions, supramolecular polymers are obtained. Although in the last decades a large number of approaches have been elaborated in order to create complex noncovalent polymeric architectures [10e,g, 11], it was only after the careful design of supramolecular polymers with multiple H-bonds that it was possible to obtain systems showing true polymer-like material properties, both in solution and in the solid state [12]. The great hope revolving around these nanomaterials lies in the possibility to combine in an easy and facile way many of the attractive properties of conventional polymers with the reversibility and dynamicity of the noncovalent bonds. Indeed, many physicochemical properties of these polymeric materials, such as the degree of polymerization and its chain conformations, can be opportunely tuned, modifying the strength of the noncovalent interactions and thus originating adaptable materials capable of responding to external stimuli in a way otherwise impossible for conventional covalent polymers [6, 13]. As a general principle, it is possible to form all the known structures of polymers, such as linear homo- and copolymers, branched structures, or cross-linked networks, using directional complementary couples (such as A-B) or self-complementary units (such as A-A) [10c, 11b, 14]. If a noncovalent association of bifunctional monomers forms the polymer, the degree of polymerization will be determined by the association constant (K_a) of the terminal groups and by the concentration. A strong prerequisite to producing high-molecular-weight macromolecules is therefore the possibility of using monomers characterized by high association constants (a K_a value higher than 10^6 M^{-1} is preferable) [11b, 15].

An additional factor influencing the properties of the resulting supramolecular polymers is the presence of aromatic molecular fragments, which give a planar shape to the single monomeric units, and therefore the possibility of self-assembly and organizing along both sides of the molecular plane [16]. Such kinds of interactions, mostly π - π interactions, result not only in an increase of the K_a of the single monomers (and therefore of the polymerization degree) but also in the formation of much stiff and rod-like morphologies [10e, 17]. Different from the standard polymerization reactions, the extent of supramolecular polymerization is directly coupled to thermodynamic parameters, such as concentration, temperature, and pressure, due to the reversible nature of the involved interactions. Thus, the major mechanisms through which supramolecular polymerization reactions usually undergo are isodesmic [18] and/or cooperative [19]. In the first mechanism, the reversible formation of every single noncovalent bond is thermodynamically identical, and thus, it is characterized by a single association constant (K_a) for each reversible step of the self-assembly process (Figure 5.1a,c).

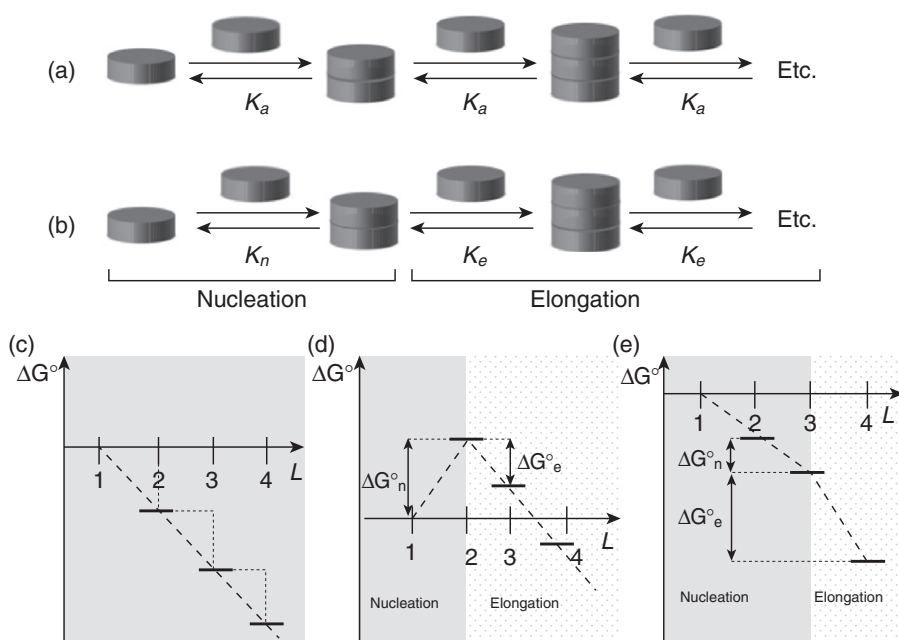


Figure 5.1. Graphic representation of the two principal mechanisms of supramolecular polymerization: (a) isodesmic supramolecular polymerization and (b) cooperative supramolecular polymerization (K_a : association constant, K_n : nucleation constant, K_e : elongation constant). Qualitative energetic diagram of an isodesmic supramolecular polymerization (c) and of the uphill (d) and downhill (e) cooperative supramolecular polymerization. The abscissa represents the supramolecular oligomer size (L) and the ordinate measures the free energy ΔG° in arbitrary units (nucleation zone is reported in gray, elongation zone with small dots, nucleus size is considered as two units in (d) and as three units in (e)).

On the other hand, the cooperative mechanism (Figure 5.1b) occurs in two distinct stages: a first stage known as “nucleation” step, characterized by a linear isodesmic supramolecular polymerization (described by an association constant K_n , describing the association of each monomer with the so-called polymerization nucleus), and a second step known as “elongation phase,” in which the addition of the monomers is governed by a different association constant K_e (elongation constant, $>K_n$). The nucleation step can be further classified in two different categories (Figure 5.1d,e). In the first, also called “uphill polymerization” (Figure 5.1d), the initial supramolecular nucleus possesses a Gibbs free energy higher than that of the monomeric units, thus resulting in an initial thermodynamic instability of the system. In the second (Figure 5.1e), also known as “downhill polymerization,” the supramolecular nucleus has a Gibbs free energy lower than that of the monomer, therefore leading to a thermodynamically more stable supramolecular entity. The stability of the nucleus, in comparison with that of the monomeric units, has been revealed to be highly influenced by the reference state and by parameters such as the monomer concentration, thus giving rise to interconversion between the two pathways [10g]. For a more detailed insight into

the physical principles of the supramolecular polymerization process, the reader is referred to the reviews and works of De Greef and coworkers [10g, 11b, 20].

Due to their high selectivity, directionality, and reversibility [10g, 15b,c, 21], H-bonds are among the most useful noncovalent interactions to self-assemble and self-organize organic molecules into nanostructured materials [15b,c, 22]. In general terms, H-bonds can be defined as noncovalent attractive interactions between a positively charged hydrogen atom bonded to an electronegative atom (defined as H-bond donor D-H) and a negatively charged/polarized atom possessing a lone pair of electrons (the H-bond acceptor A) [21b, 23]. H-bonds can vary in strength from being very weak ($1\text{--}2\text{ kJ mol}^{-1}$) to being among the strongest (161.5 kJ mol^{-1}) noncovalent intermolecular interactions [24]. Multiple H-bonds are directional and complementary and can thus simplify the engineering of specific orientations and interactions between individual H-bond donor and acceptor moieties. The strength of the supramolecular interactions deriving from H-bonds depends on a relevant number of factors such as the solvent, the total number of involved H-bonds, and their spatial disposition into the recognition site. Indeed, thanks to the cooperativity among the H-bonds present in the array, strength, selectivity, and specificity can be increased during the molecular recognition process [25]. As can be intuitively expected, the strength of the interactions arising from the molecular recognition process between two H-bond arrays can be strictly related to the (i) strength of the isolated H-bonds and (ii) the number of H-bonds formed between the two molecular units. While the first of these two factors can be associated with the basicity and acidity of the H-bond donor and acceptor sites, respectively, for (ii) it is possible to state as a general principle that the stability of an H-bond-based complex would be the highest as most of the H-bonds are formed during the molecular recognition process [15c, 26]. In any case, even though it is possible to establish a linear correlation between the number of H-bonds and the free energy association of two molecules [27], this parameter cannot be taken as the only reference principle for the correct evaluation of the strength of interactions into a multiple H-bond system. Indeed, a conspicuous number of secondary effects, such as the geometrical disposition of the H-bond donor (D) and acceptor (A) functionalities, the presence of intramolecular H-bonds, tautomerization phenomena, and the electronic effect of the substituent, can play a decisive role in the final strength of the overall interaction. In the seminal works by Jorgensen, it was shown that in multiple H-bonded arrays, the electrostatic cross interactions between adjacent polarized atoms forming the donor and acceptor functionalities of the arrays could induce a “secondary electrostatic interaction,” responsible for the increase or decrease in the H-bonded complex stability [28]. From a qualitative point of view, it is clear that the proximity of atoms bearing the same charge would induce the instauration of repulsive secondary interactions, whereas the presence of opposite charges on adjacent atoms would lead to secondary attractive interactions (Figure 5.2a).

Therefore, following this concept, a DAD-ADA array would have a lower stability in comparison with a DDA-ADA due to the presence of a higher amount of repulsive secondary interactions (Figure 5.2a,b). Although Jorgensen’s theory gives a qualitative trend, the calculated energies of the effects (-31 kJ mol^{-1} for the primary interactions, $+10.5\text{ kJ mol}^{-1}$ or -10.5 kJ mol^{-1} for each repulsive or attractive secondary interactions) were shown to be probably overestimated. In a further refinement using multiple linear regression analyses, Sartorius and Schneider refined the previous values to -8.0 kJ mol^{-1} for the primary interactions and to $\pm 2.9\text{ kJ mol}^{-1}$ for the secondary attractive/repulsive interactions [29].

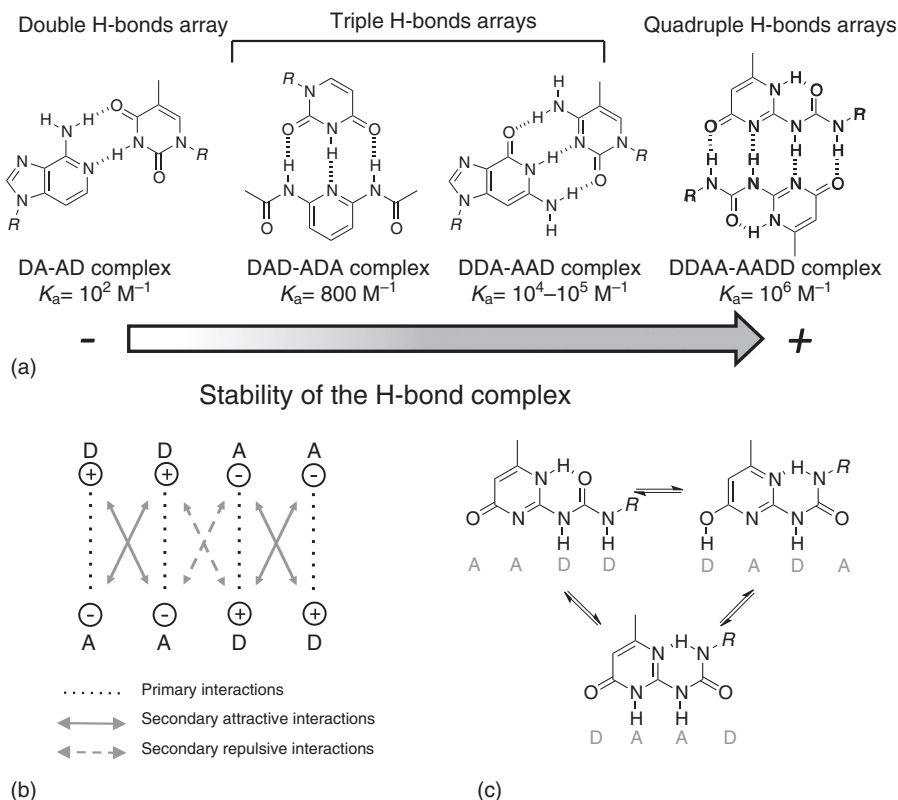


Figure 5.2. Schematic depiction (a) of the relation existing between the number and the disposition of the donor and acceptor sites in a multiple H-bond array and the stability of the resulting supramolecular complex. Graphic representation (b) showing the primary and secondary (both repulsive and attractive) interactions arising from a DDAA-AADD quadruple H-bond array (Jorgensen model). (c) Tautomeric equilibrium of the ureido pyrimidinone derivatives influencing the donor/acceptor disposition and thus the strength of the association.

A further phenomenon able to strongly influence the stability of the H-bond-based complexes is the tautomerization process that can occur when heteroaromatic systems are used as molecular recognition units. Indeed, the possibility to have different tautomers of the same recognition system can induce an interchanging equilibrium between the donor and acceptor functionalities in the array, varying their spatial orientation and therefore the strength and the specificity of the final interaction. A classical example of this is constituted by the ureido pyrimidinone (UPy) recognition motif displaying a three-tautomer equilibrium (Figure 5.2c), in which each tautomer displays a different H-bond array: AADD, DADA, and DAAD. This equilibrium ultimately diminishes the “fidelity” [30] of the H-bond array (defined as the ability of a recognition unit to produce the desired supramolecular complex over all the possible complexes obtainable) [31] and thus the association strength.

Due to the conspicuous number of developed methods toward the preparation of both linear and cross-linked supramolecular polymers based on H-bond motifs

[11a, 32], this chapter is structured on the dimensionality of the final organic architecture: the first part is focused on self-assembly/self-organization of molecular units for the nanostructuring of one-dimensional (1D) assemblies and two-dimensional (2D) networks, whereas the second section is centered on the discussion of engineering of discrete systems, such as nanoparticles, nanorings, and toroids. For the sake of completeness, one should also remember the “crystal-engineering” approach, in which H-bond interactions are engaged in three-dimensional (3D) crystalline structures [33]. Many examples of crystalline nanostructures based on H-bond molecular recognition have been developed, such as 2D and 3D networks [34], tapes, or rosettes [35], showing how slight structural modification of the molecular components can lead to the formation of different nanoscopic structures. In this respect, H-bonded crystals as prepared following the crystal-engineering approach, introduced in 1988 by Desiraju as “the understanding of intermolecular interactions in the context of crystal packing and the utilization of such understanding in the design of new solids with desired physical and chemical properties” [36], play an important role in the field of supramolecular materials, and it is therefore perfectly understandable that the concepts proper of this field are intimately connected to the general principles relative to the supramolecular chemistry treated in this chapter. For an extensive overview of the subject, the interested reader is directed to the extensive review by Desiraju and Zaworotko [37].

5.3 1D H-BONDED NANOSTRUCTURED MATERIALS

The possibility of exploiting single or multiple arrays of H-bond interactions has been known since the early 1990s, thanks to the pioneering works of Lehn and coworkers, who synthesized the first supramolecular polymers based on self-assembly between multiple H-bond recognition sites. In this work, triple H-bonding interactions between uracil derivative **5.1** and bifunctional diamidopyridine module **5.2** induced the formation of a supramolecular polymer, which underwent self-organization into fibroid objects, displaying helicity as a consequence of the chirality of the single-molecular components (Figure 5.3a) [38]. This approach based on the molecular recognition process between diamidopyridine units and imidic systems was further exploited by Lehn and coworkers to induce the assembly of different building blocks such as cyanuric derivative **5.3** and complementary Hamilton-type receptor **5.4**, inducing the formation of fibers observable through transmission electron microscopy (TEM) analysis (Figure 5.3b–f) [22e, 39].

Following the work in the last 20 years, two main approaches toward the engineering of 1D supramolecular nanostructures have been developed, mainly depending on the spatial orientation of the H-bonded recognition units with respect to the main developing axis of the supramolecular architectures: (i) nanostructures in which the H-bond systems are formed along the supramolecular chain (H-bonded main-chain polymers) and (ii) systems in which the H-bond systems are formed orthogonally to the elongation axis.

5.3.1 H-Bonded Supramolecular Main-Chain Polymers

To this class belong all the nanostructures in which the H-bond recognition systems are formed along the supramolecular chain, and the H-bond recognition unit itself is mainly responsible for the formation of the 1D nanostructure. One of the most

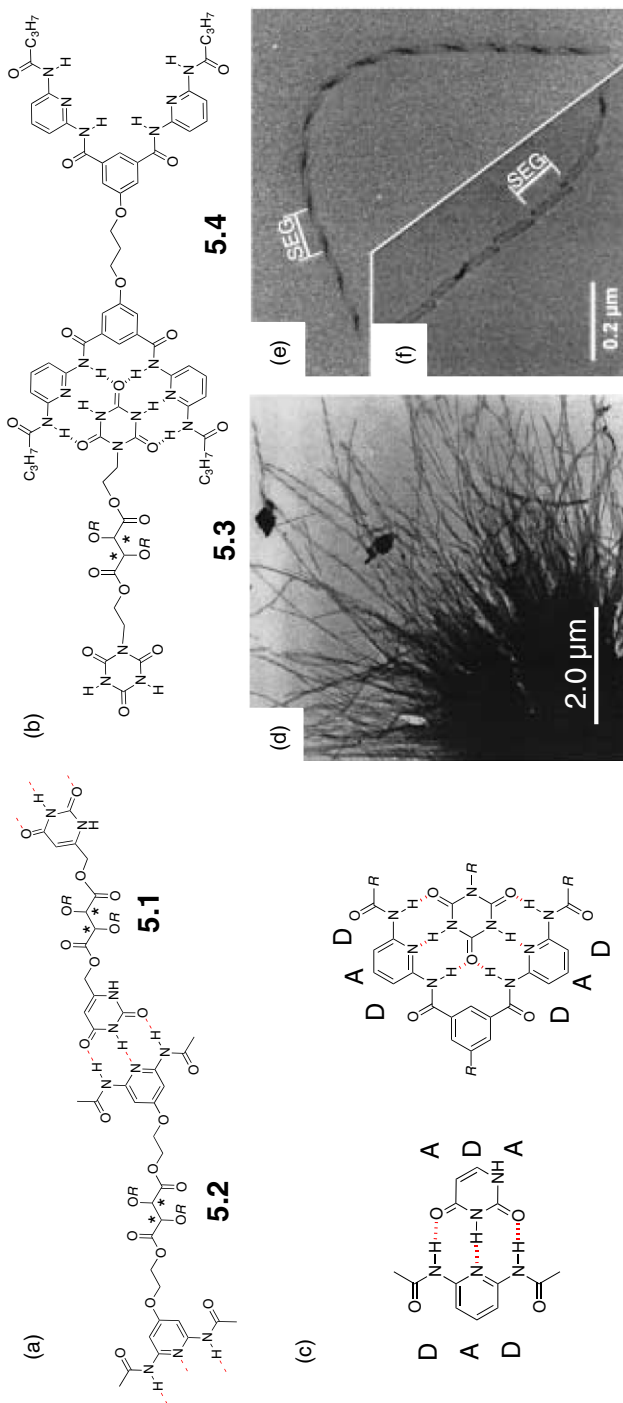


Figure 5.3. Self-assembly process (a) between the diacetylaminopyridine unit **5.2** and the uracilic molecular module **5.1** developed by Lehn through the derivatization of a tartaric acid core [22e] leading to the formation of a supramolecular polymer able to organize into helical fibroid material as a consequence of the chirality of the single building blocks (*R*: -C₁₂H₂₅). Molecular structures (b) of the supramolecular assembly between the cyanuric derivatives **5.3** and its complementary unit **5.4** (*R*: -C₁₂H₂₅). Schematic representation (c) of two different multiple H-bond arrays based on the imidic-diacetylaminopyridine recognition motifs (*R*: -alkyl). TEM images (d–f) of the helical fibers obtained from the assembly of **5.3** and **5.4** (white segment represent the helical pitch distance). Source: [39]. Reproduced with permission of Wiley-VCH Verlag GmbH & Co. KGaA.

important steps toward the preparation of main-chain H-bonded supramolecular polymers is the synthesis reported by the groups of Meijer and Sijbesma in 1998, in which UPy derivatives dimerize through the formation of a supramolecular DDAA-AADD complex based on four H-bonds, characterized by a dimerization constant exceeding 10^6 M^{-1} (Figure 5.4b) [15a]. Due to the easy synthesis and high K_a values, this discovery paved the way for the subsequent development of many different types of supramolecular homo- and copolymers based on multiple H-bond interactions. Recently, the UPy recognition unit has been used for the development of highly luminescent supramolecular polymers by the groups of Meijer and Schenning [40]. In this work, three π -conjugated supramolecular molecular modules **5.5**–**5.7** (blue, red, and green emitting, respectively) functionalized at their termini with UPy moieties were synthesized (Figure 5.4a). Specifically, upon self-assembly of these monomers, a mixed supramolecular copolymer is formed at a certain mixing ratio of the chromophores, leading to the emission of white light (Figure 5.4c–e). In fact, simultaneous addition of aliquots of **5.6** and **5.7** into a solution of **5.5** induced the formation of the supramolecular copolymer, which, at the **5.5:5.6:5.7** ratio of 33:8:59, afforded white photoluminescence (Figure 5.4d). Moreover, a spin-coated orthodichlorobenzene (ODCB) solution ($[4.5\text{--}9] \times 10^{-3} \text{ M}$) of the supramolecular polymer (ratio of **5.5:5.6:5.7** = 10:6:84) gave rise to a white photoluminescent film, showing the effective processability of such molecular systems for the preparation of luminescent devices.

Recently, the same recognition system employed by Lehn to prepare linear supramolecular assemblies in solution has been also thoroughly investigated on surface in a joint collaborative network by our group, by means of ultra-high-vacuum scanning tunneling microscopy (UHV-STM) [41]. After the codeposition of building blocks **5.8** and **5.9** on Ag(111), the formation of wirelike assemblies $[\mathbf{5.8:5.9}]_n$ occurs (Figure 5.5) as a direct consequence of the instauration of triple H-bonds between complementary diacetylaminopyridinic moieties **5.8** and uracilic recognition sites **5.9**. It was also shown that the length and the morphology of the resulting linear assemblies could be tuned by the addition of a third component, anthracenic derivative **5.10**, which, acting as a supramolecular stopper, terminates the elongation of the single supramolecular chains on the surface (Figure 5.5e,f).

Another example was developed by Pei and coworkers who synthesized aromatic hexa-acid **5.11**, capable of undergoing nanowire self-assembly, displaying a high solid-state quantum efficiency (22%) (Figure 5.6) [42]. In this case, the exploitation of a rigid tridimensional skeleton as a molecular core dramatically increases the emissive properties of the resulting nanostructure into the first known example of a luminescent supramolecular nanowire based on multiple H-bond interactions.

Another category of molecules able to induce the formation of supramolecular main-chain polymers is constituted by the simple N-unsubstituted perylene diimide (PDI). The supramolecular polymerization of these compounds in apolar solvents is mainly driven by the formation of H-bond pairs upon antiparallel arrangements of their imidic termini and the collateral interdigitation of the resulting chains. Würthner and coworkers recently synthesized a series of highly fluorescent tetraaryloxy-substituted PDI derivatives, molecules **5.12**–**5.16** (Figure 5.7a), equipped with different peripheral chains [43].

By combining different spectroscopic (UV-Vis, circular dichroism [CD], and linear dichroism [LD] spectroscopies) and microscopic (atomic force microscopy [AFM], STM) techniques, it was possible to reveal that the self-assembly between PDI units was occurring through the formation of extended double string cables, each consisting

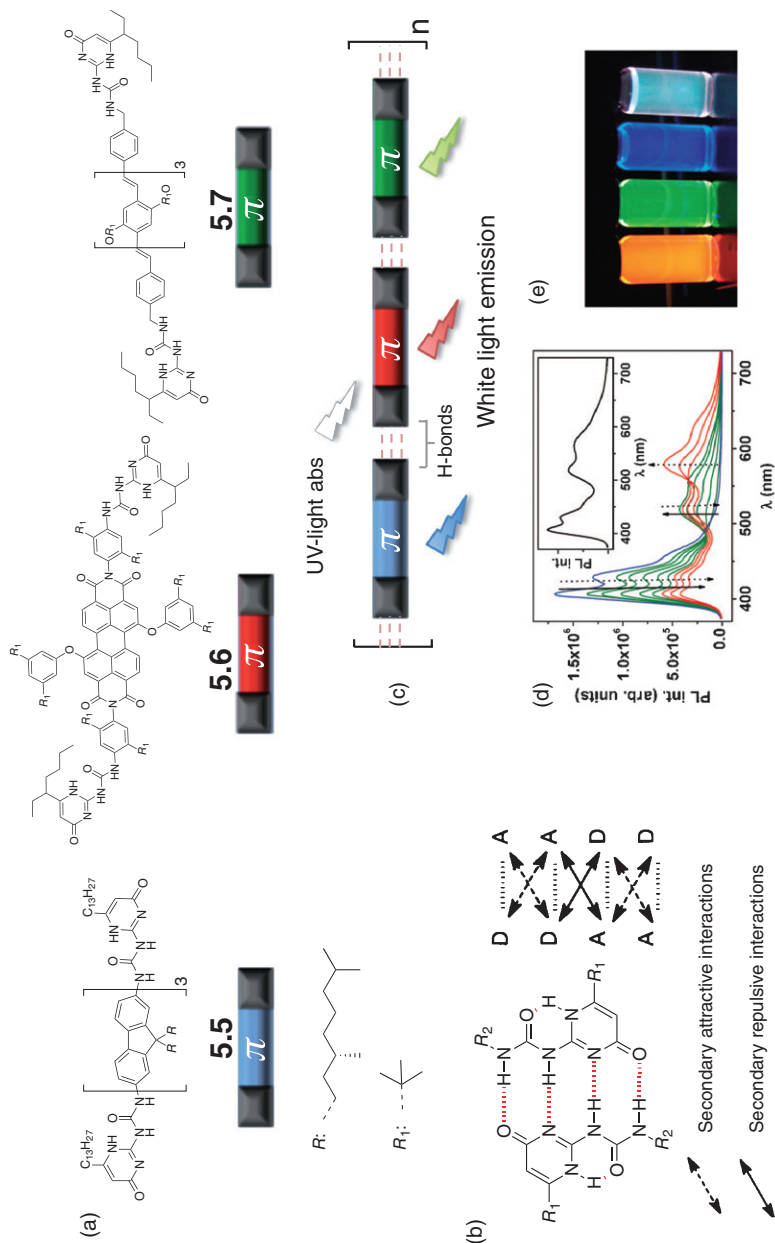


Figure 5.4. Molecular structures (a) of the UPy derivatives **5.5**, **5.6**, and **5.7**, blue, red, and green emitting, respectively [40]. Structural representation (b) of the quadruple H-bond system established within the UPy dimers (*R*: general alkyl fragment) [15a]. Schematic representation of the white-light emissive material constituted by the supramolecular polymer formed by **5.5**, **5.6**, and **5.7**. Photoluminescence titration experiment (d) in CHCl_3 (blue line: pure module **5.5**; green line: **5.7** with different amounts of **5.6**; red lines: **5.5** with different amounts of **5.6** and **5.7**) (the inset shows the spectra relative to a ratio of 59:33:8 [$c_{5.5} = 1.6 \times 10^{-6} \text{ M}$, $\lambda_{\text{exc}} = 364 \text{ nm}$)] and the solutions (e) containing the different H-bonding chromophores **5.6**, **5.7**, and **5.5** and their mixture in CHCl_3 (first from the right) when irradiated at 365 nm. Source: [40]. Adapted with permission of the American Chemical Society. See color insert.

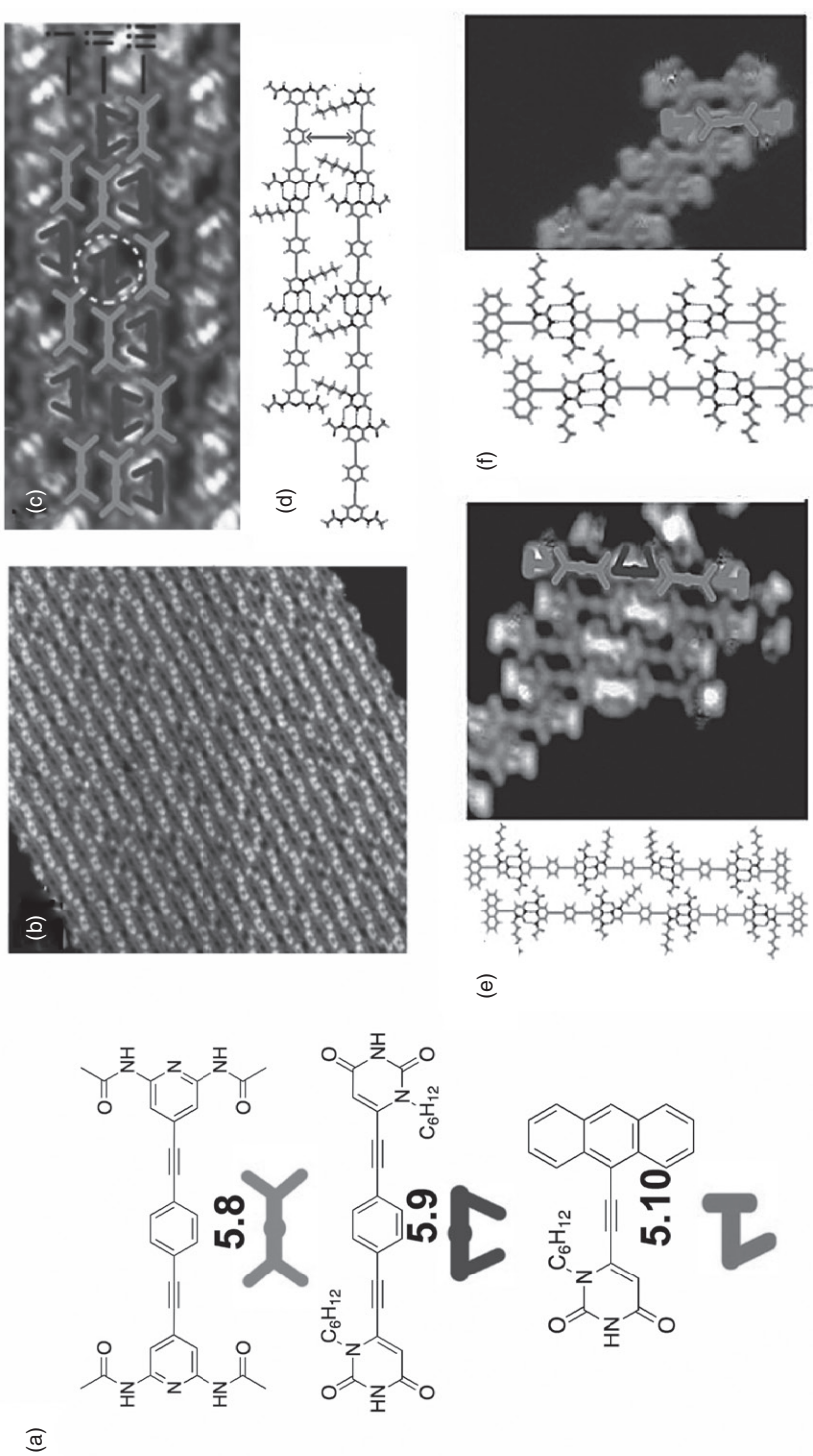


Figure 5.5. Molecular structure (a) of the modules used by Bonifazi and coworkers to induce the formation of wirelike 1D structures on a Ag(111) surface by means of multiple H-bonds. UHV-STM images (b) of the assembly **[5.8-5.9]_n** on Ag (111) after annealing at 383 K. Schematic representation of the disposition of molecule **5.8**, **5.9**, and **5.10** along the 1D assembly (c) and relative molecular models (d). UHV-STM images (e-f) of multicomponent submonolayers constructed by a sequential sublimation of molecules **5.8**, **5.9**, and **5.10** and the relative molecular modules. Source: [41]. Reproduced with permission of Wiley-VCH Verlag GmbH & Co. KGaA.

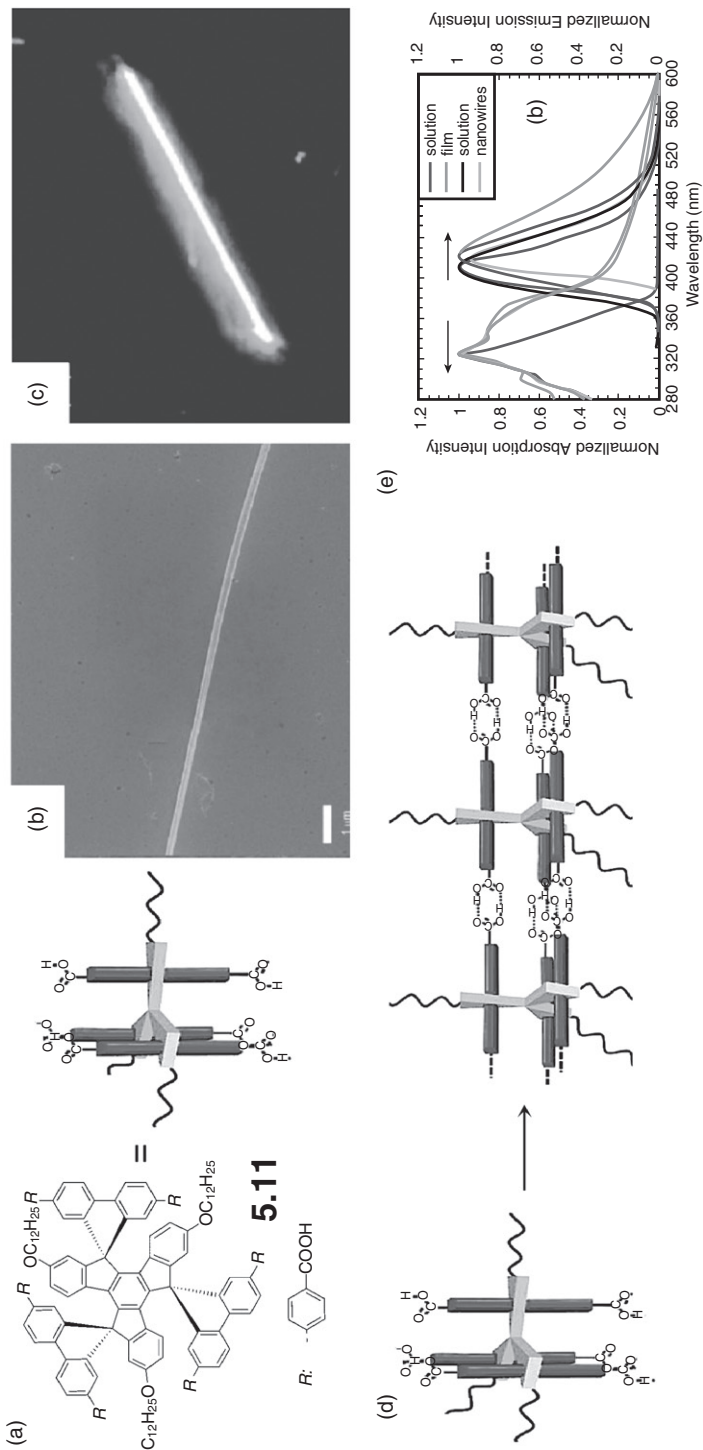


Figure 5.6. Molecular structure of hexa-acid **5.11** (a) and a SEM image (b) of the supramolecular nanowire obtained from its self-assembly through multiple H-bond interactions. Fluorescence micrograph (c) of the supramolecular nanowire (400 \times of magnitude). Schematic representation (d) of the self-assembly process between the single units of **5.11**. UV-Vis and PL spectra (e) for **5.11** and for its methyl ester precursor in THF solution and solid state. Source: [42]. Adapted with permission of the American Chemical Society.

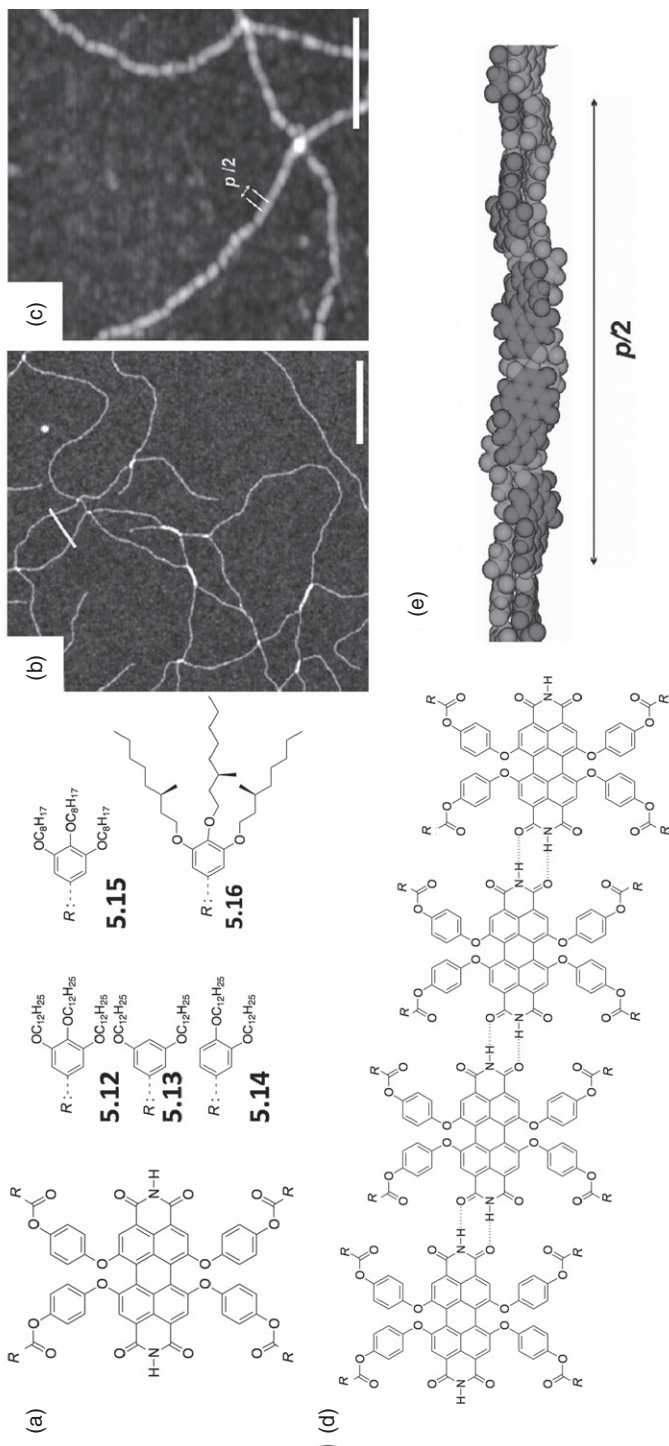


Figure 5.7. Chemical structures (a) of PDI derivatives **5.12–5.16**. TM-AFM images (b and c) at different magnifications of the self-assembled nanofibers obtained by drop casting an MCH solution of **5.15** on a silicon surface. Schematic representation (d) of the homomolecular self-assembly between the PDI units. Molecular model (e) obtained with AMBER force field for the supramolecular structure of PDI **5.12** aggregates. The half of a helical pitch $p/2$ was calculated as 6 nm. Source: [43]. Adapted with permission of the American Chemical Society.

of two H-bonded supramolecular polymeric chains of densely packed and strongly excitonically coupled PDI chromophores, featuring highly fluorescent J-aggregates (Figure 5.7b–e). The aggregation stability of the nanostructure and the photoemissive properties of the J-aggregates have proven to be in strict relation with the structure of the peripheral alkoxy substituents. Furthermore, concentration-dependent UV-Vis absorption studies proved the presence of a cooperative nucleation–elongation mechanism responsible for the aggregation of the assemblies in which the PDI core was functionalized with chiral alkoxy moieties, providing a nucleation equilibrium constant of $K_n = 13 \pm 11 \text{ L mol}^{-1}$ and an elongation constant of $K_e = 2.3 \pm 0.1 \times 10^6 \text{ L mol}^{-1}$ in methylcyclohexane (MCH).

Another important class of compounds is the 1,3,5-benzene trisamide (BTA). This aromatic module is very well known in the literature due to its ability to induce the formation of 1D supramolecular polymers both in solution and at the solid state, as a result of the threefold α -helix-type arrangement of its intermolecular H-bonds [44]. On the basis of UV-Vis and CD spectroscopies, several alkylated BTA derivatives have proven to self-assemble by means of highly cooperative processes. In this context, the highest degree of cooperativity was shown by chiral molecular derivatives that were also able to induce chiral amplifications by means of the known “sergeant-and-soldier” effect [45]. Depending on the chemical nature of the different functional groups at the level of the amidic moieties, different types of supramolecular systems can be formed, such as nanorods [46], nanofibers [47], or liquid crystals [48]. In a recent work, Nolte and coworkers were able to synthesize triporphyrinoid derivative of BTA **5.18**, which self-assembles in cyclohexane (CHX) at micromolar concentrations into long, chiral supramolecular polymers, which precipitate as fibers when the solution is drop-cast on mica surfaces (Figure 5.8) [49].

In contrast, in CHCl_3 , BTA derivative **5.18** was molecularly dissolved up to a concentration of 0.02 mM, and after drop casting on mica surface, no macroscopic precipitation of fibroid material was observed. However, when the CHCl_3 solution was subjected to a spinoidal dewetting, an equidistant pattern of 1D columnar assembly with a diameter comparable to that of the single molecule was formed (Figure 5.8c–e). Exploiting the same recognition motif, Marcellis and coworkers used BTA derivative **5.17** to organize triphenylene functions into columnar nanostructures, forming hexagonal discotic phases possessing the highest charge carrier mobility ever ($0.12 \text{ cm}^2 \text{ V}^{-1} \text{ s}^{-1}$ at 180°C) [50]. Very recently, the tris-amide functionality has been also exploited by García and Sánchez to study the transfer of chirality in different columnar nanostructures obtained with oligo(phenylene ethynylene) (OPE) derivatives [51].

For this purpose, two series of OPE derivatives, **5.19–5.22** and **5.23–5.25**, bearing different solubilizing chains have been prepared (Figure 5.9a). The first is composed of OPE trisamides with a variable number of chiral side chains that self-assemble following a cooperative mechanism, whereas the second is constituted by OPEs with a variable number of ether and amide functional groups. CD spectroscopy of the self-assembled nanostructures originating from the first series showed that the presence of only one stereogenic center in the peripheral chains is sufficient to achieve helical organization with a preferred handedness, whereas in the case of compounds **5.23–5.25**, no helical organization was observed (Figure 5.9b–d). Interestingly, mixing achiral trisamide **5.19** with chiral bisamide **5.25** generated helical nanostructures with a preferred handedness in a cooperative fashion in a process involving the transfer of helicity from **5.19** to **5.25** and the amplification of chirality from **5.25** to **5.19**. This is a rare example in which the molecular chirality is obtained from the formation of host–guest

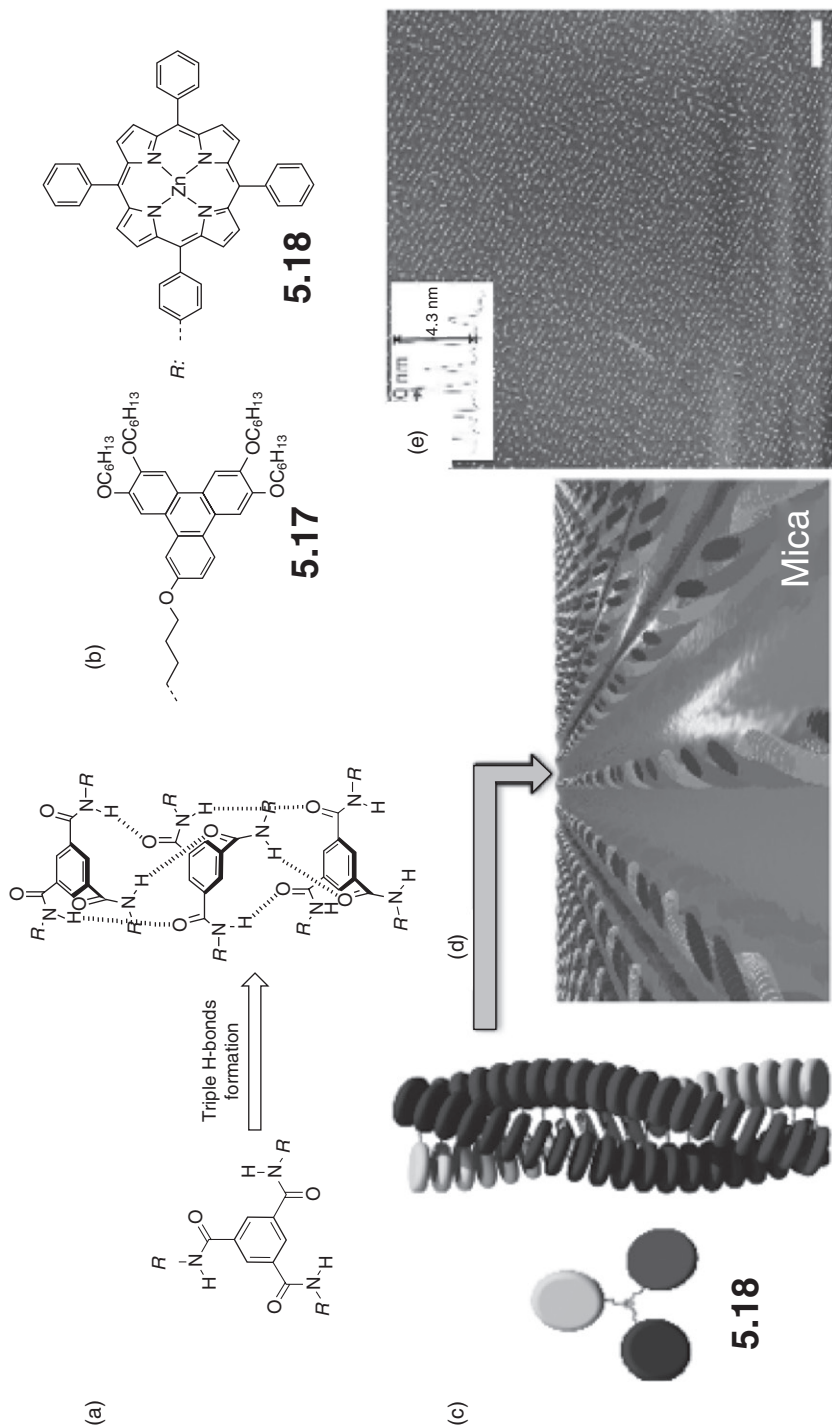


Figure 5.8. Molecular structure (a) and self-assembly mechanism of BTA modules mediated by threefold helical H-bonds [44]. Molecular structures of triphenylene BTA derivative **5.17** [50] and porphyrin derivative **5.18** [49] (b). Schematic representation of the assembly mechanism of porphyrin derivative **5.18** in solution (c) and on mica (d) surface. TM-AFM image (e) of the self-assembled nanofibers originated from the deposition of a CHCl_3 solution of **5.18** on a mica surface. Source: [49]. Adapted with permission of the American Chemical Society.

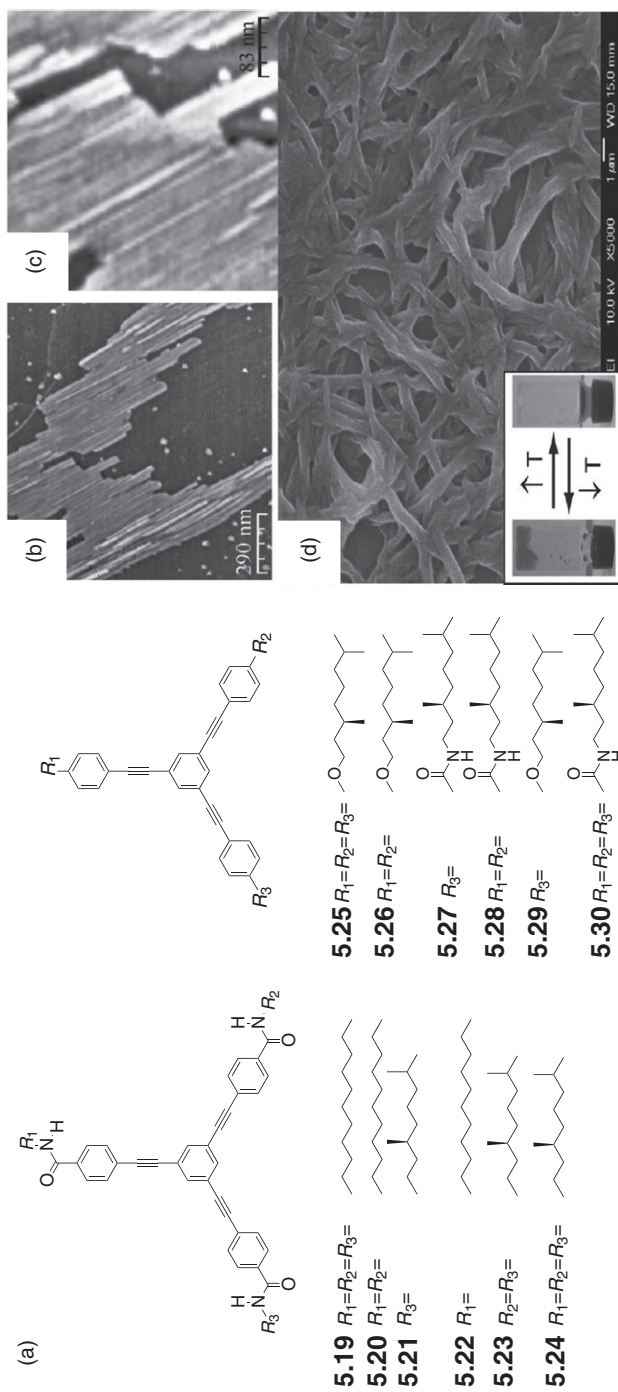


Figure 5.9. Molecular structures (a) of the two series of OPE building blocks synthesized by García and Sanchez [51]. TM-AFM images of the linear nanostructures (b and c) obtained by deposition of a toluene solution of **5.19** and **5.21** on mica surface and SEM image of an organogel structure formed by **5.19** alone (d). (Inset) Picture of the gel–sol transition of the organogel formed by **5.19** in toluene. Source: [51]. Adapted with permission of the American Chemical Society.

complexes between structurally analogous species that, alone, are CD silent. Another elaborated example of noncovalent nanostructuring took advantage of the crown-ether-based molecular recognition as developed by Stoddart and coworkers to form pseudorotaxane structures. The ability of crown ethers to originate H-bond interactions with ammonium cations has been frequently exploited in literature, with the aim of constructing supramolecular architectures possessing different geometries and functions [52]. In this context, in a very recent work, Huang and coworkers have prepared a self-complementary molecular module **5.26** containing a dibenzo-[24]crown-8 (DB24C8) moiety and a bisbenzylammonium (DBA) cation separated by a 15-term flexible alkylic chain (Figure 5.10a) [53]. Such a module undergoes self-assembly into linear supramolecular polymers in apolar solvents, further self-organizing into different kinds of nanomaterials such as rodlike nanofibers or gel (Figure 5.10b–d) as a function of the used concentration. Moreover, the supramolecular polymer showing reversible gel–sol phase transitions upon heating and cooling or addition of a base or an acid (Figure 5.10c) was successfully employed for the selective release of guest molecules such as rhodamine B.

Exploiting a similar strategy, Gibson and coworkers have developed the first type of AA-BB supramolecular polymer based on bis(*m*-phenylene)-32-crown-10-based cryptands (BMP32C10) and paraquat derivatives. The self-organization of such supramolecular polymers leads to the formation of linear nanofibers observable by scanning electron microscopy (SEM) [54].

5.3.2 Supramolecular Polymers with H-Bonds Perpendicular to the Elongation Direction

Through an accurate design of the molecular geometry, it is possible that the H-bond arrays form perpendicularly to the principal growth direction of the nanostructure, further strengthening side interactions such as the π – π contacts. As a consequence, a recognition process mediated by the concomitant action of H-bonds and π -interactions can form highly hierarchized supramolecular materials. Among all the functional systems able to polymerize through this combined action, *p*-phenylenevinylene was revealed to be the most exploited. In an extensive work of Meijer and coworkers, *p*-phenylenevinylene derivative **5.27** functionalized at one peripheral position with ureidotriazine (Figure 5.11a–c) was shown to dimerize via multiple H-bond formation and subsequently to self-organize via π – π interactions, leading to polymeric structures [55]. If opportunely functionalized with chiral lateral chains, helical nanofibers with an approximate diameter of 5 nm showing a preferred handedness could also be formed, as shown by combined AFM and computational studies [55c, 56]. Regrettably, electrical measurements of nanofibers deposited on Au–Pd electrodes showed considerably low conductive properties, most probably due to the presence of defects or to the intrinsically poor conductance of the π – π stacking arrangement [57].

The self-organization of thienylvinylene **5.28** and **5.29** originating supramolecular nanofibers featuring organic gel (Figure 5.11d,e) has been also studied by Ajayaghosh and coworkers [58]. The ability of the nanofibers to give charge-transfer phenomena was studied by means of conducting probe (CP) AFM analysis, revealing a semiconductor behavior (Figure 5.11 f,g) of these nanostructures, with the highest conductance of the nanofiber formed by **5.29**, which was of approximately 0.93 nS. In another work, Takeuchi and coworkers reported the organization of phthalhydrazide-helicene **5.30** into trimeric disks, leading to the formation of fibrous assemblies in nonpolar solvents such

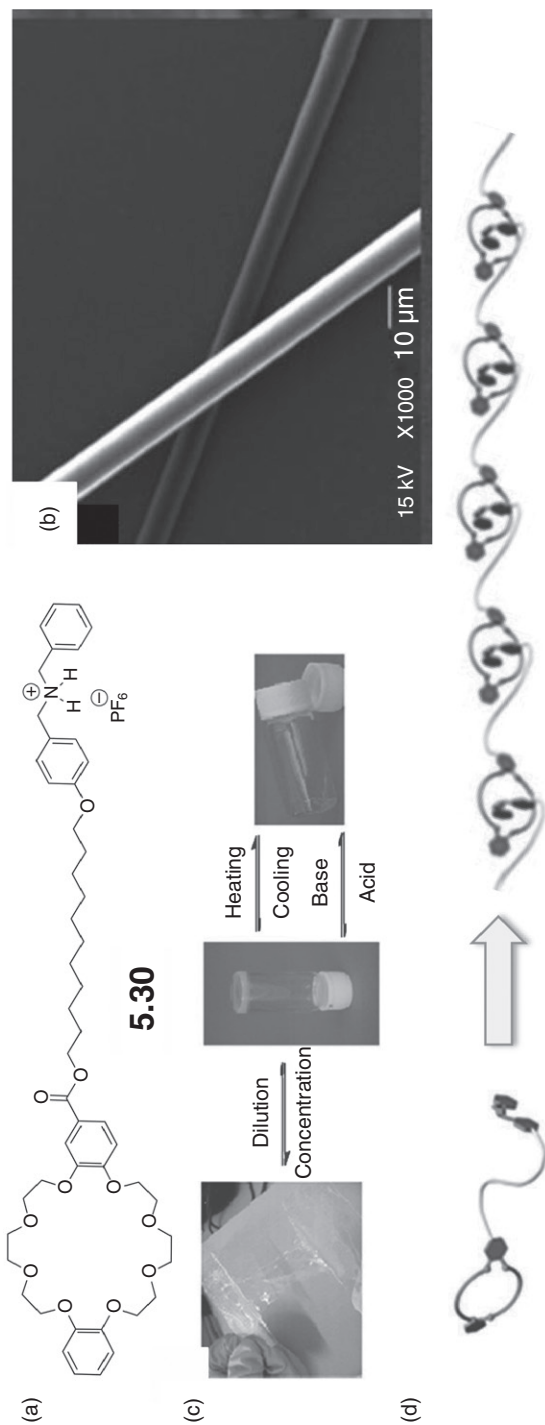


Figure 5.10. Molecular structure (a) of the pseudorotaxane building block **5.26** as synthesized by Huang and coworkers [53]. SEM image (b) of a linear rodlike nanofibers obtained from the self-assembly/self-organization of **5.26**. A polymeric film (c) prepared from **5.26**_n (left) and the schematic representation of the reversible sol-gel transition of **5.26** at different pH and at different temperatures. Schematic representation (d) of the homomolecular self-assembly process between the single units of **5.26** leading to the formation of the supramolecular polymer **5.26**_n. Source: [53]. Reproduced with permission of Wiley-VCH Verlag GmbH & Co. KGaA.

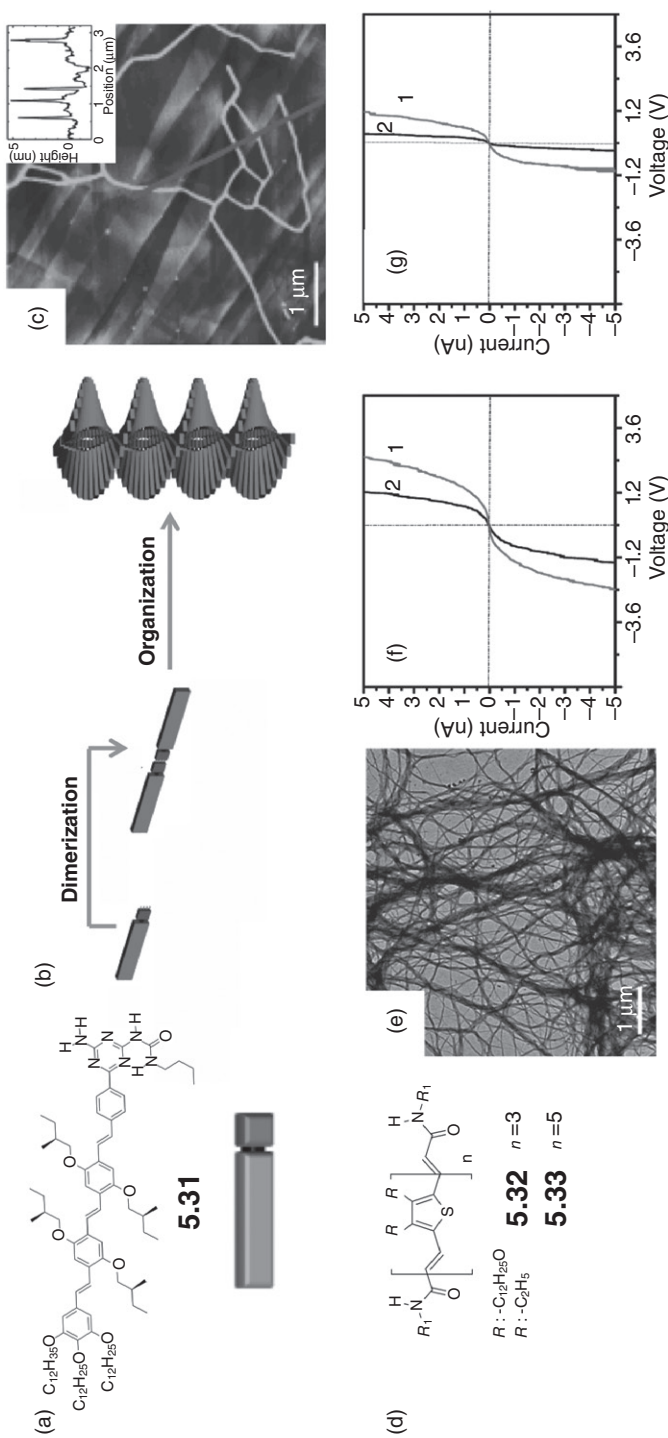


Figure 5.11. Molecular structure (a) of ureidotriazine-functionalized OPV **5.27**. Schematic representation (b) of the self-assembly/self-organization process leading to the formation of the helical nanofibers. TM-AFM image (c) of the nanofibers as obtained after spin coating on graphite (inset: lateral profile) [55c]. Molecular structures (d) of thiophenylene derivatives **5.28** and **5.29**. Representative (CP)/AFM measurements (f and g) of **5.28** and **5.29** xerogels from decane solution drop-cast on HOPG ($c = 1 \times 10^{-4}$ M) [58]. Source of panels a-c: [55c]. Source of panels d-g: [58]. Both adapted with permission of the American Chemical Society.

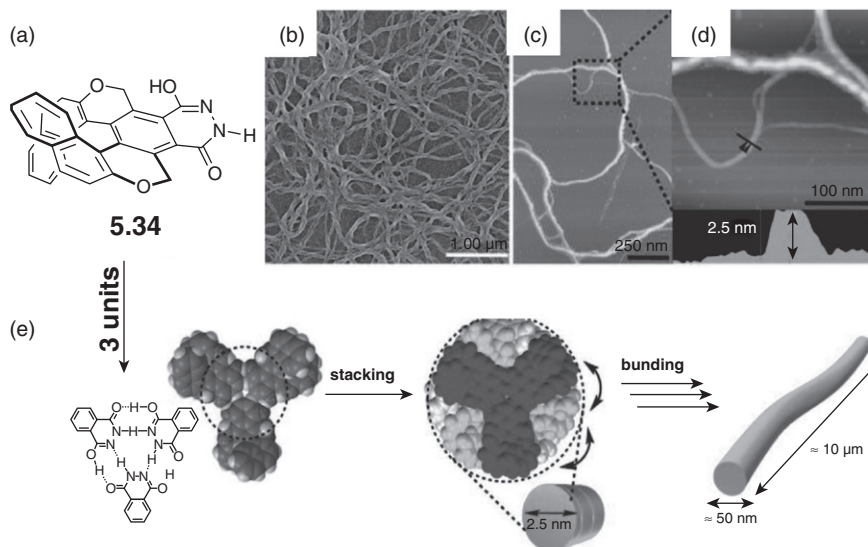


Figure 5.12. Molecular structure (a) of the helicene derivative **5.30**. SEM image (b) of the nanofiber produced by the self-assembly of (*M*)-**5.30**. TM-AFM images (c and d) at different magnifications of the nanofibers deriving from the assembly of (*M*)-**5.30** in toluene. Schematic representation (e) of the self-assembly process of helicene derivatives **5.30**, through H-bond-mediated trimerization and subsequent π - π interactions. Source: [59]. Reproduced with permission of Wiley-VCH Verlag GmbH & Co. KGaA.

as CHCl_3 and toluene (Figure 5.12) [59]. Moreover, both assemblies derived from molecules (*M*)-**5.30** and (*P*)-**5.30** showed extraordinary values of circularly polarized luminescence ($|g_{\text{um}}| = 0.035$ at the peak maxima), which can be considered as the highest value ever reported for organic molecules without a hosting matrix.

From these examples, we can thus conclude that self-complementarity between molecular modules having multiple H-bonded-based recognition sites is an excellent instrument to preorganize a discrete number of supramolecular oligomers into larger structures able to polymerize in different supramolecular nanostructures such as helix, wires, or tubes through π - π stacking interactions. As shown recently by Yagai and coworkers for the case of melamine-functionalized oligo(phenylene vinylene) (OPV) molecules **5.31** and **5.32** (Figure 5.13a), passing from a self-complementary to a coassembled supramolecular system, it was possible to tune in a dramatic way the morphology and the complexity of the resulting nanostructures (Figure 5.13d,e) [60]. After the deposition of **5.32** on highly oriented pyrolytic graphite (HOPG), the formation of fibers with a diameter of 8 nm was observed by means of AFM analysis (Figure 5.13c). On the other hand, deposition under the same experimental conditions of molecule **5.31** resulted in the formation of an ill-defined nanostructure. Nonetheless, the combination of **5.31** with cyanuric acid **5.33** induced the formation of ring-shaped nanostructures (Figure 5.13b), efficiently reconverted into fibrillar nano-objects upon increasing the concentration of the modules. This transition mainly originates from the formation

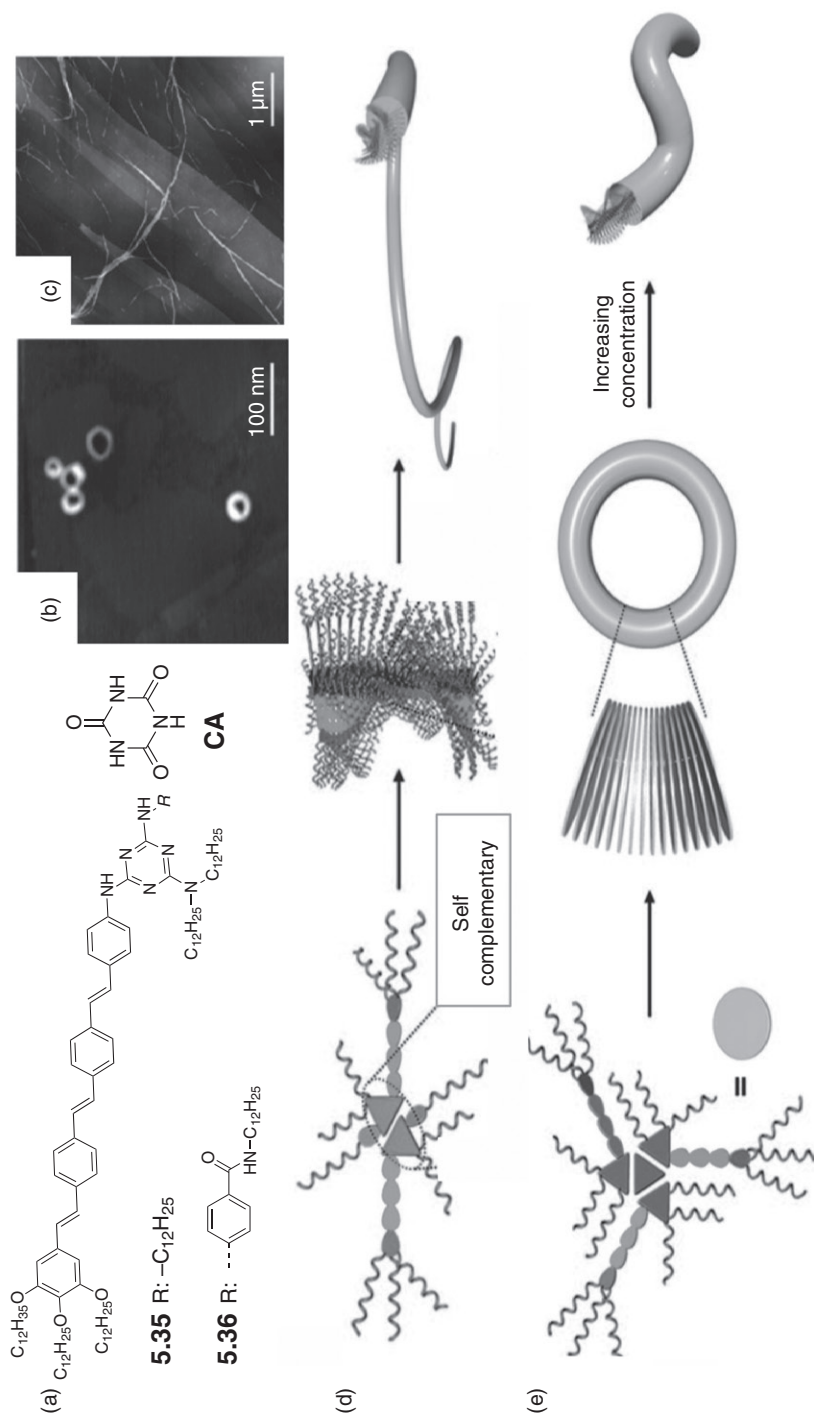


Figure 5.13. Molecular structures (a) of the OPV derivatives **5.31** and **5.32** synthesized by *Yagai* and coworkers and of the cyanuric acid **5.33** used induced the formation of ring shape nanostructures. TM-AFM images (b and c) of the nanorings and nanofibers produced by the heteromolecular assembly of **5.31** with **5.33** and of the nanofibers obtained from the homomolecular self-assembly of **5.32**. Schematic representations of the homomolecular self-assembly process of building block **5.32** (d) leading to the formation of H-bonded nanofibers, and the heteromolecular association between **5.31** and **5.33** leading to the formation of nanorings (e) that upon increase of the concentration were transformed into nanofibers. Source: [60]. Reproduced with permission of Wiley-VCH Verlag GmbH & Co. KGaA.

of a different kind of supramolecular oligomer in solution between the melamine functions of **5.31** and the imidic residues of **5.33** (Figure 5.13e). Depending on the concentration, such supramolecular heterotetramers can generate both rings and fibers, through π - π stacking interactions.

In a further development, the same recognition units composed by melamine and **5.33** were employed to engineer the organization of functional chromophores such as PDI derivatives into helical nanostructures. The formation of discotic supramolecular 3:1 complexes in MCH by mixing the melamine derivative **5.34**, equipped with two PDI chromophores, and **5.33** (Figure 5.14) was confirmed by UV-Vis and fluorescence titration [61].

Microscopic investigations (TEM and AFM) revealed that the complex hierarchically organized into fibrous columnar assemblies, which resulted in the formations of gels produced by an evaporation-induced organization process. Wide-area TEM analysis has shown the presence of different types of fibrous entities (Figure 5.14c) classified as thin fibrils, thin fibers, and thick fibers. CD investigation showed that the helicoidal

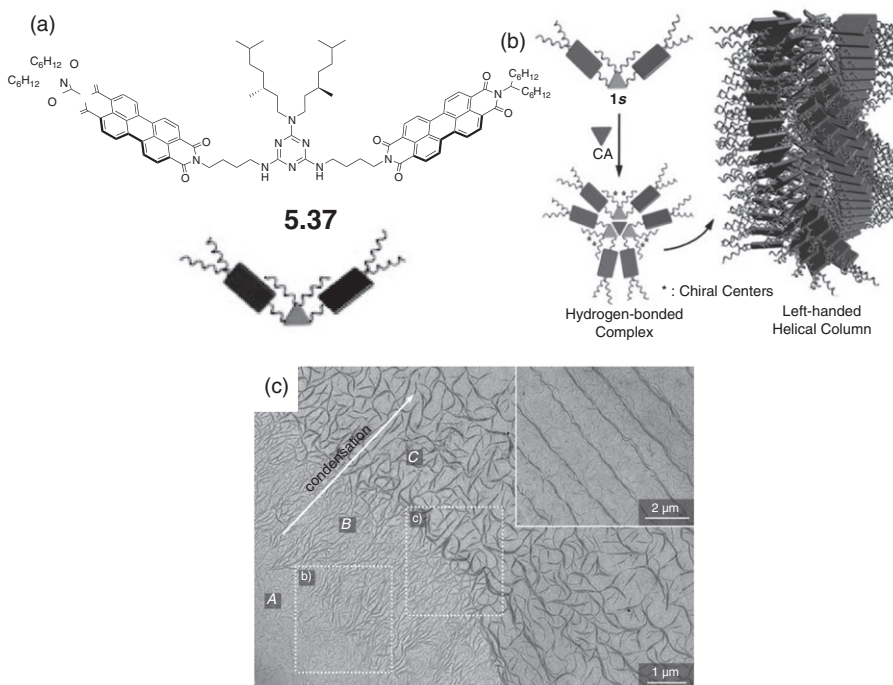


Figure 5.14. Molecular structure (a) of the melamine derivative **5.34** used by Yagai and coworkers to organize PDI molecules into helical nanostructure through H-bond interactions. Schematic representation (b) of the self-assembly process leading to the final nanohelix. SEM image of the nanofibers, showing the different morphologies of the structures along the condensation axis (highlighted by the white squares and letters). Source: [61]. Reproduced with permission of Wiley-VCH Verlag GmbH & Co. KGaA.

structuration of the columnar stacks is determined by the direction of the rotational displacement of the H-bonded core, which is commanded by the intercomplex asymmetric interaction between the internal chiral chains of the primary discotic entity. In addition, the obtained columnar aggregates have shown a remarkable retention of chirality upon dilution and in time, maintaining their CD activity up to 2 weeks after their preparation.

The π - π stacking interactions that usually originate from the organization of the molecular modules, in which the H-bonding system is orthogonally oriented to an aromatic moiety, can be efficiently exploited in order to produce ordered 1D nanostructures characterized by high electrical conductivity. Thus, organic *p-n-p* junctions prepared using diaminotriazine (DAT) and PDI have been thoroughly studied by different groups [62]. In the work of Meijer and coworkers, PDI derivative **5.36** was exploited to form an H-bonded trimer in which the two molecules of OPV **5.35** were associated at both termini of the PDI modules (Figure 5.15) [63]. After the trimerization process, due to the increase in the π -conjugated surface of the supramolecular complex, the formation of helical columnar stacks, with a diameter of approximately 7 nm, occurred. The resulting nanofibers have proven to serve as an efficient “supramolecular wire” for the antiparallel transport of both electrons and holes. The occurrence of an electron transfer phenomena within the columnar structure, from the electron donor OPV to the electron acceptor (PDI), was outlined by time-resolved transient absorption (TA) spectroscopy, proving in this way the functionality of the supramolecular system.

5.4 2D H-BONDED NETWORKS

The investigation of the electronic and geometrical properties of molecular materials bidimensionally arranged on surface can be extremely important for their potential applications in the field of fabrication of nanoelectronic devices [64]. In this context, the continuous development of scanning probe microscopy (SPM) in the last decades has allowed observation and characterization at the molecular level of the geometrical properties of 2D networks [65]. In particular, among all the SPM techniques, STM has become the chosen technique for characterizing the formation of mono- and multimolecular layers on different types of conductive surfaces [66]. In these systems, the process of formation of the first monolayer and its stability is generally ruled by both intermolecular contacts and molecule–substrate interactions. In this context, intermolecular noncovalent interactions taking place parallel to the substrate can govern the structural features of the final 2D assembly. Among all the possible strategies, the incorporation of H-bond motifs in conjugated molecules to induce a controlled self-assembly process on a surface is one of the most successful approaches due to the high directionality and reversibility of this type of interaction, which give the possibility of programming the geometrical and structural features of the resulting network [67]. So far, a conspicuous number of examples, describing the preparation of mono- and bicomponent 2D networks through the formation of H-bonding interactions, has been published [66–68]. One of the first examples of bicomponent porous networks characterized by the presence of empty hexagonal pores was reported in 2003 by Beton and coworkers [69], who described the formation of hexagonal arrays by the codeposition of the commercially available perylene derivative **5.38** and melamine **5.37** on a Ag(111)-terminated silicon surface under UHV conditions (Figure 5.16).

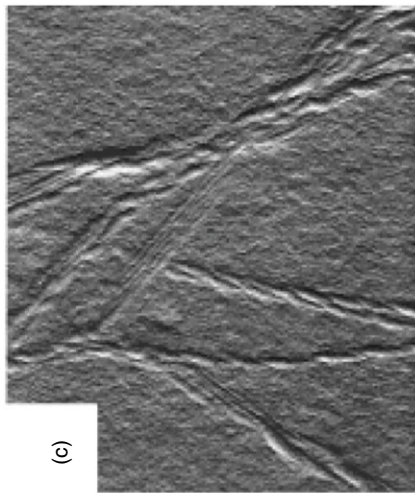
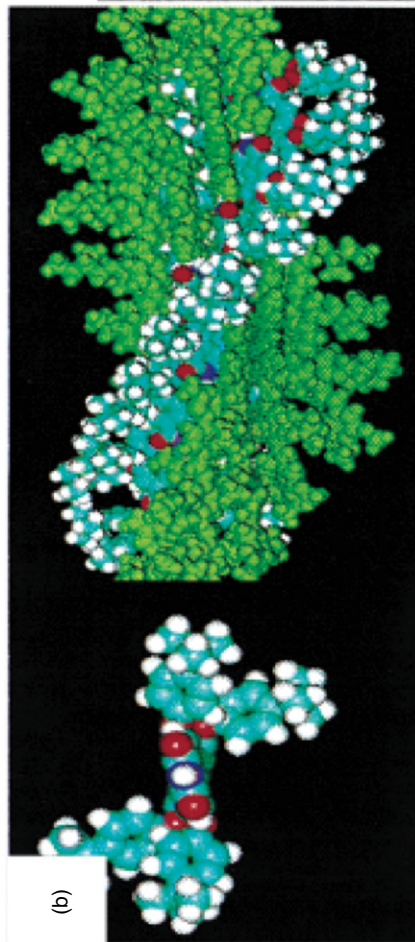
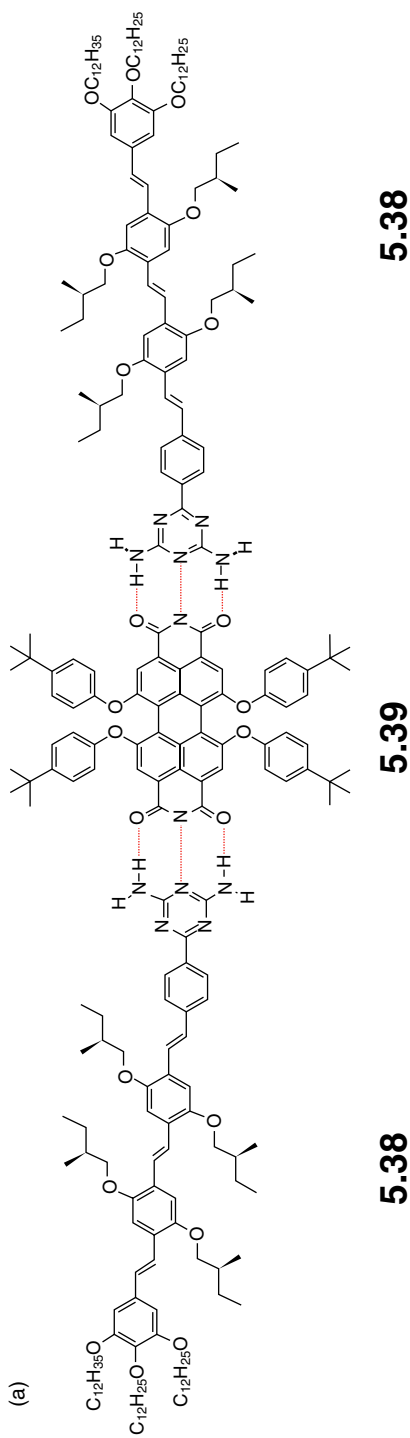


Figure 5.15. Molecular structure of the H-bond-based trimer formed by the self-assembly of PDI **5.36** and two units of melamine-functionalized OPV derivative **5.35**. Corey–Pauling–Koltun (CPK) representations (b) of the optimized PDI derivative **5.36** (left) and of its disposition along the nanofibers (right). TM-AFM images (c) of the fibers obtained upon spin coating of an MCH solution of molecule **5.36** and **5.35** in 1:2 ratio. Source: [62b]. Adapted with permission of the American Chemical Society.

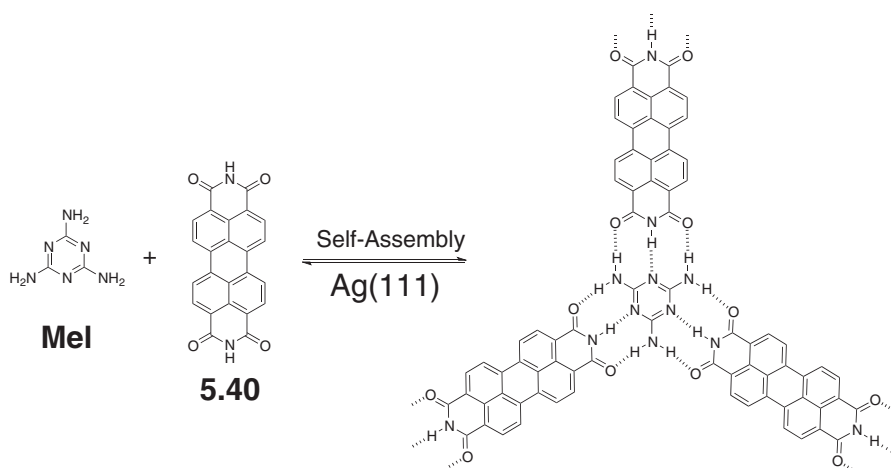


Figure 5.16. Schematic representation of the self-assembly process between **5.37** and **5.38** inducing the formation of a honeycomb network on the Ag/Si (111) $\sqrt{3} \times \sqrt{3}R30^\circ$ surface [69].

As revealed by STM images, the two molecular modules organize in such a way that hexagonal domains are formed. In this system, melamine and perylene-tetracarboxydiimide (PTCDI) module **5.38** undergo triple H-bond recognition, forming the vertices and the straight edges of the hexagonal domains, respectively.

In a recent work by Linderoth and coworkers, the first example of an extended 2D architecture formed by H-bond recognition between molecules that exhibit a pronounced 3D structure has been reported [70]. After the deposition of the diamino-triazine functionalized (hexaphenyl)benzene derivative **5.39** on a Au(111) surface, the formation of both linear and long-range-ordered 2D networks was observed by UHV-STM. The different arrangements originate from the combination of N–H \cdots N bonds between the DAT functional moieties (Figure 5.17).

The most common approach for the preparation of 2D systems with a controlled geometry consists of the deposition of molecular modules having a predefined recognition site able to induce the formation of the self-assembly process. Using a different approach, Stöhr and coworkers exploited a molecular system in which the molecular recognition sites could be activated *in situ*, enabling hydrogen-bonding interactions [71]. The authors reported that by thermal dehydrogenation of 4,9-diaminoperylenequinone-3,10-diimine (DPDI) **5.40** on a Cu(111) surface to form derivative **5.41** (Figure 5.18a), the formation of a supramolecular network based on H-bond donor and acceptor was observed by UHV-STM analysis (Figure 5.18b). The resulting periodic honeycomb structure has revealed to be thermally very stable (up to $>300^\circ\text{C}$) as a consequence of an irreversible chemical transformation and of the combination of intramolecular H-bonds and strong π -bonding between the organic molecules and metal atoms of the surface.

Our group has investigated the controlled formation of a bi-component porous network at the solid–liquid interface formed using **5.37** and bis-uracyl module **5.42** in 1,2,4-trichlorobenzene (TCB) on HOPG surfaces (Figure 5.19a) [72]. The structural characteristic of melamine, that is, its ability to form three H-bond systems oriented at

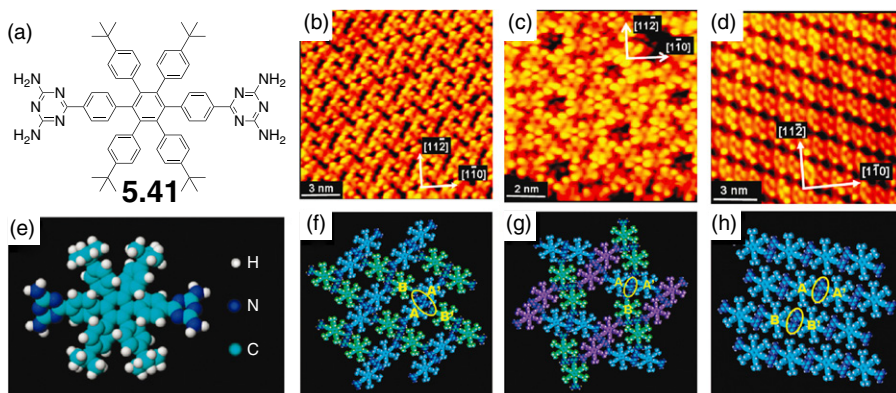


Figure 5.17. Chemical structure of molecular lander **5.39** (a) and its respective space-filling model (e) (white: hydrogen; blue: nitrogen; and cyan: carbon). STM images of three of the different bidimensional architectures obtained by the deposition of **5.39** on Au(111) (b–d). The representative molecular disposition in the supramolecular network is reported below each image (f–h), and the yellow circles are highlighting the different interactions between the DAT units of different molecules (marked as A, A', B, and B'). Source: [70]. Adapted with permission of the American Chemical Society. See color insert.

120° to each other, directs the assembly of the network forming the resulting honeycomb structure. The porous network was formed only with low concentration solutions ($\approx 2.0 \mu\text{M}$) since at higher concentration ($\approx 20 \mu\text{M}$) only tightly packed monolayers of **5.42** were formed due to the competitive surface physisorption of the two molecules. By working at the submonolayer coverage ($\approx 2.0 \mu\text{M}$), it was possible also to investigate the formation of discrete polygonal assemblies featuring porous domain at the solid–liquid interface. Two different molecular modules were exploited: tetrakis[ethynylpyrene] derivative **5.43** and diacetylaminopyridine derivative **5.44** bearing complementary triple H-bond recognition sites (Figure 5.19b–g) [73]. The nucleation of the H-bonded assemblies was performed in solution and studied at very low concentration ($< 10 \mu\text{M}$). STM analysis showed the formation of hybrid-polygonal assemblies between **5.43** and **5.44**, resulting in the formation of different types of self-assembled cyclic oligomers characterized by rhomboidal and rectangular shapes, formed as a consequence of the preprogrammed disposition of the H-bond recognition moieties into the molecular components. Taking into account the differences in the absorption energy of the single components and their tendency to minimize the occupied areas, control of the deposition of two different molecules on a surface can be considered a very difficult task. This approach, preventing the competitive adsorption between the modules, can be considered a valuable route to the future engineering of multicomponent nanostructures on a surface.

A further strategy for the preparation of 2D networks on surfaces exploits the biomimetic approach [74]. In this context, He and coworkers have used DNA to engineer an infinite 2D porous network able to induce the formation of highly extended nanostructured arrays with a length of up to 1 mm (Figure 5.20) [75]. The fundamental unit used for the preparation of the supramolecular network was characterized by a

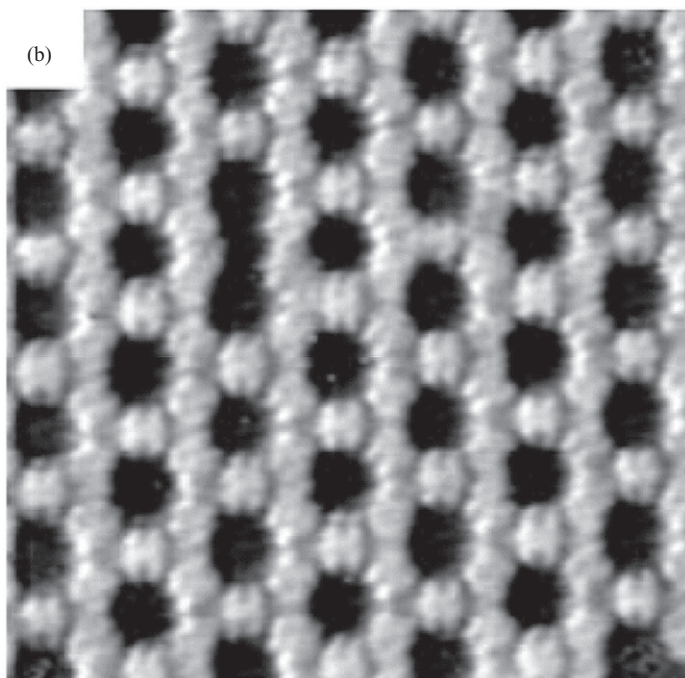
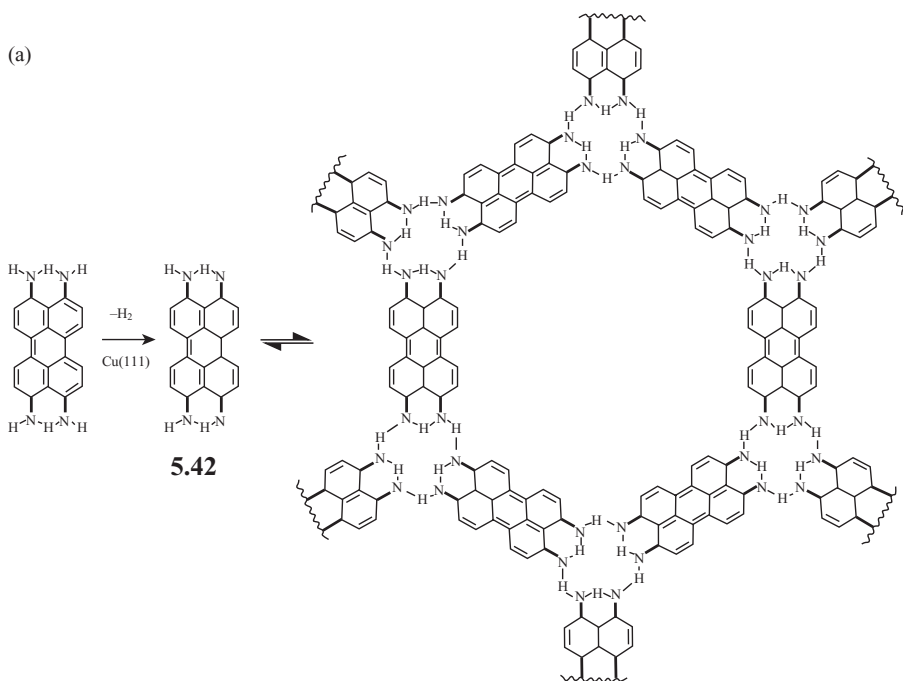


Figure 5.18. (a) Schematic representation of the hexagonal assembly formed by the dehydrogenation of DPDI forming derivative **5.41**; (b) STM image of the self-assembled architecture formed by **5.40** after thermal activation on a Cu(111) surface under UHV conditions. Source: [71a]. Reproduced with permission of Wiley-VCH Verlag GmbH & Co. KGaA.

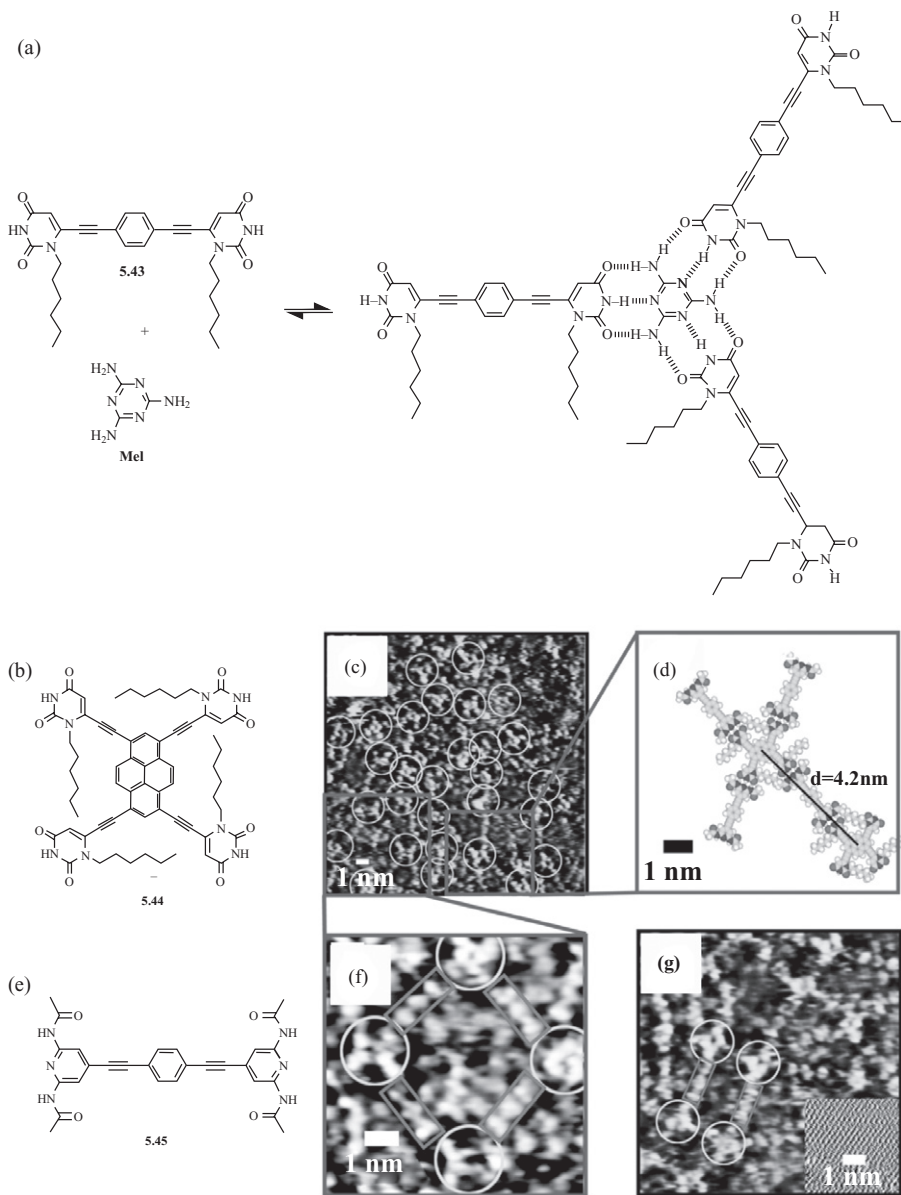


Figure 5.19. Molecular structures (a) of melamine **5.37** and bis-uracil **5.42** modules and the formation of the hybrid assembly via hydrogen bonding [72]. Molecular structures of tetrakis[ethynylpyrene] derivative **5.43** (b) and of diacetylamino pyridine derivative **5.44** (e). STM images (c, f, and g) at different magnifications of the supramolecular polygonal assemblies formed by **5.43** and **5.44** at the HOPG–TCB interface. Model assembly (d) of a hexameric hybrid complex showing the distance values as estimated by MM2-based computational geometry optimization. Source: [73]. Adapted with permission of the American Chemical Society.

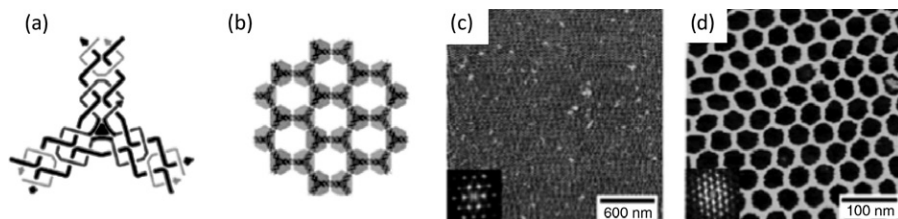


Figure 5.20. (a and b) The three-point star motif made up of seven DNA single strands; (c and d) AFM images of the self-assembly showing the hexagonal porous network on a mica surface. Source: [75]. Adapted with permission of the American Chemical Society.

three-pointed star shape and was produced by the selective association of seven DNA single strands. In this case, palindromic sequences were used to ensure that the H-bond interactions in all directions would have the same strength. After mixing the DNA strands in the appropriate proportions in a tris-acetic-EDTA- Mg^{2+} , the material was consequently deposited onto a mica surface, and AFM analysis of the surface showed the formation of an extended, highly ordered, hexagonal 2D crystalline array characterized by pore diameters of 29 ± 0.1 nm.

In the recent work of Borguet and coworkers, by STM investigation of tetracarboxylporphyrin **5.45** on Au (111) in an acidic medium ($HClO_4$ 0.01 M), the formation of three different types of ordered 2D arrays was observed as a consequence of the instauration of multiple intermolecular H-bond interactions between the carboxylic moieties (Figure 5.21a) [76]. In these ordered systems, single molecules can be slowly reduced by tuning the potential of the underlying electrode, showing that the more negative the potential was, the faster the reduction reaction occurred (Figure 5.21b–e).

These results, along with the possibility of organizing the single electroactive molecules in a very efficient way, have shed new light on the possibility of exploiting the new generations of 2D supramolecular networks for the production of high-performance solar cells or nanoelectronic devices [77].

5.5 H-BOND DISCRETE NANOSTRUCTURES

One of the principal targets in the field of supramolecular nanostructuring of organic materials consists in the possibility, through a strict control over the self-assembly process, of governing the relation between the size of the supramolecular object and the molecular properties. In this context it is important to control the number of molecules that are associating in order to induce the formation of nanostructures characterized by an extremely precise dimension and, at the same time, a relatively high monodispersity. In this section recent developments in the preparation of discrete nanostructures based on H-bond interactions are reviewed. In Section 5.5.1, the formation of discrete assembly through a templated approach will be discussed, whereas in Section 5.5.2, the formation of discrete entities by a self-assembly/self-organization process of low-molecular-weight building blocks will be reviewed.

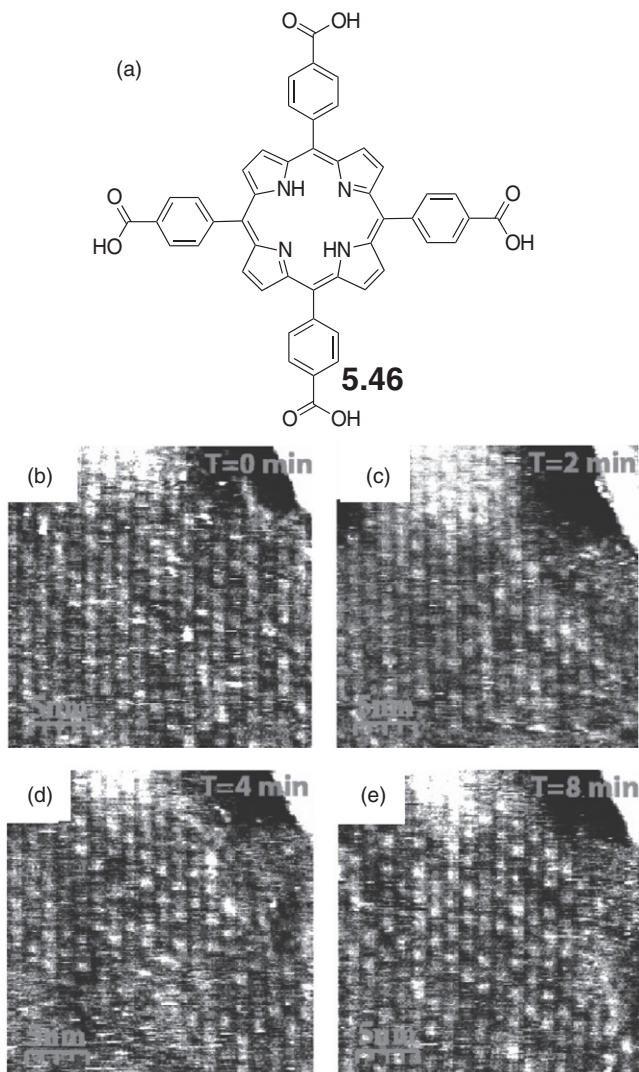


Figure 5.21. Molecular structure (a) of tetracarboxylporphyrin derivative **5.45**. STM images (b–e) relative to the slow reduction dynamic of **5.45** after the potential was stepped from 0.12 to 0.1 V ($c = 0.01\text{M HClO}_4$), revealed by the increase in the number of bright spots from b (50), c (80), d (100), to e (150). Source: [76]. Adapted with permission of the American Chemical Society.

5.5.1 Templated Supramolecular Systems

One of the most intuitive and effective approaches used for the preparation of supramolecular materials featured with a controlled dimension consists in the use of a template molecule, able to organize in precise fashion a finite number of building blocks, through the use of noncovalent interactions [17c]. In general, rigid linear molecules have been used in order to template in a monodisperse manner stacked 1D nanostructures. In this context Matile and coworkers, exploiting a combination of H-bonds and aromatic electron donor–acceptor interactions, were able to construct a supramolecular tubular nanostructure that could be exploited as a synthetic ion channel, able to be opened in response to a chemical stimulation (Figure 5.22) [78].

Rigid supramolecular templates **5.46** were synthesized incorporating a rigid *p*-octyphenyl rod molecule, eight naphthalene diimide (NDI) derivatives functionalized with amidic functions, that acting through self-recognition mediated by a complex combination of H-bonds and π - π interactions induce the formation of a closed *p*-helix channel. The addition of an electron-rich dialkyl naphthalene (DAN) derivative **5.47** (Figure 5.22b, left) resulted in its intercalation between the aromatic planes defined by

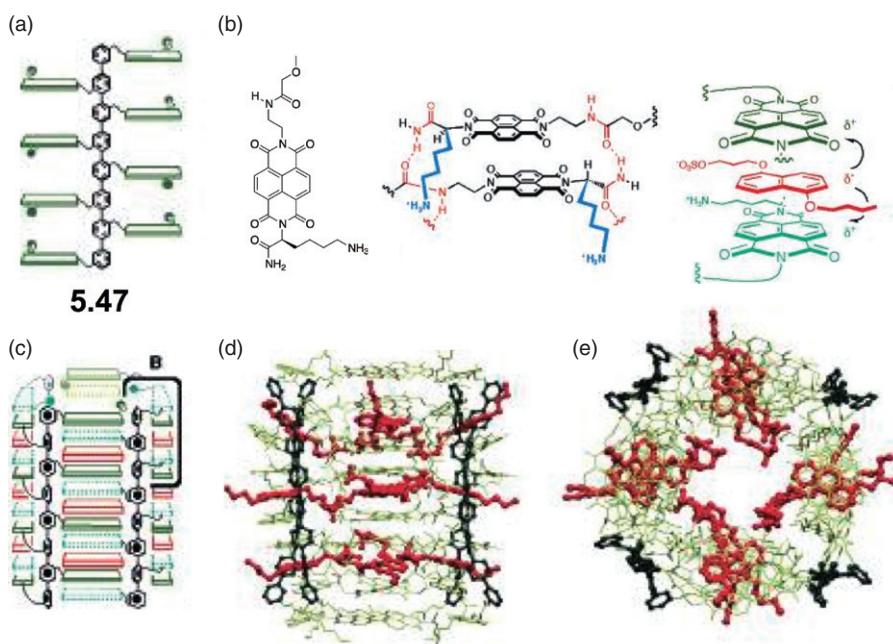


Figure 5.22. Schematic representation (a) of oligomeric template **5.46** used for the preparation of the artificial pores synthesized by Matile and coworkers. (b) Molecular structure of the DAN derivative **5.47** used (left) and schematic representation of the H-bond and aromatic donor–acceptor interactions occurring along the pore structure (center and right). Schematic depiction of the pore structure (c); red tiles represent the DAN units, whereas the green ones represent the NDI fragments. Axial (d) and top (e) views of the geometry-optimized model of the supramolecular pore (DANs units are represented in red). Source: [78]. Adapted with permission of the American Chemical Society. See color insert.

the NDI subunits, with a consequent structural change in the supramolecular architecture corresponding to the formation of an open channel. This structural modification, leading to an external control of the opening of the supramolecular pore, was attributed to the formation of a charge-transfer process between the NDI and the DAN units, able to induce the parallel disposition of their aromatic systems and therefore the opening of the channel.

Sugimoto and coworkers reported the formation of a well-defined ladder-like complex based on H-bond interactions between an oligomer having secondary dialkylammonium cations (constituting the rails of the ladder) and a porphyrin difunctionalized with 2,6-bis(2-oxazolyl)pyridine (PYBOX) moieties at the 5 and 15 *meso* positions (constituting the bars between the rails) [79]. As a further development of this work, through the introduction of chiral PYBOX moieties on the porphyrin core, the synthesis of bis-PYBOX derivative **5.48** was performed (Figure 5.23a) [80]. After mixing chiral unit **5.48** with the polycationic oligomer **5.49**, the formation of a helical nanostructure on HOPG surface was observed using AFM microscopy (Figure 5.23b,c).

CD and UV-Vis analyses of the mixture of **5.48** and **5.49** gave a further confirmation of the helical structure of the templated assembly in solution. Indeed, during titration experiments, the positive Cotton effect observed by CD in the Soret band of **5.48** was completely reverted, showing a decrease in the intensity (Figure 5.23d). This result confirmed the formation of helical arrangements as a probable consequence of the twisted π - π stacked interactions between the single units of **5.48** caused by the isopropyl groups on the oxazolyl rings. Another valid approach recently used for the preparation of H-bond-templated nanostructures takes advantage of the biomimetic exploitation of oligomeric nucleic acids as linear organic templates. This approach was demonstrated for the first time by Iwaura et al. [81], who were able to coassemble thymidine-functionalized OPV molecules using a complementary oligoadenylic eicosamer in aqueous solution. AFM analysis, in combination with CD and UV-Vis investigations, confirmed the formation of helical stacked structures. In a series of more recent works, the preparation of helical stacks formed of chromophoric conjugate molecules has been also attempted by other groups. Meijer and coworkers demonstrated that a single strand of DNA is able to template a supramolecular strand of chromophores, yielding a new type of DNA hybrid (Figure 5.24a,b). In this type of architecture, an oligothymine unit was used to template via multiple H-bond interactions the stack of different chromophores, such as naphthalene **5.50** or OPV **5.51**, each bearing a DAT unit as a molecular recognition site [82]. The formation and the stability of the supramolecular constructs were monitored by variable-temperature CD and UV-Vis spectroscopies, showing that the binding of the chromophores to the ssDNA was completely reversible and the formation of the helical stack followed a nucleation-growth mechanism.

As a further development of this work, in 2009, Schenning and coworkers developed a new type of chromophore able to respond to pH variation [83]. Diamino-purine derivative **5.52** (Figure 5.24c) was synthesized, and its ability to reversibly associate with an oligothymine template was investigated in solution by means of CD and UV-Vis spectroscopies [83]. Also in this case, both techniques confirmed the reversible association process forming right-handed supramolecular helices between the oligothymine strand and achiral guest **5.52**. Remarkably, by changing the pH from 8 to 2, the CD spectra showed a complete inversion of the Cotton effect proper of the right-handed helix, highlighting in this way the passage from a right-handed to a left-handed helix. The pH-dependent chirality inversion was hypothesized to be related to the

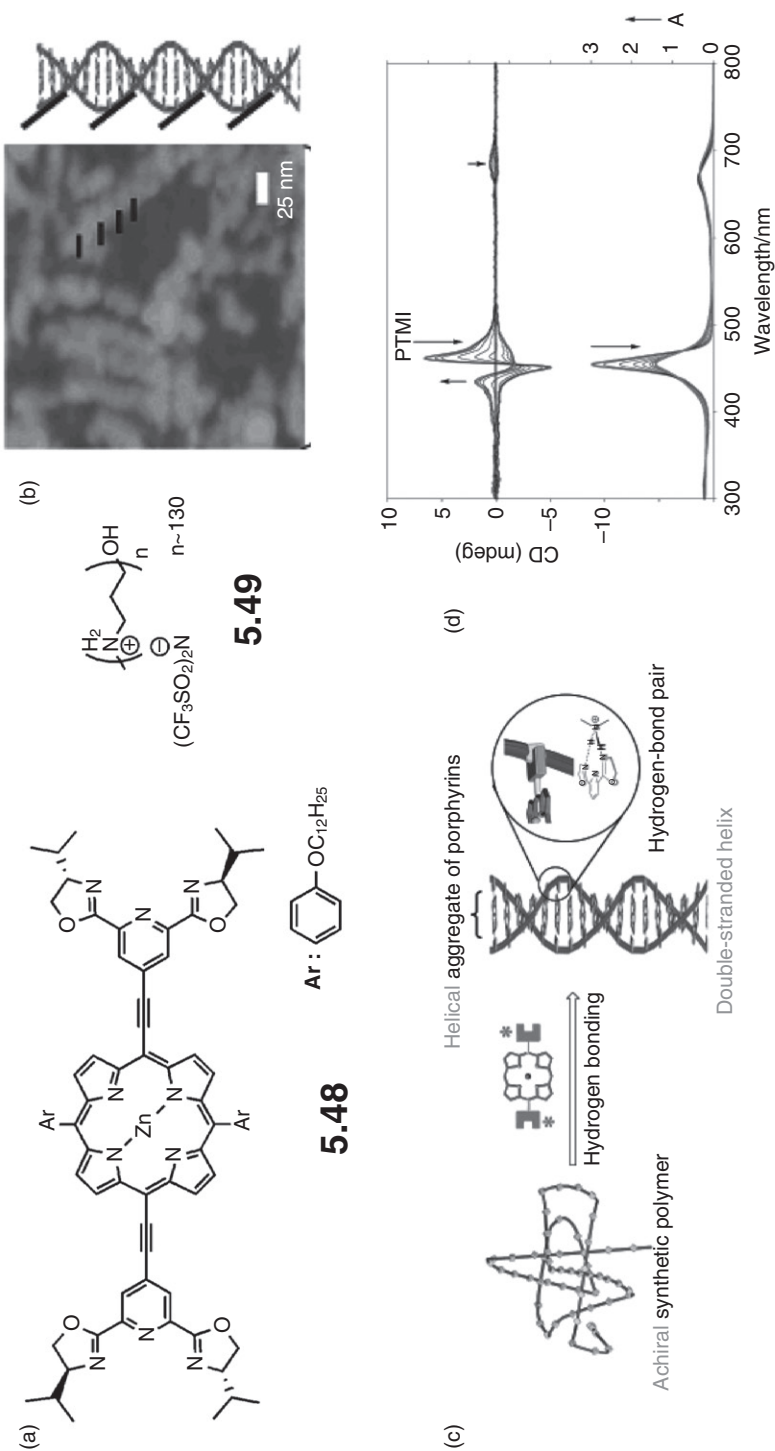


Figure 5.23. Molecular structures (a) of porphyrin derivative **5.48** (left) and of polycationic oligomer **5.49** (right), TM-AFM image (b, left) of the helical nanostructures formed by the H-bond-mediated assembly between **5.48** and **5.49**, and its schematic representation (right); black lines are used to highlight the step distance in the helix. Representative depiction (c) of the templated self-assembly process between **5.48** and oligomeric derivative **5.49**. (d) CD (top) and UV-Vis titration spectra of molecule **5.48** with module **5.49**. Source: [80]. Adapted with permission of the American Chemical Society.

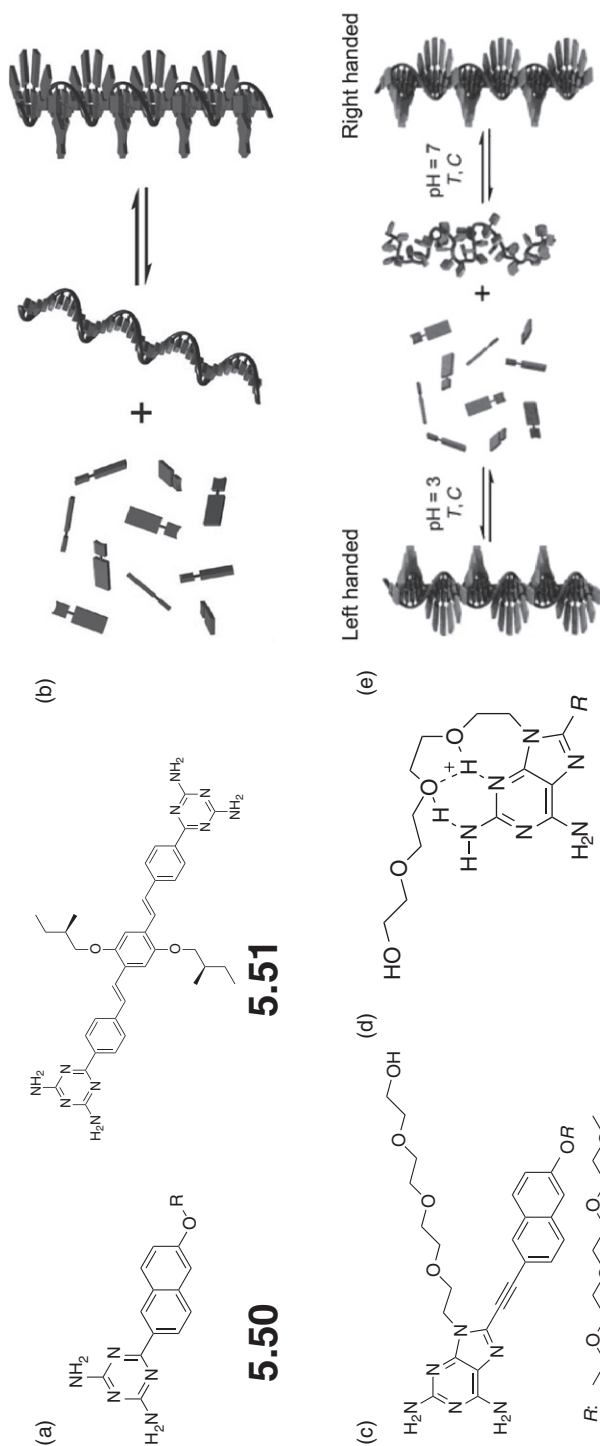
**5.53****5.52**

Figure 5.24. Molecular structures (a) of the naphthalene derivative **5.50** and of the OPV derivative **5.51** used by Meijer and Shenning for the preparation of the H-bond templated chromophoric stacks [82]. Schematic representation (b) of the assembly process between the oligothymine single strand and the DAT functionalized chromophores inducing the formation of the helical stacks. Reprinted (adapted) with permission from Janssen, P. G. A., Vandenberg, J., v. Dongen, J. L. J., Meijer, E. W., Shenning, A. P. H. J. (2007). ssDNA templated self-assembly of chromophores. *J. Am. Chem. Soc.*, *129*, 6078–6079. Copyright (2007) American Chemical Society. Molecular structure (c) of the adenosine derivative **5.52** and of its *N*-3 protonated species **5.53** (d) responsible for the pH-dependent chirality inversion of the helical stack. Schematic representation (e) of the pH-dependent handedness inversion of the helical chromophores stack. Source: [83]. Reproduced with permission of Wiley-VCH Verlag GmbH & Co. KGaA.

protonation of the *N*-3 position of the diamino-purine moieties of **5.52** leading to the formation of **5.53**. This phenomenon can be responsible for the change of conformation of the polyethyleneoxy chains present on the purine fragment that, due to electrostatic interactions, can induce a conformational rearrangement (Figure 5.24d,e) responsible for the stabilization of the left-handed helix.

5.5.2 Nontemplated Self-Organized Systems

Focusing on the use of H-bonds as principal noncovalent interactions for the preparation of discrete nanostructures, the preparation of soft nanoparticles and nanovesicles deserves particular attention. The work by Reinhoudt and coworkers on melamine functionalized calix[4]arene represents one of the first key examples of formation of discrete nano-objects through solely H-bond interactions [84]. Upon mixing three equivalents of calix[4]arene derivative **5.54** with six equivalents of mercocyanine dye **5.55**, the formation of an assembly comprising two coplanar chiral rosettes was obtained (Figure 5.25a), held together by the highly cooperative action of 36 H-bonds. Recently, Ajayaghosh and coworkers were able also to direct the self-assembly of OPE derivatives into the formation of spherical nanoparticles [85]. For this task, two OPE derivatives **5.56** and **5.57**, bearing at their termini hydroxy and methyl groups, respectively, were synthesized (Figure 5.25b). UV-Vis spectra of a solution of **5.56** in CHCl_3 showed a strong π - π^* absorption band at 377 nm, which led to redshifted bands at 385 and 419 nm, whereas no considerable differences were noticeable in the case of derivative **5.57**. These changes in the absorption spectra of compound **5.56** are attributed to the formation of J-type aggregates. Tapping mode atomic force microscopy (TM-AFM) and high-resolution transmission electron microscopy (HR-TEM) investigations of a decane solution ($c = 1 \times 10^{-6}$ M) of derivative **5.56** showed the formation of highly monodispersed nanoparticles provided with spherical geometry and a vesicular structure (Figure 5.25c-f).

Most remarkably, AFM images at higher concentration (ca. 10^{-5} M) showed a pronounced tendency of these vesicles to agglomerate and fuse, ultimately leading to the formation of a self-supporting gel with a strong blue fluorescence ($\lambda_{\text{max}} = 443$ nm). In a further development of the same work, the introduction of a chiral center into the lateral chains of the OPE core led to the selective transformation of the particle obtained by OPE derivative **5.56** into helical fibers, through a sergeant-soldier-type mechanism [86].

In a collaborative work with the group of N. Armaroli, our group has recently developed a novel approach for the preparation of both hollow and filled spherical nanostructures, through the combination of both H-bond, aromatic-aromatic, and solvophobic interactions [87]. Under temperature and solvent polarity control, supramolecular adducts between two π -conjugated units, bearing complementary H-bonding groups, can be obtained in solution and further organized into hollow spherical nano-objects provided with a vesicular structure. In this work, the possibility of changing the size distribution and shape by changing the stoichiometric ratio of the molecular components was proven to be a consequence of the solvophobic/solvophilic interaction established among the supramolecular species (Figure 5.26). For this task, molecular modules **5.58** and **5.59** bearing complementary H-bond recognition moieties were synthesized. Molecule **5.58** consisted of a *p*-disubstituted central benzene ring bearing at both sides two 2,6-bis(acetylamino)-pyridyl moieties, whereas molecule **5.59**

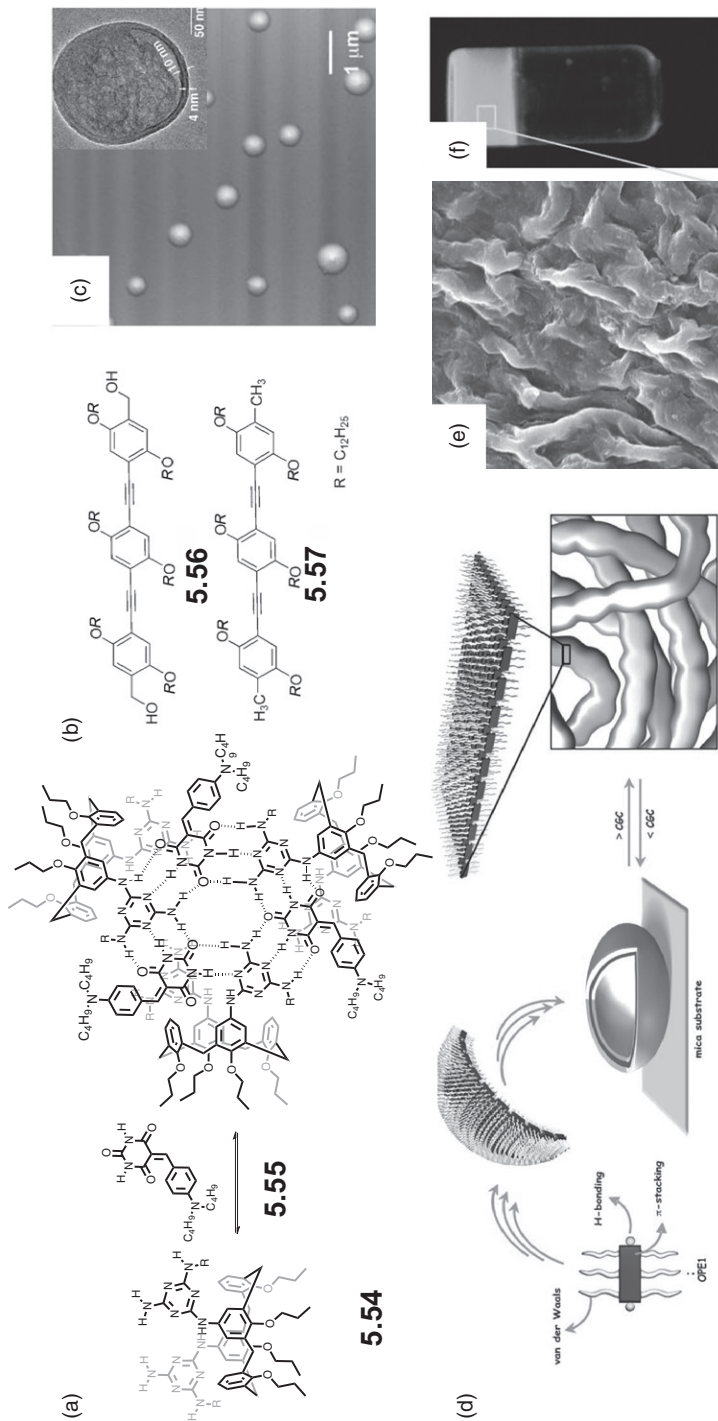


Figure 5.25. Self-assembly process (a) between calix[4]arene derivative **5.54** and the mercyanine **5.55**, producing a supramolecular discrete nonameric complex (*R* = benzyl) [84]. Molecular structures (b) of the OPE derivatives **5.56** and **5.57** and TM-AFM image (c) and HR-TEM image (inset) of the spherical nanoparticles obtained by the H-bond-mediated self-assembly of **5.57**. Schematic representation (d) of the interconversion mechanism between nanoparticles and gel structure. SEM images of the gel produced by OPE derivative **71** in decane (e) and photograph of the gel in decane (f) under UV illumination at 365 nm. Source: [85]. Reproduced with permission of Wiley-VCH Verlag GmbH & Co. KGaA.

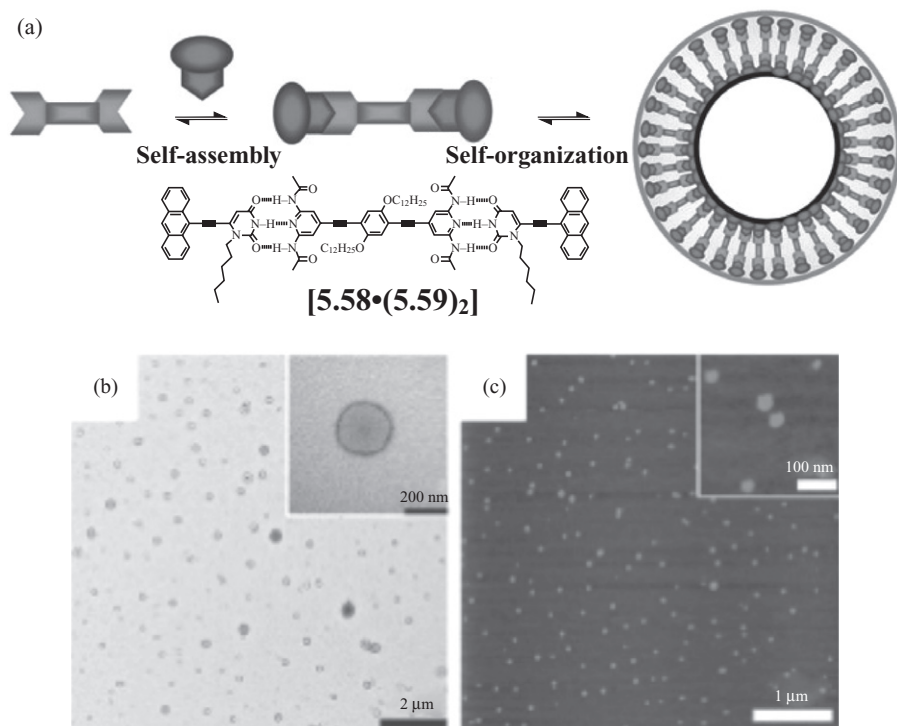


Figure 5.26. Schematic representation (a) of the self-organization process between molecular modules **5.58** and **5.59** resulting in the formation of H-bond-based vesicular nanostructures. TEM (b) and TM-AFM (c) images of a drop-casted solution of molecules **5.58** and **5.59** in 1:2 ratio (insets: detail on the single nanoparticle). Source: [87]. Adapted with permission of the Royal Society of Chemistry.

possessed only one H-bond recognition site consisting of a uracil moiety. These molecular units are known to undergo a self-assembly process through the formation of triple H-bonding systems with high association constant in apolar solvents (between 10^4 and 10^5 M^{-1}) [88].

The UV-Vis spectrum of the ternary mixture $[5.58 \cdot (5.59)_2]$ presented the formation of a new redshifted band, which was not present in the spectra of the isolated compounds, thus potentially ascribed to the formation of π - π aggregates, likely induced by the formation of the H-bonded trimers $[5.58 \cdot (5.59)_2]$. Remarkably, TEM and AFM analyses of drop-cast solutions of a 1:2 mixture of **5.58** and **5.59** showed the presence of supramolecular vesicles provided with uniform size distribution (diameter ranging from 80 to 180 nm). Such results confirm that the self-assembly between **5.58** and **5.59** increases the solute-solvent interactions as a consequence of the change of the solvophobic 2,6-di(acetylamino)-pyridyl moieties into the more solvophilic anthracenyl extremity, thermodynamically favoring the formation of the spherical supramolecular vesicles. Aiming at investigating the influence of the geometry of the single-molecular components on the morphological features of self-organized

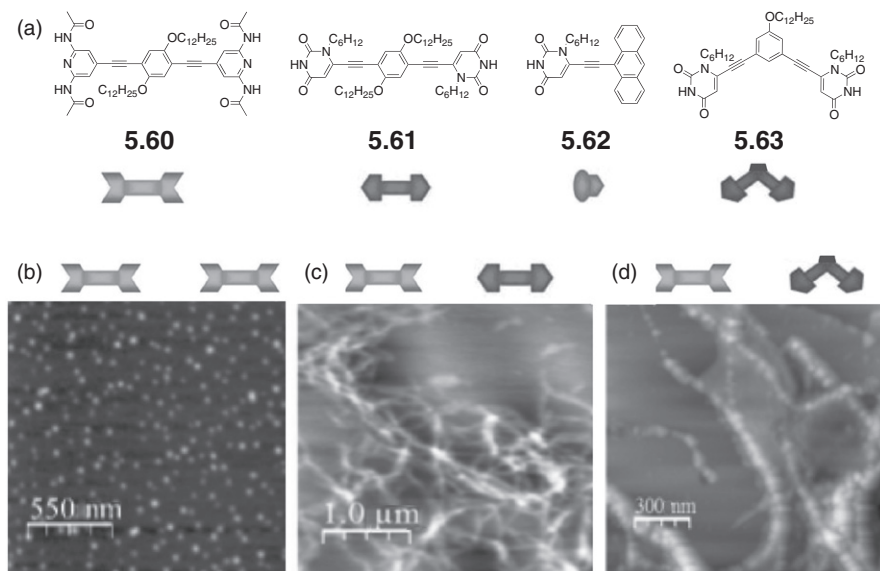


Figure 5.27. Molecular structures (a) of the different building blocks (**5.60–5.63**) bearing complementary H-bonding units. Topographic TM-AFM images (b–d) of the assemblies **[5.60]_n** (b), **[5.60-5.61]_n** (c), and **[5.60-5.63]_n** (d) on the mica surface, showing the formation of different type of nanostructures such as nanoparticles, linear, and helicoidal arranged nanofibers, respectively. Source: [10h]. Reproduced with permission of Wiley-VCH Verlag GmbH & Co. KGaA.

nanostructures, our group has synthesized a molecular library consisting of different phenylacetylenic scaffolds equipped with 2,6-di-(acetyl-amino)-pyridil or uracil moieties (**5.60–5.63**, Figure 5.27) [10h].

In this context it was clearly demonstrated that depending on the number of recognition moieties and their spatial disposition, different types of self-assembled nanostructures could be obtained through a fine tuning of the self-assembling conditions (Figure 5.27). Interestingly, by mixing the previously discussed building block **5.60** with its linear complementary unit **5.61**, it was possible to characterize by AFM analysis the formation of nanowires of length above 400 nm and width of approximately 30 nm. Upon addition of molecular stopper **5.62**, the nanostructured material turned into nanorods with length between 80 and 200 nm and width between 40 and 60 nm. In a second set of experiments, the simple exchange of the linear molecule **5.61** with bent-shaped molecule **5.63** led to the formation of self-organized nanofibers. Detailed morphological investigations showed the presence of humps and lumps on the surface, most probably originated by the presence of helicoidally organized 1D nanostructures. In the same work, a novel kind of stimuli-induced nanostructuring process has been also reported exploiting thermally labile protecting groups. In particular, *tert*-butoxycarbonyl (BOC)-protected uracil derivative **5.64** was shown to easily undergo thermal deprotection at 145°C, thus allowing H-bond formation at room

temperature [89]. Microscopy studies evidenced that the BOC-protected tetrapotic module **5.64** self-assembles and self-organizes with **5.60** into extended domains of circular nano-objects upon heating at 145°C. Confirmation of the occurrence of the self-assembly/self-organization process in solution was obtained by variable temperature (VT) steady-state UV-Vis absorption and emission measurements, which showed a progressive decrease in the absorption feature at 480 nm and the concomitant appearance of a new band centered at 505 nm as a direct consequence of the formation of H-bonded supramolecular assemblies initiated by the thermal cleavage of the BOC group (Figure 5.28).

The AFM characterization of the nanostructures originating from the self-organization of [**5.64a**•**5.60**]_n on surfaces showed the formation of very regular nano-objects possessing morphologies that resemble that of a crater. The variation of the geometrical features of such systems was monitored by AFM imaging at different temperatures, leading to the elaboration of a thermodynamic theoretical model, showing that the self-organization process is strictly correlated to the solute diffusivity D_0 , the solvent kinematic viscosity η , and the temperature.

Another important challenge in the development of discrete nanostructures is the preparation of nano-objects characterized by a circular shape such as rings or toroids. In this context, Ajayaghosh and coworkers have recently reported the hierarchized assembly of melamine-functionalized OPE derivatives in the presence of cyanuric acid derivatives, resulting in the formation of luminescent toroid nanostructures [90]. The bicomponent system formed by OPE-functionalized derivative and **5.65** is able to self-assemble into discrete H-bond-based rosettes, through which π - π stacking interaction of the final toroid structure is evolved (Figure 5.29).

Absorption measurements showed that the major driving force leading to the rosette association was the formation of H-type aggregates induced by the OPE fragments of **5.66**. Moreover, molecular modeling simulations showed that the aromatic planes defined by the OPE moieties were rotated 45° with respect to the H-bond plane, confirming that an extended association of rosettes in such tilted conformation could lead to the formation of columnar assemblies provided with a certain degree of curvature, such as in the case of toroidal objects. In a very recent paper, the preparation of H-bond-based toroidal nanostructures was also achieved by Yagai and coworkers, through the self-assembly between complementary OPV derivatives opportunely functionalized with barbiturate moieties at one of their termini [91]. Compounds **5.67**–**5.69** consisted of a barbituric acid H-bonding head group, an OPV π -conjugated segment, and a wedge-shaped tridodecyloxybenzyl (TDB) moiety (Figure 5.30a). UV-Vis spectra of an MCH solution showed a strong hypochromic effect in comparison to the one in tetrahydrofuran (THF) as a consequence of an associative phenomenon. The authors hypothesize that the formation of the ring structures was caused by the specific curvature encoded within the π - π stacked columnar nanostructures of the supramolecular macrocycle formed through H-bonds in dilute conditions.

Most notably, close AFM investigations of spin-coated solutions ($c = 1 \times 10^{-4}$ M) of **5.68** and **5.69** in MCH on HOPG showed the formation of interlocked structures made of two nanorings, whereas for the derivative **5.67**, interlocked structures were not observed (Figure 5.30b–d). This can be rationalized, taking in consideration the different types of supramolecular macrocycles formed by the different OPV building blocks. In the case of OPV derivative **5.67**, the ring structures resulting from the π - π interaction of the supramolecular macrocycles were too small (average diameter of 25 nm)

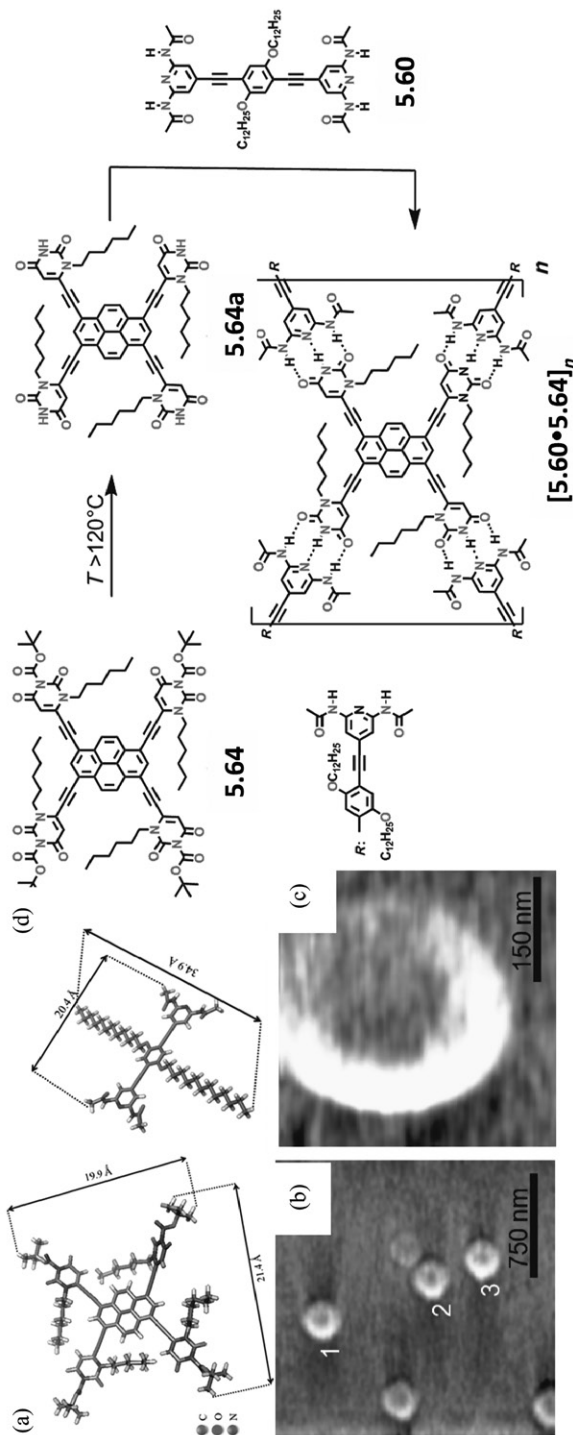


Figure 5.28. Optimized geometrical structures (a) of molecular modules **5.64** (right) and **5.60** (left). TM-AFM topography of the crater-like self-organized morphologies (b and c) as obtained from the assembly of molecules $[\mathbf{5.64}\cdot\mathbf{5.60}]_n$ from a solution deposited on mica surfaces at 145°C . Schematic representation (d) of the nanostructure process between molecules **5.64** and **5.60** triggered by the T-dependent removal of the BOC protecting group. Source: [89]. Adapted with permission of the American Chemical Society.

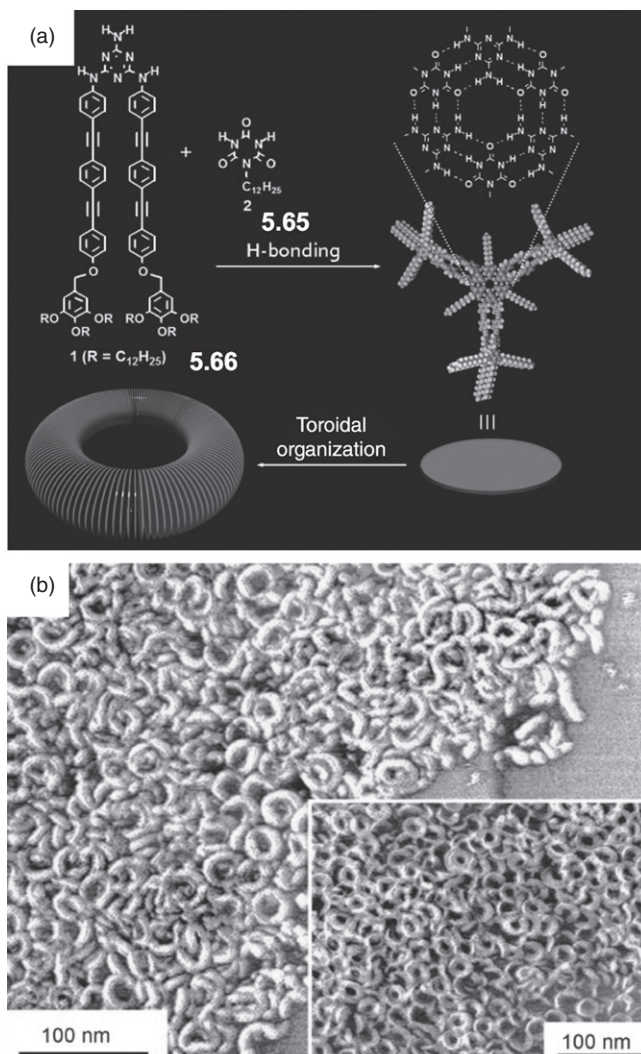


Figure 5.29. Schematic representation (a) of the self-assembly process between melamine-linked OPE **5.66** and cyanurate **5.65**, inducing the formation of toroid nano-objects. TM-AFM image (b) of an equimolar mixture of **5.66** and **5.65** as spin-coated from decane solution on HOPG (Inset: image obtained by low-force tapping mode). Source: [90]. Reproduced with permission of Wiley-VCH Verlag GmbH & Co. KGaA.

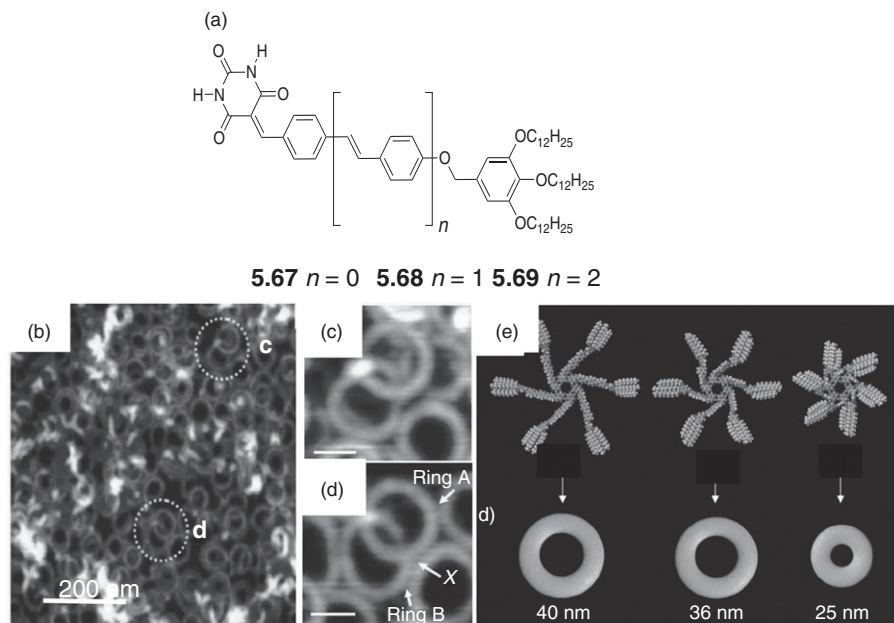


Figure 5.30. Molecular structures (a) of the barbituric derivatives **5.67**–**5.69** used by *Yagai* and coworkers to induce the formation of discrete supramolecular nanorings. TM-AFM images (b–d) of a spin-coated solution of **5.69** on HOPG surface revealing the formation of interlocked nanoring structures resembling the formation of catenanes. Schematic representation (e) of the correlation existing between the molecular structures of **5.67**–**5.69** and the size of the relative nanorings. Source: [91]. Reproduced with permission of Wiley-VCH Verlag GmbH & Co. KGaA.

to allow an effective interlocking of the single nanoring, and the resulting nanostructures were therefore constituted only by isolated circular units (Figure 5.30e).

A further strategy, recently used for the preparation of discrete nanostructures composed of an extremely restricted number of supramolecular building blocks, consists in the exploitation of surface-based methods. Indeed, the size control of H-bonded assemblies and the relative positioning of a small number of supramolecular building blocks can be achieved more easily if the self-assembly process is restricted to only two dimensions. One of the systems that is most studied so far is the one regarding the self-association of the DAT OPV derivatives **5.70**–**5.72** (Figure 5.31a) [92].

All of the derivatives self-organize at the 1-phenyloctane/HOPG interface into chiral hexameric rosettes as a result of the formation of H-bond pairs between the DAT moieties (Figure 5.31b,c). Pure enantiomers **5.70** and **5.71** lead to the exclusive formation of one of the two possible mirror-type arrangements, whereas the achiral derivative **5.72** resulted in the formation of equal amounts of mirror-image domains. Using this approach, it is also possible to induce the formation of monolayers constituted by the heteroassociation of a mixture of different building blocks. In this context, H-bonded rosettes between OPV derivative **5.74** and N-unsubstituted naphthalene bisimide (NBI) derivatives **5.73** have been visualized at the HOPG–solvent interface

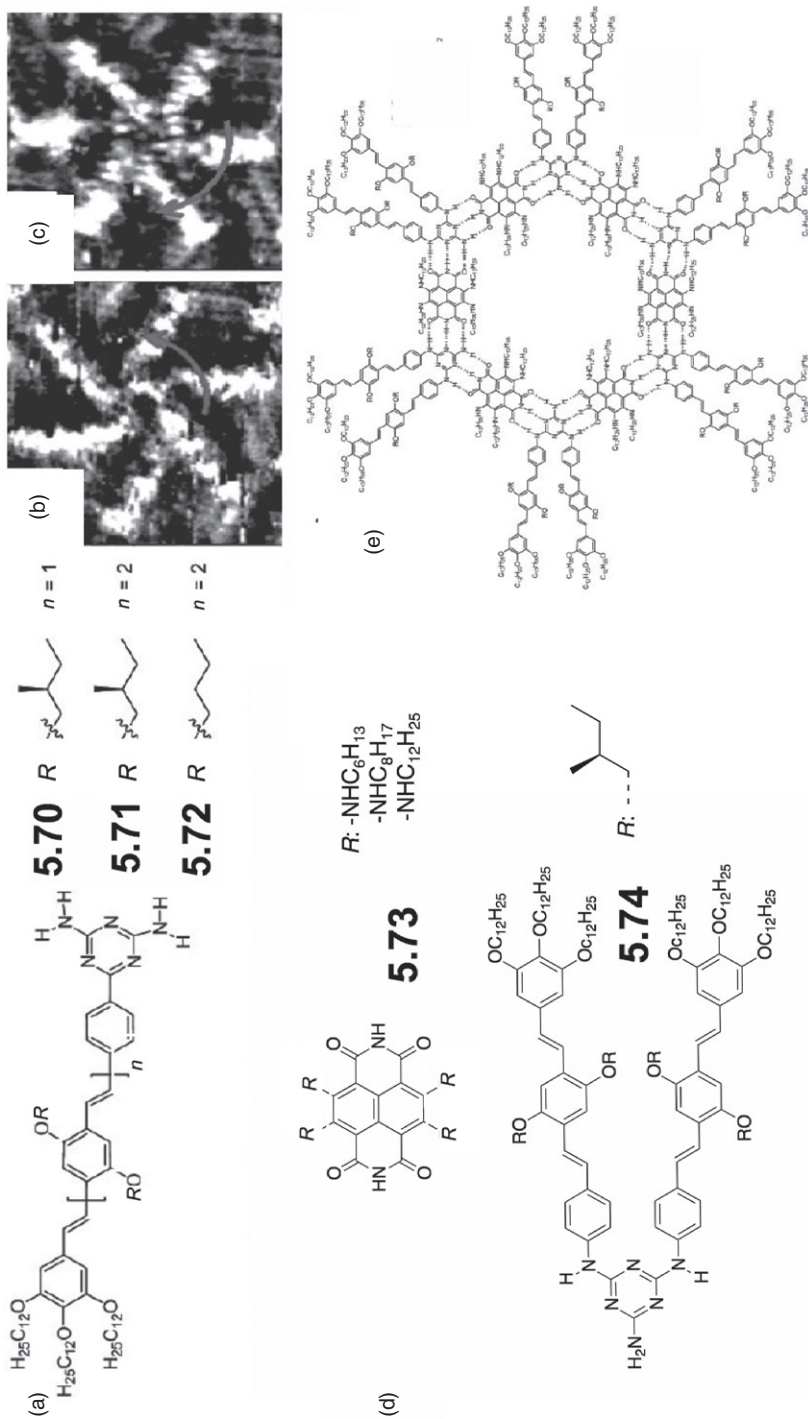


Figure 5.31. Molecular structures (a) of the OPV derivatives **5.70–5.72**. Mirror type domains (b and c) obtained at the solid–liquid interface from the deposition of **5.70** and **5.71**, respectively. Source: [92a]. Reproduced with permission of Wiley-VCH Verlag GmbH & Co. KGaA.

by STM measurements [92b]. Despite the disordered nature of the assembly, the formation of the heterocomplex at the solid–liquid interface was demonstrated using a bias-dependent imaging technique able to discriminate between the electronic properties of the single components.

5.6 CONCLUSIONS

In this chapter, the most recent advancements concerning the design and the preparation of organic nanomaterials through H-bond interactions have been reviewed. In Section 5.1, the reader was introduced to the fundamental aspects regarding the design and the preparation of supramolecular materials through H-bond interactions. In this context, the two main supramolecular polymerization mechanisms (isodesmic and cooperative) have been discussed, highlighting their basic thermodynamic features. Subsequently, the principal characteristics of the H-bond-based molecular recognition process have been discussed, with particular emphasis on the factors that are able to influence the strength, selectivity, and reversibility of this noncovalent interaction (such as the number of H bonds, their dispositions along the molecular backbone, and the presence of tautomerization phenomena). Finally, the use of multiple H-bond systems for the preparation of supramolecular polymeric materials has been discussed, showing how through an opportune design of the structural parameters of the single-molecular modules, and by a strict control of the solvent and temperature conditions, it is possible to produce organic materials possessing different geometrical structures such as nanofibers, 2D organic networks, vesicles, or toroids. The development of all of the H-bond nanostructured systems reported in this chapter has been possible thanks to the recent developments in the synthesis and preparation of increasingly more complex and elaborate building blocks, which introduced the possibility of studying with a higher degree of detail the self-assembly and self-organization process of the different kinds of supramolecular polymers.

Although nowadays this approach is still far from being exploited for the commercial production of devices in the “everyday world,” its advantages [93] (high convergence in the nanostructuring protocol, facile formation of the final nanostructures by simple mixing of the components, possibility of obtaining defect-free architecture due to the reversible nature of the interactions involved, which can induce the most thermodynamically stable phase) outline the necessity of further expanding the knowledge and technologies required for the preparation of increasingly more sophisticated supramolecular nanostructures, which in the near future could be the foundation of leading technologies in the world.

REFERENCES

- [1] Grimsdale, A. C., Müllen, K. (2005). The chemistry of organic nanomaterials. *Angewandte Chemie—International Edition*, 44, 5592–5629.
- [2] Rao, C. N. R., Kulkarni, G. U., Thomas, P. J., Edwards, P. P. (2000). Metal nanoparticles and their assemblies. *Chemical Society Reviews*, 29, 27–35.
- [3] Hamley, I. W. (2003). Nanotechnology with soft materials. *Angewandte Chemie—International Edition*, 42, 1692–1712.

- [4] Rogach, A. L., Talapin, D. V., Weller, H. *Colloids and Colloid Assemblies*, Caruso, F. (Ed.), Wiley-VCH, Weinheim, 2004.
- [5] Aymonier, C., Schlotterbeck, U., Antonietti, L., Zacharias, P., Thomann, R., Tiller, J. C., Mecking, S. (2002). Hybrids of silver nanoparticles with amphiphilic hyperbranched macromolecules exhibiting antimicrobial properties. *Chemical Communications*, 3018–3019.
- [6] Hirst, A. R., Escuder, B., Miravet, J. F., Smith, D. K. (2008). High-tech applications of self-assembling supramolecular nanostructured gel-phase materials: From regenerative medicine to electronic devices. *Angewandte Chemie—International Edition*, 47, 8002–8018.
- [7] Bishop, K. J. M., Wilmer, C. E., Soh, S., Grzybowski, B. A. (2009). Nanoscale forces and their use in self-assembly. *Small*, 5, 1600–1630.
- [8] (a) Lehn, J. M. *Supramolecular Chemistry: Concepts and Perspectives*, Wiley VCH, Weinheim, 1995; (b) Lehn, J. M. (1990). Perspectives in supramolecular chemistry: From molecular recognition towards molecular information processing and self-organization. *Angewandte Chemie—International Edition*, 29, 1304–1309.
- [9] (a) Salonen, L. M., Ellermann, M., Diederich, F. (2011). Aromatic rings in chemical and biological recognition: Energetics and structures. *Angewandte Chemie—International Edition*, 50, 4808–4842; (b) Meyer, E. A., Castellano, R. K., Diederich, F. (2003). Interactions with aromatic rings in chemical and biological recognition. *Angewandte Chemie—International Edition*, 42, 1210–1250; (c) Fischer, F. R., Schweizer, W. B., Diederich, F. (2008). Substituent effects on the aromatic edge-to-face interaction. *Chemical Communications*, 4031–4033; (d) Faul, C. F. J., Antonietti, M. (2003). Ionic self-assembly: Facile synthesis of supramolecular materials. *Advanced Materials*, 15, 673–683.
- [10] (a) Elemans, J. A. A. W., Rowan, A. E., Nolte, R. J. M. (2003). Mastering molecular matter. Supramolecular architectures by hierarchical self-assembly. *Journal of Materials Chemistry*, 13, 2661–2670; (b) Vriezema, D. M., Aragonès, M. C., Elemans, J. A. A. W., Cornelissen, J. J. L. M., Rowan, A. E., Nolte, R. J. M. (2005). Self-assembled nanoreactors. *Chemical Reviews*, 105, 1445–1490; (c) Cornelissen, J. J. L. M., Rowan, A. E., Nolte, R. J. M., Sommerdijk, N. A. J. M. (2001). Chiral architectures from macromolecular building blocks. *Chemical Reviews*, 101, 4039–4070; (d) Aida, T., Meijer, E. W., Stupp, S. I. (2012). Functional supramolecular polymers. *Science*, 335, 813–817; (e) Hoeben, F. J. M., Jonkheijm, P., Meijer, E. W., Schenning, A. P. H. J. (2005). About supramolecular assemblies of π -conjugated systems. *Chemical Reviews*, 105, 1491–1546; (f) Leclère, P., Surin, M., Viville, P., Lazzaroni, R., Kilbinger, A. F. M., Henze, O., Feast, W. J., Cavallini, M., Biscarini, F., Schenning, A. P. H. J., Meijer, E. W. (2004). About oligothiophene self-assembly: From aggregation in solution to solid-state nanostructures. *Chemistry of Materials*, 16, 4452–4466; (g) De Greef, T. F. A., Smulders, M. M. J., Wolffs, M., Schenning, A. P. H. J., Sijbesma, R. P., Meijer, E. W. (2009). Supramolecular polymerization. *Chemical Reviews*, 109, 5687–5754; (h) Yoosaf, K., Llanes-Pallas, A., Marangoni, T., Belbakra, A., Marega, R., Botek, E., Champagne, B., Bonifazi, D., Armaroli, N. (2011). From molecular to macroscopic engineering: Shaping hydrogen-bonded organic nanomaterials. *Chemistry—A European Journal*, 17, 3262–3273.
- [11] (a) Ciferri, A. *Supramolecular Polymers*, 2nd ed., CRC Press, Boca Raton, FL, 2005; (b) Brunsveld, L., Folmer, B. J. B., Meijer, E. W., Sijbesma, R. P. (2001). Supramolecular polymers. *Chemical Reviews*, 101, 4071–4098; (c) De Greef, T. F. A., Meijer, E. W. (2008). Materials science: Supramolecular polymers. *Nature*, 453, 171–173; (d) Korevaar, P. A., George, S. J., Markvoort, A. J., Smulders, M. M. J., Hilbers, P. A. J., Schenning, A. P. H. J., De Greef, T. F. A., Meijer, E. W. (2012). Pathway complexity in supramolecular polymerization. *Nature*, 481, 492–496.
- [12] Sijbesma, R. P., Beijer, F. H., Brunsveld, L., Folmer, B. J. B., Hirschberg, J. H. K. K., Lange, R. F. M., Lowe, J. K. L., Meijer, E. W. (1997). Reversible polymer formed from self complementary monomers using quadruple hydrogen bonding. *Science*, 278, 1601–1604.
- [13] (a) Cordier, P., Tournilhac, F., Soulie-Ziakovi, C., Leibler, L. (2008). Self-healing and thermoreversible rubber from supramolecular assembly. *Nature*, 451, 977–980; (b) Noro, A., Hayashi,

- M., Matsushita, Y. (2012). Design and properties of supramolecular polymer gel. *Soft Matter*, 8, 2416–2429; (c) Broer, D. J., Bastiaansen, C. M. W., Debije, M. G., Schenning, A. P. H. J. (2012). Functional organic materials based on polymerized liquid-crystal monomers: Supramolecular hydrogen-bonded systems. *Angewandte Chemie—International Edition*, 51, 7102–7109; (d) Liu, K. L., Zhang, Z., Li, J. (2011). Supramolecular hydrogels based on cyclodextrin-polymerpolypseudorotaxanes: Materials design and hydrogel properties. *Soft Matter*, 7, 11290–11297; (e) Cooke, G., Rotello, V. M. (2002). Methods of modulating hydrogen bonded interactions in synthetic host–guest systems. *Chemical Society Reviews*, 31, 275–286.
- [14] Lehn, J. M. (2002). Toward self-organization and complex matter. *Science*, 295, 2400–2403.
- [15] (a) Beijer, F. H., Sijbesma, R. P., Kooijman, H., Spek, A. L., Meijer, E. W. (1998). Strong dimerization of ureidopyrimidones via quadruple hydrogen bonding. *Journal of the American Chemical Society*, 120, 6761–6769; (b) Wilson, A. J. (2007). Non-covalent polymer assembly using arrays of hydrogen-bonds. *Soft Matter*, 3, 409–425; (c) Sijbesma, R. P., Meijer, E. W. (2003). Quadruple hydrogen bonded systems. *Chemical Communications*, 1, 5–16.
- [16] (a) Seiffert, S., Sprakelc, J. (2012). Physical chemistry of supramolecular polymer networks. *Chemical Society Reviews*, 41, 909–930; (b) Kumar, S. (2006). Self-organization of disc-like molecules: Chemical aspects. *Chemical Society Reviews*, 35, 83–109.
- [17] (a) Ryu, J. H., Hong, D. J., Lee, M. (2008). Aqueous self-assembly of aromatic rod building blocks. *Chemical Communications*, 1043–1054; (b) Chen, Z., Lohr, A., Saha-Moller, C. R., Wurthner, F. (2009). Self-assembled π -stacks of functional dyes in solution: Structural and thermodynamic features. *Chemical Society Reviews*, 38, 564–584; (c) Klosterman, J. K., Yamachi, Y., Fujita, M. (2009). Engineering discrete stacks of aromatic molecules. *Chemical Society Reviews*, 38, 1714–1725.
- [18] Gillissen, M. A. J., Hoeben, T. T., Spiering, A. J. H., Vekemans, J. A. J. M., Palmans, A. R. A., Meijer, E. W. (2011). Supramolecular chirality using both cooperative and isodesmic self-assembly: Hierarchical growth through competition. *Israel Journal of Chemistry*, 51, 1118–1127.
- [19] Hunter, C. A., Anderson, H. L. (2009). What is cooperativity? *Angewandte Chemie—International Edition*, 48, 7488–7499.
- [20] (a) Janssen, P. G. A., Jabbari-Farouji, S., Surin, M., Vila, J. G. X., De Greef, T. F. A., Vos, M. R. J., Bomans, P., Sommerdijk, N. A. J. M., Christianen, P. C. M., Leclère, P., Lazzaroni, R., van der Schoot, P., Meijer, E. W., Schenning, A. P. H. J. (2009). Insights into templated supramolecular polymerization: Binding of naphthalene derivatives to ssDNA templates of different lengths. *Journal of the American Chemical Society*, 131, 1222–1231; (b) Markvoort, A. J., Eikelder, H. M. M. T., Hilbers, P. A. J., De Greef, T. F. A., Meijer, E. W. (2011). Theoretical models of nonlinear effects in two-component cooperative supramolecular copolymerizations. *Nature Communications*, 2, 1–9.
- [21] (a) Fathalla, M., Lawrence, C. M., Zhang, N., Sessler, J. L., Jayawickramarajah, J. (2009). Base-pairing mediated non-covalent polymers. *Chemical Society Reviews*, 38, 1608–1620; (b) Prins, L. J., Reinhoudt, D. N., Timmerman, P. (2001). Noncovalent synthesis using hydrogen bonding. *Angewandte Chemie—International Edition*, 40, 2382–2426; (c) Rodríguez, D. G. A., Schenning, A. P. H. J. (2011). Hydrogen-bonded supramolecular π -functional materials. *Chemistry of Materials*, 23, 310–325.
- [22] (a) Beijer, F. H., Kooijman, H., Spek, A. L., Sijbesma, R. P., Meijer, E. W. (1998). Self-complementarity achieved through quadruple hydrogen bonding. *Angewandte Chemie—International Edition*, 37, 75–78; (b) Zimmerman, S. C., Corbin, P. S. (2000). Heteroaromatic modules for self-assembly using multiple hydrogen bonds. *Structure and Bonding*, 96, 63–94; (c) Stupp, S. (2010). Self-assembly and biomaterials. *Nano Letters*, 10, 4783–4786; (d) Palmer, L. C., Stupp, S. I. (2008). Molecular self-assembly into one-dimensional nanostructures. *Accounts of Chemical Research*, 41, 1674–1684; (e) Fouquey, C., Lehn, J. M., Levelut, A. M. (1990). Molecular recognition directed self-assembly of supramolecular liquid crystalline polymers from complementary chiral components. *Advanced Materials*, 2(5), 254–257.

- [23] Arunan, E., Desiraju, G. R., Klein, R. A., Sadlej, J., Scheiner, S., Alkorta, I., Clary, D. C., Crabtree, R. H., Dannenberg, J. J., Hobza, P., Kjaergaard, H. G., Legon, A. C., Mennucci, B., Nesbitt, D. J. (2011). Defining the hydrogen bond: An account. *Pure and Applied Chemistry*, 83, 1619–1636.
- [24] Emsley, J. (1980). Very strong hydrogen bonding. *Chemical Society Reviews*, 9, 91–124.
- [25] Archer, E. A., Gong, H., Krische, M. J. (2001). Hydrogen bonding in noncovalent synthesis: Selectivity and the directed organization of molecular strands. *Tetrahedron*, 57, 1139–1159.
- [26] Hunter, C. A. (2004). Quantifying intermolecular interactions: Guidelines for the molecular recognition toolbox. *Angewandte Chemie—International Edition*, 43, 5310–5324.
- [27] Schneider, H. J., Juneva, R. K., Simova, S. (1989). Solvent and structural effects on hydrogen bonds in some amides and barbiturates: An additive scheme for the stability of corresponding host-guest complexes. *Chemische Berichte*, 122, 1211–1213.
- [28] (a) Jorgensen, W. L., Pranata, J. (1990). Importance of secondary interactions in triply hydrogen bonded complexes: Guanine-cytosine vs uracil-2,6-diaminopyridine. *Journal of the American Chemical Society*, 112, 2008–2010; (b) Pranta, J., Wierschke, S. G., Jorgensen, W. L. (1991). OPLS potential functions for nucleotide bases. Relative association constants of hydrogen-bonded base pairs in chloroform. *Journal of the American Chemical Society*, 113, 2810–2819.
- [29] Sartorius, J., Schneider, H. J. (1996). A general scheme based on empirical increments for the prediction of hydrogen-bond associations of nucleobases and of synthetic host-guest complexes. *Chemistry—A European Journal*, 2, 1446–1452.
- [30] Todd, E. M., Quinn, J. R., Park, T., Zimmerman, S. C. (2005). Fidelity in the supramolecular assembly of triply and quadruply hydrogen-bonded complexes. *Israel Journal of Chemistry*, 45, 381–389.
- [31] (a) Beijer, F. H., Sijbesma, R. P., Kooijman, H., Spek, A. L., Meijer, E. W. (1998). Strong dimerization of ureidopyrimidones via quadruple hydrogen bonding. *Journal of the American Chemical Society*, 120, 6761–6769; (b) Söntjens, S. H. M., Sijbesma, R. P., van Genderen, M. H. P., Meijer, E. W. (2000). Stability and lifetime of quadruply hydrogen bonded 2-ureido-4[1H]-pyrimidinone dimers. *Journal of the American Chemical Society*, 122, 7487–7493.
- [32] (a) Perron, M. E., Monchamp, F., Duval, H., Boils-Boissier, D., Wuest, J. D. (2004). Controlling the assembly of hydrogen-bonded supramolecular polymers by the strategy of molecular tectonics. *Pure and Applied Chemistry*, 76, 1345–1351; (b) Brunsveld, L., Vekemans, J. A. J. M., Hirschberg, J. H. K. K., Sijbesma, R. P., Meijer, E. W. (2002). Hierarchical formation of helical supramolecular polymers via stacking of hydrogen-bonded pairs in water. *Proceedings of the National Academy of Sciences of the United States of America*, 99, 4977–4982; (c) Armstrong, G., Buggy, M. (2005). Hydrogen-bonded supramolecular polymers: A literature review. *Journal of Materials Science*, 40, 547–559.
- [33] (a) Aakeröy, C. B., Seddon, K. R. (1993). The hydrogen bond and crystal engineering. *Chemical Society Reviews*, 22, 397–407; (b) Desiraju, G. R. (2002). Hydrogen bridges in crystal engineering: Interactions without borders. *Accounts of Chemical Research*, 35, 565–573.
- [34] (a) Goldberg, I. (2000). Metalloporphyrin molecular sieves. *Chemistry—A European Journal*, 6, 3863–3870; (b) Gallant, M., Viet, M. T. P., Wuest, J. D. (1991). Hydrogen-bonded dimers. Direct study of the interconversion of pyridone dimers and hydroxypyridine monomers by low-temperature nuclear magnetic resonance spectroscopy. *Journal of the American Chemical Society*, 113, 721–723.
- [35] Zerkowsky, J. A., Withesides, G. M. (1994). Steric control of secondary, solid-state architecture in 1:1 complexes of melamines and barbiturates that crystallize as crinkled tapes. *Journal of the American Chemical Society*, 116, 4298–4304.
- [36] (a) Desiraju, G. U. *Crystal Engineering: The Design of Organic Solids*, Elsevier Scientific Publisher, Amsterdam, 1989; (b) Weissbuch, I., Lahav, M., Leiserowitz, L. (2003). Toward

- stereochemical control, monitoring, and understanding of crystal nucleation. *Crystal Growth and Design*, *3*, 125–150.
- [37] (a) Moulton, B., Zaworotko, M. J. (2001). From molecules to crystal engineering: Supramolecular isomerism and polymorphism in network solid. *Chemical Reviews*, *101*, 1629–1658; (b) Desiraju, G. R. (1995). Supramolecular synthons in crystal engineering—A new organic synthesis. *Angewandte Chemie—International Edition*, *34*, 2311–2327.
- [38] Kotera, M., Lehn, J. M., Vigneron, J. P. (1994). Self-assembled supramolecular rigid rods. *Journal of the Chemical Society, Chemical Communications*, 197–199.
- [39] Berl, V., Schmutz, M., Krische, M. J., Khoury, R. G., Lehn, J. M. (2002). Supramolecular polymers generated from heterocomplementary monomers linked through multiple hydrogen-bonding arrays—Formation, characterization, and properties. *Chemistry—A European Journal*, *8*, 1227–1244.
- [40] Abbel, R., Grenier, C., Pouderoijen, M. J., Stouwdam, J. W., Leclère, P. E. L. G., Sijbesma, R. P., Meijer, E. W., Schenning, A. P. H. J. (2009). White-light emitting hydrogen-bonded supramolecular copolymers based on π -conjugated oligomers. *Journal of the American Chemical Society*, *131*, 833–843.
- [41] Llanes-Pallas, A., Matena, M., Jung, T., Prato, M., Stöhr, M., Bonifazi, D. (2008). Trimodular engineering of linear supramolecular miniatures on Ag(111) surfaces controlled by complementary triple hydrogen bonds. *Angewandte Chemie—International Edition*, *47*, 7726–7730.
- [42] Luo, J., Lei, T., Wang, L., Ma, Y., Cao, Y., Wang, J., Pei, J. (2009). Highly fluorescent rigid supramolecular polymeric nanowires constructed through multiple hydrogen bonds. *Journal of the American Chemical Society*, *131*, 2076–2077.
- [43] Kaiser, T. E., Stepanenko, V., Würthner, F. (2009). Fluorescent J-aggregates of core-substituted perylene bisimides: Studies on structure–property relationship, nucleation–elongation mechanism, and sergeants-and-soldiers principle. *Journal of the American Chemical Society*, *131*, 6719–6732.
- [44] Lightfoot, M. P., Mair, F. S., Pritchard, R. G., Warren, J. E. (1999). New supramolecular packing motifs: π -stacked rods encased in triply-helical hydrogen bonded amide strands. *Chemical Communications*, 1945–1946.
- [45] Smulders, M. M. J., Schenning, A. P. H. J., Meijer, E. W. (2008). Insight into the mechanisms of cooperative self-assembly: The “sergeants-and-soldiers” principle of chiral and achiral C_3 -symmetrical discotic triamides. *Journal of the American Chemical Society*, *130*, 606–611.
- [46] Roosma, J., Mes, T., Leclère, P., Palmans, A. R. A., Meijer, E. W. (2008). Supramolecular materials from benzene-1,3,5-tricarboxamide-based nanorods. *Journal of the American Chemical Society*, *130*, 1120–1121.
- [47] van Gorp, J. J., Vekemans, J. A. J. M., Meijer, E. W. (2002). C_3 -symmetrical supramolecular architectures: Fibers and organic gels from discotic trisamides and trisureas. *Journal of the American Chemical Society*, *124*, 14759–14769.
- [48] Stals, P. J. M., Everts, J. C., de Bruijn, R., Pilot, I. A. W., Smulders, M. M. J., Martín-Rapffn, R., Pidko, E. A., de Gree, T. F. A., Palman, A. R. A., Meijer, E. W. (2010). Dynamic supramolecular polymers based on benzene-1,3,5-tricarboxamides: The influence of amide connectivity on aggregate stability and amplification of chirality. *Chemistry—A European Journal*, *16*, 810–821.
- [49] van Hameren, R., van Buul, A. M., Castriciano, M. A., Villari, V., Micali, N., Schön, P., Speller, S., Scolaro, L. M., Rowan, A. E., Elemans, J. A. A. W., Nolte, R. J. M. (2008). Supramolecular porphyrin polymers in solution and at the solid–liquid interface. *Nano Letters*, *8*, 253–259.
- [50] Paraschiv, I., Giesbers, M., van Lagen, B., Grozema, F. C., Abellon, R. D., Siebbeles, L. D. A., Marcelis, A. T. M., Zuilhof, H., Sudholter, E. J. R. (2006). H-bond-stabilized triphenylene-based columnar discotic liquid crystals. *Chemistry of Materials*, *18*, 968–974.

- [51] García, F., Sánchez, L. (2012). Structural rules for the chiral supramolecular organization of OPE-based discotics: Induction of helicity and amplification of chirality. *Journal of the American Chemical Society*, *134*, 734–742.
- [52] (a) Nepogodie, S. A., Stoddart, J. F. (1998). Cyclodextrin-based catenanes and rotaxanes. *Chemical Reviews*, *98*, 1959–1976; (b) Raymo, F. M., Stoddart, J. F. (1999). Interlocked macromolecules. *Chemical Reviews*, *99*, 1643–1663; (c) Dey, S. K., Beuerle, F., Olson, M. A., Stoddart, J. F. (2011). Arranging pseudorotaxanes octahedrally around [60]fullerene. *Chemical Communications*, *47*, 1425–1427; (d) Ashton, P. R., Baxter, I., Fyfe, M. C. T., Raymo, F. M., Spencer, N., Stoddart, J. F., White, A. J. P., Williams, D. J. (1998). Rotaxane or pseudorotaxane? That is the question! *Journal of the American Chemical Society*, *120*, 2297–2307.
- [53] Dong, S., Luo, Y., Yan, X., Zheng, B., Ding, X., Yu, Y., Ma, Z., Zhao, Q., Huang, F. (2011). A dual-responsive supramolecular polymer gel formed by crown ether based molecular recognition. *Angewandte Chemie—International Edition*, *50*, 1905–1909.
- [54] Niu, Z., Huang, F., Gibson, H. W. (2011). Supramolecular AA–BB-type linear polymers with relatively high molecular weights via the self-assembly of bis(*m*-phenylene)-32-crown-10 cryptands and a bisparaquat derivative. *Journal of the American Chemical Society*, *133*, 2836–2839.
- [55] (a) Schenning, A. P. H., Jonkheim, P., Peeters, E., Meijer, E. (2001). Hierarchical order in supramolecular assemblies of hydrogen-bonded oligo(*p*-phenylene vinylene)s. *Journal of the American Chemical Society*, *123*, 409–416; (b) El-ghayoury, A., Schenning, A. P. H. J., van Hal, P. A., van Duren, J. K. J., Jansse, R. A. J., Meijer, E. W. (2001). Supramolecular hydrogen-bonded oligo(*p*-phenylene vinylene) polymers. *Angewandte Chemie—International Edition*, *40*, 3660–3663; (c) Jeukens, C. R. L. P. N., Jonkheijm, P., Wijnen, F. J. P., Gielen, C. J., Christianen, P. C. M., Schenning, A. P. H. J., Meijer, E. W., Maan, J. C. (2005). Polarized emission of individual self-assembled oligo(*p*-phenylenevinylene)-based nanofibers on a solid support. *Journal of the American Chemical Society*, *127*, 8280–8281.
- [56] Jonkheijm, P., Hoeben, F. J. M., Kleppinger, R., van Herrikhuyzen, J., Schenning, A. P. H. J., Meijer, E. W. (2003). Transfer of π -conjugated columnar stacks from solution to surfaces. *Journal of the American Chemical Society*, *125*, 15941–15949.
- [57] Durkut, M., Mas-Torrent, L., Hadley, P. M., Jonkheijm, P., Schenning, A. P. H. J., Meijer, E. W., George, S. J., Ajayaghosh, A. (2006). Electrical transport measurements on self-assembled organic molecular wires. *Journal of Chemical Physics*, *124*, 154704/154701–154706.
- [58] Prasanthkumar, S., Gopal, A., Ajayaghosh, A. (2010). Self-assembly of thienylenevinylene molecular wires to semiconducting gels with doped metallic conductivity. *Journal of the American Chemical Society*, *132*, 13206–13207.
- [59] Kaseyama, T., Furumi, S., Zhang, X., Tanaka, K., Takeuchi, M. (2011). Hierarchical assembly of a phthalhydrazide-functionalized helicene. *Angewandte Chemie—International Edition*, *50*, 3684–3687.
- [60] Yagai, S., Aonuma, H., Kikkawa, Y., Kubota, S., Karatsu, T., Kitamura, A., Mahesh, S., Ajayaghosh, A. (2010). Rational design of nanofibers and nanorings through complementary hydrogen-bonding interactions of functional π systems. *Chemistry—A European Journal*, *16*, 8652–8661.
- [61] Seki, T., Asano, A., Seki, S., Kikkawa, Y., Murayama, H., Karatsu, T., Kitamura, A., Yagai, S. (2011). Rational construction of perylene bisimide columnar superstructures with a biased helical sense. *Chemistry—A European Journal*, *17*, 3598–3608.
- [62] (a) Beckers, E. H. A., Chen, Z., Meskers, S. C. J., Jonkheim, P., Schenning, A. P. H. J., Li, X. Q., Osswald, P., Würthner, F., Janssen, R. A. J. (2006). The importance of nanoscopic ordering on the kinetics of photoinduced charge transfer in aggregated π -conjugated hydrogen-bonded donor–acceptor systems. *The Journal of Physical Chemistry B*, *110*, 16967–16978; (b) Schenning, A. P. H. J., van Herrikhuyzen, J., Jonkheijm, P., Chen, Z., Würthner, F., Meijer, E. W. (2002). Photoinduced electron transfer in hydrogen-bonded oligo(*p*-phenylene

- vinylene)–perylene bisimide chiral assemblies. *Journal of the American Chemical Society*, *124*, 10252–10253.
- [63] Würthner, F., Chen, Z., Hoeben, F. J. M., Osswald, P., You, C. C., Jonkheim, P., van Herikhuyzen, J., Schenning, A. P. H. J., van der Schoot, P. P. A. M., Meijer, E. W., Beckers, E. H. A., Meskers, S. C. J., Janssen, R. A. J. (2004). Supramolecular p–n-heterojunctions by co-self-organization of oligo(*p*-phenylene vinylene) and perylene bisimide dyes. *Journal of the American Chemical Society*, *126*, 10611–10618.
- [64] Joachim, C., Gimzewski, J. K., Aviram, A. (2000). Electronics using hybrid-molecular and mono-molecular devices. *Nature*, *408*, 541–548.
- [65] Samorì, P. (2004). Scanning probe microscopies beyond imaging. *Journal of Materials Chemistry*, *14*, 1353–1366.
- [66] Feyter, S. D., Schryver, F. C. D. (2003). Two-dimensional supramolecular self-assembly probed by scanning tunneling microscopy. *Chemical Society Reviews*, *32*, 139–150.
- [67] Bonifazi, D., Mohnani, S., Llanes-Pallas, A. (2009). Supramolecular chemistry at interfaces: Molecular recognition on nanopatterned porous surfaces. *Chemistry—A European Journal*, *15*, 7004–7025.
- [68] (a) Barth, J. V., Costantini, G., Kern, K. (2005). Engineering atomic and molecular nanostructures at surfaces. *Nature*, *437*, 671–679; (b) Palma, C. A., Cecchini, M., Samorì, P. (2012). Predicting self-assembly: From empiricism to determinism. *Chemical Society Reviews*, *41*, 3713–3730; (c) Ciesielski, A., Palma, C. A., Bonini, M., Samorì, P. (2010). Towards supramolecular engineering of functional nanomaterials: Pre-programming multi-component 2D self-assembly at solid-liquid interfaces. *Advanced Materials*, *22*, 3506–3520; (d) Elemans, J. A. A. W., Lei, S., De Feyter, S. (2009). Molecular and supramolecular networks on surfaces: From two-dimensional crystal engineering to reactivity. *Angewandte Chemie—International Edition*, *48*, 7298–7332.
- [69] Theobald, J. A., Oxtoby, N. S., Phillips, M. A., Champness, N. R., Beton, P. H. (2003). Controlling molecular deposition and layer structure with supramolecular surface assemblies. *Nature*, *424*, 1029–1031.
- [70] Yu, M., Kalashnyk, N., Xu, W., Barattin, R., Benjalal, Y., Lægsgaard, E., Stensgaard, I., Hliwa, M., Bouju, X., Gourdon, A., Joachim, C., Besenbacher, F., Linderoth, T. R. (2010). Supramolecular architectures on surfaces formed through hydrogen bonding optimized in three dimensions. *ACS Nano*, *4*, 4097–4109.
- [71] (a) Stöhr, M., Wahl, M., Galka, C. H., Riehm, T., Jung, T. A., Gade, L. H. (2005). Controlling molecular assembly in two dimensions: The concentration dependence of thermally induced 2D aggregation of molecules on a metal surface. *Angewandte Chemie—International Edition*, *44*, 7394–7398; (b) Stöhr, M., Wahl, M., Spillmann, H., Gade, L. H., Jung, T. A. (2007). Lateral manipulation for the positioning of molecular guests within the confinements of a highly stable self-assembled organic surface network. *Small*, *3*, 1336–1340.
- [72] Palma, C. A., Bonini, M., Llanes-Pallas, A., Breiner, T., Prato, M., Bonifazi, D., Samorì, P. (2008). Pre-programmed bicomponent porous networks at the solid–liquid interface: The low concentration regime. *Chemical Communications*, 5289–5291.
- [73] Llanes-Pallas, A., Palma, C. A., Piot, L., Belbakra, A., Listorti, A., Prato, M., Samorì, P., Armaroli, N., Bonifazi, D. (2009). Engineering of supramolecular H-bonded nanopolygons via self-assembly of programmed molecular modules. *Journal of the American Chemical Society*, *131*, 509–520.
- [74] (a) Gothelf, K. V., LaBean, T. H. (2005). DNA-programmed assembly of nanostructures. *Organic and Biomolecular Chemistry*, *3*, 4023–4037; (b) Krishnan, Y., Sethuramasundaram, P. (2006). First blueprint, now bricks: DNA as construction material on the nanoscale. *Chemical Society Reviews*, *35*, 1111–1121.
- [75] He, Y., Chen, Y., Liu, H., Ribbe, A. E., Mao, C. (2005). Self-assembly of hexagonal DNA two-dimensional (2D) arrays. *Journal of the American Chemical Society*, *127*, 12202–12203.

- [76] Yuan, Q., Xing, Y., Borguet, E. (2010). An STM study of the pH dependent redox activity of a two-dimensional hydrogen bonding porphyrin network at an electrochemical interface. *Journal of the American Chemical Society*, *132*, 5054–5060.
- [77] (a) Tian, J. H., Yang, Y., Zhou, X., Schöllhorn, B., Maisonhaute, E., Chen, Z., Yang, F., Chen, Y., Amatore, C., Mao, B., Tian, Z. (2010). Electrochemically assisted fabrication of metal atomic wires and molecular junctions by MCBJ and STM-BJ methods. *ChemPhysChem*, *11*, 2745–2755; (b) Puigmartí-Luis, J., Minoia, A., Le, S., Geskin, V., Li, B., Lazzaroni, R., De Feyter, S., Amabilino, D. B. (2011). Self-assembly of supramolecular wires and cross-junctions and efficient electron tunnelling across them. *Chemical Science*, *2*, 1945–1951; (c) Drain, C. M., Varotto, A., Radivojevic, I. (2009). Self-organized porphyrinic materials. *Chemical Reviews*, *109*, 1630–1658.
- [78] Talukdar, P., Bollot, G., Mareda, J., Sakai, N., Matile, S. (2005). Synthetic ion channels with rigid-rod π -stack architecture that open in response to charge-transfer complex formation. *Journal of the American Chemical Society*, *127*, 6528–6529.
- [79] Sugimoto, T., Sada, K., Tateishi, Y., Suzuki, T., Sei, Y., Yamaguchi, K., Shinkai, S. (2005). Template-assisted control of porphyrin aggregation by ladder-type supramolecular assemblies. *Tetrahedron Letters*, *46*, 5347–5350.
- [80] Sugimoto, T., Suzuki, T., Shinkai, S., Sada, K. (2007). A double-stranded helix by complexation of two polymer chains with a helical supramolecular assembly. *Journal of the American Chemical Society*, *129*, 270–271.
- [81] Iwaura, R., Hoeben, F. J. M., Masuda, M., Schenning, A. P. H. J., Meijer, E. W., Shimizu, T. (2006). A two-unnatural-base-pair system toward the expansion of the genetic code. *Journal of the American Chemical Society*, *126*, 13298–13304.
- [82] Janssen, P. G. A., Vandenbergh, J., van Dongen, J. L. J., Meijer, E. W., Schenning, A. P. H. J. (2007). ssDNA templated self-assembly of chromophores. *Journal of the American Chemical Society*, *129*, 6078–6079.
- [83] Janssen, P. G. A., Ruiz-Carretero, A., González-Rodríguez, D., Meijer, E. W., Schenning, A. P. H. J. (2009). pH-switchable helicity of DNA-templated assemblies. *Angewandte Chemie—International Edition*, *48*, 8103–8106.
- [84] Prins, L. J., Thalacker, C., Wurthner, F., Timmerman, P., Reinhoudt, D. N. (2001). Chiral exciton coupling of merocyanine dyes within a well defined hydrogen-bonded assembly. *Proceedings of the National Academy of Sciences of the United States of America*, *98*, 10042–10045.
- [85] Ajayaghosh, A., Varghese, R., Praveen, V. K., Mahesh, S. (2006). Evolution of nano- to micro-sized spherical assemblies of a short oligo(*p*-phenyleneethynylene) into superstructured organogels. *Angewandte Chemie—International Edition*, *45*, 3261–3264.
- [86] Ajayaghosh, A., Varghese, R., Mahesh, S., Praveen, V. K. (2006). From vesicles to helical nanotubes: A sergent-and-soldiers effect in the self-assembly of oligo(*p*-phenyleneethynylene)s. *Angewandte Chemie—International Edition*, *45*, 7729–7732.
- [87] Yoosaf, K., Belbakra, A., Armaroli, N., Llanes-Pallas, A., Bonifazi, D. (2009). Engineering spherical nanostructures through hydrogen bonds. *Chemical Communications*, *20*, 2830–2832.
- [88] Wurthner, F., Thalacker, C., Sautter, A., Scharl, W., Ibachand, W., Hollricher, O. (2000). Hierarchical self-organization of perylene bisimide–melamine assemblies to fluorescent mesoscopic superstructures. *Chemistry—A European Journal*, *6*, 3853–3886.
- [89] Marangoni, T., Mezzasalma, S. A., Llanes-Pallas, A., Yoosaf, K., Armaroli, N., Bonifazi, D. (2011). Thermosolutal self-organization of supramolecular polymers into nanocraters. *Langmuir*, *27*, 1513–1523.
- [90] Yagai, S., Mahesh, S., Kikkawa, Y., Unoike, K., Karatsu, T., Kitamura, A., Ajayaghosh, A. (2008). Toroidal nanoobjects from rosette assemblies of melamine-linked oligo(*p*-phenyleneethynylene)s and cyanurates. *Angewandte Chemie—International Edition*, *47*, 4691–4694.

- [91] Yagai, S., Goto, Y., Karatsu, T., Kitamura, A., Kikkawa, Y. (2011). Catenation of self-assembled nanorings. *Chemistry—A European Journal*, 17, 13657–13660.
- [92] (a) Miura, A., Jonkheijm, P., De Feyter, S., Schenning, A. P. H. J., Meijer, E. W., De Schryver, F. C. (2005). 2D self-assembly of oligo(*p*-phenylene vinylene) derivatives: From dimers to chiral rosettes. *Small*, 1, 131–137; (b) De Cat, I., Röger, C., Lee, C. C., Hoeben, F. J. M., Pouderoijen, M. J., Schenning, A. P. H. J., Würthner, F., De Feyter, S. (2008). Identification of oligo(*p*-phenylene vinylene)–naphthalene diimide heterocomplexes by scanning tunneling microscopy and spectroscopy at the liquid–solid interface. *Chemical Communications*, 5496–5498.
- [93] Whitesides, G., Grzybowski, B. (2002). Self-assembly at all scales. *Science*, 295, 2418–2424.

CHAPTER 6

MOLECULAR SYSTEMS FOR SOLAR THERMAL ENERGY STORAGE AND CONVERSION

KASPER MOTH-POULSEN

6.1 INTRODUCTION

In 2001, the world energy consumption was estimated to be 425×10^{18} J, corresponding to a consumption rate of approximately 13.5 terawatts (TW) [1, 2]. The energy consumption rate is estimated to grow from 13.5 TW in 2001 to about 27 TW in 2050 [1]. The majority (81%) of today's primary energy production is based on fossil fuels such as oil, natural gas, and coal, while nuclear (5.8%) and hydropower (2.2%) are much less important. Other renewable energy sources (wind, photovoltaics, and solar thermal) add up to 0.7% [3]. Growing energy consumption based on finite amounts of fossil fuels is not sustainable—first, due to simple availability issues, and second, problems with pollution might impose irreversible damage to the planet. Development of large-scale renewable energy technologies is therefore a requirement for the sustainability of the world society. Hydropower and wind turbines are already implemented on a large scale, but limitations on their geographical location imply that these technologies alone cannot produce the needed energy output [4]. Solar energy technologies in the form of photovoltaics have seen an impressive development during the last decades, and it is estimated that the cost of solar energy for power production will be able to compete directly with fossil fuel technologies as early as 2016–2018 [5]. The decreasing cost of photovoltaics together with government incentives are leading to large-scale implementation in some countries, for example, 3.2% of Germany's total electric power production in 2011 [6]. As a larger fraction of the energy production stems from solar energy, energy storage and load leveling is becoming increasingly important due to challenges with daily large variations in both solar energy flux and on energy demand [7–12].

Technologies for storing electrical energy (in the case of photovoltaic energy generation) or thermal energy (in the case of solar thermal energy generation) have not

been widely implemented on a large scale due to high cost and/or limited energy storage time [4, 9, 13]. Relatively low energy density storage, geographic limitations, and high cost make large-scale pumped hydroelectric storage impractical [4, 9, 14]. Similarly, the high cost and the need to consume other energy sources for stable power generation limit compressed air energy storage from large-scale applications [4, 9, 14]. Storage of solar energy in the form of energetic chemical bonds is currently being studied using several approaches, such as photoinduced water splitting [1, 15, 16], CO reduction [1, 15], CO₂ reduction [1, 15], and more biologically inspired approaches [15, 17, 18].

In this chapter we will discuss a related, but so far much less explored approach where photoinduced chemical reaction sequences are used to store large amounts of heat in molecular materials (closed-cycle storage) [19] and also molecular solar thermal (MOST) systems [20]. In MOST systems, a photoactive molecule (the parent) is exposed to photons and is thus photochemically transformed into a high-energy photoisomer, which should ideally have a long lifetime. Using external stimuli such as heat or catalysis, the energy stored in the photoisomer can then be recovered in a controlled way along with regeneration of the parent. In the schematic illustration of this concept in Figure 6.1, the parent **A** is first activated by a photon to isomerize it to a high-energy photoisomer **B**. The difference in energy between the parent and the photoisomer is given as $\Delta H_{\text{storage}}$. The long-term stability of the photoisomer is determined by the energy barrier for back-conversion E_a . Back-conversion to **A** is achieved either by thermal activation or catalysis. The MOST strategy attracted considerable attention several decades ago, but fundamental problems, largely related to molecular design, proved to be insurmountable at the time [19].

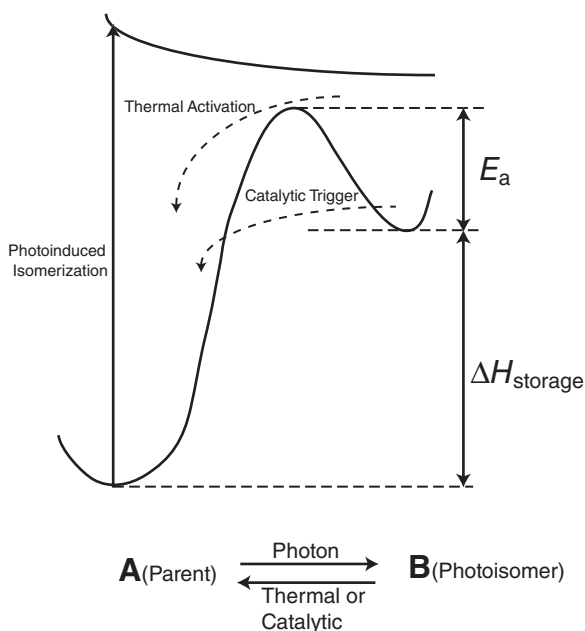


Figure 6.1. General energy profile for a MOST system.

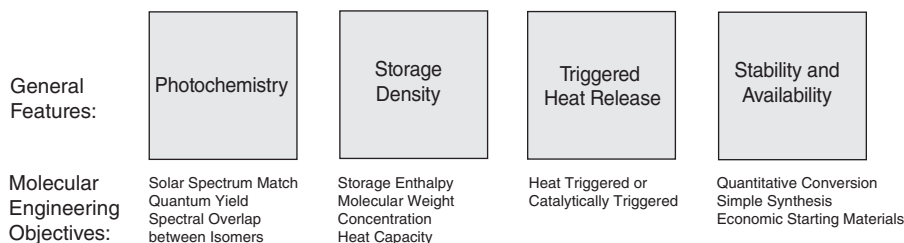


Figure 6.2. Key requirements and molecular engineering challenges for a MOST system.

Several chemical systems have been proposed as candidates for solar thermal energy storage, such as stilbenes [21, 22], anthraquinones [23], linked anthracenes [24], limonene [25], norbornadiene–quadricyclanes (NQ) [26–32], ruthenium fulvalenes [33–36], and inorganic systems such as dinitrogen tetroxide (N_2O_4 to NO_2) [37], nitrosyl chloride ($NOCl$ to NO and Cl_2) [38, 39], and drying of zeolites [40, 41]. The NQ system has also been incorporated into photoresponsive polymers [42, 43]. Recently, the use of carbon nanotubes functionalized with azobenzenes has also been proposed as a material for solar energy storage [44]. The focus of this chapter is on the design of molecules for MOST, and in keeping with the “molecular” theme of this book, the scope of the chapter is focused on molecular systems with the exclusion of inorganic and polymeric systems.

6.2 BASIC ENGINEERING CHALLENGES

A number of requirements need to be fulfilled for a successful MOST system [24, 29, 45, 46], each associated with molecular engineering challenges. In brief, the challenges fall into four categories (Figure 6.2):

- photochemistry
- energy storage
- heat release
- stability and availability.

Each requirement imposes constraints and challenges on the design of the molecular system, and it is challenging to develop a molecular system satisfying all the requirements. The implications of the basic requirements for molecular design are discussed in the following.

6.2.1 Photochemistry

From a photochemical perspective, the design of molecules for MOST is related to three parameters: (i) solar spectrum match, (ii) quantum yield, and (iii) spectral overlap of photoisomers.

Solar spectrum match is a general challenge for all solar light-harvesting technologies. Figure 6.3 illustrates the solar spectrum energy flux as a function of wavelength

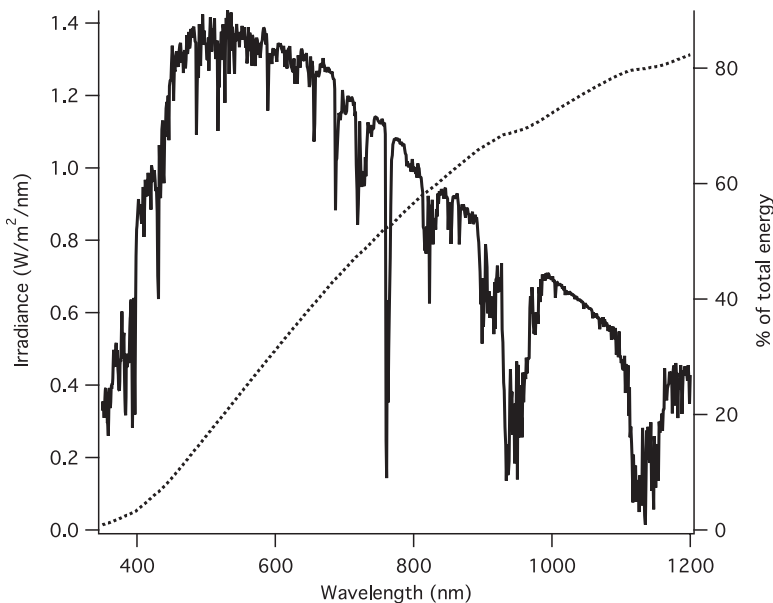


Figure 6.3. Black, spectral distribution of the intensity for AM 1.5 solar radiation (direct + circumsolar) (black). Dotted curve shows the percentage of all incident photons below the absorption onset wavelength.

(AM 1.5, solid line). The dotted line is an integration of total energy flux from 250 nm to the onset wavelength. As 50% of solar energy is in the 300–700 nm range, a challenge from a chemical design perspective is to have a system that can absorb as many photons as possible. In traditional chromophores, redshifted absorption maxima are typically achieved using molecules with extended π -conjugation or by the introduction of donor–acceptor systems. In the context of MOST, it is an extra challenge to tailor the absorption while keeping the molecular weight low [29] and the storage enthalpy $\Delta H_{\text{storage}}$ as high as possible.

The quantum yield, ϕ , of a photochemical process is given by Equation 6.1 [47]:

$$\phi = \frac{n_{\text{converted}}}{n_{\text{photons}}}, \quad (6.1)$$

where $n_{\text{converted}}$ is the number of converted molecules and n_{photons} is the number of incident photons.

In an ideal system, all photons induce an isomerization reaction and ϕ approaches unity. Depending on the molecular system and the detailed mechanism of isomerization, other reaction paths that do not lead to the desired photoisomer might compete in the process, for example, fluorescence, vibrational relaxation, quenching, and others.

The third requirement with regard to photochemical properties is that the photoisomer ideally should have little or no spectral overlap with the parent molecule. The reason for this requirement is that the MOST system should be able to operate in highly concentrated and optically dense systems. If there is too much spectral overlap

between photoisomer and parent, it would not be possible to reach full conversions in the system due to inner filtering effects. The overall efficiency (η_E) of a molecular system to store solar energy is described in Equation 6.2 [30]:

$$\eta_E = \frac{\Delta H_{\text{storage}} \Phi}{E_{hv}} \frac{\int_0^{\infty} I_{\lambda} (\lambda/\lambda_{\text{lim}}) d\lambda}{\int_0^{\infty} I_{\lambda} d\lambda} \eta_{\text{abs}} 100. \quad (6.2)$$

Here, η_E is the efficiency, $\Delta H_{\text{storage}}$ the storage enthalpy, E_{hv} the energy of the absorbed photons, λ_{lim} is the long wavelength limit of absorption, I_{λ} is the distribution of power in the solar spectrum, and η_{abs} is the fraction of absorbed photons with respect to the total number of photons in the solar spectrum. For a full evaluation of the efficiency of a MOST system, additional effects have to be taken into account. For example, the energy storage density and heat capacities together determine the maximum adiabatic temperature rise ($\Delta T_{\text{adiabatic}}$) one can expect from the system.

6.2.2 Energy Storage

Several factors come into play when considering the energy storage capabilities of a MOST system. The quantity that one seeks to optimize is the maximal adiabatic temperature change ($\Delta T_{\text{adiabatic}}$) achievable, which for a MOST system is described by Equation 6.3:

$$\Delta T_{\text{adiabatic}} = \frac{m_{\text{solu}} \Delta H_{\text{storage}}}{m_{\text{solu}} c_{\text{solu}} + m_{\text{solv}} c_{\text{solv}}}. \quad (6.3)$$

Here, $\Delta H_{\text{storage}}$ is the storage enthalpy of the molecular system (in J/g), m_{solu} is the mass of the active molecular material in the system, and c_{solu} and c_{solv} are the heat capacities of the involved molecules and solvents. To achieve the best performance, $\Delta H_{\text{storage}}$ should be maximized and the amount of solubilizing solvent minimized; ideally, this could be a neat system with no solvent at all. Maximizing molar enthalpy alone, however, is not relevant if it comes at the expense of higher molecular weight. Ideally, the storage enthalpy should be higher than 300 J/g [30], which exceeds the solar heating ($\Delta T = 50^\circ\text{C}$) of water ($\Delta H_{\text{storage}} = 209$ J/g), sand ($\Delta H_{\text{storage}} = 42$ J/g), and salt hydrates ($\Delta H_{\text{storage}} = 250$ J/g) [30].

6.2.3 Heat Release

One important aspect of MOST is that the photoisomer should be stable for extended periods of time. Therefore, there should be a high energetic activation barrier E_a for back-conversion to the parent compound (Figure 6.1). Likewise, it should be possible to initiate back-conversion and thereby release the stored energy in a fast and efficient way. The triggered back-reaction can be initiated by heat, or more beneficially, by a heterogeneous catalyst. A solid-state catalyst is ideal since it simplifies device design and implementation [29].

6.2.4 Stability and Availability

Considering the design challenges described earlier, concurrently with long-term stability, recyclability (quantitative chemical reactions) and availability also have to be considered. For practical reasons, a MOST system should be able to operate on a daily basis for extended periods (e.g., 10 years), meaning that the molecular material should be robust and able to withstand more than 10^3 cycles without significant degradation. Availability is also important, since the target molecules should be synthesized from cheap and abundant starting materials.

6.3 MOLECULAR SYSTEMS

Several photochemical isomerization reactions and molecular systems have been proposed for MOST. In the following sections, some of these systems are described, with emphasis on examples where “molecular engineering” has been used to optimize the molecular properties and where trends in molecular structure–property relations can be extracted.

6.3.1 Stilbene Systems

The photoisomerization of “stilbene-like” compounds has been considered as a potential chemical system for solar energy storage [48]. Most stilbene derivatives have absorptions in the visible range from 300 to 700 nm [21, 22], making them interesting in the context of this chapter. The basic isomerization of the stilbene C=C double bond has an enthalpy difference of only a few kilojoule/mole [21, 22], but Mancini and coworkers [21, 22] have discovered that some stilbene-like molecules possess surprisingly high storage enthalpies in their *Z/E* conversion. The discovery is based on two concomitant but opposing effects: the *E* isomer is stabilized by electronic delocalization, whereas the *Z* form is destabilized due to steric interactions [21]. These results, in terms of molecular structure and energy storage enthalpy, are summarized in Figure 6.4. Introducing bulky methyl groups on the benzene ring, which destabilizes the *Z* form, results in an increased storage enthalpy when going from unsubstituted ($\Delta H_{\text{storage}} = 5$ kJ/mol) to tetrasubstituted ($\Delta H_{\text{storage}} = 55$ kJ/mol) phenyl groups (Figure 6.4 and Scheme 6.1). The energy difference between *Z* and *E* isomers is further enhanced by introducing an amino group on the benzene moiety ($\Delta H_{\text{storage}} = 18$ kJ/mol) or a naphthyl group ($\Delta H_{\text{storage}} = 20$ kJ/mol). The aminophenyl and naphthyl groups are thought to stabilize the *E* forms of the molecules due to extended electronic delocalization. This delocalization does not play as big a role in the *Z* isomers due to their strained angular geometry [21] (Scheme 6.1). In the most promising case, where both electronic and steric effects are combined in the same molecular system, an impressive storage enthalpy of 104 kJ/mol is achieved, which is comparable to the energy of a covalent chemical bond.

6.3.2 Linked Anthracenes

Anthracene dimerizes by a photoinduced [4 + 4] cycloaddition reaction. The reaction is reversible when the dimer is exposed to heat or irradiated below 300 nm. The

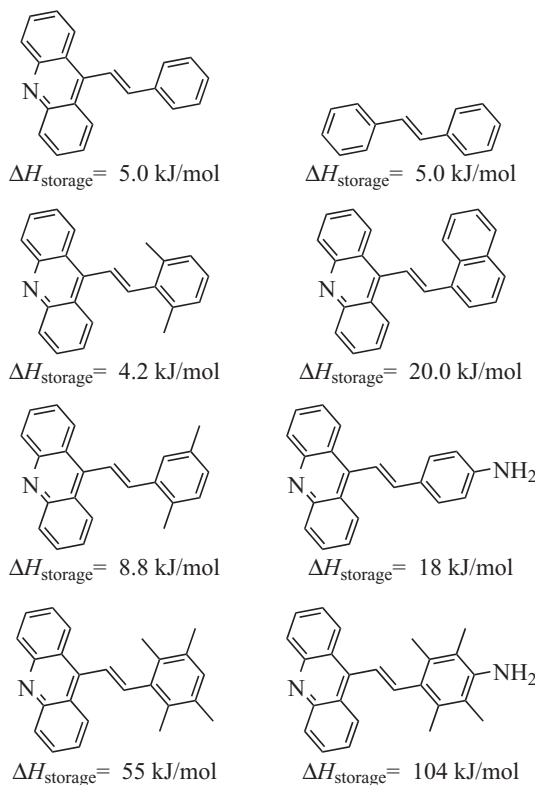
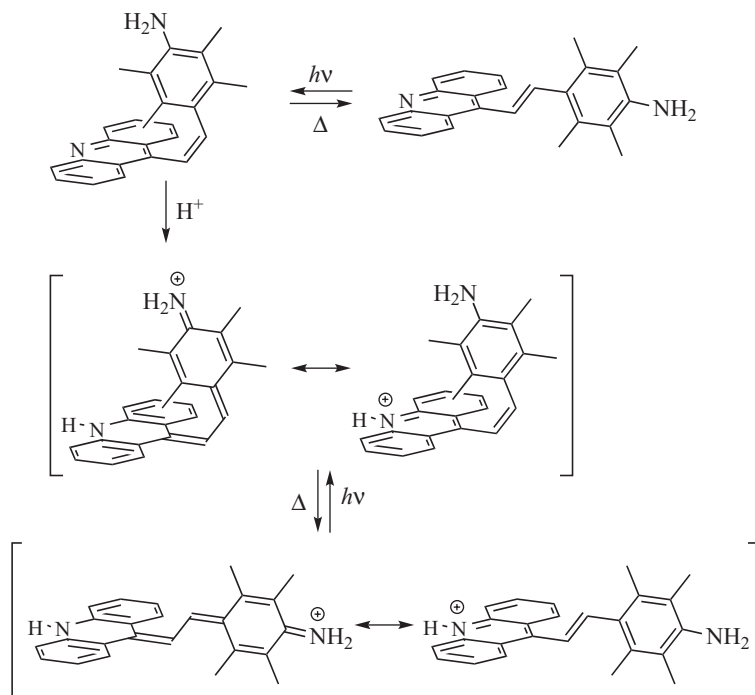


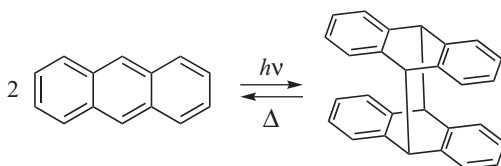
Figure 6.4. Engineering the storage enthalpy of *cis/trans* isomerization of “stilbene-like” molecules [21].

energetics and reversibility of this reaction led to a suggestion that anthracenes could be used for photon energy storage (Scheme 6.2) [24].

Jones et al. studied the dimerization reaction and measured the quantum yields and storage enthalpies ($\Delta H_{\text{storage}}$) for a number of linked anthracene derivatives (Scheme 6.3) [24]. The unsubstituted anthracene dimerizes with a quantum yield of 0.3 in highly concentrated solutions, and the system possesses a storage enthalpy of $\Delta H_{\text{storage}} = 65 \text{ kJ/mol}$. By adding donor and acceptor units to anthracene, the storage enthalpy could be enhanced to 84 kJ/mol . Jones et al. wanted to develop a system where the quantum yield was independent of concentration and prepared a number of linked anthracene derivatives (Scheme 6.3). The quantum yield of linked anthracenes was independent of concentration, and being in the 0.15–0.36 range, it was comparable to the unlinked system. The storage enthalpy of the linked anthracenes with a methylene bridge ($\Delta H_{\text{storage}} = 72 \text{ kJ/mol}$) was higher than for the ethyl-bridged system ($\Delta H_{\text{storage}} = 61 \text{ kJ/mol}$), probably due to the formation of a strained three-carbon ring in the photoisomer of the methylene bridged anthracene. The double bridge “sandwich” compound had much lower storage enthalpy ($\Delta H_{\text{storage}} = 35.5 \text{ kJ/mol}$), perhaps owing to destabilization of the parent compound due to both proximity of the two anthracene units in this system and the formation of two very strained four-membered rings.



Scheme 6.1. Illustration of the chemical structures and resonance forms that contribute to the increased storage enthalpy in “stilbene-like” molecules containing the 4-aminodurene moiety [21].

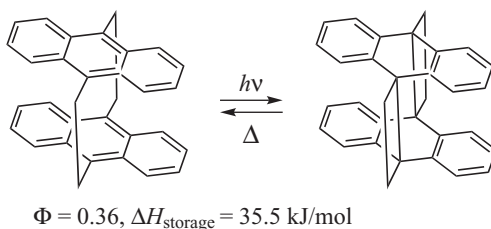
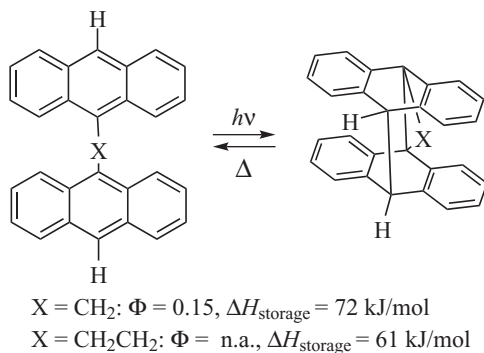
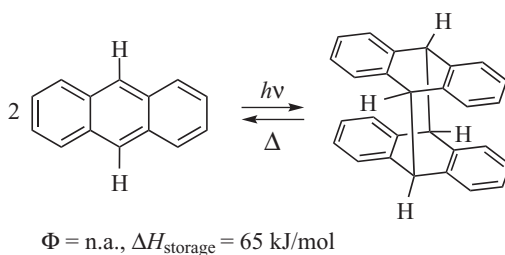


Scheme 6.2. Light-induced dimerization of anthracene.

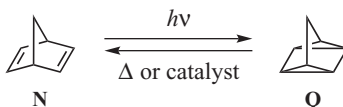
6.3.3 Norbornadiene–Quadricyclane System

The photoinduced valence bond isomerization of norbornadiene to quadricyclane, observed by Dauben and Cargil in 1961 [49] in the unsubstituted system and by Crystol and Snell for the carboxy-substituted derivative [50], has been extensively studied. The photoinduced intramolecular [2 + 2] cycloaddition reaction has been found to proceed both without [49] and with [51, 52] auxiliary photosensitizers (Scheme 6.4) [53].

The unsubstituted NQ system features a low-molecular-weight and high-storage enthalpy (96 kJ/mol [54]). Also, both norbornadiene and quadricyclane are liquids at room temperature, which is an advantage from a device implementation perspective. Challenges associated with the system are lack of robustness, a low quantum yield in



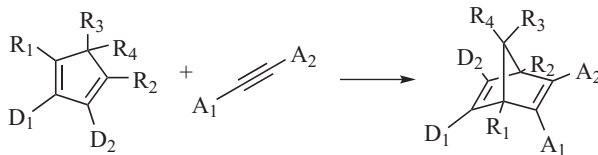
Scheme 6.3. Quantum yields (Φ) of the forward reaction and storage enthalpy ($\Delta H_{\text{storage}}$) for a number of substituted anthracenes. It should be noted that the photodimerization quantum yield of unlinked anthracenes is concentration dependent. Values taken from Reference 24.



Scheme 6.4. The photoinduced isomerization and back-conversion of the norbornadiene (N)–quadricyclane (Q) system.

the absence of sensitizers, and that UV photons below 300 nm are needed to convert the system [55], meaning that virtually no photoconversion of norbornadiene takes place under natural solar irradiation conditions [26].

The synthesis of substituted norbornadienes is typically achieved via a Diels–Alder [4 + 2] cycloaddition reactions [29, 31, 42, 43, 56] (Scheme 6.5). The key starting materials are derivatives of cyclopentadiene and acetylene.



Scheme 6.5. Key step in the synthesis of substituted norbornadienes via the Diels–Alder cycloaddition reaction of a cyclopentadiene with a substituted acetylene. D = donor and A = acceptor groups.

Improving the photophysical properties via molecular engineering has been attempted with success using two different strategies: (i) chemical modification of the system by the introduction of donor and acceptor units [30, 32] and (ii) by the use of sensitizers and other auxiliary intermolecular energy transfer agents [30, 32]. In some examples, the sensitizer has been bound to the NQ system via noncovalent interactions [57, 58]. Notably, both approaches have led to improved quantum yields, and the absorption spectra of the modified systems show that they are capable of absorbing in the visible range with onset of absorption above 500 nm [26, 30, 32, 55].

Figure 6.5 summarizes some of the results with donor–acceptor NQ systems with the chemical structures, quantum yields, and the wavelength for the onset of photon absorption. Notably, the quantum yield is very high for all these compounds and is unaffected by solvent polarity [29]. The onset of absorption is redshifted by the introduction of donors and acceptors with increasing strength: donors ($H < CH_3 < C_6H_5 < C_6H_4OCH_3$) and acceptors ($H < CO_2CH_3 < CN$). The findings by Yoshida [29] corroborates the later results by Nagai, who employed various other donors and acceptors [31]. The molar storage enthalpy of the donor–acceptor norbornadienes is not affected much by variations in the substitution pattern [29]. Interestingly, the promising properties of the donor–acceptor norbornadienes led to early investigations of the viability of using this system as an energy storage media for house heating [29].

6.3.4 Fulvalene Diruthenium System

(Fulvalene)tetracarbonyldiruthenium photoisomerizes via an unusual chemical rearrangement to the corresponding fulvene (Scheme 6.6). The reaction is fully reversible by thermal heating or by exposure to a catalyst. The storage enthalpy of the reaction is ≈ 87 kJ/mol [34].

The high storage enthalpy and general robustness of the system have led to the proposed use of these types of compounds for MOST systems [20, 33, 34, 36, 59, 60]. The reaction mechanism of the photoinduced isomerization has been scrutinized using a combination of computational techniques and experimental observations (time-resolved IR and X-ray measurements), leading to the proposed photoinduced reaction sequence shown in Figure 6.6 [60].

First, when a photon hits the parent compound, **1a**, excitation leads to rapid metal–metal bond dissociation and the formation of a *syn*-singlet state or a *syn*-triplet state. The *syn*-singlet state decays on the ≈ 30 ps timescale either by recombination to reform **1a** or via intersystem crossing to form the longer lived ($\approx ns$) *syn*-triplet state. The *syn*-triplet state proceeds via thermal activation through the crossing point (CP) to form the *anti* intermediate **B**. This intermediate proceeds then via transition state **C** to form photoisomer **2a** [60].

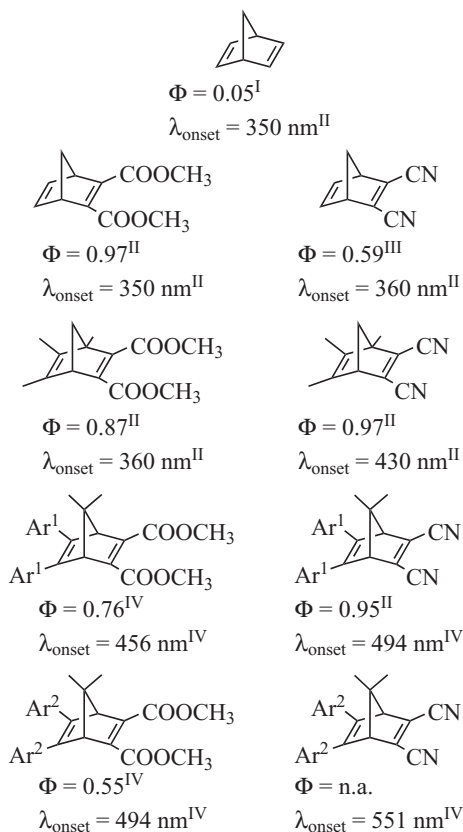
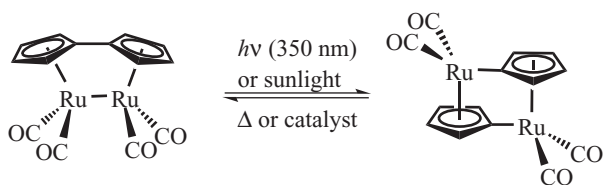


Figure 6.5. Engineering the NQ system by introducing donor–acceptor groups. The figure illustrates the effect of increased donor–acceptor strength on the quantum yield and on the onset of the absorption wavelength. Ar¹ denotes a phenyl group and Ar² a *p*-methoxyphenyl group. Values taken from references: I (Dilling et al. [55]), II (Harel et al. [54]), III (Yoshida [29]), and IV (Miki et al. [63]).



Scheme 6.6. Photoinduced isomerization of the fulvalenediruthenium system.

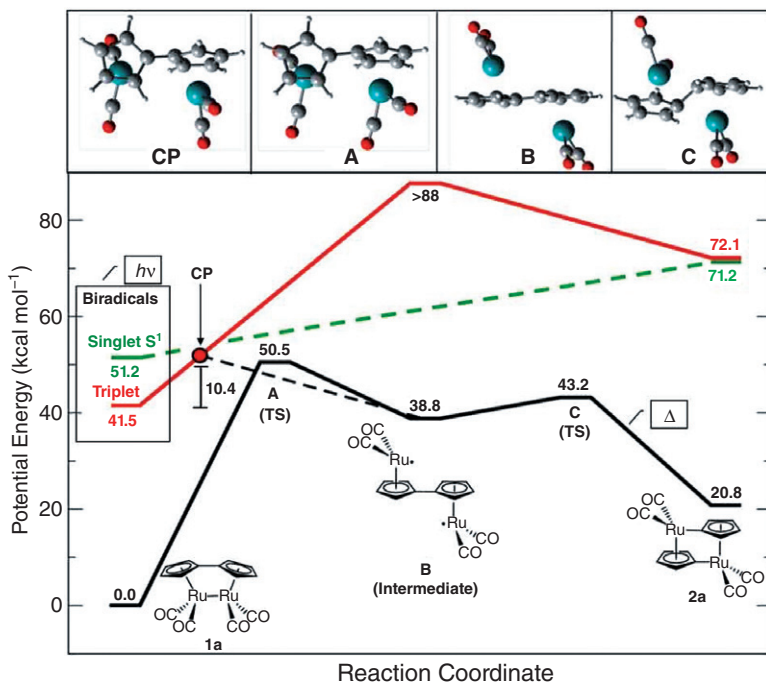


Figure 6.6. Potential energy profiles for the isomerization of (fulvalene)tetracarbonyldiruthenium. Source: [60]. Reproduced with permission of Wiley-VCH Verlag GmbH & Co. KGaA. See color insert.

The thermal back-reaction was investigated by Grossman, Vollhardt, and coworkers [34] both computationally and experimentally. The reaction mechanism follows the black energy profile on Figure 6.6. Both calculations and kinetic studies showed that a thermal activation energy of ≈ 125 kJ/mol is needed to overcome the activation barrier (C) in order to generate the parent compound **1a** [34].

6.4 ENERGY RELEASE

The photoisomer in a MOST system should be stable over extended periods of time. Therefore, the activation energy barrier (E_a) for heat release back to the parent compound should be sufficiently high. Meanwhile, for practical applications, it should be possible to release the stored heat in a fast and efficient way. One option is to heat the photoisomer to a temperature high enough to ensure thermal activation. From a device perspective, thermal activation requiring a heating stage might require additional energy and thus complicate the design. A more favorable concept is to trigger the heat release via a catalytic reaction [29]. For practical reasons, the catalyst should be immobilized on a solid support and reused repeatedly [29].

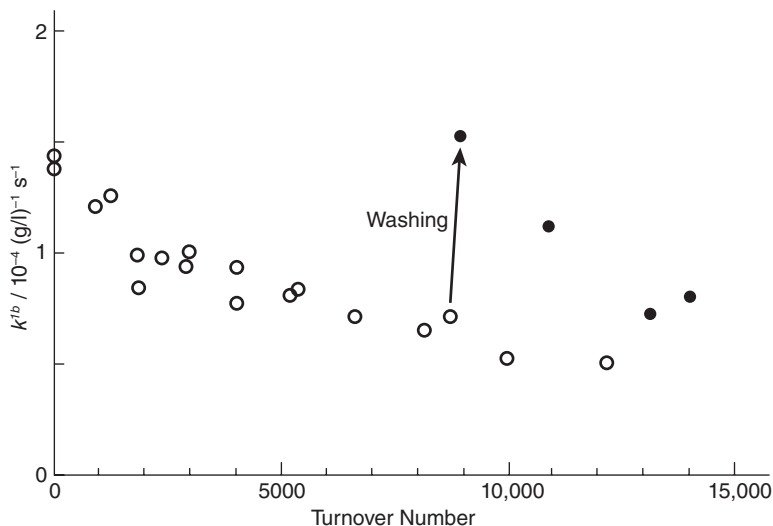


Figure 6.7. Catalytic reaction rate of conversion from quadricyclane to norbornadiene using a copper phthalocyanine catalyst on activated carbon. Source: [61]. Reproduced with permission of the Royal Society of Chemistry.

For the NQ system, catalytic systems based on $\text{Rh}_2(\text{CO})_4\text{Cl}_2$ [26], silver ions [61], and cobalt porphyrins [62] have been presented. Some of the catalysts have been immobilized on a solid support and the activity and turnover numbers (TON's) monitored [61, 62]. Figure 6.7 illustrates the activity of a copper phthalocyanine catalyst on a solid support as a function of TON. The catalyst is capable of inducing the heat release reaction at room temperature. The activity of the catalyst drops to half after about 8000 reactions but, interestingly, the activity of the catalyst can be fully recovered by washing with a solvent.

6.5 STABILITY TESTS

Robustness of the molecular structures and reversibility of the isomerization reactions through multiple cycles are of paramount importance if MOST systems should be developed from research lab demonstrations to real-world applications [30, 32]. If the MOST system is used as load-leveling energy storage system in conjunction with photovoltaic systems for example, one can assume that the system will be charged and discharged once every day. Also, for practical reasons, the lifetime should be at least 5–10 years and preferably longer. With this point in mind, the relevant number of cycles a system should be able to withstand is $2\text{--}4 \times 10^3$. In terms of stability tests, the NQ system is the most widely studied. Decomposition and side reactions have been reported for some systems, while especially the donor–acceptor norbornadienes (Figure 6.5) have shown impressive stability with almost no degradation both in solution [56, 63] and in solid-state polymer matrix [63] (Figure 6.8).

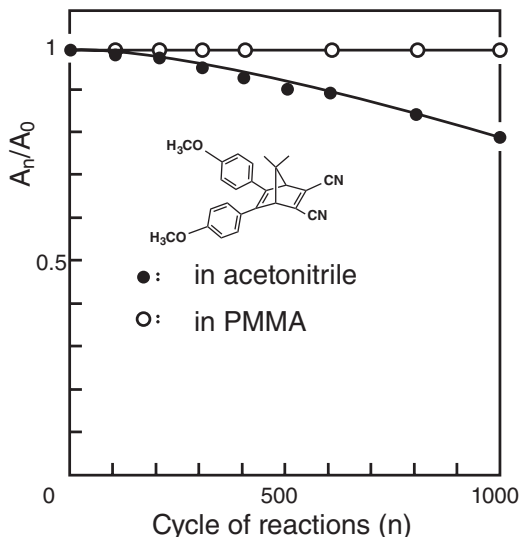


Figure 6.8. Stability tests of NO donor–acceptor system (donor: *p*-methoxyphenyl, acceptor: cyano) embedded in a polymer matrix or acetonitrile. Source: [63]. Reproduced with permission of the Chemical Society of Japan.

6.6 CONCLUSIONS AND OUTLOOK

Since the introduction of MOST systems several decades ago, the world has changed in many ways. The scientific and engineering fields have evolved while the world demand for and cost of energy has continuously increased. Recently, new concepts have been proposed [44], which has led to a reappraisal of MOST systems for energy production [10, 19].

The design and synthesis of new and improved MOST systems are associated with the molecular engineering challenges of photochemistry, energy storage, heat release and stability, and availability, as discussed in Section 6.2. Synthetic chemistry methods and computational methods as design aids have improved much since most of these systems were first prepared three to four decades ago. On the device side, the development of low temperature thermoelectrics might enable devices that efficiently produce power from the released heat.

With these points in mind, it is hoped this chapter can be a source of inspiration for a new generation of scientists working on the molecular engineering of new molecular systems for solar energy storage and conversion.

REFERENCES

- [1] Lewis, N. S., Nocera, D. G. (2006). Powering the planet: Chemical challenges in solar energy utilization. *Proceedings of the National Academy of Sciences of the United States of America*, 103, 15729–15735.
- [2] Administration, E. I. (2005). *Annual Energy Outlook*. US Dept. Energy, Washington, DC.

- [3] Agency, I. E. (2010). *Key World Energy Statistics 2010*.
- [4] Lindley, D. (2010). The energy storage problem. *Nature*, *463*, 18–20.
- [5] Wolden, C. A., Kurtin, J., Baxter, J. B., Repins, I., Shaheen, S. E., Torvik, J. T., Rockett, A. A., Fthenakis, V. M., Aydil, E. S. (2011). Photovoltaic manufacturing: Present status, future prospects, and research needs. *Journal of Vacuum Science and Technology A*, *29*, 030801.
- [6] Böhme, D. (2011). Zeitreihen zur Entwicklung der erneuerbaren Energien in Deutschland. *Arbeitsgruppe Erneuerbare Energien*.
- [7] Chen, H. S., Cong, T. N., Yang, W., Tan, C. Q., Li, Y. L., Ding, Y. L. (2009). Progress in electrical energy storage system: A critical review. *Progress in Natural Science*, *19*, 291–312.
- [8] Crabtree, G. W., Lewis, N. S. (2007). Solar energy conversion. *Physics Today*, *60*, 37–42.
- [9] Cook, T. R., Dogutan, D. K., Reece, S. Y., Surendranath, Y., Teets, T. S., Nocera, D. G. (2010). Solar energy supply and storage for the legacy and non legacy worlds. *Chemical Reviews*, *110*, 6474–6502.
- [10] Gur, I., Sawyer, K., Prasher, R. (2012). Searching for a better thermal battery. *Science*, *335*, 1454–1455.
- [11] Mondol, J. D., Yohanis, Y. G., Norton, B. (2007). Comparison of measured and predicted long term performance of grid: A connected photovoltaic system. *Energy Conversion and Management*, *48*, 1065–1080.
- [12] Yohanis, Y. G., Mondol, J. D., Wright, A., Norton, B. (2008). Real-life energy use in the UK: How occupancy and dwelling characteristics affect domestic electricity use. *Energy and Buildings*, *40*, 1053–1059.
- [13] Armand, M., Tarascon, J. M. (2008). Building better batteries. *Nature*, *451*, 652–657.
- [14] Dresselhaus, M. S., Thomas, I. L. (2001). Alternative energy technologies. *Nature*, *414*, 332–337.
- [15] Blankenship, R. E., Tiede, D. M., Barber, J., Brudvig, G. W., Fleming, G., Ghirardi, M., Gunner, M. R., Junge, W., Kramer, D. M., Melis, A., Moore, T. A., Moser, C. C., Nocera, D. G., Nozik, A. J., Ort, D. R., Parson, W. W., Prince, R. C., Sayre, R. T. (2011). Comparing photosynthetic and photovoltaic efficiencies and recognizing the potential for improvement. *Science*, *332*, 805–809.
- [16] Osterloh, F. E. (2008). Inorganic materials as catalysts for photochemical splitting of water. *Chemistry of Materials*, *20*, 35–54.
- [17] Fukuzumi, S. (2008). Bioinspired energy conversion systems for hydrogen production and storage. *European Journal of Inorganic Chemistry*, 1351–1362.
- [18] Larkum, A. W. D., Ross, I. L., Kruse, O., Hankamer, B. (2012). Selection, breeding and engineering of microalgae for bioenergy and biofuel production. *Trends in Biotechnology*, *30*, 198–205.
- [19] Kucharski, T. J., Tian, Y. C., Akbulatov, S., Boulatov, R. (2011). Chemical solutions for the closed-cycle storage of solar energy. *Energy and Environmental Science*, *4*, 4449–4472.
- [20] Moth-Poulsen, K., Coso, D., Börjesson, K., Vinokurov, N., Meier, S., Majumdar, A., Vollhardt, K. P. C., Segalman, R. A. (2012). Molecular solar thermal (MOST) energy storage and release system. *Energy and Environmental Science*, *5*, 8534–8537.
- [21] Bastianelli, C., Caia, V., Cum, G., Gallo, R., Mancini, V. (1991). Thermal-isomerisation of photochemically synthesized (Z)-9-styrylacridines—An unusually high enthalpy of Z-E conversion for stilbene-like compounds. *Journal of the Chemical Society-Perkin Transactions 2*, 679–683.
- [22] Caia, V., Cum, G., Gallo, R., Mancini, V., Pitoni, E. (1983). A high enthalpy value in thermal-isomerisation of photosynthesized cis-9-styrylacridines. *Tetrahedron Letters*, *24*, 3903–3904.
- [23] Miki, S., Matsuo, K., Yoshida, M., Yoshida, Z. (1988). Novel anthraquinone derivatives undergoing photochemical valence isomerisation. *Tetrahedron Letters*, *29*, 2211–2214.
- [24] Jones, G., Reinhardt, T. E., Bergmark, W. R. (1978). Photon energy-storage in organic materials—Case of linked anthracenes. *Solar Energy*, *20*, 241–248.

- [25] Ndiaye, S. A., Aaron, J. J., Garnier, F. (1986). Sensitized photoisomerisation of limonene as a model for a light energy-storage process. *Journal of Photochemistry*, 35, 389–394.
- [26] Maruyama, K., Terada, K., Yamamoto, Y. (1981). Highly efficient valence isomerisation between norbornadiene and quadricyclane derivatives under sunlight. *Chemistry Letters*, 10, 839–842.
- [27] Canas, L. R., Greenberg, D. B. (1985). Determination of the energy-storage efficiency of the photoisomerisation of norbornadiene to quadricyclane as a potential means for the trapping of solar-energy. *Solar Energy*, 34, 93–99.
- [28] Maruyama, K., Tamiaki, H., Kawabata, S. (1985). Development of a solar-energy storage process—Photoisomerisation of a norbornadiene derivative to a quadricyclane derivative in an aqueous alkaline-solution. *The Journal of Organic Chemistry*, 50, 4742–4749.
- [29] Yoshida, Z. (1985). New molecular energy storage systems. *Journal of Photochemistry*, 29, 27–40.
- [30] Bren, V. A., Dubonosov, A. D., Minkin, V. I., Chernouvanov, V. A. (1991). Norbornadiene-quadricyclane as efficient molecular-system of accumulation of solar energy. *Uspekhi Khimii*, 60, 913–948.
- [31] Nagai, T., Takahashi, I., Shimada, M. (1999). Trifluoromethyl-substituted norbornadiene, useful solar energy material. *Chemistry Letters*, 28, 897–898.
- [32] Dubonosov, A. D., Bren, V. A., Chernouvanov, V. A. (2002). Norbornadiene: Quadricyclane as an abiotic system for accumulation of the solar energy. *Uspekhi Khimii*, 71, 1040–1050.
- [33] Boese, R., Cammack, J. K., Matzger, A. J., Pflug, K., Tolman, W. B., Vollhardt, K. P. C., Weidman, T. W. (1997). Photochemistry of (fulvalene)tetracarbonyldiruthenium and its derivatives: Efficient light energy storage devices. *Journal of the American Chemical Society*, 119, 6757–6773.
- [34] Kanai, Y., Srinivasan, V., Meier, S. K., Vollhardt, K. P. C., Grossman, J. C. (2010). Mechanism of thermal reversal of the (fulvalene)tetracarbonyldiruthenium photoisomerization: Toward molecular solar-thermal energy storage. *Angewandte Chemie—International Edition*, 49, 8926–8929.
- [35] Vollhardt, K. P. C., Weidman, T. W. (1983). Synthesis, structure, and photochemistry of tetracarbonyl(fulvalene)diruthenium—Thermally reversible photo-isomerisation involving carbon-carbon bond activation at a dimetal center. *Journal of the American Chemical Society*, 105, 1676–1677.
- [36] Zhu, B. L., Miljanic, O. S., Vollhardt, K. P. C., West, M. J. (2005). Synthesis of 2,2',3,3'-tetramethyl- and 2,2',3,3'-tetra-tert-butylfulvalene: Attractive platforms for dinuclear transition metal fragments, as exemplified by (eta(5):eta(5)-2,2',3,3'-t-Bu₄C₁₀H₄)M-2(CO)_n (M = Fe, Ru, Os, Mo) and first X-ray crystal structures of fulvalene diiron and diosmium complexes. *Synthesis-Stuttgart*, 3373–3379.
- [37] Ragaini, V. (1982). Solar-energy storage by the reversible-reaction—N₂O₄ reversible 2NO₂—Theoretical and experimental results. *Solar Energy*, 29, 535–540.
- [38] Marcus, R. J., Wohlers, H. C. (1960). A new solar furnace—Design and operation. *Industrial and Engineering Chemistry*, 52, 825–826.
- [39] Marcus, R. J., Wohlers, H. C. (1961). Photochemical systems for solar energy conversion—Nitrosyl chloride. *Solar Energy*, 5, 44–57.
- [40] Shigeishi, R. A., Langford, C. H., Hollebhone, B. R. (1979). Solar-energy storage using chemical-potential changes associated with drying of zeolites. *Solar Energy*, 23, 489–495.
- [41] Tchernev, D. I. (2001). Natural zeolites in solar energy heating, cooling, and energy storage. *Natural Zeolites: Occurrence, Properties, Applications*, 45, 589–617.
- [42] Nagai, T., Shimada, M., Nishikubo, T. (2001). Synthesis of new photoresponsive polymers containing trifluoromethyl-substituted norbornadiene moieties. *Chemistry Letters*, 2001, 1308–1309.

- [43] Nagai, T., Shimada, M., Ono, Y., Nishikubo, T. (2003). Synthesis of new photoresponsive polymers containing trifluoromethyl-substituted norbornadiene moieties. *Macromolecules*, *36*, 1786–1792.
- [44] Kolpak, A. M., Grossman, J. C. (2011). Azobenzene-functionalized carbon nanotubes as high-energy density solar thermal fuels. *Nano Letters*, *11*, 3156–3162.
- [45] Jones, G., Chiang, S. H., Xuan, P. T. (1979). Energy-storage in organic photoisomers. *Journal of Photochemistry*, *10*, 1–18.
- [46] Scharf, H. D., Fleischhauer, J., Leismann, H., Ressler, I., Schleker, W., Weitz, R. (1979). Criteria for the efficiency, stability, and capacity of abiotic photo-chemical solar-energy storage-systems. *Angewandte Chemie—International Edition*, *18*, 652–662.
- [47] Suppan, P. *Chemistry and Light*, The Royal Society of Chemistry, London, 1994.
- [48] Schwerzel, R. E., Klosterman, N. E., Kelly, J. R., Hillenbrand, L. J. (1978) U.S. Patent 4105014/1978.
- [49] Dauben, W. G., Cargill, R. L. (1961). Photochemical transformations 8. Isomerisation delta 2,5-Bicyclo 2.2.1 heptadiene to quadricyclo 2.2.1 heptane (quadricyclene). *Tetrahedron*, *15*, 197–201.
- [50] Cristol, S. J., Snell, R. L. (1958). Bridged polycyclic compounds 6. The photoisomerisation of bicyclo 2,2,1 hepta-2,5-diene-2,3-dicarboxylic acid to quadricyclo 2,2,1 heptane-2,3-dicarboxylic acid. *Journal of the American Chemical Society*, *80*, 1950–1952.
- [51] Hammond, G. S., Turro, N. J., Fischer, A. (1961). Photosensitized cycloaddition reactions. *Journal of the American Chemical Society*, *83*, 4674–4675.
- [52] Hammond, G. S., Turro, N. J., Wyatt, P., Deboer, C. D. (1964). Photosensitized isomerisation involving saturated centers. *Journal of the American Chemical Society*, *86*, 2532–2533.
- [53] Smith, C. D. (1988). Quadricyclane. *Organic Syntheses*, *50*, 962–964.
- [54] Harel, Y., Adamson, A. W., Kutal, C., Grutsch, P. A., Yasufuku, K. (1987). Photocalorimetry 6. Enthalpies of isomerisation of norbornadiene and substituted norbornadienes to corresponding quadricyclenes. *Journal of Physical Chemistry*, *91*, 901–904.
- [55] Dilling, W. L. (1966). Intramolecular photochemical cycloaddition reactions of nonconjugated olefins. *Chemical Reviews*, *66*, 373–393.
- [56] Nagai, T., Fujii, K., Takahashi, I., Shimada, M. (2001). Trifluoromethyl-substituted donor-acceptor norbornadiene, useful solar energy material. *Bulletin of the Chemical Society of Japan*, *74*, 1673–1678.
- [57] Franceschi, F., Guardigli, M., Solari, E., Floriani, C., ChiesiVilla, A., Rizzoli, C. (1997). Designing copper(I) photosensitizers for the norbornadiene-quadricyclane transformation using visible light: An improved solar energy storage system. *Inorganic Chemistry*, *36*, 4099–4107.
- [58] Han, L., Wei, H. X., Li, S. Y., Chen, J. P., Zeng, Y., Li, Y. Y., Han, Y. B., Li, Y., Wang, S. Q., Yang, G. Q. (2010). Remote sensitized photoisomerization via through-bond triplet-triplet energy transfer mediated by a salt bridge in a supramolecular dyad. *Chemphyschem*, *11*, 229–235.
- [59] Cho, J., Berbil-Bautista, L., Pechenezhskiy, I. V., Levy, N., Meier, S. K., Srinivasan, V., Kanai, Y., Grossman, J. C., Vollhardt, K. P. C., Crommie, M. F. (2011). Single-molecule-resolved structural changes induced by temperature and light in surface-bound organometallic molecules designed for energy storage. *ACS Nano*, *5*, 3701–3706.
- [60] Harpham, M. R., Nguyen, S. C., Hou, Z., Grossman, J. C., Harris, C. B., Mara, M. W., Stickrath, A. B., Kanai, Y., Kolpak, A., Lee, D., Liu, D.-J., Lomont, J. P., Moth-Poulsen, K., Vinokurov, N., Chen, L. X., Vollhardt, K. P. C. (2012). X-ray transient absorption and picosecond IR spectroscopy of fulvalene(tetracarbonyl)diruthenium on photoexcitation. *Angewandte Chemie—International Edition*, *51*, 7692–7696.

- [61] Maruyama, K., Tamiaki, H., Kawabata, S. (1986). Exothermic isomerisation of water-soluble quadricyclanes to norbornadienes by soluble and insoluble catalysts. *Journal of the Chemical Society-Perkin Transactions 2*, 543–549.
- [62] Maruyama, K., Tamiaki, H. (1986). Catalytic isomerisation of water-soluble quadricyclane to norbornadiene derivatives induced by cobalt porphyrin complexes. *The Journal of Organic Chemistry*, 51, 602–606.
- [63] Miki, S., Asako, Y., Yoshida, Z. (1987). Photochromic solid films prepared by doping with donor-acceptor norbornadienes. *Chemistry Letters*, 16, 195–198.

CHAPTER 7

STRATEGIES TO SWITCH FLUORESCENCE WITH PHOTOCHROMIC OXAZINES

ERHAN DENIZ, JANET CUSIDO, MASSIMILIANO TOMASULO, MUTLU BATTAL, IBRAHIM YILDIZ, MARCO PETRIELLA, MARIANO L. BOSSI, SALVATORE SORTINO, and FRANÇISCO M. RAYMO

7.1 FLUORESCENCE IMAGING AT THE NANOSCALE

The introduction of fluorescent labels [1] within a sample of interest offers the opportunity to reconstruct an image of the specimen in real time with the aid of an optical microscope [2]. Indeed, the microscope optics can be exploited to illuminate a relatively small area of the labeled sample at an appropriate wavelength and excite the individual fluorescent probes. The same optics can then collect the emission of the excited labels and map their spatial distribution in two dimensions within the illuminated area. Relying on the sectioning ability of confocal optics [3], the third dimension can also be explored with the consecutive acquisition of two-dimensional maps offset in the vertical direction. In fact, the fluorescence microscope has become an indispensable analytical tool in the biomedical laboratory for the investigation of the structural features and dynamic processes associated with a diversity of biological samples.

The illumination of the sample and the collection of its fluorescence demand the use of lenses to focus the exciting and emitted radiation [2]. The phenomenon of diffraction [4], however, prevents the focusing of light within volumes of subwavelength dimensions. As a result, the wavelength of the emitted radiation (as well as that of the exciting one when confocal optics are employed) ultimately dictates the resolution of a conventional fluorescence image, rather than the actual dimensions of the emissive probes. It follows that the acquisition of images with visible light translates into the inability to distinguish features separated by less than a few hundred nanometers. These physical dimensions are at least two orders of magnitude larger than those of most molecules and, therefore, conventional fluorescence microscopes cannot provide structural information at the molecular level.

Organic Synthesis and Molecular Engineering, First Edition.

Edited by Mogens Brøndsted Nielsen.

© 2014 John Wiley & Sons, Inc. Published 2014 by John Wiley & Sons, Inc.

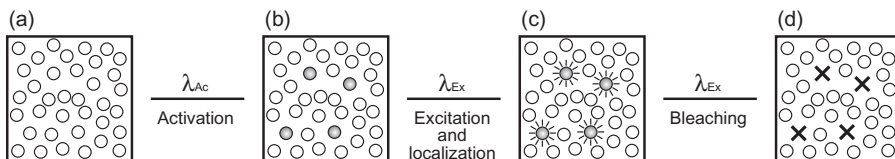


Figure 7.1. Illumination at an activating wavelength (λ_{Ac}) switches the probes from a nonemissive to an emissive state (a \rightarrow b). Irradiation at an exciting wavelength (λ_{Ex}) permits the localization of the emissive species at the single-molecule level (c) and then the bleaching of the localized probes (d). Reiterative sequences of activation, excitation/localization, and bleaching steps offer the opportunity to map sequentially the spatial distribution of the photoactivatable probes with resolution at the nanometer level.

The phenomenon of diffraction is inherent to focusing and cannot be avoided [4]. However, it can be overcome with the aid of single-molecule localization, switchable probes, and time [5–12]. Indeed, multiple fluorescent labels positioned within the same subdiffraction volume can be localized one by one with the sequential acquisition of snapshots, if they are designed to emit individually in turn at different times. This stringent requirement can be satisfied with labels that switch from a nonemissive state to an emissive one under illumination at an activating wavelength (λ_{Ac}) and then fluoresce upon irradiation at an exciting wavelength (λ_{Ex}). Under these conditions, the illumination of a labeled sample at λ_{Ac} can be exploited to activate a relatively small fraction of probes at a given time (a \rightarrow b in Figure 7.1). If the population of active probes is sufficiently small and sparse, then the probability of having more than one within the same subdiffraction volume is negligible. As a result, the subsequent illumination at λ_{Ex} can be exploited to excite the active species and localize them individually (b \rightarrow c in Figure 7.1). If the active probes are sufficiently bright, the spatial coordinates of each one of them can be identified with nanoscale precision. Further illumination at λ_{Ex} can then bleach permanently the localized probes (c \rightarrow d in Figure 7.1). At this point, the sequence of activation, excitation/localization, and bleaching steps can be reiterated multiple times until a sufficient number of coordinates is available to compile a map of the spatial distribution of the labels in two dimensions. In fact, this clever protocol* [13, 14] to overcome diffraction ultimately culminates with the reconstruction of a complete image of the sample with resolution at the nanometer level.

7.2 FLUORESCENCE SWITCHING WITH PHOTOCHROMIC COMPOUNDS

Photochromic compounds [15–20] switch reversibly between states with distinct absorption properties in the visible region under the influence of optical stimulation. Their photoinduced transformations are accompanied by pronounced stereoelectronic modifications that can be engineered to control the emission of complementary fluorophores [20–23]. Indeed, fluorescent and photochromic components can be integrated within the same molecular skeleton or supramolecular construct to generate multicomponent systems with photoswitchable fluorescence. The operating principles to switch

*These operating principles for the reconstruction of fluorescence images with subdiffraction resolution were originally reported in References 13 and 14.

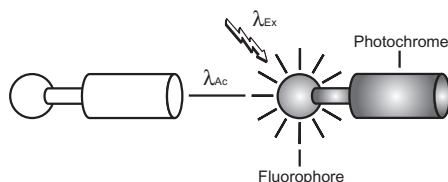


Figure 7.2. Illumination at an activating wavelength (λ_{Ac}) switches the photochromic component, alters the electronic structure of the adjacent fluorophore, and enables absorption at an exciting wavelength (λ_{Ex}) with concomitant fluorescence.

the emission of these fluorophore–photochrome assemblies are generally designed around either electron or energy transfer* [24–32]. Specifically, one of the interconvertible states of the photochromic component can be designed to either exchange an electron with or accept energy from the excited fluorescent component and quench its emission. Under these conditions, the photochromic transformation alters the quantum yield of the emissive process and modulates fluorescence.

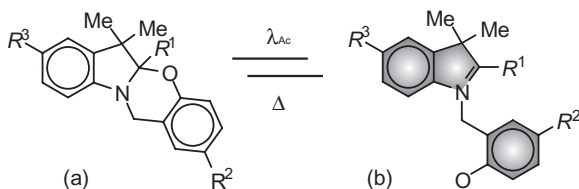
Mechanisms based on electron and energy transfer control the excitation dynamics of the emissive component to regulate fluorescence. Alternatively, the photochromic process can be designed to alter the electronic structure of the fluorescent component in the ground state. Specifically, illumination at an activating wavelength (λ_{Ac}) can induce the photochromic transformation to extend conjugation within the emissive chromophore and shift bathochromically its main absorption. In turn, the photoinduced bathochromic shift can enable the absorption of the fluorescent component at an exciting wavelength (λ_{Ex}) with concomitant fluorescence. Indeed, the interplay of beams at λ_{Ac} and λ_{Ex} translates into the opportunity to photoactivate fluorescence (Figure 7.2) with these photochromic systems and permits the reconstruction of fluorescence images with subdiffraction resolution, according to the protocol outlined in Figure 7.1† [33, 34].

7.3 DESIGN AND SYNTHESIS OF FLUOROPHORE–OXAZINE DYADS

In search of viable structural designs to implement photochromic transformations with fast switching speeds, we developed a family of photochromic compounds based on the photoinduced opening and thermal closing of oxazine rings [35]. These molecules fuse a *2H,3H*-indole heterocycle to a benzo-*2H,3H*-oxazine ring in their covalent skeleton (a in Scheme 7.1). The local excitation of their phenoxy chromophore cleaves the [C–O] bond at the junction of the two heterocyclic fragments and opens the oxazine ring on a subnanosecond timescale. The resulting zwitterionic isomer (b in Scheme 7.1) incorporates anionic and cationic chromophores that can be designed to absorb in the visible region with the manipulation of their substituents (R^1 , R^2 , and R^3). This species

*Mechanisms for fluorescence switching with photochromic compounds are reviewed in Reference 22. Representative examples of fluorophore–photochrome dyads operating on the basis of electron and energy transfer are reported in References 24–32.

†The use of photochromic compounds to reconstruct images with subdiffraction resolution is reviewed in Reference 22e. Representative examples of subdiffraction images acquired with photochromic fluorescent probes are reported in References 33 and 34.



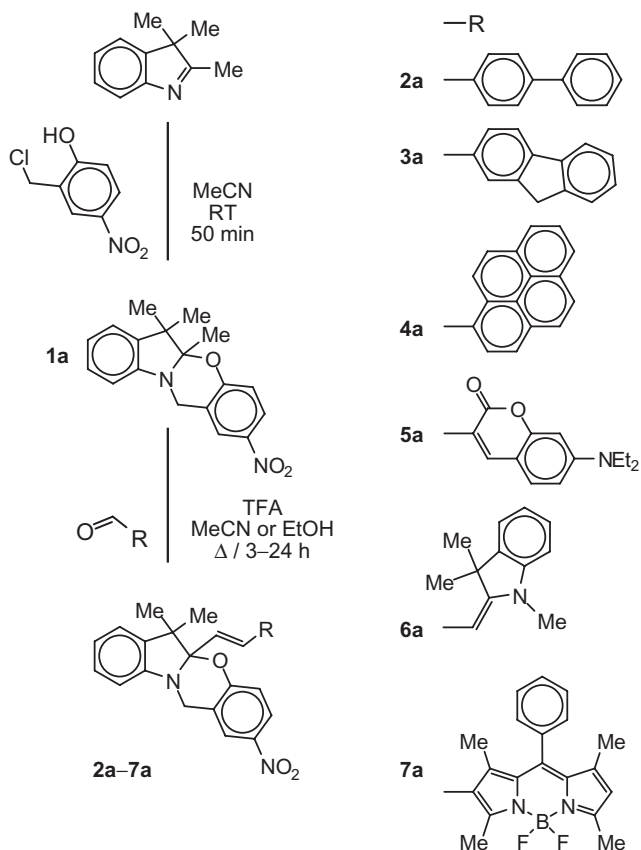
Scheme 7.1. Illumination at an activating wavelength (λ_{Ac}) opens the oxazine ring of one isomer (a) to generate a zwitterionic species (b). The photogenerated isomer reverts to the original one after the spontaneous closing of the oxazine ring.

reverts spontaneously to the original one with first-order kinetics on timescales ranging from few tens of nanoseconds to several microseconds, depending on the nature of R^1 , R^2 , and R^3 .

The photoinduced opening of the oxazine ring of our compounds can be exploited to activate the emission of an adjacent fluorophore, according to the operating principles outlined in Figure 7.2 [36]. Indeed, this structural transformation brings R^1 in conjugation with the 3*H*-indolium cation of the zwitterionic isomer. Therefore, the electronic structure of an emissive chromophore, introduced at this particular position, can change with the state of the photochromic component. Specifically, the illumination at an activating wavelength (λ_{Ac}) can open the oxazine ring, shift bathochromically the band associated with the $S_0 \rightarrow S_1$ transition of R^1 , and enable its absorption at an exciting wavelength (λ_{Ex}). On the basis of these considerations, we designed a general synthetic strategy to condense a preformed oxazine to formylated fluorophores and prepared six compounds differing in the nature of R^1 . In particular, the reaction of 2,3,3-trimethyl-3*H*-indole with 2-chloromethyl-4-nitrophenol gives the oxazine **1a** (Scheme 7.2) in a yield of 58% [35a, 37]. The subsequent coupling of **1a** with commercial or readily accessible aldehydes, under the assistance of trifluoroacetic acid (TFA), affords the target compounds **2a–7a** (Scheme 7.2) in yields ranging from 10% to 63% [36].

7.4 FLUORESCENCE ACTIVATION WITH FLUOROPHORE–OXAZINE DYADS

The chiral center within the oxazine ring of **2a–7a** prevents electronic communication between the fluorescent and photochromic components of these dyads in the ground state [36]. As a result, their absorption spectra are essentially the sum of those of their constituent components. Specifically, the spectra of **2a–5a** and **7a** in acetonitrile show bands centered at wavelengths (λ_{Ab} in Table 7.1) ranging from 288 to 520 nm for the fluorescent appendages and an absorption centered at ca. 310 nm for the 4-nitrophenoxy chromophore. Illumination in the tail of this band with a pulsed laser, operating at 355 nm (λ_{Ac} in Scheme 7.1), opens the oxazine ring of **2a**, **3a**, and **5a** to generate the corresponding zwitterionic isomers **2b**, **3b**, and **5b** with quantum yields (ϕ_p in Table 7.1) of 0.08, 0.02, and 0.02, respectively. This structural transformation brings the fluorescent appendage in conjugation with the cationic fragment of **2b**, **3b**, and **5b** and elongates its absorption wavelength by more than 120 nm. Indeed, the spectroscopic signature of the resulting extended chromophores is essentially equivalent to that of the model 3*H*-indolium cations **8**, **9**, and **11** (Figure 7.3). As an example, the absorption spectra



Scheme 7.2. The fluorophore–photochrome dyads **2a–7a** can be prepared in two synthetic steps, starting from commercial precursors and accessible aldehydes.

TABLE 7.1. Photochemical and Photophysical Parameters of the Ring-Closed Isomers **2a–5a and **7a**, the Ring-Open Species **6b**, and Their Models **8–13** in Acetonitrile at 20°C**

	λ_{Ab}^a (nm)	ϕ_{P}^b	τ_{P}^c (μs)		λ_{Ab}^a (nm)	λ_{Em}^a (nm)	ϕ_{F}^d
2a	288	0.08	0.1	8	412	542	<0.01
3a	299	0.02	0.1	9	431	559	<0.01
4a	362	–	–	10	501	630	<0.01
5a	412	0.02	0.2	11	573	645	0.09
6b	548	–	–	12	543	565	0.03
7a	520	–	31	13	558	–	–

^aThe absorption (λ_{Ab}) and emission (λ_{Em}) wavelengths were estimated from the corresponding spectra.

^bThe quantum yield (ϕ_{P}) for the photochromic transformation was determined with a benzophenone standard.

^cThe lifetime (τ_{P}) of the photogenerated isomer was determined from the temporal absorbance evolutions.

^dThe fluorescence quantum yield (ϕ_{F}) was determined with fluorescein and rhodamine B standards.

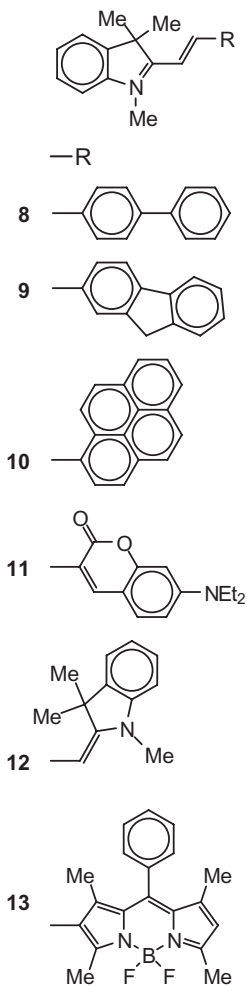


Figure 7.3. The model compounds **8–13** incorporate essentially the same 3*H*-indolium chromophore of the ring-opened isomers **2b–7b**.

of an acetonitrile solution of **5a** recorded before (a in Figure 7.4) and 30 ns after (b in Figure 7.4) laser illumination clearly reveal the photoinduced bathochromic shift imposed on the absorption band of the fluorescent component. Furthermore, the absorption band observed after irradiation (b in Figure 7.4) closely resembles that of the model compound **11** (c in Figure 7.4).

The photogenerated isomers **2b**, **3b**, and **5b** have lifetimes (τ_p in Table 7.1) ranging from 0.1 to 0.2 μs and eventually revert to the original species **2a**, **3a**, and **5a** with first-order kinetics. Consistently, the band associated with the extended cationic chromophores of **2b**, **3b**, and **5b** decays monoexponentially. As an example, the absorbance of **5b** in the visible region decays within few microseconds from laser illumination (Figure 7.5). In fact, these particular fluorophore–photochrome dyads can be switched between

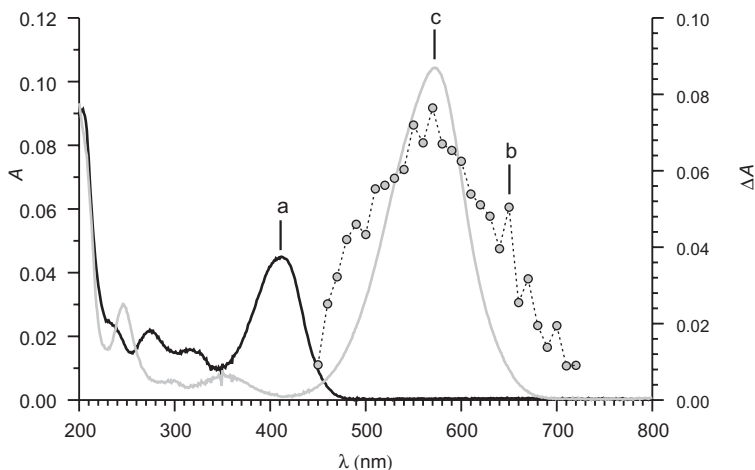


Figure 7.4. Absorption spectra of solutions (MeCN, 20°C) of **5a**, recorded before ([a] 2.5 μM) and 30 ns after ([b] 10 μM) illumination at λ_{Ac} (355 nm) with a pulsed laser (6 ns, 10 mJ), and of **11** ([c] 2.5 μM).

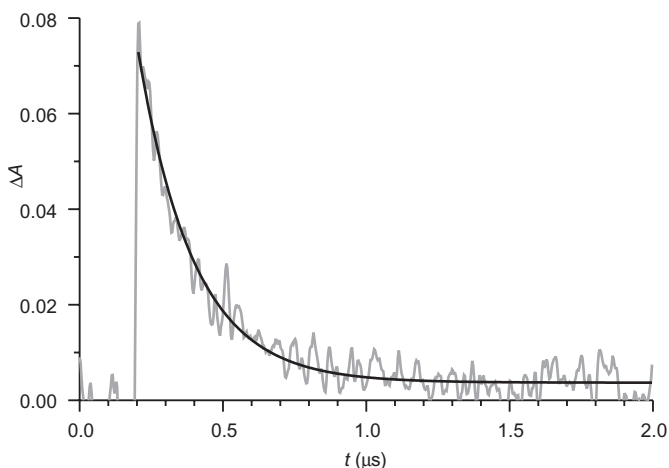


Figure 7.5. Evolution of the absorbance at 580 nm for a solution (10 μM, MeCN, 20°C) of **5a** upon illumination at λ_{Ac} (355 nm) with a pulsed laser (6 ns, 10 mJ).

their two interconvertible states on microsecond timescales simply turning on and off a laser operating at λ_{Ac} . Furthermore, they tolerate hundreds of switching cycles without any sign of degradation even in aerated solutions.

In contrast to the behavior of **2a**, **3a**, and **5a**, the fluorophore–photochrome dyads **4a** and **7a** do not switch to the corresponding zwitterionic isomers **4b** and **7b**, under otherwise identical illumination conditions [36b,c]. Rather than the expected ground-state absorption of their 3*H*-indolium chromophores, the absorption spectra of **4a** and **7a**, recorded after illumination with a pulsed laser, reveal transient absorptions in the

triplet manifold of their fluorescent components. Comparison of the time-resolved spectrum of **7a** with that of an appropriate model demonstrates that the local excitation of the 4-nitrophenoxy chromophore of the photochromic component encourages the population of the triplet state of the fluorescent component [36c]. Thus, the excitation energy of the former is transferred to the latter, sensitizing the formation of its triplet state. However, further comparison of the excitation spectrum of **7a** with that of a model fluorophore indicates the lack of any intramolecular energy transfer in the singlet state. These observations demonstrate that the excited photochromic component undergoes intersystem crossing first and then transfers energy to the fluorescent component in the triplet state, instead of opening its oxazine ring. In fact, the excitation dynamics of **7a** prove unequivocally that the photochemistry of this particular family of photochromic oxazines evolves along the potential energy surface of their triplet state.

In the case of the cyanine derivative, the absorption spectrum in acetonitrile shows bands for the anionic and cationic chromophores of the zwitterionic isomer **6b** [36b]. Consistently, the ^1H NMR spectrum reveals a single peak for the pair of homotopic protons on the methylene bridge between the two chromophoric fragments of this species, rather than an AB system expected for the very same protons in the chiral ring-closed isomer **6a**. Thus, the extended conjugation of the *3H*-indolium cation encourages the preferential population of **6b** relative to **6a** for this particular fluorophore–photochrome dyad.

The bathochromic shift associated with the transformation of **2a**, **3a**, and **5a** into **2b**, **3b**, and **5b**, respectively, upon illumination at λ_{Ac} can be exploited to activate fluorescence, according to the operating principles in Figure 7.2 [36a,b]. Specifically, the simultaneous illumination at λ_{Ac} and a λ_{Ex} positioned within the absorption band of the photogenerated isomer results in the excitation of its fluorescent appendage with concomitant fluorescence. Indeed, the emission spectra of acetonitrile solutions of **2a**, **3a**, and **5a** recorded upon irradiation at both λ_{Ac} and λ_{Ex} reveal bands essentially identical to those observed upon illumination of the corresponding models **8**, **9**, and **11**, respectively at λ_{Ex} only. In fact, these particular model compounds incorporate *3H*-indolium cations equivalent to those of the zwitterionic isomers **2b**, **3b**, and **5b** and emit at wavelengths (λ_{Em} in Table 7.1) ranging from 542 to 645 nm. As an example, the emission spectrum (a in Figure 7.6) recorded upon illumination of an acetonitrile solution of **5a** at $\lambda_{\text{Ac}} = 355$ nm, to open its oxazine ring, and at $\lambda_{\text{Ex}} = 532$ nm, to excite the photogenerated isomer, shows a band that resembles the one (b in Figure 7.6) observed for the model **11** upon illumination exclusively at λ_{Ex} .

The fluorescence quantum yield (ϕ_{F} in Table 7.1) of the model compounds **8** and **9** is smaller than 0.01, while that of **11** approaches 0.09 [36a,b]. This particular value, together with a molar extinction coefficient of $83 \text{ mM}^{-1} \text{ cm}^{-1}$ at 573 nm, translates into a brightness of $8 \text{ mM}^{-1} \text{ cm}^{-1}$. In turn, the relatively large brightness of this extended *3H*-indolium cation suggests that the corresponding zwitterionic species **5b** is sufficiently bright to be detected at the single-molecule level. Indeed, individual molecules of **5b**, trapped within a poly(methyl methacrylate) (PMMA) matrix, can clearly be observed in fluorescence images recorded after activation at λ_{Ac} and excitation at λ_{Ex} . Specifically, the continuous illumination at λ_{Ac} of a portion of the doped polymer film switches stochastically individual molecules from the nonemissive state **5a** to the emissive state **5b** within the irradiated area. The concomitant acquisition of multiple frames in sequence with irradiation at λ_{Ex} offers the opportunity to identify the fluorescent species photogenerated at different times in distinct positions within the activated area.

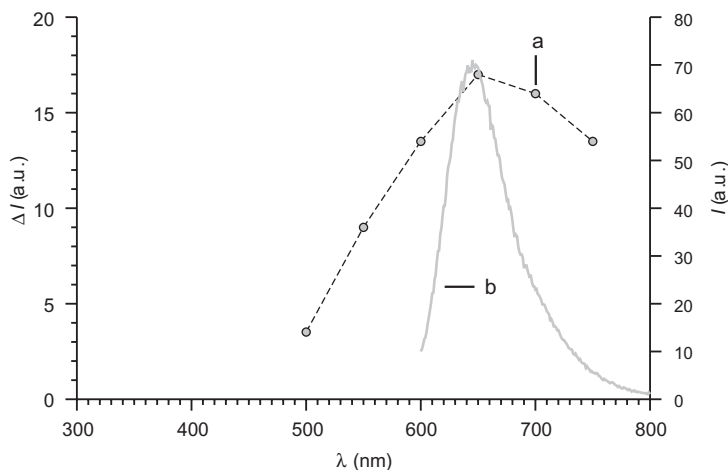


Figure 7.6. Emission spectra of solutions (MeCN, 20°C) of **5a** ([a] 10 μM), recorded upon simultaneous illumination at λ_{Ac} (355 nm, 10 mJ) and λ_{Ex} (532 nm, 30 mJ) with a pulsed laser (6 ns), and of **11** ([b] 2.5 μM), recorded upon excitation at λ_{Ex} (593 nm) only.

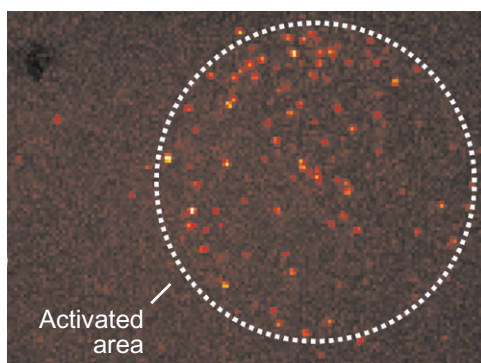


Figure 7.7. Sum of 2000 images (frame time = 10 ms) of a PMMA film doped with **5a** (1×10^{-5} % w/w), recorded upon illumination at λ_{Ac} (355 nm, 10 W cm^{-2}) of a circular area with a radius of ca. $6 \mu\text{m}$ and at λ_{Ex} (532 nm, 5 kW cm^{-2}) of the entire imaging field. See color insert.

The acquired frames can then be summed to map the many species localized within the activated area in a single image (Figure 7.7).

7.5 DESIGN AND ASSEMBLY OF PHOTOSWITCHABLE NANOPARTICLES

Amphiphilic copolymer **14** (Figure 7.8) incorporates multiple hydrophobic decyl and hydrophilic oligo(ethylene glycol) chains along a common poly(methacrylate) backbone [38]. In aqueous environment, this macromolecule assembles into micellar constructs with nanoscaled dimensions capable of trapping hydrophobic guests in their interior. Furthermore, these nanoparticles can cross the membrane of living cells and

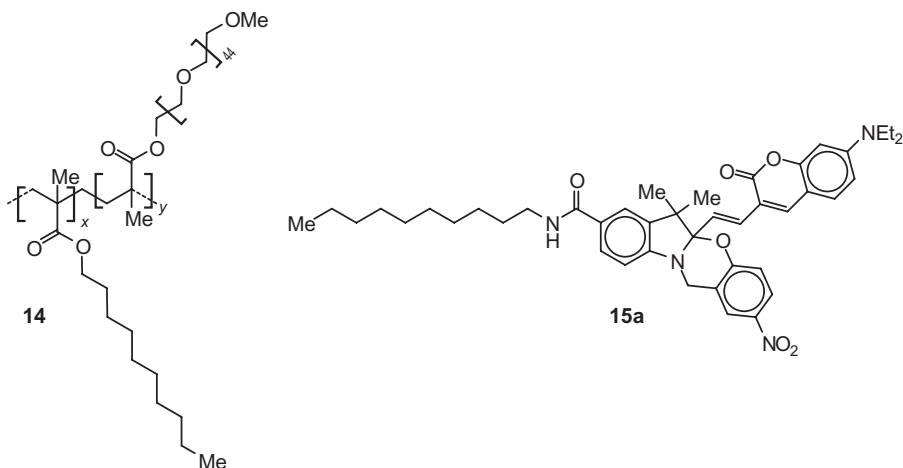


Figure 7.8. The amphiphilic copolymer **14** forms nanoscaled micellar assemblies in water able to encapsulate the fluorophore–photochrome dyad **15a** in their hydrophobic core.

transport their cargo unaffected into the cytosol. In principle, such supramolecular strategy for intracellular delivery could be extended to the fluorophore–photochrome dyad **5a** in order to permit the subdiffraction imaging of the intracellular environment, according to the operating principles outlined in Figure 7.1. On the basis of these considerations, we assessed the ability of **14** to capture either **5a** or its hydrophobic analog **15a** (Figure 7.8) and transfer them into aqueous solutions [39].

The decyl tail of **15a** was expected to enhance the hydrophobic character of the overall fluorophore–photochrome dyad and facilitate its encapsulation within micellar assemblies of **14** [39]. Nonetheless, both **5a** and **15a** turned out to be optimal guests for this particular polymeric host. Indeed, both molecules are virtually insoluble in aqueous environments, but readily dissolve in neutral phosphate buffer saline (PBS) in the presence of **14**. The absorption spectra of the resulting micellar dispersions are similar to those of **5a** and **15a** in acetonitrile. Under both set of conditions, the absorption band of the coumarin appendage can clearly be observed at ca. 400 nm. Upon illumination of the PBS dispersions at $\lambda_{Ac} = 355$ nm, the oxazine ring of the dyads entrapped within the micelles opens to generate the corresponding zwitterionic isomers **5b** and **15b**. As observed in acetonitrile, this structural transformation is accompanied by the appearance of a band at ca. 600 nm for the extended *3H*-indolium cation of **5b** and **15b**. This transient absorption decays monoexponentially with the spontaneous reversion of **5b** and **15b** back to **5a** and **15a**. Interestingly, the quantum yield for the photoinduced ring opening of the dyads entrapped within the micelles and the lifetime of the photo-generated isomers are essentially identical to those measured in acetonitrile (ϕ_p and τ_p in Table 7.1). Thus, the polymeric host protects the encapsulated guests effectively from the aqueous phase and provides an environment similar to that experienced by the dyads in acetonitrile.

The photochemical response of the fluorophore–photochrome dyads **5a** and **15a**, entrapped within the micellar assemblies, offers the opportunity to photoactivate fluorescence in aqueous environments [39]. As observed in acetonitrile, simultaneous illumination at λ_{Ac} , to open the oxazine ring, and at λ_{Ex} , to excite the photogenerated

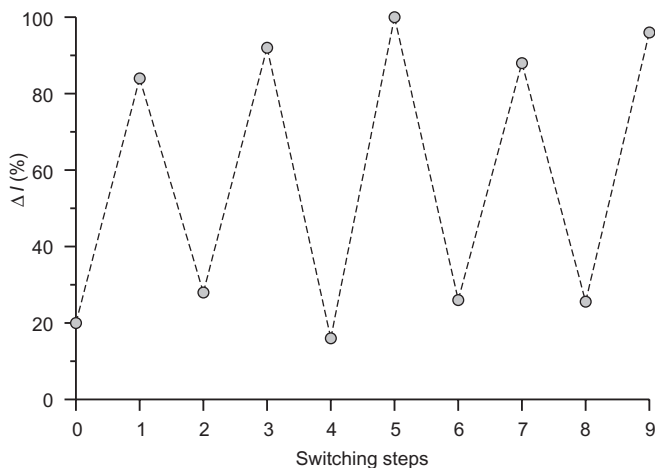


Figure 7.9. Relative emission intensity at 650 nm of a dispersion (H_2O , 25°C) of **14** (2 mg mL^{-1}) and **15a** ($9\text{ }\mu\text{g mL}^{-1}$), recorded upon pulsed irradiation at λ_{ex} (532 nm, 6 ns, 30 mJ) without and with simultaneous pulsed illumination at λ_{Ac} (355 nm, 6 ns, 15 mJ).

isomer, results in the appearance of the characteristic band of the extended *3H*-indolium cation at ca. 650 nm in the corresponding emission spectrum. In fact, the fluorescence of these nanostructured constructs can be switched on and off simply by turning a laser operating at λ_{Ac} on and off, while illuminating the sample at λ_{ex} . As an example, Figure 7.9 shows the changes in the emission intensity of an aqueous dispersion of **14** and **15a** for nine consecutive switching steps.

The ability to photoactivate the fluorescence of the dyads trapped within the micellar assemblies permits the implementation of the operating principles in Figure 7.1 and the visualization of these nanoscaled constructs with subdiffraction resolution [36b]. Specifically, micellar assemblies of **14** with **5a** in their interior were deposited on a glass slide and imaged for thousands of consecutive frames under illumination at $\lambda_{\text{Ac}} = 355\text{ nm}$, to open the oxazine ring, and at $\lambda_{\text{ex}} = 532\text{ nm}$, to excite the resulting zwitterionic isomer **5b**. The coordinates of the fluorescent species localized at the single-molecule level in each frame were then combined to produce an image of the specimen with resolution at the nanometer level. The resulting map (Figure 7.10a) shows objects of nanoscaled dimensions that cannot otherwise be distinguished in the corresponding diffraction-limited image (Figure 7.10b). Indeed, the spatial profile (Figure 7.10c) of the emission intensity reveals that the peak-to-peak separation between two of the three objects in the field of view is only 110 nm. This value is well below the limit imposed by diffraction on the resolution of the conventional fluorescence image. Thus, the unique combination of photochemical and photophysical properties associated with the fluorophore-photochrome dyads entrapped within the micelles offers the opportunity to overcome diffraction and resolve structural features at the nanoscale.

7.6 CONCLUSIONS

A photochromic oxazine can be assembled in a single synthetic step from commercial precursors and condensed to fluorescent aldehydes under acidic conditions. The local

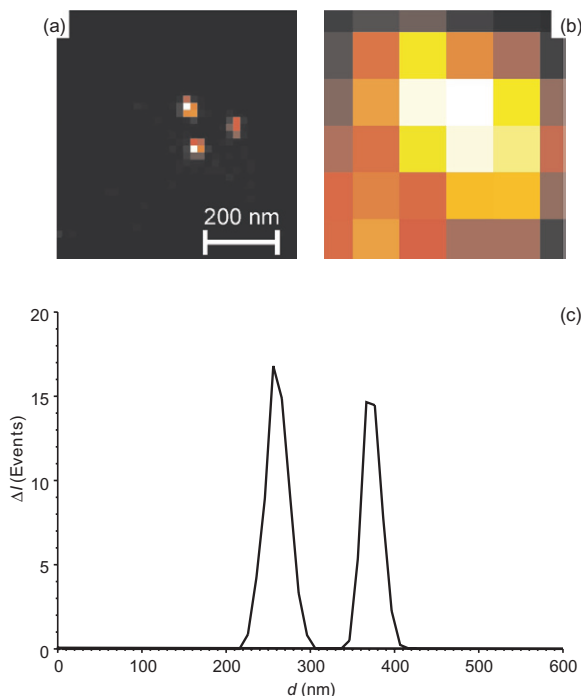


Figure 7.10. A dispersion of **5a** and **14** in neutral PBS was deposited on a glass slide. After the evaporation of the solvent, the resulting nanoparticles were imaged for 90,000 consecutive frames (frame time = 10 ms) with simultaneous wide-field illumination at $\lambda_{Ac} = 355 \text{ nm}$ ($1 \rightarrow 100 \text{ W cm}^{-2}$) and $\lambda_{Ex} = 532 \text{ nm}$. The super-resolution image (a), reconstructed from the sum of the acquired frames, shows individual micellar assemblies that cannot be distinguished in the diffraction-limited counterpart (b). The profile (c) of the emission intensity, measured along the two brightest nanoparticles, indicates a peak-to-peak separation of ca. 110 nm with an average full width at half maximum of ca. 30 nm. See color insert.

excitation of the photochromic component of the resulting fluorophore–photochrome dyads opens the oxazine ring to produce a zwitterionic isomer. This structural transformation extends the conjugation of the fluorescent component and shifts its main absorption band bathochromically. Illumination at a wavelength positioned within this band excites exclusively the fluorescent component of the photogenerated isomer. As a result, the emission of such fluorophore–photochrome dyads can be switched under optical control, relying on the interplay of activating and exciting beams designed to address the photochromic and fluorescent components, respectively. In the case of a coumarin derivative, the photogenerated isomer is sufficiently bright to be localized at the single-molecule level. Furthermore, this particular fluorophore–photochrome dyad can be encapsulated within micellar assemblies of an amphiphilic copolymer, and the resulting supramolecular constructs can be operated in aqueous environments. Indeed, the fluorescence of these nanoparticles can be switched on and off with the photoinduced interconversion of the photochromic component. Furthermore, the photoswitchable character of these supramolecular constructs offers the opportunity to overcome

diffraction and reconstruct fluorescence images with resolution at the nanometer level. Thus, our strategies for fluorescence activation with photochromic oxazines can eventually lead to the realization of an entire family of photoswitchable fluorophores for the visualization of biological samples with subdiffraction resolution.

REFERENCES

- [1] Lakowicz, J. R. *Principles of Fluorescence Spectroscopy*, Springer, New York, 2006.
- [2] Murphy, D. B. *Fundamentals of Light Microscopy and Electronic Imaging*, Wiley-Liss, New York, 2001.
- [3] Pawley, J. B. (Ed.). *Handbook of Biological Confocal Microscopy*, Springer, New York, 2006.
- [4] Born, M., Wolf, E. *Principles of Optics*, Cambridge University Press, Cambridge, 2002.
- [5] (a) Hell, S. W. (2003). Toward fluorescence nanoscopy. *Nature Biotechnology*, *21*, 1347–1355; (b) Hell, S. W. (2007). Far-field optical nanoscopy. *Science*, *316*, 1153–1158; (c) Hell, S. W. (2009). Microscopy and its focal switch. *Nature Methods*, *6*, 24–32.
- [6] (a) Sauer, M. (2005). Reversible molecular photoswitches: A key technology for nanoscience and fluorescence imaging. *Proceedings of the National Academy of Sciences of the United States of America*, *105*, 9433–9434; (b) Heilemann, M., Dedecker, P., Hofkens, J., Sauer, M. (2009). Photoswitches: Key molecules for subdiffraction-resolution fluorescence imaging and molecular quantification. *Laser & Photonics Reviews*, *3*, 180–202; (c) van de Linde, S., Wolter, S., Sauer, M. (2011). Single-molecule photoswitching and localization. *Australian Journal of Chemistry*, *64*, 503–511.
- [7] Fernández-Suárez, M., Ting, A. Y. (2008). Fluorescent probes for super-resolution imaging in living cells. *Nature Reviews. Molecular Cell Biology*, *9*, 929–943.
- [8] (a) Bates, M., Huang, B., Zhuang, X. (2008). Super-resolution microscopy by nanoscale localization of photo-switchable fluorescent probes. *Current Opinion in Chemical Biology*, *12*, 505–514; (b) Huang, B., Bates, M., Zhuang, X. (2009). Super-resolution fluorescence microscopy. *Annual Review of Biochemistry*, *78*, 993–1016; (c) Vaughan, J. C., Zhuang, X. (2011). New fluorescent probes for super-resolution imaging. *Nature Biotechnology*, *29*, 880–881.
- [9] Toomre, D., Bewersdorf, J. (2010). A new wave of cellular imaging. *Annual Review of Cell and Developmental Biology*, *26*, 285–314.
- [10] Vogelsang, J., Steinhauer, C., Forthmann, C., Stein, H. I., Person-Skerger, B., Cordes, T., Tinnefeld, P. (2010). Make them blink: Probes for super-resolution microscopy. *Chemphyschem: A European Journal of Chemical Physics and Physical Chemistry*, *11*, 2475–2490.
- [11] Thompson, M. A., Biteen, J. S., Lord, S. J., Conley, N., Moerner, W. E. (2010). Molecules and methods for super-resolution imaging. *Methods in Enzymology*, *475*, 27–59.
- [12] Cusido, J., Impellizzeri, S., Raymo, F. M. (2011). Molecular strategies to read and write at the nanoscale with far-field optics. *Nanoscale*, *3*, 59–70.
- [13] Hess, S. T., Girirajan, T. P. K., Mason, M. D. (2006). Ultra-high resolution imaging by fluorescence photoactivation localization microscopy. *Biophysical Journal*, *91*, 4258–4272.
- [14] Betzig, E., Patterson, G. H., Sougrat, R., Lindwasser, O. W., Olenych, S., Bonifacino, J. S., Davidson, M. W., Lippincott-Schwartz, J., Hess, H. F. (2006). Imaging intracellular fluorescent proteins at nanometer resolution. *Science*, *313*, 1642–1645.
- [15] Dorian, G. H., Wiebe, A. F. *Photochromism*, Focal Press, New York, 1970.
- [16] Brown, G. H. (Ed.). *Photochromism*, Wiley, New York, 1971.
- [17] El'tsov, A. V. (Ed.). *Organic Photochromes*, Consultants Bureau, New York, 1990.
- [18] Bouas-Laurent, H., Dürr, H. (Eds.). *Photochromism: Molecules and Systems*, Elsevier, Amsterdam, 1990.

- [19] Crano, J. C., Guglielmetti, R. (Eds.). *Organic Photochromic and Thermochromic Compounds*, Plenum Press, New York, 1999.
- [20] Irie, M. (Ed.). (2000). Photochromism: Memories and switches—Introduction. *Chemical Reviews*, 100, 1683–1890.
- [21] Kuz'min, M. G., Koz'menko, M. V. Luminescence of photochromic compounds. In *Organic Photochromes*, El'tsov, A. V. (Ed.), Consultants Bureau, New York, 1990; pp. 245–265.
- [22] (a) Raymo, F. M., Tomasulo, M. (2005). Electron and energy transfer modulation with photochromic switches. *Chemical Society Reviews*, 34, 327–336; (b) Raymo, F. M., Tomasulo, M. (2005). Fluorescence modulation with photochromic switches. *Journal of Physical Chemistry A*, 109, 7343–7352; (c) Cusido, J., Deniz, E., Raymo, F. M. (2009). Fluorescent switches based on photochromic compounds. *European Journal of Organic Chemistry*, 2031–2045; (d) Yildiz, I., Deniz, E., Raymo, F. M. (2009). Fluorescence modulation with photochromic switches in nanostructured constructs. *Chemical Society Reviews*, 38, 1859–1867; (e) Cusido, J., Deniz, E., Raymo, F. M. (2011). Photochromic compounds for fluorescence nanoscopy. *Current Physical Chemistry*, 1, 232–241.
- [23] Yun, C., You, J., Kim, J., Huh, J., Kim, E. (2009). Photochromic fluorescence switching from diarylethenes and its applications. *Journal of Photochemistry and Photobiology C: Photochemistry Reviews*, 10, 111–129.
- [24] Inada, T., Uchida, S., Yokoyama, Y. (1997). Perfect on/off switching of emission of fluorescence by photochromic reaction of a binaphthol-condensed fulgide derivative. *Chemistry Letters*, 26, 321–322.
- [25] (a) Myles, A. J., Branda, N. R. (2001). Controlling photoinduced electron transfer within a hydrogen-bonded porphyrin-phenoxynaphthacenequinone photochromic system. *Journal of the American Chemical Society*, 123, 177–178; (b) Myles, A., Branda, N. R. (2002). 1,2-Dithienylethene photochromes and non-destructive erasable memory. *Advanced Functional Materials*, 12, 167–173.
- [26] (a) Bahr, J. L., Kodis, G., de la Garza, L., Lin, S., Moore, A. L., Moore, T. A., Gust, D. (2001). Photoswitched singlet energy transfer in a porphyrin-spiropyran dyad. *Journal of the American Chemical Society*, 123, 7124–7133; (b) Andréasson, J., Kodis, G., Terazono, Y., Liddell, P. A., Bandyopadhyay, S., Mitchell, R. H., Moore, T. A., Moore, A. L., Gust, D. (2004). Molecule-based photonically switched half-adder. *Journal of the American Chemical Society*, 126, 15926–15927; (c) Terazono, Y., Kodis, G., Andréasson, J., Jeong, G., Brune, A., Hartmann, T., Dürr, H., Moore, T. A., Moore, A. L., Gust, D. (2004). Photonic control of photoinduced electron transfer via switching of redox potentials in a photochromic moiety. *Journal of Physical Chemistry B*, 108, 1812–1814; (d) Straight, S. D., Andréasson, J., Kodis, G., Bandyopadhyay, S., Mitchell, R. H., Moore, T. A., Moore, A. L., Gust, D. (2005). Molecular AND and INHIBIT gates based on control of porphyrin fluorescence by photochromes. *Journal of the American Chemical Society*, 127, 9403–9409.
- [27] (a) Giordano, L., Jovin, T. M., Irie, M., Jares-Erijman, E. A. (2002). Diheteroarylethenes as thermally stable photoswitchable acceptors in photochromic fluorescence resonance energy transfer (pcFRET). *Journal of the American Chemical Society*, 124, 7481–7489; (b) Jares-Erijman, E. A., Giordano, L., Spagnuolo, C., Kawior, J., Vernej, R. J., Jovin, T. M. (2004). Photochromic fluorescence resonance energy transfer (pcFRET): Formalism, implementation, and perspectives. *Proceedings of the Society of the Photo-Optical Instrumentation Engineers (SPIE)*, 5323, 13–26.
- [28] (a) Irie, M., Fukaminato, T., Sasaki, T., Tamai, N., Kawai, T. (2002). Organic chemistry: A digital fluorescent molecular photoswitch. *Nature*, 420, 759–760; (b) Kim, M.-S., Kawai, T., Irie, M. (2003). Fluorescence switching of photochromic diarylethenes. *Optical Materials*, 21, 275–278; (c) Fukaminato, T., Sasaki, T., Kawai, T., Tamai, N., Irie, M. (2004). Digital photoswitching of fluorescence based on the photochromism of diarylethene derivatives at a single-molecule level. *Journal of the American Chemical Society*, 126, 14843–14849; (d) Odo, Y., Fukaminato, T., Irie, M. (2007). Photoswitching of fluorescence based on intramolecular electron transfer.

- Chemistry Letters*, 36, 240–241; (e) Fukaminato, T., Umemoto, T., Iwata, Y., Yokojima, S., Yoneyama, M., Nakamura, S., Irie, M. (2007). Photochromism of diarylethene single molecules in polymer matrices. *Journal of the American Chemical Society*, 129, 5932–5938; (f) Fukaminato, T., Doi, T., Tanaka, M., Irie, M. (2009). Photocyclization reaction of diarylethene-perylenebisimide dyads upon irradiation with visible (>500 nm) light. *Journal of Physical Chemistry C*, 113, 11623–11627; (g) Fukaminato, T., Tanaka, T., Doi, T., Tamaoki, N., Katayama, T., Mallick, A., Ishibashi, Y., Miyasaka, H., Irie, M. (2010). Fluorescence photoswitching of a diarylethene-perylenebisimide dyad based on intramolecular electron transfer. *Photochemical & Photobiological Sciences*, 9, 181–187; (h) Fukaminato, T., Doi, T., Tamaoki, N., Okuno, K., Ishibashi, Y., Miyasaka, H., Irie, M. (2011). Single-molecule fluorescence photoswitching of a diarylethene-perylenebisimide dyad: Non-destructive fluorescence readout. *Journal of the American Chemical Society*, 133, 4984–4990.
- [29] Jukes, R. T., Adamo, V., Hartl, F., Belser, P., De Cola, L. (2004). Photochromic dithienylethene derivatives containing Ru(II) or Os(II) metal units. Sensitized photocyclization from a triplet state. *Inorganic Chemistry*, 43, 2779–2792.
- [30] (a) Bossi, M., Belov, V., Polyakova, S., Hell, S. W. (2006). Reversible red fluorescent molecular switches. *Angewandte Chemie (International ed. in English)*, 45, 7462–7465; (b) de Meijere, A., Zhao, L., Belov, V. N., Bossi, M., Noltemeyer, M., Hell, S. W. (2007). 1,3-bicyclo[1.1.1]pentanediyl: The shortest rigid linear connector of phenylated photochromic units and a 1,5-dimethoxy-9,10-di(phenylethynyl)anthracene fluorophore. *Chemistry (Weinheim an der Bergstrasse, Germany)*, 13, 2503–2516; (c) Fölling, J., Polyakova, S., Belov, V., von Blaaderen, A., Bossi, M. L., Hell, S. W. (2008). Synthesis and characterization of photoswitchable fluorescent silica nanoparticles. *Small*, 4, 134–142.
- [31] Liu, L.-H., Nakatani, K., Pansu, R., Vachon, J.-J., Tauc, P., Ishow, E. (2007). Fluorescence patterning through photoinduced migration of squaraine-functionalized azo derivatives. *Advanced Materials*, 19, 433–436.
- [32] Berberich, M., Krause, A.-M., Orlandi, M., Scandola, F., Würthner, F. (2008). Toward fluorescent memories with nondestructive readout: Photoswitching of fluorescence by intramolecular electron transfer in a diarylethene-perylene bisimide photochromic system. *Angewandte Chemie (International edition in English)*, 47, 6616–6619.
- [33] (a) Fölling, J., Belov, V. N., Kunetsky, R., Medda, R., Schönle, A., Egner, A., Eggeling, C., Bossi, M., Hell, S. W. (2007). Photochromic rhodamines provide nanoscopy with optical sectioning. *Angewandte Chemie (International ed. in English)*, 46, 6266–6270; (b) Fölling, J., Belov, V. N., Riedel, D., Schönle, A., Egner, A., Eggeling, C., Bossi, M., Hell, S. W. (2008). Fluorescence nanoscopy with optical sectioning by two-photon induced molecular switching using continuous-wave lasers. *Chemphyschem: A European Journal of Chemical Physics and Physical Chemistry*, 9, 321–326; (c) Bossi, M., Fölling, J., Belov, V. N., Boyarskiy, V. P., Medda, R., Egner, A., Eggeling, C., Schönle, A., Hell, S. W. (2008). Multicolor far-field fluorescence nanoscopy through isolated detection of distinct molecular species. *Nano Letters*, 8, 2463–2468; (d) Testa, I., Schönle, A., von Middendorf, C., Geisler, C., Medda, R., Wurm, C. A., Stiel, A. C., Jakobs, S., Bossi, M., Eggeling, C., Hell, S. W., Egner, A. (2008). Nanoscale separation of molecular species based on their rotational mobility. *Optics Express*, 16, 21093–21104; (e) Belov, V. N., Bossi, M. L., Fölling, J., Boyarskiy, V. P., Hell, S. W. (2009). Rhodamine spiroadamides for multicolor single-molecule switching fluorescent nanoscopy. *Chemistry (Weinheim an der Bergstrasse, Germany)*, 15, 10762–10776; (f) Aquino, D., Schönle, A., Geisler, C., von Middendorf, C., Wurm, C. A., Okamura, Y., Lang, T., Hell, S. W., Egner, A. (2011). Two-color nanoscopy of three-dimensional volumes by 4Pi detection of stochastically switched fluorophores. *Nature Methods*, 8, 353–359.
- [34] (a) Hu, D., Tian, Z., Wu, W., Wan, W., Li, A. D. Q. (2008). Photoswitchable nanoparticles enable high-resolution cell imaging: PULSAR microscopy. *Journal of the American Chemical Society*, 130, 15279–15281; (b) Tian, Z., Li, A. D. Q., Hu, D. (2011). Super-resolution fluorescence nanoscopy applied to imaging core-shell photoswitching nanoparticles and their self-assemblies. *Chemical Communications*, 47, 1258–1260.

- [35] (a) Tomasulo, M., Sortino, S., White, A. J. P., Raymo, F. R. (2005). Fast and stable photochromic oxazines. *The Journal of Organic Chemistry*, *70*, 8180–8189; (b) Tomasulo, M., Sortino, S., Raymo, F. M. (2005). A fast and stable photochromic switch based on the opening and closing of an oxazine ring. *Organic Letters*, *7*, 1109–1112; (c) Tomasulo, M., Sortino, S., White, A. J. P., Raymo, F. M. (2006). Chromogenic oxazines for cyanide detection. *The Journal of Organic Chemistry*, *71*, 744–753; (d) Tomasulo, M., Sortino, S., Raymo, F. M. (2007). Fast and stable photochromic switches based on the opening and closing of [1,3]oxazine rings. *Asian Chemistry Letters*, *11*, 219–222; (e) Tomasulo, M., Sortino, S., Raymo, F. M. (2008). Amplification of the coloration efficiency of photochromic oxazines. *Advanced Materials*, *20*, 832–835; (f) Tomasulo, M., Sortino, S., Raymo, F. M. (2008). Bichromophoric photochromes based on the opening and closing of a single oxazine ring. *The Journal of Organic Chemistry*, *73*, 118–126; (g) Tomasulo, M., Sortino, S., Raymo, F. M. (2008). A new family of photochromic compounds based on the photoinduced opening and thermal closing of [1,3]oxazine rings. *Journal of Photochemistry and Photobiology A*, *200*, 44–49; (h) Tomasulo, M., Deniz, E., Benelli, T., Sortino, S., Raymo, F. M. (2009). Photochromic polymers based on the photoinduced opening and thermal closing of [1,3]oxazine rings. *Advanced Functional Materials*, *19*, 3956–3961; (i) Åxman Petersen, M. Å., Deniz, E., Brøndsted Nielsen, M., Sortino, S., Raymo, F. M. (2009). Photochromic oxazines with extended conjugation. *European Journal of Organic Chemistry*, 4333–4339; (j) Deniz, E., Tomasulo, M., Sortino, S., Raymo, F. M. (2009). Substituent effects on the photochromism of bichromophoric oxazines. *Journal of Physical Chemistry C*, *113*, 8491–8497; (k) Deniz, E., Ray, S., Tomasulo, M., Impellizzeri, S., Sortino, S., Raymo, F. M. (2010). Photoswitchable fluorescent dyads incorporating BODIPY and [1,3]oxazine components. *Journal of Physical Chemistry A*, *114*, 11567–11575; (l) Deniz, E., Sortino, S., Raymo, F. M. (2010). Fast fluorescence photoswitching in a BODIPY–oxazine dyad with excellent fatigue resistance. *Journal of Physical Chemistry Letters*, *1*, 1690–1693; (m) Tomasulo, M., Deniz, E., Sortino, S., Raymo, F. M. (2010). Hydrophilic and photochromic switches based on the opening and closing of [1,3]oxazine rings. *Photochemical & Photobiological Sciences*, *9*, 136–140; (n) Deniz, E., Impellizzeri, S., Sortino, S., Raymo, F. M. (2011). A photoswitchable bichromophoric oxazine with fast switching speeds and excellent fatigue resistance. *Canadian Journal of Chemistry*, *89*, 110–116; (o) Deniz, E., Tomasulo, M., Cusido, J., Sortino, S., Raymo, F. M. (2011). Fast and stable photochromic oxazines for fluorescence switching. *Langmuir: The ACS Journal of Surfaces and Colloids*, *27*, 11773–11783; (p) Deniz, E., Cusido, J., Swaminathan, S., Battal, M., Impellizzeri, S., Sortino, S., Raymo, F. M. (2012). Synthesis and properties of molecular switches based on the opening and closing of oxazine rings. *Journal of Photochemistry and Photobiology A*, *229*, 20–28.
- [36] (a) Deniz, E., Sortino, S., Raymo, F. M. (2010). Fluorescence switching with a photochromic auxochrome. *Journal of Physical Chemistry Letters*, *1*, 3506–3509; (b) Deniz, E., Tomasulo, M., Cusido, J., Yildiz, I., Petriella, M., Bossi, M. L., Sortino, S., Raymo, F. M. (2012). Photoactivatable fluorophores for super-resolution imaging based on oxazine auxochromes. *Journal of Physical Chemistry C*, *116*, 6058–6068; (c) Deniz, E., Battal, M., Cusido, J., Sortino, S., Raymo, F. M. (2012). Insights on the isomerization of photochromic oxazines from the excitation dynamics of BODIPY oxazine dyads. *Physical Chemistry Chemical Physics*, *14*, 10300–10307.
- [37] The synthesis of 1a was originally reported in (a) Shachkus, A. A., Degutis, J., Jezerskaite, A. 5a,6-Dihydro-12H-indolo[2,1-b]-1,3-benzoxazines. In *Chemistry of Heterocyclic Compounds*, Vol. 35, Kovac, J., Zalupsky, P. (Eds.), Elsevier, Amsterdam, 1987; pp. 518–520; (b) Shachkus, A. A., Degutis, J., Urbonavichyus, A. G. (1989). Synthesis and Study of 5a,6-dihydro-12H-indolo[2,1-b][1,3]-benzoxazines. *Chemistry of Heterocyclic Compounds*, *25*, 562–565.
- [38] Yildiz, I., Impellizzeri, S., Deniz, E., McCaughan, B., Callan, J. F., Raymo, F. M. (2011). Supramolecular strategies to construct biocompatible and photoswitchable fluorescent assemblies. *Journal of the American Chemical Society*, *133*, 871–879.
- [39] Cusido, J., Battal, M., Deniz, E., Yildiz, I., Sortino, S., Raymo, F. M. (2012). *Chemistry (Weinheim an der Bergstrasse, Germany)*, *18*, 10399–10407.

CHAPTER 8

SUPRAMOLECULAR REDOX TRANSDUCTION: MACROCYCLIC RECEPTORS FOR ORGANIC GUESTS

SÉBASTIEN GOEB, DAVID CANEVET, and MARC SALLÉ

8.1 INTRODUCTION

The growth of supramolecular chemistry over the last decades has been materialized by the production of an extraordinary wide variety of macrocyclic receptors designed for binding ionic or neutral guests [1, 2]. More and more sophisticated macrocyclic hosts are prepared, and synthetic routes to their functionalization have been extensively developed. Within this field, specific efforts have been produced to transduce the host–guest recognition process in a redox event [3, 4], paving the way to various families of sensors, smart materials, or devices for molecular electronics. Most often, the related molecular structure is conceptually rather simple, since it essentially associates a binding subunit (host) and a functional redox probe capable of interacting, directly or not, with the bound species. Obviously, a critical issue lies on the nature of the communication between both subunits, in order that the binding process efficiently interferes with the electroactive moiety. A broad range of redox-active units can be integrated in such systems, providing they are oxidized or reduced at readily accessible potentials and preferably, according to reversible redox processes. Basically, two working modes can be envisaged for the corresponding redox-active host assemblies, which actually function either as *detectors* or as *effectors*. In the first case (*responsive mode*), the redox properties of the probe are modified upon host–guest binding process (*output signal*). In this context, the recognition of ionic guests is particularly illustrative. Indeed, due to electrostatic interactions, the ion binding is accompanied by a perturbation of the distribution of the charge density on the neighboring redox unit, which results in a modification of the redox potential ($E_{1/2}$) of the electroactive reporter. Noteworthy, useful thermodynamic information can be extracted from the magnitude of the electrochemical shift $\Delta E_{1/2}$. In particular, the latter can be directly correlated to the host–

Organic Synthesis and Molecular Engineering, First Edition.

Edited by Mogens Brøndsted Nielsen.

© 2014 John Wiley & Sons, Inc. Published 2014 by John Wiley & Sons, Inc.

guest binding constants corresponding to each redox state. This shift is described by the equation $\Delta E_{1/2} = (RT/nF)\ln(K_{\text{red}}/K_{\text{ox}})$, for which K_{red} and K_{ox} correspond to the association constants in the reduced and oxidized states, respectively. A second working mode has to be considered for redox-active receptors, and concerns the electrochemical control over the binding intensity between host and guest units. In this case, the redox unit is considered to be tantamount to an effector and is used to promote an *input* stimulus. Tuning electrochemically, the redox state of the electroactive unit allows for controlling the association constant between the receptor and the guest, the limit cases being the trapping and the expulsion of the latter [5]. This redox-*switchable* working mode has been explored in conformationally flexible or dynamic systems, such as interlocked molecules [6]. Finally, it is worth noting that a given redox-active receptor can function under each of the responsive- and switchable-working modes.

Compared to small ion recognition, binding organic substrates is known to be more difficult to address from a general viewpoint given (i) their larger sizes, (ii) their higher surfaces available for interacting with solvent molecules, and sometimes (iii) their three-dimensional (3D) structures. Therefore, the specific case of responsive receptors for organic molecules must address another challenging issue, by the additional need to communicate the binding information to the redox center. At this stage, charged and neutral organic guests have to be considered separately for two major reasons. In the former case, as mentioned earlier, ion binding is prone to significantly modify the electronic distribution of the electroactive unit and the presence of a charge, all the more when localized, affords a way to recognize a binding site through electrostatic interactions [7]. Unlike charged species, neutral guests only display partial charges which result from bond polarization. Consequently, the related binding interactions are weaker than in ionic complexes, and this makes the design of neutral guest receptors more delicate. Using a combination of noncovalent forces along the recognition process is often essential to increase the enthalpic contribution of Gibbs energy, but remains an intricate issue since these supramolecular interactions may be as well synergistic or antagonistic. In addition, whatever the charge of the guest, one should have in mind that organic substrates have larger surface areas than small ions and thus, many solvent molecules may interact with the host or the guest. Therefore, the choice of the solvent is even more important in the case of organic guests since solvent molecules can impede and sometimes prevent the desired binding if the guest-solvent or the host-solvent interactions are too strong. On the contrary, it is also possible to take advantage of solvophobic interactions to force the formation of the complex if the guest has a poor affinity toward solvent molecules. Having in mind that the enthalpic term is usually limited because of the weakness of the related interactions, a valuable strategy to get round this issue consists in utilizing preorganized receptors. With macrocycles endowed with well-defined cavities, the receptor does not have to experience any significant conformational change to be able to bind the guest and, consequently, the binding event is favored from an entropic point of view. Nevertheless, one should not forget this strategy is a double-edged sword since it makes the receptor more rigid and thus, more selective toward potential guests. On this ground, a wide variety of receptors for neutral molecules involving hollows or cavities with an intrinsic curvature prone to generate a three-dimensional encapsulation of the guest has been reported in the literature (e.g., cavitands, carcerands, cryptophanes, cucurbiturils, and cyclodextrins [CDs]). In this context, some redox-active receptors for organic guests undergo a conformational change along the recognition process, which results in a modification of their redox properties (responsive mode). Reciprocally, the binding properties of some

of them can be electrochemically tuned upon reduction or oxidation [6], either through a conformational change (case of interlocked molecules) or through an assembly/disassembly process of the supramolecular complex (*redox-switchable* mode).

In this chapter, the specific case of macrocyclic redox-responsive reporters for organic molecules, be they charged or neutral, will be covered through illustrative examples of the recent literature. The recognition of small organic molecules, possibly chiral, and of macromolecules of biological interest will be successively considered, with a special emphasis on selected applications. The recognition of redox-active organic guests by macrocyclic receptors will also be addressed through various examples.

8.2 REDOX-RECOGNITION/TRANSDUCTION WITH ORGANIC GUEST MOLECULES

Binding organic molecular guests requires specific interactions [1, 3a,b, 4a,d] which have to be considered when designing a receptor. Recent trends in the elaboration of macrocyclic redox-active receptors are proposed through few illustrative and recent examples of the literature.

8.2.1 Molecular Receptors Incorporating a Redox-active Subunit

8.2.1.1 Based on Tetrathiafulvalene (TTF) Derivatives Tetrathiafulvalene **1** (Figure 8.1) is a well-established fully organic π -donor, originally studied for the electrical solid-state conduction of its corresponding cation-radical salts [8]. This unit has known a growing interest as a key redox-reporter for a broad range of supramolecular processes, and many examples of redox-responsive/switchable receptors incorporating this unit have been described during the last decade [9].

In this context, TTF-calix(4)pyrrole conjugates have focused much attention and will be discussed in the following chapter. Other TTF-based receptors involving a rigid prebuilt cavity have been produced, and are therefore of potential interest to probe the presence of neutral molecules (e.g., CD [10], calix(4)arene [11], or resorcinarene [12] derivatives). Nevertheless, these receptors have been mostly studied for the recognition of inorganic ions rather than neutral organic guests. In this regard, the case of the so-called extended-tetrathiafulvalene (exTTF) derivatives is particularly appealing. Such structures incorporate a conjugated analog of the above-encountered TTF unit, for which both 1,3-dithiolylydene moieties are separated by an anthracene-based linker (Figure 8.2a). The short 1,6-H,S periplanar distance is responsible for the butterfly shape of exTTFs, and obviously, the electrochemical

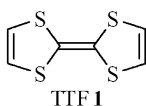


Figure 8.1. Tetrathiafulvalene (TTF).

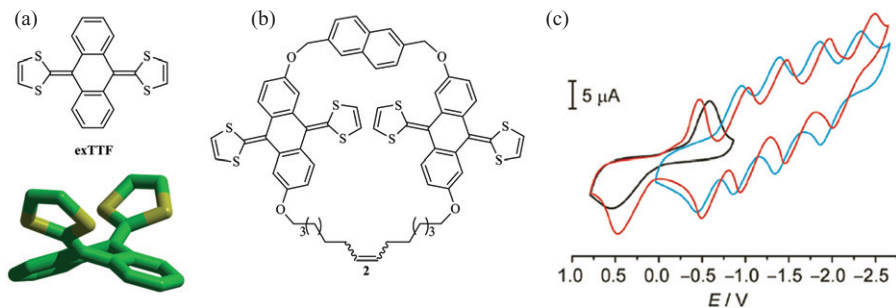


Figure 8.2. (a) Chemical structure of exTTF and its optimized geometry (*Hyperchem*, PM3); (b) chemical structure of compound **2**; (c) cyclic voltammograms of **2** (black), C₆₀ (blue), and **2**•C₆₀ (red); chlorobenzene, TBAPF₆ 0.1 M, 100 mV·s⁻¹, V versus Ag/AgNO₃. Source: [13a]. Reproduced with permission of the American Chemical Society. See color insert.

behavior of these compounds is strongly modified related to TTF derivatives. Unlike TTF and its two successive one-electron oxidations, exTTF displays a single and poorly electrochemically reversible two-electron process, associated with a direct oxidation into exTTF²⁺ cation. The concave geometry of exTTF, together with its electron-donating properties, makes it an interesting building block for the recognition of convex acceptors such as fullerenes. With this in mind, Pérez, Martín and coworkers have recently developed macrocyclic molecules, which display very high binding constants toward C₆₀ and C₇₀ [13]. They can be distinguished in two families, whether the exTTF units are part of the macrocycle or are decorating moieties grafted on a macrocyclic structure. With the first family, the authors have found the highest binding constant reported to date for all-organic hosts of C₆₀ and C₇₀, with binding constants as high as $\log K_a = 6.5 \pm 0.5$ in chlorobenzene. In few cases, fullerenes are tightly bound to the macrocycles and thus, it is not surprising that clear electrochemical responses could be measured. For instance, the fourth reduction wave of C₇₀ was cathodically shifted by 150 mV in the presence of one equivalent of compound **2** (Figure 8.2).

The related molecules **3** and **4** belonging to the second family display valuable features supported by a strong ability to bind fullerenes and to transduce the recognition process into an electrochemical signal (Figure 8.3). Indeed, from a basic point of view, the corresponding complexes **3**•C₆₀ and **3**•C₇₀ are very nice examples of synergistic interactions ($n-\pi$ and $\pi-\pi$), which allow the stabilization of an inclusion complex despite a limited preorganization. In the case of **4**, one should focus on the inherent chirality of this cyclotrimeratrylene scaffold, given that one of the major current challenges [14] concerning fullerenes is the resolution of racemic mixtures of higher fullerenes (e.g., C₇₆) in a supramolecular manner.

8.2.1.2 Based on Ferrocene (Fc) Another demanding task regarding the recognition of organic guests concerns the specific case of carboxylate anions. Such systems are indeed of potential broad interest in biology, medicine, catalysis, or environment, and several reviews have addressed this issue [15]. In this case, the recognition process is mainly governed by hydrogen bonding and/or electrostatic interactions with suitable

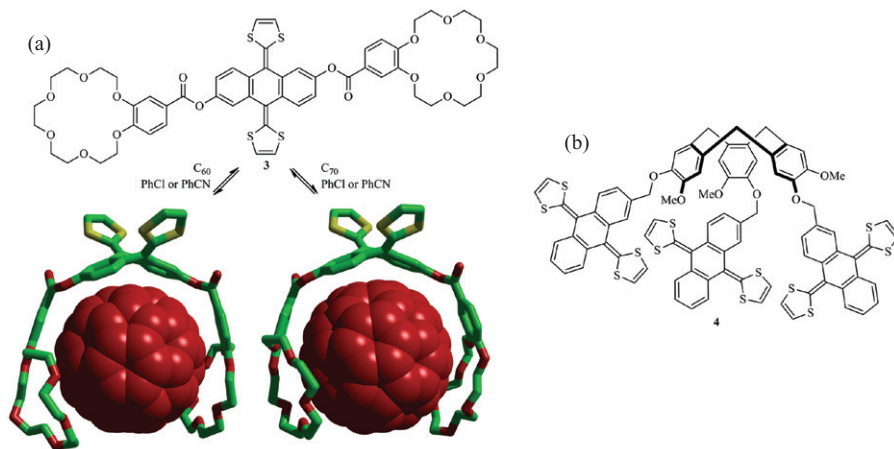


Figure 8.3. (a) Compound 3 and the corresponding host–guest associations with C₆₀ and C₇₀; (b) Chemical structure of cyclotrimeratrylene 4 [14].

groups, such as amide, urea, or polyammoniums. An interesting illustration is provided by compound 5 which associates a tetraaza macrocyclic residue to ferrocene (Fc) units and which is able to bind various carboxylate aromatic derivatives (Figure 8.4) [16]. The reversibly oxidized Fc framework has largely proved its efficiency for the preparation of electrochemical sensors [17]. The recognition of the dicarboxylate derivatives *ph*²⁻, *iph*²⁻, *dipic*²⁻ by the tetraprotonated ligand **5**•4H⁺, which occurs outside the cavity, is accompanied by a strong cathodic shift of the redox potential associated to the Fc probe (from -168 (*dipic*²⁻) to -275 mV (*ph*²⁻)). This electrochemical behavior is assigned to the binding of the carboxylate anions by the RR'NH₂⁺ groups in the vicinity of the Fc units, which increases the electron density on the Fc center, facilitating thereof the oxidation of the latter.

A complementary interesting case of specific carboxylic acid recognition with a Fc-based receptor is provided by receptor 6 (Figure 8.5) [18]. This ditopic host system is designed to simultaneously bind the carboxylic acid and the ammonium groups of an amino-acid (phenylalanine, L-Phe), thanks to an amidopyridyl and a crown ether moiety, respectively. The binding is efficient even in acetonitrile and operates through a guest-to-host proton transfer reaction. Noteworthy, the recognition process is accompanied by a large positive shift (+129 mV) of the reversible redox process associated to Fc oxidation as followed by cyclic voltammetry (Figure 8.5). This value reaches a maximum for one equivalent of L-Phe added, suggesting a 1:1 stoichiometry in the resulting complex. The positive shift contrasts with the previous case (receptor 5) for which a negative shift was observed. This result is consistent with a host-to-guest proton transfer from the L-Phe carboxylic acid function to the pyridine, which results in the introduction of a positive charge in close vicinity of the Fc unit and therefore in a more difficult oxidation of the latter. Interestingly, the proton transfer from the guest to the amidopyridine unit only occurs with strongly acidic carboxylic functions, as this is the case of amino acids like L-Phe, whereas no binding is observed with a structurally close carboxylic acid (hydrocinnamic acid).

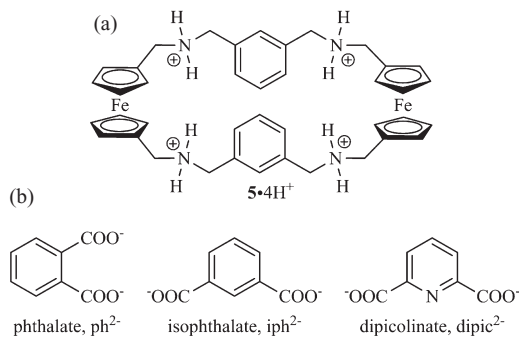


Figure 8.4. (a) Redox-active responsive ligand $5\bullet 4H^+$; (b) Organic dicarboxylate guests under study.

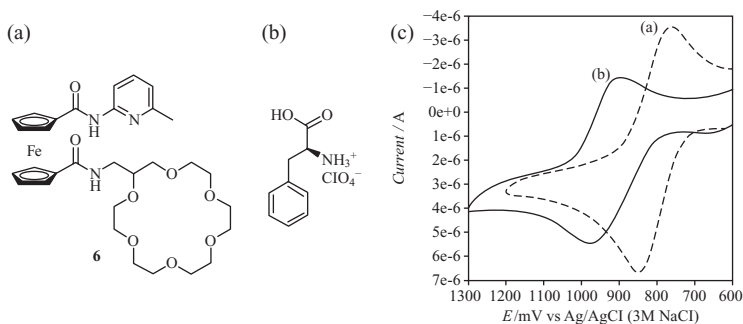


Figure 8.5. (a) Redox-active responsive ligand **6**; (b) Organic guest under study (L-Phe); (c) Cyclic voltammograms without (a) and with (b) 5 equivalents of the perchlorate salt of L-Phe (CH_3CN). Source: [18]. Reproduced with permission of The Royal Society of Chemistry.

8.2.1.3 Derived from Cyclobis(Paraquat-*p*-Phenylene) ($CBPQT^{4+}$) Macrocyclic electrochemical transducers have also been used in the field of biodetection. This is particularly true in the case of cyclobis(paraquat-*p*-phenylene) $CBPQT^{4+}$, a well-known receptor for electron donating guests [19]. If $CBPQT^{4+}$ is a well-established neurotransmitter binder [20], to the best of our knowledge, its possible affinity toward adenosine triphosphate (ATP) has never been studied. This seems particularly puzzling since various analogs (compounds **7–10**) have proven to be good ATP binders (Figure 8.6) [21].

Moutet, Royal, and coworkers have reported the organometallic macrocycle **7** [21c]. Instead of the phenylene spacers encountered in $CBPQT^{4+}$, ferrocenyl units link up viologen moieties in such a way that four electroactive moieties make up the macrocycle. In principle, the supramolecular recognition of ATP^{2-} by **7** (or **8**) can be followed according to three redox processes related to viologen (V) and Fc units. However, both $V^{2+}/V^{•+}$ and $V^{•+}/V^0$ processes lead to strong adsorption phenomena onto the electrode and complicates the reading of the binding event. Conversely, no adsorption was pro-

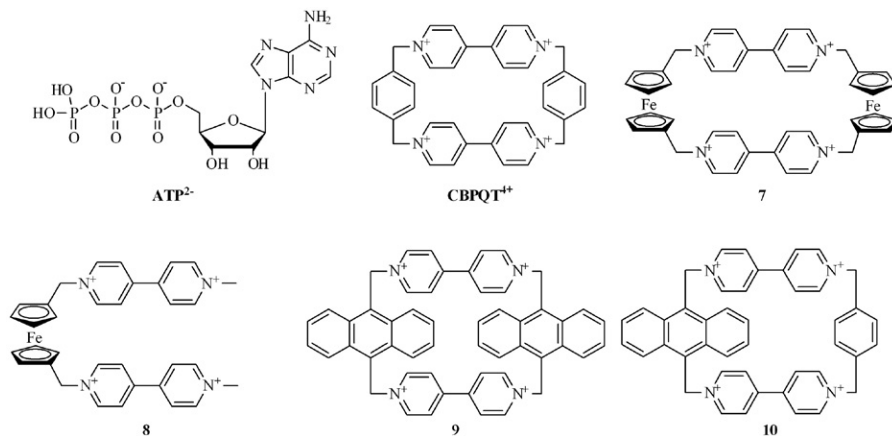


Figure 8.6. ATP²⁻ and several paraquat-based receptors.

voked by Fc oxidation. Thus, by comparing macrocycle **7** and its acyclic analog **8**, the authors demonstrated the importance of using a preorganized cavity when aiming to bind ATP²⁻. Indeed, the Fc oxidation in **7** undergoes a larger cathodic shift upon binding ATP²⁻ (25 and 10 mV for **7** and **8**, respectively). In other words, noncovalent interactions are facilitated when viologen subunits are maintained in the most suitable conformation to bind ATP²⁻. This assessment raises questions about the forces involved to form the ATP²⁻•macrocycle complex and the positioning of the guest in the cavity. In order to get hints about this problematic, NMR spectroscopy can be a valuable tool, as shown by Ramaiah and coworkers with macrocycle **9** [21b]. By performing NMR titrations at different ionic strengths, the authors demonstrated that ATP binding mainly results from electrostatic interactions. Furthermore, as shown by cyclic voltammetry, **9** exhibits significant interactions with the doubly charged ADP²⁻ and ATP²⁻, whereas it does not with AMP⁻, PO₄³⁻, or adenosine.

From a fundamental point of view, studying compound **10** [21a], which corresponds to a hybrid system between CBPQT⁴⁺ and compound **9**, looks worthwhile in order to evaluate the role of π - π stacking in the supramolecular recognition of ATP²⁻ and its impact on the redox properties of the system. Curiously, the authors reported the decrease of the redox signals upon addition of ATP²⁻, but no cathodic or anodic shift of any redox waves was commented in this article. Finally, this system appears as particularly appropriate for recognizing 3,4-dihydroxyphenylacetic acid (DOPAC), another neurotransmitter, since it can selectively bind the latter when competing with other biomolecules of interest, namely ascorbic acid and dopamine [22].

8.2.2 Case of Electrochemical Chiral Recognition

Chiral discrimination between enantiomers is of crucial importance in analytical chemistry, with a heavy impact in various applied fields such as analysis of drugs [23]. Therefore, the development of efficient methods allowing a rapid determination of enantiomeric excess corresponds to a strong demand. Beside the well-established

chromatographic or NMR techniques, various electrochemical techniques have been applied to this field [24]. The discrimination between both enantiomers of a racemic to analyze is supported by the difference in stability constants of intermediate diastereomeric complexes which are formed between each enantiomer and a chiral selector designed on purpose. The chiral recognition at the asymmetric center is governed by a minimum of three-point attractive or repulsive interactions. On this ground, voltammetric recognition of enantiomers by redox-active receptors constitutes a very promising outlook in this field, as depicted in several examples of the recent literature. Compared to the above-mentioned redox-responsive ligands, the receptor integrates one or more chiral centers in its structure.

An example of a chiral redox-responsive ligand incorporating a Fc unit and capable to discriminate between both enantiomers of alanine methyl ester hydrochloride (AlaOMe•HCl) is provided with compound **11** (Figure 8.7) [25]. This system combines a chiral crown ether unit to a secondary H-bond donating group. A host–guest interaction model is proposed by the authors, based on a combination of H bonds, and allows for anticipating a higher affinity of host **11** for D-AlaOMe in front of the L-enantiomer. Indeed, cyclic voltammetry studies in presence of D- and L-AlaOMe show a moderate shift of the redox potential of the Fc probe (ca. 20 mV) in the case of the D-enantiomer

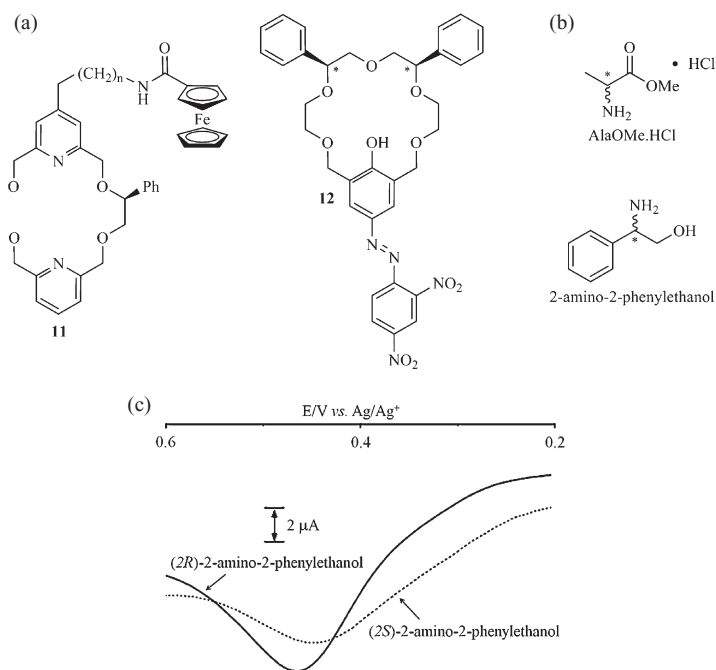


Figure 8.7. (a) Redox-active responsive ligands **11** and **12** designed for voltammetric chiral discrimination; (b) chiral analytes under study; (c) Square-wave voltammograms of **12** in the presence of (2*R*)-2-amino-2-phenylethanol (solid curve) and (2*S*)-2-amino-2-phenylethanol (dotted curve). Source: [26]. Reproduced with permission of the American Chemical Society.

whereas no change is observed with *L*-enantiomer. Though very limited in intensity, this different behavior is assigned to a discrimination between the *D* and the *L* isomers of AlaOMe.

A step further is proposed with receptor **12** which contains a crown-ether macrocycle with asymmetric centers and a dinitroazophenol group. The latter can act as an indicator by changing in color and by signaling the guest complexation electrochemically with various alkyl amines [26]. Spectrophotometric analyses show that the binding of a given amino-derivative modifies the electronic configuration of the chromogenic dinitroazophenol group, and that the two enantiomers give rise to complexes with distinctive stabilities. This molecular recognition process is also followed by cyclic voltammetry. The host oxidation occurs on the phenol group, and the progressive addition of an enantiomerically pure alkyl amine is accompanied by a new oxidation wave at potentials that are specific of each enantiomer. This difference in redox potentials between both enantiomers of 2-amino-2-phenylethanol reaches 43 mV (Figure 8.7) and is assigned to a chiral-selective complexation with **12**. Despite this moderate difference between pure enantiomers, the authors suggest that this method allows quantifying the ratios of enantiomers in an *R/S* mixture of the analyte, based on the fact that the peak potential of **12** shifts continuously and proportionally with the ratio of each enantiomer.

Recent significant achievements in this field have been accomplished by the group of J. H. R. Tucker, who designed α -ferrocenylalkylurea-based chiral receptors, from which compound **13** is a representative example [27]. Receptor **13** does not include any macrocyclic cavity but presents a suitable combination of complementary H-bonding interactions with carboxylate anions. This host undergoes a pronounced cathodic shift in acetonitrile upon introduction of either enantiomer of various carboxylates, providing an additional example of the sensing of organic molecules by redox-active supramolecular receptor (see § 8.2.1). Similar to the carboxylate recognition by the above-mentioned receptor **5**, the negative shift in potential in the case of **13** is attributed to the carboxylate anion which increases the electron density on the Fc center, resulting in an easier oxidation of the complex compared to the free ligand. Interestingly, the two enantiomers of proline derivative **14** produce distinct electrochemical titration profiles of receptor **13** (Figure 8.8d). Although the redox potential shifts provoked by each enantiomer are not strongly different (ΔE_{obs}), this work offers promising perspectives regarding electrochemical chiral discrimination.

A major achievement in this field was possible, thanks to compound **15** (Figure 8.9a) [28]. In this case, not only electrochemical chiral discrimination was performed, but also a proof of principle for the accurate determination of *ee* using an electrochemical method was demonstrated. Receptor **15** contains a Fc redox center attached to a chiral boronic acid, a known functionalized group used in NMR shift reagents for the determination of *ee* of diols and amines. Compound **15** is able to bind either enantiomers of Binol, which is accompanied by a clear signature upon electrochemical analysis (cyclic voltammetry and square wave voltammetry) (Figure 8.9). Remarkably, each enantiomer behaves distinctively, as shown by positive shifts of +95 mV and +44 mV with introduction of (*R*)- and (*S*)-Binol, respectively, to a solution of **15**, illustrating a clear electrochemical enantiomeric discrimination. Of striking interest is the difference in binding strength that can be used to determine the enantiomeric composition of various mixtures of (*R*)- and (*S*)-Binol. As shown in Figure 8.9b, the redox potential associated to the Fc probe linearly shifts to positive values upon gradual increasing of the (*R*)-Binol ratio Figure 8.9c. This linear dependence allows to discriminate between

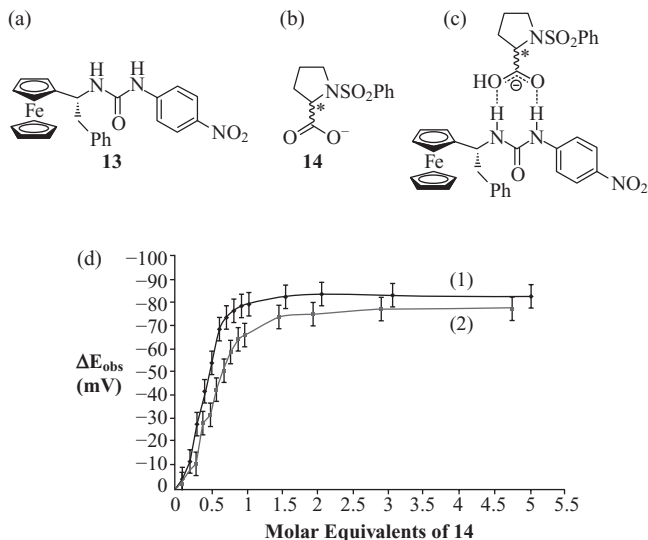


Figure 8.8. (a) Redox-active responsive ligand **13** designed for voltammetric chiral discrimination; (b) Proline guest **14** under study; (c) Recognition model between **13** and **14**; (d) Plot of the ΔE_{obs} value observed for receptor **13** against molar equivalents of (*S*)-**14** (1) and (*R*)-**14** (2). Source: [27]. Reproduced with permission of the American Chemical Society.

mixtures containing 98% and 90% ee of (*S*)-Binol and allows the detection of small amounts (<5%) of (*R*)-Binol at very low concentration (10^{-5} M). This result paves the way to very promising studies on various chiral analytes and nicely illustrates the scope of the electrochemical approach to chiral discrimination as an alternative to the chromatographic or NMR techniques.

8.3 ELECTROCHEMICALLY TRIGGERED MACROCYCLIC SYSTEMS

Controlling motion in interlocked systems such as catenanes or rotaxanes constitutes a field of intense interest, in particular in connection with molecular electronics. The following paragraphs focus on electrochemically triggered macrocyclic systems, either purely organic or constructed around inorganic metal complexes.

8.3.1 Interlocked Assemblies Based on Organic Compounds

The above-mentioned **CBPQT**⁴⁺ system (“blue box”) has focused much attention in this field because of its excellent ability to incorporate electron-rich substrate [19]. In this context, the π -donating TTF constitutes a complementary building block and forms with **CBPQT**⁴⁺ a strong green 1:1 complex in solution or in the solid state. Since the seminal example by Stoddart and coworkers [29], a myriad of pseudo-rotaxanes,

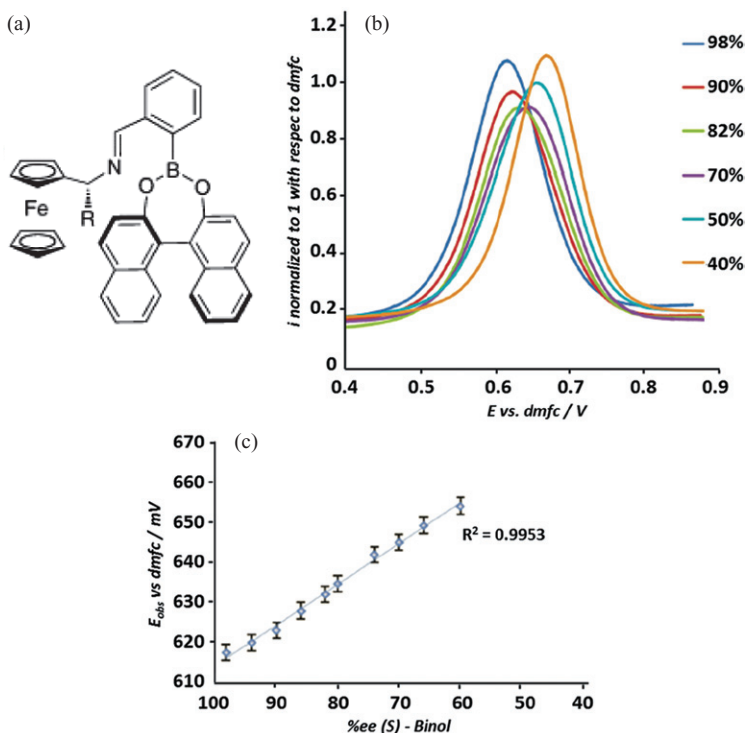


Figure 8.9. (a) Redox-active responsive ligand **15** designed for voltammetric chiral discrimination; (b) square wave voltammograms of (R) -**15** (CH_2Cl_2 , 3.14×10^{-5} M, 0.1 M $TBAPF_6$), each in the presence of a 10-fold excess of Binol with varying enantiomeric composition, as expressed by % ee of (S) -Binol in the legend (-40% equates to 40% ee of (R) -Binol); (c) plot of E_{obs} against % ee of (S) -Binol showing the linear dependence between 60% and 98% ee. Source: [28]. Reproduced with permission of the American Chemical Society. See color insert.

rotaxanes, and catenanes involving these two units have been produced, some being electrochemically triggered. Different reviews have been dedicated to the always-increasing level of complexity of these fascinating interlocked systems [6, 30], and only some selected recent examples are developed below. The mechanical motion in such systems is typically supported by a modulation of π - π interactions depending on the oxidation state of redox-active moieties, in particular neutral and dicationic states of a TTF unit. A recent additional achievement regarding the electrochemical control of a molecular movement is provided with the [3]catenane system **16**, which contains two TTF units and two dialkoxynaphthalene (DNP) units interlocked with two $CBPQT^{4+}$ macrocycles (Figure 8.10) [31]. Tuning electrochemically, the oxidation degree of the TTF units allows for controlling the three stable ring positions reversibly. Since TTF is a better electron donor than DNP, the electron withdrawing $CBPQT^{4+}$ units occupy the TTF stations when the latter are neutral (**16** in Figure 8.10). On the contrary, when

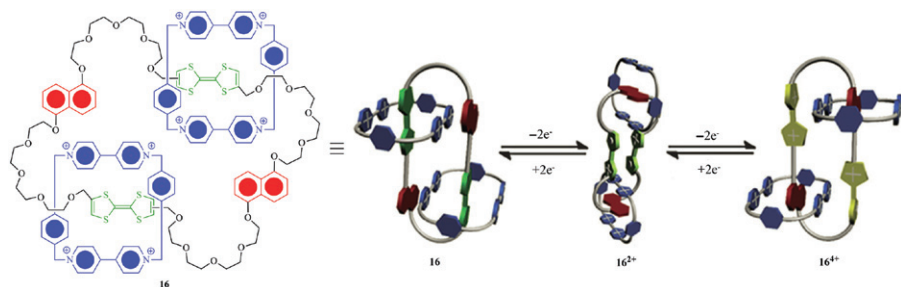


Figure 8.10. Schematic representation of the redox-controlled switching behavior of catenane **16**. Source: [31]. Reproduced with permission of The Royal Society of Chemistry.

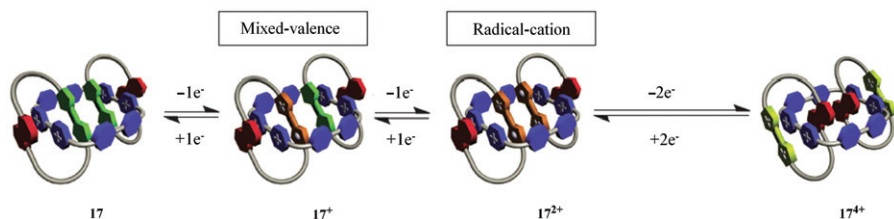


Figure 8.11. Schematic representation of the redox-controlled switching behavior of catenane **17**. Source: [32]. Reproduced with permission of the Nature Publishing Group.

TTF units are oxidized to their dicationic state (16^{4+}), they lose their electron-donating ability, and DNP moieties become the better donor. Therefore, CBPQT^{4+} rings are shifted toward these new stations. Remarkably, a more original situation arises from the mono-electronic oxidation of both TTF units (16^{2+}). In this case, a less explored type of interactions takes place and results in the formation of a $(\text{TTF}^{+\bullet})_2$ dimer. Such kind of interaction, largely unexplored to date, offers promising perspective in terms of motion control, as shown with catenane **17** (Figure 8.11).

Expanding the electron-poor CBPQT^{4+} by one phenylene unit to form cyclobis(paraquat-4,4'-biphenylene) (CBPQTP^{4+}) in compound **17** allows co-accommodation in the ring of two electron-rich TTF units, a recognition process which is not only driven by a host-guest recognition but also by a guest-guest interaction within the paraquat cavity (Figure 8.11) [32]. Thus, the successive electrochemical oxidations of both TTF units inside the cationic macrocycle lead to the formation of stable mixed valence and radical-cation dimers ($(\text{TTF})_2^{+\bullet}$ and $(\text{TTF}^{+\bullet})_2$, respectively), and rotation of the electron-rich guests around the CBPQTP^{4+} ring occurs only after complete oxidation of the TTF units to the TTF^{2+} state (17^{4+}).

Based on the same approach, a multistable switchable [3]rotacatenane **18**, which associates both rotary and translational motion, has been very recently reported (Figure 8.12a) [33]. Compared to catenane **17**, one electron-rich TTF-DNP macrocycle is unrolled in **18** to constitute a rotaxane axis. The first two electrochemical oxidation steps successively lead to the mixed valence $(\text{TTF})_2^{+\bullet}$ dimer (18^+) and the $(\text{TTF}^{+\bullet})_2$ one

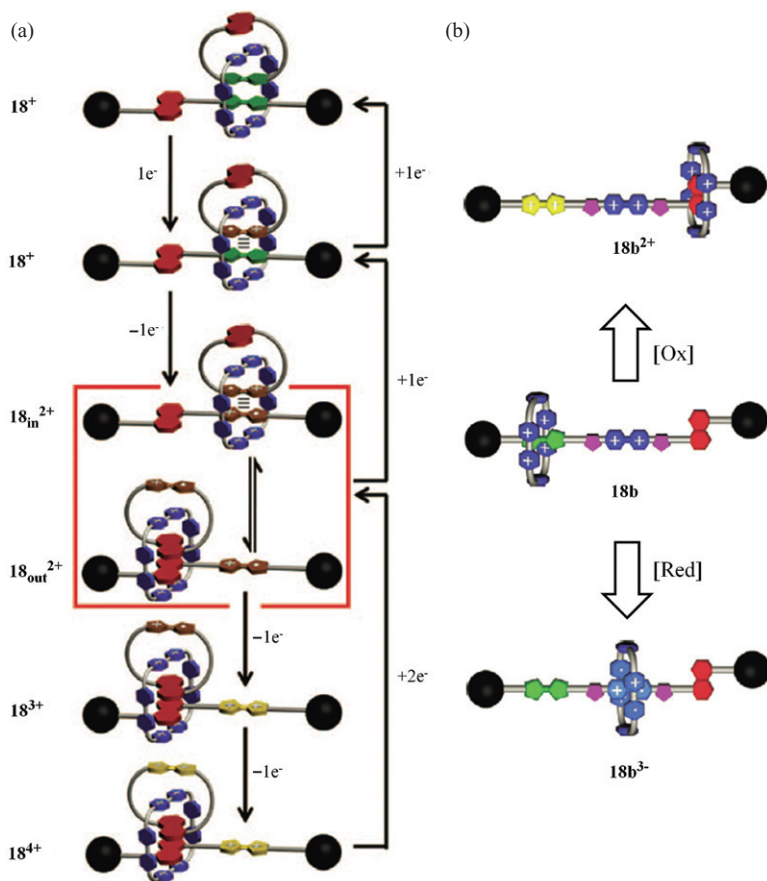


Figure 8.12. Schematic representations of the redox-controlled switching behavior of (a) a multistable switchable [3]rotacatenane **18** and (b) a tristable [2]rotaxane **18b**. Source of panel a: [33]. Reproduced with permission of Wiley-VCH Verlag GmbH & Co. KGaA. Source of panel b: [34]. Reproduced with permission of the Nature Publishing Group.

(18_{in}^{2+}), the latter being in equilibrium with compound 18_{out}^{2+} . This observation suggests that in this case, $TTF^{+} - TTF^{+}$ interactions are not only competing with host-guest electrostatic repulsions between dimethylviologen DMV^{2+} and TTF^{+} , but also with DNP-DNP $\pi-\pi$ stacking. To force both the translational motion of the paraquat to the DNP station and the rotation of the TTF-DNP ring (compound 18^{3+}), the authors nicely demonstrated by EPR that the only TTF unit which had to be oxidized was the one composing the axle. These examples (**17**, **18**) illustrate the fact that paraquat macrocycles may be well-suited hosts for supramolecular dimers made up of radical-cation species. Such feature, observed in those cases with donor derivatives (TTF), could also be demonstrated with electron-deficient units, such as dimethylviologen [34]. On this ground, the same group proposed a step forward in the construction of advanced

molecular machines by incorporating a viologen unit within the rotaxane axle in order to dispose of a third station (compound **18b**, Figure 8.12b) [34]. This strategy proves to be relevant given that the reduction of the DMV^{2+} units into $\text{DMV}^{\bullet+}$ results in the formation of a stable supramolecular trimer, allowing thus a full control over the ring movement, not only by oxidizing the TTF moiety but also by reducing the DMV^{2+} to the $\text{DMV}^{\bullet+}$ form.

8.3.2 Interlocked Assemblies Based on Transition Metals

Apart from the successful examples involving TTF and DMV^{2+} moieties, it is worth mentioning that alternative redox-active units have been integrated to reach electrochemically triggered macrocyclic systems. In particular, those based on transition metals are of interest. For instance, Wozniak et al. described a molecular shuttle **19** for which the movement of an interlocked electron-rich aromatic crown ether with a face-to-face macrocyclic heterodinuclear complex is controlled by the oxidation state of the metal centers (Figure 8.13) [35]. The oxidation of Cu(II) center leads to a translocation of the crown ether from its nickel initial docking station to the more positively charged metal center. At low temperature or at shorter timescale, the translocation is slow, and a part of the Ni-centers still interacts with the electron-donating ring, resulting in a wave splitting. After the Ni(II/III) oxidation, the crown ether moves back to its original position. This same concept was subsequently utilized to electrochemically thread and unthread a crown-ether derivative interacting with a surface-immobilized mononuclear Cu(II) complex [36a,b].

Examples treated so far in this paragraph are related to a modification of the electron-donating ability of a station which provokes *in fine* a shuttling movement. Another strategy based on coordination chemistry has also largely proved to be relevant in this context. Indeed, the coordination sphere of a metal center strongly depends on its oxidation state. Consequently, it appears possible to electrochemically tune the latter in order to induce a modification of the metal chelating environment, which may be accompanied with a rotational or a translational motion. On this ground, Sauvage and coworkers have described series of molecular shuttles over the last decades. Most recent advances have notably implied interlocked systems based on a long axis containing two or three binding sites and a ring endowed with a bidentate ligand that coordinates a copper ion (Figure 8.14) [37a,b]. Based on their initial result with ring **20** and axle **22a** [38], the authors designed more elaborated systems to get insight on the factors that control the gliding motion of the shuttle between two stations. They demonstrated first that the nature of the ring could impact significantly the translation kinetics. Electrochemical studies revealed that the nonhindered bis-isoquinoline ring **21** translocates over axle **22a** on the milliseconds to seconds timescale, at least four orders of magnitude

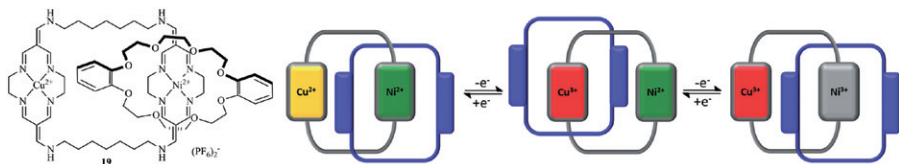


Figure 8.13. Catenane **19** based on a dibenzo [24]crown-8 and a heterodinuclear macrocycle [35].

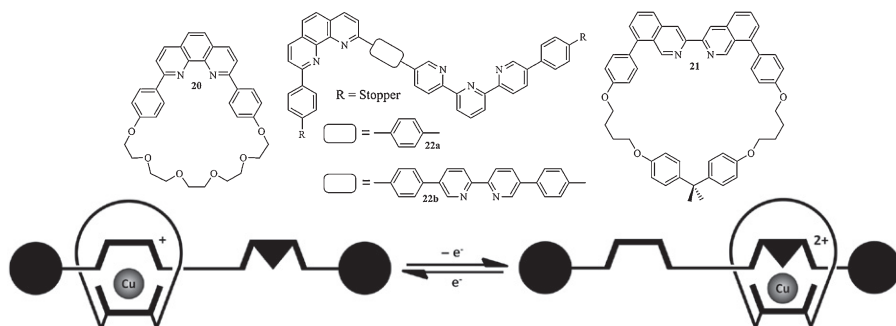


Figure 8.14. Rings **20**, **21** and axles **22a**, **22b**; Principle of the electrochemically driven molecular shuttles based on copper (I) and copper (II) coordination.

faster than the original ring **20**. This improvement is of particular interest in the fields of information storage and nanoscale mechanical switches which necessitate a rapid answer to the external stimuli. Another issue of particular interest lies on the information transfer over long distances. This step further has been proposed with an intermediary chelating group placed in the axle between the two external stations (compound **22b**) [37a]. Its role has not been clearly determined yet, but in this case, shuttle **21** is capable to translocate as fast as in the precedent example over a larger distance of 23 Å.

The same team reported very recently another nice example with rotaxane **23** constituted by two bichelating stations connected to a triazole unit (Figure 8.15) [39]. The geometry of the chelating nitrogens is designed in order that the triazole groups can either take part or not to the coordination process. Thus, Cu(I) is only bound by the bipyridyl unit, while the oxidized Cu(II) is also coordinated by the triazole moiety. The fast and quantitative reversible flapping motion (Figure 8.15) generated by this redox process results in a strong angle modification between both macrocycles. Besides, it has been shown that the corresponding advanced [4]rotaxane **24** (Figure 8.15) forms a host–guest complex with the flat electron-rich TTF, which is accommodated between the two aromatic platforms [40].

8.4 ELECTROACTIVE GUESTS

The electrochemical recognition of non-redox-active analytes with electroactive macrocycles has been tackled through the first part of this chapter. This strategy, which requires the incorporation of a redox reporter within or onto the macrocyclic scaffold, proved to be sound. Reciprocally, one can consider the possibility of using the guest electroactivity to transduce the recognition phenomenon. In this regard, two tracks have to be distinguished, namely, the detection of intrinsically electroactive analytes and the recognition of given species incorporating a redox probe.

Cucurbit [7]uril (CB7) and cucurbit [8]uril (CB8) were first isolated in 2000 by Kim and coworkers [41] and have been extensively utilized as organic substrate receptors since then. These hosts have focused much attention as they present well-suited cavity sizes for the incorporation of small organic molecules. In particular, an interesting

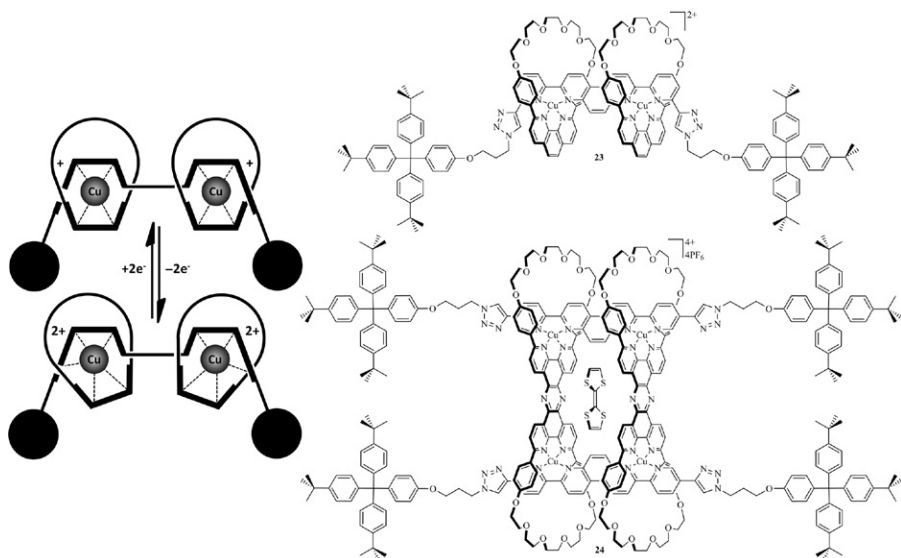


Figure 8.15. Rotaxane **23**, cartoon representation of the two macrocycles motion and intercalation of TTF in bisrotaxane **24**.

feature of CBs lies on their 3D hollow, which makes them efficient receptors for two-dimensional guests. Studies dedicated to interactions that take place in these inclusion complexes in water are of prime importance. In this context, Kaifer and coworkers recently studied [42] different inclusion complexes between CB7 and the electron-poor paraquat **25**²⁺ and diquat **26**²⁺, as a complementary study to a previous work by Kim and coworkers [43]. By means of cyclic voltammetry and ¹H NMR, they were able to determine the corresponding binding constants in water (CB7•**25**²⁺, $K = 1.2 \times 10^5 \text{ M}^{-1}$; CB7•**26**²⁺, $K = 3.5 \times 10^2 \text{ M}^{-1}$). The significantly higher value with guest **25**²⁺ can arise from two major differences: (i) **26**²⁺ is a bit larger than **25**²⁺ and is not planar, and (ii) as demonstrated by the surface electrostatic plots of **25**²⁺ and **26**²⁺, their charge distributions are deeply different. Regarding the first item, ¹H NMR showed that **26**²⁺ does not fit entirely in CB7 [42] whereas **25**²⁺ does. Unlike diquat **26**²⁺, paraquat **25**²⁺ displays a convenient distance between its quaternized nitrogen atoms so that ion-dipole interactions take place with the oxygen atoms of CB openings. Both electrodeficient dicationic guest species undergo two consecutive one-electron reductions that are electrochemically reversible at ca. 0.5 and 1.0 V (vs. Ag/AgCl) to form a cation radical and a fully reduced neutral species. This behavior enabled the use of alternative investigation techniques to study the binding process, and Figure 8.16a shows the electrochemical behavior of **26**²⁺ in the presence of various concentrations of CB7. The first reduction (**26**²⁺/**26**^{•+}) process is shifted to less negative values while the second (**26**^{•+}/**26**) shifts in the opposite direction. This observation is consistent with a more stable complex CB7•**26**^{•+} ($K = 1.0 \times 10^4 \text{ M}^{-1}$) than CB7•**26**²⁺. Indeed, the reduction process decreases the hydrophilic character of the cation and allows a better interaction with the hydrophobic midsection of the host. The same experiment performed with **25**²⁺

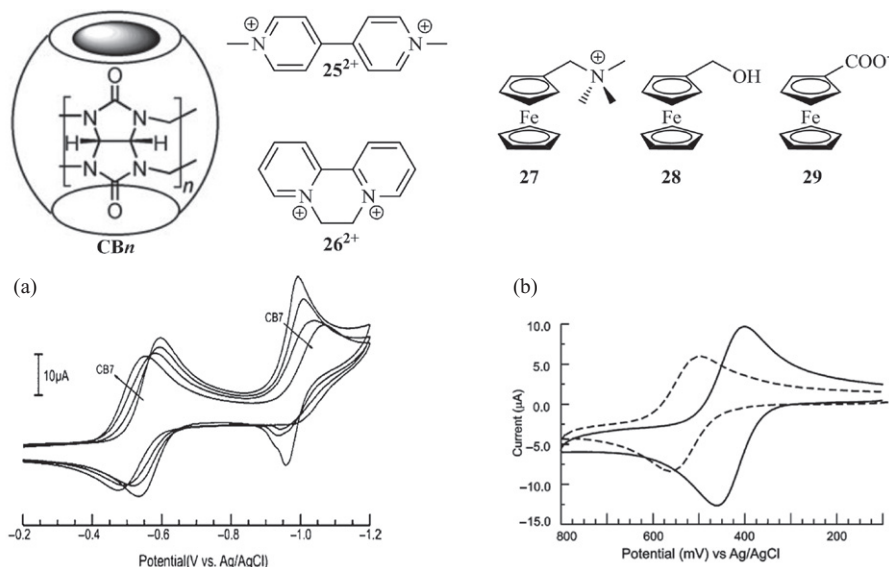


Figure 8.16. Schematic representation of cucurbit[*n*]uril, bispyridinium guests paraquat **25**²⁺, diquat **26**²⁺, and ferrocene-based guests **27–29**; CV responses of (a) **26**²⁺ (1.29 mM) in the presence of 0, 0.5, 1.0, and 2.0 equivalents of CB7 (0.1 M phosphate buffer, scan rate 0.1 V/s, glassy carbon working electrode). Source: [42]. Reproduced with permission of Wiley-VCH Verlag GmbH & Co. KGaA. CV responses of (b) **27** (1.0 mM) without (continuous line) and with CB [7] (1.1 mM) (dashed line) (0.1 M NaCl, scan rate 0.1 V s⁻¹, glassy carbon working electrode). Source: [44]. Reproduced with permission of the American Chemical Society.

revealed an opposite behavior with a CB7•**25**⁺ complex ($K = 6.1 \times 10^4 \text{ M}^{-1}$) less stable than the CB7•**25**²⁺ due to a decrease of its peripheral positive charge that reduces the interactions with the CB7 oxygen atoms.

In order to estimate the importance of electrostatics with these hosts, a valuable strategy has also consisted in studying closely related guests, be they ionic or not. This was done with Fc-based derivatives **27–29** which are cationic, neutral, and anionic, respectively (Figure 8.16) [44a,b]. As determined by NMR spectroscopy and cyclic voltammetry, both **27** and **28** form strong associations with CB7 in water, while the negatively charged guest **29** is not bound at all. This observation is consistent with the morphology of CBs and their peripheral negative potential, which generates electrostatic repulsions and precludes the anion entrance. The CV response of **27** confirms the high affinity of this unit for CB7, as shown by the positive shift (+110 mV) of the redox potential observed for the corresponding complex. In addition, only the host–guest redox signal remains visible after the addition of one equivalent of CB7 illustrating the stability of the complex (Figure 8.16b).

By taking advantage of CB7 affinity toward Fc on the one hand, and cations on the other hand, Kaifer and coworkers subsequently reported a nice extension of this work with the synthesis and study of electrochemically -triggered rotaxanes **30a–d** (Figure 8.17) [45]. The concept lies on the preparation of a molecular axle made up of an alkyl

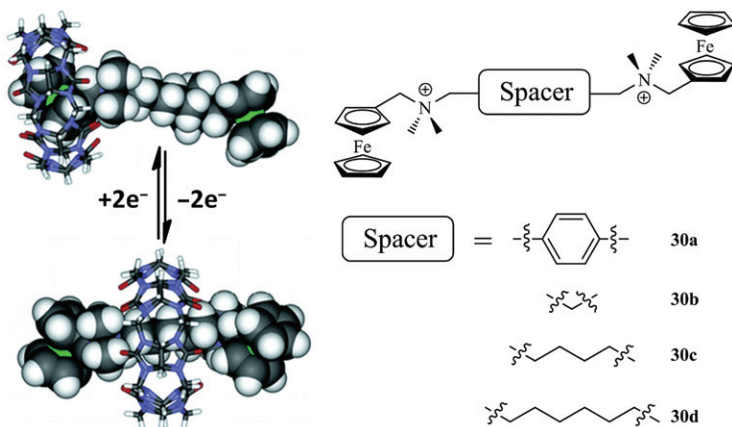


Figure 8.17. Electrochemically-triggered rotaxanes **30a-d**. Source: [45]. Reproduced with permission of the American Chemical Society.

or an aromatic spacer surrounded by two quaternized (ferrocenylmethyl)dimethylamine units. In this manner, CB7 binds one of the lateral ferrocenyl moieties when the latter are neutral, whereas it binds the central alkylendiammonium (or the arylene-diammonium) part when Fc units are oxidized.

Another recent work from Kaifer's team concerns the so-called (Ferrocenylmethyl)tempammonium guests **31a-c**, which therefore associate two distinctive electroactive units linked through an ammonium bridge (Figure 8.18) [46]. These derivatives are different by the methylation degree of the ammonium bridge, which proved to be critical regarding the recognition phenomenon with cucurbit [8]uril. Cyclic voltammetry of compounds **31a-c** shows two signals corresponding to the oxidations of the Fc at +0.43 V and the nitroxide at +0.77 V versus Ag/AgCl. Based on the ^1H NMR spectra and the voltammograms of the inclusion complexes, the authors concluded that **31a** forms a very stable complex with CB8, with the tempo unit included in the cavity, while the Fc moiety is predominantly hosted in the case of **31c**. To get a deeper insight on this process, the authors prepared and studied a structurally intermediate guest, **31b**, endowed with a tertiary ammonium bridge. Interestingly, a middle situation was noticed with two competing binding modes: Fc@CB8 and TEMPO@CB8 . Unfortunately, CV experiments in the presence of CB8 were impossible because of the insolubility of the complexes in the supporting electrolyte solution. Nevertheless, the inclusion of the Fc residue in the lower size cucurbituril CB7 could be confirmed with the voltammetric data (Figure 8.18). Addition of CB7 to a solution of **31b** leads to a positive shift of the Fc redox potential while the TEMPO unit is almost not affected. This result is consistent with the data collected on the water soluble **27** derivative for which a positive shift of the half-wave potential was consecutive to the guest inclusion. Even though there is so far no indication about the exact role of the nitrogen methylation degree, one could imagine that hydrogen bonds between the oxygen atoms of the cucurbituril openings and the $\text{R}_1\text{R}_2\text{R}_3\text{NH}^+$ and the $\text{R}_1\text{R}_2\text{NH}_2^+$ might be involved in the recognition behavior with such guests.

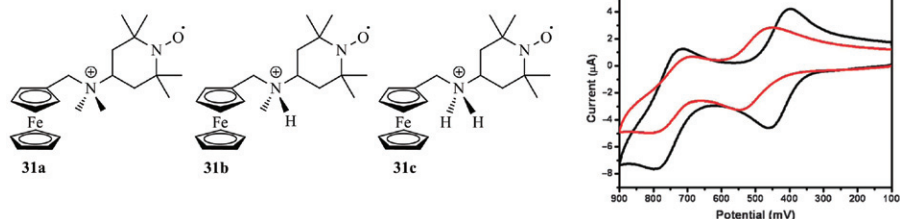


Figure 8.18. Compounds 31a-c and cyclic voltammetric response of 31b (1.0 mM) in 50 mM NaCl without (black) and with 1.0 equiv CB7 (red) (E vs. Ag/AgCl). Source: [46]. Reproduced with permission of The Royal Society of Chemistry.

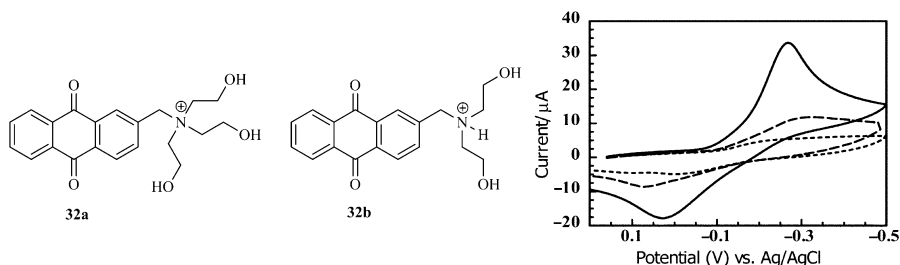


Figure 8.19. Molecular structure of water soluble anthraquinone guests; cyclic voltammetric response on glassy carbon (0.071 cm²) of guest **32b** in 0.1 M HCl solution without (continuous line) and with 1.0 equiv. (discontinuous line) and 2.0 equiv. (dotted lined) of CB7. Scan rate: 0.1 V s⁻¹. Source: [47]. Reproduced with permission of The Royal Society of Chemistry.

The inclusion of reducible anthraquinone guests (compounds **32a**, **32b**) has also been studied (Figure 8.19) [47]. Cucurbit [7]uril is characterized by an internal diameter of 7.3 Å and peripheral openings of 5.4 Å, while 5.3 Å separate the oxygen atoms of anthraquinone derivatives. Thus, the inclusion of the guest within the cavity is necessarily associated to a distortion of the host. This explains the moderate binding constants observed for **32a** ($K_a = 1.3 \times 10^3 \text{ M}^{-1}$) and **32b** ($K_a = 2.8 \times 10^3 \text{ M}^{-1}$) in chlorhydric acid. In addition to steric effects, hydrogen bonding may once again intervene and explain, at least in part, why **32b** is more strongly bound by CB7 than its tetraalkylated analog **32a**. Both guests exhibit one wave centered at 0.13 V versus Ag/AgCl in acidic solution, corresponding to the two electron reduction process to give the anthradihydroquinone. Addition of the CB7 host impedes the electrochemical process, indicating the progressive inclusion of the guest in the cavity (Figure 8.19). In this case and contrary to what was previously observed, the redox potential of the guest is not affected. This example underlines the arising complexity when aiming to clearly identify the role of different complementary interactions since even a small modification of the guest molecular structure modifies various parameters, such as solvation or steric hindrance.

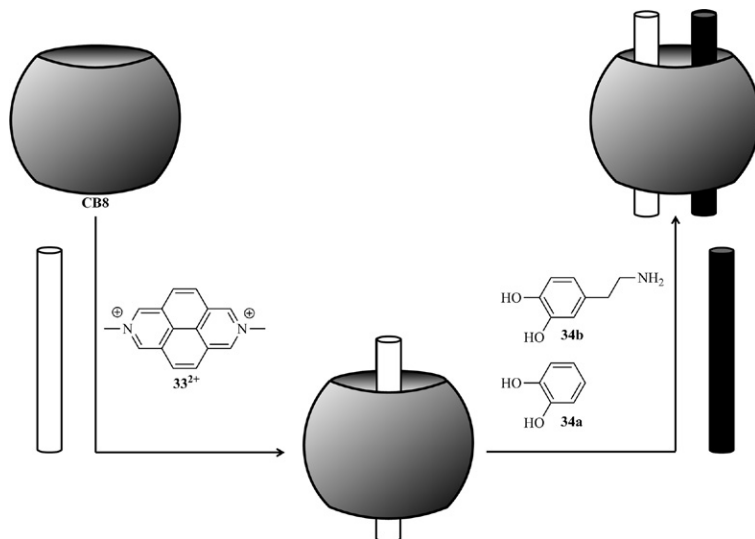


Figure 8.20. Formation of binary and ternary inclusion complexes with CB8 [49].

Such detection strategy, which results from the modification of the redox properties of the guest upon inclusion, has been commonly used for neurotransmitter recognition [48]. Nevertheless, the detection mechanism lies sometimes on more elaborate concepts. In this regard, Raymo, Kaifer, and coworkers have reported a unique example with a cucurbit [8]uril accommodating both a dimethyldiazapyrenium 33^{2+} unit and a catechol derivative (**34a**: catechol; **34b**: dopamine) (Figure 8.20) [49]. While one could expect that both guests would compete to enter the cavity, they form a π -dimer within the cucurbituril ring. From an electrochemical point of view, authors chose to study dimethylviologen 25^{2+} instead of 33^{2+} because of the complicated and nonfully understood voltammogram of the latter in water. Anyhow, they were able to identify the redox signature of the $25^{2+} \cdot 34b$ complex and demonstrated that the presence of catechol **34a** or dopamine **34b** inhibits the formation of the radical-cation dimer (33^{+})₂ which exists in cucurbit [8]uril after a one-electron reduction process.

Cyclodextrins (CDs) are naturally occurring macrocycles, which result from the enzymatic degradation of starch. These hosts represent a class of oligosaccharides usually made up of six, seven, or eight D-glucose units linked through α -1,4-glucose bonds to form α -, β -, and γ -CDs, respectively. Their inner cavity diameters are similar of those of the CB [6], CB [7], and CB [8]. However, cucurbituril are perfectly symmetrical, while CDs are conical and endowed with two rims that differ in chemical nature. It is well known that hydrophobic and van der Waals interactions are predominant in host–guest associations involving CDs. But, unlike cucurbituril openings, the peripheral hydroxyl groups of CDs do not seem to play a key role in the guest binding. However, it is possible to use their reactivity to introduce new functionalities and tune CD environment.

To date, many supramolecular Fc–CD associations have been reported, and their stoichiometry mainly depends on the cavity size. Indeed, α - and β -CDs form 1:1 com-

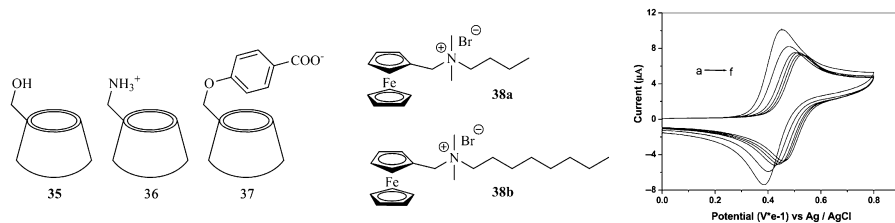


Figure 8.21. Cyclic voltammograms of **38a** (1.0 mM) obtained on a GC electrode immersed in phosphate aqueous buffer solution (pH 7.20, 50 mM NaCl as supporting electrolyte) in presence of **36** (0, 1.0, 3.0, 5.0, 7.0, 10.0 mM from a to f). Scan rate = 50 mV s⁻¹. Source: [51]. Reproduced with permission of the American Chemical Society.

plexes whereas γ -CD incorporates two electroactive guests. Another important parameter controlling the related supramolecular interactions lies on the solvent nature. In particular, V. Kolivoska et al. showed the strong influence of the solvent dielectric constant over the Gibbs free energy [50]. Just like for cucurbiturils, this statement suggests an important contribution of electrostatic interactions. In this regard, Liu and coworkers have recently compared the complexation behaviors of the native β -CD to functionalized β -CDs **35–37** with cationic Fc derivatives **38a,b**, by means of isothermal titration calorimetry (ITC) and cyclic voltammetry (Figure 8.21) [51]. Experiments were run at pH = 7.2 so that **36** bears an ammonium group whereas **37** exists as a carboxylate. As expected, binding constants depend on the electrostatic interactions between the positively charged Fc derivatives **38a** or **38b**, and the CDs. The unsubstituted CD **35** shows K_a values of 4137 and 5122 M⁻¹ toward these guests, respectively. These values increase to 7679 and 9328 M⁻¹ with the anionic macrocycle **37** due to favorable electrostatic interactions. Conversely, this value decreases to 3130 and 3680 M⁻¹ when the rim is positively charged (**36**). By cyclic voltammetry, the **36**•**38a** host–guest complex presents a similar behavior than the CB/Fc inclusion complex **CB7**•**27** reported earlier. The sequential addition of the CD derivative over a solution of **38a** decreases the peak current and shifts the wave to more positive potentials (Figure 8.21). This behavior indicates that the complex diffusion is lower than the free guest and that the equilibrium constant is thermodynamically favorable. Besides, a similar behavior has been reported by J. M. Casas-Solvas et al. with thioglycosylated Fc's derivatives [52].

As seen earlier, TTF is a well-known electroactive unit, which can be successively and reversibly oxidized at readily accessible potentials to afford the TTF^{•+} radical cation and the TTF²⁺ dication. In a recent work dedicated to the study of electron transfers in host–guest inclusion complexes [53], Bergamini et al. examined the TTF oxidation behavior in presence of the hydroxypropyl- β -cyclodextrin (HP β CD). Almost insoluble in water, TTF becomes soluble in the presence of the HP β CD, which suggests the formation of the TTF@HP β CD inclusion complex. Electrochemical measurements demonstrated that increasing the concentration of the CD derivative in a TTF solution anodically shifts the first oxidation wave and results in a current decrease for both oxidation processes (Figure 8.22).

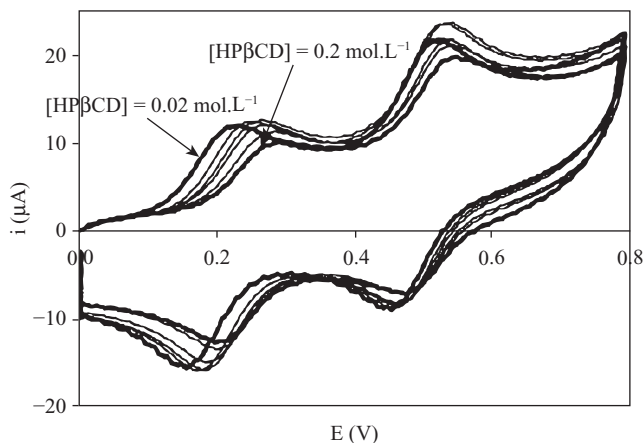


Figure 8.22. Cyclic voltammetry of TTF (5×10^{-4} M), LiClO_4 (0.1 M), H_2O , 1 V s^{-1} in the presence of increasing concentrations of HP β CD from 0.02 to 0.2 M on a 0.7 mm diameter GC disk electrode (E vs. SCE). Source: [53]. Reproduced with permission of Elsevier.

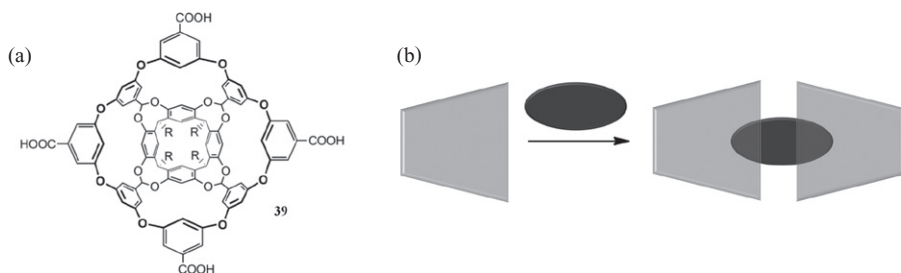


Figure 8.23. Representation of (a) the octaacid cavitaand **39**, (b) the corresponding dimeric capsule including a guest. Source: [56]. Reproduced with permission of the American Chemical Society.

Another interesting macrocycle used to incorporate electroactive guest is the water-soluble octaacid cavitaand **39** (Figure 8.23a) developed by B. C. Gibb [54]. This host forms in solution a dimeric container, which is stabilized when a guest is incorporated in its hydrophobic cavity (Figure 8.23b).

The formation of this capsule, mostly driven by hydrophobic forces, reduces the contact of the guest and of the inner cavity surface with water molecules. When cavitaand **39** and Fc are mixed in solution, the rapid solubilization of the electroactive unit suggests the formation of the host–guest capsule [55]. This result was confirmed by pulse gradient-stimulated echo (PGSE) NMR that allows the determination of diffusion coefficients. Surprisingly, the electrochemical experiments showed a silent voltammogram in the case of the capsule as a result of slow electron transfer kinetics. This situation probably arises from the host acting as a neutral barrier. As a consequence, Kaifer et al. developed a simple strategy to get partially round this issue [56]. To do so,

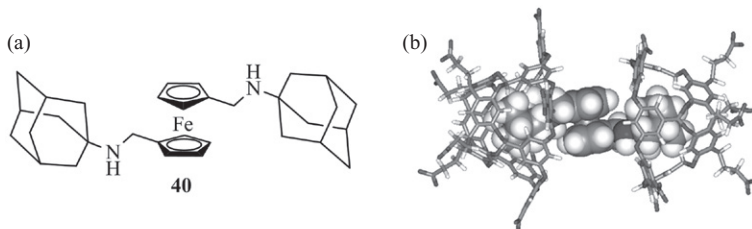


Figure 8.24. (a) Structure of the adamantyl-substituted ferrocene **40** and (b) the corresponding energy minimized structure (PM3) of the supramolecular capsule. Source: [56]. Reproduced with permission of the American Chemical Society.

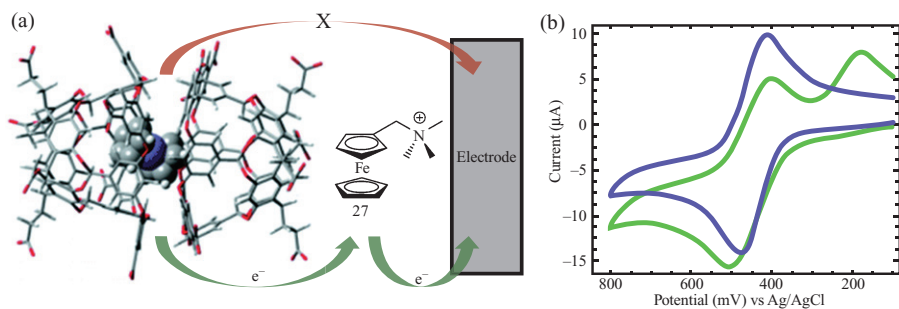


Figure 8.25. (a) Scheme of the electron transfer in the dimeric capsule•Fc/**27** system; (b) CV responses on glassy carbon of 50 mM NaCl aqueous solutions buffered at pH 9 with 10 mM sodium borate of **27** (1.0 mM) in the absence (blue) and in the presence (green) of 1.0 equiv of dimeric capsule•Fc. Scan rate: 0.1 V s^{-1} . Source: [57]. Reproduced with permission of the American Chemical Society. See color insert.

they synthesized a new bulky Fc derivative **40** grafted with two adamantyl units, well-known moieties for their strong interactions with cavitands. In this manner, the guest is able to maintain a larger distance between the two cavitands, preventing electrochemical isolation of the redox reporter, which consequently is clearly detected in this case (Figure 8.24).

Finally, the oxidation of the incorporated naked Fc has been possible with the use of a cationic mediator, the water-soluble Fc derivative **27** (Figure 8.25) [57]. Addition of the latter to a solution of the host–guest complex dimeric capsule•Fc was followed by PGSE NMR. This experiment indicates that the complex does not dissociate upon addition of compound **27** and that the latter stands outside the cavity. The electrochemical behavior of this mixture was studied by cyclic voltammetry and shows the oxidation of free **27** only at 0.44 V versus Ag/AgCl (Figure 8.25b). The reverse scan reveals the reduction of two species. The first is assigned to reduction of 27^+ to **27** with a current level lower than the corresponding anodic wave, when the second takes place in the region of the free Fc reduction (0.2 V vs. Ag/AgCl). From these findings, it has been concluded that the encapsulated Fc transfers an electron to the oxidized 27^+ to

generate the corresponding less hydrophobic Fc^+ species inside the capsule (Figure 8.25a), which leads to the destruction of the assembly.

In a different context, neurotransmitters are small redox-active molecules found in the synaptic region, which allow communication between neurons, thanks to oxidation and reduction reactions. Given their importance in neural science, their electrochemical detection has focused much attention, and there have been thousands of examples reported so far. Nevertheless, the utilization of macrocycles to host these species and gain for example in selectivity remains less frequent in the literature. In this regard, different kinds of receptors have been studied, such as CDs. With the latter, seminal papers were used to describe the study of the neurotransmitter binding in solution. From now on, scientists mainly focus their attention on modified electrodes, which may have advantages in terms of experiment, cost, or reusability. A recent example was published by Abbaspour and coworkers with a multilayer electrode made up of carbon paste, multiwall carbon nanotubes (MWCNTs), poly(*N*-acetylaniline), and β -cyclodextrin [58]. This work is particularly interesting since it benefits from two synergistic effects. On the one hand, MWCNTs catalyze the oxidation reaction of dopamine and serotonin and, on the other hand, β -cyclodextrins allow for selectively recognizing these neuromediators among other possible interfering analytes (e.g., ascorbic acid, ibuprofen, and glutamine) and make the oxidation potentials of dopamine and serotonin sufficiently different to isolate their own electrochemical signatures.

8.5 REDOX-RECOGNITION/TRANSDUCTION WITH NUCLEIC ACIDS

Nucleic acids are ubiquitous in living organisms and have central roles in most biological processes. Consequently, their lacks, excesses, or dysfunctions are likely to induce horrendous diseases at different levels. Therefore, it appears essential to be capable of determining their concentrations and probing possible modifications of their chemical structures. During the last two decades, chemists and biologists have developed new methods and derivatives in order to recognize nucleic acids with very high selectivities and sensitivities. This proves to be a very elaborate task, given the considered molecular structures which often impose the utilization of multivalent systems. Indeed, these macromolecules display peculiar arrangements with tridimensional binding sites that can be considered as cavities or macrocycles.

From the medical point of view, major breakthroughs may be possible if one succeeds in improving ability to detect major nucleic acids (e.g., DNA and RNA). For instance, this would offer interesting outlooks regarding the treatment and the prevention of genetic diseases. In this context, electrochemical methods are often qualified as promising because of their cheaper implementation compared with optical devices. An interesting school case lies on a DNA-based molecular beacon labeled with a *Fc* unit at the terminal position and attached to a gold surface (Figure 8.26) [59]. In the absence of the complementary nucleic acid, the grafted DNA forms a macrocycle through weak intramolecular interactions and the latter maintain the *Fc* unit in vicinity of the electrode (strong current). Then, upon addition of a perfectly matching 17-base target, nucleic acids hybridize together; this provokes the macrocycle opening, imposing a larger distance between the terminal *Fc* reporter and the gold electrode, which eventually results in a decreased current (Figure 8.26). Authors demonstrated their chip could

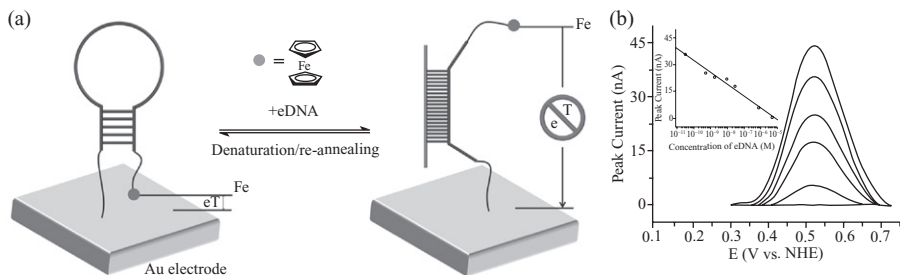


Figure 8.26. (a) Modulation of the redox probe-electrode distance by addition of a complementary DNA strand on a DNA-modified electrode; (b) Evolution of the square-wave voltammetry in the presence of increasing concentrations of complementary DNA (from top to bottom: 0 pM, 30 pM, 500 pM, 30 nM, 800 nM and 5 μ M). Source: [59]. Reproduced with permission of the National Academy of Sciences, U.S.A.

detect nucleic acid concentrations as low as 10^{-15} mol L $^{-1}$, but this system suffers from a drawback regarding the reusability: by using sodium chloride and heating, only 80% of the initial signal could be regenerated after one cycle.

Reusability is also a key point when aiming at generalizing a technique because it may have a strong economic impact but more importantly, because it allows the experimenter to perform control experiments to avoid false positives that could be due to nonspecific interactions or denaturation of the strand. This is the reason why the same team proposed few years later a valuable improvement with the utilization of an electrode-bound DNA pseudoknot [60]. It consists in a nucleic acid secondary structure made up of a single strand which includes at least two stem loops, with half of one comprised in the other loop (Figure 8.27). The redox-active tag in this case corresponds to methylene-blue **41**. Unlike the previous system, this SAM-based chip works as a “signal-on” sensor. When free, the electroactive methylene blue **41** unit is far from the gold electrode and isolated from the latter by the pseudoknot thickness. Conversely, hybridization with a complementary strand makes the supramolecular complex more flexible and allows tag **41** to approach the electrode, which is responsible for the current increase. This method displays a very high selectivity. For instance, a solution of a 17-base target with three mismatches produces only a 2% variation compared with a 20 times more diluted solution of the perfectly matched target, whether in water or in blood serum (Figure 8.27b). This system also proved to be more robust than the previous example, which would be due to the replacement of the Fc tag by a methylene blue redox unit **41**. As a consequence, the chip can be readily reemployed after a simple and fast rinsing with distilled water.

As seen previously, the electrochemical behavior of Fc may also be modulated provided the formation of an inclusion complex with CD. Such a recognition phenomenon classically induces a decrease of the measured current and sometimes a shift of the Fc electrochemical signal. Thus, different teams have recently taken advantage of these features for developing new strategies to detect nucleic acid sequences. For instance, Aoki and coworkers have studied Fc-DNA- β -cyclodextrin conjugate **42**, which experiences a dramatic conformational change upon binding a complementary

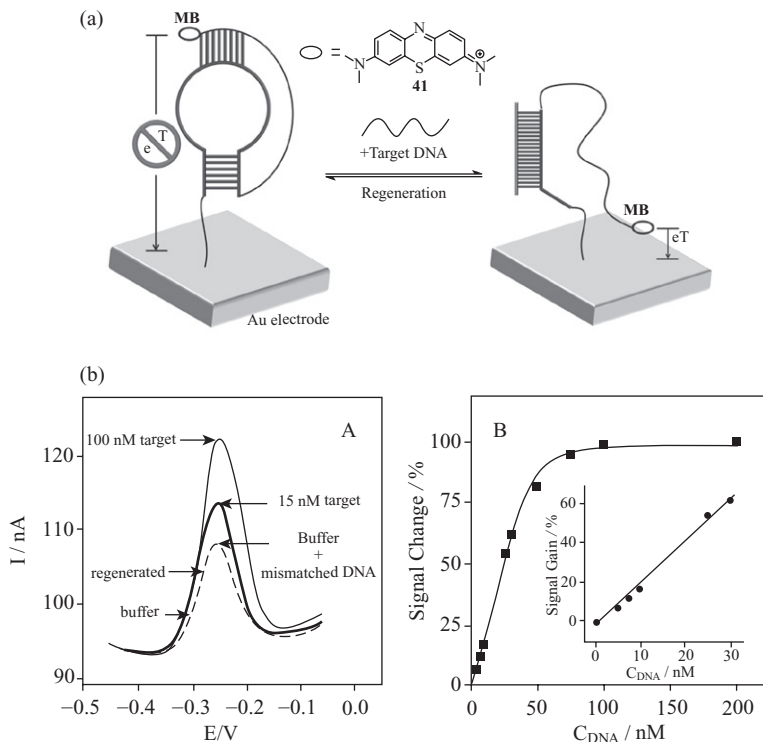


Figure 8.27. (a) Modulation of the redox probe-electrode distance by addition of a complementary DNA strand on a DNA-modified electrode; (b) Evolution of the square-wave voltammetry in the presence of complementary target DNA and mismatched DNA. MB stands for methylene blue. Source: [60]. Reproduced with permission of the American Chemical Society.

strand (Figure 8.28) [61]. When free, **42** behaves as an Ouroboros: the molecule is conformationally flexible and this makes the intramolecular Fc- β -CD recognition process possible. On the contrary, when **42** is in the presence of a complementary nucleic acid, DNA hybridization causes the dethreading of the Fc- β -cyclodextrin inclusion complex. Consequently, the current intensity decreases significantly because of the larger hydrodynamic radius and the oxidation potential is cathodically shifted (62 mV) (Figure 8.28c), which may be ascribed to the negative charges brought by DNA.

As mentioned in the introduction of this part, being able to probe small chemical modifications of DNA strands (for instance, the replacement of a nucleotide by another one) remains challenging with electrochemical methods. In this regard, an elegant work was recently reported by Ihara et al. [62], who were able to differentiate the four sequences presented in Figure 8.29. As one can observe, these 22-base oligonucleotides have the same structures with the exception of one base. Thanks to the hybridization of these oligonucleotides **target22N** with two other compounds, the DNA- β -CD conjugate **43** on the one hand, and the Fc-DNA one **44** on the other hand, authors were able to show that a perfect match between these strands was a *sine qua non* condition

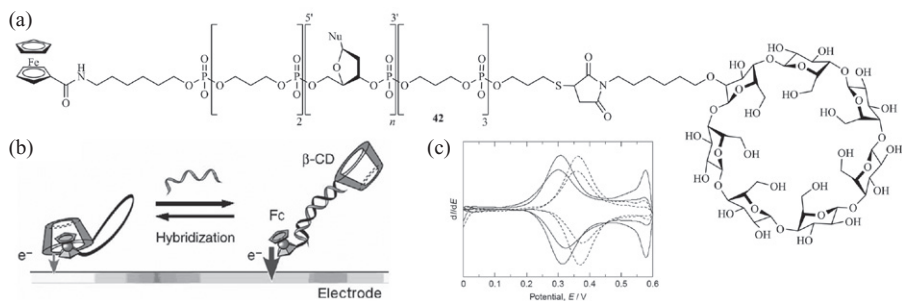


Figure 8.28. (a) Chemical structure of compound **42**; (b) Schematic representation of the functioning of the DNA responsive transducer; (c) Deconvoluted cyclic voltammograms of **42** in the absence (dashed line) and in the presence (solid line) of the target oligonucleotide (carbon-based microelectrode, E versus Ag/AgCl , 0.01 V s^{-1}) [61]. Reprinted with permission from Aoki, H., Kitajima, A., Tao, H. (2010). Label-free and “signal-on” DNA detection using a probe DNA terminated with ferrocene and β -cyclodextrin. *Supramolecular Chemistry*, 22, 455–460. Copyright (2010) Taylor & Francis, Ltd.

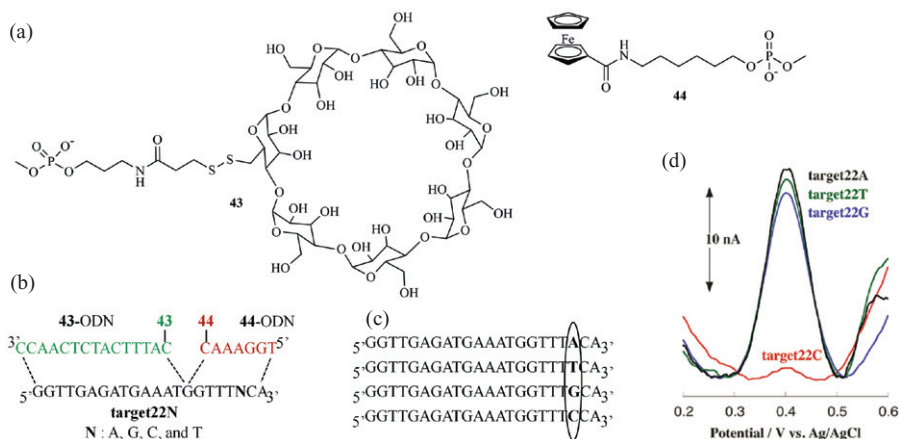


Figure 8.29. (a) Chemical structure of βCyD - and Fc-fragments; (b) Schematic representation of the tandem duplex; (c) targets **22A**, **22T**, **22G** and **22C**; (d) Square wave voltammograms of **44** in the presence of **43** and targets **22A**, **22T**, **22G**, **22C**. Source: [62]. Reproduced with permission of The Royal Society of Chemistry.

to observe the formation of the Fc- β -CD inclusion complex, that is, the tandem duplex. This was nicely proved through electrochemical measurements, which show the Fc is electrochemically silent when perfect complementarity is reached (Figure 8.29d). A similar observation had already been reported by Liu, Leumann, Fermín, and coworkers, who had shown that the formation of the duplex could be accompanied by the electrical isolation of a TTF redox probe [63]. These promising results pave the way for the development of new electrochemical sensors to probe small mutations, for instance.

When using a redox reporter to probe DNA, the electroactive unit nature and its position relative to the recognition unit can be decisive. Thus, fully label-free strategies, that is, approaches that do not require the chemical grafting of a redox transducer, look particularly promising [64]. In spite of their relatively high oxidation potentials, one should not forget that adenine, thymine, cytosine, and guanine are electroactive moieties. Consequently, the “label-free” method consists in this case in exploring their own electrochemical signature to detect nucleic acids. In this context, Abbaspour and collaborators recently reported a nice study by modifying a screen-printed electrode (SPE) with a composite made up of β -cyclodextrin, poly(*N*-acetylaniline) (PNAANI), and multiwalled carbon nanotubes (MWNTs) in order to differentiate ss-DNA (single-strand DNA) and ds-DNA (double-strand DNA) among other things (Figure 8.30a) [65]. Their strategy lies on the supramolecular interaction existing between adenine or guanine and a β -cyclodextrin ring. Unlike the nucleobases of a ds-DNA, the ones composing an ss-DNA are available to penetrate the hydrophobic cavity of a β -CD and hence, be efficiently oxidized at the modified electrode. Their strategy proved to be relevant since they demonstrated that a lower current was measured with ds-DNA. Authors were even able to show the influence of base-complementarity by comparing the cyclic voltammograms of a single strand (ss-DNA; green line) in the presence of (i) its perfectly complementary sequence (ds-DNA; black line), (ii) a two-base mismatching sequence (partially ds-DNA; red line), and (iii) another noncomplementary one (two independent ss-DNA; blue line) (Figure 8.30b).

8.6 SELF-ASSEMBLED MACROCYCLIC REDOX-ACTIVE RECEPTORS

The self-assembly methodology, more particularly when assisted by metals, constitutes a very efficient synthetic tool to reach macrocyclic structures, otherwise very challenging to prepare through classical step-by-step covalent synthesis. In the recent past, chemists have extensively used this strategy to synthesize host structures of increased complexity. If a metal is required in the process, this methodology is supported by coordination bonds between suitable metal complexes and polytopic ligands which often incorporate two or more pyridyl units. The resulting discrete structures, namely molecular polygons or polyhedra, intrinsically present a cavity prone to bind a complementary guest. Interestingly, the use of redox-active ligands along the self-assembly process offers the possibility to reach macrocyclic structures endowed with redox-active panels. Therefore, this situation potentially allows a control over the ionic charge of the cavity, which can be tuned electrochemically. This feature may also be valuable to probe the presence of a guest within the cavity. The former issues are of particular importance regarding potential applications in terms of controlling the encapsulation/delivery processes of various guests. The redox-active units encountered in the previous paragraphs of this chapter are in principle concerned by this part, providing they are chemically functionalized with appropriate chemical functions prone to allow self-assembly. The latter being driven by thermodynamics, can be essentially performed using either (i) reversible chemical reactions between the starting building blocks or (ii) through coordination of a polytopic ligand to a transition-metal complex which assists the self-assembly process. In the following are presented several illustrative examples of redox-active self-assembled macrocycles.

A case falling in the first category is provided with the recently described macrocycles **45a-b** which integrate three redox metallic centers and which were prepared

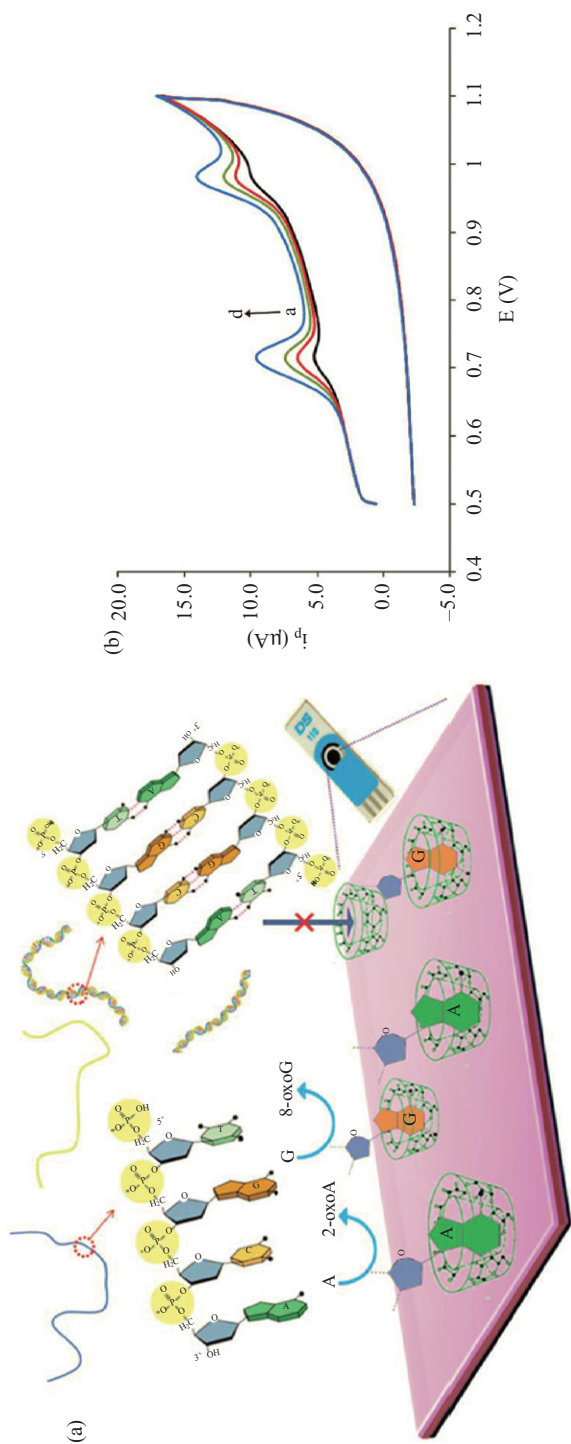


Figure 8.30. (a) Schematic representation of the detection mode: contrary to what is observed in the case of ds-DNA, adenine and guanine fragments from ss-DNA can enter cyclodextrins and be efficiently oxidized at the electrode-liquid interface; (b) cyclic voltammograms recorded for a given DNA-strand alone (green line), with a perfectly matching sequence (black line), with a two-base mismatching one (red line), and with a noncomplementary one (blue line). Source: [65]. Reproduced with permission of The Royal Society of Chemistry. See color insert.

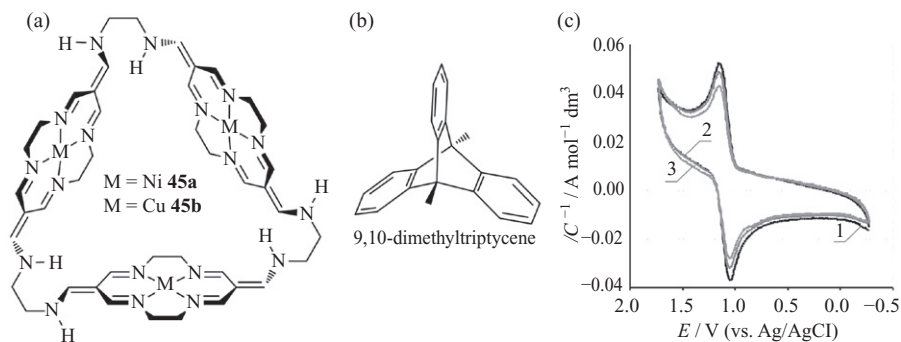


Figure 8.31. (a) Self-assembled redox-active triangle **45a-b**; (b) 9,10-dimethyltriptycene guest under study; (c) Cyclic voltammograms of **45b** without (1) and after addition of 9,10-dimethyltriptycene in 1:10 (2) and 1:20 ratios (3); 0.1 M TBAPF₆ in CH₃CN, 0.2 V s⁻¹. Source: [66]. Reproduced with permission of Wiley-VCH Verlag GmbH & Co. KGaA.

through a self-assembly process from a Ni (respectively Cu) tetraazamacrocyclic mononuclear unit and ethylene diamine as building blocks [66]. Regarding the triangular shape of the resulting tris-macrocyclic hosts (Figure 8.31), the authors have found a strong affinity with the structurally complementary 9,10-dimethyltriptycene, as demonstrated by electrochemical studies. Interestingly, the latter are not based on the usual variation of the redox potentials of the host–guest complex compared to the free receptor, but rather on the evolution of the corresponding diffusion coefficient upon inclusion of dimethyltriptycene. Both complexes **45a** and **45b** undergo a nearly reversible M²⁺/M³⁺ oxidation processes at 1.15 and 1.37 V versus Ag/AgCl, respectively, with each of the three redox centers oxidized at the same potential in both cases. Introduction of the triptycene guest onto an acetonitrile solution of hosts **45a** or **45b** leads to a decreasing of the corresponding peak currents in the cyclic voltammogram. Exploring this evolution, the authors could determine the association constants ($K_{\text{ass}} = 454 (+/- 42)$ and $322 (+/- 27)$ for the Ni and the Cu complexes, respectively). Noteworthy, these values, determined electrochemically, reasonably correspond to those obtained from NMR titration, providing a new lighting on analytical tools dedicated to host–guest interactions and illustrating an additional interest in the use of redox-active receptors.

As pointed out previously, the TTF unit is a highly π -donating building block showing unique redox properties, with occurrence of three distinct stable redox states at easily reachable potentials. Moreover, this unit is compatible with a wide range of reaction conditions, a favorable issue for various types of functionalization. In this context, in Angers, we have recently developed several examples of self-assembled redox-active electron-rich macrocyclic receptors. Their synthesis is based on the metal-driven self-assembly methodology. Only some examples of self-assembled host structures involving electroactive side walls are depicted [67], and they are mostly built from electron-acceptor ligands (typically of the 1,3,5-triazine or quinone family). On the other hand, only few cavities are built from electron-rich panels, and compounds **47** and **48** belong to this category (Figure 8.32a) [68]. Triangle **47** and square **48** are independently isolated from the same self-assembly reaction, through reaction between a

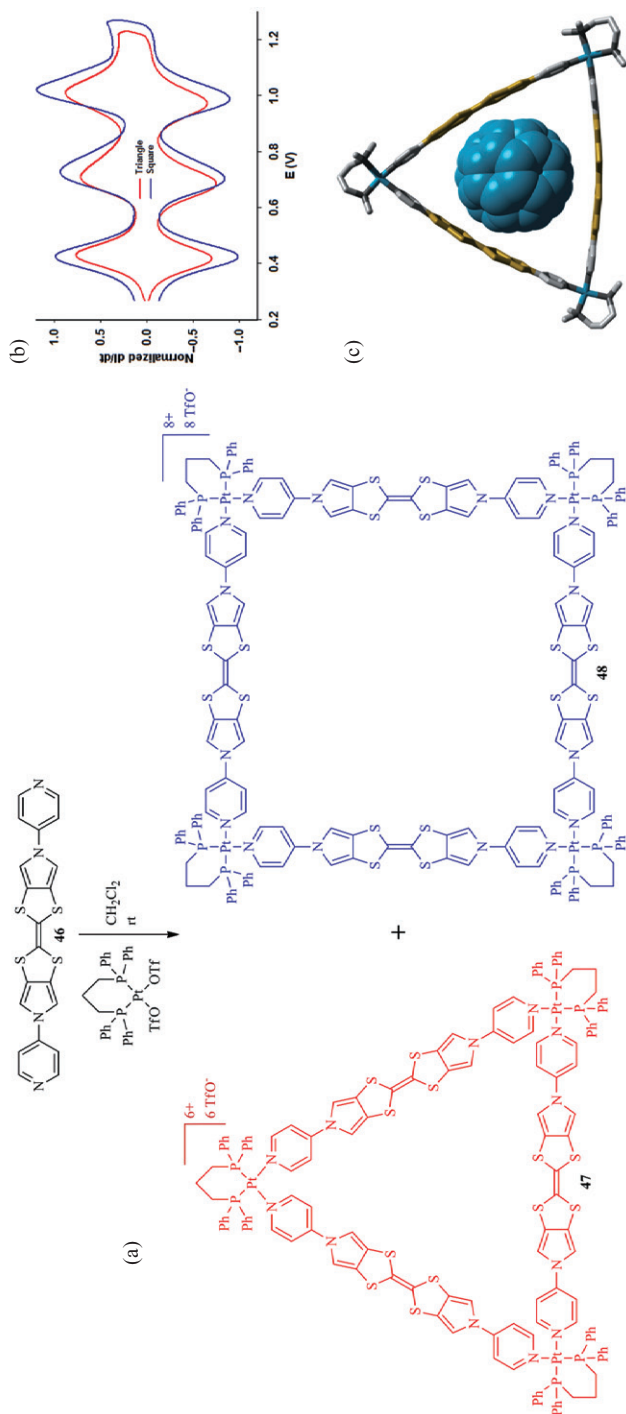


Figure 8.32. (a) Metal-driven self-assembly of redox-active triangle **47** and square **48**; (b) deconvoluted cyclic voltammograms of triangle **47** (0.5 mM) and square **48** (0.5 mM) in presence of ferrocene (3 eq. and 4 eq., respectively); (c) optimized geometry (Hyperchem, MM+) of the $\mathbf{47} \cdot \text{C}_{60}$ complex. Source: [68]. Reproduced with permission of The Royal Society of Chemistry. See color insert.

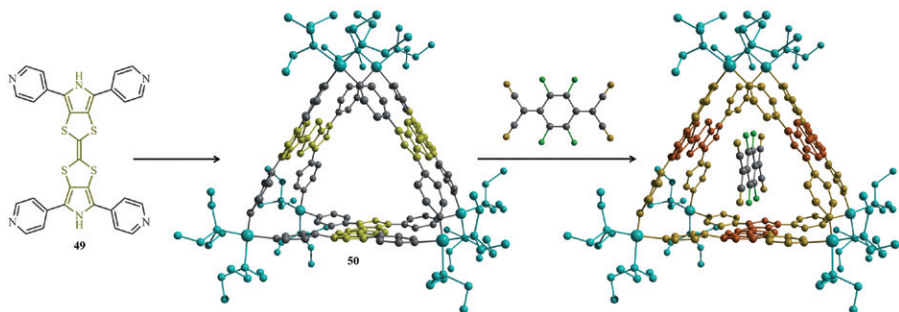


Figure 8.33. Metal-driven self-assembly of the redox-active trigonal prismatic structure **50** and inclusion of organic guest TCNQF₄ within the electron-rich cavity of **50**. Source: [69]. Reprinted with permission of the American Chemical Society.

TTF-based linear ditopic ligand **46** and a *cis*-coordinated square-planar Pt(II) complex. Both polygons **47** and **48** are reversibly oxidized through two successive independent three (respectively four) electron redox processes (Figure 8.32), giving rise to a reversible control over the charge state of the cavity which can be tuned between **47** to **47⁶⁺** (**48** to **48⁸⁺**). The electron-rich cavity of triangle **47** shows a good affinity for the electrodeficient fullerene C₆₀ as shown by UV-vis titration studies (log K_a = 4.2 in a CS₂/CH₂Cl₂ 8/2 (v/v) solution). On the contrary, square **48**, though presenting a similar π -donating ability than triangle **47**, does not exhibit any affinity for C₆₀. This difference is assigned to an inappropriate cavity size to match C₆₀ in the case of the square which exhibits an inner diameter of 22 Å versus 13 Å for **47**. This observation illustrates that in addition to favorable interaction between redox-antagonists, a good size matching is essential in the case of a preorganized rigid cavity.

From an analogous metal-driven self-assembly strategy, the trigonal-prismatic polyhedron **50** could be recently prepared from a tetrapyrridyl-TTF derivative **49** [69]. This metallo-based structure corresponds to the first example of a TTF-based self-assembled cage and the corresponding electron-rich cavity can be used to incorporate one electrodeficient molecule as shown in the case of tetrafluorotetracyano-*p*-quinodimethane (TCNQF₄) (Figure 8.33). This example illustrates both the potentiality offered by the metal-driven self-assembly methodology to reach electron donating cages and in addition shows the ability of the latter to bind electron-poor guests. Given that each panel making up the cavity can be oxidized twice, a step forward now concerns the access to new related 3D host structures for which the guest could be switch-on/off electrochemically.

In addition to these cavities constructed from electroactive side panels, considerable efforts have also been produced in direction of polygons appended with redox probes, be they internal or external to the cavity, such as in the case of representative assemblies **51** [70], **52** [71], and **53** [72], respectively, or even with the 3D cuboctahedral redox-system **54** [73], designed as a model to explore protein encapsulation, and for which presence of redox-groups can potentially provide an extra means of characterizing the guest-encapsulated species (Figure 8.34).

Though their electrochemistry has not been specifically addressed in the literature, several other examples of redox-active cages capable of including various guests have

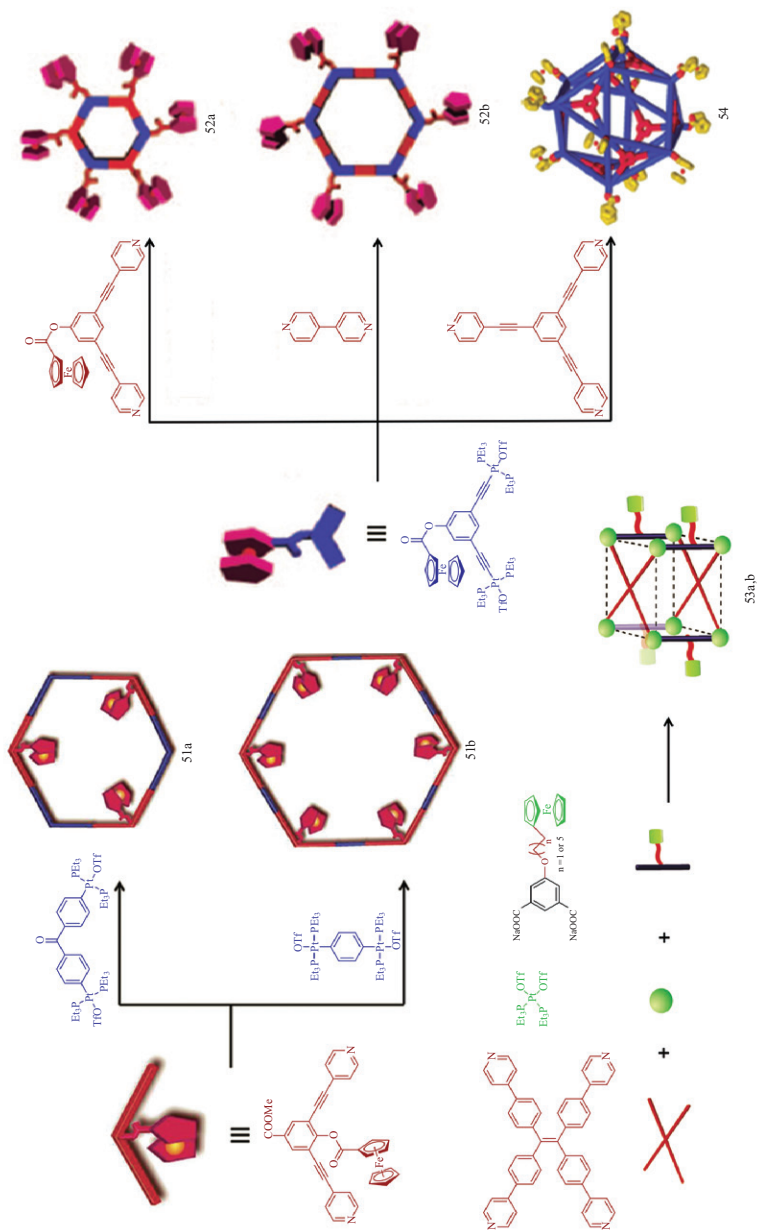


Figure 8.34. Self-assembled discrete structures **51–54** bearing pendant Fc redox probes. Figure sources: [70–73]. All adapted with permission of the American Chemical Society. See color insert.

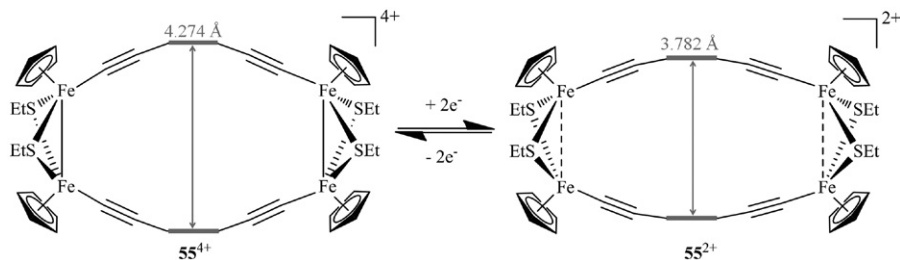


Figure 8.35. Redox-controlled cavity modulation of the rectangular complex **55**.

been recently produced. For instance, (i) porphyrin-based boxes, be they covalent [74] or self-assembled [75], exhibit an excellent binding ability for fullerenes or large aromatic guests, a behavior which is supported by the enriched π -electron density of the cavity; (ii) many examples of metalla-cages based on the electrodeficient 2,4,6-tripyridyl-1,3,5-triazine ligand have been produced and have allowed spectacular results in terms of inclusion of organic substrates [76, 77].

Finally, one can note that self-assembled structures also provide an opportunity to electrochemically control the cavity size such as in the recent rectangular iron thiolate aryldiisocyanide metallo-cyclic structure **55** (Figure 8.35), which also opens interesting perspectives in terms of electrochemical-triggering of guest binding [78].

8.7 CONCLUSIONS AND PERSPECTIVES

Through this chapter, a sampling of covalent or self-assembled redox-active macrocyclic receptors for organic molecules has been proposed. As shown with those examples, various topical application fields are concerned, ranging from electrochemical sensors of potential interest in environmental or medical sciences, to controlled motions in electrochemically-triggered systems, a key issue in the field of molecular electronics. Efforts in those fields are continuously produced and several emerging further studies can be identified:

- The design of the redox-receptor itself remains of critical importance, in particular in connection with the structural characteristics of the targeted guests. From this point of view, this chapter has essentially focused on redox-receptors integrating an electron-rich cavity, designed to bind electrodeficient organic compounds. It is worth mentioning that in principle, complementary electron-poor receptors can also be designed, beside those derived from **CBPQT**⁴⁺ already mentioned. On this ground, the pyromellitic diimide framework has recently attracted a strong interest as a π -accepting building block widely used in supramolecular chemistry [79]. Several examples of a pyromellitic diimide-based macrocyclic receptors have been developed [80], and an illustrative example is provided with compound **56** (Figure 8.36). The host-cavity in **56** [80b], with a transannular distance of 7.3 Å between two diimide π -faces, is π -electron poor and favors intercalation of electron-rich aromatic guests with occurrence of a charge transfer interaction. On

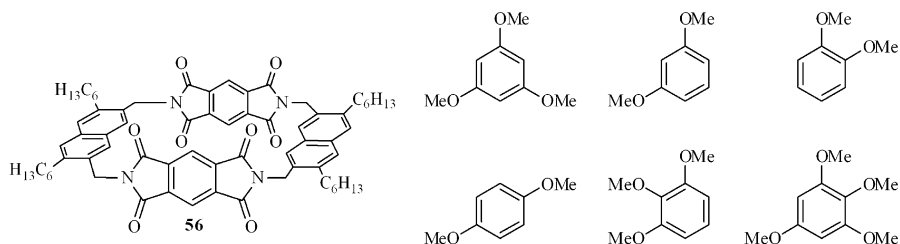


Figure 8.36. Redox-active ligand **56** and studied organic guests.

this basis, extension to new families of π -electron poor receptors can be envisaged as a promising complementary approach to electron-donating macrocycles

- Chiral electrochemical recognition is particularly topical from the fundamental and practical point of view, in particular regarding the need to alternative easy-to-run *ee* determination analytical tools. Though this topic has focused an intense interest for long, it is only recently that a striking achievement was accomplished [28], which opens promising perspectives in terms of synthesis of new families of redox-active macrocyclic chiral receptors.
- Beyond electrochemical transduction led in solution, which has constituted the guideline of this book chapter, material sciences provide an additional promising field of application for electroactive macrocyclic receptors in the solid state. Modifying the electronic properties in the solid state is of course of interest for a wide range of applications, such as molecular conductors, organic field-effect transistors (OFETs) or organic solar cells (OSCs). In this context, fullerene is a well-known electron acceptor which is utilized as an electron transporter in photovoltaic devices. However, fullerene containing devices often suffer from their tendency to aggregate. As a consequence, there has been in the recent years a growing interest in the search for fullerene hosts, which would be capable of preventing this phenomenon. In this regard, macrocyclic receptors [13b] have contributed to significant advances. During the last decade, outstanding discoveries have been allowed regarding fullerene recognition, thanks to bisporphyrinic macrocycles [74c]. In particular, Fumito Tani and collaborators have recently described the utilization of such a host to produce interesting materials [81]. As illustrated in Figure 8.37, molecule **57** forms channels through hydrogen bonding in the crystalline state, and fullerene nicely fits within these tubes when cocrystallized.

In the case of the nonmetallated macrocycle, the redox potentials of the inclusion complex were studied by cyclic voltammetry. Both oxidation (porphyrin) and reduction (C₆₀) processes were affected compared to the unfilled **57** and C₆₀, transducing an interaction in the ground state between both species. Moreover, the macrocyclic structure prevents fullerene aggregation and allows for aligning these electron acceptors. This peculiar supramolecular arrangement generates anisotropy, and as a matter of fact, it clearly explains why the conducting properties were so different depending on the crystal orientation. Indeed, when the conductivity was measured in a parallel

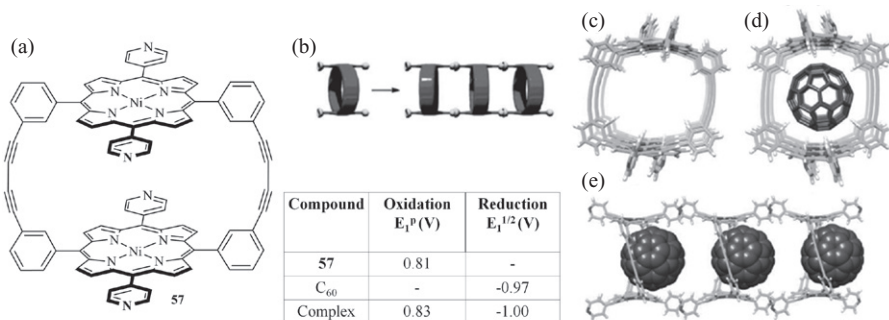


Figure 8.37. (a) Compound **57**; (b) Channels based on **57**; (c) X-Ray structure of **57**; (d and e) X-Ray structure of complex **57**• C_{60} . Table 1: [a] The oxidation potentials were analyzed by DPV of film states of the samples on platinum electrodes in acetonitrile with 0.1 M nBu_4NClO_4 . [b] The reduction potentials were determined by cyclic voltammetry in *o*-dichlorobenzene/pyridine (1:1) with 0.1 M nBu_4NClO_4 . Scan rate = 0.1 V s⁻¹. [**57**] = 0.2 mM. Source: [13b]. Reproduced with permission of Wiley-VCH Verlag GmbH & Co. KGaA.

manner compared to the fullerene axis, the σ value was as high as $\sigma = 0.72 \text{ cm}^2 \text{ V}^{-1} \text{ s}^{-1}$, whereas it was only $0.12 \text{ cm}^2 \text{ V}^{-1} \text{ s}^{-1}$ in a perpendicular direction. Such example, and others [82], illustrate how redox-active macrocyclic host–guest systems can also interfere at the solid state, giving rise to promising applications in the field of materials sciences.

- Important efforts are currently produced in preparing self-assembled redox-active cages. Beyond the synthetic interest of this strategy which allows reaching functionalized cavities which are otherwise difficult to prepare through multistep covalent synthesis, the resulting redox-active cavities are promising in the field of redox-driven recognition processes. First, following the inclusion of a guest within the cavity, they may allow an electrochemical detection of the host–guest process through the response of the redox-probes surrounding or constituting the cavity (responsive mode, §II.1). It is worth mentioning that in addition to sensor applications, a valuable extension of the concept can be envisaged by an electrochemical control over the binding ability between the redox cavity and a given guest. One could expect that controlling the redox state—that is, the ionic level—of the cavity can switch on and off the guest binding, by modifying interactions between both counterparts. For instance, cationic cavities would bind cations more weakly than reduced ones, a concept which has already been demonstrated in the case of ionic species with molecular organocyanometalate boxes which allow a redox-switch of the complexation/decomplexation of K^+ and Cs^+ [83]. Extension of this strategy to organic guests definitely constitutes a promising further challenge.

REFERENCES

- [1] Steed, J. W., Atwood, J. L. *Supramolecular Chemistry*, John Wiley and Sons, Chichester, 2009; p. 307.

- [2] (a) Wenzel, M., Hiscock, J. R., Gale, P. A. (2012). Anion receptor chemistry: Highlights from 2010. *Chemical Society Reviews*, 41, 480–520; (b) Gale, P. A. (2010). Anion receptor chemistry: Highlights from 2008 and 2009. *Chemical Society Reviews*, 39, 3746–3771; (c) Steed, J. W. (2009). Coordination and organometallic compounds as anion receptors and sensors. *Chemical Society Reviews*, 38, 506–519.
- [3] (a) Bernhardt, P. V., Moore, E. G. (2003). Functionalized macrocyclic compounds: Potential sensors of small molecules and ions. *Australian Journal of Chemistry*, 56, 239–258; (b) Beer, P. D., Gale, P. A., Chen, G. Z. (1999). Electrochemical molecular recognition: Pathways between complexation and signalling. *Journal of the Chemical Society—Dalton Transactions*, 28, 1897–1909.
- [4] (a) Tucker, J. H. R., Collinson, S. R. (2002). Recent developments in the redox-switched binding of organic compounds. *Chemical Society Reviews*, 31, 147–156; (b) Kaifer, A. E. (1999). Interplay between molecular recognition and redox chemistry. *Accounts of Chemical Research*, 32, 62–71; (c) Boulas, P. L., Gomez-Kaifer, M., Echegoyen, L. (1998). Electrochemistry of supramolecular systems. *Angewandte Chemie (International ed. in English)*, 37, 216–247; (d) Kaifer, A. E., Mendoza, S. Redox-switchable receptors. In *Comprehensive Supramolecular Chemistry*, Vol. 1, Gokel, G. W. (Ed.), Pergamon, Tarrytown, NY, 1996; pp. 701–732.
- [5] Lyskawa, J., Le Derf, F., Levillain, E., Mazari, M., Sallé, M., Dubois, L., Viel, P., Bureau, C., Palacin, S. (2004). Univocal demonstration of the electrochemically mediated binding of Pb^{2+} by a modified surface incorporating a TTF-based redox-switchable ligand. *Journal of the American Chemical Society*, 126, 12194–12195.
- [6] Nijhuis, C. A., Ravoo, B. J., Huskens, J., Reinhoudt, D. N. (2007). Electrochemically controlled supramolecular systems. *Coordination Chemistry Reviews*, 251, 1761–1780.
- [7] Hunter, C. A. (2004). Quantifying intermolecular interactions: Guidelines for the molecular recognition toolbox. *Angewandte Chemie (International ed. in English)*, 43, 5310–5324.
- [8] Batail, P. (2004). Special issue on molecular conductors. *Chemical Reviews*, 104, 4887–4890.
- [9] (a) Canevet, D., Sallé, M., Zhang, G., Zhang, D., Zhu, D. (2009). Tetrathiafulvalene (TTF) derivatives: Key building-blocks for switchable processes. *Chemical Communications*, 45, 2245–2269; (b) Herranz, M. A., Sánchez, L., Martín, N. (2005). Tetrathiafulvalene: A paradigmatic electron donor molecule. *Phosphorus, Sulfur, and Silicon and the Related Elements*, 180, 1133–1148; (c) Yamada, J., Sugimoto, T. *TTF Chemistry: Fundamentals & Applications of Tetrathiafulvalene*, Kodansha, Tokyo and Springer, Berlin, Heidelberg, New York, 2004.; (d) Martín, N., Segura, J.-L. (2001). New concepts in tetrathiafulvalene chemistry. *Angewandte Chemie (International ed. in English)*, 40, 1372–1409; (e) Bryce, M. R. (2000). Functionalised tetrathiafulvalenes: New applications as versatile (-electron systems in materials chemistry. *Journal of Materials Chemistry*, 10, 589–598; (f) Nielsen, M. B., Lomholt, C., Becher, J. (2000). Tetrathiafulvalenes as building blocks in supramolecular chemistry II. *Chemical Society Reviews*, 29, 153–164.
- [10] Surpateanu, G. G., Landy, D., Lungu, C. N., Fourmentin, S., Surpateanu, G., Rethore, C., Avarvari, N. (2006). Synthesis and inclusion capability of a β -cyclodextrin-tetrathiafulvalene derivative. *Tetrahedron*, 62, 9701–9704.
- [11] (a) Sun, F., Hu, F., Zhang, G., Zhang, D. (2012). Metal-Ion-promoted electron transfer between tetrathiafulvalene and quinone units within a calix[4]arene framework and tuning through coordination of the neighboring crown ether with a sodium cation. *Chemistry—An Asian Journal*, 7, 183–189; (b) Flídrová, K., Tkadlecová, M., Lang, K., Lhoták, P. (2012). Anion complexation by calix[4]arene–TTF conjugates. *Dyes and Pigments*, 92, 668–673; (c) Sun, F., Hu, F., Zhang, G., Zheng, Q., Zhang, D. (2011). Calix[4]arenes with electroactive tetrathiafulvalene and quinone units: Metal-ion-promoted electron transfer. *The Journal of Organic Chemistry*, 76, 6883–6888; (d) Lee, M. H., Cao, Q. Y., Kim, S. K., Sessler, J. L., Kim, J. S. (2011). Anion responsive TTF-appended calix[4]arenes. synthesis and study of two different conformers. *The Journal of Organic Chemistry*, 76, 870–874; (e) Düker, M. H., Gómez, R., Vande

- Velde, C. M. L., Azov, V. A. (2011). Upper rim tetrathiafulvalene-bridged calix[4]arenes. *Tetrahedron Letters*, 52, 2881–2884; (f) Lyskawa, J., Canevet, D., Allain, M., Sallé, M. (2010). An electron-rich three dimensional receptor based on a calixarene-tetrathiafulvalene assembly. *Tetrahedron Letters*, 51, 5868–5872; (g) Zhao, B.-T., Zhou, Z., Yan, Z.-N., Belhadj, E., Le Derf, F., Sallé, M. (2010). Synthesis and electrochemical behavior of a model redox-active thiacalix[4]arene-tetrathiafulvalene assembly. *Tetrahedron Letters*, 51, 5815–5818; (h) Zhao, B. T., Blesa, M. J., Le Derf, F., Canevet, D., Benhaoua, C., Mazari, M., Allain, M., Sallé, M. (2007). Carboxylic acid derivatives of tetrathiafulvalene: Key intermediates for the synthesis of redox-active calixarene-based anion receptors. *Tetrahedron*, 63, 10768–10777; (i) Blesa, M. J., Zhao, B. T., Allain, M., Le Derf, F., Sallé, M. (2006). Bis(calixcrown)tetrathiafulvalene receptors. *Chemistry—A European Journal*, 12, 1906–1914; (j) Lyskawa, J., Sallé, M., Balandier, J.-Y., Le Derf, F., Levillain, E., Allain, M., Viel, P., Palacin, S. (2006). Monitoring the formation of TTF dimers by Na⁺ complexation. *Chemical Communications*, 42, 2233–2235; (k) Zhao, B. T., Blesa, M. J., Mercier, N., Le Derf, F., Sallé, M. (2005). A calixarene-amide-tetrathiafulvalene assembly for the electrochemical detection of anions. *New Journal of Chemistry*, 29, 1164–1167.
- [12] (a) Frei, M., Diederich, F., Tremont, R., Rodriguez, T., Echegoyen, L. (2006). Tetrathiafulvalene (TTF)-bridged resorcin[4]arene cavitands: Towards new electrochemical molecular switches. *Helvetica Chimica Acta*, 89, 2040–2057; (b) Mendoza, S., Godínez, L. A., Kaifer, A. E. (2004). Tetrathiafulvalene-functionalized cavitands as building blocks for redox active hemiacarcerands. *Supramolecular Chemistry*, 16, 165–169; (c) Moon, K., Kaifer, A. E. (2004). Dimeric molecular capsules under redox control. *Journal of the American Chemical Society*, 126, 15016–15017.
- [13] (a) Canevet, D., Gallego, M., Isla, H., de Juan, A., Pérez, E. M., Martín, N. (2011). Macrocyclic hosts for fullerenes: Extreme changes in binding abilities with small structural variations. *Journal of the American Chemical Society*, 133, 3184–3190; (b) Canevet, D., Pérez, E. M., Martín, N. (2011). Wraparound hosts for fullerenes: Tailored macrocycles and cages. *Angewandte Chemie (International ed. in English)*, 50, 9248–9259; (c) Huerta, E., Isla, H., Pérez, E. M., Bo, C., Martín, N., de Mendoza, J. (2010). Tripodal exTTF-CTV hosts for fullerenes. *Journal of the American Chemical Society*, 132, 5351–5353; (d) Isla, H., Gallego, M., Pérez, E. M., Viruela, R., Orti, E., Martín, N. (2010). A bis-exTTF macrocyclic receptor that associates C₆₀ with micromolar affinity. *Journal of the American Chemical Society*, 132, 1772–1773; (e) Grimm, B., Santos, J., Illescas, B. M., Munoz, A., Guldi, D. M., Martín, N. (2010). A new exTTF-crown ether platform to associate fullerenes: Cooperative n- π and π - π effects. *Journal of the American Chemical Society*, 132, 17387–17389.
- [14] Shoji, Y., Tashiro, K., Aida, T. (2010). One-pot enantioselective extraction of chiral fullerene C₇₆ using a cyclic host carrying an asymmetrically distorted, highly π -basic porphyrin module. *Journal of the American Chemical Society*, 132, 5928–5929.
- [15] (a) Amendola, V., Fabbrizzi, L., Mosca, L. (2010). Anion recognition by hydrogen bonding: Urea-based receptors. *Chemical Society Reviews*, 39, 3889–3915; (b) Blondeau, P., Segura, M., Perez-Fernandez, R., de Mendoza, J. (2007). Molecular recognition of oxoanions based on guanidinium receptors. *Chemical Society Reviews*, 36, 198–210; (c) Casnati, A., Sansone, F., Ungaro, R. (2003). Peptido- and glycolixarenes: playing with hydrogen bonds around hydrophobic cavities. *Accounts of Chemical Research*, 36, 246–254; (d) Schmuck, C., Geiger, L. (2003). Carboxylate binding by guanidiniocarbonyl pyrroles: From self assembly to peptide receptors. *Current Organic Chemistry*, 7, 1485–1502.
- [16] Cui, X. L., Delgado, R., Carapuca, H. M., Drew, M. G. B., Felix, V. (2005). Carboxylate anions binding and sensing by a novel tetraazamacrocycle containing ferrocene as receptor. *Dalton Transactions*, 34, 3297–3306.
- [17] (a) Martic, S., Labib, M., Shipman, P. O., Kraatz, H.-B. (2011). Ferrocene-peptido conjugates: From synthesis to sensory applications. *Dalton Transactions*, 40, 7264–7290; (b) Molina, P., Tárraga, A., Caballero, A. (2008). Ferrocene-based small molecules for multichannel molecu-

- lar recognition of cations and anions. *European Journal of Inorganic Chemistry*, 2008, 3401–3417; (c) Beer, P. D., Hayes, E. J. (2003). Transition metal and organometallic anion complexation agents. *Coordination Chemistry Reviews*, 240, 167–189; (d) Beer, P. D., Cadman, J. (2000). Electrochemical and optical sensing of anions by transition metal based receptors. *Coordination Chemistry Reviews*, 205, 131–155.
- [18] Miyaji, H., Gasser, G., Green, S. J., Molard, Y., Strawbridge, S. M., Tucker, J. H. R. (2005). Selective electrochemical sensing of acidic organic molecules via a novel guest-to-host proton transfer reaction. *Chemical Communications*, 41, 5355–5357. [19] Andersen, S. S., Jensen, M., Sørensen, A., Miyazaki, E., Takimiya, K., Laursen, B. W., Flood, A. H., Jeppesen, J. O. (2012). Anion effects on the cyclobis(paraquat-p-phenylene) host. *Chemical Communications*, 48, 5157–5159.
- [20] Bernardo, A. R., Stoddart, J. F., Kaifer, A. E. (1992). Cyclobis(paraquat-p-phenylene) as a synthetic receptor for electron-rich aromatic compounds: Electrochemical and spectroscopic studies of neurotransmitter binding. *Journal of the American Chemical Society*, 114, 10624–10631.
- [21] (a) Ma, Y., Zhao, H., Yu, P., Su, L., Zhang, D., Mao, L. (2009). Electrochemical sensing of ATP with synthetic cyclophane as recognition element. *Science in China Series B: Chemistry*, 52, 741–745; (b) Neelakandan, P. P., Hariharan, M., Ramaiah, D. (2005). Synthesis of a novel cyclic donor–acceptor conjugate for selective recognition of ATP. *Organic Letters*, 7, 5765–5768; (c) Reynes, O., Bucher, C., Moutet, J.-C., Royal, G., Saint-Aman, E. (2004). Redox sensing of anions in pure aqueous environment by ferrocene-containing 4,4'-bipyridinium-based receptors and polymer films. *Chemical Communications*, 40, 428–429.
- [22] Yan, J., Zhou, Y., Yu, P., Su, L., Mao, L., Zhang, D., Zhu, D. (2008). An electrochemical sensor for 3,4-dihydroxyphenylacetic acid with carbon nanotubes as electronic transducer and synthetic cyclophane as recognition element. *Chemical Communications*, 44, 4330–4332.
- [23] Izake, E. L. (2007). Chiral discrimination and enantioselective analysis of drugs: An overview. *Journal of Pharmaceutical Sciences*, 96, 1659–1676.
- [24] Trojanowicz, M., Kaniewska, M. (2009). Electrochemical chiral sensors and biosensors. *Electroanalysis*, 21, 229–238.
- [25] Jo, S., Jin, Y., Kim, J., Suh, H. (2007). Synthesis of ferrocenyl and diphenyl substituted bispyridino-18-crown-6 ether for chiral recognition. *Bulletin of the Korean Chemical Society*, 28, 2015–2019.
- [26] Chun, K. M., Kim, T. H., Lee, O. S., Hirose, K., Chung, T. D., Chung, D. S., Kim, H. (2006). Structure-selective recognition by voltammetry: Enantiomeric determination of amines using azophenolic crowns in aprotic solvent. *Analytical Chemistry*, 78, 7597–7600.
- [27] Willener, Y., Joly, K. A., Moody, C. J., Tucker, J. H. R. (2008). An exploration of ferrocenyl ureas as enantioselective electrochemical sensors for chiral carboxylate anions. *The Journal of Organic Chemistry*, 73, 1225–1233.
- [28] Mirri, G., Bull, S. D., Horton, P. N., James, T. D., Male, L., Tucker, J. H. R. (2010). Electrochemical method for the determination of enantiomeric excess of binol using redox-active boronic acids as chiral sensors. *Journal of the American Chemical Society*, 132, 8903–8905.
- [29] Anelli, P.-L., Asakawa, M., Ashton, P. R., Bissell, R. A., Clavier, G., Górski, R., Kaifer, A. E., Langford, S. J., Mattersteig, G., Menzer, S., Philp, D., Slawin, A. M. Z., Spencer, N., Stoddart, J. F., Tolley, M. S., Williams, D. J. (1997). Toward controllable molecular shuttles. *Chemistry—A European Journal*, 3, 1113–1135.
- [30] (a) Barin, G., Forgan, R. S., Stoddart, J. F. (2012). Mechanostereochemistry and the mechanical bond. *Proceedings of the Royal Society A: Mathematical, Physical and Engineering Science*, 468, 2849–2880; (b) Forgan, R. S., Sauvage, J.-P., Stoddart, J. F. (2011). Chemical topology: Complex molecular knots, links, and entanglements. *Chemical Reviews*, 111, 5434–5464.

- [31] Wang, C., Cao, D., Fahrenbach, A. C., Grunder, S., Dey, S. K., Sarjeant, A. A., Stoddart, J. F. (2012). The effects of conformation on the noncovalent bonding interactions in a bistable donor-acceptor [3]catenane. *Chemical Communications*, 48, 9245–9247.
- [32] Spruell, J. M., Coskun, A., Friedman, D. C., Forgan, R. S., Sarjeant, A. A., Trabolsi, A., Fahrenbach, A. C., Barin, G., Paxton, W. F., Dey, S. K., Olson, M. A., Benitez, D., Tkatchouk, E., Colvin, M. T., Carmielli, R., Caldwell, S. T., Rosair, G. M., Hewage, S. G., Duclairoir, F., Seymour, J. L., Slawin, A. M. Z., Goddard, W. A., Wasielewski, M. R., Cooke, G., Stoddart, J. F. (2010). Highly stable tetrathiafulvalene radical dimers in [3]catenanes. *Nature Chemistry*, 2, 870–879.
- [33] Barin, G., Coskun, A., Friedman, D. C., Olson, M. A., Colvin, M. T., Carmielli, R., Dey, S. K., Bozdemir, O. A., Wasielewski, M. R., Stoddart, J. F. (2011). A multistate switchable [3]rotacatenane. *Chemistry—A European Journal*, 17, 213–222.
- [34] Trabolsi, A., Khashab, N., Fahrenbach, A. C., Friedman, D. C., Colvin, M. T., Coti, K. K., Benitez, D., Tkatchouk, E., Olsen, J. C., Belowich, M. E., Carmielli, R., Khatib, H. A., Goddard, W. A., Wasielewski, M. R., Stoddart, J. F. (2010). Radically enhanced molecular recognition. *Nature Chemistry*, 2, 42–49.
- [35] Korybut-Daszkiewicz, B., Więckowska, A., Bilewicz, R., Domagała, S., Woźniak, K. (2004). An electrochemically controlled molecular shuttle. *Angewandte Chemie (International ed. in English)*, 43, 1668–1672.
- [36] (a) Wawrzyniak, U. E., Wozny, M., Mames, I., Palys, B., Korybut-Daszkiewicz, B., Bilewicz, R. (2010). Interactions of dithiolated tetraazamacrocyclic copper(II) and nickel(II) complexes self-assembled on gold electrodes with π -electron deficient molecules in solution. *Dalton Transactions*, 39, 730–735; (b) Korybut-Daszkiewicz, B., Bilewicz, R., Wozniak, K. (2010). Tetraimine macrocyclic transition metal complexes as building blocks for molecular devices. *Coordination Chemistry Reviews*, 254, 1637–1660.
- [37] (a) Collin, J.-P., Durola, F., Lux, J., Sauvage, J.-P. (2009). A rapidly shuttling copper-complexed [2]rotaxane with three different chelating groups in its axis. *Angewandte Chemie (International ed. in English)*, 48, 8532–8535; (b) Durola, F., Sauvage, J.-P. (2007). Fast electrochemically induced translation of the ring in a copper-complexed [2]rotaxane: The bisoquinoline effect. *Angewandte Chemie (International ed. in English)*, 46, 3537–3540.
- [38] Collin, J. P., Gavina, P., Sauvage, J. P. (1996). Electrochemically induced molecular motions in a copper(I) complex pseudorotaxane. *Chemical Communications*, 2005–2006.
- [39] Joosten, A., Trolez, Y., Collin, J.-P., Heitz, V., Sauvage, J.-P. (2012). Copper(I)-assembled [3]rotaxane whose two rings act as flapping wings. *Journal of the American Chemical Society*, 134, 1802–1809.
- [40] Sauvage, J.-P., Trolez, Y., Canevet, D., Sallé, M. (2011). Intercalation of tetrathiafulvalene between the two plates of a copper(I)-complexed [4]rotaxane. *European Journal of Organic Chemistry*, 2011, 2413–2416.
- [41] Kim, J., Jung, I. S., Kim, S. Y., Lee, E., Kang, J. K., Sakamoto, S., Yamaguchi, K., Kim, K. (2000). New cucurbituril homologues: Syntheses, isolation, characterization, and X-ray crystal structures of cucurbit[n]uril (n=5, 7, and 8). *Journal of the American Chemical Society*, 122, 540–541.
- [42] Ling, Y., Mague, J. T., Kaifer, A. E. (2007). Inclusion complexation of diquat and paraquat by the hosts cucurbit[7]uril and cucurbit[8]uril. *Chemistry—A European Journal*, 13, 7908–7914.
- [43] Jeon, W. S., Kim, H.-J., Lee, C., Kim, K. (2002). Control of the stoichiometry in host-guest complexation by redox chemistry of guests: Inclusion of methylviologen in cucurbit[8]uril. *Chemical Communications*, 38, 1828–1829.
- [44] (a) Cui, L., Gadde, S., Li, W., Kaifer, A. E. (2009). Electrochemistry of the inclusion complexes formed between the cucurbit[7]uril host and several cationic and neutral ferrocene derivatives†† Part of the “Langmuir 25th Year: Molecular and macromolecular self-assemblies”

- special issue. *Langmuir: The ACS Journal of Surfaces and Colloids*, 25, 13763–13769; (b) Jeon, W. S., Moon, K., Park, S. H., Chun, H., Ko, Y. H., Lee, J. Y., Lee, E. S., Samal, S., Selvapalam, N., Rekharsky, M. V., Sindelar, V., Sobransingh, D., Inoue, Y., Kaifer, A. E., Kim, K. (2005). Complexation of ferrocene derivatives by the cucurbit[7]uril host: A comparative study of the cucurbituril and cyclodextrin host families. *Journal of the American Chemical Society*, 127, 12984–12989.
- [45] Sobransingh, D., Kaifer, A. E. (2006). Electrochemically switchable cucurbit[7]uril-based pseudorotaxanes. *Organic Letters*, 8, 3247–3250.
- [46] Yi, S., Captain, B., Kaifer, A. E. (2011). The importance of methylation in the binding of (ferrocenylmethyl)tempammonium guests by cucurbit[n]uril (n=7, 8) hosts. *Chemical Communications*, 47, 5500–5502.
- [47] Sindelar, V., Parker, S. E., Kaifer, A. E. (2007). Inclusion of anthraquinone derivatives by the cucurbit[7]uril host. *New Journal of Chemistry*, 31, 725–728.
- [48] Colliver, T. L., Ewing, A. G. *Encyclopedia of Analytical Chemistry*, John Wiley & Sons, Ltd, 2006. Published online. DOI: 10.1002/9780470027318.a5309
- [49] Sindelar, V., Cejas, M. A., Raymo, F. M., Chen, W., Parker, S. E., Kaifer, A. E. (2005). Supramolecular assembly of 2,7-dimethyldiazapyrenium and cucurbit[8]uril: A new fluorescent host for detection of catechol and dopamine. *Chemistry—A European Journal*, 11, 7054–7059.
- [50] Kolivoska, V., Gal, M., Hromadova, M., Valasek, M., Pospisil, L. (2011). Correlation of the formation constant of ferrocene-cyclodextrin complexes with dielectric properties of the aqueous DMSO solution. *Journal of Organometallic Chemistry*, 696, 1404–1408.
- [51] Liu, Y., Cao, R., Chen, Y., He, J. Y. (2008). Effect of β -cyclodextrin charge type on the molecular recognition thermodynamics of reactions with (ferrocenylmethyl)dimethylammonium derivatives. *Journal of Physical Chemistry B*, 112, 1445–1450.
- [52] Casas-Solvas, J. M., Ortiz-Salmerón, E., Giménez-Martínez, J. J., García-Fuentes, L., Capitán-Vallvey, L. F., Santoyo-González, F., Vargas-Berenguel, A. (2009). Ferrocene-carbohydrate conjugates as electrochemical probes for molecular recognition studies. *Chemistry—A European Journal*, 15, 710–725.
- [53] Bergamini, J. F., Hapiot, P., Lorcy, D. (2006). Direct versus indirect electron transfers in host-guest-inclusion complexes: Example of the oxidation of TTF- β -CD complexes. *Journal of Electroanalytical Chemistry*, 593, 87–98.
- [54] Gibb, C. L. D., Gibb, B. C. (2004). Well-defined, organic nanoenvironments in water: the hydrophobic effect drives a capsular assembly. *Journal of the American Chemical Society*, 126, 11408–11409.
- [55] Podkoscielny, D., Philip, I., Gibb, C. L. D., Gibb, B. C., Kaifer, A. E. (2008). Encapsulation of ferrocene and peripheral electrostatic attachment of viologens to dimeric molecular capsules formed by an octaacid, deep-cavity cavitand. *Chemistry—A European Journal*, 14, 4704–4710.
- [56] Qiu, Y., Yi, S., Kaifer, A. E. (2012). Trapping of bulky guests inside dimeric molecular capsules formed by a deep-cavity cavitand. *The Journal of Organic Chemistry*, 77, 4622–4627.
- [57] Podkoscielny, D., Gadde, S., Kaifer, A. E. (2009). Mediated electrochemical oxidation of a fully encapsulated redox active center. *Journal of the American Chemical Society*, 131, 12876–12877.
- [58] Abbaspour, A., Noori, A. (2011). A cyclodextrin host-guest recognition approach to an electrochemical sensor for simultaneous quantification of serotonin and dopamine. *Biosensors and Bioelectronics*, 26, 4674–4680.
- [59] Fan, C., Plaxco, K. W., Heeger, A. J. (2003). Electrochemical interrogation of conformational changes as a reagentless method for the sequence-specific detection of DNA. *Proceedings of the National Academy of Sciences*, 100, 9134–9137.

- [60] Xiao, Y., Qu, X., Plaxco, K. W., Heeger, A. J. (2007). Label-free electrochemical detection of DNA in blood serum via target-induced resolution of an electrode-bound DNA pseudoknot. *Journal of the American Chemical Society*, *129*, 11896–11897.
- [61] Aoki, H., Kitajima, A., Tao, H. (2010). Label-free and “signal-on” DNA detection using a probe DNA terminated with ferrocene and β -cyclodextrin. *Supramolecular Chemistry*, *22*, 455–460.
- [62] Ihara, T., Wasano, T., Nakatake, R., Arslan, P., Futamura, A., Jyo, A. (2011). Electrochemical signal modulation in homogeneous solutions using the formation of an inclusion complex between ferrocene and β -cyclodextrin on a DNA scaffold. *Chemical Communications*, *47*, 12388–12390.
- [63] Schnippering, M., Zahn, A., Liu, S.-X., Leumann, C., Decurtins, S., Fermin, D. J. (2009). Synthesis and electrochemical properties of TTF modified oligodeoxynucleotides. *Chemical Communications*, *45*, 5552–5554.
- [64] Das, J., Cederquist, K. B., Zaragoza, A. A., Lee, P. E., Sargent, E. H., Kelley, S. O. (2012). An ultrasensitive universal detector based on neutralizer displacement. *Nature Chemistry*, *4*, 642–648.
- [65] Abbaspour, A., Noori, A. (2012). A cyclodextrin host-guest recognition approach to a label-free electrochemical DNA hybridization biosensor. *The Analyst*, *137*, 1860–1865.
- [66] Malecka, J., Lewandowska, U., Kaminski, R., Mames, I., Wieckowska, A., Bilewicz, R., Korybut-Daszkiwicz, B., Wozniak, K. (2011). Macrocyclic multicenter complexes of nickel and copper of increasing complexity. *Chemistry—A European Journal*, *17*, 12385–12395.
- [67] (a) Bhattacharya, D., Chang, C.-H., Cheng, Y.-H., Lai, L.-L., Lu, H.-Y., Lin, C.-Y., Lu, K.-L. (2012). Multielectron redox chemistry of a neutral, NIR-active, indigo-pillared re^1 -based triangular metalloprism. *Chemistry—A European Journal*, *18*, 5275–5283; (b) Mattson, J., Govindaswamy, P., Renfrew, A. K., Dyson, P. J., Stepnicka, P., Suss-Fink, G., Therrien, B. (2009). Synthesis, molecular structure, and anticancer activity of cationic arene ruthenium metal-larectangles. *Organometallics*, *28*, 4350–4357; (c) Amijs, C. H. M., van Klink, G. P. M., van Koten, G. (2006). Metallasupramolecular architectures, an overview of functional properties and applications. *Dalton Transactions*, *35*, 308–327.
- [68] (a) Goeb, S., Bivaud, S., Dron, P. I., Balandier, J.-Y., Chas, M., Sallé, M. (2012). A BPTTF-based self-assembled electron-donating triangle capable of C_{60} binding. *Chemical Communications*, *48*, 3106–3108; (b) Balandier, J.-Y., Chas, M., Goeb, S., Dron, P. I., Rondeau, D., Belyasmine, A., Gallego, N., Sallé, M. (2011). A self-assembled bis(pyrrolo)tetrathiafulvalene-based redox active square. *New Journal of Chemistry*, *35*, 165–168.
- [69] Bivaud, S., Balandier, J.-Y., Chas, M., Allain, M., Goeb, S., Sallé, M. (2012). A metal-directed self-assembled electroactive cage with bis(pyrrolo)tetrathiafulvalene (BPTTF) side walls. *Journal of the American Chemical Society*, *134*, 11968–11970.
- [70] Chen, L.-J., Li, Q.-J., He, J., Tan, H., Abliz, Z., Yang, H.-B. (2012). Design and construction of endo-functionalized multiferrocenyl hexagons via coordination-driven self-assembly and their electrochemistry. *The Journal of Organic Chemistry*, *77*, 1148–1153.
- [71] Ghosh, K., Zhao, Y., Yang, H.-B., Northrop, B. H., White, H. S., Stang, P. J. (2008). Synthesis of a new family of hexakisferrocenyl hexagons and their electrochemical behavior. *The Journal of Organic Chemistry*, *73*, 8553–8557.
- [72] Wang, M., Zheng, Y.-R., Cook, T. R., Stang, P. J. (2011). Construction of Functionalized metallosupramolecular tetragonal prisms via multicomponent coordination-driven self-assembly. *Inorganic Chemistry*, *50*, 6107–6113.
- [73] Ghosh, K., Hu, J., White, H. S., Stang, P. J. (2009). Construction of multifunctional cuboctahedra via coordination-driven self-assembly. *Journal of the American Chemical Society*, *131*, 6695–6697.

- [74] (a) Zhang, C. X., Wang, Q., Long, H., Zhang, W. (2011). A highly C_{70} selective shape-persistent rectangular prism constructed through one-step alkyne metathesis. *Journal of the American Chemical Society*, *133*, 20995–21001; (b) Gil-Ramirez, G., Karlen, S. D., Shundo, A., Porfyrakis, K., Ito, Y., Briggs, G. A. D., Morton, J. J. L., Anderson, H. L. (2010). A cyclic porphyrin trimer as a receptor for fullerenes. *Organic Letters*, *12*, 3544–3547; (c) Tashiro, K., Aida, T. (2007). Metalloporphyrin hosts for supramolecular chemistry of fullerenes. *Chemical Society Reviews*, *36*, 189–197.
- [75] (a) Meng, W. J., Breiner, B., Rissanen, K., Thoburn, J. D., Clegg, J. K., Nitschke, J. R. (2011). A self-assembled M8L6 cubic cage that selectively encapsulates large aromatic guests. *Angewandte Chemie (International ed. in English)*, *50*, 3479–3483; (b) Song, J. X., Aratani, N., Shinokubo, H., Osuka, A. (2010). A porphyrin nanobarrel that encapsulates C_{60} . *Journal of the American Chemical Society*, *132*, 16356–16357.
- [76] (a) Yoshizawa, M., Klosterman, J. K., Fujita, M. (2009). Functional molecular flasks: New properties and reactions within discrete, self-assembled hosts. *Angewandte Chemie (International ed. in English)*, *48*, 3418–3438; (b) Therrien, B. (2009). Arene ruthenium cages: Boxes full of surprises. *European Journal of Inorganic Chemistry*, *2009*, 2445–2453.
- [77] (a) Amouri, H., Desmarests, C., Moussa, J. (2012). Confined nanopspaces in metallocages: Guest molecules, weakly encapsulated anions, and catalyst sequestration. *Chemical Reviews*, *112*, 2015–2041; (b) Chakrabarty, R., Mukherjee, P. S., Stang, P. J. (2011). Supramolecular coordination: Self-assembly of finite two- and three-dimensional ensembles. *Chemical Reviews*, *111*, 6810–6918.
- [78] Lin, P.-C., Chen, H.-Y., Chen, P.-Y., Chiang, M.-H., Chiang, M. Y., Kuo, T.-S., Hsu, S. C. N. (2011). Self-assembly and redox modulation of the cavity size of an unusual rectangular iron thiolate arylidithiocyanide metallocyclophane. *Inorganic Chemistry*, *50*, 10825–10834.
- [79] (a) Koshkakarayan, G., Parimal, K., He, J., Zhang, X., Abliz, Z., Flood, A. H., Liu, Y. (2008). π -Stacking enhanced dynamic and redox-switchable self-assembly of donor–acceptor metallo-[2]catenanes from diimide derivatives and crown ethers. *Chemistry—A European Journal*, *14*, 10211–10218; (b) Kaiser, G., Jarrosson, T., Otto, S., Ng, Y.-F., Bond, A. D., Sanders, J. K. M. (2004). Lithium-templated synthesis of a donor–acceptor pseudorotaxane and catenane. *Angewandte Chemie (International ed. in English)*, *43*, 1959–1962.
- [80] (a) Nakagaki, T., Harano, A., Fuchigami, Y., Tanaka, E., Kidoaki, S., Okuda, T., Iwanaga, T., Goto, K., Shinmyozu, T. (2010). Formation of nanoporous fibers by the self-assembly of a pyromellitic diimide-based macrocycle. *Angewandte Chemie (International ed. in English)*, *49*, 9676–9679; (b) Nakagaki, T., Shin-ichiro, K., Harano, A., Shinmyozu, T. (2010). Molecular recognition of polymethoxybenzenes by host molecule comprised of two pyromellitic diimides and two dialkoxynaphthalenes. *Tetrahedron*, *66*, 976–985; (c) Kato, S. I., Nonaka, Y., Shimasaki, T., Goto, K., Shinmyozu, T. (2008). Novel pyromellitic diimide-based macrocycle with a linear π -electronic system and bis(phenylethynyl)pyromellitic diimide: Syntheses, structures, photophysical properties, and redox characteristics. *The Journal of Organic Chemistry*, *73*, 4063–4075; (d) Kato, S., Matsumoto, T., Ideta, K., Shimasaki, T., Goto, K., Shinmyozu, T. (2006). Supramolecular assemblies and redox modulation of pyromellitic diimide-based cyclophane via noncovalent interactions with naphthol. *The Journal of Organic Chemistry*, *71*, 4723–4733.
- [81] (a) Nobukuni, H., Shimazaki, Y., Tani, F., Naruta, Y. (2007). A nanotube of cyclic porphyrin dimers connected by nonclassical hydrogen bonds and its inclusion C_{60} in a linear arrangement. *Angewandte Chemie (International ed. in English)*, *46*, 8975–8978; (b) Nobukuni, H., Tani, F., Shimazaki, Y., Naruta, Y., Ohkubo, K., Nakanishi, T., Kojima, T., Fukuzumi, S., Seki, S. (2009). Anisotropic high electron mobility and photodynamics of a self-assembled porphyrin nanotube including C_{60} molecules. *Journal of Physical Chemistry C*, *113*, 19694–19699; (c) Nobukuni, H., Shimazaki, Y., Uno, H., Naruta, Y., Ohkubo, K., Kojima, T., Fukuzumi, S., Seki, S., Sakai, H., Hasobe, T., Tani, F. (2010). Supramolecular structures and

photoelectronic properties of the inclusion complex of a cyclic free-base porphyrin dimer and C₆₀. *Chemistry—A European Journal*, 16, 11611–11623.

- [82] Scheer, M., Schindler, A., Merkle, R., Johnson, B. P., Linseis, M., Winter, R., Anson, C. E., Virovets, A. V. (2007). Fullerene C₆₀ as an endohedral molecule within an inorganic supramolecule. *Journal of the American Chemical Society*, 129, 13386–13387.
- [83] Boyer, J. L., Ramesh, M., Yao, H. J., Rauchfuss, T. B., Wilson, S. R. (2007). Redox-switched complexation/decomplexation of K⁺ and Cs⁺ by molecular cyanometalate boxes. *Journal of the American Chemical Society*, 129, 1931–1936.

CHAPTER 9

DETECTION OF NITROAROMATIC EXPLOSIVES USING TETRATHIAFULVALENE-CALIX[4]PYRROLES

KARINA R. LARSEN, KENT A. NIELSEN, JONATHAN L. SESSLER,
and JAN O. JEPPESEN

9.1 INTRODUCTION

Current international public awareness of terrorist attacks using explosives has resulted in an increasing interest in the development of quick and reliable methods to detect explosives. In addition, explosives are commonly used in land mines and large quantities of explosives have been dumped in the environment. In both cases, the availability of improved sensing systems would be beneficial. This has led to efforts to develop new chemical-based sensor systems, so-called chemosensors. One approach taken within this broader effort involves the development of tetrathiafulvalene (TTF) calix[4]pyrrole-based chemosensors for nitroaromatic explosives. In this chapter, we describe the molecular engineering that underlies the design of TTF-calix[4]pyrroles and summarize their application as colorimetric chemosensors for nitroaromatic explosives. These systems not only exploit fundamental donor–acceptor interactions between the electron-rich TTF moieties and the electron-deficient nitroaromatic explosive analytes but also rely heavily on the principles of supramolecular chemistry.

The advent of supramolecular chemistry [1] has stimulated interest in the development of sensors—devices, molecule sized or larger, that signal the presence of matter or energy in a way discernible by one of the human senses. Chemosensors capable of recognizing a specific substrate, that is, the chemical species one wishes to detect [2], have received increasing attention as alternatives to biosensors. Occasionally, the motivation to develop a chemosensor reflects the fact that no biological receptor exists for the targeted analyte. More often, biological-based sensor systems exist, but lack the properties needed to make the systems useful outside of a controlled laboratory

Organic Synthesis and Molecular Engineering, First Edition.

Edited by Mogens Brøndsted Nielsen.

© 2014 John Wiley & Sons, Inc. Published 2014 by John Wiley & Sons, Inc.

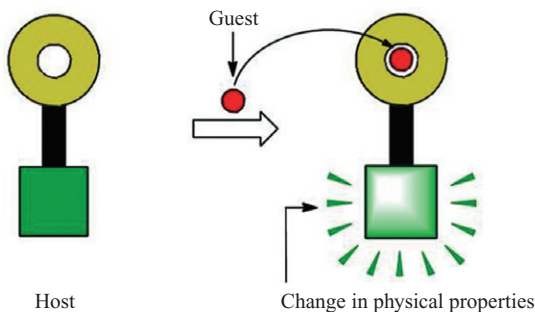


Figure 9.1. Schematic view of a chemosensor composed of receptor unit and a transducer unit.

environment. For instance, antibodies often display high affinities for specific substrates but are usually available only on small scale and are easily subject to denaturing or degradation. In contrast, chemosensors, which are typically the product of dedicated synthesis, can, in principle, be manufactured on large scale and generally expected to be more stable than their biological counterparts.

As shown in Figure 9.1, chemosensors can be produced *inter alia* from the covalent association of a receptor unit and a transducer unit. Perturbation of the physical properties of the transducer unit upon complexation of the substrate then produces a detectable signal, such as a color change. There are now many chemosensors available, and for a wide range of analytes, based on this fundamental design. This chapter will focus exclusively on systems based on TTF-calix[4]pyrroles.

9.1.1 Calix[4]pyrroles

In 1886 Baeyer synthesized a white crystalline material by condensing pyrrole with Me_2CO in the presence of a catalytical amount of hydrochloric acid [3]. Thirty years later, Chelintzev and Tronov repeated this experiment and proposed a cyclic tetrameric porphyrinogen structure **1**, which later proven to be correct [4]. In 1955 Rothmund and Gage improved this synthesis by using methanesulfonic acid as the catalyst [5]. Beyond these specific findings, this class of compounds was only studied sporadically in the 100 years following their discovery [6]. This situation changed in the early 1990s when Floriani and Floriani-Moro began exploring their metal coordination chemistry extensively [7]. These seminal studies served to revive interest in these macrocycles after a long dormant period. Interest in calix[4]pyrroles increased further when Sessler and coworkers reported in 1996 that this kind of macrocycle could bind anions in organic solution while likewise proposing that this macrocycle could prove useful in a number of applications where anion recognition would be beneficial [8]. Sessler and coworkers introduced the name calix[4]pyrrole to highlight the fact that these macrocycles displayed conformational behavior similar to that of the calix[4]arenes. Since the 1996 report, many new calix[4]pyrrole-based anion receptors have been synthesized and studied in a number of research groups throughout the world. A summary of this effort is beyond the scope of this chapter. However, a brief review of some of the key features of calix[4]pyrroles is needed to understand the recognition attributes of their more complex, TTF-functionalized derivatives.

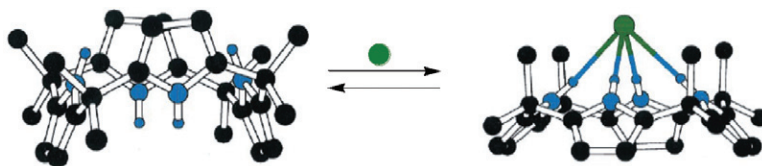
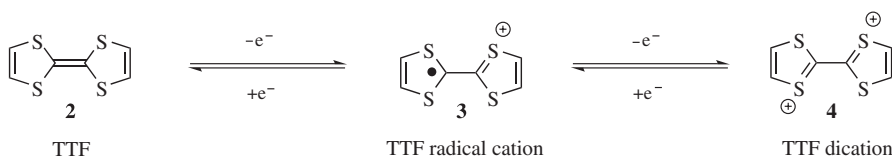


Figure 9.2. X-ray crystal structure of calix[4]pyrrole **1** in the absence (1,3-alternate conformation) and in the presence of Cl^- anion (cone conformation). Source: [9]. Reproduced with permission of The Royal Society of Chemistry. Link: <http://pubs.rsc.org/en/content/articlelanding/1998/cc/a706280j>.



Scheme 9.1. The sequential and reversible oxidation of TTF (**2**) affords the stable cationic species **3** and **4**.

X-ray crystal analysis revealed that without anions, calix[4]pyrrole **1** adopts a 1,3-alternate conformation (Figure 9.2) wherein adjacent rings are oriented in opposite directions. In the presence of anions (e.g., Cl^- anion), the molecule undergoes a dramatic change in geometry and adopts a cone-like conformation such that the four NH protons are involved in hydrogen-bonding interactions to the Cl^- anion. Single-crystal X-ray diffraction analyses revealed this conformation (Figure 9.2) and revealed distance parameters consistent with the presence of strong hydrogen-bonding interactions between the four pyrrolic NH protons and the Cl^- anion in the solid state.

9.1.2 Tetrathiafulvalene (TTF)

During the past decades, the sulfur-containing heterocycle, TTF [10], and its derivatives have been intensively studied on account of their unique π -electron-donating properties. Derivatives of TTF were originally prepared as strong electron-donor molecules for the development of electrically conducting materials. However, recently TTF derivatives have been used increasingly as building blocks in macrocyclic and supramolecular chemistry, and this work has revealed the utility of the TTF unit in application areas beyond the field of materials chemistry [10b–d]. TTF has been incorporated into a number of molecular and supramolecular systems to give complex entities and ensembles with fascinating properties, including various macrocycles [11], interlocked compounds [12], and polymers [13]. Systems incorporating the TTF unit capable of forming host–guest interactions also show promise, for example, as chemosensors and as molecular switches [14]. Some examples hereof were shown in the previous chapter.

Although TTF is a planar 14 π -electron system, it is nonaromatic according to Hückel definition because the 14 π -electrons lack cyclic conjugation [11a]. Oxidation to the radical cation and dication occurs sequentially and reversibly at low potentials. In contrast to the neutral TTF molecule, both the radical cation and dication (Scheme 9.1) are aromatic in the Hückel sense as the result of the 6 π -electron heteroaromaticity of the 1,3-ditholium cation that results upon oxidation.

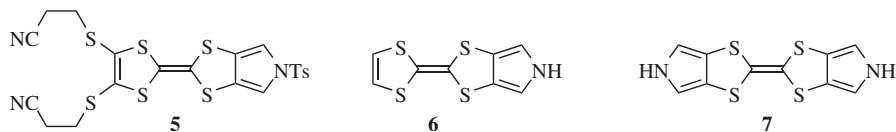


Figure 9.3. Pyrrolo-TTF building blocks 5–7.

Neutral TTF is also a π -strong electron donor; this allows it to form charge-transfer (CT) complexes with electron-deficient molecules such as nitroaromatic explosives. It is this feature that has allowed for the development of TTF-calix[4]pyrrole sensors for nitroaromatic explosives.

9.1.2.1 Pyrrolo-Annulated TTFs TTF has four identical potential attachment sites. This makes the regioselective functionalization of TTF a challenge. In fact, incorporation of TTF into new molecular and supramolecular systems often results in a mixture of *cis* and *trans* isomers. Moreover, separating the two isomeric products is often impossible. On the other hand, the ongoing quest for well-defined molecular and supramolecular materials has provided an incentive to develop new TTF-containing building blocks for which the regiochemical issues associated with substitution are addressed. One of the most successful realizations of this generalized objectives involves the synthesis [15] of pyrrolo-annulated TTFs (Figure 9.3). Derivatives of pyrrolo-TTFs, such as monopyrrolo-TTF (MPTTF) **5** carrying cyanoethyl thiolate and tosyl protecting groups, have proven to be some of the most useful building blocks in TTF chemistry [16].

Because of the fact that sequential and selective deprotecting of the two cyanoethyl and the tosyl protecting groups followed by efficient *S*- and *N*-alkylations can be carried out, the MPTTF unit has been incorporated into several molecular and supramolecular systems, such as electrochemical sensors [17], porphyrins [18], and rotaxanes [19].

9.1.3 MPTTF Macrocycles, Belts, and Cages

Cyclophanes are fundamentally important compounds in many aspects of macrocyclic and supramolecular chemistry, and research in this field has expanded rapidly [20]. Cyclophanes with rigid frameworks, often reflecting the presence of aromatic subunits, and large internal cavities have been frequently exploited to accommodate charged or neutral guest molecules [21]. Incorporation of the redox-active TTF unit into cyclophanes may serve a dual purpose, namely, increasing the host–guest interaction with a complementary electroactive guest and at the same time providing an electrochemical signal for the complexation event; this makes such systems attractive for use in, for example, sensor development [22].

By using MPTTF building block **5**, a TTF belt **12** was prepared in relatively few steps (Scheme 9.2). This was done by linking the two MPTTF units together with glycol chains [23].

TTF belt **12** was designed to recognize the electron acceptor 7,7,8,8-tetracyano-*p*-quinodimethane (TCNQ) and bind it within its central cavity. However, a solid-state X-ray crystal structure analysis (Figure 9.4) of the CT complex revealed that the TCNQ guest is associated outside the center, being located specifically alongside one of the TTF electron donors in the solid state [23].

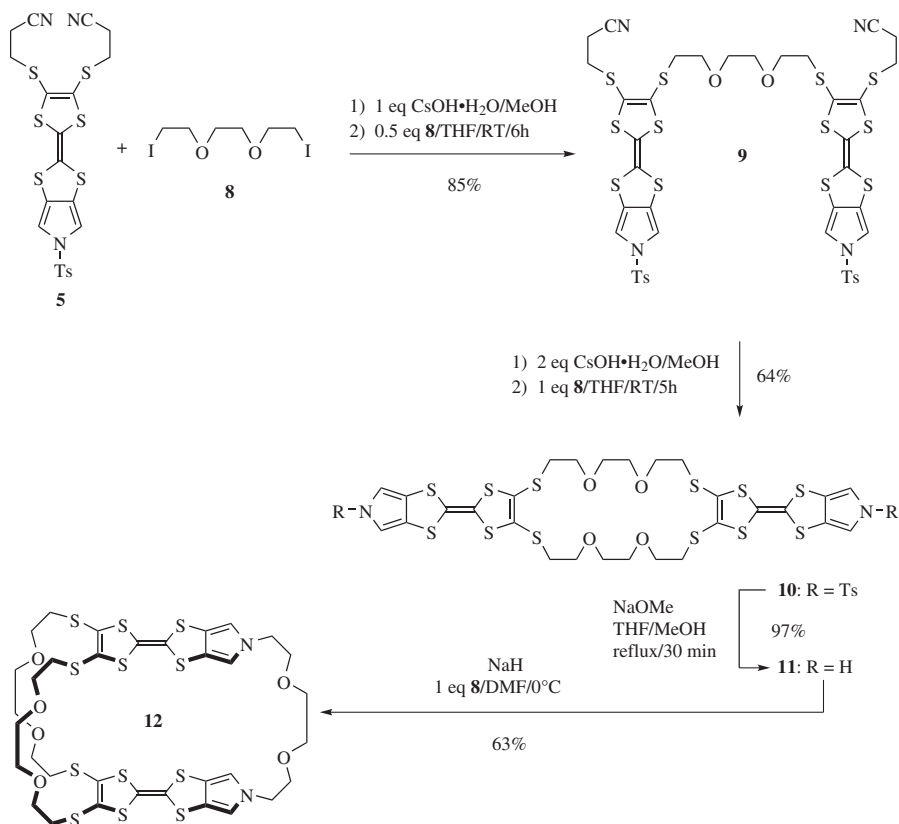
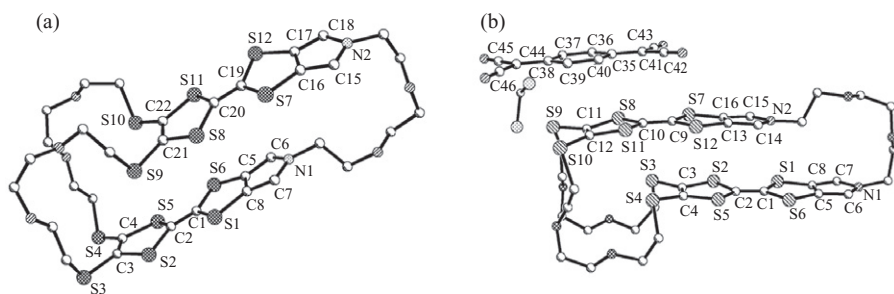
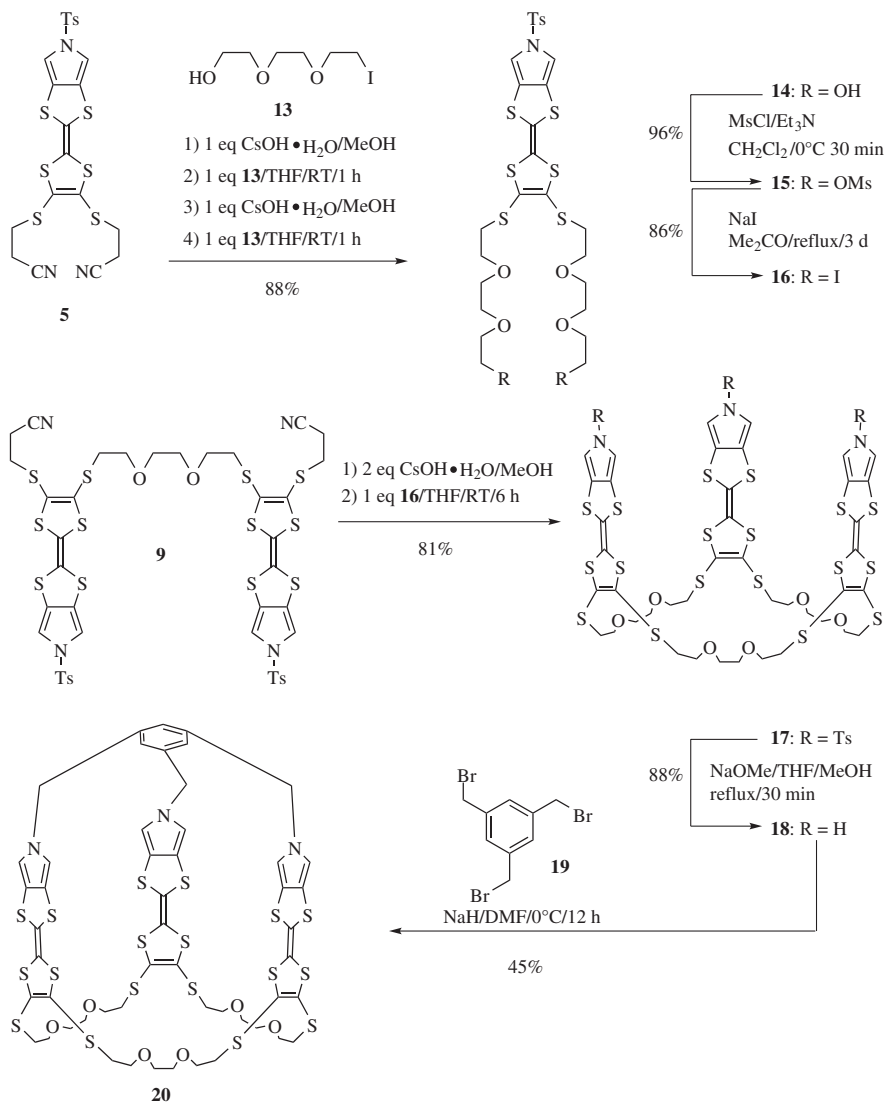
Scheme 9.2. Synthesis of a TTF belt **12**.

Figure 9.4. (a) Single-crystal X-ray structure of the TTF belt **12**. (b) X-ray crystal structure of the CT complex **12**·TCNQ [23]. Hydrogen atoms are omitted for clarity. Source: [23]. Reproduced with permission of the American Chemical Society.



Scheme 9.3. Synthesis of a TTF cage **20**.

By applying the synthetic methodology used for the preparation of TTF belt **12**, the synthesis of a TTF-cage molecule was later accomplished. Specifically, tris-TTF-cage molecule **20** (Scheme 9.3) was prepared [24]. This system was designed to have a larger and more flexible cavity than present in the TTF belt **12**. This, in turn, was expected to increase the likelihood that receptor **20** would be able to accommodate electron-deficient guests inside its cavity.

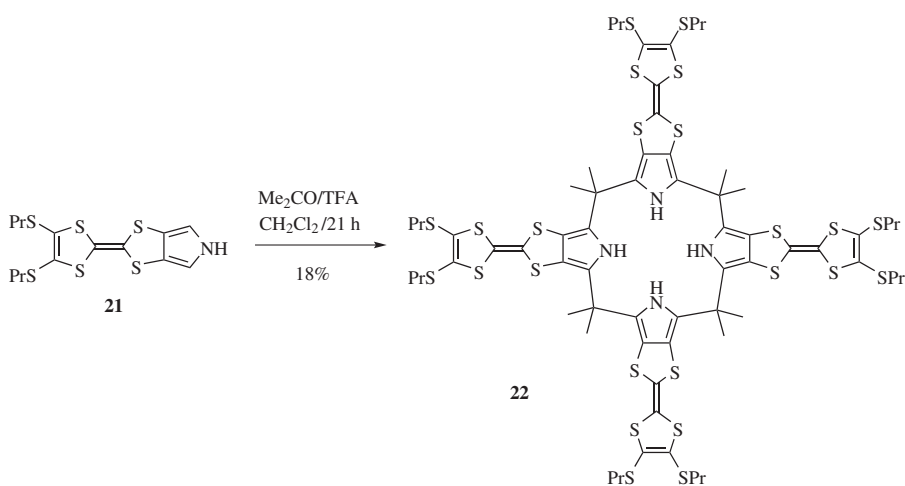
UV-Vis-NIR absorption studies carried out [24] on a mixture of tris-TTF cage **20** and 1,3,5-trinitrobenzene (TNB), chosen as a test explosive, revealed the appearance

of a weak CT band, accompanied by a color change from orange to light green when TNB is added to a CHCl_3 solution of the cage. Unfortunately, in spite of the underlying design expectations and these experimental findings, it proved impossible to determine whether TNB was being captured within the cage or was simply associating with **20** via an outside binding mode [24]. In light of this ambiguity, a dedicated effort was made to design, synthesize, and test functional TTF-based receptors for nitroaromatic explosives, such as TNB.

9.2 SYMMETRIC TETRA-TTF-CALIX[4]PYRROLES

In order to find a receptor suitable for TNB, more rigidity in the receptor design was introduced, since belts and cages such as **12** and **20** seemed to be too flexible to ensure encapsulation of the guest(s) inside their cavities. This led to the design of a new class of MPTTF receptors, namely, tetra-TTF-calix[4]pyrroles. These systems were expected to have a more rigid structure than the TTF belts and TTF cages described above by virtue of the fact that the TTF units are attached directly to the calix[4]pyrrole scaffold. The first tetra-TTF-calix[4]pyrrole, **22** (Scheme 9.4), was reported in 2004 [25]. This system was found to be an effective receptor for neutral electron acceptors, such as TNB, tetrafluoro-*p*-benzoquinone, tetrachloro-*p*-benzoquinone, and *p*-benzoquinone in CH_2Cl_2 solution.

Receptor **22** was designed to be more rigid than the TTF-derived belts and cages, such as **12** and **20**, but still to be sufficiently flexible so as to accommodate substrates, such as TNB. In point of fact, system **22**, like other calix[4]pyrroles, can exist potentially in many conformations including the four limiting conformations designated as 1,3-alternate, partial-cone, 1,2-alternate, and cone (Figure 9.5). As detailed below, it was the 1,3-alternate conformation that proved most effective for TNB binding, whereas little appreciable affinity was observed in the case of the cone conformation.



Scheme 9.4. Synthesis of tetra-TTF-calix[4]pyrrole **22**.

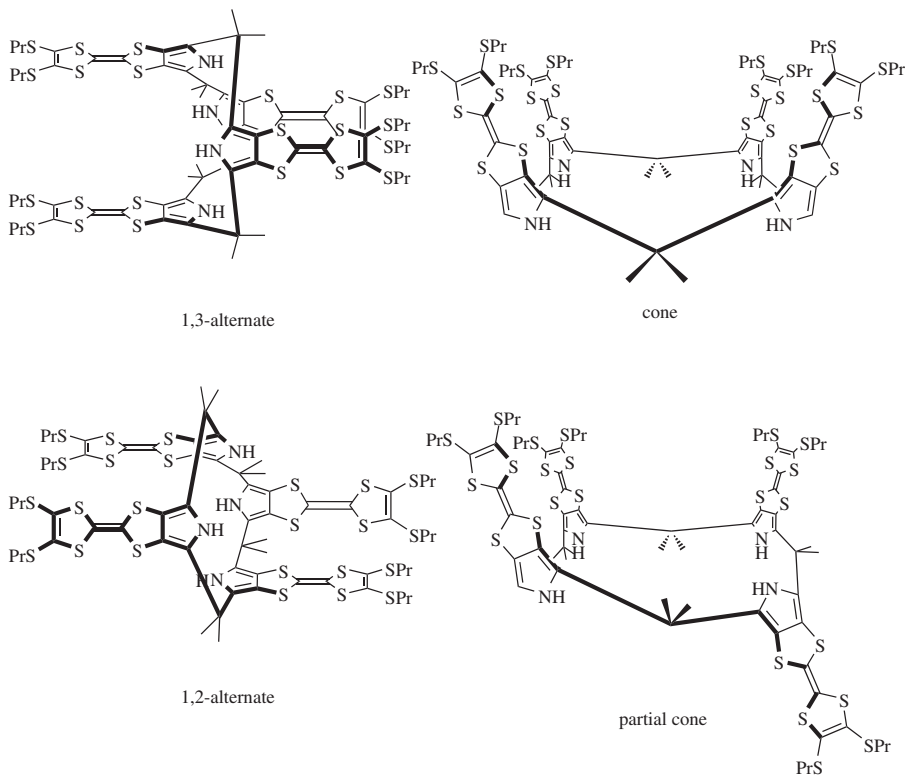


Figure 9.5. The four limiting conformations possible for tetra-TTF-calix[4]pyrrole **22**.

The synthesis (Scheme 9.4) of tetra-TTF-calix[4]pyrrole **22** was carried out in one step from MPTTF **21** [25] by treatment with an excess of trifluoroacetic acid (TFA) in a mixture of CH_2Cl_2 and Me_2CO . This produced tetra-TTF-calix[4]pyrrole as a yellow solid in 18% yield.

Receptor **22** was designed to take advantage of the fact that as a rule calix[4]pyrroles exist preferentially in the 1,3-alternate conformation [26] in the absence of anions. In this conformation, each pair of identical TTF electron donors was expected to hold an electron-deficient guest in a sandwich-like fashion via CT interactions. Additional stabilization was also expected to be provided by the pyrrole-NH protons acting as hydrogen-bond donors.

X-ray crystallography revealed (Figure 9.6) a solid-state structure in which TNB guest molecules were sandwiched between each pair of TTF “arms,” thus forming a 1:2 CT complex [25].

The interactions between the receptor and TNB were studied in CH_2Cl_2 solution using UV-Vis-NIR spectroscopy (Figure 9.7). Neither tetra-TTF-calix[4]pyrrole **22** nor TNB gave rise to any notable visible absorption bands at $\lambda \geq 500$ nm. Addition of 2 equiv of TNB to the yellow solution of **22** resulted in an immediate color change to green and the appearance of a CT absorption band centered at $\lambda = 677$ nm in the

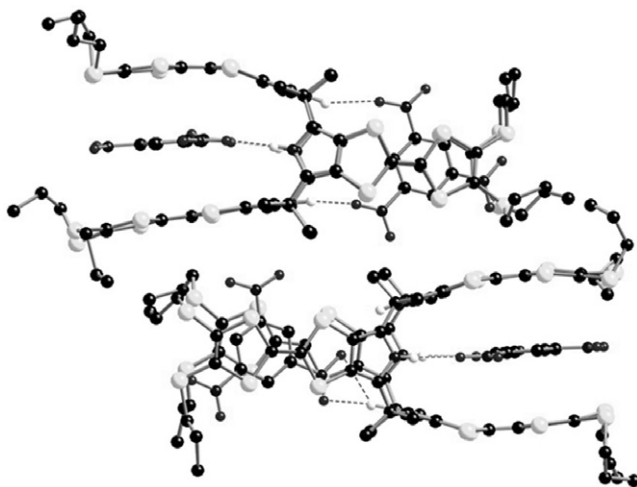


Figure 9.6. View of a single-crystal X-ray structure illustrating the H-bonding interactions (dashed lines) between **22** and TNB in the 1:2 complex. Source: [25]. Reproduced with permission of the American Chemical Society.

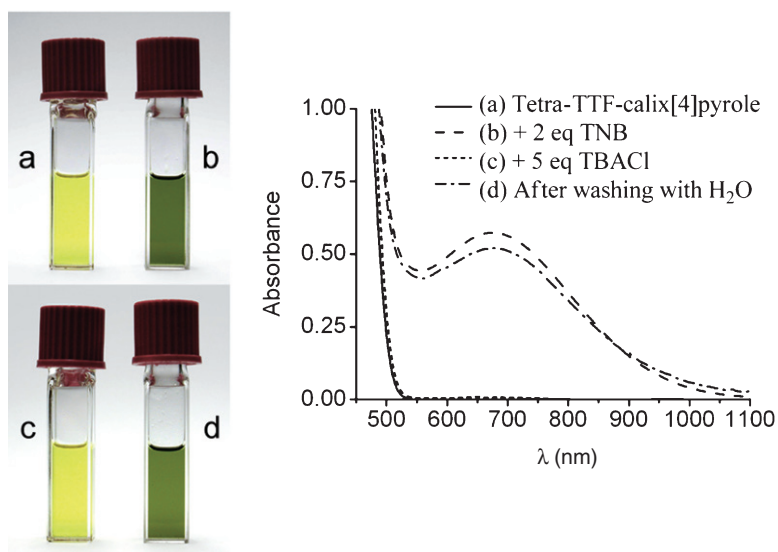


Figure 9.7. Absorption spectra and pictures (CH₂Cl₂, 25°C) of (a) **22** (1.0 mM), (b) **22** + 2 equiv of TNB, (c) **22** + 2 equiv of TNB + 5 equiv of TBACl, and (d) after washing with H₂O. Source: [25]. Reproduced with permission of the American Chemical Society. See color insert.

UV-Vis-NIR spectrum. It was concluded [25] that this latter feature reflects CT interactions between the donor and acceptor units present in **22** and TNB, respectively. The binding constants for the formation of the 1:2 complex between **22** and TNB were found to be 20 and 900 M⁻¹ for K_1 and K_2 , respectively, as determined in CDCl₃ at 298 K [25].

As expected given the anion recognition and inherent conformational “switchable” nature of calix[4]pyrroles, the complex formed between receptor **22** and TNB was found to be unstable in the presence of chloride anions. Addition of 5 equiv of tetrabutylammonium chloride (TBACl) to a CH₂Cl₂ solution containing tetra-TTF-calix[4]pyrrole **22** and TNB induced a color change from green back to yellow and the disappearance of the CT absorption band centered at $\lambda = 677$ nm in the UV-Vis-NIR spectrum. This observation was rationalized by a competition between the chloride anions and the electron-deficient guests for hydrogen-bonding interactions with the NH protons of **22** when chloride anions were added to the solution containing TNB and **22**. However, because of the high binding constant ($K_a = 2.5 \times 10^6$ M⁻¹, CH₂Cl₂, 298 K) [25] between **22** and chloride anions, the equilibrium was largely shifted in favor of the cone conformation. Conversion to this latter form leads to the release of the electron-deficient TNB guests since the cavities present in **22** in its 1,3-alternate conformation are no longer available for binding. Extracting the TBACl salt from the organic CH₂Cl₂ phase by washing with H₂O served to regenerate the CT complex (Figure 9.7d), and as a consequence, the green color of the CH₂Cl₂ solution was reestablished. On the basis of these combined observations, it is inferred that the host–guest complex between tetra-TTF-calix[4]pyrrole **22** and TNB observed in the absence of anions is enhanced by hydrogen-bonding interactions between the NH protons of receptor **22** and the nitro groups present in the TNB guests.

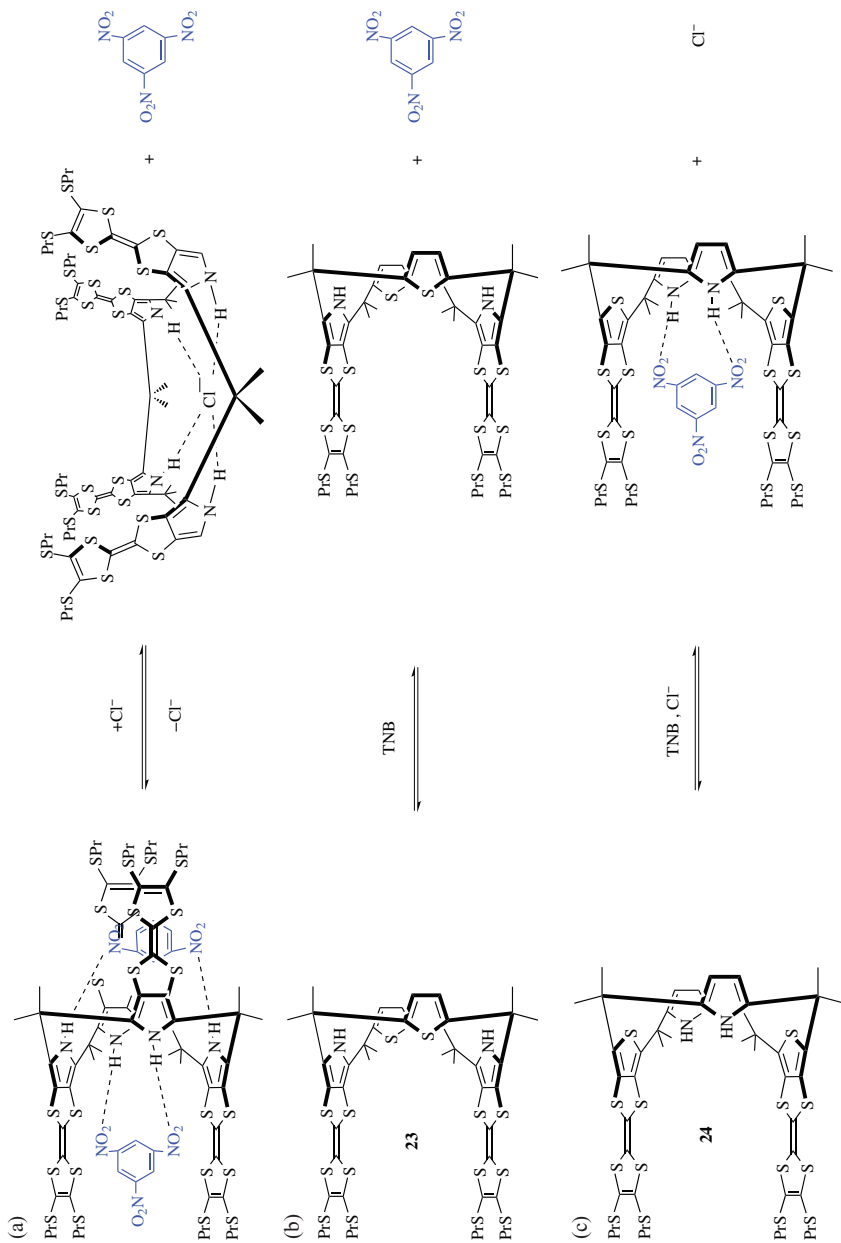
While the release of TNB upon addition of chloride anions is interesting as a molecular switching phenomenon, it, however, limits the use of this system as a chemosensor for explosive materials, since anions are ubiquitous in nature. On the other hand, this limitation provided an incentive to refine further tetra-TTF-calix[4]pyrrole-based nitroaromatic sensing systems.

9.3 ASYMMETRIC TETRA-TTF-CALIX[4]PYRROLES

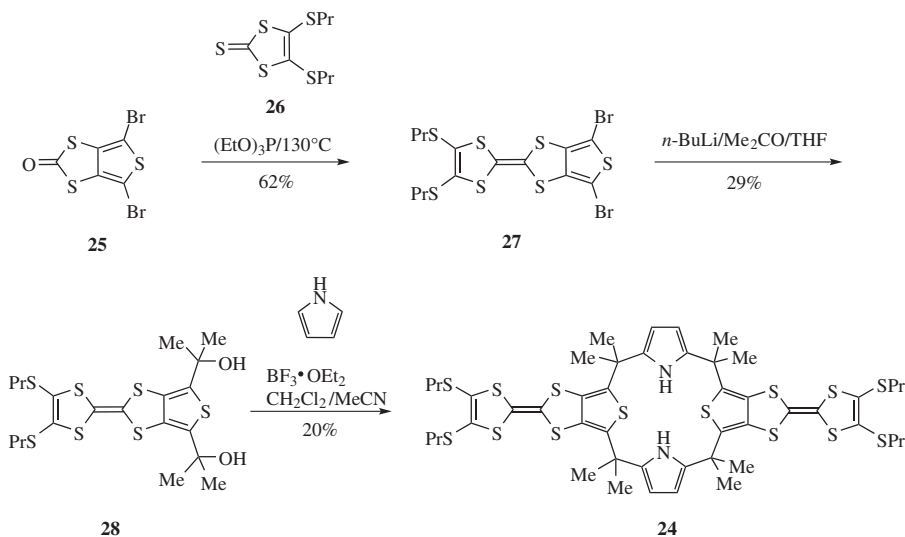
Since the complex between tetra-TTF-calix[4]pyrrole **22** and TNB was found to be unstable in the presence of chloride anions, efforts were made to develop systems that were not plagued by this limitation. These efforts were driven by a rational appreciation of the underlying chemistry.

Anion (X⁻) recognition by calixpyrrole-type receptors is known to be a result of N–H•••X⁻ interactions [8]. These N–H•••X⁻ interactions switch the receptor from the 1,3-alternate conformation, which favors TNB binding, to the corresponding cone conformation, which lack binding sites toward TNB [25, 27].

Based on this knowledge, it was expected that reducing the number of NH units in tetra-TTF-calix[4]pyrrole would serve to overcome the chloride anion recognition problem, producing an anion-insensitive sensor for TNB. This resulted in the design and synthesis of a bis-TTF-calix[2]pyrrole[2]thiophene derivative **23**, where two of the MPTTF units were replaced by thiophene units (Scheme 9.5) [28]. It was found to form a weak 1:1 complex with TCNQ in the solid state. However, it failed to produce any detectable complex with TNB in solution, an observation which was ascribed [28] to



Scheme 9.5. Schematic illustration of (a) change in conformation associated with the addition and removal of chloride anion to a CH₂Cl₂ solution of tetra-TTF-calix[4]pyrrole **22** and TNB. (b) No interaction between receptor **23** and TNB is observed in a CH₂Cl₂ solution. (c) Proposed complexation between receptor **24** and TNB observed in the presence of added chloride anion.



Scheme 9.6. Synthesis of bis-TTF-calix[2]thiophene[2]pyrrole receptor **24**.

removal of potential NH hydrogen-bond donors pointing into the cavity (Scheme 9.5b) defined by the two TTF units in the 1,3-alternate conformation of **23**.

The above findings provided an incentive to design and synthesize the isomeric bis-TTF-calix[2]thiophene[2]pyrrole **24** [29] in which the location of the pyrrole NH and thiophene S atoms are “reversed” in a configurational sense. Receptor **24**, in contrast to **23**, can adopt a 1,3-alternate conformation (Scheme 9.5c) where the two TTF electron-donor subunits are orientated in such a way that they may bind TNB in a sandwich-like fashion via a combination of TTF-derived π - π donor-acceptor interactions and pyrrole-NH-nitro-oxygen hydrogen-bond interactions. These interactions were expected to compete effectively with those involving added chloride anion.

The synthesis of bis-TTF-calix[2]thiophene[2]pyrrole **24** is provided in Scheme 9.6. A phosphite-mediated cross coupling of dithiophene **25** and bispropylthio derivative **26** [29] afforded the annelated thieno-TTF derivative **27** in 62% yield. Treatment of **27** with *n*-BuLi and Me₂CO produced 2,5-bis(1-hydroxymethylethyl)thiopheno-TTF **28** in 29% yield. Stirring a mixture of **28**, pyrrole, and a catalytic amount of Et₂O·BF₃ afforded receptor **24** as a yellow solid in 20% yield.

Initial evidence for the interaction between the receptor and TNB came from X-ray crystallography (Figure 9.8). The structural analysis revealed that the complex formed between **24** and TNB was characterized by the presence of one TNB guest sandwiched between the pair of TTF arms provided by the receptor. In the solid state, the bound TNB guest appears stabilized by π - π donor-acceptor interactions, as well as specific hydrogen-bonding interactions between the oxygen atoms of one of the three TNB nitro groups and the NH protons of the receptor.

The interactions between **24** and the test explosives TNB and picric acid (PA) were studied in CHCl₃ solution using absorption spectroscopy. Addition of 5 equiv of TNB to a solution of receptor **24** resulted in the appearance of a new absorption band cen-

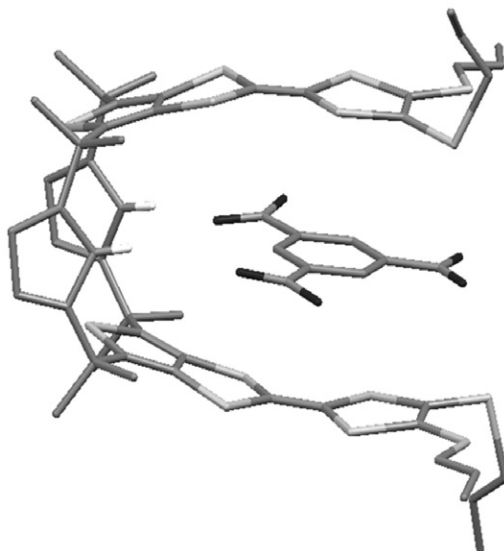


Figure 9.8. View of the solid-state structure of the complex between **24** and TNB derived from single-crystal X-ray diffraction analysis [29]. Hydrogen atoms bound to carbon atoms are omitted for clarity. Source: [29]. Reproduced with permission of Springer Science and Business Media.

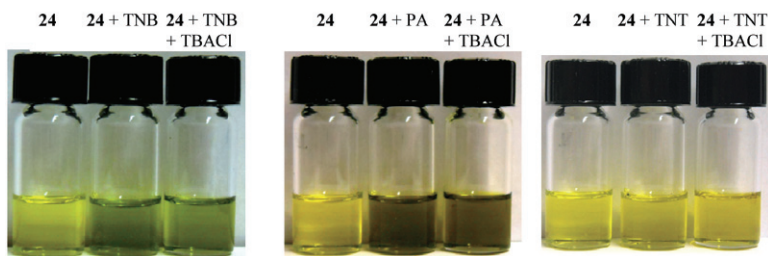


Figure 9.9. Photographs of solutions (CHCl_3 , 298 K) containing 2.5 mM **23** (leftmost vial in each set) in the presence of 5 equiv of various test substrates in the absence (middle vial in each set) and in the presence of 10 equiv of TBACl (rightmost vial in each set). From left to right the substrates in each set of photographs were TNB, PA, and TNT, respectively. Source: [29]. Reproduced with permission of Springer Science and Business Media. See color insert.

tered at $\lambda = 649 \text{ nm}$ ($\epsilon = 72 \text{ M}^{-1} \text{ cm}^{-1}$). It was concluded that this spectral feature and the associated color changes from yellow to green (Figure 9.9) arise from CT interactions between the TTF donor units of **24** and the bound TNB guest. Addition of excess TBACl to a solution of **24** and TNB did not result in a disruption of the CT absorption band centered at $\lambda = 649 \text{ nm}$, nor did this addition serve to change the color of the solution. This lack of interference was completely consistent with the design expectations noted above.

TABLE 9.1. Binding Constant (K_a , M^{-1}) Corresponding to the Interaction between Guests (TNB, PA, and TNT) and Receptors **22 and **24** as Determined by 1H NMR Titrations Carried Out in $CDCl_3$ at 298 K, and between Receptor **22** and TBACl Determined by Isothermal Titration Calorimetry (ITC) in $ClCH_2CH_2Cl$ at 298 K**

	TNB	PA	TNT	TBACl
Receptor 24	3	6	<1	— ^a
Receptor 22	$K_1 = 20$ $K_2 = 900$	$K_1 = 50$ $K_2 = 930$	$K_1 = 25$ $K_2 = 130$	2.5×10^6

NMR, nuclear magnetic resonance.

^aToo small to be determined by 1H NMR titrations.

This insensitivity toward addition of chloride anions was also observed [29] in the case of PA. When receptor **24** was mixed with PA in $CHCl_3$, the color of the solution changed from yellow to dark green. This color change, along with the associated CT band at $\lambda = 746$ nm ($\epsilon = 72$ M^{-1} cm^{-1}), was observed to occur in the presence and absence of excess TBACl. Unfortunately, analogous experiments carried out with 2,4,6-trinitrotoluene (TNT) did not reveal any evidence of binding interactions between **24** and TNT.

Estimation of the binding constants between **24** and the nitroaromatic compounds TNB, PA, and TNT were made using the chemical shift changes for the signal associated with the NH protons upon addition of increasing amounts of the nitroaromatic compound in question to receptor **24** in $CDCl_3$.

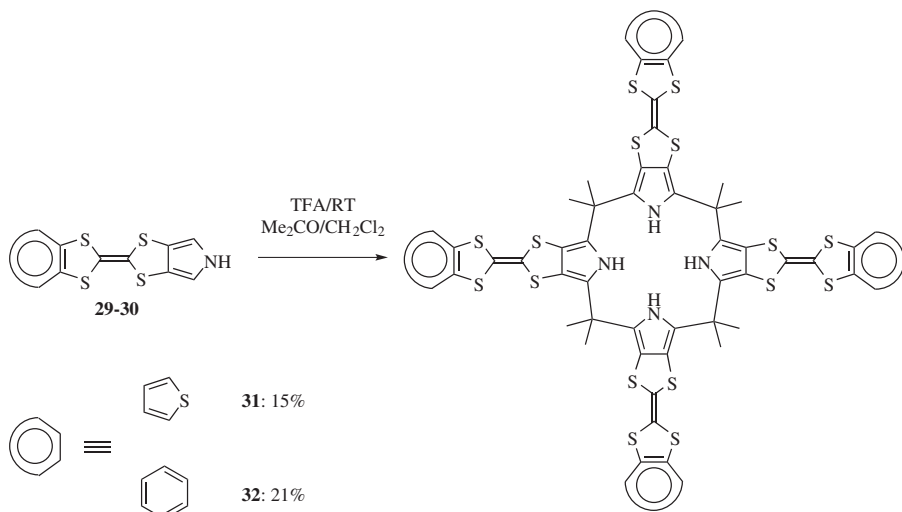
As can be seen from an inspection of Table 9.1, the K_a values for **24** are reduced compared to those for the first binding event in the case of **22**. This observation can be accounted for by the fact that the total number of NH donors and TTF units present in **24** is lower than in **22**.

Although the design and synthesis of **24** as a chloride anion-insensitive colorimetric chemosensor for TNB and PA proved successful, its sensitivity toward the substrates TNB/PA is far too low. Since high sensitivity is crucial for a practical chemosensor, there remained an incentive to prepare a TTF-calixpyrrole receptor with high sensitivity toward nitroaromatic explosives.

9.4 EXTENDED Π -SYSTEMS

As noted above, tetra-TTF-calix[4]pyrrole **22** was found to undergo a fast and easy-to-visualize color change (from yellow to green) when exposed to TNB. However, the receptor is characterized by only modest binding affinity, as well as sensitivity toward choride anion as an interferant. To address issues of sensitivity, the electronics of the system were modified in order to exploit cooperative effects and to increase the sensitivity toward nitroaromatic explosives.

Tetra-TTF-calix[4]pyrroles **31** and **32** (Scheme 9.7) [30] were designed based on the idea that first-generation tetra-TTF-calix[4]pyrrole **22** could be modified through annulation of different aromatic moieties directly onto the TTF subunit. This approach was expected to enlarge and rigidify the TTF walls, making them a better match in



Scheme 9.7. Synthesis of tetra-TTF-calix[4]pyrrole derivatives **31** and **32**.

terms of size and shape for the flat electron-deficient nitroaromatic substrates TNB, PA, and TNT. Specifically, these changes were expected to modulate the electronic properties of the system and provide flat π surfaces that were extended relative to those present in **22**.

As in the case of **22**, the modified tetra-TTF-calix[4]pyrrole **31** and **32** were found [30] to form 1:2 complexes with nitroaromatic explosives. For instance, X-ray crystallographic analysis revealed that **32** forms a sandwich-shaped complex with PA, wherein the electron-deficient guest is captured between the two TTF arms of the calix[4] pyrrole, which is found in the 1,3-alternate conformation (Figure 9.10). In addition, short distances of 3.2809(74)–3.4900(75) Å between the two imaginary planes defined by the electron-rich benzo-TTF-pyrroles and the electron-deficient PA guests were seen. This is consistent with the presence of strong face-to-face π -electron donor–acceptor interactions between receptor **32** and PA. For both PA guests, hydrogen-bond interactions are present between the oxygen atoms of the nitro groups in the 2- and 4-positions and two of the pyrrolic protons provided by tetrabenzo-TTF-calix[4]pyrrole **32**.

The interaction of the three different tetra-TTF-calix[4]pyrroles **22**, **31**, and **32** with the test explosives TNB, PA, and TNT was investigated using UV-Vis-NIR spectrometric titration experiments carried out in CHCl₃ solution. The binding of the guest was easily visualized by following the progressive color change as the nitroaromatic compounds were added to solutions of the receptors. Plots of the associated changes in absorption intensity as a function of TNB, PA, and TNT concentrations were used [30] to estimate the binding constants K_a .

A comparison of first-generation tetra-TTF-calix[4]pyrrole **22** with the two new annulated tetra-TTF-calix[4]pyrroles **31** and **32** revealed a significant enhancement of the binding affinity for all three nitroaromatic compounds in the case of the latter systems, with binding constants as high as $3.7 \times 10^6 \text{ M}^{-2}$ ($K_1 = 640 \text{ M}^{-1}$, $K_2 = 2.0 \times 10^4 \text{ M}^{-1}$)

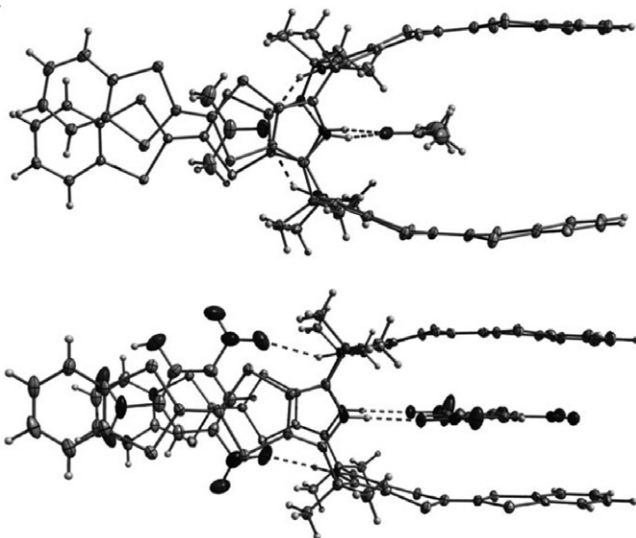


Figure 9.10. X-ray crystal structure of $32 \cdot \text{Me}_2\text{CO}$ (top) and $32 \cdot \text{2PA}$ (bottom) shown with the thermal ellipsoids at 30%. Source: [30]. Reproduced with permission of Wiley-VCH Verlag GmbH & Co. KGaA.

for the $31 \cdot \text{2PA}$ complex being observed. This overall enhancement was ascribed [30] to the larger π surface and more suitable orientation of the receptor surfaces in the case of **31** and **32**.

To test the utility of **22**, **31**, and **32** as possible sensors, 0.1 mM CHCl_3 solutions of each of the receptors were mixed with 0.2 mM aqueous solutions of the three test nitroaromatic explosives. As can be seen from Figure 9.11, this mixing results in an immediate color change, with the actual variations depending on the specific choice of receptor and guest. The observed color changes correspond to the CT interaction observed in the UV-vis-NIR spectra.

The annulated tetra-TTF-calix[4]pyrroles **31** and **32** displayed changes significantly greater than those observed for first-generation tetra-TTF-calix[4]pyrrole **22**. Furthermore, addition of salts (NaHCO_3 , K_2CO_3 , MgSO_4 , CaCl_2 , and NH_4Cl , each at a concentration of 2 mM) to the aqueous phase did not inhibit the colorimetric response.

9.5 SELF-COMPLEXATION AND SWITCHING

The ability of tetra-TTF-calix[4]pyrroles to bind different anions through intermolecular hydrogen-bonding interactions between the four NH protons and the anion in question has been used to create unique intramolecular self-associated systems.

The design, synthesis (Scheme 9.8), and characterization of a nonsymmetric tetra-TTF-calix[4]pyrrole (receptor **37**) bearing an appended phenol moiety were reported in 2011 [31]. This system was used to show how deprotonation/protonation at a “remote”



Figure 9.11. Visual color changes induced by the addition of 2 mL of 0.1 mM solutions of **22**, **31**, and **32** in CHCl_3 to 3 mL of 0.2 mM aqueous solutions of the test nitroaromatic explosives TNB, PA, and TNT in the absence and presence of salts [30]. Here, “salts” refer to a mixture of NaHCO_3 , K_2CO_3 , MgSO_4 , CaCl_2 , and NH_4Cl , 2 mM in each experiment. The contents of the vials from left to right are as follows: (1) pure **22**, (2) **22** + TNB, (3) **22** + TNB + salts, (4) **22** + TNT, (5) **22** + PA, (6) pure **31**, (7) **31** + TNB, (8) **31** + TNB + salts, (9) **31** + TNT, (10) **31** + PA, (11) pure **32**, (12) **32** + TNB, (13) **32** + TNB + salts, (14) **32** + TNT, and (15) **32** + PA. Source: [30]. Reproduced with permission of Wiley-VCH Verlag GmbH & Co. KGaA. See color insert.

site can be utilized to lock/unlock the molecular receptor. Deprotonation of the phenol moiety in calix[4]pyrrole receptor **37** changes its ability to bind guest molecules as a result of a conformational change (Scheme 9.9) induced by a self-complexation event taking place between the phenolate anion “tail” and the calix[4]pyrrole “head” [31]. Since this receptor design allows the calix[4]pyrrole head to bite its own tail (phenolate), it was named as an *ouroboros* (“tail eater” in Greek).

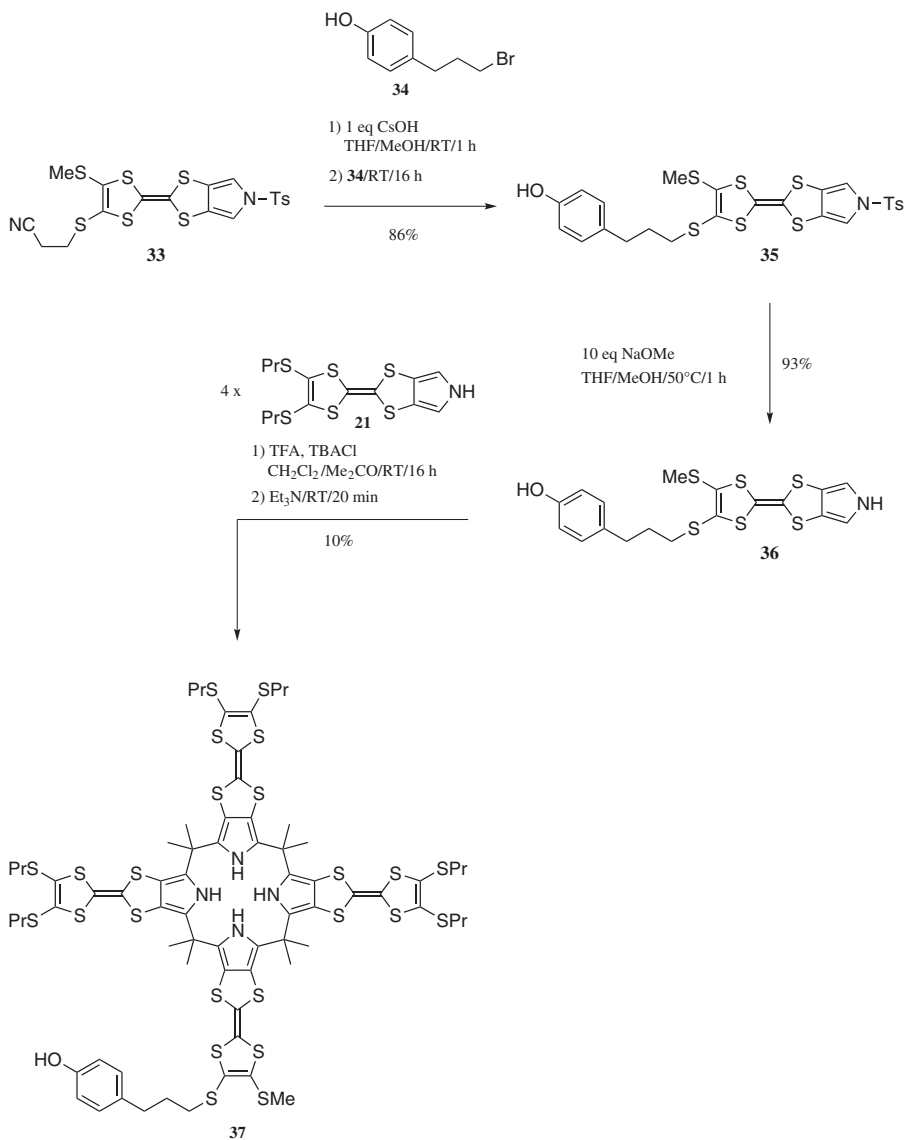
The mechanistic scheme for the proposed locking/unlocking of molecular receptor **37** is shown in Scheme 9.9. In its neutral form, receptor **37** exists predominantly in the 1,3-alternate conformation. This allows electron-deficient guests, such as TNB, to access the two cavities of **37**, which leads to formation of a 2:1 complex. Deprotonation of the phenol moiety leads to the formation of **37⁻**, which undergoes conformational changes, from the 1,3-alternate to the self-complexing conformation **37⁻** with a concomitant release of the two TNB guests. This release takes place since no cavities in self-complexing conformation **37⁻** are available for TNB binding. Finally, protonation of **37⁻** regenerates the neutral 1,3-alternate conformation of the receptor.

Functionalization of **37** with 3,5-dinitrobenzoylchloride produced tetra-TTF-calix[4]pyrrole **38** [32], which was found to undergo self-assembly into a dimeric supramolecular structure (Scheme 9.10).

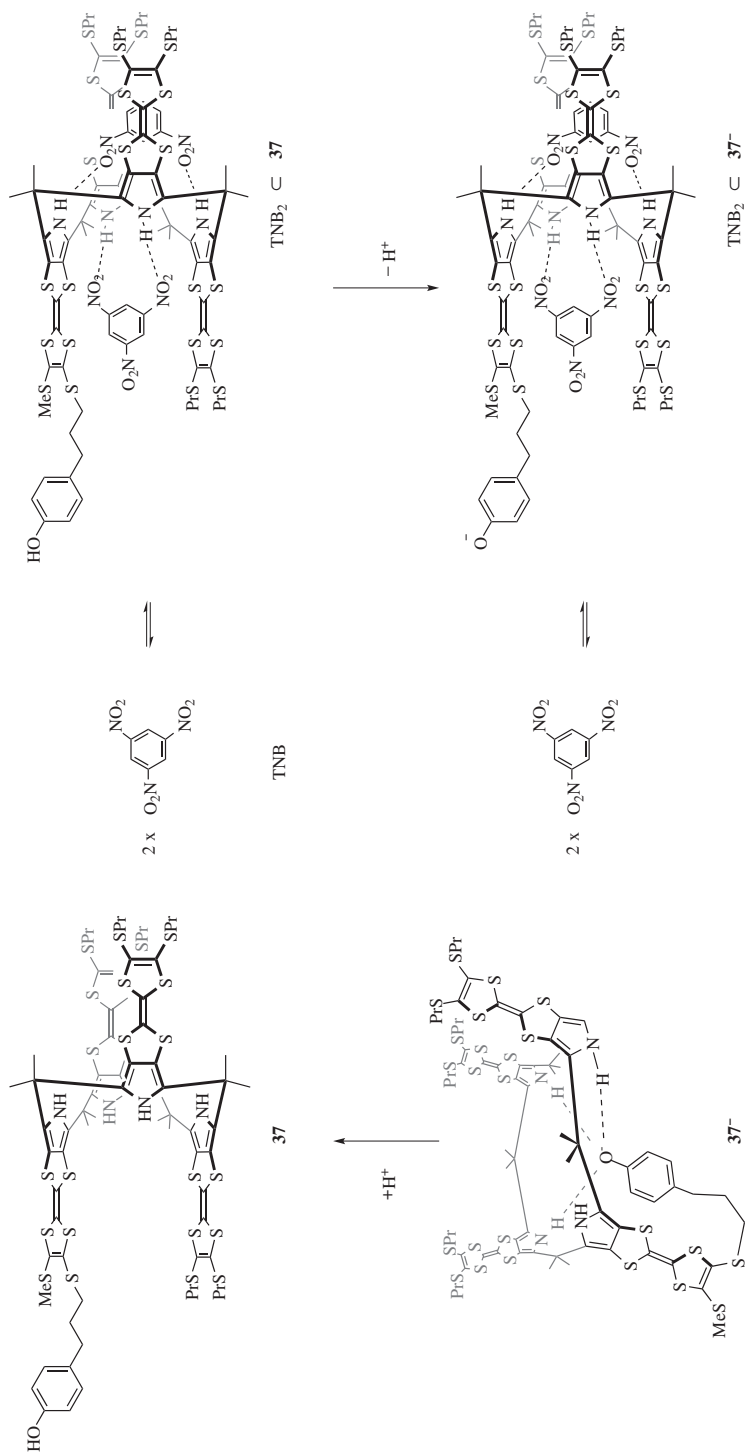
It was concluded [32] that the self-complexation event involving receptor **38** preorganizes the dimeric structure **38•38** in a 1,3-alternate conformation, a form that is more suitable for the accommodation of TNB guests. It was shown [32] that the dimeric receptor **38•38** displays a two-order magnitude higher binding affinity toward TNB as compared to first-generation tetra-TTF-calix[4]pyrrole receptor **22**. Such a finding provides support for the notion that a rationally designed supramolecular approach can be used to increase the sensitivity of TTF-calix[4]pyrrole-based receptors.

9.6 TOWARD A POTENTIAL APPLICATION

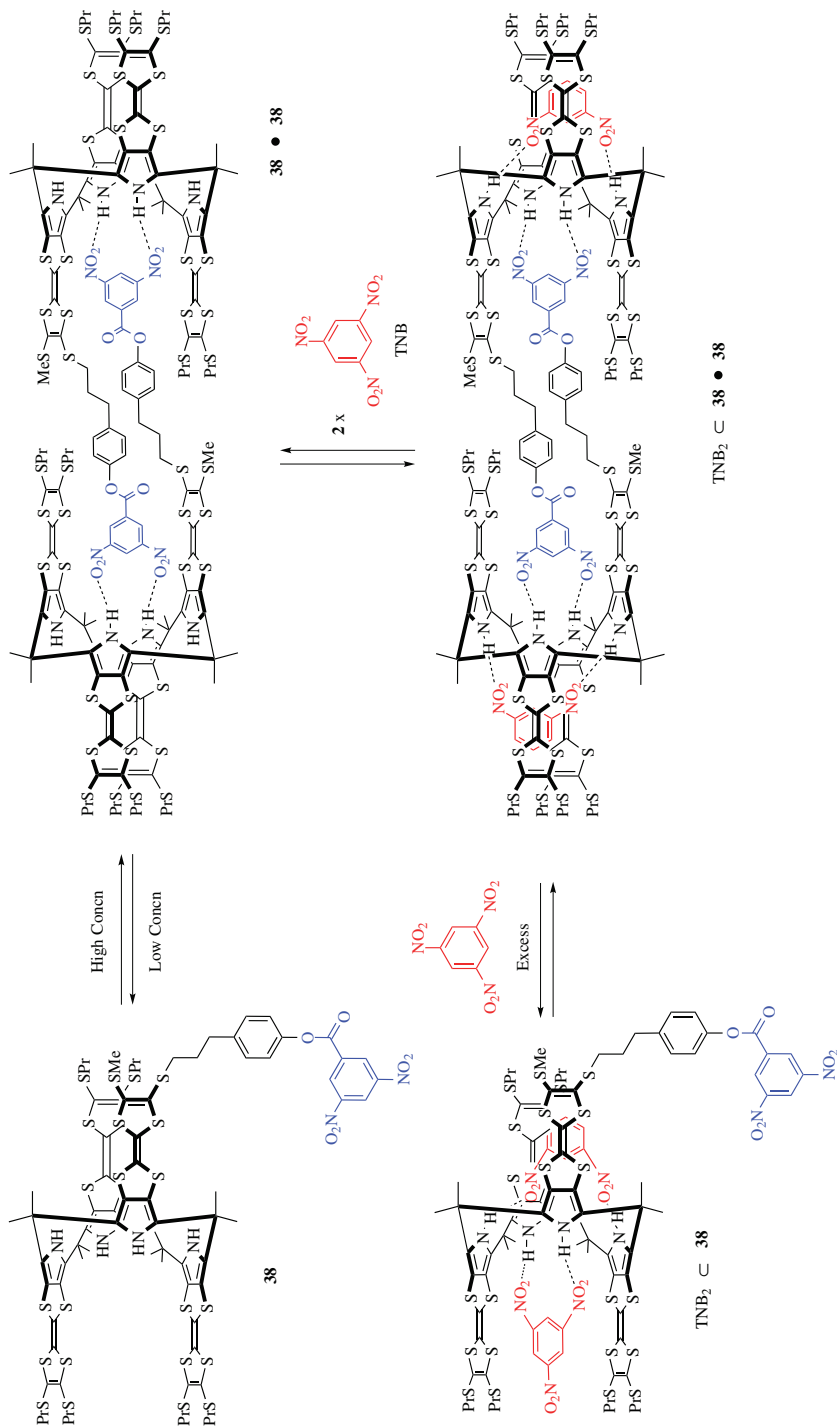
Investigations of the different tetra-TTF-calix[4]pyrroles presented so far in this chapter have all been carried out in solution. From a practical perspective, the sensing



Scheme 9.8. Synthesis of receptor 37.



Scheme 9.9. Mechanistic scheme for the acid/base controlled conformational locking and unlocking of molecular receptor **37**. These changes allow for the decomplexation and complexation of TNB guests.



Scheme 9.10. Schematic illustration of dimeric ensemble **38•38** and its subsequent monomerization following complexation with TNB.

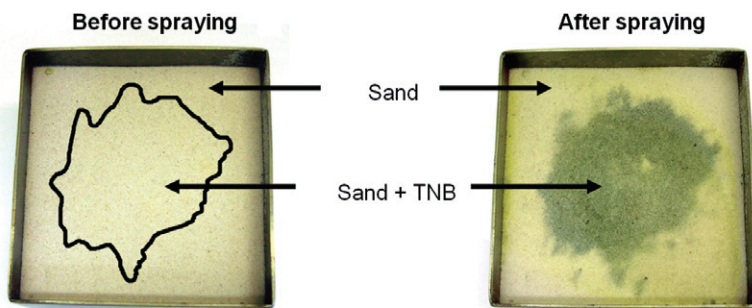
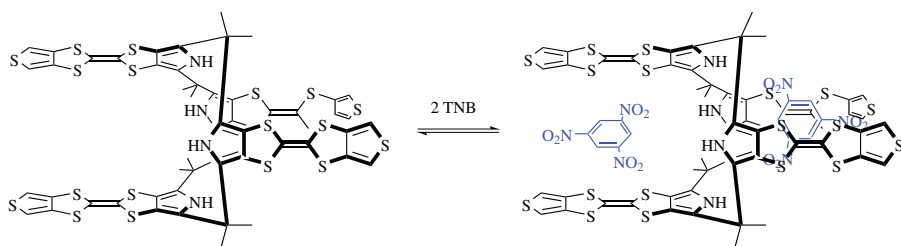


Figure 9.12. Detection of TNB in the solid state. A sand sample containing TNB in a defined area (inside the area defined by the black line). Upon spraying an aerosol of tetra-TTF-calix[4]pyrrole **22** the sand turns green as a result of the interaction between **22** and TNB [33].



Scheme 9.11. Molecular structure of tetra-TTF-calix[4]pyrrole **31** and its TNB binding mode observed in organic solvents.

event needs to take place in either the solid state or in the gas phase. Many nitroaromatic explosives have a rather high vapor pressure and thus can be spotted by analyzing the surrounding air. Water supplies might also be contaminated by explosives. Therefore, in order to ensure water quality and to spot land mines, the underground water is often tested for traces of explosives. It has been demonstrated (Figure 9.12) that tetra-TTF-calix[4]pyrrole **22** can be used to detect TNB in a layer of sand [33].

The sample of sand contains TNB in a defined area. Tetra-TTF-calix[4]pyrrole **22** in a CHCl_3 solution was sprayed on to the sand using a simple paint spray, which resulted (Figure 9.12, right) in the appearance of a green color in the TNB-containing sand area. These results were taken as evidence that tetra-TTF-calix[4]pyrrole **22** can be used to detect TNB in the solid state.

While the above results are promising, there are situations, such as the testing of passengers and luggage at airports, where spray-based applications are not viable. Economics of scale likely makes this true in the case of land mines. Therefore, in order to obtain a more viable sensing system, tetra-TTF-calix[4]pyrrole **31** (Scheme 9.11) was incorporated into cantilever devices.

Cantilever-based sensors are well established in the area of trace chemicals detection, including the area of explosives detection [34]. In 2011, a cantilever sensor incorporating tetra-TTF-calix[4]pyrrole **31** was reported [35]. The resulting device was found

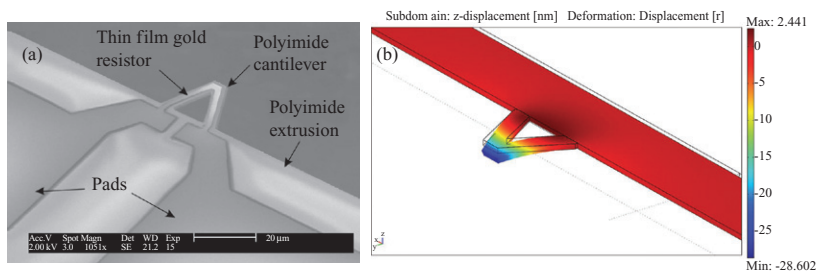


Figure 9.13. (a) Scanning electron microscopy image of the polyimide cantilever. (b) FEM simulation of the surface stress of cantilever. Source: [35]. Reproduced with permission of the American Institute of Physics. See color insert.

capable of detecting TNB in the vapor phase via a process that involves a change in the surface stress of the cantilever.

The V-shape polyimide cantilever used to generate this sensing device (Figure 9.13) contains an ultrathin film gold sensor integrated within the top of the cantilever. The resulting cantilever can be used to measure very small deflections. However, in the absence of a specific receptor, the response is not strong. On the other hand, by applying receptor **31** onto the cantilever surface the signal is enhanced, rendering the cantilever technique potentially viable for the purposes of nitroaromatic explosive detection.

The system was tested using a mixture of TNB vapor in 99% pure nitrogen. The saturated vapor employed contains TNB at 6.44×10^{-6} Torr and 298 K. Figure 9.14b shows the response of the cantilever when a 20 mL TNB gas mixture is slowly injected in the chamber, which contains the cantilever. Additional experiments showed that the system did not respond to air or acetone-saturated vapors. The results showed an improvement in the detection limit of 30-fold compared to the achievable level when tetra-TTF-calix[4]pyrrole **31** is used as a bulk receptor in organic solution.

Very recently, the single-cantilever-based tetra-TTF-calix[4]pyrrole technology has been expanded to include (Figure 9.15) a series of cantilever receptors (up to 27) working simultaneously [36]. In explosive detection high reliability is needed and thus a statistical measurement approach has considerable advantages. With the above considerations and results in mind, a DVD-based readout system capable of generating large sets of cantilever data for vapor- and liquid-phase detection of 2,4-dinitrotoluene (DNT) was developed (Figure 9.15). Gold-coated cantilevers were initially functionalized with tetra-TTF-calix[4]pyrrole **22**, a system that is known to bind TNB and TNT (*vide supra*). The results from these experiments provided evidence that the system also responds to DNT. The binding of DNT on the chemically treated surfaces resulted in a bending of the cantilever and in a decrease in its resonant frequency.

The experiments showed good reproducibility of the results, where over 80% of the independent cantilevers showed the same bending behavior, when monitored under the same conditions in different experimental batches. The DVD-ROM-based sensing system proved to be able to generate large data sets and to be compatible with both dry- and wet-phase experimentation.

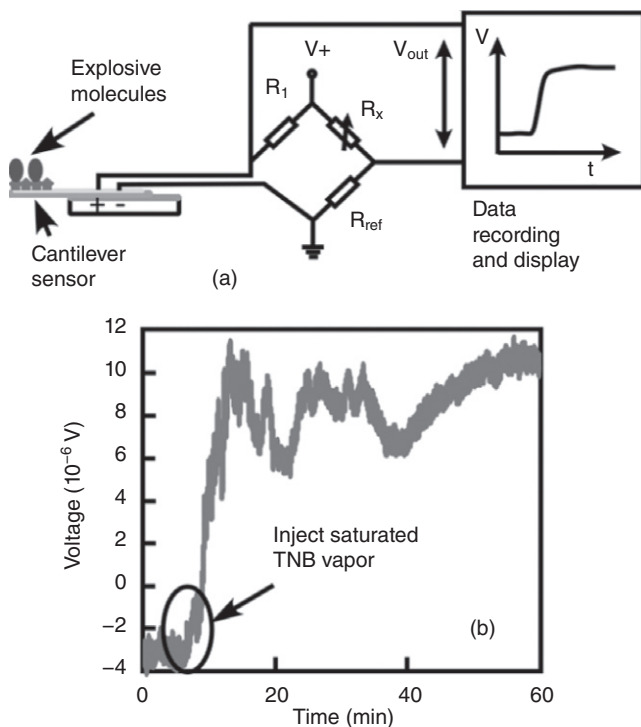


Figure 9.14. (a) Schematic diagram of the experimental cantilever-based detection setup, which includes a Wheatstone bridge circuit with a reference and a detection cantilever. (b) Graph of the response of the V-shape polyimide cantilever when exposed to TNB. The vertical axis corresponds to the normalized values of the change in resistance of the sensing element and the horizontal axis represents time in minutes. Source: [35]. Reproduced with permission of the American Institute of Physics.

9.7 CONCLUSIONS AND OUTLOOK

Almost ten years ago the first TTF-calixpyrroles were reported. They displayed promise for nitroaromatic sensing, with substantial improvements having been made in the intervening years. In this chapter, we have shown that careful design can produce chemosensors with unique properties, and that small changes can have a big impact on both sensitivity and selectivity of the TTF-calixpyrroles toward nitroaromatic explosives and anions. Although much more research is required before TTF-calixpyrroles can be used as practical chemosensors for nitroaromatic explosives, it has already been demonstrated that TTF-calixpyrroles can be integrated into different solid-state devices, an advance that allows for the detection event to be monitored using a nonoptical readout. These recent findings provide support for the notion that in the not-too-distant future the receptor systems described in this chapter will emerge as a viable approach to nitroaromatic explosive detection.

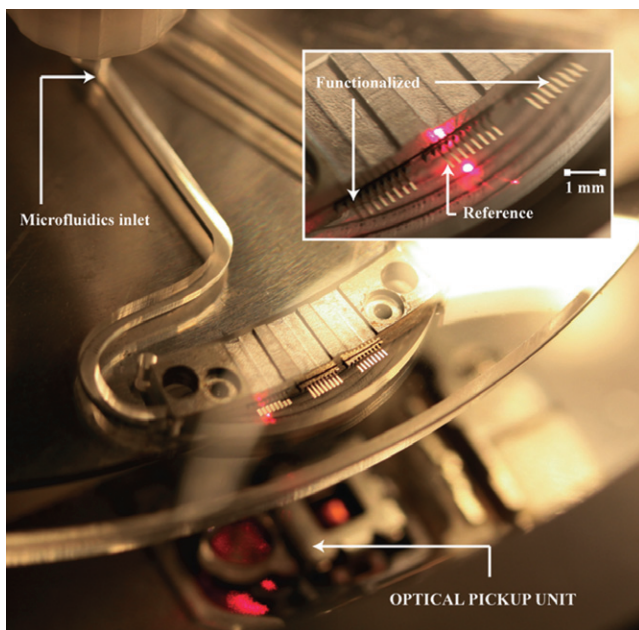


Figure 9.15. Photograph of rotating CD-like platform aligned above DVD-ROM readout optics. The inset shows a close-up of stainless steel holder with two functionalized cantilever chips (16 cantilevers) and one reference chip (8 cantilevers). Source: [36]. Reproduced with permission of Elsevier.

REFERENCES

- [1] Lehn, J.-M. *Supramolecular Chemistry*, VCH, Weinheim, 1995.
- [2] Beer, P. D., Gale, P. A. (2001). Anion recognition and sensing: The state of the art and future perspectives. *Angewandte Chemie (International ed. in English)*, 40, 486–516.
- [3] Baeyer, A. (1886). Ueber ein condensationsproduct von pyrrol mit acetone. *Berichte der Deutschen Chemischen Gesellschaft*, 19, 2184–2185.
- [4] Chelintzev, V. V., Tronov, B. V. (1916). Process of condensation of pyrrole with acetone. Constitution of the resulting products. *Zhurnal Russkago Fiziko-Khimicheskago Obshchestva*, 48, 105–155.
- [5] Rothmund, P., Gage, C. L. (1955). Concerning the structure of “acetonepyrrole”. *Journal of the American Chemical Society*, 77, 3340–3342.
- [6] (a) Dietrich, B., Viout, P., Lehn, J. M. Tetraheterocyclic Compounds Similar to Phorphyrins. In *Macrocyclic Chemistry*, Dietrich, B., Viout, P., Lehn, J. M. (Eds.), VCH, Weinheim, 1993 pp. 82
- [7] Floriani, C., Floriani-Moro, R. (2000). Metalation and metal-assisted modifications of the porphyrinogen skeleton using meso-octaalkylporphyrinogen. *Porphyrin Handbook*, 3, 385–403.
- [8] Gale, P. A., Sessler, J. L., Král, V., Lynch, V. (1996). Calix[4]pyrroles: Old yet new anion-binding agents. *Journal of the American Chemical Society*, 118, 5140–5141.
- [9] Gale, P. A., Sessler, J. L., Kral, V., Lynch, V. (1998). Calixpyrroles. *Chemical Communications*, 1–8.

- [10] (a) Schukat, G., Fanghänel, E. (1996). Synthesis, reactions, and selected physico-chemical properties of 1,3- and 1,2-tetrachalcogenafulvalenes. *Sulfur Reports*, 18, 1–294; (b) Bryce, M. R. (2000). Functionalised tetrathiafulvalenes. New applications as versatile π -electron systems in materials chemistry. *Journal of Materials Chemistry*, 10, 589–598; (c) Nielsen, M. B., Lomholt, C., Becher, J. (2000). Tetrathiafulvalenes as building blocks in supramolecular chemistry II. *Chemical Society Reviews*, 29, 153–164; (d) Segura, J. L., Martín, N. (2001). New concepts in tetrathiafulvalene chemistry. *Angewandte Chemie (International ed. in English)*, 40, 1372–1409; (e) Inagi, S., Naka, K., Chujo, Y. (2007). Functional polymers based on electron-donating TTF and derivatives. *Journal of Materials Chemistry*, 17, 4122–4135; (f) Martín, N., Sánchez, L., Herranz, M. Á., Illescas, B., Guldi, D. M. (2007). Electronic communication in tetrathiafulvalene (TTF)/C60 systems: Toward molecular solar energy conversion materials? *Accounts of Chemical Research*, 40, 1015–1024; (g) Lorcy, D., Bellec, N., Fourmigué, M., Avarvari, N. (2009). Tetrathiafulvalene-based group XV ligands: Synthesis, coordination chemistry and radical cation salts. *Coordination Chemistry Reviews*, 253, 1398–1438.
- [11] (a) Simonsen, K. B., Becher, J. (1997). Tetrathiafulvalene thiolates: Important synthetic building blocks for macrocyclic and supramolecular chemistry. *Synlett: Accounts and Rapid Communications in Synthetic Organic Chemistry*, 1211–1220; (b) Jeppesen, J. O., Nielsen, M. B., Becher, J. (2004). Tetrathiafulvalene cyclophanes and cage molecules. *Chemical Reviews*, 104, 5115–5132.
- [12] (a) Perkins, J., Collier, P. C., Heath, J. R., Jeppesen, J. O., Luo, Y., Nielsen, K. A., Pease, A. R., Stoddart, J. F., Wong, E. W. (2001). Toward artificial molecular devices. *Molecular Electronics and Bioelectronics*, 12, 69–74; (b) Li, Z.-T., Stein, P. C., Becher, J., Jensen, D., Mørk, P., Svenstrup, N. (1996). Self-assembling tetrathiafulvalene-based rotaxanes and catenanes. *Chemistry—A European Journal*, 2, 624–633; (c) Asakawa, M., Ashton, P. R., Balzani, V., Credi, A., Hamers, C., Mattersteig, G., Montalti, M., Shipway, A. N., Spencer, N., Stoddart, J. F., Tolley, M. S., Venturi, M., White, A. J. P., Williams, D. J. (1998). A chemically and electrochemically switchable [2]catenane incorporating a tetrathiafulvalene unit. *Angewandte Chemie (International ed. in English)*, 37, 333–337; (d) Jeppesen, J. O., Perkins, J., Becher, J., Stoddart, J. F. (2001). Slow shuttling in an amphiphilic bistable [2]rotaxane incorporating a tetrathiafulvalene unit. *Angewandte Chemie (International ed. in English)*, 40, 1216–1221; (e) Wang, C., Olson, M. A., Fang, L., Benítez, D., Tkatchouk, E., Basu, S., Basuray, A. N., Zhang, D., Zhu, D., Goddard, W. A., Stoddart, J. F. (2010). Isolation by crystallization of translational isomers of a bistable donor-acceptor [2]catenane. *Proceedings of the National Academy of Sciences U.S.A.*, 107, 13991–13996.
- [13] (a) Frenzel, S., Arndt, S., Gregorious, R. M., Müllen, K. (1995). Synthesis of tetrathiafulvalene polymers. *Journal of Materials Chemistry*, 5, 1529–1537; (b) Kanibolotsky, A. L., Forgie, J. C., Gordeyev, S., Vilela, F., Skabara, P. J., Lohr, J. E., Petersen, B. M., Jeppesen, J. O. (2008). The introduction of pyrrolotetrathiafulvalene into conjugated architectures: Synthesis and electronic properties. *Macromolecular Rapid Communications*, 29, 1226–1230.
- [14] Canevet, D., Salle, M., Zhang, G., Zhang, D., Zhu, D. (2009). Tetrathiafulvalene (TTF) derivatives: Key building-blocks for switchable processes. *Chemical Communications*, 2245–2269.
- [15] (a) Jeppesen, J. O., Takimiya, K., Jensen, F., Becher, J. (1999). Pyrrolo annelated tetrathiafulvalenes: The parent systems. *Organic Letters*, 1, 1291–1294; (b) Jeppesen, J. O., Takimiya, K., Jensen, F., Brimert, T., Nielsen, K., Thorup, N., Becher, J. (2000). Pyrrolo-annelated tetrathiafulvalenes: The parent systems. *The Journal of Organic Chemistry*, 65, 5794–5805.
- [16] (a) Jeppesen, J. O., Becher, J. (2003). Pyrrolo-tetrathiafulvalenes and their applications in molecular and supramolecular chemistry. *European Journal of Organic Chemistry*, 3245–3266; (b) Gopee, H., Nielsen, K. A., Jeppesen, J. O. (2005). Complete sequential functionalization of monopyrrolotetrathiafulvalenes. *Synthesis*, 1251–1260.
- [17] Trippé, G., Levillain, E., Le Derf, F., Gorgues, A., Sallé, M., Jeppesen, J. O., Nielsen, K., Becher, J. (2002). Electrochemical recognition of cations by bis(pyrrolo)tetrathiafulvalene macrocycles. *Organic Letters*, 4, 2461–2464.

- [18] Li, H., Jeppesen, J. O., Levillain, E., Becher, J. (2003). A mono-TTF-annulated porphyrin as a fluorescence switch. *Chemical Communications*, 846–847.
- [19] Collier, C. P., Jeppesen, J. O., Luo, Y., Perkins, J., Wong, E. W., Hearsh, J. R., Stoddart, J. F. (2001). *Journal of the American Chemical Society*, 123, 12632–12641.
- [20] (a) Keehn, P. M., Rosenfeld, S. M. (Eds.). *Cyclophanes I, Topics in Current Chemistry*, Vol. 113, Springer, Berlin, 1983; pp. 1–357; (b) Kehn, P. M., Rosenfeld, S. T. (Eds.). *Cyclophanes II, Topics in Current Chemistry*, Vol. 115, Springer, Berlin, 1983; pp. 359–725; (c) Diederich, F. In *Cyclophanes, Monographs in Supramolecular Chemistry*, Stoddart, J. F. (Ed.), The Royal Society of Chemistry, London, 1991.
- [21] Seel, C., Vögtle, F. (1992). Molecules with large cavities in supramolecular chemistry. *Angewandte Chemie (International ed. in English)*, 31, 528–549.
- [22] Boulas, P. L., Gómez-Kaifer, M., Echegoyen, L. (1998). Electrochemistry of Supramolecular Systems. *Angewandte Chemie (International ed. in English)*, 37, 216–247.
- [23] Nielsen, K., Jeppesen, J. O., Thorup, N., Becher, J. (2002). A pyrrolo-tetrathiafulvalene belt and its TCNQ complex: Syntheses and X-ray crystal structures. *Organic Letters*, 4, 1327–1330.
- [24] Nielsen, K. A., Jeppesen, J. O., Levillain, E., Thorup, N., Becher, J. (2002). A pyrrolo-tetrathiafulvalene cage: Synthesis and X-ray crystal structure. *Organic Letters*, 4, 4189–4192.
- [25] Nielsen, K. A., Cho, W. S., Jeppesen, J. O., Lynch, V. M., Becher, J., Sessler, J. L. (2004). Tetra-TTF calix[4]pyrrole: A rationally designed receptor for electron-deficient neutral guests. *Journal of the American Chemical Society*, 126, 16296–16297.
- [26] (a) Pichierri, F. (2008). Effect of fluorine substitution in calix[4]pyrrole: A DFT study. *Journal of Molecular Structure: THEOCHEM*, 870, 36–42; (b) Hong, J., Son, M., Ham, S. (2009). Computational study on the conformational characteristics of calix[4]pyrrole derivatives. *Bulletin of the Korean Chemical Society*, 30, 423–428; (c) Blas, J. R., Marquez, M., Sessler, J. L., Luque, F. J., Orozco, M. (2002). Theoretical study of anion binding to calix[4]pyrrole: The effects of solvent, fluorine substitution, cosolute, and water traces. *Journal of the American Chemical Society*, 124, 12796–12805.
- [27] Nielsen, K. A., Cho, W.-S., Lyskawa, J., Levillain, E., Lynch, V. M., Sessler, J. L., Jeppesen, J. O. (2006). Tetrathiafulvalene-calix[4]pyrroles: Synthesis, anion binding, and electrochemical properties. *Journal of the American Chemical Society*, 128, 2444–2451.
- [28] Poulsen, T., Nielsen, K. A., Bond, A. D., Jeppesen, J. O. (2007). Bis(tetrathiafulvalene)-calix[2]pyrrole[2]-thiophene and its complexation with TCNQ. *Organic Letters*, 9, 5485–5488.
- [29] Dae-Sik, K., Lynch, V. M., Nielsen, K. A., Johnsen, C., Jeppesen, J. O., Sessler, J. L. (2009). A chloride-anion insensitive colorimetric chemosensor for trinitrobenzene and picric acid. *Analytical & Bioanalytical Chemistry*, 395, 393–400.
- [30] Park, J. S., Le Derf, F., Bejger, C. M., Lynch, V. M., Sessler, J. L., Nielsen, K. A., Johnsen, C., Jeppesen, J. O. (2010). Positive homotropic allosteric receptors for neutral guests: Annulated tetrathiafulvalene-calix[4]pyrroles as colorimetric chemosensors for nitroaromatic explosives. *Chemistry—A European Journal*, 16, 848–854.
- [31] Nielsen, K. A., Bähring, S., Jeppesen, J. O. (2011). Acid/base controllable molecular recognition. *Chemistry—A European Journal*, 17, 11001–11007.
- [32] Nielsen, K. A., Stein, P. C. (2011). Self-assembly of dimeric tetrathiafulvalene-calix[4]pyrrole: Receptor for 1,3,5-trinitrobenzene. *Organic Letters*, 13, 6176–6179.
- [33] Jeppesen, J. O., Nielsen, K. A. (2006) Explosives detection markers US Patent 8378093.
- [34] (a) Pinnaduwege, L. A., Hai-Feng, J., Thundat, T. (2005). Moore's law in homeland defense: An integrated sensor platform based on silicon microcantilevers. *Sensors Journal, IEEE*, 5, 774–785; (b) Li, M., Tang, H. X., Roukes, M. L. (2007). Ultra-sensitive NEMS-based cantilevers for sensing, scanned probe and very high-frequency applications. *Nature Nanotechnol-*

- ogy, 2, 114–120; (c) Berger, R., Delamarche, E. (1997). Surface stress in the self-assembly of alkanethiols on gold. *Science*, 276, 2021–2024; (d) Fritz, J., Baller, M. K., Lang, H. P., Rothuizen, H., Vettiger, P., Meyer, E., Guntherodt, H. J., Gerber, C., Gimzewski, J. K. (2000). Translating biomolecular recognition into nanomechanics. *Science*, 288, 316–318; (e) Moulin, A. M., O’Shea, S. J., Welland, M. E. (2000). Microcantilever-based biosensors. *Ultramicroscopy*, 82, 23–31.
- [35] Zhu, W., Park, J. S., Sessler, J. L., Gaitas, A. (2011). A colorimetric receptor combined with a microcantilever sensor for explosive vapor detection. *Applied Physics Letters*, 98, 123501–123503.
- [36] Bosco, F. G., Bache, M., Hwu, E. T., Chen, C. H., Andersen, S. S., Nielsen, K. A., Keller, S. S., Jeppesen, J. O., Hwang, I. S., Boisen, A. (2012). Statistical analysis of DNT detection using chemically functionalized microcantilever arrays. *Sensors and Actuators. B, Chemical*, 171–172, 1054–1059.

CHAPTER 10

RECOGNITION OF CARBOHYDRATES

MARTINA CACCIARINI

10.1 INTRODUCTION

Starting a new research field is always a big challenge. Collection of both the literature published “up to now” on the subject and the methods employed to investigate it are the most demanding issues. When I first became interested in molecular recognition of carbohydrates it was 2002, at which point a lot of research had been already done on this topic and excellently described by the review of Davis and Wareham in 1999 [1]. Later on, advances in the field have been reported focusing on different aspects of the problem: some of more general and broad approach [2], some more specific on biomimetic receptors, and on recent results [3–8].

The aim of this chapter is to provide a small guide to the different techniques used to evaluate molecular recognition of carbohydrates by artificial receptors through a selection of the most recent and innovative papers published in the field.

But why is saccharide recognition so important? Which goals have already been reached? Which are still far from being achieved? And more important, why should researchers keep trying? I hope by the end of the chapter to have given the reader some answers and to provide an overview of the state of the art in this fascinating and expanding field.

10.2 WHY? KEY ROLE IN LIFE PROCESSES

Carbohydrates are involved in the metabolic pathways of living organisms [9–13], and the detection of biologically relevant saccharides is essential to investigate their role in numerous natural processes, as well as to give insights into the mechanisms involved and the diseases provoked. Since the seminal idea of Hakomori [14] on the role of carbohydrate–carbohydrate interactions in cell adhesion and signal transduction events, scientists have walked a long way, and the crucial function of saccharides in the first step of cell–cell, cell–virus, and cell–bacteria interactions is nowadays generally accepted (Figure 10.1) [15].

Organic Synthesis and Molecular Engineering, First Edition.

Edited by Mogens Brøndsted Nielsen.

© 2014 John Wiley & Sons, Inc. Published 2014 by John Wiley & Sons, Inc.

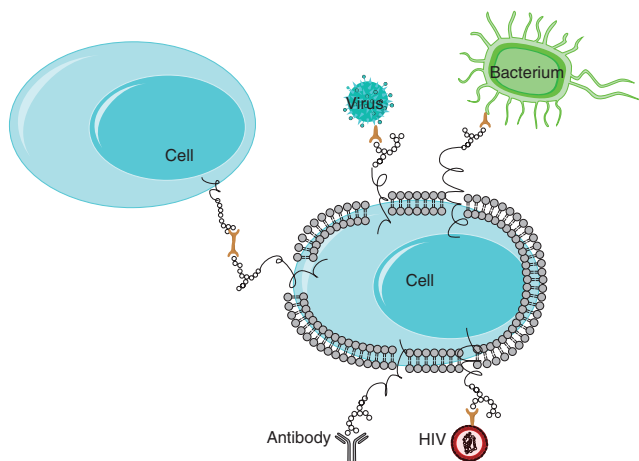


Figure 10.1. Cartoon representation of cell-surface-carbohydrate interactions. See color insert.

There is no doubt on the potential of the structural features possessed by saccharides and their intrinsic characteristics can give rise to a wide complexity of structural building blocks, as depicted in Figure 10.2. If the simple saccharides (i.e., monosaccharides) can be numerous and present preferentially as cyclic pyranose (such as saccharides **1–7** and **10–12**) or furanose rings (such as **8** and **9**), the number of possible combinations solely for dimers (i.e., disaccharides) is already extremely high. Indeed it varies according to (i) the constituent monosaccharides, (ii) the position of the bond, (iii) the bridging atom involved (mainly oxygen, but nitrogen and sulfur can be found as well), and (iv) the stereochemistry of the linkage (axial or equatorial). As a result, the variety of oligosaccharides and polysaccharides is enormous.

A challenge on the recognition of carbohydrates by synthetic receptors is related to their chemical similarity to water (the physiological medium) due to the presence of multiple hydroxyl groups in the structure. Hence effective receptors must be able to discriminate between water and saccharides, compete with the strong hydration of carbohydrates in water, and be able to select closely related isomers. In fact, biological recognition of carbohydrates is therefore driven both by direct interactions and hydrophobic effect [16–18].

In the early days of research in this field, all efforts have been directed on developing artificial receptors for monosaccharide recognition, in particular, glucose **1**, the most abundant saccharide in nature and the one widely available in every organism [1]. Targeting glucose by an artificial receptor, coupled to a response signal, in practical terms results in a glucose sensor, which can find application in different areas, from blood glucose monitoring, food industry quality control, bioprocess, and to the development of renewable, sustainable biofuel cells; the number and value of potential applications explain why carbohydrate receptors are considered an attractive area of sensor research (and evaluated as 85% of the biosensor industry). In food industry measuring the amount of different sugars to evaluate the quality and nutritional value of the product is considered essential by the new legislation. However, blood glucose monitoring remains the main application of glucose sensors. To the best of our knowledge, there

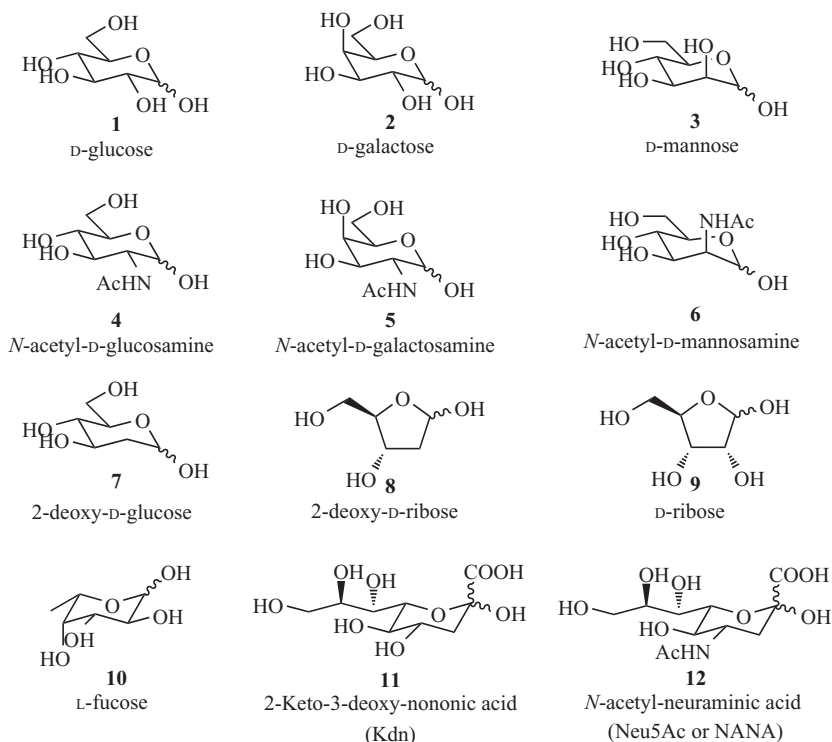


Figure 10.2. Most common monosaccharides in nature.

are three main systems for blood glucose monitoring on the market, all applying enzymatic reactions and consisting of disposable finger-stick sensors that allow a self-test from the patient. If the higher selectivity and relative nontoxicity of enzyme-based sensors in comparison with nonenzymatic ones has driven the market up to now, the next step is focused on continuous glucose sensing by *in vivo* sensors, able to monitor blood glucose fluctuations in real time [19].

In the last decade attention has been attracted by receptors for disaccharides (Figure 10.3, R = monosaccharide), such as cellobiose and maltose [20–27], and more recently by mannose **3** and dimannoside receptors [28–32].

Cellobiose and maltose are constituents of the two main biopolymers, cellulose and starch; hence receptors able to bind those substrates could be exploited in processing and biorefining of cellulose biomass, modulating their solubility properties [27].

Mannose has attracted attention since it has been identified as one of the most common terminal saccharide in glycans and it was found to be densely expressed on the glycocalix of several viral infections (such as human immunodeficiency virus [HIV] and hepatitis C virus [HCV]) [33]. In fact, molecules able to interact with glycans on the viral envelope (better defined as carbohydrate-binding agents) may affect the infection of a target cell from the virus at different levels; both blocking the communication between cell and virus, and cheating the immune system to produce a response against previously hidden immunogenic epitopes of the viral envelope. Hence,

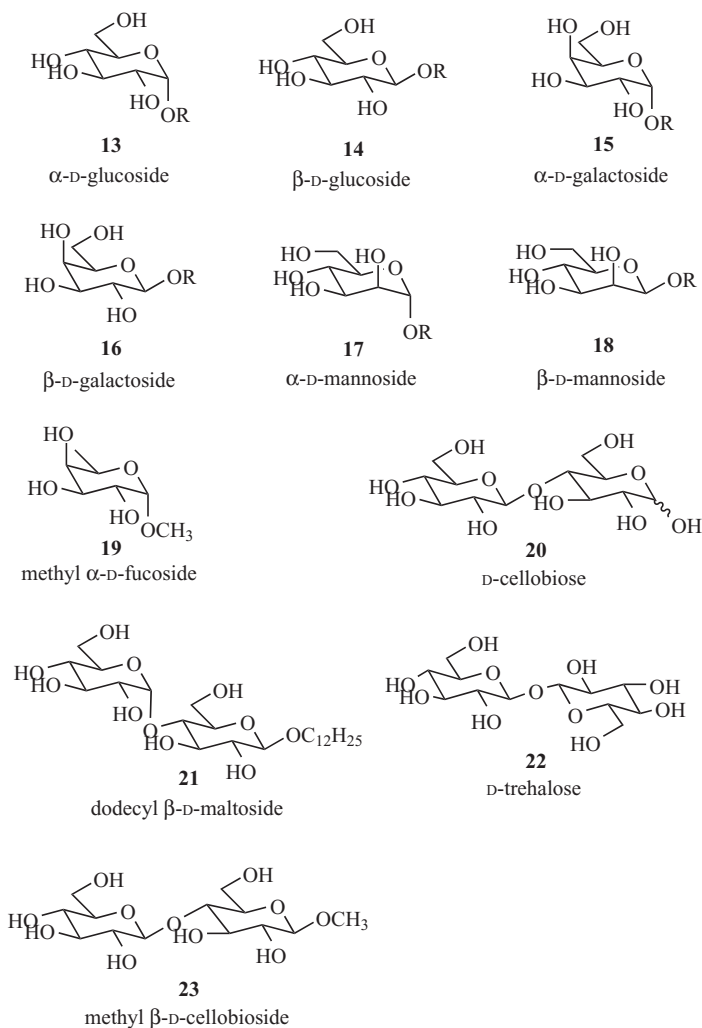


Figure 10.3. Mono- and disaccharides used in the reported recognition studies.

carbohydrate-binding agents are considered to have potential both in diagnosis and as double-functional agents, by direct inhibition upon virus entry, inducing an antiviral action, and as promoter of an unconventional immune response [34].

10.3 WHAT? NONCOVALENT INTERACTIONS

Although an extensive amount of work has been reported on the use of reversible covalent-bond formation in water, in particular, through the formation of boron–oxygen bonds [2, 35], the focus of this chapter will be on systems that use a combination

of multiple noncovalent intermolecular interactions for binding carbohydrates in organic solvents and water.

Investigation of protein–carbohydrate binding sites through crystallography has revealed that protein–carbohydrate complex formation is induced by simultaneous single weak interactions, the majority of which are hydrogen-bonding interactions often stabilized by hydrophobic interactions, CH- π interactions, and coordination of metal ions such as Ca^{2+} and Mg^{2+} [36–38]. Thus, new artificial receptors, often defined as synthetic lectins due to their mimicry of natural lectins, are generally designed with multiple effective donor–acceptor units, complementary to the hydroxyl moieties of saccharides, to provide a unique and strong binding from a large number of weak interactions. In other words, researchers have been taking inspiration from nature, applying its old tricks in the design of new carbohydrate-binding structures.

10.4 HOW? METHODS

Nuclear magnetic resonance (NMR) has been one of the main techniques used to investigate molecular recognition of carbohydrates by artificial receptors through one-dimensional (1D) and two-dimensional (2D) NMR experiments. This powerful method gives information not only on the strength of the binding event but also on the exact binding geometry. In the last decade it has increased the number of papers where the authors present results confirmed by different techniques to support the validity of their findings and to demonstrate they are consistent independently by the chosen method.

The results herein reported are divided according to the main technique described in the original paper, and then a description of the complementary techniques used, if any, is briefly mentioned.

10.4.1 Nuclear Magnetic Resonance (NMR)

A recognition event that implies the binding between a host and a guest can be characterized by slow or fast exchange rate on the NMR timescale. The slow exchange is manifested by separate signals for the bound and the free species and is less frequently encountered, while the fast exchange is evidenced by time-averaged signals, that is, a change of NMR shielding upon complexation. In practical terms, it is more common to observe fast exchange complexation/decomplexation with flexible synthetic receptors, while rigid and preorganized structures can facilitate slow exchange processes on the NMR timescale. When slow exchange is present, association constants can be directly calculated from the NMR signal integrals on the spectra. However, in the case of fast exchange, a full titration followed by a nonlinear least-squares fitting analysis of the chemical shifts of the monitored nuclei is needed to calculate the binding constants.

In spite of the high-field spectrometers now available, NMR requires quite high sample concentrations (0.3–1 mM) for the spectra acquisition, and binding constants higher than 10^6 M^{-1} cannot be precisely evaluated. To overcome this problem without changing technique, one option is to change to a more polar solvent (or solvent mixture) where the hydrogen-bonding interactions are weaker, and consequently, the binding constants are lower. Of course this trick implies, as essential condition, the solubility of the receptor in the more polar medium and cannot be used when the initial

studies have already been performed in water. But, so far, systems that have been successful operating in water are few [21, 22, 27, 39–45], and the affinities are not as strong to face this problem. Besides, the use of NMR can be nontrivial and nonresolutive when the receptor forms aggregates in solution, since they will produce broad signals and hence affect resolution of the spectra and interpretation of the results. Misleading results could also be provoked by exchange phenomena of slightly acidic protons with water or if the carbohydrate receptor promotes solvation of the hydrogen-bonding groups into its cavity.

Ground-breaking research has been reported by Davis and Wareham in 1998, particularly on the development of the so-called temple architecture (Figure 10.4) [46]. Such architecture has produced the best results to date in carbohydrate recognition by artificial receptors. The concept involves a rigid tridimensional structure constituted by four polar “columns,” possessing H-bonding acceptor–donor units such as isophthalamides, and by an apolar “roof” and an apolar “floor,” constituted by biphenyl units

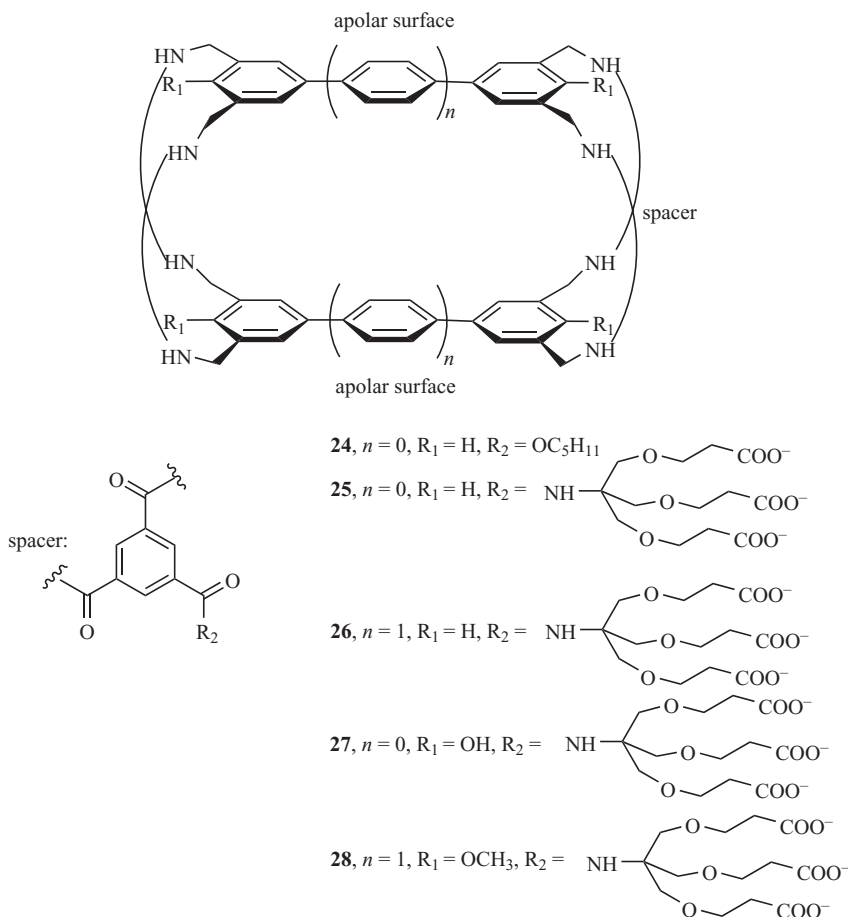


Figure 10.4. Davis temple architecture: $n = 0$, first prototype; $n = 1$, linear extended apolar surface.

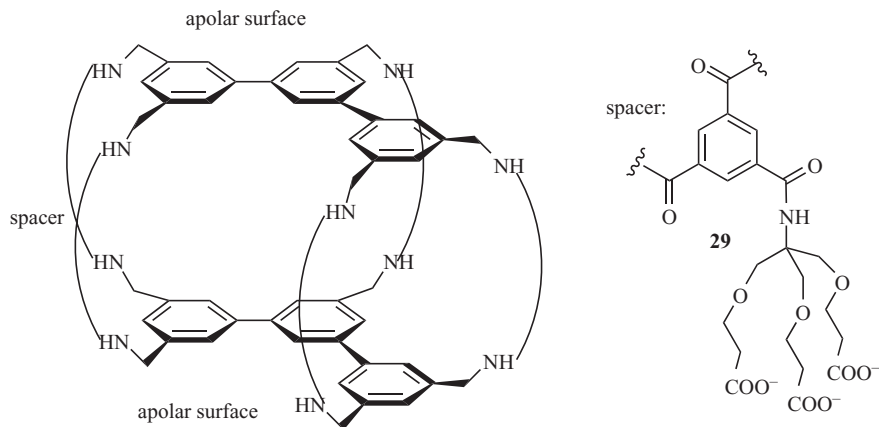


Figure 10.5. Extended apolar surface of the temple.

TABLE 10.1. Association Constants (K_a [M^{-1}]) for 1:1 Complex of Receptors 25–29 with Carbohydrates in Water Measured by 1H NMR Titration

	K_a (M^{-1})				
	25	26	27	28	29
D-Glucose 1	9	–	43	2	11
NAC-D-glucosamine 4	56	–	–	9	24
Methyl β -D-glucoside 14	28	–	90	–	–
Methyl α -D-glucoside 13	7	–	15	–	–
D-Cellobiose 20	17	3140	–	3340	580
Methyl β -D-cellobioside 23	–	–	–	4500	850

and aimed to induce CH– π interactions with the saccharides. This type of design has produced compounds able to bind selectively all equatorial-substituted saccharides, from methyl β -D-glucoside to D-xylose, 2-deoxyglucose, and β -D-N-acetylglucosamine; moreover, an evident preference for the β -anomer of glycosides has been always evidenced.

The original temple-based skeleton **24** has been properly modified in the last decade to achieve both solubility in water and the best results for selective monosaccharide and disaccharide recognition in water (Figure 10.4 and Figure 10.5). In particular, changes in the roof and in the floor of the temple have been designed to achieve disaccharide recognition by means of extension of the apolar surfaces in linear ($n = 1$, Figure 10.4) or bent manner (Figure 10.5), while modification of the side chain on the polar “columns” (R_2 , Figure 10.4) have induced water solubility. Substituent effects have been recently explored to study the role of CH– π interactions in carbohydrate recognition (R_1 , Figure 10.4) [44].

A table with the most relevant association constants measured in D_2O by 1H NMR titration with the different temple receptors **25–29** is here reported (Table 10.1).

Comparison of the association constants for compounds **25** and **27**, both constituted by biphenyl apolar surfaces but with **27** bearing additional hydroxyl groups in the biphenyl 4,4' positions, has revealed that the binding event can be just slightly modulated by electronic effects and that the electron density of the system is not the predominant effect to influence the binding energy. Indeed the corresponding association constant values of **25** and **27** slightly increased from 9 to 43 M^{-1} for D-glucose **1**, from 28 to 90 M^{-1} for methyl β -D-glucoside **14**, and from 7 to 15 M^{-1} for methyl α -D-glucoside **13**.

On the contrary, initial extension of the apolar surface in bent manner to temple **29** (Figure 10.5) allowed Davis and coworkers to achieve selectivity toward D-cellobiose **20** ($K_a = 580 M^{-1}$) and methyl β -D-cellobioside **23** ($K_a = 850 M^{-1}$) with respect to D-glucose **1** ($K_a = 11 M^{-1}$) and NAc-D-glucosamine **4** ($K_a = 24 M^{-1}$).

Recent findings reported by Davis and Wareham involve extended linear structures **26** and **28** ($n = 1$, Figure 10.4). Although modeling studies using MacroModel predicted a collapsed conformation of such a skeleton being more stable than the corresponding open structure, which contains a cavity prone to binding, the authors decided to undertake the study. Despite the modeling prevision, their determination has been rewarded by excellent results with these structures. Since broad signals detected in the 1H NMR spectra prevented a correct evaluation of the binding event in most cases for **26**, tetramethoxy analog **28** was prepared. Association constants of 4500 and 3340 M^{-1} have been calculated for **28** by 1H NMR titration in D_2O toward methyl β -D-cellobioside **23** and D-cellobiose **20**, respectively, the data being confirmed as well by isothermal calorimetry (ITC) and fluorescence studies.

An important message that can be extrapolated from these findings concerns a more positive approach to the use of less rigid and preorganized structures. Indeed, receptors more flexible, not rigidly organized, but designed to adjust in the presence of the guest, can be a frontier to explore more deeply, despite the less predictable behavior by molecular-modeling studies.

The results reported independently by Roelens and by Mazik by means of acyclic tripodal receptors support this concept. Although the affinities obtained have not reached the level of "temple" receptors, modulation of selectivity toward different saccharides has been achieved.

Mazik has designed and developed acyclic receptors inspired by the analysis of the binding motifs observed in the natural protein-carbohydrate crystal structures. A systematic study through careful introduction of protein-binding groups has been performed by means of symmetrical and asymmetrical tripodal scaffolds, with interesting results [7, 8]. The system showing the most relevant findings is **30** (Figure 10.6) and consists of two aminopyridine units and a bicarboxylic arm on the benzene-based platform. In spite of the multiple-stoichiometry system, apparent association constants were evaluated in water toward methyl β -D-glucoside **14** ($R = CH_3$, $K_a = 2 M^{-1}$) and D-cellobiose **20** ($K_a = 305 M^{-1}$) [41].

A similar approach has been used by Roelens and coworkers, investigating carbohydrate recognition by means of benzene-based tripodal receptors [47]. The initial paper described a tripodal molecule bearing three convergent ureidic groups **31** (Figure 10.7) as H-bonding donor-acceptor system and showed millimolar affinities in $CDCl_3$, calculated by NMR titration, and a significant selectivity toward octyl β -D-galactoside **16** ($R = C_8H_{17}$) [48]. In this report a thorough description of the NMR titration protocol and the difficulties encountered in order to achieve reliable association constants for saccharides are included, and an affinity index (BC_{50}^0) [49], useful to compare

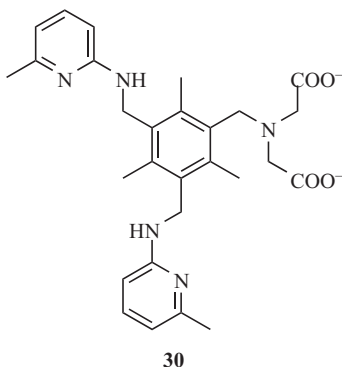


Figure 10.6. Mazik's carbohydrate receptor studied in water.

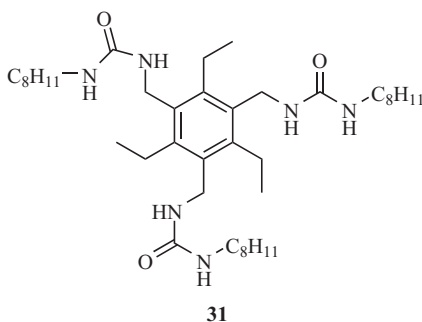


Figure 10.7. Ureidic tripodal receptor.

dimensionally heterogeneous binding data (i.e., host–guest systems described by single- or multiple-binding equilibria) and calculated from the cumulative binding constants β , is introduced.

Later studies focused on different H-bonding groups [50, 51], from catecholic to sulfonamidic, oxypyrrolic, imidazolic, and indolic groups, but the most promising and effective have been aminopyrrole units. Amines properly combined with pyrrolic ring, on cage structure **32** [52] or on acyclic tripodal receptors **33** and **34** [29, 53] (Figure 10.8), showed the best complementary interactions with carbohydrates. Receptor **33** showed effective recognition properties toward octyl β -D-glucoside **14** ($R = C_8H_{17}$) in $CDCl_3$ in the micromolar range and still efficient in CD_3CN in the millimolar range; cage **32** showed an affinity of 20 μM toward octyl β -D-glucoside **14** ($R = C_8H_{17}$) in $CDCl_3$ and in addition was able to partially dissolve insoluble methyl- β -D-glucoside **14** ($R = CH_3$) in $CDCl_3$ by complexation, and triacetalic receptor **34** exhibited an affinity for octyl β -D-mannoside **18** ($R = C_8H_{17}$) estimated in the nanomolar range in $CDCl_3$ and measured in the micromolar range (BC_{50}^0 : 680 μM) in CD_3CN . Association constants were measured by NMR titrations following the previously established protocol [48] and combining other techniques, from ITC to mass-spectroscopy collision-induced dissociation (MS-CID) (see later discussion).

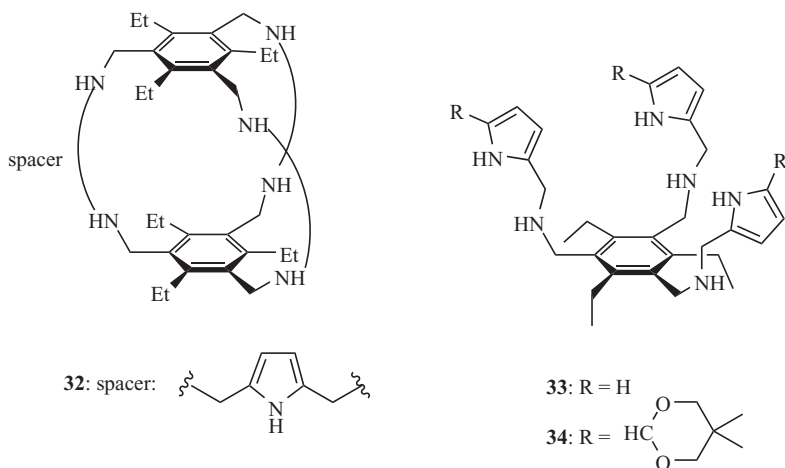


Figure 10.8. Pyrrolic tripodal receptors.

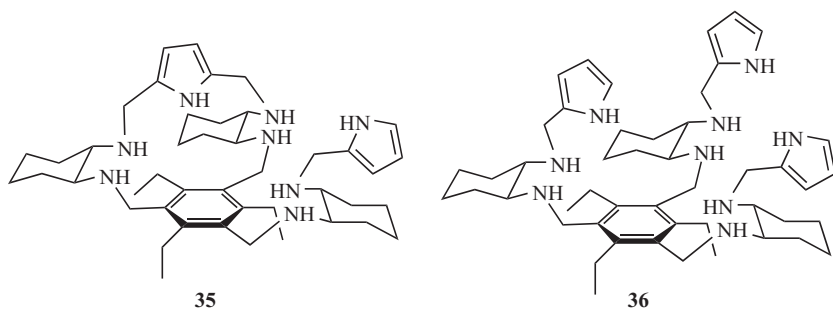


Figure 10.9. Second-generation tripodal receptors.

Structural and functional modifications have been attempted on the progenitor structures **32** and **33** based on the replacement of (*S,S*)- or (*R,R*)-*trans*-1,2-diaminocyclohexane for the amino groups and provided a second generation of chiral receptors **35** and **36** prepared and investigated both in the enantiomerically pure forms (enantiomer (*S,S,S,S,S,S*) named as (*S*)-**35**, and analogously (*R*)-**35**, (*S*)-**36**, (*R*)-**36**). The introduction of additional hydrogen-bonding groups and chirality allowed modulation in the carbohydrate selectivity and provided for compound (*S*)-**35** the highest affinity reported up to date toward octyl β -D-mannoside **18** ($R = C_8H_{17}$) in CD_3CN ($BC_{50}^0 = 83 \mu M$) (Figure 10.9) [29–32].

The potential importance of aminopyrrolic artificial receptors has been further underlined by recent biological studies [54], where the antibiotic activity and cytotoxicity of these receptors, structurally related to **33**, have been analyzed and reported. The findings showed that this family of carbohydrate-binding agents actually possesses antibiotic activity against yeast and yeast-like pathogens, moving forward the field of carbohydrate recognition by artificial receptor toward effective application.

Furthermore, the antibiotic activity measured by **33** is comparable to polyene (amphotericin B) or azole (ketoconazole) drugs.

Although attempts to find a direct correlation between minimum inhibitory concentrations and the affinities recorded toward mannosides failed, it has been observed that compounds showing no affinity for mannosides lack inhibitory activity, while compounds showing some type of affinity also show antibiotic activity.

Fluorescence microscopy experiments performed on this class of receptors underlined the essential role of the pyrrolic groups with respect to permeability, antibiotic activity, and toxicity. Since both active aminopyrrolic receptor **33** and the parent amino receptor, lacking the pyrrole units and inactive, were localized in the cytoplasm, the authors could state that pyrrolic groups are responsible not only for the permeability but also for the antibiotic activity and toxicity. Moreover, the authors suggested that although the origin of the antibiotic activity does not reside in the ability to bind mannosides, the carbohydrate-binding event must be involved at some stage of the process, either helping the approach of the inhibitor or its access onto the cell surface [54].

The ability of aminomethylpyrroles to be an appropriate and complementary group in the binding of carbohydrates has been recently confirmed by Joshi and Davis [55]. In this case, two of the four prototype isophthalamide columns in the temple architecture, responsible of polar interactions, have been replaced by bis-aminomethylpyrroles, bearing two carboxylic groups for solubility reason, giving receptor **37** (Figure 10.10). These units can act both as acceptor–donor–acceptor (A–D–A) or donor–donor–donor

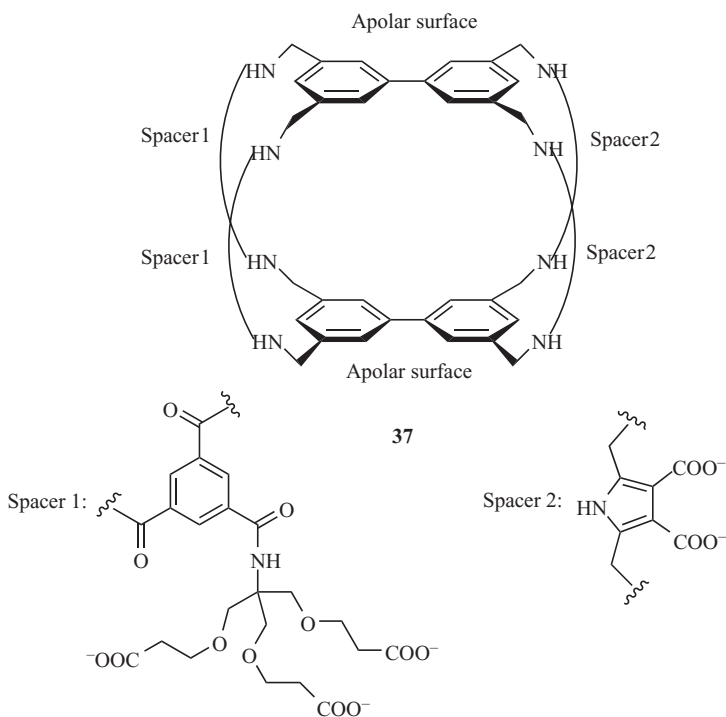


Figure 10.10. Temple-bearing aminomethylpyrrole units.

(D–D–D) unit depending on the pH of the aqueous solution. Only the A–D–A bonding arrangement has been reported, showing unprecedented selectivity in D₂O at pD 13 ($K_a = 18 \text{ M}^{-1}$) for glucose with respect to other monosaccharides tested.

Once the chapter was almost completed, a recent publication from Roelens has underlined the crucial role of the functional groups chosen for carbohydrate binding. Aminomethylpyrrole units resulted forming stronger hydrogen bonds toward saccharides, that is, having higher affinity and hence being more complementary as donor–acceptor groups, than aminomethylpyridine or aminomethylbenzene, when isostructural substitution is introduced in a cage system [56].

10.4.2 UV-Vis Spectroscopy

UV-Vis titrations have been used to evaluate carbohydrate recognition in several contexts, although mostly as complementary technique to NMR. The recognition event takes place quickly, on picosecond timescale, which implies the observation of individual signals for the free and the bound species. The possibility to use low-concentration solutions (10^{-5} M) is a big advantage, and the necessity of strong chromophores on the receptor is an essential requisite to use this technique. The changes in absorbance at λ_{max} are monitored for different concentrations of the carbohydrate and their fitting allowed the determination of the binding constants.

In 2002, Ladomenou and Bonar-Law [57] and Kim and Hong [58] have, independently, reported aspartate urea appended porphyrin receptors for carbohydrate recognition. Recently, Hong and coworkers described new porphyrin-based synthetic carbohydrate receptor architecture (Figure 10.11) bearing urea, carbamate, or amide groups as hydrogen-bonding sites [59]. Investigation of the binding interactions has been performed by different techniques (UV, NMR, circular dichroism [CD]). Upon addition of the saccharidic guests, the UV-Vis spectra showed a shift and a change in intensity, and isosbestic points, indicating the existence of two states by formation of a 1:1 complex, were registered. The absorbances at λ_{max} were reported as a function of the different carbohydrate concentrations and the curve fitting provided the corresponding apparent association constants. Ureidic zinc porphyrin receptor **38** showed the highest affinity, measuring a K_a value of $6.8 \times 10^5 \text{ M}^{-1}$ in chloroform toward octyl β -galactoside **16** ($R = \text{C}_8\text{H}_{17}$) and $5.7 \times 10^5 \text{ M}^{-1}$ toward octyl β -D-glucoside **14** ($R = \text{C}_8\text{H}_{17}$). The binding events were confirmed by NMR and CD, and recognition in more polar solvent mixtures ($\text{CD}_3\text{OD}/\text{CDCl}_3$, 1/10) still remained effective, even in the presence

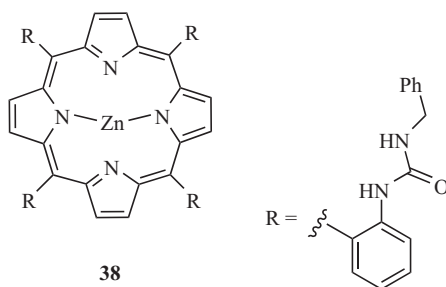


Figure 10.11. Porphyrin-based carbohydrate receptor.

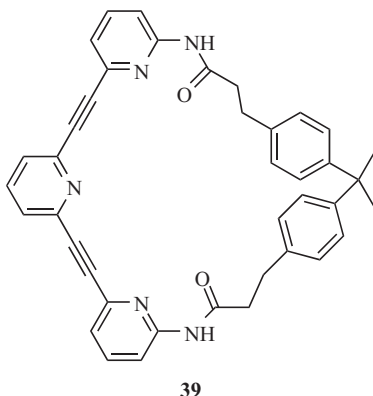


Figure 10.12. Inouye receptor bearing acceptor–acceptor–acceptor unit.

of competing methanol ($K_a = 250$ and 470 M^{-1} , respectively, for octyl β -galactoside **16** and octyl β -D-glucoside **14**). The results reported by Hong conclude that the ureidic NHs on **38** behave as hydrogen-bonding donors, while the porphyrin plane and the flexible phenyl groups can give rise to CH- π interactions with the CHs of the sugar.

10.4.3 Circular Dichroism (CD)

Registering the presence of a change, named as Cotton effect, in the CD spectrum can give insight in the formation of chiral complexes between an achiral receptor and the chiral saccharide, which does not absorb at the specific wavelength region.

Abe, Inouye and coworkers have broadly used this method, in conjunction with UV–Vis experiments, to evaluate carbohydrate recognition [26, 40, 60–64]. A macrocyclic framework, preorganized and rigid, containing hydrogen-bonding donor or acceptor multiple-binding sites (acceptor–acceptor–acceptor or A–D–A) given by pyridone/pyridine moieties was found to be effective toward hexose, ribose, and 2-deoxyribose recognition. Receptor **39** is one of the first examples reported (Figure 10.12) [61].

Most recent findings by Inouye and coworkers involve acetylene-linked pyridone/pyridine macrocycles able to selectively detect maltoside in dichloromethane (Figure 10.13) [26]. In this type of receptors, the pyridone NHs behave as hydrogen-bonding donors while the pyridine nitrogen atoms as hydrogen-bonding acceptors and are responsible for the recognition event as showed by the authors through a Monte Carlo simulation of a model compound. UV–Vis experiments in CH_2Cl_2 and CD bands were registered around 350 nm when macrocyclic receptor **40** was in the presence of a saccharide and gave a binding constant $K_a = 1.4 \times 10^6 \text{ M}^{-1}$ toward dodecyl- β -maltoside **21**, while in the more polar CH_3CN , a lower $K_a = 1.8 \times 10^3 \text{ M}^{-1}$ was observed. However, in spite of the receptor's high solubility in water, no association with saccharides was detected in this solvent by CD analysis.

10.4.4 Isothermal Calorimetry (ITC)

Due to the development of highly sensitive microcalorimeters that can operate with small sample volumes, ITC has become popular in the determination of equilibrium

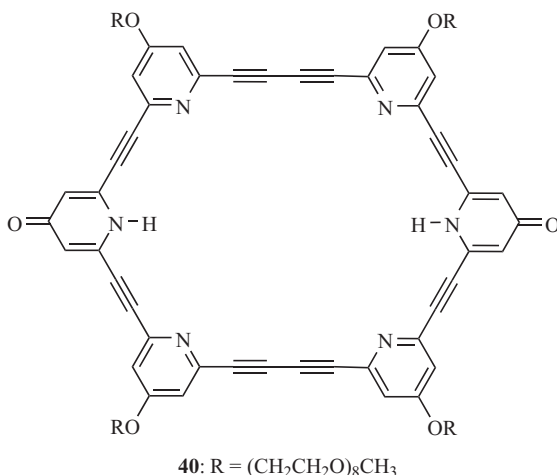
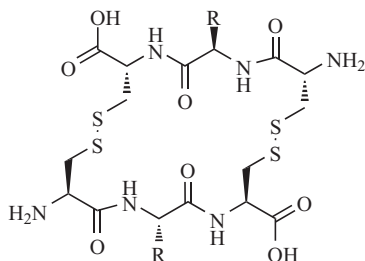


Figure 10.13. Abe–Inouye receptor bearing A–D–A units.

constants. The main advantage of this technique consists in the determination of free energy and enthalpy changes at a specific temperature, and in the determination of heat capacity changes from measurements at different temperatures. It is a necessary condition that the reaction heat effect must be big enough to produce a measurable temperature change and that essentially entropy-driven equilibria needs to be sufficiently endothermic to allow detection. Furthermore, calorimetric measurements are more difficult in nonaqueous solvents since the heat exchange is not as fast as in water [65]. Hence, only in the presence of strong carbohydrate receptor, able to bind saccharides in water, water–solvent mixture, or in a polar organic solvent, such as acetonitrile, is possible to use this technique.

One of the most relevant contributions to the recent literature on carbohydrate recognition by means of ITC has been published by Ravoo et al. [66]. The use of dynamic combinatorial chemistry with various mono- and disaccharides as templates allowed Ravoo et al. to obtain peptide-based receptors for molecular recognition of saccharides in water. This approach followed the reversible disulfide exchange pioneered by Sanders and coworkers [67, 68] using the disulfide-exchange reaction of cysteine. The best results were found with neurotransmitter *N*-acetyl neuraminic acid **12** (NANA); in fact, a number of significant changes to the composition of the dynamic combinatorial library in the presence of **12** as template were observed (Figure 10.14). Each library was monitored by high-performance liquid chromatography/MS (HPLC/MS) using hydrophilic interaction liquid chromatography and electrospray spray ionization MS (HILIC/ESI-MS) in the SIM mode. In particular, cyclic homodimer HisHis **41** was amplified by a factor of 2.0 in the presence of **12** (Figure 10.12). This interaction was investigated more deeply after conventional preparation of **41** as mixture of two constitutional isomers. The ITC titration experiment of 2.0 mM **41** with 40 mM NANA **12** at pH 7.4 showed an exothermic interaction where one molecule of cyclic **41** binds two molecules of **12** (1 : 2 stoichiometry). The interpretation of the ITC data was confirmed by NMR experiments. The job plot of the NMR data confirmed a 1 : 2 stoichiometry of the complex rather than 1 : 1, and data fitting of ¹H NMR titration experiments



41: R = side chain of His

42: R = side chain of Tyr

43: R = side chain of Thr

Figure 10.14. Peptide-based receptors selected by dynamic combinatorial chemistry with saccharides as templates.

(following the shifts of the signals of the imidazole protons of **41** upon addition of NANA at pH 7.6) provided two independent binding constants, $K_1 = 70.4 \text{ M}^{-1}$ and $K_2 = 5.52 \times 10^3 \text{ M}^{-1}$, between the strongest reported to date. Ravoo and coworkers concluded that **41** binds two molecules of **12** in a cooperative way, since the second **12** is bound much more tightly than the first.

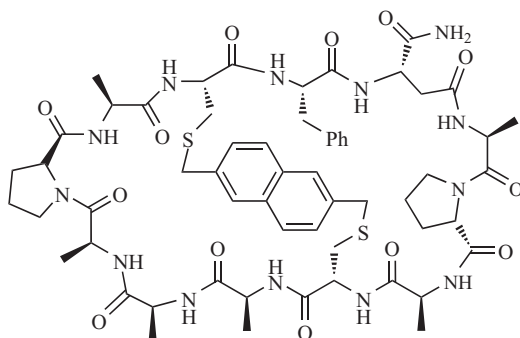
Two other cyclic peptides were found to be selective receptors for carbohydrates in water from the set of tripeptides selected by Ravoo et al. and were similarly analyzed. TyrTyr **42** was selected with the natural disaccharide D-trehalose **22** and ThrThr **43** was selected by methyl α -D-fucoside **19**. In both cases 1 : 1 stoichiometry was observed. As for **42**, in addition to ITC and NMR experiments, fluorescence experiments were performed and revealed a significant loss of fluorescence intensity of **42** upon addition of D-trehalose **22**. Fluorescence, ITC, and NMR measurements were consistent and demonstrated a strong interaction of the peptidic receptor and D-trehalose **22** in water. The strength of the complex can be ascribed to a combination of hydrogen-bonding and CH- π interactions with the peptide side chain.

On the contrary an ITC titration of **43** with methyl α -D-fucoside **19** was inconclusive owing to the very small heat effect observed. Therefore, in this particular case, only NMR experiments allowed the determination of the binding constant. However, this last result shows the limit of the ITC technique and implies that the interaction of **43** and **19** is entropy driven.

10.4.5 Other Methods (MS and Liquid-Liquid and Liquid-Solid Extractions)

In the last decade excellent progress and results have been obtained in mass spectrometry through ESI, and lately, CID have been performed to analyze carbohydrate-receptor complex stability in gas phase [53]. CID experiments consist in the selection of the saccharide-receptor complex ion produced by ESI, its acceleration, and collision in a cell containing neutral gas atoms. The higher is the potential to apply to disrupt the complex, the stronger is its stability [69].

A thorough description of the method and interesting findings on disaccharide recognition have been recently reported by Meldal and coworkers [22]. They described



44

Figure 10.15. Meldal's cyclic peptide for carbohydrate recognition.

the solid-phase synthesis of cyclic peptide **44**, able to provide hydrogen-bonding donor–acceptor interactions, and containing a rigid aromatic bridge, properly introduced to help the binding through CH– π interactions (Figure 10.15). According to the authors, the cyclization of the peptide chain and the aromatic bridge induce less flexibility to the system and provide a conformationally stable receptor molecule.

The specificity for 1-4-linked disaccharides, suggesting that most likely the receptor interacts with both the terminal sugar and the aglycon, was revealed by MS-CID experiments on a set of mono-, di-, and trisaccharides. The binding properties of **44** toward saccharides have been also confirmed in the liquid phase by 1D and 2D NMR experiments. The highest association constant was calculated toward D-cellobiose **20** ($K_a = 7.7 \text{ M}^{-1}$) in 10% deuterated acetic acid in water. Despite the modest affinity and specificity, an appropriate modification of the scaffold by change of the constituent amino acids and the easy synthetic accessibility through solid-phase methods justify the interest in this type of systems.

Although sometimes the lack of solubility of carbohydrate receptors in water does not allow the determination of their binding ability or selectivity in the physiological media, it is indeed possible to utilize them to extract saccharides from water solution, inducing a phase transfer in organic solvent through complexation by means of non-covalent interactions. Several examples can be found in the scientific literature, among them one of the first templates reported by Davis, **25**, has been used to measure the different saccharides extractability from water into chloroform solution. The mole equivalent of monosaccharide extracted by the receptor was evaluated by integration of the proton NMR signals of the guest with respect to the host. Since the extractability diverged from the estimated degree of solvation of the saccharides, the author suggested a stereospecific glucose interaction with the receptor [70].

10.5 CONCLUSIONS AND PERSPECTIVES

Although the main issues in the design of carbohydrate receptors remain the discrimination between saccharide and the physiological solvent water, as well as between different saccharides, the primary goal for researchers nowadays is to utilize them in

effective applications. Of course, only once carbohydrates can be strongly and selectively bound in their natural environment, it is realistic to consider applications. Nevertheless, interesting results on antibiotic activity against yeast and yeast-like pathogens by mannose-binding systems have been reported, even if the initial evaluation of the binding ability was performed on model mannosides in acetonitrile, a most unnatural system

The expectations on this field of research remain high and the development of glucose sensors based on nonenzymatic glucose-selective receptors, important in the management of diabetes, is close at hand. As a matter of fact, in a recent publication from Davis and coworkers, an anthracene-based temple, synthetically more simple and accessible than the previous temple receptors, having a K_a value of 56 M^{-1} for glucose (calculated by ^1H NMR titration in D_2O), sensing at concentration found in blood, and showing a guest-dependent fluorescent emission has been reported [71].

Considering the general up-growing interest toward the concept of multivalency [72–75], in particular, for biomedical applications, we believe that multivalent systems (water soluble or on solid support) bearing multiple effective carbohydrate-binding units can move forward this field of research and bring new effective and determinant developments.

REFERENCES

- [1] Davis, A. P., Wareham, R. S. (1999). Carbohydrate recognition through noncovalent interactions: A challenge for biomimetic and supramolecular chemistry. *Angewandte Chemie (International ed. in English)*, *38*, 2978–2996.
- [2] Jin, S., Cheng, Y., Reid, S., Li, M., Wang, B. (2010). Carbohydrate recognition by boronolactins, small molecules, and lectins. *Medicinal Research Reviews*, *30*, 171–257.
- [3] Davis, A. P., James, T. D. Carbohydrate receptors. In *Functional Synthetic Receptors*, Schrader, T., Hamilton, A. D. (Eds.), Wiley-VCH, Weinheim, 2005; pp. 45–109.
- [4] Davis, A. P. (2009). Synthetic lectins. *Organic & Biomolecular Chemistry*, *7*, 3629–3638.
- [5] Walker, D. B., Joshi, G., Davis, A. P. (2009). Progress in biomimetic carbohydrate recognition. *Cellular and Molecular Life Sciences*, *66*, 3177–3191.
- [6] Kubik, S. (2009). Synthetic lectins. *Angewandte Chemie (International ed. in English)*, *48*, 1722–1725.
- [7] Mazik, M. (2009). Molecular recognition of carbohydrates by acyclic receptors employing noncovalent interactions. *Chemical Society Reviews*, *38*, 935–956.
- [8] Mazik, M. (2012). Recent developments in the molecular recognition of carbohydrates by artificial receptors. *RSC Advances*, *2*, 2630–2642.
- [9] Gabius, H.-G. (Ed.). *The Sugar Code. Fundamentals of Glycosciences*, Wiley-VCH, Weinheim, 2009.
- [10] Ernst, B., Hart, W., Sinaÿ, P. *Carbohydrates in Chemistry and Biology*, Part I, Vol. 2, and Part II, Vol. 4, Wiley-VCH, Weinheim, Germany, 2000.
- [11] Lindhorst, T. K. *Essentials of Carbohydrate Chemistry and Biochemistry*, 1st ed., Wiley-VCH, Weinheim, 2000.
- [12] Penadés, S. Host–guest chemistry. Mimetic approaches to study carbohydrate recognition. In *Topics in Current Chemistry*, Vol. 218, Springer-Verlag, Heidelberg, 2002.
- [13] Lutzen, A. Carbohydrate recognition by artificial receptors. In *Highlights in Bioorganic Chemistry: Methods and Applications*, Schmuck, C., Wennemers, H. (Eds.), Wiley-VCH, Weinheim, 2004; pp. 109–119.

- [14] Hakomori, S. (1991). Carbohydrate-carbohydrate interaction as an initial step in cell recognition. *Pure and Applied Chemistry*, 5, 741–764.
- [15] Hakomori, S. (2002). The glycosynapse. *Proceedings of the National Academy of Sciences*, 99, 225–232.
- [16] Lemieux, R. U. (1996). How water provides the impetus for molecular recognition in aqueous solution. *Accounts of Chemical Research*, 29, 373–380.
- [17] Garcia-Hernandez, E., Hernandez-Arana, A. (1999). Structural bases of lectin-carbohydrate affinities: Comparison with protein folding energetics. *Protein Science*, 8, 1075–1086.
- [18] Ambrosi, M., Cameron, N. R., Davis, B. G. (2005). Lectins: Tools for the molecular understanding of the glycode. *Organic & Biomolecular Chemistry*, 3, 1593–1608.
- [19] Toghiani, K. E., Compton, R. G. (2010). Electrochemical non-enzymatic glucose sensors: A perspective and an evaluation. *International Journal of Electrochemical Science*, 5, 1246–1301.
- [20] Klein, E., Ferrand, Y., Auty, E. K., Davis, A. P. (2007). Selective disaccharide binding by a macrocyclic receptor. *Chemical Communications*, 43, 2390–2392.
- [21] Ferrand, Y., Crump, M. P., Davis, A. P. (2007). A synthetic lectin analog for biomimetic disaccharide recognition. *Science*, 318, 619–622.
- [22] Reenberg, T., Nyberg, N., Duus, J. Ø., van Dongen, J. L. J., Meldal, M. (2007). Specific recognition of disaccharides in water by an artificial bicyclic carbohydrate receptor. *European Journal of Organic Chemistry*, 2007, 5003–5009.
- [23] Mazik, M., Buthe, A. C. (2007). Oxime-based receptors for mono- and disaccharides. *The Journal of Organic Chemistry*, 72, 8319–8326.
- [24] Mazik, M., Buthe, A. C. (2008). Highly effective receptors showing di- vs. monosaccharide preference. *Organic & Biomolecular Chemistry*, 6, 1558–1568.
- [25] Striegel, S., Gichinga, M. G. (2008). Disaccharide recognition by binuclear copper(II) complexes. *Chemical Communications*, 44, 5930–5932.
- [26] Abe, H., Chida, Y., Kurokawa, H., Inouye, M. (2011). Selective binding of D_{2h} -symmetrical, acetylene-linked pyridine/pyridone macrocycles to maltoside. *The Journal of Organic Chemistry*, 76, 3366–3371.
- [27] Sookcharoenpinyo, B., Klein, E., Ferrand, Y., Walker, D. B., Brotherhood, P. R., Ke, C., Crump, M. P., Davis, A. P. (2012). High-affinity disaccharide binding by tricyclic synthetic lectins. *Angewandte Chemie (International ed. in English)*, 51, 4586–4590.
- [28] Striegel, S., Dittel, M. (2003). A sugar discriminating binuclear copper(II) complex. *Journal of the American Chemical Society*, 125, 11518–11524.
- [29] Nativi, C., Cacciarini, M., Francesconi, O., Moneti, G., Roelens, S. (2007). A beta-mannoside-selective pyrrolic tripodal receptor. *Organic Letters*, 9, 4685–4688.
- [30] Arda, A., Venturi, C., Nativi, C., Francesconi, O., Gabrielli, G., Canada, F. J., Jimenez-Barbero, J., Roelens, S. (2010). A chiral pyrrolic tripodal receptor enantioselectively recognizes β -mannose and β -mannosides. *Chemistry—A European Journal*, 16, 414–418.
- [31] Nativi, C., Francesconi, O., Gabrielli, G., Vacca, A., Roelens, S. (2011). Chiral diaminopyrrolic receptors for selective recognition of mannosides, part 1: Design, synthesis, and affinities of second-generation tripodal receptors. *Chemistry—A European Journal*, 17, 4814–4820.
- [32] Arda, A., Canada, F. J., Nativi, C., Francesconi, O., Gabrielli, G., Ienco, A., Jimenez-Barbero, J., Roelens, S. (2011). Chiral diaminopyrrolic receptors for selective recognition of mannosides, Part 2: A 3D view of the recognition modes by X-ray, NMR spectroscopy, and molecular modeling. *Chemistry—A European Journal*, 17, 4821–4829.
- [33] Balzarini, J. (2005). Targeting the glycans of gp120: A novel approach aimed at the Achilles heel of HIV. *The Lancet Infectious Diseases*, 5, 726–731.
- [34] Balzarini, J. (2007). Targeting the glycans of glycoproteins: A novel paradigm for antiviral therapy. *Nature Reviews. Microbiology*, 5, 583–597.

- [35] James, T. D., Phillips, M. D., Shinkai, S. *Boronic Acids in Saccharide Recognition*, Royal Society of Chemistry, Cambridge, 2006; p. 1.
- [36] Quijochó, F. A. (1986). Carbohydrate-binding proteins—tertiary structures and protein-sugar interactions. *Annual Review of Biochemistry*, 55, 287–315.
- [37] Meyer, E. A., Castellano, R. K., Diederich, F. (2003). Interactions with aromatic rings in chemical and biological recognition. *Angewandte Chemie (International ed. in English)*, 42, 1210–1250.
- [38] Asensio, J. L., Ardá, A., Cañada, F. J., Jiménez-Barbero, J. (2012). Carbohydrate-aromatic interactions. *Accounts of Chemical Research*, 48, 946–954.
- [39] Klein, E., Crump, M. P., Davis, A. P. (2005). Carbohydrate recognition in water by a tricyclic polyamide receptor. *Angewandte Chemie (International ed. in English)*, 44, 298–302.
- [40] Waki, M., Abe, H., Inouye, M. (2006). Helix formation in synthetic polymers by hydrogen bonding with native saccharides in protic media. *Chemistry—A European Journal*, 12, 7839–7847.
- [41] Mazik, M., Cavga, H. (2006). Carboxylate-based receptors for the recognition of carbohydrates in organic and aqueous media. *The Journal of Organic Chemistry*, 71, 2957–2963.
- [42] Klein, E., Ferrand, N., Barwell, N. P., Davis, A. P. (2008). Solvent effects in carbohydrate binding by synthetic receptors; implications for the role of water in natural carbohydrate recognition. *Angewandte Chemie (International ed. in English)*, 47, 2693–2696.
- [43] Davis, A. P. (2010). Supramolecular chemistry: Sticking to sugars. *Nature*, 464, 169–170.
- [44] Barwell, N. P., Davis, A. P. (2011). Substituent effects in synthetic lectins—Exploring the role of CH- π interactions in carbohydrate recognition. *The Journal of Organic Chemistry*, 76, 6548–6557.
- [45] Corzana, F., Fernandez-Tejada, A., Busto, J. H., Joshi, G., Davis, A. P., Jimenez-Barbero, J., Avenoza, A., Peregrina, J. M. (2011). Molecular recognition of β -O-GlcNAc glycopeptides by a lectin-like receptor: Binding modulation by the underlying ser or thr amino acids. *ChemBioChem: A European Journal of Chemical Biology*, 12, 110–117.
- [46] Davis, A. P., Wareham, R. S. (1998). A tricyclic polyamide receptor for carbohydrates in organic media. *Angewandte Chemie (International ed. in English)*, 37, 2270–2273.
- [47] Hennrich, G., Anslyn, E. V. (2002). 1,3,5-2,4,6-functionalized, facially segregated benzenes—Exploitation of sterically predisposed systems in supramolecular chemistry. *Chemistry—A European Journal*, 8, 2218–2224.
- [48] Vacca, A., Nativi, C., Cacciarini, M., Pergoli, R., Roelens, S. (2004). A new tripodal receptor for molecular recognition of monosaccharides. A paradigm for assessing glycoside binding affinities and selectivities by H-1 NMR spectroscopy. *Journal of the American Chemical Society*, 126, 16456–16465.
- [49] Definition of BC_{50}^0 according to Reference 48: total concentration of receptor necessary for binding 50% of the ligand when the fraction of bound receptor is zero, that is, when forming the first complex molecule and, for 1:1 systems, coincides with the dissociation constant K_d . The lower is BC_{50}^0 , the higher is the affinity.
- [50] Cacciarini, M., Cordiano, E., Nativi, C., Roelens, S. (2007). A tricatecholic receptor for carbohydrate recognition: Synthesis and binding studies. *The Journal of Organic Chemistry*, 72, 3933–3936.
- [51] Cacciarini, M., Nativi, C., Norcini, M., Staderini, S., Francesconi, O., Roelens, S. (2011). Pyrrolic tripodal receptors for carbohydrates. Role of functional groups and binding geometry on carbohydrate recognition. *Organic & Biomolecular Chemistry*, 9, 1085–1091.
- [52] Francesconi, O., Ienco, A., Moneti, G., Nativi, C., Roelens, S. (2006). A self-assembled pyrrolic cage receptor specifically recognizes beta-glucopyranosides. *Angewandte Chemie (International ed. in English)*, 45, 6693–6696.

- [53] Nativi, C., Cacciarini, M., Francesconi, O., Vacca, A., Moneti, G., Ienco, A., Roelens, S. (2007). Pyrrolic tripodal receptors effectively recognizing monosaccharides. Affinity assessment through a generalized binding descriptor. *Journal of the American Chemical Society*, *129*, 4377–4385.
- [54] Nativi, C., Francesconi, O., Gabrielli, G., De Simone, I., Turchetti, B., Mello, T., Di Cesare Mannelli, L., Ghelardini, C., Buzzini, P., Roelens, S. (2012). Aminopyrrolic synthetic receptors for monosaccharides: A class of carbohydrate-binding agents endowed with antibiotic activity versus pathogenic yeasts. *Chemistry—A European Journal*, *18*, 5064–5072.
- [55] Joshi, G., Davis, A. P. (2012). New H-bonding patterns in biphenyl-based synthetic lectins; pyrroliediamine bridges enhance glucose-selectivity. *Organic & Biomolecular Chemistry*, *10*, 5760–5763.
- [56] Francesconi, O., Gentili, M., Roelens, S. (2012). Synthetic tripodal receptors for carbohydrates. pyrrole, a hydrogen bonding partner for saccharidic hydroxyls. *The Journal of Organic Chemistry*, *77*, 7548–7554.
- [57] Ladomenou, K., Bonar-Law, R. P. (2002). Urea porphyrins as simple receptors for sugars. *Chemical Communication*, *38*, 2108–2109.
- [58] Kim, Y. H., Hong, J. I. (2002). Molecular recognition of carbohydrates through directional hydrogen bonds by urea-appended porphyrins in organic media. *Angewandte Chemie (International ed. in English)*, *41*, 2947–2950.
- [59] Lee, J. D., Kim, Y. H., Hong, J. I. (2010). Carbohydrate recognition through H-bonding and CH- π interactions by porphyrin-based receptors. *The Journal of Organic Chemistry*, *75*, 7588–7595.
- [60] Waki, M., Abe, H., Inouye, M. (2007). Translation of mutarotation into induced circular dichroism signals through helix inversion of host polymers. *Angewandte Chemie (International ed. in English)*, *46*, 3059–3061.
- [61] Inouye, M., Miyake, T., Furusyo, M., Nakazumi, H. (1995). Molecular recognition of β -ribofuranosides by synthetic polypyridine-macrocyclic receptors. *Journal of the American Chemical Society*, *117*, 12416–12425.
- [62] Abe, H., Horii, A., Matsumoto, S., Shiro, M., Inouye, M. (2008). D_{3h} -symmetrical hydrogen-bonding unit as a saccharide recognition and self-assembling module. *Organic Letters*, *10*, 2685–2688.
- [63] Abe, H., Takashima, S., Yamamoto, T., Inouye, M. (2009). Azacrown-attached meta-ethynylpyridine polymer: Saccharide recognition regulated by supramolecular device. *Chemical Communications*, *45*, 2121–2123.
- [64] Abe, H., Aoyagi, Y., Inouye, M. (2005). A rigid C_{3v} -symmetrical host for saccharide recognition: 1,3,5-tris(2-hydroxyaryl)-2,4,6-trimethylbenzenes. *Organic Letters*, *7*, 59–61.
- [65] Schneider, H. J., Yatsimirsky, A. *Principles and Methods in Supramolecular Chemistry*, John Wiley and Sons, England, 2000; p. 205.
- [66] Rauschenberg, M., Bomke, S., Karst, U., Ravoo, B. J. (2010). Dynamic peptides as biomimetic carbohydrate receptors. *Angewandte Chemie (International ed. in English)*, *49*, 7340–7345.
- [67] Otto, S., Furlan, R. L. E., Sanders, J. K. M. (2000). Dynamic combinatorial libraries of macrocyclic disulfides in water. *Journal of the American Chemical Society*, *122*, 12063–12064.
- [68] Otto, S., Sanders, J. K. M. (2002). Selection and amplification of hosts from dynamic combinatorial libraries of macrocyclic disulfides. *Science*, *297*, 590–593.
- [69] Daniel, J. M., Friess, S. D., Rajagopalan, S., Wendt, S., Zenobi, R. (2002). Quantitative determination of noncovalent binding interactions using soft ionization mass spectrometry. *International Journal of Mass Spectrometry*, *216*, 1–27.
- [70] Ryan, T. J., Lecollinet, G., Velasco, T., Davis, A. P. (2002). Phase transfer of monosaccharides through noncovalent interactions: Selective extraction of glucose by a lipophilic cage receptor. *Proceedings of the National Academy of Sciences*, *99*, 4863–4866.

- [71] Ke, C., Destecroix, H., Crump, M. P., Davis, A. P. (2012). A simple and accessible synthetic lectin for glucose recognition and sensing. *Nature Chemistry*, 4, 718–723.
- [72] Mulder, A., Huskens, J., Reinhoudt, D. N. (2004). Multivalency in supramolecular chemistry and nanofabrication. *Organic & Biomolecular Chemistry*, 2, 3409–3424.
- [73] Huskens, J. (2006). Multivalent interactions at interfaces. *Current Opinion in Chemical Biology*, 10, 537–543.
- [74] Martos, V., Castreno, P., Valero, J., de Mendoza, J. (2008). Binding to protein surfaces by supramolecular multivalent scaffolds. *Current Opinion in Chemical Biology*, 102, 698–706.
- [75] Uhlenheuer, D. A., Petkau, K., Brunsveld, L. (2010). Combining supramolecular chemistry with biology. *Chemical Society Reviews*, 39, 2817–2826.

CHAPTER 11

CYCLODEXTRIN-BASED ARTIFICIAL ENZYMES: SYNTHESIS AND FUNCTION

CHRISTIAN MARCUS PEDERSEN and MIKAEL BOLS

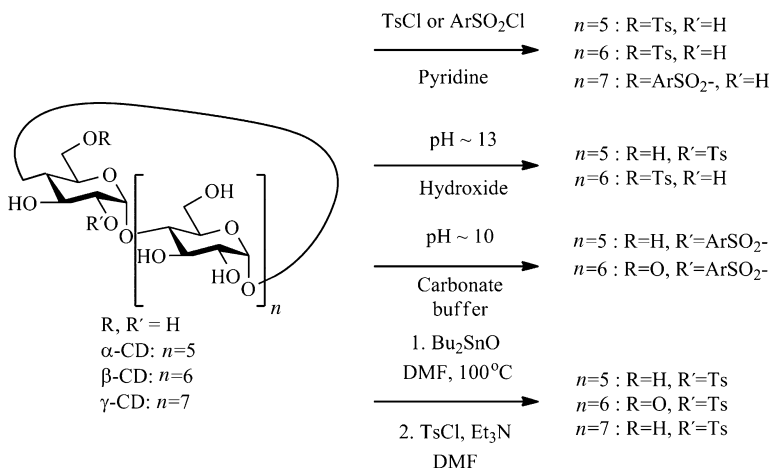
11.1 INTRODUCTION

The most common and hence commercially available cyclodextrins consist of 6, 7, or 8 α -1,4-linked D-glucosyl units, which form a conical bucket-like structure. The remaining hydroxyl groups, that is, 2-OH, 3-OH, and 6-OH, are all placed on the outside of the bucket, making it polar and hydrophilic. The cavity, however, is apolar and can therefore bind small hydrophobic compounds. The ability to complex apolar molecules in their cavity, thereby making them soluble in aqueous solvents, has been studied extensively. This property of cyclodextrins has led to many industrial uses, especially as a food ingredient and as a flavor/aroma stabilizer. The ability of cyclodextrins to function as molecular hosts has also interested the academic community. In particular, the complexation of compounds in aqueous solutions has gained interest, and cyclodextrin-based artificial enzymes (chemzymes) have been developed during the last three decades.

11.2 FUNCTIONALIZATION ON THE PRIMARY RIM

11.2.1 Unprotected Cyclodextrins

The interest in mimicking enzymes, where one or more often two functional groups participate in the catalysis, has required the development of selective functionalization of cyclodextrins. This has led to a number of different approaches, which can be divided into two major groups: the direct and the indirect approach. The direct method refers to the functionalization of native cyclodextrins to obtain the mono-, di-, tri-, and other modified products, which can then be further protected or modified. The indirect



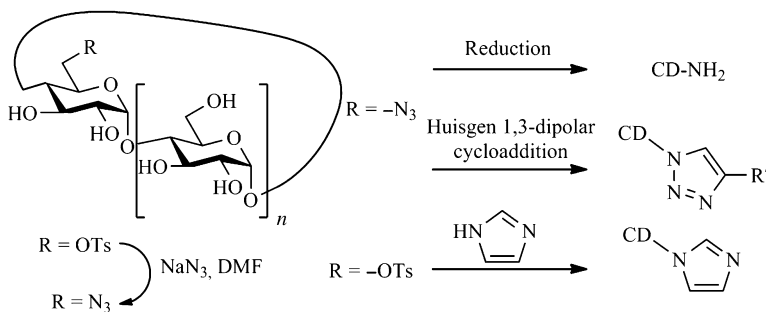
Scheme 11.1. Selective arylsulfonylation of cyclodextrins under various conditions.

approach is based on the stripping of protective groups in a selective manner from a fully protected cyclodextrin, giving one or a few available hydroxyl groups for further modification.

11.2.1.1 OH Activation and Substitution The first successful approach to the selective functionalization of cyclodextrins relied on complexation followed by reaction of an apolar electrophilic reagent such as a sulfonate or acyl derivative. These methods have been refined over the years and represent a valuable toolset for building up artificial enzymes.

The most widely studied modification of the primary hydroxyl groups in cyclodextrins is tosylation, which provides a useful starting point for further modifications. Over the years, numerous modifications in the procedures have appeared, but there are some general trends for the optimal facial selectivity and monofunctionalization (multiple functionalizations are generally unselective) (Scheme 11.1) [1].

Taking advantage of the fact that the primary rim is easily accessible and more nucleophilic than the secondary, a modification here is advantageous. Using the standard conditions in carbohydrate chemistry for tosylation, that is, tosyl chloride in pyridine, a selective mono-6-*O*-tosylation takes place in reasonable yields. Melton and Slessor reported the first selective monotosylation of α -cyclodextrin using the conditions above and isolated the product in approximately 45% yield [2]. The β -cyclodextrin-6-*O*-tosylate could be prepared by using excess cyclodextrin (1.4 equiv), giving the product in 31% yield (based on cyclodextrin, 42% based on TsCl) [3]. Performing the tosylation reactions in alkaline aqueous solution (pH 13) results in a 1:1 complex formation followed by site-selective tosylation. β -Cyclodextrin preferentially gives the 6-*O*-tosylate, whereas α -cyclodextrin is tosylated on the 2-OH [4]. Many modifications of these procedures have appeared over the years, but with only a few improvements. Using tosyl imidazole instead of tosyl chloride is one of the more noticeable contributions [5]. Recently, however, an elegant approach involving a copper complex formation of two β -cyclodextrins (tail to tail), leaving the primary site available, followed by a monotosylation, has appeared [6]. The procedure yields 48% of the desired product



Scheme 11.2. Common reactions with the cyclodextrin monotosylates.

isolated by a simple crystallization from water. The method has furthermore been used on kilogram-scale synthesis, where the reuse of copper salts is another advantage.

Bulky arylsulfonyl chlorides have also been found useful, especially for the larger γ -cyclodextrins, where the monofunctionalized products can be obtained in around 70% yield [7]. Despite the bulkier reagent, unsymmetric difunctionalization was still practically unselective, giving a mixture of all combinations in yields from 2.2% to 4% [8].

With the relatively easy access to monotosylated cyclodextrins, this has been the main entrance to modifications and hence artificial enzymes. The substitutions of the tosylates are normally unproblematic, and a vast number of examples have been described. In addition to using azide as nucleophile for substitution in a one-pot approach [9], other nitrogen nucleophiles such as hydrazine [10] and amines have been widely used. Azides, in particular, have been synthesized and used as building blocks, since they are easily reduced to the corresponding amines [11] and even more importantly used in copper-catalyzed Huisgen 1,3-dipolar cycloadditions (Scheme 11.2) [12]. Monointroduction of azide onto cyclodextrins has also been successfully performed using triphenylphosphine-carbontetrabromide reagent system for activation followed by azide substitution. This provided the monoazide in up to 53% yield (β -cyclodextrin) from the unprotected cyclodextrin [13]. Substitution of the tosyl with imidazole has provided an artificial serine protease (enzyme cleaving peptides via the nucleophilic OH of a serine at the active site). Interestingly, it was observed that the imidazole moiety could regioselectively acylate or mesylate in an intramolecular fashion in the D (α -cyclodextrin) or E (β - and γ -cyclodextrin) position of cyclodextrins [14].

The lack of regioselectivity in difunctionalization of unprotected cyclodextrins has been solved by using intramolecular directed reactions. Fujita and coworkers used mesitylenedisulfonyl chloride for the capping of two adjacent primary hydroxyl groups in β -cyclodextrin (A and B) [15]. With yields of around 20%, the method is superior compared with, for example, a ditosylation, which gave 6% (Figure 11.1) [1]. Even more useful is the selective ring opening (10:1) of the mesitylenedisulfonyl capped β -cyclodextrin, which turned out to be selective toward opening at the B-6-O site (42% yield) when imidazole was used as the nucleophile. Substitution of the remaining sulfonate with benzyl sulfide gave the heterofunctionalized β -cyclodextrin.

Another interesting aspect of the AB-di-6-O-tosylates is their dimerization using sodium sulfide, which gives the “head-head” dimer in 21% yield, whereas the dimerization of the corresponding A,B-diiodide and A,B-disulfide gives the topoisomer selectively in 19% yield [16]. When using the linear diphenylmethane-*p,p'*-disulfonylchloride,

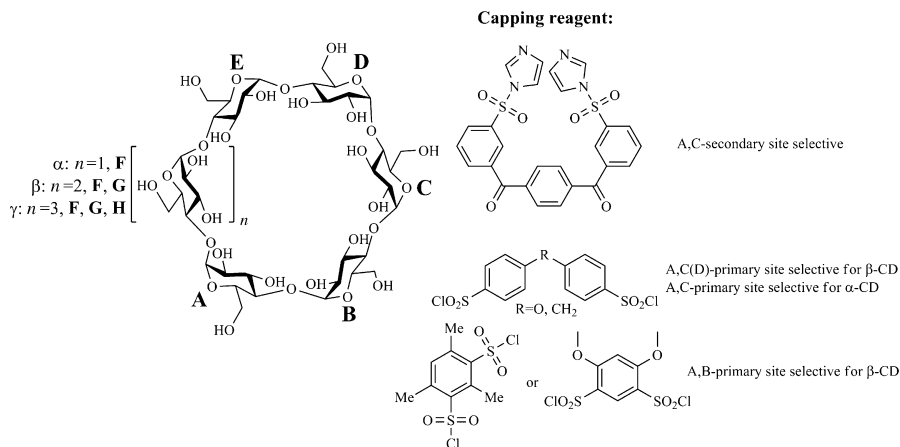
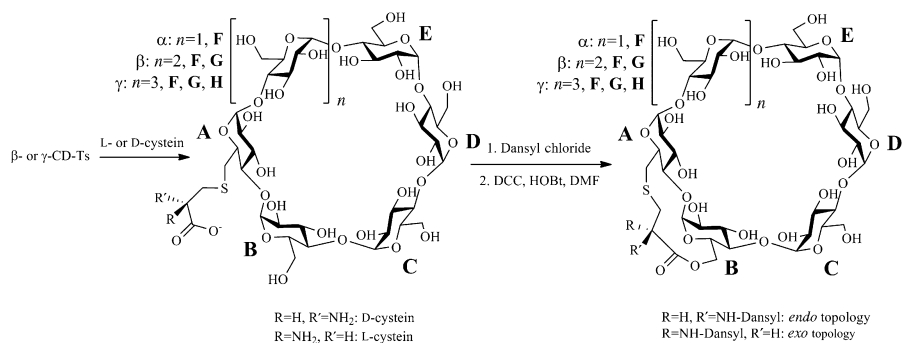


Figure 11.1. Examples of selective capping reagents used in cyclodextrin chemistry.



Scheme 11.3. Synthesis of β - and γ -cyclodextrin with *exo* and *endo* isomerism: “vector-selective” functionalization.

a capping of opposite hydroxyl groups was favored over the adjacent ones, giving reasonable yields of the monocapped cyclodextrins (α -cyclodextrin 43% [17]; β -cyclodextrin 20% [18]). The concept of capping cyclodextrins has been refined over the years and represents an important tool for selective cyclodextrin functionalization [19].

Regioselectivity in heterodifunctionalization of cyclodextrins has additionally been obtained by intramolecular macrolactone formation, also termed “vector”-selective reaction [20]. Starting from 6-*O*-tosyl- β -cyclodextrin, which was substituted by L- or D-cysteine, followed by conversion to the sulfonamide using dansyl chloride, activation of the remaining carboxylic acid with *N,N'*-dicyclohexylcarbodiimide (DCC) and 1-hydroxybenzotriazole (HOBT) resulted in a selective macrolactone formation with the 6-B-OH. The reaction is highly “clockwise” selective, giving the A–B macrocycle in around 80% yield independent of the cysteine stereochemistry. The L-cysteine gives the *exo* isomer, whereas the D gives the *endo* isomer (Scheme 11.3). This is of major interest in developing preorganized artificial enzymes.

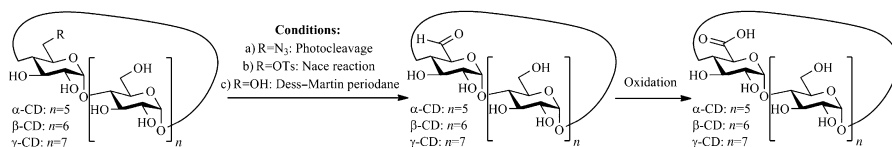
The problem regarding clockwise/counterclockwise selectivity has also been investigated in γ -cyclodextrin [21]. The first approach involved unselective formation of the A–B ditosylate, which was then monosubstituted by cysteine, giving two regioisomers. The obtained isomers were treated with dansyl chloride to give the sulfonamides and thoroughly analyzed using α -amylase degradation followed by post-source decay mass spectrometry (PSD-MS) as well as nuclear magnetic resonance (NMR) studies. Attempts to perform intramolecular substitution of the tosyl by the carboxylic acid were not successful, and the topoisomeric lactones had to be prepared in another way. Using the same approach as for the β -cyclodextrin, as described above, selectively gave the *exo* and *endo* isomers in about 60% yield [22].

Recently, a solid-phase approach for the monofunctionalization of cyclodextrin appeared. This involves the buildup of the linker part on solid phase using phosphoramidite chemistry followed by a reaction with the native cyclodextrin [23]. The cyclodextrin carrying the phosphate-linked label can then be isolated by high-performance liquid chromatography (HPLC) in yields ranging from 36% to 43%, which is superior to a traditional route involving protective chemistry and multiple steps.

11.2.1.2 Oxidation Mono-oxidation of unprotected cyclodextrins is an alternative way to obtain a monofunctionalization that is orthogonal to the hydroxyl groups in reactivity. An aldehyde, for example, can be conjugated to other molecules via imine (or iminium ion) formation and subsequent reduction to the respective amines. These reactions can be performed in water and are therefore suitable for ligation with, for example, biomolecules.

The first reports on cyclodextrin monoaldehydes date back to the mid-1970s, where it was shown that cyclodextrin monoaldehydes could be synthesized from photocleavage of an azide, obtained from the monotosylate, or oxidation of the corresponding amine by ninhydrin [24]. This approach was significantly improved by the direct conversion of the monotosylate to the aldehyde by the Nace reaction conditions, that is, dimethyl sulfoxide (DMSO) and amine base. In this way, the aldehyde could be prepared in up to 64% yield (Scheme 11.4) [25, 26].

The obtained aldehydes were further oxidized to the carboxylic acid, reduced to the native cyclodextrin, and treated with NaHSO_3 and amines [27]. β -Elimination was observed as a side product in the Nace reaction; this pathway could be favored by using N-oxides instead of amine bases. In this way the cyclodextrin could be opened to a linear oligosaccharide. The normally undesired β -elimination could be avoided by a direct and selective mono-oxidation of the native cyclodextrin using Dess–Martin periodane as the reagent [28]. The yields in the reactions were near quantitative, and only the monoaldehydes were isolated. Blocking of the remaining primary hydroxyl groups by the complexation of the reagent could be a plausible explanation for this selectivity.



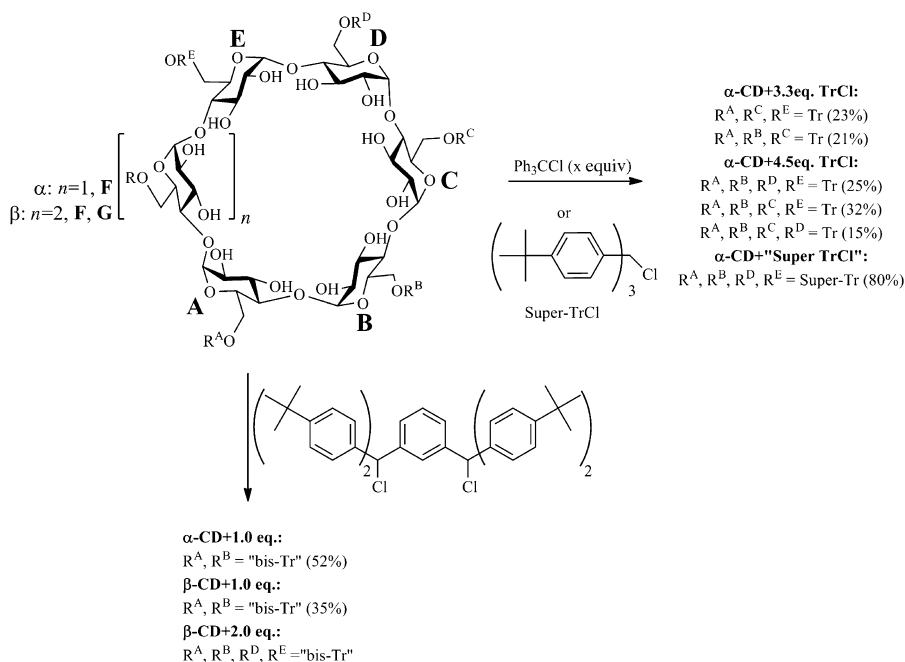
Scheme 11.4. Synthesis of cyclodextrin monoaldehydes by different methods.

11.2.1.3 OH Protection Selective protection of one or more primary hydroxyl groups is an alternative (indirect method) approach in contrast to the direct functionalization described above. Selective acylations of cyclodextrins have been investigated, but the regioselectivity obtained in carbohydrate chemistry has so far not been achieved. By taking advantage of the complexation properties, a reasonable selective acylation of the primary hydroxyl groups can nevertheless be obtained with, for example, palmitoyl or valeryl esters [29].

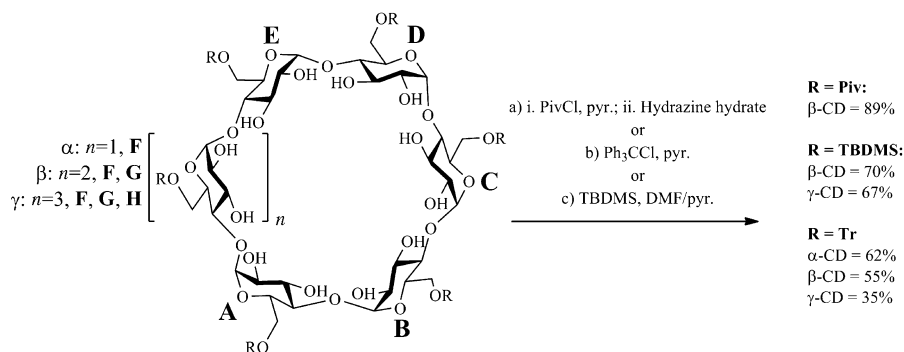
Since the primary hydroxyl groups are more nucleophilic and more accessible; it is possible to regioselectively protect them by using bulky protective groups. In particular, trityl and related compounds have successfully been used, not only to per-protect the primary hydroxyl groups but also to distinguish between them. Tri- and tetratrylated α -cyclodextrins have been prepared by tritylation using trityl chloride in pyridine at elevated temperatures followed by methylation. The tritrylation gave a separable mixture of the ACE isomer (23%), the ABC isomer (21%), and an inseparable mixture of ABD and ABE (Scheme 11.6) [30, 31]. Tetratrylation under the same conditions but with 4.5 equiv trityl chloride resulted in a mixture of the methylated ABDE isomer (25%), the ABCD isomer (15%), and the ABCE isomer (32%), all separable by column chromatography. When peracetylation of the tetratrylated products was performed, an interesting shift of the two anomeric protons was observed. Due to the anisotropic effect from the neighboring trityl group, an upfield shift to 2.88 ppm was observed (these signals are normally observed at around 5.5 ppm). These abnormal shifts provided information about the conformation of tritylated cyclodextrins [32]. The importance of bulkiness in the applied protective groups has been underlined with the use of the "supertrityl" protective group (*tris*(4-*tert*-butylphenyl)methyl chloride), which afforded the ABDE-tetraalkylated α -cyclodextrin in approximately 80% yield (Scheme 11.5) [33].

The trityl approach has been expanded with a bis-trityl reagent, which can selectively tether two neighboring 6-OHs together, giving the AB-protected cyclodextrin in 52% for α -cyclodextrin and 35% for the β -cyclodextrin (Scheme 11.5) [34]. Further reaction with one additional equivalent gave the ABDE tetraprotected cyclodextrin. Methylation and purification of the crude product gave the β -cyclodextrin derivative in 50% yield. Acid-mediated deprotection gave the tetraols (α - and β -cyclodextrin), which can then be further functionalized. Tetramesylation followed by substitution by dianions, such as PhP^{2-} and S^{2-} , provided the phenylphosphane- and sulfur-doubly capped cyclodextrins, respectively, in a regiospecific manner [35]. When cyclic sulfates were used instead of mesylates, a regioselective nucleophilic substitution was observed. Bulky nucleophiles such as Ph_2P^- or the phthalimide anion gave excellent yields and regioisomeric excess, whereas small nucleophiles (N_3^-) gave a moderate regioselectivity [36].

Selective per-protection of the primary side of cyclodextrins can also be achieved by using bulky protective groups. Pivaloyl has successfully been used: for example, β -cyclodextrin was treated with pivaloyl chloride (9.1 equiv) in pyridine at 60°C overnight. The pivaloylated secondary hydroxyl groups were subsequently selectively removed with hydrazine hydrate, giving the per-6-O-pivoylated product in 89% yield (Scheme 11.6) [37]. *tert*-Butyldimethylsilylation of the primary hydroxyl groups is another excellent method for facial protection of cyclodextrins. Thus, α -, β -, and γ -cyclodextrins have been protected in good to excellent yields. More forceful conditions with excess reagent regioselectively protect the secondary O-2 hydroxyl groups (Scheme 11.6) [38–40]. Even the per-6-O-tritylated cyclodextrins have recently been



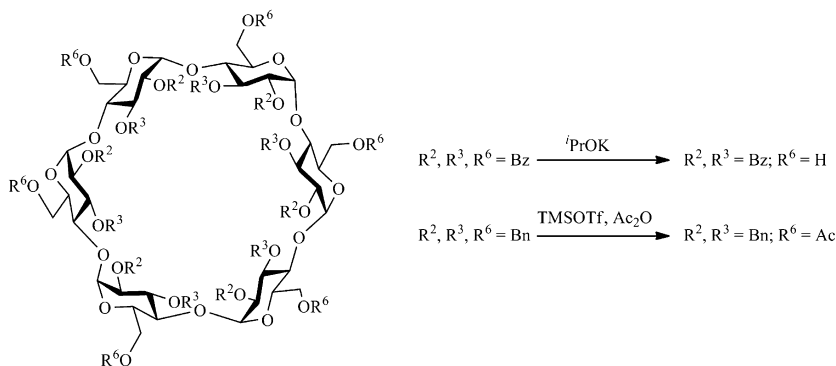
Scheme 11.5. Regioselective tritylation, "supertritylation," and "bistritylation" of α - and β -cyclodextrins.



Scheme 11.6. Site-selective per-protection of cyclodextrins.

synthesized in good yields ranging from 35% (γ -cyclodextrin) to 55% (β -cyclodextrin) and 62% (α -cyclodextrin) [41]. The tritylated compounds have the advantage over the silylated and acylated in being inert under basic conditions (e.g., alkylations) but still easily removed under mild acidic conditions.

Per-protection of the native cyclodextrins is often the first step in more sophisticated syntheses of artificial enzymes (or other complex cyclodextrin derivatives). Permethylation and peracetylation can be performed uneventfully using standard methods



Scheme 11.7. Site-selective deprotection of per-protected α -cyclodextrin.

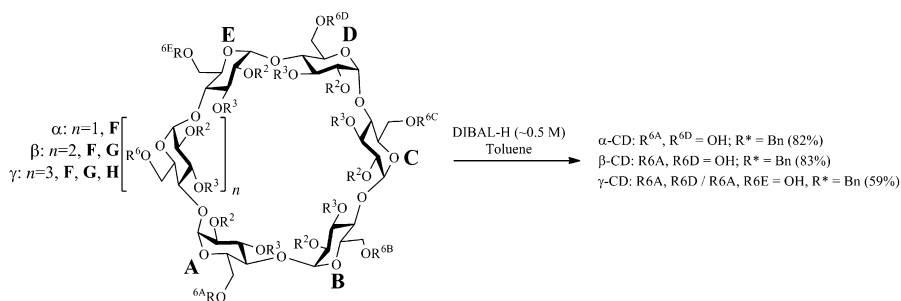
known from carbohydrate chemistry. Perbenzylation, however, can be trickier; that is, it is essential to use benzyl chloride as the alkylation reagent and not benzyl bromide. As a solvent, DMSO is preferred over dimethylformamide (DMF) [42].

11.2.2 Synthesis with Protected Cyclodextrins

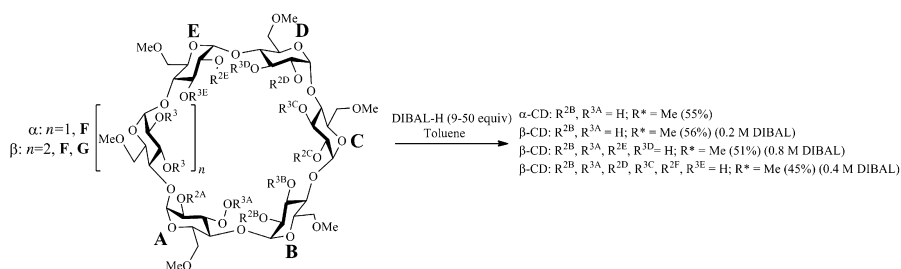
11.2.2.1 Selective Deprotection and Migration Per-protection followed by a selective deprotection has become an important route to pure isomers of cyclodextrins having several functional groups installed. Discussed earlier was one of the early examples involving selective removal of pivaloyl groups from the secondary hydroxyl groups with hydrazine hydrate described. The face-selective removal of benzoyl esters has also been developed. Treating a perbenzoylated α -cyclodextrin with potassium isopropoxide gave, after purification, the α -cyclodextrin-dodeca(2,3)benzoate in 61% yield (Scheme 11.7).

Applying the same conditions to the β -cyclodextrin was not successful, however [43]. Acid-mediated regioselective debenylation of a perbenzoylated α -cyclodextrin has been performed [44]. When treating the fully protected cyclodextrin with trimethylsilyl trifluoromethanesulphonate (TMSOTf) in acetic anhydride at -35°C , 95% of the hexakis(6-*O*-acetyl-2,3-di-*O*-benzyl)cyclomaltohexaose could be isolated (Scheme 11.7). This could then be deacetylated to give the hexaol or debenzylated to the dodecaol, leaving the 6-*O*-acetyls intact.

A milestone in the regioselective deprotection of cyclodextrins was reached by Sinaÿ and Pearce [45], who developed a reductive debenylation method that has had an immense influence on the synthesis of sophisticated artificial enzymes. When a perbenzoylated cyclodextrin (α , β , or γ) was treated with diisobutylaluminium-hydride (DIBAL-H) in toluene, excellent yields of the A–D (+A–E for the γ -cyclodextrin) were obtained (Scheme 11.8). The reaction conditions proved to be crucial for the outcome; that is, the optimal conditions for diol formation from perbenzoylated α -cyclodextrin was a DIBAL-H concentration of 0.5 M (120 equiv) at 50°C for 2 h, which gave the diol in 82%. The β -diol was obtained under slightly different conditions (140 equiv and 30°C), which resulted in 83% yield. The γ -cyclodextrin demanded slightly higher temperature (55°C) and 150 equiv DIBAL-H, and gave a moderate yield of 59%. The



Scheme 11.8. Regioselective reductive debenzoylation of perbenzylated cyclodextrins.



Scheme 11.9. Regioselective demethylation of per-methylated α - and β -cyclodextrin.

original procedure has been refined over the years; for example, it has been demonstrated that the use of 4 Å molecular sieves can lower the concentration and thereby the amount needed of DIBAL-H [46]. More recently, μ -wave heating has lowered the required amount of DIBAL-H to 5 equiv [47].

Applying the reductive debenzoylation conditions on a 6-O-methylated perbenzylated α -cyclodextrin, the A–D diol was isolated in 59% yield; the primary methyl ethers are cleaved more readily than the secondary benzyl ethers [48]. However, the facial selectivity was rendered when using permethylated cyclodextrin. Demethylation from the primary face was observed only as a minor product (approximately 20% for α - and β -cyclodextrin). The major product was 2B-3A-diol, which could be isolated in around 55% [49]. When increasing the amount of DIBAL-H together with decreasing the reaction temperature from 50°C to room temperature, a regioselective removal of 4-methyl groups from the secondary rim could be achieved in more than 50% yield (Scheme 11.9) [50]. Longer reaction times gave the hexaol 2B-3A-2D-3C-2F-3E in one step in 45% yield [51]. It should be pointed out that although the reactions are selective and give good yields, the purifications are very tedious and lengthy [52]. The reductive dealkylation of per-protected cyclodextrins has provided several tools for selective modification of cyclodextrins. A particularly interesting observation was the influence of the cyclodextrins' circular chirality on the outcome of the reactions. The differentiation between the primary hydroxyl groups based on this has been illustrated with DIBAL-H-mediated deprotection on AD-functionalized perbenzylated cyclodextrins. For instance, with A–D-dideoxy perbenzylated α -cyclodextrin, clockwise debenzoylation takes place [53].

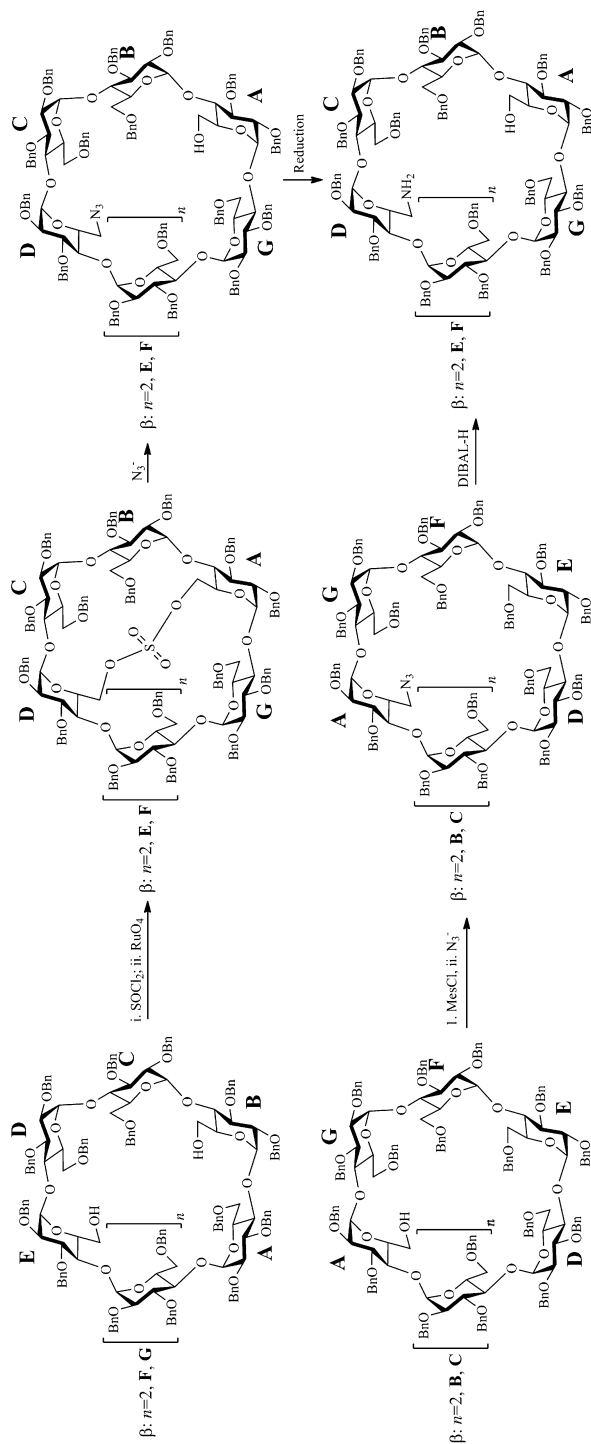
Similar selectivity was seen when an A–D-bridged α -cyclodextrin is treated with DIBAL-H; the C–F diol was isolated in 86% yield [54]. Further refinement of the deprotection methods has led to heterotrifunctionalization and tetradifferentiation of α -cyclodextrin in a selective and controlled manner beyond what is possible when starting with native cyclodextrin by selective introduction of protective groups [55].

Recently, Ling and coworkers studied the DIBAL-H-mediated debenzoylation of perbenzoylated α -cyclodextrin beyond the diol product originally described by Sinaÿ and coworkers. When the reaction was performed with DIBAL-H in hexanes, instead of toluene, side products were observed [56]. Prolonging the reaction time to 96 h made it possible to obtain two new products in yields of 32% and 10%, respectively. NMR studies revealed that the new products corresponded to the 3A, 6A, and 6E triol and the 3A, 6A, 3E, and 6E tetraol, which both are highly interesting for artificial enzyme synthesis. Performing the reaction on β - and γ -cyclodextrins surprisingly resulted not in secondary rim debenzoylation, but instead in additional debenzoylation on the primary rim, giving 6-*O*-triols and 6-*O*-tetra-ols in moderate yields and as inseparable mixtures [57].

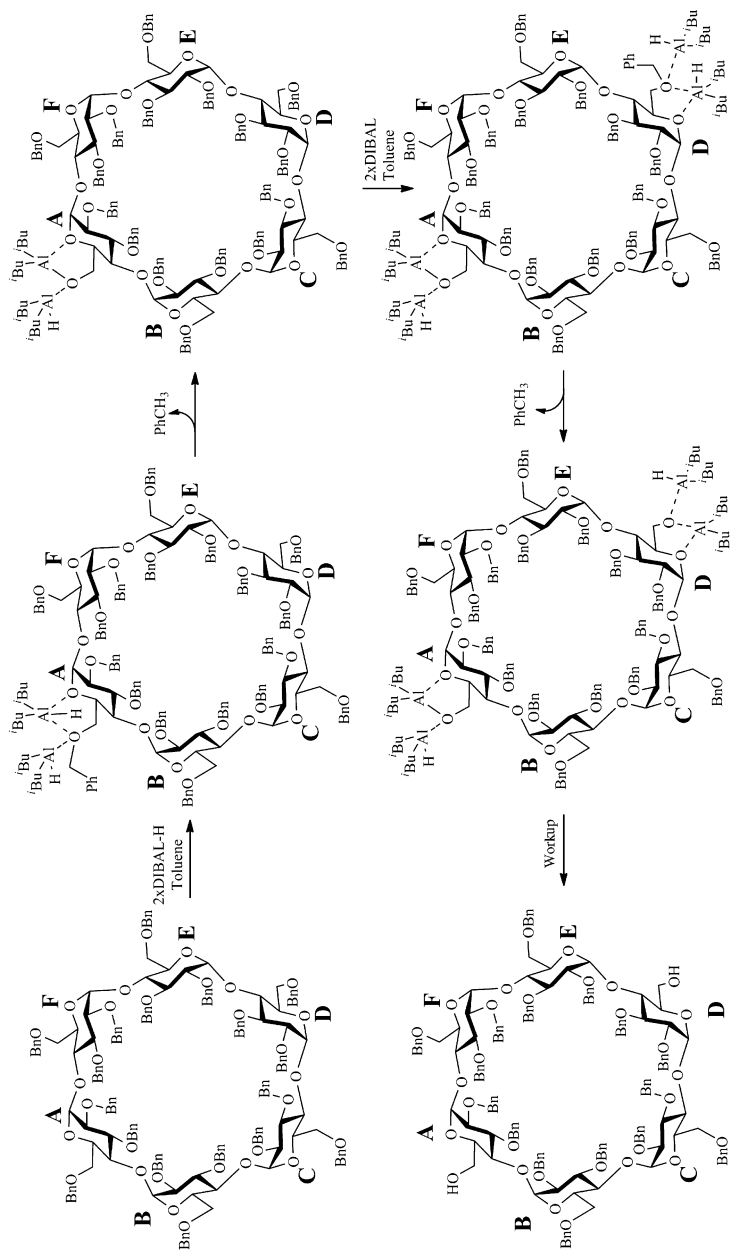
The regioselective reductive debenzoylation is not limited to alkyl ethers. Perbenzoylated cyclodextrin-monoazides (6A) are easily obtained from the mono-ol via activation and substitution. DIBAL-H-mediated deprotection of the azide under the standard conditions reduced the azide to the amine together with a regioselective monodebenzoylation (Scheme 11.10) [58]. The selectivity is as for the diol formation toward the diametrically opposed sugar ring due to steric hindrance. Due to the rotational chirality of the cyclodextrins, two regioisomeric products are possible with the β -cyclodextrin, but interestingly only the A–D azido alcohol is obtained and not the A–E. Another approach to the same azido alcohol has been developed by Bols and coworkers [59]. In this method the much more accessible A–D- β -cyclodextrin diol is used as the substrate, which is transformed into the cyclic sulfite by treatment with thionyl chloride. RuO₄-mediated oxidation to the cyclic sulfate and subsequent opening with azide provided the A–E product in excellent yields and regioselectivity (Scheme 11.10). The striking regioselectivity for nucleophilic opening of the cyclic sulfate was explained by steric arguments obtained from modeling.

The mechanism and hence the explanation for the amazing selectivities obtained with the DIBAL-H has been intriguing chemists in the field since the first reports on reductive debenzoylation. Since the mono-ol could be isolated in good yields, depending on the conditions, and resubmitted to the reaction conditions to afford the diol, it was clear that the process was stepwise. By studying the reaction in a more simple system, it became clear that the ring oxygen (O5) participates in the complexation of DIBAL-H and that two equivalents of DIBAL-H are required (Scheme 11.11) [60].

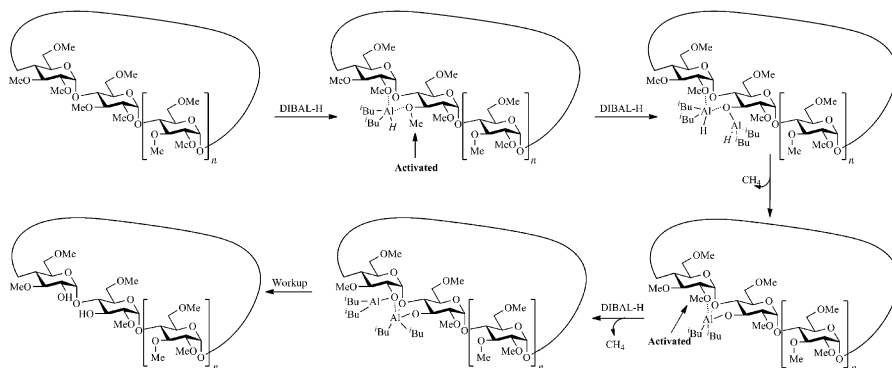
The proposed mechanism for the DIBAL-H-mediated secondary rim demethylation of cyclodextrin is slightly different from the one suggested for debenzoylation (Scheme 11.12) [61]. bis-de-*O*-methylation, for instance, is preferred and only the diol, tetraol, and hexaol are isolated as major products from the corresponding optimized procedures. Another interesting observation was that only the 3-hydroxy-cyclodextrin affords the diol when treated with DIBAL-H; starting from the 2-hydroxy-cyclodextrin no reaction took place. The diol formation from the 3-hydroxy-cyclodextrin was also found to be much faster than when starting from permethylated cyclodextrin. This suggests that the process is stepwise, with initial demethylation on the 3A-position followed by a fast demethylation on the 2B-position. As outlined in Scheme 11.13, two aluminum atoms take part in complex formation before the 3A-*O*-methyl is



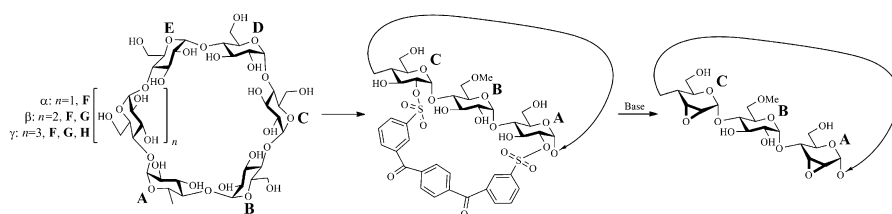
Scheme 11.10. A–D selective synthesis of amino alcohols from β -cyclodextrin.



Scheme 11.11. Proposed mechanism for A-D selective debenzylation.



Scheme 11.12. Proposed mechanism for the DIBAL-H-mediated demethylation of cyclodextrins.



Scheme 11.13. Regioselective A–C functionalization of cyclodextrins.

deprotected, giving an intermediate, which is already activated for the next deprotection; hence, this reaction takes place much faster than the first step.

Recently, the scope of DIBAL-H-mediated deprotection has been expanded to silyl ethers [62]. Since the cyclodextrins with *tert*-butyldimethyl silyl ethers on the primary rim and methyl ethers on the secondary are readily available, they were used as starting material for the reductive deprotection. When 3 equiv DIBAL-H were used in a concentration of 0.1 M, a monodeprotection was observed for the α -, β -, and γ -cyclodextrins in 71%, 62%, and 58% yield, respectively. These results are superior to the original debenzoylation method, where the mono-ol is hardly obtained in more than 60% and demands significantly more of the costly DIBAL-H reagent. By doubling the amount of DIBAL-H and tripling the concentration, a dideprotection took place in good yields: 68% for α -cyclodextrin and 71% for β -cyclodextrin.

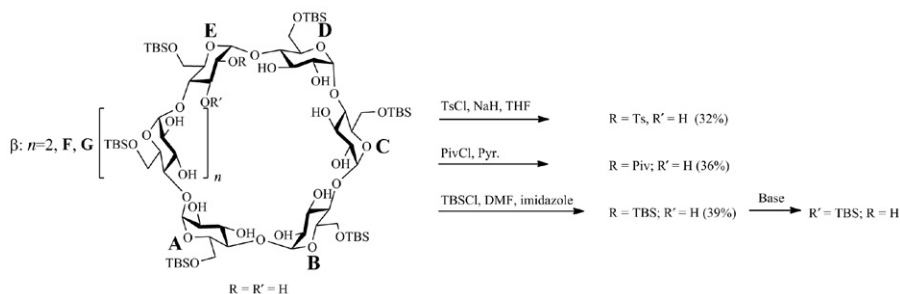
11.3 FUNCTIONALIZATION ON THE SECONDARY RIM

11.3.1 Unprotected Cyclodextrins

11.3.1.1 OH-Activation and Substitution As was the case with selective monofunctionalization of the primary rim in cyclodextrins, sulfonate esters played a central role in the early methods. The first report on a selective sulfonation of a secondary hydroxyl group of β -cyclodextrin describes the reaction of native cyclodextrin dissolved

in DMF together with a carbonate buffer (pH 9.9) with *m*-nitrophenyl tosylate at 60°C. After neutralization and workup, the 2-*O*-sulfonate could be isolated in around 10% by precipitation [63]. As discussed earlier [4], tosylation using tosyl chloride under alkaline conditions in water (or water DMF) preferentially gives the 2-*O*- α -cyclodextrin monotosylate in low yield as a mixture containing regioisomers [64]. Changing the sulfonylation reagent was shown to alter the selectivity; hence, β -naphthalenesulfonyl chloride in aqueous acetonitrile gave mainly the 3-*O*-sulfonate of β -cyclodextrin in 18% yield [65]. The regioselectivity and yield was significantly improved by a two-step procedure involving the formation of the 2,3-di-*O*-dibutylstanylidene in DMF followed by selective monotosylation of the 2-*O* by tosyl chloride [66]. This method proved to be general for all three cyclodextrins; that is, the α -, β -, and γ -cyclodextrin mono-2-*O*-tosylates were prepared in 30%, 32%, and 28%, respectively. The reactions have been only sparsely developed in the last two decades. Recently reported improvements include the use of *N*-tosyl imidazole as the reagent; the yield, however, is enhanced only to 34% for the β -cyclodextrin [67]. Disulfonylation reagents have also been applied for regioselective difunctionalization of the secondary rim. 1,4-Debenzoylbenzene-3',3''-disulfonyl imidazole has successfully been used for the selective sulfonylation of the C2A and C2C hydroxyl groups [68]. Reasonable yields, ranging from 39% to 58%, were obtained for the three common cyclodextrins (Scheme 11.13).

The facial selectivity toward the secondary rim has been improved by selective per *tert*-butyldimethylsilylation of the primary hydroxyl groups, leaving the secondary hydroxyl groups free for functionalization. Besides blocking the more accessible and reactive primary hydroxyl groups, the cyclodextrin is also becoming more soluble in organic solvents, which are required for many reactions. Monotosylation of the heptakis-6-*O*-(*tert*-butyldimethylsilyl)- β -cyclodextrin could then be performed in tetrahydrofuran (THF) with tosyl chloride as the reagent and NaH as the base to give the 2-*O*-tosylated product in 32% yield (Scheme 11.14) [69]. Monopivaloylation and mono-*tert*-butyldimethylsilylation were similarly obtained in 36% and 39% yields, respectively [70]. The obtained 2-*O*-*tert*-butyldimethylsilylether can, under strongly basic conditions, migrate to the 3-position (Scheme 11.14). This migration has also been observed in per 2,6-di-*O*-*tert*-butyldimethylsilylated cyclodextrins and hence provided a method for the selective functionalization of O2 or O3 [71]. The migration has been proposed to proceed either intra- or interglucosidically, depending on the substrate and conditions [72].



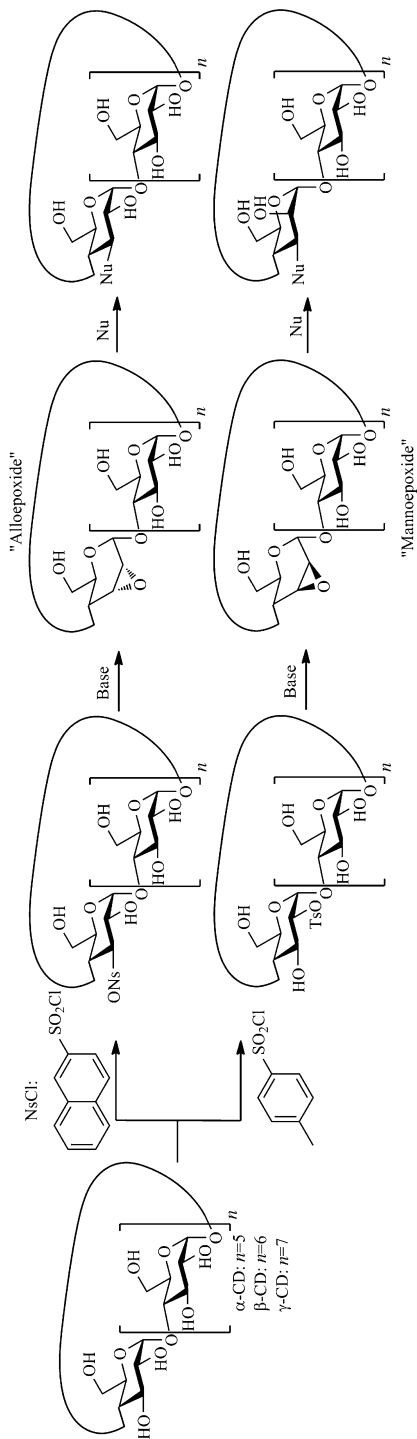
Scheme 11.14. Monofunctionalization of secondary hydroxyl groups in β -cyclodextrin.

The relatively efficient synthesis of 2-*O*-tosyl derivatives of cyclodextrins has paved the way for new secondary rim cyclodextrin derivatives. With the tosyl being a good leaving group, it can readily be substituted intramolecularly by the neighboring 3-OH under strongly basic conditions to form the 2,3 epoxide, which can then be regioselectively opened at the 3-position by another nucleophile (Scheme 11.15). Histidine has been introduced on the secondary rim in such a way to furnish the α -cyclodextrin-3-His derivative [73]. The opening of the epoxide on the C3 results in inversion of stereochemistry, hence the *altro* configuration is obtained. In this case the conformation of the *altro* side unit was determined to be in the 1C_4 conformation rather than the initial 4C_1 (in the parent glucoside). The catalytic activity as a hydrolase was found to be more than four times larger than the corresponding α -cyclodextrin-6-His derivative. The corresponding manno-2,3-epoxide of β -cyclodextrin has been obtained from the corresponding 2-*O*-tosylate and used for artificial enzyme synthesis. Opening of the epoxide with hydroxyl amine to the C3-hydroxyl amine group gave a mixture of products in 62% yield, which could catalyze transesterification [74]. The reactions of 2,3-anhydrocyclodextrins have been investigated under many conditions and with many nucleophiles. Both the 2,3-mannoepoxy- and the 2,3-alloepoxy- β -cyclodextrin derivatives are preferentially attacked by the nucleophile on the C3, since it is more accessible than C2 (Scheme 11.15) [75]. This regioselectivity has been observed with amine, azide, sulfur, hydroxyl, and halide nucleophiles. An interesting side reaction was observed under basic conditions where an attack on the 2,3-manno-epoxide, from the 3-OH on the neighboring glucoside, took place to give a tricyclic ring system. The corresponding 2A-3A-mannoepithio derivative has been obtained from 2A,3A-alloepoxy- β -cyclodextrin by treatment with thiourea [76].

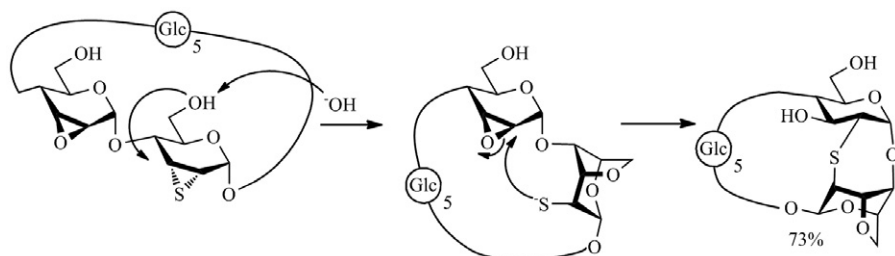
Base-mediated intramolecular nucleophilic attack from the neighboring 3G-alkoxide-gluco afforded the 3A,2B-anhydro-3B-deoxy-3B-thio- β -cyclodextrin, with a thiol group for further functionalization and a distorted cavity due to the tricyclic ring system. The product showed enhanced catalytic activity in hydrolysis compared with the undistorted thiol-cyclodextrin and the distorted cyclodextrin without the thiol group. The cross-linking of C2A and C2B via a sulfur atom has been achieved by a tandem reaction involving first a nucleophilic attack of the 6A-OH on the C3A of the epithio residue, which generates a 2B-thiolate anion that attacks the neighboring 2B,3B-mannoepoxy residue to form a tetracyclic ring system (Scheme 11.16) [77].

Monoalkylation of the secondary rim in a native cyclodextrin is another alternative to the approaches described above. Since the 2-OH is the more acidic of the hydroxyl groups, it can be selectively deprotonated and subsequently attack an electrophile. β -Cyclodextrin, for instance, can be selectively 2-*O*-benzylated in 33% yield followed by a permethylation and debenylation, giving the free OH for further modifications [78]. There are examples, however, of selective monoalkylations of the 3OH; for instance, D'Souza and coworkers has alkylated heptakis(6-*O*-*tert*-butyldimethylsilyl)- β -cyclodextrin with *N*-methyl-4-chloromethyl-2-nitroaniline to get the 3-*O*-mono-modified cyclodextrin in 28% yield after desilylation [79]. The unusual selectivity was explained by a complexation, which orients the electrophilic center toward the 3OH.

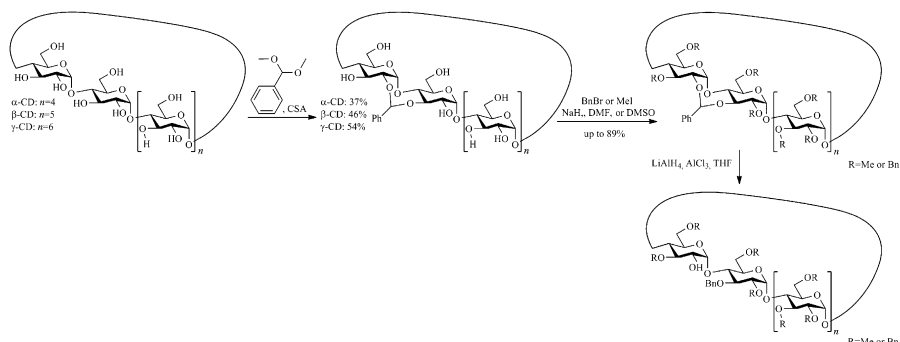
A method for the monofunctionalization of native β -cyclodextrin has recently been developed; hence, a copper complex formation followed by the addition of an alkylating reagent (benzyl bromide derivatives) provided the monofunctionalization of the 3-OH in up to 42% yield (for *p*-bromobenzyl ether formation) [80]. When allyl derivatives were used as the electrophiles, a change in regioselectivity was observed; that is,



Scheme 11.15. 2,3-Anhydro-cyclodextrin formation and reaction with nucleophile.



Scheme 11.16. Formation of tetracyclic segment in β -cyclodextrin mediated by basic conditions.



Scheme 11.17. Regioselective benzylidene formation, alkylation, and regioselective reductive benzylidene opening to give the mono-ol.

allyl bromide preferentially reacted with the 2-OH, whereas the 1-bromoallylbromide reacted with the 3-OH.

The regioselective direct protection of two hydroxyl groups on the secondary rim, giving a specific diol after protective group manipulations, is very attractive for artificial enzyme development. The method developed by Sollogoub for regioselective 2B-3A didemethylation on the secondary rim has earlier been described in this chapter. The same diol pattern can be obtained, in a few steps, starting from β -cyclodextrin. Heptakis(6-*O*-pivaloyl)- β -cyclodextrin was benzylidenated using α,α -dimethoxytoluene in DMF with camphorsulphonic acid (CSA) as the acid catalyst [37]. This yielded the 2B,3A-benzylidene in 46%, which was stable enough for pivaloyl removal and perbenzylation of the remaining hydroxyl groups (Scheme 11.17). The diol could easily be removed by CSA in MeOH-THF or reductively opened by $\text{LiAlH}_4\text{-AlCl}_3$ to give the 2A-OH in 87% yield.

11.4 SELECTIVELY MODIFIED CYCLODEXTRINS AS ARTIFICIAL ENZYMES: CHEMZYMES

As mentioned earlier, cyclodextrins have many advantages as the substrate-binding moiety in artificial enzymes due to their water solubility and environmentally friendly

character. The use of modified cyclodextrins as artificial enzymes has been long-standing [81, 82], and progress has been slow in large part due to the significant experimental challenges involved in preparing cyclodextrin derivatives. We will describe our latest progress (within the last 10 years) in the area where artificial enzymes have been made using novel cyclodextrin synthesis methods.

11.4.1 Glycosidases

Glycosidases or glycoside hydrolases are a widespread group of enzymes that perform an important biochemical role by catalysis of the hydrolytic cleavage of glycoside bonds. Glycosidases are responsible for catalyzing the degradation of polysaccharides, such as cellulose, starch, and glycogen, into glucose for the trimming of cell-surface oligosaccharides and for promoting many other important reactions. The glycosidase lysozyme was the first enzyme to have its three-dimensional structure determined, and the catalytic machineries of glycosidases are fairly well understood [83]. In the most common types of glycosidases, there are two carboxylic acid groups in the glycosidase active site that are important for catalyzing the reaction. One catalytic acid group acts as a general acid that protonates the glycosidic bond, and the other acts either as a nucleophile (in the so-called retaining glycosidases) or as a general base (in the inverting glycosidases) (Figure 11.2).

The comparatively simple catalytic machinery of glycosidases makes them almost ideal targets for synthetic enzyme mimics. The distance between the carboxylic acids in a retaining glycosidase is 5.5 Å, while it is 10.5 Å in an inverting glycosidase [83]. Since the diameter across the primary rim of the cyclodextrin is 5.0 Å in α -cyclodextrin and 6.5 Å in the β -cyclodextrin and thus is close to the distance in the retaining glycosidase [84], one can envision a retaining glycosidase model based on attaching two

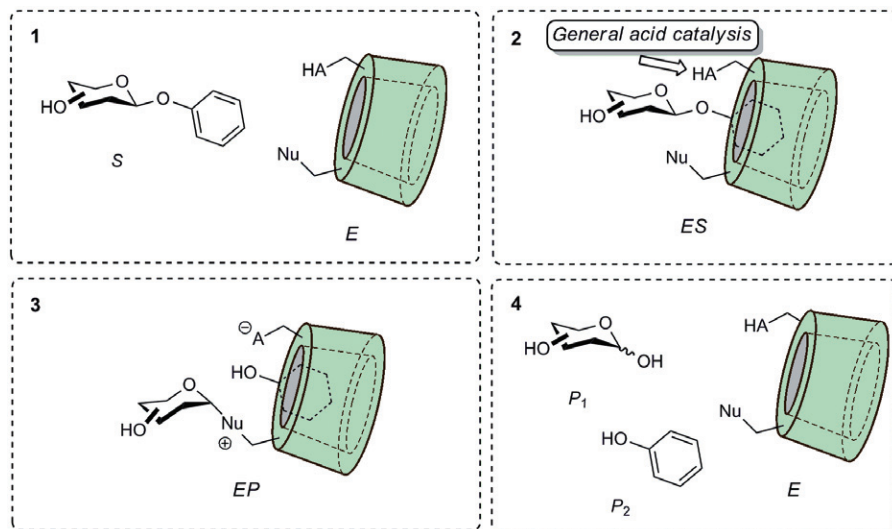
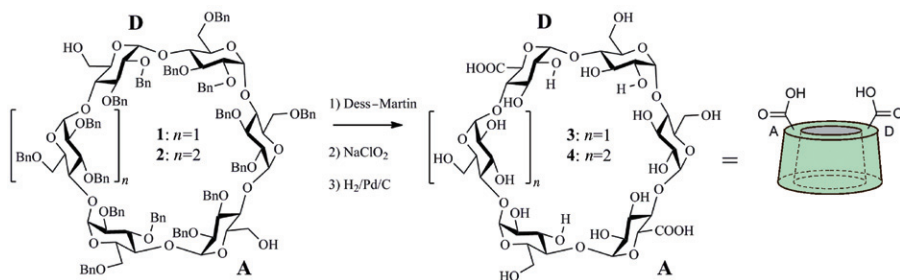


Figure 11.2. Glycosidase model performing catalysis with retention of configuration.



Scheme 11.18. Synthesis of cyclodextrin acids.

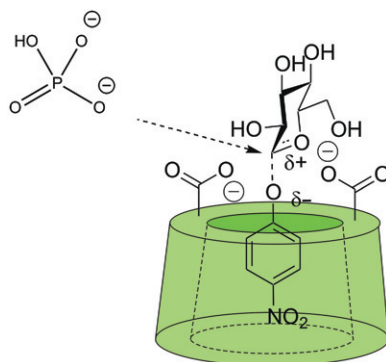
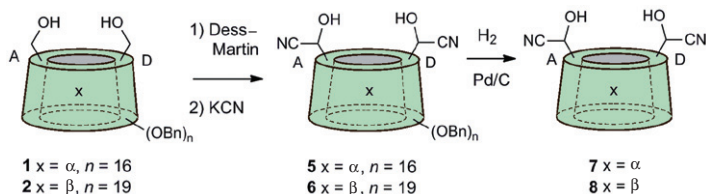


Figure 11.3. Proposed mechanism for the hydrolysis of glycosides by a cyclodextrin diacid in the presence of phosphate ions.

catalytic groups to the primary face (Figure 11.2). Such an enzyme model would accept substrates with lipophilic aglycons, for example, aryl glycosides.

This idea was tested by a synthesis of cyclodextrins with carboxylic acids at the C-6 position of the A and D residues. Two compounds, **3** and **4**, were prepared from α - and β -cyclodextrin using the benzylation-/DIBAL-promoted debenylation methodology [45], followed by oxidation and deprotection (Scheme 11.18). Diacids **3** and **4** were found to catalyze the hydrolysis of various 4-nitrophenyl glycosides. The hydrolysis followed Michaelis–Menten kinetics, and Michealis–Menten constants of 0.6–13.4 mM and k_{cat} values of $(1.1\text{--}3.4) \times 10^{-7} \text{ s}^{-1}$ were found. This means that compared with the uncatalyzed reaction, the reaction inside the cyclodextrin is 12–35 times faster [84].

Subsequently, it was found that the concentration of phosphate in the buffer was important for this reaction. A linear increase in rate was observed when the reaction was performed in increasing concentrations of phosphate buffer, and the pH dependency revealed that it was the increase in HPO_4^{2-} that was important for the rate [46]. At a concentration of phosphate buffer of 0.5 M, the rate increase ($k_{\text{cat}}/k_{\text{uncat}}$) caused by **4** was 989. The mode of catalysis shown in Figure 11.3 was proposed. The enzyme model does not perform general acid or nucleophilic catalysis but rather stabilizes the transition state through electrostatic interactions, while the phosphate is a nucleophilic catalyst. Other negatively charged groups can also cause catalysis. A cyclodextrin di-*O*-sulfate gave some activity [46], but diphosphates were inactive [85].



Scheme 11.19. Synthesis of cyclodextrin cyanohydrins.

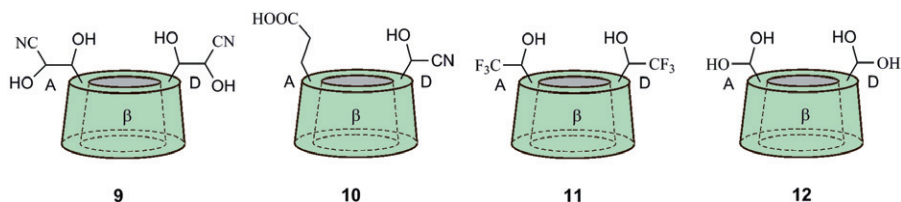


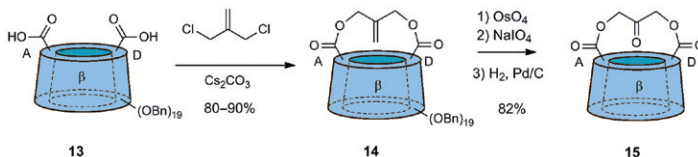
Figure 11.4. Artificial enzymes based on cyclodextrin derivatives containing acidic hydroxyl groups.

Acids **4.3** and **4.4** are too strong (pK_a 3.5) to function as general acid catalysts in buffer solution near neutrality. Therefore, weaker acids, such as cyanohydrins, were investigated. Two dicyanohydrins, **7** and **8**, were prepared from **1** and **2** by oxidation with Dess–Martin periodinane to the aldehyde followed by reaction with cyanide (to generate **5** and **6**) and hydrogenation (Scheme 11.19) [86]. These compounds were found to catalyze glycoside hydrolysis with high rate accelerations: The hydrolysis of 4-nitrophenyl α -D-glucopyranoside was found to be 7922 times faster inside the cavity of **8** than outside. Similarly, the hydrolysis of 4-nitrophenyl- β -D-glucopyranoside, its epimer, was 7101 times faster inside the cavity of α -cyclodextrin **7** than in the surrounding buffer [87]. A wide variety of aryl glycoside substrates were investigated and were generally cleaved. Natural substances such as toxic coumarin glycosides were hydrolyzed with k_{cat}/k_{uncat} up to 10,000 [88]. Based on the structure activity data, it was concluded that the cyanohydrin group is responsible for the catalysis by acting as a general acid catalyst. Two cyanohydrins, as in **7** and **8**, cause a faster hydrolysis simply because the probability of having a bound substrate close to the catalytic group is higher.

Changing the position of cyanohydrin by inserting an extra carbon in the attachment (and an extra hydroxyl group) produced another good and perhaps even more powerful catalyst [89]. Despite being a mixture of epimers, cyanohydrin **9** (Figure 11.4) caused a rate acceleration of ca. 3500 of the hydrolysis of 4-nitrophenyl- β -D-glucopyranoside.

In an attempt to establish both nucleophilic and acid catalysis in the artificial enzyme, compounds with both a carboxylate and a cyanohydrin group were prepared, with **10** being one of them (Figure 11.4) [90]. The attempt was unsuccessful, however, as **10** (and an analog) underwent self-decomposition in the buffer solution.

An analog, **11**, with trifluoromethyl groups rather than cyano groups, was also studied in this reaction (Figure 11.4) [91]. However, the ability of the CF_3 group in increasing the protonation ability of the hydroxyl group was apparently much smaller, as **11** accelerated the reaction only 56 times in the best case. A similar catalyst is the



Scheme 11.20. Synthesis of bridged cyclodextrin **15**.

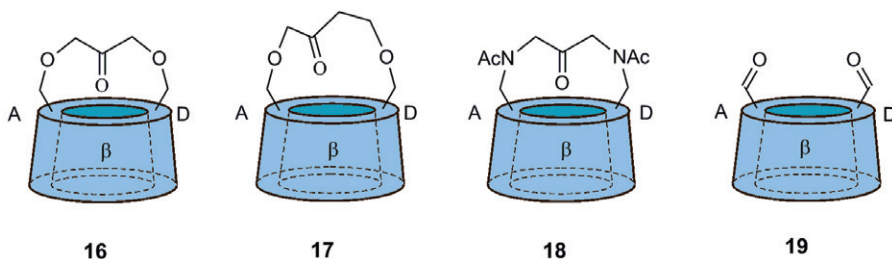


Figure 11.5. Some cyclodextrin ketones and aldehydes.

dialdehyde hydrate **12** (Figure 11.4). This compound also catalyzes aryl glycoside hydrolysis with a $k_{\text{cat}}/k_{\text{uncat}}$ of 50 [87].

11.4.2 Oxidases

Controlled oxidation is crucial in the chemistry of life, and enzymes that catalyze oxidation are widespread and varied in terms of substrates and type of reaction. Natural oxidases are not easy to employ in chemical synthesis either due to lack of substrate promiscuity and/or the requirement of costly cofactors. Artificial oxidases may overcome such problems.

A number of amine oxidases based on cyclodextrins have recently been made. Ketone **15** was prepared from diacid **13** by alkylative esterification with methallyl dichloride in the presence of cesium carbonate, followed by oxidative cleavage of the double bond, and finally deprotection (Scheme 11.20) [92]. Ketone **15** was found to be an excellent catalyst of amine oxidation [93]. In a buffer at pH 7 and in the presence of H_2O_2 , it catalyzed oxidation of 2-aminophenol to 2-aminophenoxazin-3-one with a $k_{\text{cat}}/k_{\text{uncat}}$ of 1068, and other aminophenols to nitrophenols with $k_{\text{cat}}/k_{\text{uncat}}$ values of 100–300. The oxidation was proposed to occur by addition of hydrogen peroxide to the ketone, binding of the aminobenzene derivative to the cyclodextrin, and subsequent oxidation.

Ketone **15** can also catalyze oxidation of alcohols. Under reaction conditions similar to those described above (dilute aqueous H_2O_2 , pH 7, 25°C), 2-hydroxybenzyl alcohol was oxidized to 2-hydroxybenzaldehyde with $k_{\text{cat}}/k_{\text{uncat}}$ of 28,600, and upon adjusting the temperature, even higher rate accelerations were accomplished [94].

A number of variations in the structure of the bridge were performed without any crucial improvement in catalysis. Compounds such as **16** and **17**, with an ether-linked bridge [95, 96], were comparatively poor (presumably due to the higher electron density of the ketone compared with the diester in **15**), while an *N*-acetyl-amino-linked bridge (in **18**, Figure 11.5) was a potent catalyst of alcohol oxidation [97]. This catalyst

could oxidize alcohols to aldehydes or ketones with rate accelerations of 7000–15,000.

Cyclodextrin aldehydes were found to be quite efficient oxidation catalysts as well. With a dialdehyde such as **19** (Figure 11.5), rate accelerations of amino oxidations of 3000–5000 were observed [98–100].

11.4.3 Miscellaneous

Cyclodextrin derivatives have also recently been used to catalyze epoxidation reactions. In the presence of oxone, ketones **15** [101] and **16** catalyzed epoxidation of styrene and indene in good yield and with some stereoselectivity [92].

A cyclodextrin with a ketone bridge attached to the secondary face was found to catalyze epoxidation of stilbenes [102].

11.5 CONCLUDING REMARKS

The chemistry of cyclodextrins has been undergoing an impressive development in the last three decades, from low-yielding monomodifications to regioselective installation of multiple functionalities. The development has been partly due to improved analytic instrumentation, especially high-field NMR facilities, but mainly due to the innovative chemists in the field, who have developed completely new methods for regioselective modifications of the densely functionalized and complex cyclodextrins. With the improved methods for synthesis, it has been possible to prepare sophisticated artificial enzymes with more catalytic groups at well-defined positions, and this has led to the next generation of cyclodextrin-based artificial enzymes and paved the way for tailor-made enzymes.

REFERENCES

- [1] Fujita, K., Matsunaga, A., Imoto, T. (1984). 6A6B, 6A6C, and 6A6D-ditosylates of β -cyclodextrin. *Tetrahedron Letters*, 25, 5533–5536.
- [2] Melton, L. D., Slessor, K. N. (1971). Synthesis of monosubstituted cyclohexaamyloses. *Carbohydrate Research*, 18, 29–37.
- [3] Matsui, Y., Okimoto, A. (1978). The binding and catalytic properties of a positively charged cyclodextrin. *Bulletin of the Chemical Society of Japan*, 51, 3030–3034.
- [4] Takahashi, K., Hattori, K., Toda, F. (1984). Monotosylated α - and β -cyclodextrins prepared in alkaline aqueous solution. *Tetrahedron Letters*, 25, 3331–3334.
- [5] Byun, H.-S., Zhong, N., Bittman, R. (2000). 6A-O-*p*-toluenesulfonyl- β -cyclodextrin. *Organic Syntheses*, 77, 225–230.
- [6] Law, H., Benito, J. M., Fernández, J. M. G., Jicsinszky, L., Crouzy, S., Defaye, J. (2011). Copper(II)-complex directed regioselective mono-*p*-toluenesulfonylation of cyclomaltoheptaose at a primary hydroxyl group: An NMR and molecular dynamics-aided design. *The Journal of Physical Chemistry B*, 115, 7524–7532.
- [7] Palin, R., Grove, S. J. A., Prosser, A. B., Zhang, M.-Q. (2001). Mono-6-(O-2,4,6-triisopropylbenzenesulfonyl)- γ -cyclodextrin, a novel intermediate for the synthesis of mono-functionalized γ -cyclodextrins. *Tetrahedron Letters*, 42, 8897–8899.

- [8] Himeno, Y., Miyagawa, A., Kawai, M., Yamamura, H. (2009). γ -Cyclodextrin possessing an azido group and a triisopropylbenzenesulfonyl group as useful synthetic and authentic intermediates for unsymmetrically functionalized derivatives. *Tetrahedron*, 65, 9474–9480.
- [9] Martina, K., Trotta, F., Robaldo, F., Belliardi, N., Jicsinszky, L., Cravotto, G. (2007). Efficient regioselective functionalizations of cyclodextrins carried out under microwaves or power ultrasound. *Tetrahedron Letters*, 48, 9185–9189.
- [10] Fikes, L. E., Winn, D. T., Sweger, R. W., Johnson, M. P., Czarnik, A. W. (1992). Preassociating α -nucleophiles. *Journal of the American Chemical Society*, 114, 1493–1495.
- [11] Hannesian, S., Benalil, A., Laferrrière, C. (1995). The synthesis of functionalized cyclodextrins as scaffolds and templates for molecular diversity, catalysis, and inclusion phenomena. *The Journal of Organic Chemistry*, 60, 4786–4797.
- [12] Rawal, G. K., Zhang, P., Ling, C.-C. (2010). Controlled synthesis of linear α -cyclodextrin oligomers using copper-catalyzed Huisgen 1,3-dipolar cycloaddition. *Organic Letters*, 12, 3096–3099.
- [13] Blanco, J. L. J., Fernández, J. M. G., Gabelle, A., Defaye, J. (1997). A mild one-step selective conversion of primary hydroxyl groups into azides in mono- and oligo-saccharides. *Carbohydrate Research*, 303, 367–372.
- [14] Yuan, D.-Q., Kitagawa, Y., Aoyama, K., Douke, T., Fukudome, M., Fujita, K. (2007). Imidazolyl cyclodextrins: Artificial serine proteases enabling regiospecific reactions. *Angewandte Chemie (International ed. in English)*, 46, 5024–5027.
- [15] Yuan, D.-Q., Yamada, T., Fujita, K. (2001). Amplification of the reactivity difference between two methylene groups of cyclodextrins via a cap. *Chemical Communications*, 2706–2707.
- [16] Yuan, D.-Q., Koga, K., Kouno, I., Fujioka, T., Fukudome, M., Fujita, K. (2007). The first topologically controlled synthesis of doubly bridged β -cyclodextrin dimers. *Chemical Communications*, 828–830.
- [17] Tabushi, I., Shimokawa, K., Fujita, K. (1977). Specific bifunctionalization on cyclodextrin. *Tetrahedron Letters*, 18, 1527–1530.
- [18] Tabushi, I., Shimokawa, K., Shimizu, N., Shirakata, H., Fujita, K. (1976). Capped cyclodextrins. *Journal of the American Chemical Society*, 98, 7855–7856.
- [19] Engeldinger, E., Armspach, D., Matt, D. (2003). Capped cyclodextrins. *Chemical Reviews*, 103, 4147–4173.
- [20] Yuan, D.-Q., Kitagawa, Y., Fukudome, M., Fujita, K. (2007). A vector-selective reaction enables efficient construction of specific topology upon the primary side of β -cyclodextrin. *Organic Letters*, 9, 4591–4594.
- [21] Yu, H., Makino, Y., Fukudome, M., Xie, R.-G., Yuan, D.-Q., Fujita, K. (2007). Hetero-bifunctional γ -cyclodextrins having dansylcysteine and tosyl groups at the two adjacent sugar units: Synthesis and determination of regio-chemistry. *Tetrahedron Letters*, 48, 3267–3271.
- [22] Yu, H., Yuan, D.-Q., Makino, Y., Fukudome, M., Xie, R.-G., Fujita, K. (2006). Clockwise-counterclockwise differentiation on the upper rim of a monofunctional γ -cyclodextrin: Efficient topological control of capped cyclodextrins. *Chemical Communications*, 5057–5059.
- [23] Di Fabio, G., Malgieri, G., Isernia, C., D'Onofrio, J., Gaglione, M., Messere, A., Zarrelli, A., De Napoli, L. (2012). A novel synthetic strategy for mono substituted cyclodextrin derivatives. *Chemical Communications*, 48, 3875–3877.
- [24] Gibson, A. R., Melton, L. D., Slessor, K. N. (1974). ω -Aldehyde sugars prepared by ninhydrin oxidation. *Canadian Journal of Chemistry*, 52, 3905–3912.
- [25] Martin, K. A., Czarnik, A. W. (1994). Facile preparation of the β -cyclodextrinyl aldehyde. *Tetrahedron Letters*, 35, 6781–6782.

- [26] Huff, J. B., Bieniarz, C. (1994). Synthesis and reactivity of 6-b-cyclodextrin monoaldehyde: An electrophilic cyclodextrin for the derivatization of macromolecules under mild conditions. *The Journal of Organic Chemistry*, *59*, 7511–7516.
- [27] Yoon, J., Hong, S., Martin, K. A., Czarnik, A. W. (1995). A general method for the synthesis of cyclodextrinyl aldehydes and carboxylic acids. *The Journal of Organic Chemistry*, *60*, 2792–2795.
- [28] Cornwell, M. J., Huff, J. B., Bieniarz, C. (1995). A one-step synthesis of cyclodextrin monoaldehydes. *Tetrahedron Letters*, *36*, 8371–8374.
- [29] Glazyrin, A. E., Syrtsev, A. N., Kurochkina, G. I., Kononov, L. O., Grachev, M. K., Nifant'ev, E. E. (2003). Unusual regioselective acylation of the primary hydroxyl groups of β -cyclodextrin. *Russian Chemical Bulletin International Edition*, *52*, 237–246.
- [30] Boger, J., Brenner, D. G., Knowles, J. R. (1979). Symmetrical triamino-per-O-methyl- α -cyclodextrin: Preparation and characterization of primary trisubstituted α -cyclodextrins. *Journal of the American Chemical Society*, *101*, 7630–7631.
- [31] Ling, C.-C., Coleman, A. W., Miocque, M. (1992). Multiple tritylation: A convenient route to polysubstituted derivatives of cyclomaltohexose. *Carbohydrate Research*, *223*, 287–291.
- [32] Ward, S., Zhang, P., Ling, C.-C. (2009). The conformation of a tetratrylated α -cyclodextrin with an unusual proton NMR. *Carbohydrate Research*, *344*, 808–814.
- [33] Poorters, L., Armspach, D., Matt, D. (2003). Selective tetrafunctionalisation of α -cyclodextrin using the supertrityl protecting group—Synthesis of the first C2-symmetric tetraphosphate based on a cavitand (α -TEPHOS). *European Journal of Organic Chemistry*, 1377–1381.
- [34] Armspach, D., Matt, D. (2011). Methylated cyclodextrins as preorganisation platforms for the synthesis of multidentate chelating ligands aimed at transition metal coordination and industrially relevant catalysis. *Comptes Rendus. Chimie*, *14*, 135–148.
- [35] Gramage-Doria, R., Rodriguez-Lucena, D., Armspach, D., Egloff, C., Jouffroy, M., Matt, D., Toupet, L. (2011). Regioselective double capping of cyclodextrin scaffolds. *Chemistry—A European Journal*, *17*, 3911–3921.
- [36] Jouffroy, M., Gramage-Doria, R., Armspach, D., Matt, D., Toupet, L. (2012). Regioselective opening of proximally sulfato-capped cyclodextrins. *Chemical Communications*, *48*, 6028–6030.
- [37] Sakairi, N., Kuzuhara, H. (1993). Efficient and regioselective preparation of an eight-membered interglycosidic benzylidene derivative of β -cyclodextrin. *Chemistry Letters*, 2077–2080.
- [38] Michalski, T. J., Kendler, A., Bender, M. L. (1983). A silyl- α -cyclodextrin intermediate. Preparation and characterization of dodeca-*t*-butyldimethylsilyl-hexahydroxy- α -cyclodextrin. *Journal of Inclusion Phenomena and Macrocyclic Chemistry*, *1*, 125–128.
- [39] Takeo, K., Mitoh, H., Uemura, K. (1989). Selective chemical modification of cyclomalto-oligosaccharides via *tert*-butyldimethylsilylation. *Carbohydrate Research*, *187*, 203–221.
- [40] Fügedi, P. (1989). Synthesis of heptakis(6-*O*-*tert*-butyldimethylsilyl)cyclomaltoheptaose and octakis(6-*O*-*tert*-butyldimethylsilyl)cyclomalto-octaose. *Carbohydrate Research*, *192*, 366–369.
- [41] Zhang, P., Wang, A., Cui, L., Ling, C.-C. (2012). First per-*O*-tritylation of cyclodextrins. *Organic Letters*, *14*, 1612–1615.
- [42] Sato, T., Nakamura, H., Ohno, Y., Endo, T. (1990). Synthesis of 1,4-anhydro-2,3,6-tri-*O*-benzyl- α -D-glucopyranose by cis-ring-closure of a glycosyl bromide. *Carbohydrate Research*, *199*, 31–35.
- [43] Boger, J., Corcoran, R. J., Lehn, J.-M. (1978). Cyclodextrin chemistry: Selective modification of all primary hydroxyl groups of α - and β -cyclodextrins. *Helvetica Chimica Acta*, *61*, 2190–2218.

- [44] Angibeaud, P., Utille, J. P. (1991). Cyclodextrin chemistry: Part I. Application of a regioselective acetylation method for benzyl ethers. *Synthesis*, 737–738.
- [45] Pearce, A. J., Sinaÿ, P. (2000). Diisobutylaluminium-promoted regioselective de-O-benylation of perbenzylated cyclodextrins: A powerful new strategy for the preparation of selectively modified cyclodextrins. *Angewandte Chemie (International ed. in English)*, 39, 3610–3612.
- [46] Rousseau, C., Ortega-Caballero, F., Nordstrøm, L. U., Christensen, B., Petersen, T. E., Bols, M. (2005). Artificial glycosyl phosphorylases. *Chemistry—A European Journal*, 11, 5094–5101.
- [47] Zaborova, E., Blériot, Y., Sollogoub, M. (2010). μ -Waves avoid large excess of diisobutylaluminium-hydride (DIBAL-H) in the debenylation of perbenzylated α -cyclodextrin. *Tetrahedron Letters*, 51, 1254–1256.
- [48] Wang, W., Pearce, A. J., Zhang, Y., Sinaÿ, P. (2001). Diisobutylaluminium-promoted regioselective de-O-methylation of cyclodextrins: An expeditious entry to selectively modified cyclodextrins. *Tetrahedron, Asymmetry*, 12, 517–523.
- [49] Du Roizel, B., Baltaze, J.-P., Sinaÿ, P. (2002). Diisobutylaluminium-promoted secondary rim selective de-O-methylation of permethylated cyclodextrins. *Tetrahedron Letters*, 43, 2371–2373.
- [50] Luo, X., Chen, Y., Huber, J. G., Zhang, Y., Sinaÿ, P. (2004). Diisobutylaluminium hydride as a molecular scalpel: The regioselective stripping of four methyl groups from permethylated β -cyclodextrin. *Comptes Rendus Chimie*, 7, 25–28.
- [51] Chen, Y., Huber, J. G., Chang, Y., Sinaÿ, P. (2005). Regioselective one-step synthesis of hexahydroxy permethylated β -cyclodextrin and unambiguous NMR analysis. *Comptes Rendus Chimie*, 7, 27–30.
- [52] Zhou, Y. (2012). Selectively modified cyclodextrins as artificial enzymes and catalysts. PhD thesis, University of Copenhagen.
- [53] Bistri, O., Sinaÿ, P., Sollogoub, M. (2005). Diisobutylaluminium hydride (DIBAL-H) is promoting a selective clockwise debenylation of perbenzylated 6A,6D-dideoxy- α -cyclodextrin. *Tetrahedron Letters*, 46, 7757–7760.
- [54] Bistri, O., Sinaÿ, P., Barbero, J. J., Sollogoub, M. (2007). Chemical clockwise tridifferentiation of α - and β -cyclodextrins: Bascule-bridge or deoxy-sugars strategies. *Chemistry—A European Journal*, 13, 9757–9774.
- [55] Guieu, S., Sollogoub, M. (2008). Multiple homo- and hetero-functionalizations of α -cyclodextrin through oriented deprotections. *The Journal of Organic Chemistry*, 73, 2819–2828.
- [56] Rawal, G. K., Rani, S., Ling, C.-C. (2009). Unexpected regioselective debenylation leading to modification on both rims of α -cyclodextrin. *Tetrahedron Letters*, 50, 4633–4636.
- [57] Rawal, G. K., Rani, S., Ward, S., Ling, C.-C. (2010). DIBAL-H mediated triple and quadruple debenzylations of perbenzylated cyclodextrins. *Organic and Biomolecular Chemistry*, 8, 171–180.
- [58] Guieu, S., Sollogoub, M. (2008). Regiospecific tandem azide-reduction/deprotection to afford versatile amino alcohol-functionalized α - and β -cyclodextrins. *Angewandte Chemie (International ed. in English)*, 47, 7060–7063.
- [59] Petrillo, M., Marinescu, L., Rousseau, C., Bols, M. (2009). Selective discrimination of cyclodextrin diols using cyclic sulfates. *Organic Letters*, 11, 1983–1985.
- [60] Lecourt, T., Hérault, A., Pearce, A. J., Sollogoub, M., Sinaÿ, P. (2004). Triisobutylaluminium and diisobutylaluminium hydride as molecular scalpels: The regioselective stripping of perbenzylated sugars and cyclodextrins. *Chemistry—A European Journal*, 10, 2960–2971.
- [61] Xiao, A., Yang, M., Sinaÿ, P., Blériot, Y., Sollogoub, M., Zhang, Y. (2010). Diisobutylaluminium hydride (DIBAL-H) promoted secondary rim regioselective demethylations of

- permethylated β -cyclodextrin: A mechanistic proposal. *European Journal of Organic Chemistry*, 1510–1516.
- [62] Ghosh, R., Zhang, P., Wang, A., Ling, C.-C. (2012). Diisobutylaluminum hydride mediated regioselective O desilylations: Access to multisubstituted cyclodextrins. *Angewandte Chemie (International ed. in English)*, 51, 1548–1552.
- [63] Ueno, A., Breslow, R. (1982). Selective sulfonation of a hydroxyl group of β -cyclodextrin. *Tetrahedron Letters*, 23, 3451–3454.
- [64] Fujita, K., Nagamura, S., Imoto, T. (1984). Convenient preparation and effective separation of the C-2 and C-3 tosylates of α -cyclodextrin. *Tetrahedron Letters*, 25, 5673–5676.
- [65] Fujita, K., Tahara, T., Imoto, T., Koga, T. (1986). Regiospecific sulfonation onto C-3 hydroxyls of β -cyclodextrin. Preparation and enzyme-based structural assignment of 3A,3C and 3A,3D disulfonates. *Journal of the American Chemical Society*, 108, 2030–2034.
- [66] Murakami, T., Harata, K., Morimoto, S. (1987). Regioselective sulfonation of a secondary hydroxyl group of cyclodextrins. *Tetrahedron Letters*, 28, 321–324.
- [67] Wang, Z.-Z., Fu, X.-Y., Dai, G.-D., Quan, H.-F. (2011). Efficient and improved syntheses of two key intermediates for functionalization of β -cyclodextrin at the secondary hydroxyl face. *Monatshefte für Chemie*, 142, 317–319.
- [68] Teranishi, K. (2003). Practical and convenient modification of the A,C-secondary hydroxyl face of cyclodextrins. *Tetrahedron*, 59, 2519–2538.
- [69] Van Dienst, E., Snellink, B. H. M., von Piekartz, I., Gansey, M. H. B. G., Venema, F., Feiters, M. C., Nolte, R. J. M., Engbersen, J. F. J., Reinhoudt, D. N. (1995). Selective functionalization and flexible coupling of cyclodextrins at the secondary hydroxyl face. *The Journal of Organic Chemistry*, 60, 6537–6545.
- [70] Chiu, S.-H., Myles, D. C. (1999). Efficient monomodification of the secondary hydroxyl groups of β -cyclodextrin. *The Journal of Organic Chemistry*, 64, 332–333.
- [71] Ashton, P. R., Boyd, S. E., Gattuso, G., Hartwell, E. Y., Königer, P., Spencer, N., Stoddart, J. F. (1995). A novel approach to the synthesis of some chemically-modified cyclodextrins. *The Journal of Organic Chemistry*, 60, 3898–3903.
- [72] Icheln, D., Gehrcke, B., Piprek, Y., Mischnick, P., König, W. A., Desso, M. A., Morel, A. F. (1996). Migration of secondary *tert*-butyldimethylsilyl groups in cyclomalto-heptaose and -octaose derivatives. *Carbohydrate Research*, 280, 237–250.
- [73] Ikeda, H., Nagano, Y., Du, Y. Q., Ikeda, T., Toda, F. (1990). Modifications of the secondary hydroxyl side of α -cyclodextrin and NMR studies of them. *Tetrahedron Letters*, 31, 5045–5048.
- [74] Mortellaro, M. A., Czarnik, A. W. (1992). Hydrogen bonding effects on the reactivity of a preassociating α -nucleophile. The secondary-side β -cyclodextrin hydroxylamine. *Bioorganic & Medicinal Chemistry Letters*, 2, 1635–1638.
- [75] Yuan, D. Q., Tahara, T., Chen, W.-H., Okabe, Y., Yang, C., Yagi, Y., Nogami, Y., Fukudome, M., Fujita, K. (2003). Functionalization of cyclodextrins via reactions of 2,3-anhydrocyclodextrins. *The Journal of Organic Chemistry*, 68, 9456–9466.
- [76] Fukudome, M., Shimosaki, K., Koga, K., Yuan, D.-Q., Fujita, K. (2007). Selective synthesis and ester cleavage property of 3^A,2^B-anhydro-3^B-deoxy-3^B-thio- β -cyclodextrin. *Tetrahedron Letters*, 48, 7493–7497.
- [77] Fukudome, M., Yoshikawa, K., Koga, K., Yuan, D. Q., Fujita, K. (2007). Selective modification of β -cyclodextrin: An unexpected tandem reaction enables the cross-linking of C2^A and C2^B via a sulphur bridge. *Chemical Communications*, 3157–3159.
- [78] Suzuki, M., Nozoe, Y. (2002). Facile preparation of mono-2-O-modified eicosa-O-methylcyclomaltoheptaoses (β -cyclodextrin). *Carbohydrate Research*, 337, 2393–2397.
- [79] Tian, A., Forgo, P., D'Souza, T. (1996). Selective modification at the 3-position of β -cyclodextrin. *Tetrahedron Letters*, 37, 8309–8312.

- [80] Masurier, N., Lafont, O., Le Prevost, R., Lesur, D., Masson, P., Djedaïni-Pilard, F., Estour, F. (2009). Regioselective access to 31-O-substituted- β -cyclodextrin derivatives. *Chemical Communications*, 589–591.
- [81] Breslow, R., Dong, S. D. (1998). Biomimetic reactions catalyzed by cyclodextrins and their derivatives. *Chemical Reviews*, 98, 1997–2011.
- [82] Kirby, A. J., Hollfelder, F. *From Enzyme Models to Model Enzymes*, RSC, Cambridge, UK, 2009.
- [83] Zechel, D. L., Withers, S. G. (2000). Glycosidase mechanisms: Anatomy of a finely tuned catalyst. *Accounts of Chemical Research*, 33, 11–18.
- [84] Rousseau, C., Nielsen, N., Bols, M. (2004). An artificial enzyme that catalyses hydrolysis of aryl glycosides. *Tetrahedron Letters*, 45, 8709–8711.
- [85] López, Ó., Bols, M. (2008). Effective synthesis of negatively-charged cyclodextrins. Selective access to phosphate cyclodextrins. *Tetrahedron*, 64, 7587–7593.
- [86] Caballero, F. O., Rousseau, C., Christensen, B., Pedersen, T. E., Bols, M. (2005). Remarkable supramolecular catalysis of glycoside hydrolysis by a cyclodextrin cyanohydrin. *Journal of the American Chemical Society*, 127, 3238–3239.
- [87] Ortega-Caballero, F., Bjerre, J., Laustsen, L. S., Bols, M. (2005). Four orders of magnitude rate increase in artificial enzyme catalysed aryl glycoside hydrolysis. *The Journal of Organic Chemistry*, 70, 7217–7226.
- [88] Bjerre, J., Nielsen, E. H., Bols, M. (2008). Hydrolysis of toxic natural glucosides catalyzed by cyclodextrin dicyanohydrins. *European Journal of Organic Chemistry*, 745–752.
- [89] Bjerre, J., Bols, M. (2010). Substantial spatial flexibility and hydrogen bonding within the catalysis exerted by cyclodextrin artificial glycosidases. *European Journal of Organic Chemistry*, 3487–3500.
- [90] Ortega-Caballero, F., Bols, M. (2006). Cyclodextrin derivatives with cyanohydrin and carboxylate groups as artificial glycosidases. *Canadian Journal of Chemistry*, 84, 650–658.
- [91] Bjerre, J., Fenger, T., Marinescu, L. V., Bols, M. (2007). Synthesis of some trifluoromethylated cyclodextrin derivatives and analysis of their properties as artificial glycosidases and oxidases. *European Journal of Organic Chemistry*, 704–710.
- [92] Rousseau, C., Christensen, B., Bols, M. (2005). Artificial epoxidase II. Synthesis of cyclodextrin ketoesters and epoxidation of alkenes. *European Journal of Organic Chemistry*, 2734–2739.
- [93] Marinescu, L., Mølbach, M., Rousseau, C., Bols, M. (2005). Supramolecular oxidation of anilines using hydrogen peroxide as stoichiometric oxidant. *Journal of the American Chemical Society*, 127, 17578–17579.
- [94] Marinescu, L. G., Bols, M. (2006). Very high rate acceleration of benzyl alcohol oxidation by an artificial enzyme. *Angewandte Chemie (International ed. in English)*, 45, 4590–4597.
- [95] Fenger, T. H., Marinescu, L. G., Bols, M. (2009). Cyclodextrin ketones as oxidation catalysts: Investigation of bridged derivatives. *Organic and Biomolecular Chemistry*, 933–943.
- [96] Lopez, O., Marinescu, L., Bols, M. (2007). New cup-shaped α -cyclodextrin derivatives and a study of their catalytic properties in oxidation reactions. *Tetrahedron*, 63, 8872–8880.
- [97] Marinescu, L., Doyagüez, E. G., Petrillo, M., Fernandez-Mayorales, A., Bols, M. (2010). Amino-acetone-bridged cyclodextrins—Artificial alcohol oxidases. *European Journal of Organic Chemistry*, 157–167.
- [98] Fenger, T. H., Bjerre, J., Bols, M. (2009). Cyclodextrin aldehydes are oxidase mimics. *ChemBioChem: A European Journal of Chemical Biology*, 10, 2494–2503.
- [99] Fenger, T. H., Bols, M. (2011). Simple cyclodextrin aldehydes as excellent artificial oxidases. *Journal of Inclusion Phenomena and Macrocyclic Chemistry*, 69, 397–402.

- [100] Bjerre, J., Bols, M. (2011). Substrate structure governs maximum rate of catalysis exerted by cyclodextrin oxidase chemzymes. *Journal of Inclusion Phenomena and Macrocyclic Chemistry*, 69, 417–423.
- [101] Rousseau, C., Christensen, B., Pedersen, T. E., Bols, M. (2004). Cyclodextrins containing an acetone bridge. Synthesis and study as epoxidation catalysts. *Organic and Biomolecular Chemistry*, 2, 3476–3482.
- [102] Fenger, T. H., Marinescu, L. G., Bols, M. (2011). Cyclodextrin ketones with the catalytic group at the secondary rim and their effectiveness in enzyme-like epoxidation of stilbenes. *European Journal of Organic Chemistry*, 2339–2345.

CHAPTER 12

ORGANOZYMES: MOLECULAR ENGINEERING AND COMBINATORIAL SELECTION OF PEPTIDIC ORGANO- AND TRANSITION-METAL CATALYSTS

MORTEN MELDAL

12.1 INTRODUCTION

There is a significant conceptual difference in the mode of action of the catalysts found in nature, that is, the enzymes, and most of the catalysts are traditionally designed and employed for organic synthesis. The catalysts employed in synthesis are often general catalysts with little structural specificity that will convert a particular set of functional groups, while the enzymes generally show high structural specificity and often only convert a few or even a single substrate in the entire organism. Enzymes are extremely efficient at low physiological concentrations, while most catalysts for synthesis are used in comparatively high concentrations. The high efficiency at low concentrations of enzymes is associated with the many contributions to substrate binding offered by an extended binding site. These constitute a network of hydrophobic, hydrophilic, and hydrogen bonding interactions, and the driving force for substrate binding resides to a large extent in the reorganization and relief of entropy in the organized solvation shell surrounding the substrate and binding site. The reaction coordinate is assisted by several core functional mechanistic groups in the enzyme working in beautiful concert. Furthermore, the enzymes, as well as their biological substrates, often display a certain degree of plasticity, allowing the induced fit and support of transition-state structure leading to conversion to product. Therefore, enzymes can often perform reactions the organic chemist can only dream of.

Most catalysts for synthesis, on the other hand, have a single-core element such as an amine or a transition metal mainly responsible for the actual catalysis. The decoration around the core serves to activate the core and impose steric interaction to prevent unwanted transformation. This is particularly true in stereoselective catalysis of C–C bond formation.

Organic Synthesis and Molecular Engineering, First Edition.

Edited by Mogens Brøndsted Nielsen.

© 2014 John Wiley & Sons, Inc. Published 2014 by John Wiley & Sons, Inc.

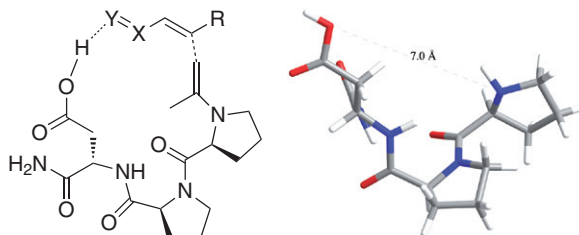


Figure 12.1. The enantioselectivity of the Wennemers organocatalyst, PPD-NH₂, a tripeptidyl amide selected by combinatorial chemistry, in 1,4-conjugate addition is obtained through distant coordination of the Michael acceptor by aspartic acid. This differs from Pro-NH₂ which preferentially catalyzes 1,2-additions.

In recent years, a variety of peptide-based catalysts that display some of the qualities of enzyme conversions have been developed. This was partly promoted through the application of combinatorial methods. Combinatorial chemistry has its strength in the fine-tuning of molecular interaction through engineering of a suitable selection process and can alleviate the problems associated with the solvent shell in a molecular design of a catalyst.

12.2 PEPTIDES IN ORGANO-CATALYSIS

Proline-based organocatalysts were developed by combinatorial selection from moderately active proline catalysts for the aldol family of reactions to a highly efficient peptide catalyst for selective 1,4-Michael additions. This was achieved through coimmobilization of catalysts and one of the substrate partners in a split mix catalyst library on beads [1, 2]. By application of a colored reaction partner in solution, colored beads that could be isolated contained active compounds among which the amino acid sequence Pro-Pro-Asp-NH₂ (PPD-NH₂) (Figure 12.1) could be identified as particularly active.

In these tripeptide catalysts, in addition to the N-terminal proline forming an enamine with a carbonyl group during aldol-type condensations, the tripeptide contained a carboxylic acid ideally situated for hydrogen bonding to a nitrovinyl [3] or an acrylic moiety, thereby directing a stereoselective 1,4-addition of the prolyl enamine formed intermediately from aldehyde. This reminds us of the simultaneous action of several distant core functionalities of an enzyme active site and can lead to great acceleration of rate and selectivity. The catalyst was active while bound to a solid support, and with Tentagel® as a carrier, stereoselectivities (ee) of reaction >95% and excellent *syn/anti* ratios (>99/1) were obtained for a variety of substrate structures. The *syn/anti* ratios varied with subtle changes in structural properties of the substrates as expected for a complex catalytic mechanism. Furthermore, this catalyst may be used at concentrations significantly lower than those used in conventional proline-based organocatalysis.

A similar approach of catalyst coimmobilization was described later in 2003 for the Diels–Alder reaction [4]. Arg-rich peptides were identified through combinatorial screening. In this study, a diene was immobilized on Tentagel together with a tripeptide library and screened for reaction with a fluorescence-labeled maleimide (Figure 12.2).

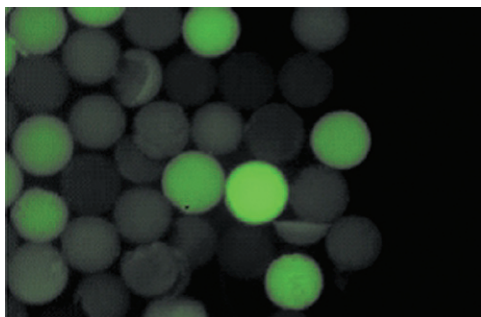
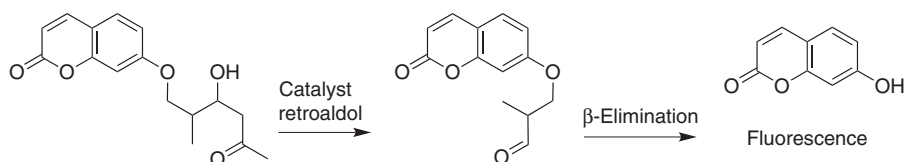


Figure 12.2. Diels–Alder reaction monitored on solid support in coimmobilization assay introduced by both Bradley’s and Wennemer’s groups in 2003. Source: [4]. Reproduced with permission of The Royal Society of Chemistry. See color insert.



Scheme 12.1. Fluorescent solution assay used to screen for catalysis of retro-aldol reactions and thereby also for the inverse catalysis of aldol reaction.

However, the catalytic activity of the identified tripeptides was rather low (3.4-fold rate increase compared to the uncatalyzed reaction), and therefore the interaction with substrate may not be very substrate specific.

In another approach [5], catalysts for the retro-aldol reaction were identified through β -elimination of fluorescent umbelliferone from the ether of the retro-aldol product (Scheme 12.1).

In turn, these proline-terminated catalysts were then used to catalyze the inverse aldol reaction. The most efficient peptide catalysts for enantioselective formation of aldol products were Pro-Glu-Leu-Phe (PELF), 96% ee 66%; Pro-Asp-Leu-Phe (PDLF), 95% ee 50%; and Pro-Gly (PG), 99% ee 46%, all presenting carboxylate favorably positioned for coordination of the incoming carbonyl electrophile for 1,2-addition, similar to the Wennemers catalyst for 1,4-aldol addition described earlier, however, with less selectivity. Other groups have designed di-, tri-, or tetrapeptides for relatively good enantio- [6] and also regioselective aldol reactions [7].

While proline may be considered the archetypal organocatalyst for aldol reactions, screening of a variety of dipeptides has demonstrated [8, 9] that dipeptides such as Val–Val also can provide high selectivity in aldol condensations, leading to selective formation of D-erythrose with an ee of 80% from glycol aldehyde.

Using phage display libraries, Tanaka and Barbas III [10] improved the catalytic activity of an 18-residue Lys-rich α -helical peptide acting as retro-aldol catalysts approximately 10-fold by addition of six more residues (YKLLKELLAKLKWLLRKL-SDHLCL-NH₂) at the C-terminal end. In a similar manner, Akagawa et al. [11] increased the efficiency of a catalyst for Fielde–Crafts C-alkylation of indoles and

pyrroles with acrylates by C-terminal extension of the catalytic peptide, Pro-D-Pro-Aib-Trp-Trp with poly-leucine (Leu_{25,4}). The yield (ee) increased from 19 (30) to 85 (>88) for the reaction. The examples demonstrate the importance of structural order of the peptide catalysts for the maintenance of both selectivity and activity. The conclusion of all these studies is that the size of the peptide seems to influence the catalytic efficiency. The same catalysts were effective in enantioselective, resin-supported α -oxyamination of carbonyl compounds using 2,2,6,6-tetramethylpiperidin-1-yl)oxyl (TEMPO) in water [12]. In a seminal study, 2,2,6,6-tetramethylpiperidine-1-oxyl-4-amino-4-carboxylic acid (TOAC) was incorporated into peptides and used for oxidative resolution of racemic alcohols [13].

Kelly and Roberts [14] and Berkessel et al. [15] have reviewed the application of α -helical homo-oligo-peptides (poly-L-Leu) in enantioselective epoxidation reactions. In these reactions, it is envisaged that the two reactants, hydrogen peroxide and a carbonyl-conjugated olefin, are brought together by hydrogen bond coordination to the N-terminal part of the chiral helix, resulting in directional delivery of the oxidant to the olefin, with enantioselectivity in the range of 60–98%. Use of α -methyl-Leu oligomers increased steric congestion and thereby destabilized α -helix, resulting in significant decrease in both rate and enantioselectivity of reaction [13].

Peptide α -helix scaffolding of functional groups was combined with cyclodextrin binding of 4-nitrophenyl esters to effect artificial esterase activity [16]. A glutamic acid, a histidine, and glutamyl-6-monoamino- β -cyclodextrin spaced four amino acids apart constituted the active residues in the structure presented by modeling in Figure 12.3.

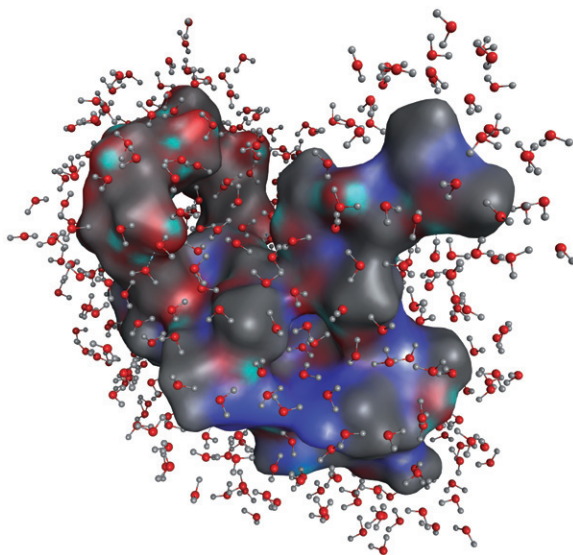


Figure 12.3. Artificial esterase Ac-AAAEAEARAHAEAE(β -CD)ARAAA-NH₂ combining three functional groups, His, Glu, and β -cyclodextrin for increased rate of hydrolysis of 4-nitrophenyl acetate. However, according to extensive MD in water, the cyclodextrin moiety (top right) and the intended catalytic His residue (bottom) are most likely located on opposite surfaces of the structure, and observed weak increase in hydrolysis rate most probably is a result of interaction with other and more distant parts of the peptide.

It was demonstrated that in the absence of Glu (6) of this structure, the reaction rate for hydrolysis of 4-nitrophenyl acetate decreased only fourfold. The effect of the catalysis is therefore limited. This may be explained by inefficient relative positioning of the three residues Glu(6), His(10), and Glu(β -CD), which should act in concert during the catalytic reaction.

Significant catalysis of 4-nitrophenyl acetate hydrolysis was observed with nanofibers formed through large self-assemblies of C-terminally palmitoylated peptides modified with an N-terminal branch of lysine derivatized with two catalytic His residues [17]. The catalysis was found to occur at the surface of the nanofibers.

Clouet et al. [18] developed dendrimer esterases through combinatorial screening of supported peptide dendrimers (resin- $A^1A^2(A^3A^4(A^5A^6(A^7A^8)_2)_2)_2$, where A's were selected from a variety of amino acids) and used fluorogenic 8-acyloxypyrene-1,3,6-trisulfonate as the ester substrates. They employed His as the active residues and had excellent catalysis of several linear acyl groups, while branched esters were less reactive. There was a significant rate enhancement by the presence of basic residues in the vicinity of the catalytic His, and it was argued that these lowered the pK_a of the imidazoles situated at the periphery of the dendrimer.

An interesting aspect of peptide catalysis is that of autocatalytic peptide ligation [19] in which self-assembly on a peptide ligation product is employed to promote ligation of two peptide fragments. The fragments form an autocatalytic product by proximity-driven ligation of a peptide thioester fragment with a fragment containing an N-terminal cysteine, and during the reaction, both fragments are binding to one product molecule.

The most comprehensive studies on peptides in organocatalysis are those of Miller et al. In 1998, Miller et al. first reported on the use of N^6 -alkyl histidines as the catalytic residue in enantioselective peptides for acylation of alcohols [20]. Very efficient and selective catalysts with properties approaching those of natural enzymes were developed through design and combinatorial screening. Most importantly, they developed a screening method for split mix libraries [21–23] based on proton-activated fluorescence (PAF) and bead sorting (Figure 12.4). The beads were aminomethyl anthracene functionalized, and during acylation, the release of acid lowered the pH locally and increased the fluorescence. Initially, this was performed as a diffusion zone assay [24]

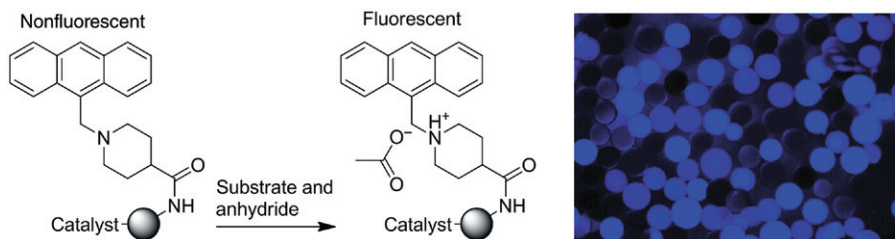
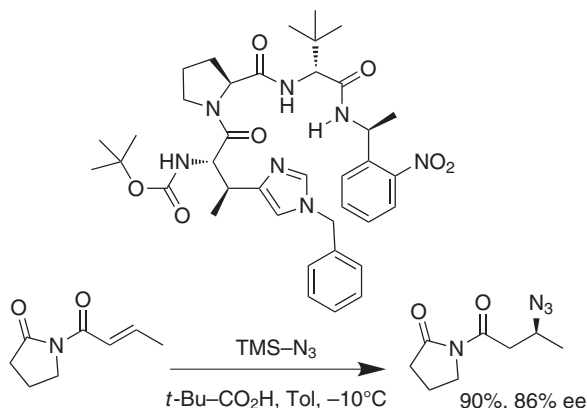


Figure 12.4. The incorporation of a pH-sensitive sensor in resin material allowed Copeland and Miller to monitor a large variety of reactions in supported catalyst libraries. The ingenious combination of combinatorial selection and molecular design has provided Copeland and Miller with a range of spectacular catalysts for some of the more difficult enantio- and regioselective reactions. Source: [21]. Reproduced with permission of the American Chemical Society.



Scheme 12.2. The β -methylation of *N*-alkylhistidine in catalytic peptide catalysts restricted the motion of the catalytic alkylimidazol side chain and produced the most efficient catalysts for enantioselective azidation of conjugated double bonds [31].

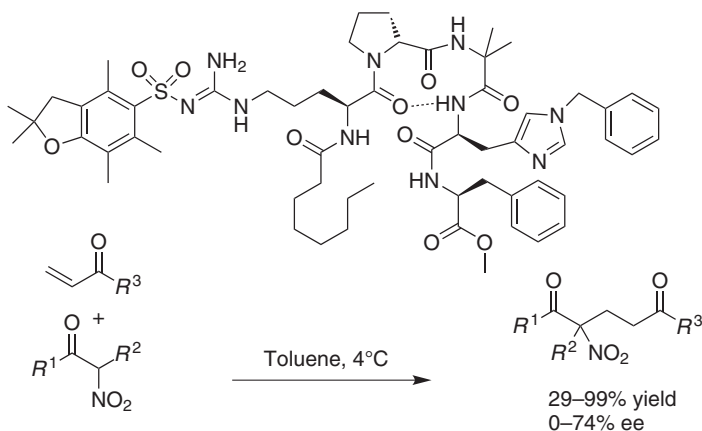
in polyethylene glycol polyacrylamide (PEGA) polymer [25, 26], but it was soon realized that the acid essentially remains in the bead where it is released and the PAF probe was coimmobilized with catalyst in Wang resin [27]. The acylation catalysts were used in resolving racemic tertiary alcohols with excellent enantiomeric ratios (k_{relative}) near 50 and ee's of the products in the range 90–99%, and the structure activity relationship was thoroughly investigated [28–31].

In any event, arrays of catalytic peptides were identified and these, during the last decade, have been developed to organocatalysts for a wide range of biogenic and organic reaction. More catalytic residues were introduced in addition to the *N*-alkyl histidines, including 3-(*N*-methylthiazolium-4-yl)alanine for aldehyde tosylamide cross couplings [32], pyridylalanine for alleneoate addition to aldehydes [33], aspartic acid for epoxidations [34–36], and tetrazol-5-ylalanine for phosphite transfer from phosphoramidites [37]. This impressive work has been reviewed in several excellent reviews by Miller and coworkers [23, 29, 38–41].

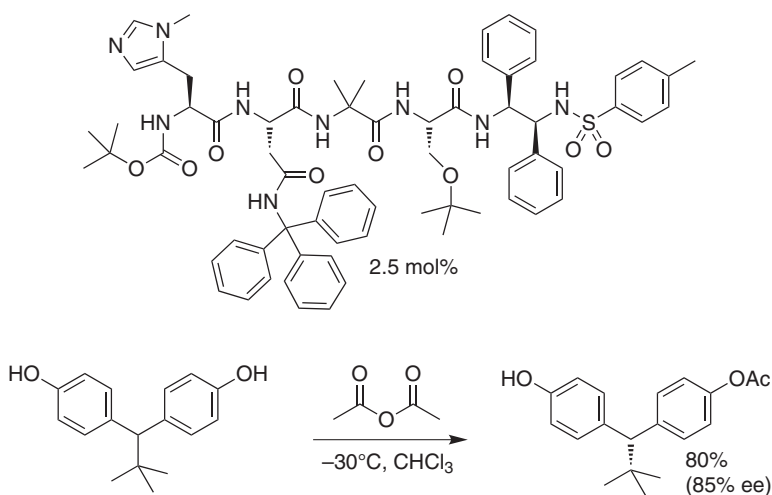
Azidation of substituted allylic carbamates is an entry to β -amino acids and, as presented in Scheme 12.2, this could be performed with excellent yield and enantioselectivity using a tetrapeptide containing β -substituted N^5 -benzyl histidine as a catalyst [31, 42, 43].

Linton et al. [44] attempted the nucleophilic Michael addition of 2-nitroketones to acrylates catalyzed with a complex *N*-methylhistidine-containing peptide with good yields and intermediate ee's depending on the structure of R^1 , Scheme 12.3.

In the first example of remote chiral induction with peptidic catalysts, Miller and coworkers desymmetrized a *meso* form of a bis-phenol, Scheme 12.4, in a remarkable ee of 95% [45, 46]. The *N*-methyl histidine type of peptide catalyst once again proved efficient in selective acylation and selectively transferred acetate to the pro-*R* hydroxyl of the bis-phenol to selectively provide the *R*-monoacetate under remote control of a *t*-butyl group. In a seminal paper [47], they described the very selective acetylation in 88% yield of the 3-hydroxyl over 4-hydroxyl group in carbohydrate derivatives, as presented in Scheme 12.5.

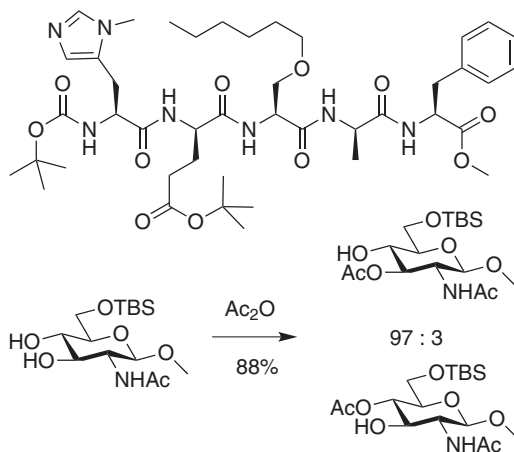


Scheme 12.3. Enantioselective C-nucleophilic Michael addition catalyzed by *N*-benzyl histidine containing peptide derivative.

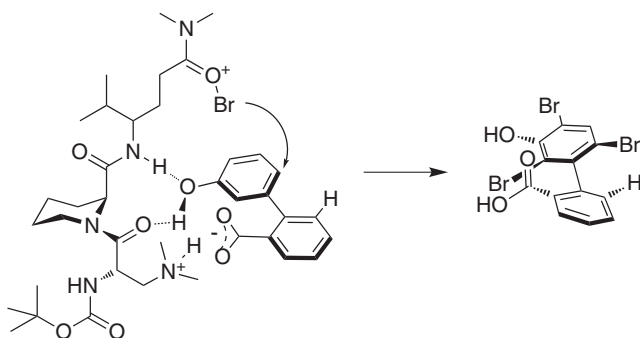


Scheme 12.4. Desymmetrization of bisphenol with a catalyst exerting remote control of the enantioselectivity through optimized interactions between functional groups and substrate.

In a very impressive demonstration of organocatalysis, Miller and coworkers showed the selective dynamic kinetic resolution of biaryl atropisomers via peptide-catalyzed asymmetric bromination [48]. In this catalysis, the peptide induced a conformation of the biaryl through coordination of a meta-hydroxyl and an ortho-carboxylate group during peptide-induced transfer of bromonium ions to the ortho and para positions of the phenol ring. As presented in Scheme 12.6, the catalyst coordinated carboxylate with charge-charge interaction with an ammonium group and the hydroxyl was engaged in two hydrogen bonds, resulting in directional delivery of bromonium ions to only one of the two possible rotamers. A relatively high concentration of 10 mol% was required



Scheme 12.5. Regioselective acylation of carbohydrates was realized with enzyme-like precision using an optimized Pmh-peptide catalyst. A catalyst for selective acylation of the 4-position of octyl β -D-glucopyranoside has also been presented.



Scheme 12.6. Peptide-catalyzed bromination of biaryl compounds can result in kinetic dynamic resolution of the compound through coordination to functional groups on the biaryl orchestrating delivery of an oxybromonium ion from a C-terminal peptide bond in the peptide. See Table 12.1 for results.

for efficient transformation. However, the reaction was general, and a wide variety of biaryl substrates were brominated and resolved in very high ee and excellent yields (see Table 12.1).

When replacing *N*-methyl histidine with a pyridyl alanine as the catalytic residue, Miller and coworkers [33] obtained a series of catalysts that catalyzed the chiral formation of C–C bonds by reaction of an *N*-acyl imine with *O*-benzyl butadienoate (Scheme 12.7). The product was formed with ee of 95%, and this constitutes a new route to chiral β -amino acids.

In one of the most spectacular demonstrations of the versatility of peptide catalysis, Miller and coworkers [49, 50] developed selective catalysts for synthesis of inositol

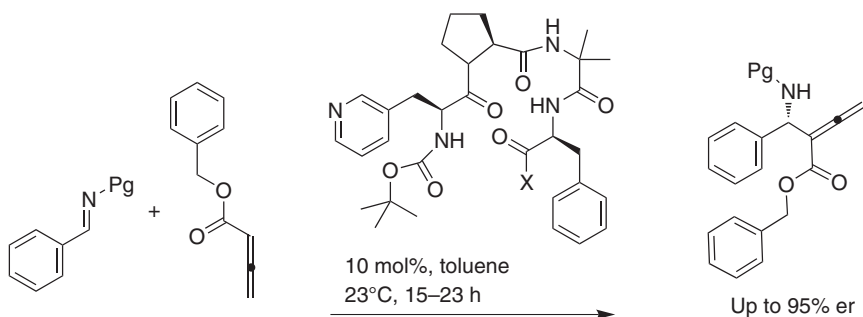
TABLE 12.1. The Kinetic Dynamic Resolution of Biaryl Substrates by Catalytic Bromination Using 10 mol% of Peptide Catalyst [48]

Entry	Racemic Starting Material	Product	Yield (%)	E.r.
1			80	97.0:3.0
2			85	97.0:3.0
3			75	96.5:3.5
4			70	96.0:4.0
5			80	94.0:6.0
6			70	97.0:3.0
7			65	96.5:3.5
8			85	87.0:13.0

(Continued)

TABLE 12.1. (Continued)

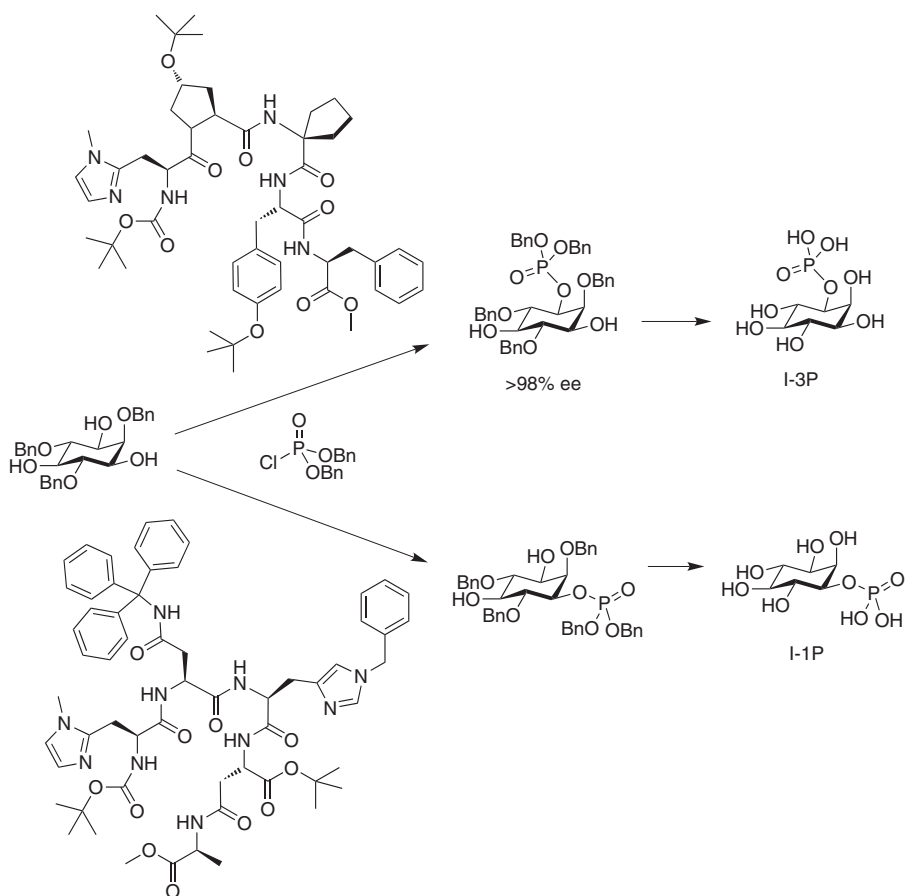
Entry	Racemic Starting Material	Product	Yield (%)	E.r.
9			77	85.0:15.0
10			70	95.0:5.0



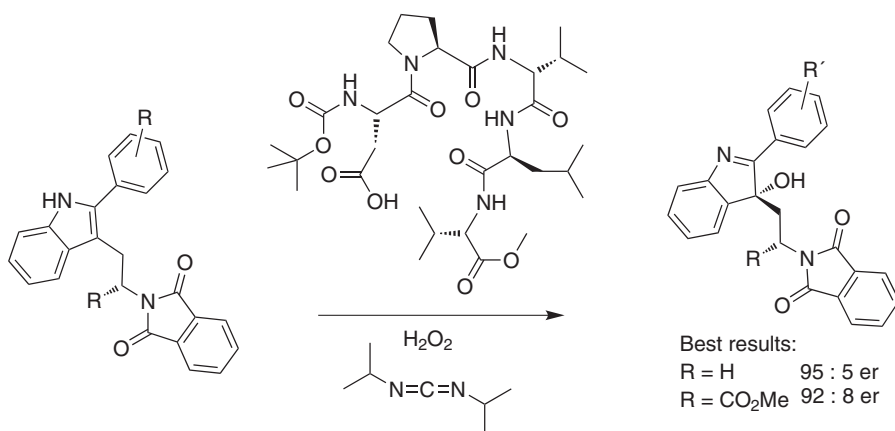
Scheme 12.7. Pyridyl alanine peptides were superior in the enantioselective reaction between imine and allenolate.

1- or 3-monophosphate. They employed the known *meso*-tri-*O*-benzyl inositol derivative, and by reaction with diphenyl chlorophosphate, their best two catalysts presented in Scheme 12.8 were capable of monophosphorylation in the 3 or the 1 positions neighboring the axial benzyl group, respectively. Depending on the catalyst they obtained more than 98% ee, and they achieved this with only 2 mol% of the catalyst. Miller and coworkers also described a comprehensive unified high yield synthesis of the important inositol triphosphates [51] and lipid-anchored inositol diphosphates [52] using these two catalysts for selective phosphorylations.

Finally, during their long survey of the landscape of opportunities in peptide catalysis, Miller and coworkers have developed a series of aspartate-containing peptides for catalysis of oxidation processes such as epoxidation [35, 36] and indole oxidation [53]. One example is the enantioselective installation of a hydroxyl group on 2,3-disubstituted indole derivatives presented in Scheme 12.9. The terminal aspartate is converted into the peracid using a diisopropyl carbodiimide (DIC) activation protocol and 10 mol% catalyst. The activated chiral peptide catalyst coordinates the substrate through hydrogen bonding and allows transfer of hydroxyl radical only from aspartate peracid approaching one particular face of the indol leading to the *S*-enantiomer in up to 95% ee.



Scheme 12.8. The reaction of 2,4,6-tribenzyl inositol with diphenylchlorophosphate in the presence of *N*-alkyl histidine type of catalysts yielded monophosphorylated inositol derivatives.



Scheme 12.9. The carboxylate of the shown catalyst is reacting with hydrogen peroxide, and upon coordination of the substrate on the peptide template, a hydroxyl radical is transferred regio- and stereoselectively to the 3-position of the indolyl moiety.

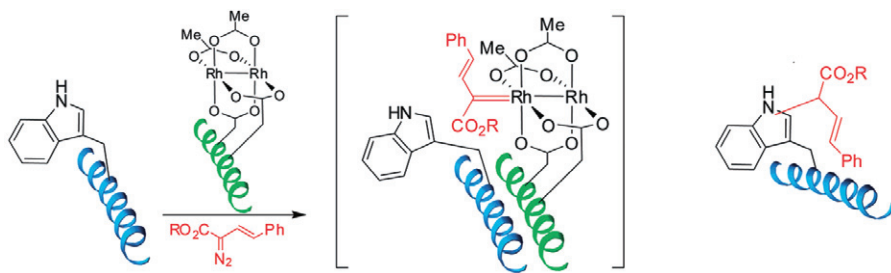
The work of Miller and coworkers is truly groundbreaking and indicates the wide range of biomimetic reactions that we can perform with peptide-based organocatalysis. However, it is obvious that we have only just touched upon the opportunities available in this area of biomimetic catalysis with peptides. By application of combinatorial approaches with the many unnatural amino acids available today and with more rigorous combinatorial screening, we should eventually be able to simulate many of the biological processes and reactions with simple small molecules.

12.3 ORGANOZYMES: PEPTIDE MIMETIC METAL COMPLEXES

While organocatalysis with peptide-based catalysts described earlier can provide excellent activity and selectivity in biomimetic reactions, including acylations, phosphorylations, oxidations, and brominations with efficiencies approaching those of the natural enzymes, the combination of peptide templates with coordination of transition metals opens up entirely new opportunities. Transition metals are inherently involved in many types of bond remodeling reactions and offer a myriad of new and highly selective chemical transformations in addition to catalysis of biomimetic reactions. These include catalysis of any C–C bond forming organic reaction. We combine the catalytic activity of the metal with the structural features, and substrate coordination of the peptide catalysis can be established at very low catalyst concentrations with high regio- and stereoselectivities.

Ball and coworkers [54, 55] demonstrated the bridging of an α -helical peptide with dirhodium dicarboxylate stabilized the secondary peptide structure. They demonstrated the formation of the stable rhodium peptide complex. This was subsequently used in an elegant and very regioselective transfer from (*E*)-alkyl 2-diazo-4-phenylbut-3-enoate to alkylate a Tyr, Phe, or Trp residue in a proximate position of an α -helical peptide matching the catalyst α -helix with hydrophobic and charge interactions to orient this position to the catalytic Rh complex (Scheme 12.10). Similarly, a report [56] described the use of bipyridyl and phenanthroline to attach Rh to the N-terminal of a peptide, and the complex was used for oxidative cleavage of DNA.

The shorter Co(3)-containing peptide shown in Figure 12.5 was selected from a library of compounds as a catalyst for selective oxidation/decarboxylation of N-terminal



Scheme 12.10. Template-assisted catalysis of alkyl transfer from (*E*)-alkyl 2-diazo-4-phenylbut-3-enoate to approximate Trp residue during temporary formation of a peptide heterodimer (2 mol% catalyst).

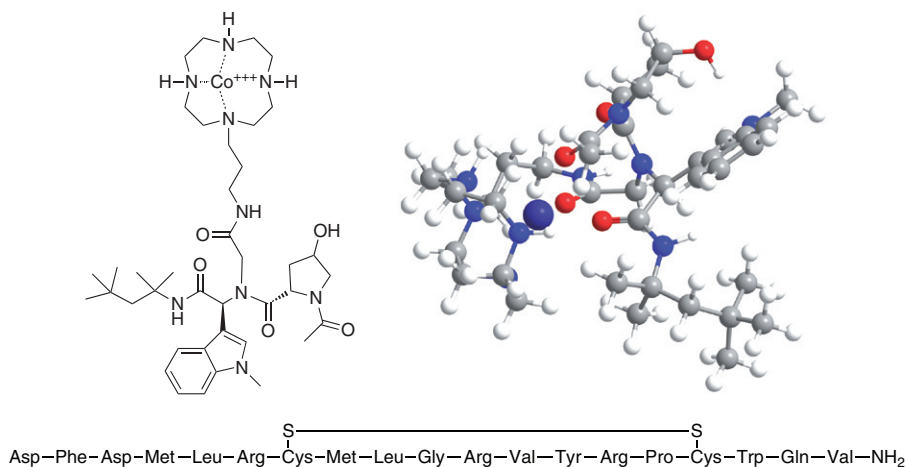


Figure 12.5. A cobalt(3) containing artificial enzyme able to oxidatively decarboxylate the N-terminal aspartic acid side chain of melanocortin. The cobalt may, according to simple molecular dynamic (MD) calculations, be coordinated both by the aza-crown and the dense carbonyl environment.

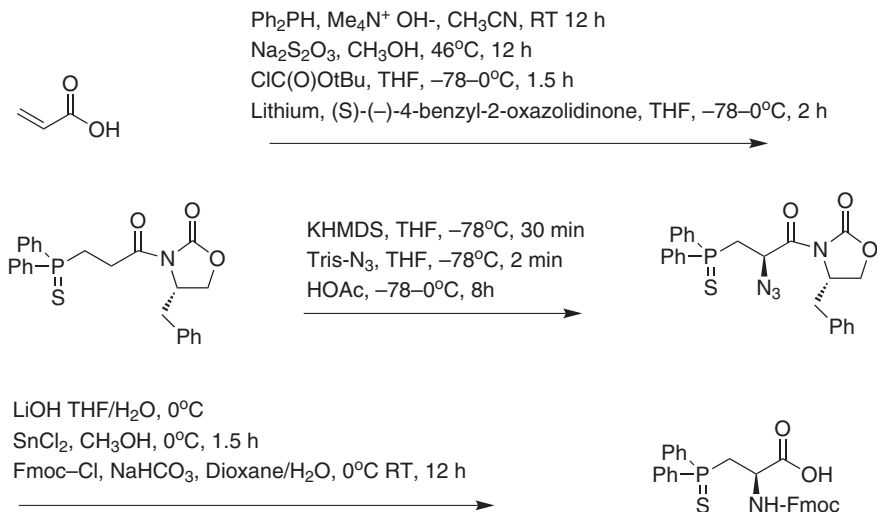
aspartates in peptides, such as melanocortin-concentrating hormone (MCH) [57]. The molecule coordinates Co(3) through the aza-crown, but the peptide structure is compact and probably also involved in metal coordination.

In this reaction, the catalyst interacts with the N-terminal of the MCH molecule, and aspartate is slowly converted into a pyruvate residue, which is useful for further chemical transformation into MCH analogs. The catalysis is selective, but quite large amounts of catalyst are required in order to achieve reasonable reaction rates.

Hoveyda and coworkers [58] described the design of dipeptides, N-terminally derivatized with 2-diphenylphosphineyl phenyl methylamine, for *in situ* Cu complex formation and catalysis of Michael addition of dialkyl zinc. The Cu catalyst was remarkably effective and afforded the products with up to 98% ee and high yields.

Gilbertson and coworkers designed secondary structure peptides, for example, β -turns containing palladium ligands [59]. The ligands were phosphines linked to carbon in the side chains of amino acid building blocks engineered for optimal *in situ* coordination of palladium in the folded structure (Scheme 12.11). They adapted an approach where the phosphine building blocks were protected as phosphine sulfides, as presented in Scheme 12.11, and they described the synthesis in detail for a variety of phosphine derivatives [60]. The difference in complexity between the preparation of peptide-based organocatalysts and transition-metal binding peptides is mainly in the requirement for elaborate synthesis of the appropriately protected building blocks for the introduction of metal ligands in the peptide. Gilbertson selected a true building block approach for the assembly of peptide phosphine ligand.

In our laboratory, we devised a route to phosphine peptides, which circumvents the elaborate synthesis of the protected phosphine building. This route takes advantage of the postassembly procedure where different phosphines are attached at the end of the peptide assembly, as presented in Scheme 12.12 [61].



Scheme 12.11. One of several reaction schemes developed by Gilbertson's group to access phosphinoylated peptides for metal complex formation.

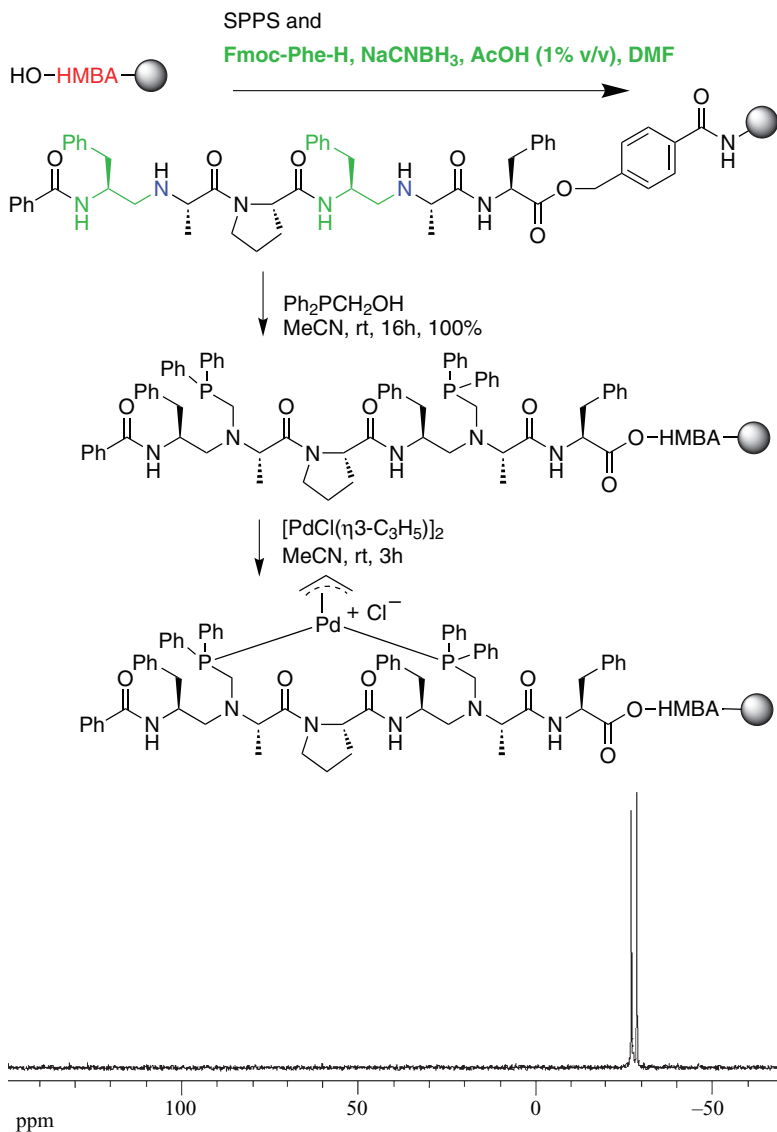
It has the advantage of being compatible with a combinatorial approach and the synthesis of libraries, simply by portioning the initial peptide library and introducing a variety of phosphines and a number of different transition metals into each portion of the peptide library.

On the other hand, we aimed also at more stable peptides containing *N*-heterocyclic carbenes (NHCs) in the backbone, and here we were forced to take a synthetic route to dipeptide mimetic building blocks, as presented in Scheme 12.13 [62].

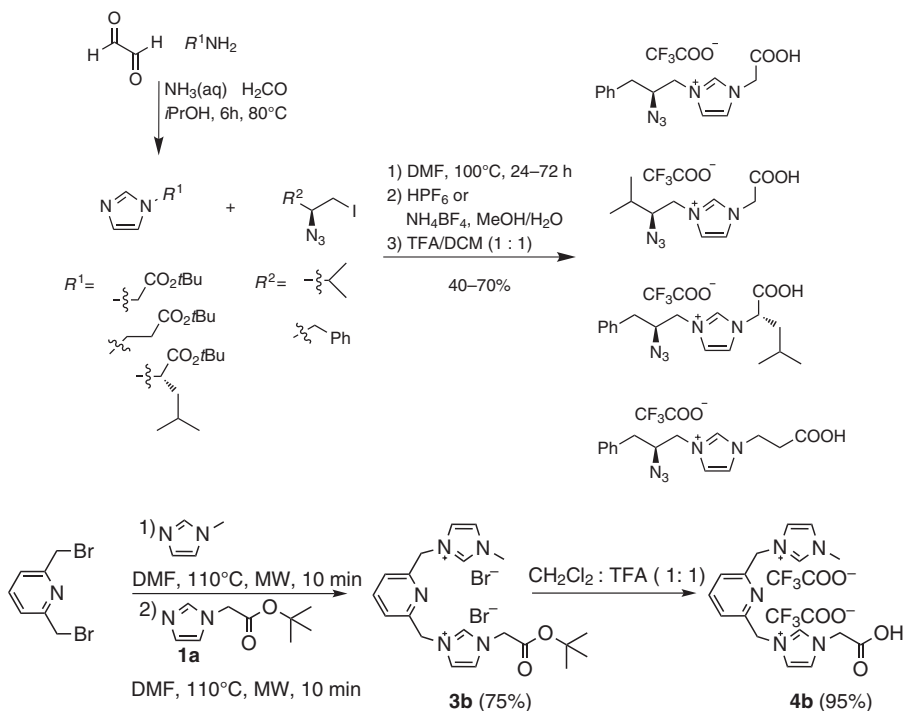
We performed a four-component Arduengo condensation [63] where one nucleophile is an amino acid and the amine was converted to an imidazole. In a subsequent step, this could be alkylated on the free nitrogen, with 2-azido iodides also derived from amino acids. The dipeptide mimetics could be directly used to introduce carbene precursor into peptide synthesis.

Gilbertson's group synthesized a variety of ligands on solid support using sulfide-protected phosphine building blocks, for example, the ligand presented in Figure 12.6. This palladium-coordinated ligand was successfully used in chiral C-allylation reactions. However, side chains of amino acids usually protrude away from the chiral fold of the peptide backbone, and this may well affect the degree of chiral induction obtained.

In an early study, Gilbertson and coworkers obtained ~50% ee in chiral C-allylations using the solid-phase bound catalyst in Figure 12.6 [13]. By engineering modifications to the aromatic phosphine substituents, changing the peptide template to Boc-D-Phe-Xps-Pro-D-Val-Pps-D-Leu-OME (Xps and Pps, 3,5-xylene and phenyl substituted phosphine building blocks, respectively), Gilbertson and coworkers optimized the C-allylation to 95% yield and 88% ee on *syn* phase polyamide support and 91% yield with an impressive ee of 95% using the purified catalyst in solution [64]. They also investigated the influence of phosphine building blocks and their chirality on catalysis



Scheme 12.12. The postpeptide assembly phosphinylation strategy developed for synthesis of combinatorial libraries of phosphinylated peptides and their transition-metal complexes. An “on-bead” phosphor NMR shows the clean crude product formed on solid support. Source: [61]. Reproduced with permission of Wiley-VCH Verlag GmbH & Co. KGaA.



Scheme 12.13. Engineering of two different types of NHC building blocks, one type for incorporation of a dipeptide mimetic in a peptide during assembly and one for postassembly, N-terminal or side chain attachment.

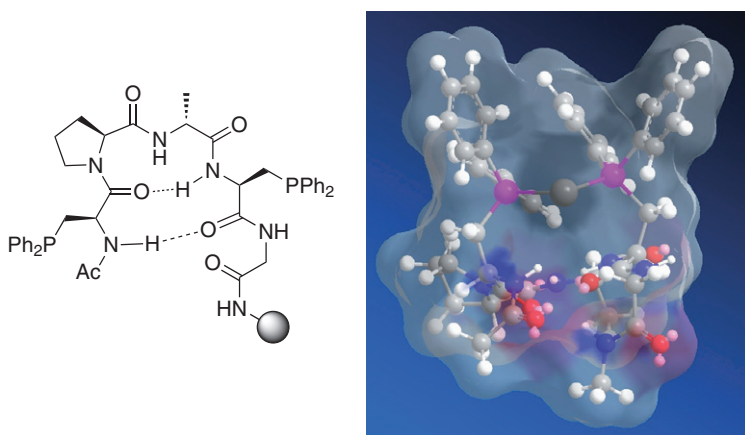
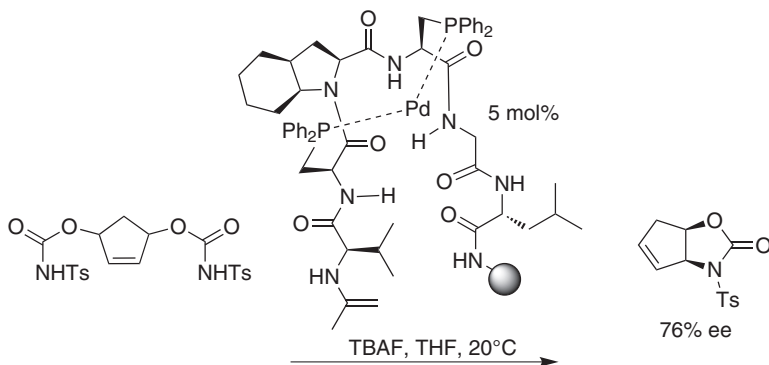


Figure 12.6. Gilbertson's solid-phase ligand for *in situ* complex formation with allyl palladium dichloride. A model of the complex indicates that the chirality of the environment surrounding palladium is limited. See color insert.



Scheme 12.14. Desymmetrization of a diol using a catalyst derived through the Gilbertson approach of parallel screening a large number of supported chiral catalyst analogs.

and found that the catalytic complex is indeed the bis-phosphine palladium complex and that the phosphines are not coordinated to other functional groups in the peptide. One of the two phosphines (e.g., Xps in the sequence above) dominated the chiral induction.

In a similar study, Gilbertson and coworkers investigated 75 supported catalysts for desymmetrization of the diol in Scheme 12.14 and derived at the efficient catalyst Ac-D-Val-Pps-Oic-Pps-Gly-D-Leu-NH-resin, which gave ~70% yield and 76% ee in the reaction [65, 66].

A thorough investigation of turn motifs in these types of peptide template palladium phosphine complexes showed that the exact nature of the turn structure is crucial for catalysis [59]. Furthermore, each substrate used in the model C-allylation reaction requires subtle optimization of template structure for quality performance, similar to the observations we find for analogous enzymatic reactions.

Based on the results from the Gilbertson and Miller laboratories, we concluded that the optimized condition for effective and selective catalysis would be one where the transition metal coordinated directly with atoms in the vicinity of the chiral peptide backbone [61]. It was also argued that, considering the subtleties of complex catalysis, the effective catalyst would preferably be derived by selection from combinatorial catalyst libraries. Therefore, the catalyst structure and synthetic protocol should be suitable for combinatorial synthesis. A synthetic approach was engineered where at least two ligand precursors for metal coordination were introduced during peptide assembly. After assembly of the peptide providing the structure of the ligand and immediately prior to metal complex formation, the precursors were converted into powerful ligands for transition metals such as palladium. This strategy resulted in clean metal coordination with, for example, Al₂Pd₂Cl₂ or CodPdCl₂ and, through coordination, folding of the peptide chain. Initially, secondary amines were introduced in the backbone of the peptide using reductive amination reactions during peptide assembly. This provided attachment points for the introduction of phosphines directly to the chiral backbone of the peptide. We used either phosphinylation of the amine with diaryl phosphine chloride or an *O*- to *N*-methylphosphine transfer reaction starting from hydroxymethyl diphenylphosphine (Scheme 12.12). Gel phase P³¹-NMR showed both solid-phase phosphinylation reactions to be quantitative. Several phosphine-containing

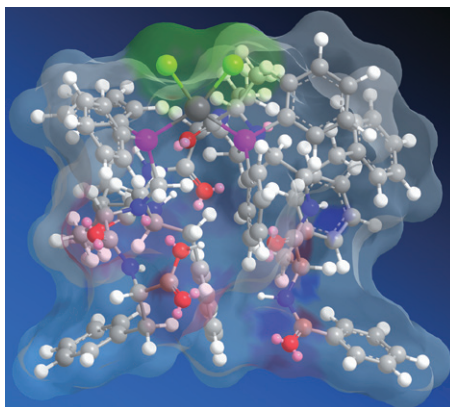
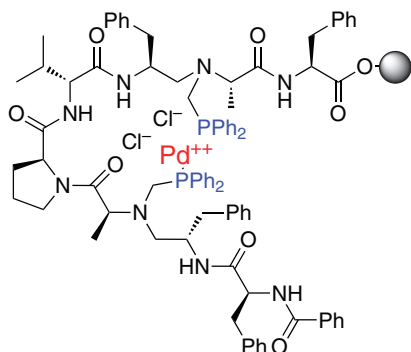


Figure 12.7. Solid-phase bis-phosphinyl peptide palladium synthesized by quantitative convergent solid-phase procedures suitable for combinatorial catalyst preparation. Molecular modeling indicates the palladium assist in peptide folding and is presented at the surface for catalysis. See color insert.

ligands, for example, the one presented in Figure 12.7, were synthesized and used on solid support for metal coordination. The addition of 1 equiv of palladium to a peptide resin containing two phosphines attached to the peptide backbone cleanly converted the phosphine compounds into their palladium complexes on the solid support.

The conversion was followed by color change of the resin from transparent to deep red. The resin did not leak any palladium after complexation. The catalysts were used in stereoselective C-allylation, but although the solid-phase conversion of the substrate to product was quantitative, the enantioselectivity was only 20–30% ee when using 5 mol% catalyst. More success was obtained when a proline-bound phosphine was combined with oxazoline formed in the peptide backbone [67]. Then, quantitative conversion and 70% ee could be obtained, slightly better than results obtained by Gilbertson and Yamada using a similar catalyst [68].

The combination of phosphine ligands with oxazoline [67], sulfides [69], or pyridyl [70] residues, as shown in Figure 12.8, provided highly active catalysts for C-allylation. We synthesized peptides with six- to eight-membered palladium ring structure and varied the stereochemistry of two marked amino acids. Interestingly, while maintaining the stereochemistry of the chiral centers in the thioether compounds, upon changing from six- to seven-membered palladium ring structure, the stereochemical outcome of catalysis was inverted [69]. Similarly, the stereochemical outcome was inverted between the seven-membered thioether and pyridyl-containing catalysts. The major determinant for selectivity was the chiral centers in the palladium-containing ring of the proline, cysteine, and pyridyl alanine residues, respectively.

While phosphine-containing ligands provided highly active catalysts for C–C bond formation, the stability of the phosphinylated ligands toward oxygen was a major concern for catalyst handling, recycling, and shelf life. We therefore developed building blocks for incorporation of carbene precursors as described earlier and incorporated these into peptides [62]. Initially, we attempted to convert the precursor to carbenes using silver carbonate, but addition of palladium compounds to the resin resulted in precipitation of palladium black. Therefore, a procedure involving carbene

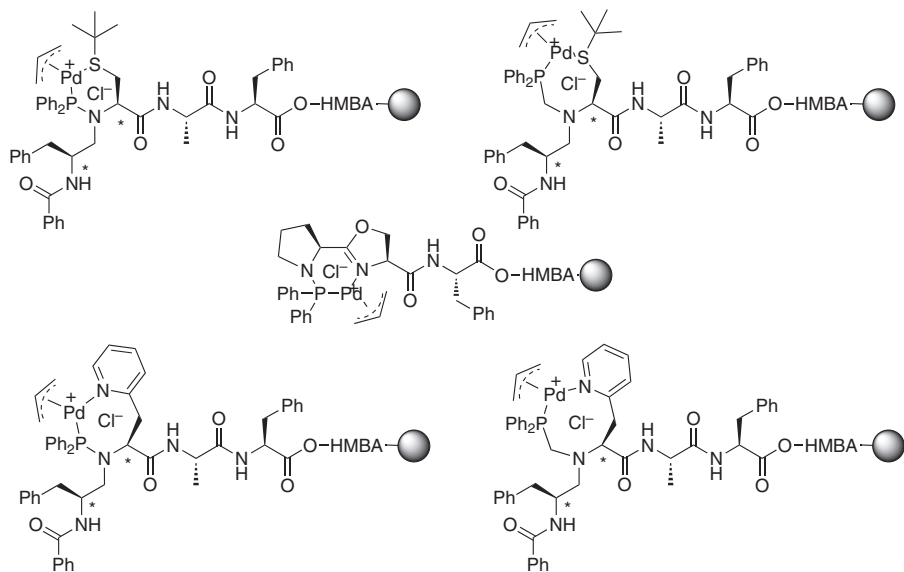


Figure 12.8. Mixed phosphine and heterocycle catalysts presenting peptide ligands coordinated to palladium. All four isomers of the chiral centers marked with stars were synthesized and showed a broad spectrum of enantioselectivities in C-allylation reactions.

formation by addition of equivalent amounts of 2-*tert*-butylimino-2-diethylamino-1,3-dimethylperhydro-1,3,2-diazaphosphorine (BEMP), followed by palladation with $\text{AlI}_2\text{Pd}_2\text{Cl}_2$, was adapted. This procedure cleanly converted the ligand to a palladium complex. The NHC–palladium catalysts were completely stable under the standard handling conditions, and the catalyst could be cleaved from the support and purified by high-performance liquid chromatography (HPLC).

The bis-carbene catalyst presented in Figure 12.9 was prepared, characterized, and used in C-allylation at 25°C but showed limited activity at the low temperature due to the strong coordination of the NHCs to palladium. Furthermore, in this structure, the palladium is most probably buried within the peptide fold, according to results from molecular modeling.

In contrast, when peptidic structures were terminated with pyridyl containing mono- or bis-carbene precursors, complex formation with $\text{AlI}_2\text{Pd}_2\text{Cl}_2$ gave highly active solid-phase-bound catalysts which were used for high-turnover Suzuki and Sonogashira reactions, Figure 12.10 [71]. The resin-bound catalysts were particularly useful for catalyst recovery. The Suzuki reaction between 4-tolyl boronic acid and phenyl iodide was performed eight times with no loss of palladium or catalyst efficiency. The resin was recovered by simple steps of filtering and washing. In aqueous solution and at elevated temperature, the best catalysts gave quantitative conversion in Suzuki reactions at as little as 0.05 mol% catalyst in less than 10 min. These are reaction rates approaching those of natural enzymes (see Table 12.2).

Ligand-based palladium catalysis is prominent in organic chemistry, particularly in C–C bond forming hetero-cross-coupling reactions. The peptidic nature of the catalysts described in this chapter opens up new opportunities for catalysis due to their

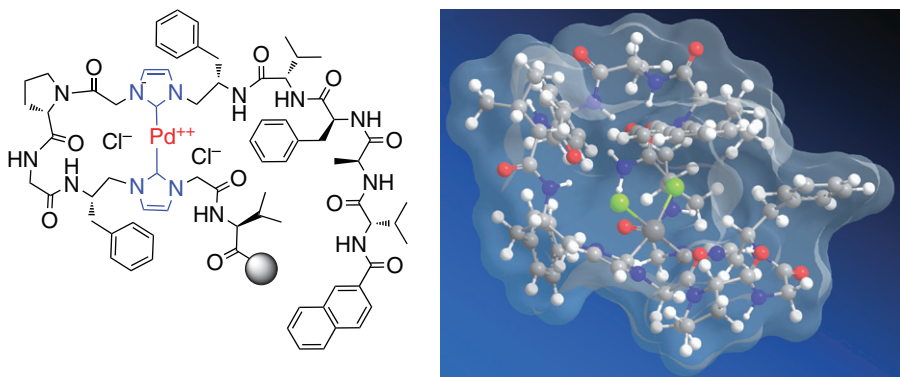


Figure 12.9. With the incorporation of carbene precursor dipeptide mimetic building blocks in peptide assembly, a folded palladium complex can be formed. The products are highly stable and may be used in supported catalytic chemical conversions in aqueous solution. See color insert.

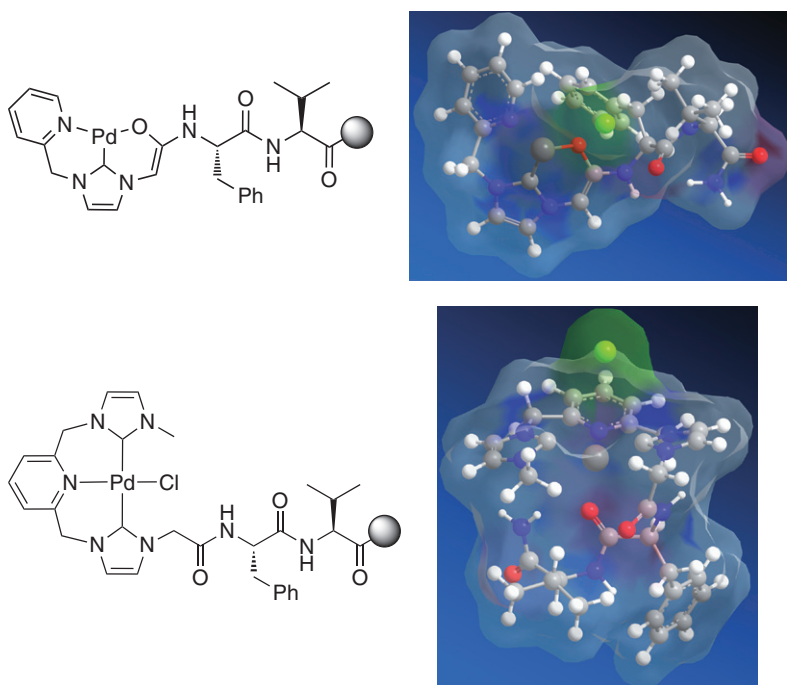
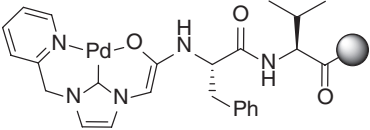
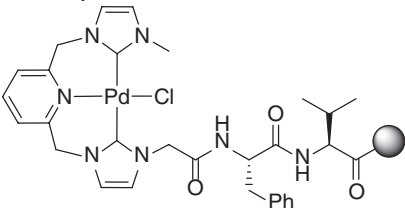


Figure 12.10. Peptide carbene palladium complexes showing very high efficiency in C–C bond forming Suzuki and Sonogashira reactions. The catalysts can be used under microwave conditions and may be recycled. See color insert.

TABLE 12.2. Solid-Phase Peptide Carbene Palladium Catalysts in Suzuki Reactions. The Catalysis Was Performed under Aqueous Microwave Conditions with Very High Turnovers

Catalyst	Temperature (°C)	Equiv	Time	Yield (isol.) (%)
	50	–	12 h	0
	50	0.02	6 h	96
	90 (μW)	0.01	15 min	95
	90 (μW)	–	30 min	0
	50	0.01	6 h	91
	90 (μW)	0.0005	10 min	95

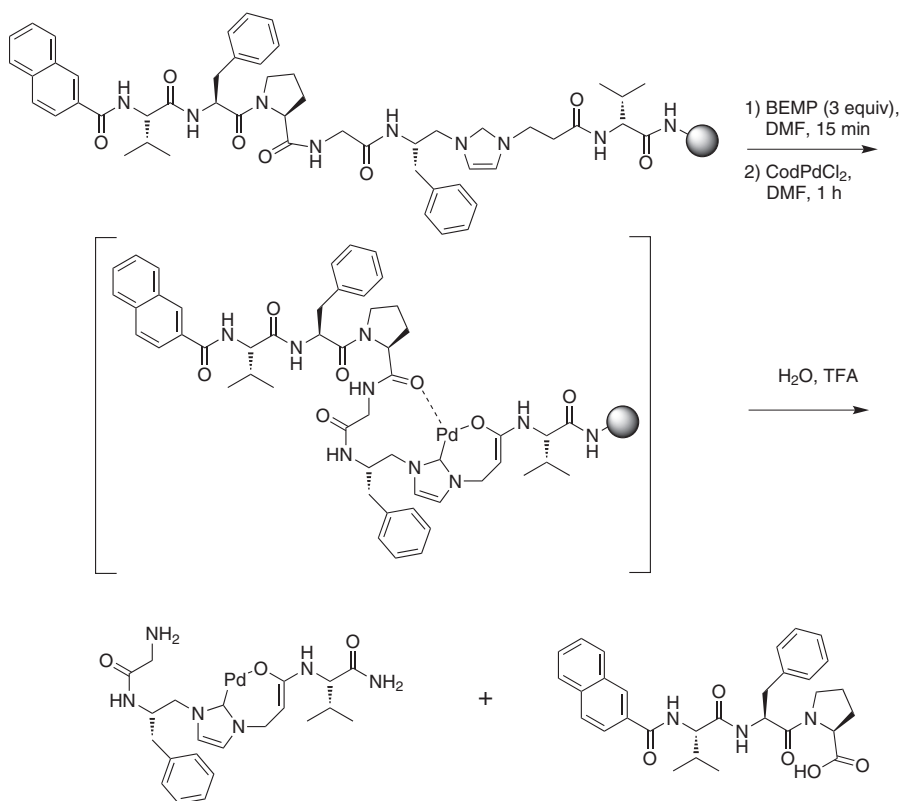
structural resemblance with bioderived peptides, and we envisage that some of nature's most prominent reactions employed in signaling and control of biofunction may be addressed with peptide-based transition-metal catalysts [72]. One such target could be hydrolytic reactions on biopolymers, for example, the exquisite function of the proteolytic enzymes [73].

The peptide ligand presented in Scheme 12.15 was synthesized and characterized. The carbene was formed, and upon addition of 1 equiv of CodPdCl_2 , the peptide spontaneously (prior to any analysis could be performed) and selectively cleaved at a proline located two amino acids toward the N-terminal from the carbene.

This is a unique structural feature of precisely the ligand presented in Figure 12.11, while all other peptide palladium complexes investigated were stable. It is an important observation that indicates an opportunity to synthesize artificial proteases by appropriate structural variation of this catalyst, by preparing peptide carbene ligand libraries and screen for the catalytic ability to cleave target-derived peptide sequences. Reactions can be monitored using Förster resonance energy transfer (FRET) substrates derived from target proteins [74].

12.4 CONCLUSIONS AND OUTLOOK

In conclusion, both peptide organocatalysts and peptide transition metal complexes offer catalysts for a wide variety of chemical transformations, with high efficiencies and selectivities approaching those of natural enzymes. Common for these two types of catalysts are the added substrate interaction resulting from the increased size and polarity of the peptide scaffold compared to normal catalysts and presumably the enhanced binding during transition state of reaction. While the natural enzymes have evolved to be efficient and selective through millions of years, combinatorial evolution



Scheme 12.15. Peptide carbene palladium complexes have a potential as artificial proteases as indicated by the quantitative, unique, and selective internal cleavage of a single peptide bond upon complex formation with palladium.

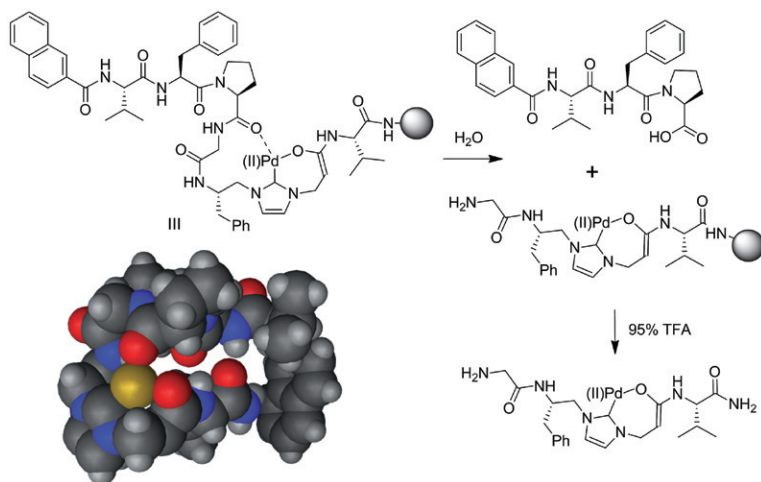


Figure 12.11. Molecular model obtained through molecular dynamics indicating a structure where carboxyl of proline amide coordinate to the palladium in turn leads to cleavage of the peptide bond. See color insert.

in the laboratory can be performed rapidly in a matter of a few years with designed evolutionary pressure and efficient selection. The combinatorial process takes advantage of careful design and molecular engineering of the overall structural features required for catalysis, while the combinatorial approach allows the subtleties of the catalytic process to be interrogated properly. So far, the described organocatalytic peptides were relatively easy to assemble from easily available building blocks, which is a great advantage when considering the major effort required to develop and perform the combinatorial synthesis, screening, selection, and validation. In the split-mix approach, the choice of resin may influence the reliability of the screening results, the most important factor being proper solvation of the resin, catalyst, and reactants in the reaction medium during the reaction. Linear peptides investigated were expected to show structural flexibility and could be excellent for induced fit catalysis. However, thorough investigation of the effect on selectivity and turnover of structurally constraining the peptidic organocatalysts is still missing. Currently, the major differences between peptide transition metals and organocatalysts are the requirement for tedious synthesis of ligand-containing building blocks and the ability to perform a large variety of reactions generally considered organic, with these “organozymes” and frequently under aqueous conditions. Currently, mainly phosphines, carbenes, crowns, and phenanthrolines have been used for metal binding, but a wide range of other tight-binding ligands for various metals has been described or are awaiting future discovery. The metal coordination has the additional advantage of restricting the conformational flexibility of the peptides and leading to expected increase in selectivity of their chemical transformations. The use of split-mix approaches where the catalysts are linked to a solid support can be a great advantage, since the selection process includes the resin effects and provides catalysts that can be easily assembled and employed for catalysis on solid support. The support [75] facilitates catalyst recycling and green aqueous chemistry. In preparation of transition-metal peptide complexes, we exploit combinatorial chemistry at three levels: (i) the scaffolding peptide structure, (ii) the ligand building blocks, and (iii) the use of various transition metals and co-ligands. The chemical space for development of catalysts is therefore immense, and it can be expected that appropriate catalysts can be found for most chemical transformations.

One great advantage of chemical assembly of catalyst libraries is the unlimited use of artificial building blocks, including D- and the α -, β -, and γ -amino acids. Therefore, we may produce catalysts that are not readily transformed by metabolic processes and may last. This could be advantageous in antifouling and surface modification and if selective catalytic drugs could be produced. One of the great challenges in the metal-coordinated peptide catalyst development lies in the selection of efficient catalysts based on the more abundant transition metals. A particular challenge is to balance the catalytic efficiency in important large-scale industrial reactions against the relative abundance of the metals.

With the prospect of enhancing this efficiency through selection by screening, we may consider the less rare metals such as Sc, Cu, Cr, Mn, Fe, Co, Ni, Zn, Mo, and Yt for chemical conversion conventionally performed with the noble metal catalysts. It is also interesting to note that the lanthanides are quite prevalent metals with abundance of 0.1–10 on the relative scale used in Table 12.3. Ce (30), Sm (2), and Yb (1) are lanthanides that have frequently been used in catalysis. Fe- or Zn-based catalysts [76, 77] would appear to have a high biocompatibility, and are of particular interest as part of a catalytic drug [72]. Our combinatorial technology is only just reaching a level where complex catalysts can be prepared, screened, and decoded on single beads in split-mix

TABLE 12.3. The Approximate Relative Abundance of the Transition Metals Is Not Favorable for Those Metals with Superior Catalytic Performance and with Increased Efficiency of Peptide-Based Catalysts

Element	Relative Occurrence	Element	Relative Occurrence	Element	Relative Occurrence
Boron	120	Silicon	1,000,000	Tin	3
Scandium	20	Yttrium	20	Lanthanum	13
Titanium	8000	Zirconium	180	Hafnium	3
Vanadium	100	Niobium	22	Tantalum	1
Chromium	80	Molybdenum	2	Tungsten	1
Manganese	900	Technetium	0	Rhenium	0.0003
Iron	60,000	Ruthenium	0.001	Osmium	0.00003
Cobalt	12	Rhodium	0.0002	Iridium	0.00001
Nickel	20	Palladium	0.0004	Platinum	0.0005
Copper	20	Silver	0.04	Gold	0.0009
Zinc	100	Cadmium	0.09	Mercury	0.03

More abundant metals such as iron and zinc may be considered as alternatives to the rare noble metal catalysts for large-scale industrial reactions or medicinal applications.

libraries. Due to the structural complexity and the binding of metals, these catalysts cannot readily be analyzed by mass-spectrometry techniques. One solution to this problem is resin encoding, preferably with optical techniques [78].

The field of molecular engineering of peptide-based catalysts is only at the beginning, and it holds significant promise for future green chemistry, medicine, and materials.

REFERENCES

- [1] Krattiger, P., McCarthy, C., Pfaltz, A., Wennemers, H. (2003). Catalyst-substrate coimmobilization: A strategy for catalyst discovery in split-and-mix libraries. *Angewandte Chemie (International edition in English)*, 42, 1722–1724.
- [2] Krattiger, P., Kovásy, R., Revell, J. D., Wennemers, H. (2005). Using catalyst—Substrate coimmobilization for the discovery of catalysts for asymmetric aldol reactions in split-and-mix libraries. *QSAR & Combinatorial Science*, 24, 1158–1163.
- [3] Wiesner, M. (2009). Peptides as catalysts for asymmetric 1,4-addition reactions of aldehydes to nitroolefins. Dissertation: University of Basel, 1–237.
- [4] Lingard, I., Bhalay, G., Bradley, M. (2003). Dyad beads and the combinatorial discovery of catalysts. *Chemical Communications*, 2310–2311.
- [5] Kofoed, J., Nielsen, J., Reymonda, J. L. (2003). Discovery of new peptide-based catalysts for the direct asymmetric aldol reaction. *Bioorganic & Medicinal Chemistry Letters*, 13, 2445–2447.
- [6] Chen, Y.-H., Sung, P.-H., Sung, K. (2010). Synthesis of proline-derived dipeptides and their catalytic enantioselective direct aldol reactions: Catalyst, solvent, additive and temperature effects. *Amino Acids*, 38, 839–845.
- [7] Tang, Z., Yang, Z.-H., Cun, L.-F., Gong, L.-Z., Mi, A.-Q., Jiang, Y.-Z. (2004). Small peptides catalyze highly enantioselective direct aldol reactions of aldehydes with hydroxyacetone: Unprecedented regiocontrol in aqueous media. *Organic Letters*, 6, 2285–2287.

- [8] Weber, A. L., Pizzarello, S. (2006). The peptide-catalyzed stereospecific synthesis of tetroses: A possible model for prebiotic molecular evolution. *Proceedings of the National Academy of Sciences of the United States of America*, *123*, 12713–12717.
- [9] Zou, W., Ibrahim, I., Dziedzic, P., Sunden, H., Cordova, A. (2005). Small peptides as modular catalysts for the direct asymmetric aldol reaction: Ancient peptides with aldolase enzyme activity. *Chemical Communications*, 4946–4948.
- [10] Tanaka, F., Barbas, C. F., III. (2001). Phage display selection of peptides possessing aldolase activity. *Chemical Communications*, 769–770.
- [11] Akagawa, K., Yamashita, T., Sakamoto, S., Kudo, K. (2009). Friedel–Crafts-type alkylation in aqueous media using resin-supported peptide catalyst having polyisoleucine. *Tetrahedron Letters*, *50*, 5602–5604.
- [12] Akagawa, K., Fujiwara, T., Sakamoto, S., Kudo, K. (2011). Efficient asymmetric α -oxyamination of aldehydes by resin-supported peptide catalyst in aqueous media. *Organic Letters*, *12*, 1804–1807.
- [13] Gilbertson, S. R., Collibee, S. E., Agarkov, A. (2000). Asymmetric catalysis with libraries of palladium b-turn phosphine complexes. *Journal of the American Chemical Society*, *122*, 6522–6523.
- [14] Kelly, D. R., Roberts, S. M. (2006). Oligopeptides as catalysts for asymmetric epoxidation. *Biopolymers*, *84*, 74–89.
- [15] Berkessel, A., Koch, B., Toniolo, C., Rainaldi, M., Broxterman, Q. B., Kaptein, B. (2006). Asymmetric enone epoxidation by short solid-phase bound peptides: Further evidence for catalyst helicity and catalytic activity of individual peptide strands. *Biopolymers*, *84*, 90–96.
- [16] Tsutsumi, H., Hamasaki, K., Mihara, H., Ueno, A. (2000). Cyclodextrin-peptide hybrid as a hydrolytic catalyst having multiple functional groups. *Bioorganic & Medicinal Chemistry Letters*, *10*, 741–743.
- [17] Guler, M. O., Stupp, S. I. (2007). A self-assembled nanofiber catalyst for ester hydrolysis. *Journal of the American Chemical Society*, *129*, 12082–12083.
- [18] Clouet, A., Darbre, T., Reymond, J.-L. (2005). Combinatorial synthesis, selection, and properties of esterase peptide dendrimers. *Biopolymers*, *84*, 114–123.
- [19] Kennan, A. J., Haridas, V., Severin, K., Lee, D. H., Ghadiri, M. R. (2011). A de novo designed peptide ligase: A mechanistic investigation. *Journal of the American Chemical Society*, *123*, 1797–1803.
- [20] Copeland, G. T., Jarvo, E. R., Miller, S. J. (1998). Minimal acylase-like peptides: Conformational control of absolute stereospecificity. *The Journal of Organic Chemistry*, *63*, 6784–6785.
- [21] Copeland, G. T., Miller, S. J. (1999). A chemosensor-based approach to catalyst discovery in solution and on solid support. *Journal of the American Chemical Society*, *121*, 4306–4307.
- [22] Copeland, G. T., Miller, S. J. (2001). Selection of enantioselective acyl transfer catalysts from a pooled peptide library through a fluorescence-based activity assay: An approach to kinetic resolution of secondary alcohols of broad structural scope. *Journal of the American Chemical Society*, *123*, 6496–6502.
- [23] Evans, C. A., Miller, S. J. (2011). Proton-activated fluorescence as a tool for simultaneous screening of combinatorial chemical reactions. *Current Opinion in Chemical Biology*, *6*, 333–338.
- [24] Harris, R. F., Nation, A. J., Copeland, G. T., Miller, S. J. (2000). A polymeric and fluorescent gel for combinatorial screening of catalysts. *Journal of the American Chemical Society*, *122*, 11270–11271.
- [25] Meldal, M. (1992). PEGA: A flow stable polyethylene glycol dimethyl acrylamide copolymer for solid phase synthesis. *Tetrahedron Letters*, *33*, 3077–3080.

- [26] Auzanneau, F.-I., Meldal, M., Bock, K. (1995). Synthesis, characterization and biocompatibility of PEGA resins. *Journal of Peptide Science*, *1*, 31–44.
- [27] Wang, S. S. (1973). p-Alkoxybenzyl alcohol resin and p-alkoxybenzyloxycarbonylhydrazide resin for solid phase synthesis of protected peptide fragments. *Journal of the American Chemical Society*, *95*, 1328–1333.
- [28] Fierman, M. B., O’Leary, D. J., Steinmetz, W. E., Miller, S. J. (2004). Structure-selectivity relationships and structure for a peptide-based enantioselective acylation catalyst. *Journal of the American Chemical Society*, *126*, 6967–6971.
- [29] Blank, J. T., Miller, S. J. (2006). Studies of folded peptide-based catalysts for asymmetric organic synthesis. *Biopolymers*, *84*, 38–47.
- [30] Jarvo, E. R., Vasbinder, M. M., Miller, S. J. (2000). Asymmetric acylation reactions catalyzed by conformationally biased octapeptides. *Tetrahedron*, *56*, 9773–9779.
- [31] Angione, M. C., Miller, S. J. (2006). Dihedral angle restriction within a peptide-based tertiary alcohol kinetic resolution catalyst. *Tetrahedron*, *62*, 5254–5261.
- [32] Mennen, S. M., Gipson, J. D., Kim, Y. R., Miller, S. J. (2005). Thiazolylalanine-derived catalysts for enantioselective intermolecular aldehyde-imine cross-couplings. *Journal of the American Chemical Society*, *127*, 1654–1655.
- [33] Cowen, B. J., Saunders, L. B., Miller, S. J. (2009). Pyridylalanine (Pal)-peptide catalyzed enantioselective allenolate additions to N-acyl imines. *Journal of the American Chemical Society*, *131*, 6105–6107.
- [34] Lichtor, P. A., Miller, S. J. (2011). One-bead-one-catalyst approach to aspartic acid-based oxidation catalyst discovery. *ACS Combinatorial Science*, *13*, 321–326.
- [35] Jakobsche, C. E., Peris, G., Miller, S. J. (2008). Functional analysis of an aspartate-based epoxidation catalyst with amide-to-alkene peptidomimetic catalyst analogues. *Angewandte Chemie (International edition in English)*, *47*, 6707–6711.
- [36] Peris, G., Jakobsche, C. E., Miller, S. J. (2007). Aspartate-catalyzed asymmetric epoxidation reactions. *Journal of the American Chemical Society*, *129*, 8710–8711.
- [37] Jordan, P. A., Kayser-Bricker, K. J., Miller, S. J. (2010). Asymmetric phosphorylation through catalytic P(III) phosphoramidite transfer: Enantioselective synthesis of D-myo-inositol-6-phosphate. *Proceedings of the National Academy of Sciences of the United States of America*, *107*, 20620–20624.
- [38] Davie, E. A. C., Mennen, S. M., Xu, Y., Miller, S. J. (2007). Asymmetric catalysis mediated by synthetic peptides. *Chemical Reviews*, *107*, 5759–5812.
- [39] Miller, S. J. (2004). In search of peptide-based catalysts for asymmetric organic synthesis. *Accounts of Chemical Research*, *37*, 601–610.
- [40] Sculimbrene, B. R., Morgan, A. J., Miller, S. J. (2003). Nonenzymatic peptide-based catalytic asymmetric phosphorylation of inositol derivatives. *Chemical Communications*, 1781–1785.
- [41] Jarvo, E. R., Miller, S. J. (2002). Amino acids and peptides as asymmetric organocatalysts. *Tetrahedron*, *58*, 2481–2495.
- [42] Guerin, D. J., Miller, S. J. (2002). Asymmetric azidation-cycloaddition with open-chain peptide-based catalysts. A sequential enantioselective route to triazoles. *Journal of the American Chemical Society*, *124*, 2134–2136.
- [43] Horstmann, T. E., Guerin, D. J., Miller, S. J. (2000). Asymmetric conjugate addition of azide to α,β -unsaturated carbonyl compounds catalyzed by simple peptides. *Angewandte Chemie (International edition in English)*, *39*, 3635–3638.
- [44] Linton, B. R., Reutershan, M. H., Aderman, C. M., Richardson, E. A., Brownell, K. R., Ashley, C. W., et al. (2007). Asymmetric Michael addition of α -nitro-ketones using catalytic peptides. *Tetrahedron Letters*, *48*, 1993–1997.
- [45] Lewis, C. A., Gustafson, J. L., Chiu, A., Balsells, J., Pollard, D., Murry, J., et al. (2008). A case of remote asymmetric induction in the peptide-catalyzed desymmetrization of a bis(phenol). *Journal of the American Chemical Society*, *130*, 16355–16368.

- [46] Lewis, C. A., Chiu, A., Kubryk, M., Balsells, J., Pollard, D., Esser, C. K., et al. (2006). Remote desymmetrization at near-nanometer group separation catalyzed by a miniaturized enzyme mimic. *Journal of the American Chemical Society*, *128*, 16454–16455.
- [47] Griswold, K. S., Miller, S. J. (2003). A peptide-based catalyst approach to regioselective functionalization of carbohydrates. *Tetrahedron*, *59*, 8869–8875.
- [48] Gustafson, J. L., Lim, D., Miller, S. J. (2010). Dynamic kinetic resolution of biaryl atropisomers via peptide-catalyzed asymmetric bromination. *Science*, *328*, 1251–1255.
- [49] Sculimbrene, B. R., Miller, S. J. (2001). Discovery of a catalytic asymmetric phosphorylation through selection of a minimal kinase mimic: A concise total synthesis of D-myo-inositol-1-phosphate. *Journal of the American Chemical Society*, *123*, 10125–10126.
- [50] Kayser-Bricker, K. J., Jordan, P. A., Miller, S. J. (2008). Catalyst-dependent syntheses of phosphatidylinositol-5-phosphate–DiC8 and its enantiomer. *Tetrahedron*, *64*, 7015–7020.
- [51] Morgan, A. J., Komiya, S., Xu, Y., Miller, S. J. (2006). Unified total syntheses of the inositol polyphosphates: D-I-3,5,6P3, D-I-3,4,5P3, D-I-3,4,6P3, and D-I-3,4,5,6P4 via catalytic enantioselective and site-selective phosphorylation. *The Journal of Organic Chemistry*, *71*, 6923–6931.
- [52] Xu, Y., Sculimbrene, B. R., Miller, S. J. (2006). Streamlined synthesis of phosphatidylinositol (PI), PI3P, PI3,5P2, and deoxygenated analogues as potential biological probes. *The Journal of Organic Chemistry*, *71*, 4919–4928.
- [53] Kolundzic, F., Noshi, M. N., Tjandra, M., Movassaghi, M., Miller, S. J. (2011). Chemoselective and enantioselective oxidation of indoles employing aspartyl peptide catalysts. *Journal of the American Chemical Society*, *133*, 9104–9111.
- [54] Zaykov, A. N., Popp, B. V., Ball, Z. T. (2010). Helix induction by dirhodium: Access to bio-compatible metallopeptides with defined secondary structure. *Chemistry—A European Journal*, *16*, 6651–6659.
- [55] Popp, B. V., Ball, Z. T. (2010). Structure-selective modification of aromatic side chains with dirhodium metallopeptide catalysts. *Journal of the American Chemical Society*, *132*, 6660–6662.
- [56] Copeland, K. D., Fitzsimons, M. P., Houser, R. P., Barton, J. K. (2002). DNA hydrolysis and oxidative cleavage by metal-binding peptides tethered to rhodium intercalators. *Biochemistry*, *41*, 343–356.
- [57] Kim, M. G., Kim, M.-S., Lee, S. D., Suh, J. (2006). Peptide-cleaving catalyst selective for melanin-concentrating hormone: Oxidative decarboxylation of N-terminal aspartate catalyzed by Co(III)cyclen. *Journal of Biological Inorganic Chemistry*, *11*, 867–875.
- [58] Degrado, S. J., Mitzutani, J., Hoveyda, A. H. (2001). Modular peptide-based phosphine ligands in asymmetric catalysis: Efficient and enantioselective Cu-catalyzed conjugate additions to five-, six-, and seven-membered cyclic enones. *Journal of the American Chemical Society*, *123*, 755–756.
- [59] Agarkov, A., Gilbertson, S. R. (2005). Coordination mode for turn-based phosphine ligands: The origin of selectivity in Pd catalysis. *Tetrahedron Letters*, *46*, 181–183.
- [60] Agarkov, A., Greenfield, S., Xie, D., Pawlick, R., Starkey, G., Gilbertson, S. R. (2006). Synthesis of phosphine containing amino acids: Utilization of peptide synthesis in ligand design. *Biopolymers*, *84*, 48–73.
- [61] Christensen, C. A., Meldal, M. (2005). Efficient solid-phase synthesis of peptide based phosphine ligands: Towards combinatorial libraries of selective transition metal catalysts. *Chemistry—A European Journal*, *11*, 4121–4131.
- [62] Jensen, J. F., Worm-Leonhard, K., Meldal, M. (2008). Optically active (peptido-carbene) palladium complexes: Towards true solid-phase combinatorial libraries of transition metal catalysts. *European Journal of Organic Chemistry*, *2008*, 3785–3797.
- [63] Bao, W., Wang, Z., Li, Y. (2003). Synthesis of chiral ionic liquids from natural amino acids. *The Journal of Organic Chemistry*, *68*, 591–593.

- [64] Agarkov, A., Greenfield, S. J., Ohishi, T., Collibee, S. E., Gilbertson, S. R. (2004). Catalysis with phosphine-containing amino acids in various "turn" motifs. *The Journal of Organic Chemistry*, *69*, 8077–8085.
- [65] Greenfield, S. J., Agarkov, A., Gilbertson, S. R. (2003). High asymmetric induction with β -turn-derived palladium phosphine complexes. *Organic Letters*, *5*, 3096–3072.
- [66] Agarkov, A., Uffman, E. W., Gilbertson, S. R. (2003). Parallel approach to selective catalysts for palladium-catalyzed desymmetrization of 2,4-cyclopentenediol. *Organic Letters*, *5*, 2091–2094.
- [67] Benito, J. M., Christensen, C. A., Meldal, M. (2004). Versatile solid-phase synthesis of peptide-derived 2-oxazolines: Application in the synthesis of ligands for asymmetric catalysis. *Organic Letters*, *7*, 581–584.
- [68] Gilbertson, S. R., Yamada, S. (2004). A study of catalyst selectivity with polymer bound palladium phosphine complexes on various solid phase synthesis supports. *Tetrahedron Letters*, *45*, 3917–3920.
- [69] Christensen, C. A., Meldal, M. (2007). Solid-phase synthesis of a P,S-ligand system designed for generation of combinatorial peptide-based catalyst libraries. *Journal of Combinatorial Chemistry*, *9*, 79–85.
- [70] Meldal, M., Tornøe, C. W., Nielsen, T. E., Diness, F., Le Quement, S., Christensen, C. A., et al. (2010). Ralph F. Hirschmann award address 2009: Merger of organic chemistry with peptide diversity. *Biopolymers*, *94*, 161–182.
- [71] Worm-Leonhard, K., Meldal, M. (2008). Green catalysts: Solid-phase peptide carbene ligands in aqueous transition metal catalysis. *European Journal of Organic Chemistry*, *2008*, 5244–5253.
- [72] Suh, J., Chei, W. S. (2008). Metal complexes as artificial proteases: Toward catalytic drugs. *Current Opinion in Chemical Biology*, *12*, 207–213.
- [73] Grant, K. B., Kassai, M. (2006). Major advances in the hydrolysis of peptides and proteins by metal ions and complexes. *Current Organic Chemistry*, *10*, 1035–1049.
- [74] Meldal, M., Breddam, K. (1991). Anthranilamide and nitrotyrosine as a donor acceptor pair in internally quenched fluorescent substrates for endopeptidases: Multicolumn peptide synthesis of enzyme substrates for subtilisin Carlsberg and pepsin. *Analytical Biochemistry*, *195*, 141–147.
- [75] Leadbeater, N. E., Marco, M. (2002). Preparation of polymer-supported ligands and metal complexes for use in catalysis. *Chemical Reviews*, *102*, 3217–3274.
- [76] Sissi, C., Rossi, P., Felluga, F., Formaggio, F., Palumbo, M., Tecilla, P., et al. (2001). Dinuclear Zn²⁺ complexes of synthetic heptapeptides as artificial nucleases. *Journal of the American Chemical Society*, *123*, 3169–3170.
- [77] Rossi, P., Felluga, F., Tecilla, P., Formaggio, F., Crisma, M., Toniolo, C., et al. (2000). An azacrown-functionalized peptide as a metal ion based catalyst for the cleavage of a RNA-model substrate. *Biopolymers*, *55*, 496–501.
- [78] Meldal, M., Christensen, S. F. (2010). Micro-particle matrix encoding of beads. *Angewandte Chemie (International edition in English)*, *49*, 3473–3476.

CHAPTER 13

DENDRIMERS IN BIOLOGY AND NANOMEDICINE

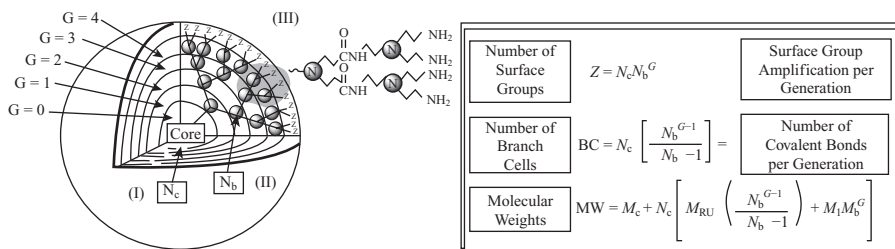
JØRN BOLSTAD CHRISTENSEN

13.1 INTRODUCTION

Dendrimers and dendrons are names that cover a very broad area of molecules that have only their molecular connectivity in common. More specifically, they are classes of highly branched “tree-shaped” nanosized molecules, where the structure branches out from the central core of the molecule toward the periphery in a well-defined manner, the dendrimer being the molecular tree and the dendrons being the branches. It is also evident from this description that the resulting molecular structures can have very different physical, chemical, and biological properties. Dendrimers and dendrons are interesting because they are synthetic macromolecules that can have sizes and molecular weights similar to proteins. They can be synthesized as pure compounds in contrast to the polymers and are some of the only well-defined nanoscale molecules available that are not of biological origin. A schematic structure of a dendrimer is shown in Figure 13.1; the molecule has a surface, an interior, and a core. The structure can be described as consisting of repeating branch-cell units. The layers in the structure are coined “generations.”

13.2 PROPERTIES

The molecular weight and the number of end groups of dendrimers increase rapidly on increasing the generation, as shown in Figure 13.1. The large number of end groups present at the surface of the dendrimer provides a platform for using multivalency for improved binding to a desired receptor simply by having a multivalent display of the weakly binding ligand at the surface. The surface groups can also be utilized for host–guest chemistry in supramolecular chemistry allowing noncovalent functionalization of the dendrimer surface, as illustrated in Figure 13.2. This phenomenon is also called exocomplexation and provides a way to use dendrimers for targeted drug delivery.



Gen	No. of NH ₂ Surface Groups	Molecular Formula	MW	Hydrodynamic Diameter (nm)
0	4	C ₂₄ H ₃₂ N ₁₀ O ₄ S ₂	609	1.5
1	8	C ₆₄ H ₁₃₂ N ₂₆ O ₁₂ S ₂	1,522	2.2
2	16	C ₁₄₄ H ₂₉₂ N ₅₈ O ₂₈ S ₂	3,348	2.9
3	32	C ₃₄₄ H ₆₁₂ N ₁₂₂ O ₆₈ S ₂	7,001	3.6
4	64	C ₄₂₄ H ₁₂₅₂ N ₂₅₈ O ₁₃₄ S ₂	14,307	4.5
5	128	C ₁₂₆₄ H ₂₅₃₂ N ₅₀₄ O ₁₅₂ S ₂	28,918	5.4
6	256	C ₁₅₄₄ H ₃₄₀₁ N ₁₀₁₈ O ₃₀₄ S ₂	58,140	6.7
7	512	C ₅₁₄₄ H ₁₀₀₁₂ N ₂₄₄₂ O ₁₀₂₀ S ₂	116,585	8.1

Z = monomer-shell-saturation level, N_c = core (cystamine) multiplicity, N_b = branch-cell (BC) multiplicity, G = generation.

Figure 13.1. Schematic representation of a PAMAM dendrimer with a cystamine core. Properties such as the number of surface groups, branch cells, and molecular weight can all be calculated using the Mansfield–Tomalia–Rakesh equation given in the box. Source: [1]. Reproduced with permission of Elsevier.

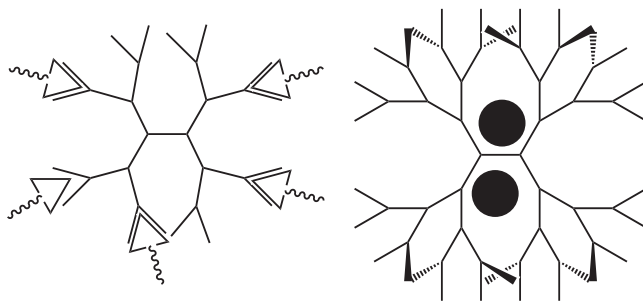


Figure 13.2. Cartoons showing binding of a ligand to receptors at the surface of a dendrimer (left) and a dendrimer encapsulating a smaller molecule also known as a dendritic box (right).

Increasing the number of receptors/ligands is not a guarantee, however, for improved binding because there may be negative cooperativity leading to weaker binding constants for additional guests. Depending on the branch-cell unit, a dendrimer can have internal voids capable of hosting smaller molecules. This can be utilized for encapsulation of smaller molecules that may be released from the interior of the dendrimer on changing the surrounding environment. Such systems were coined “dendritic boxes” and are illustrated in Figure 13.2. For references to dendrimers, in general, see References 1–6, and for guest–host chemistry with dendrimers, see References 7–10.

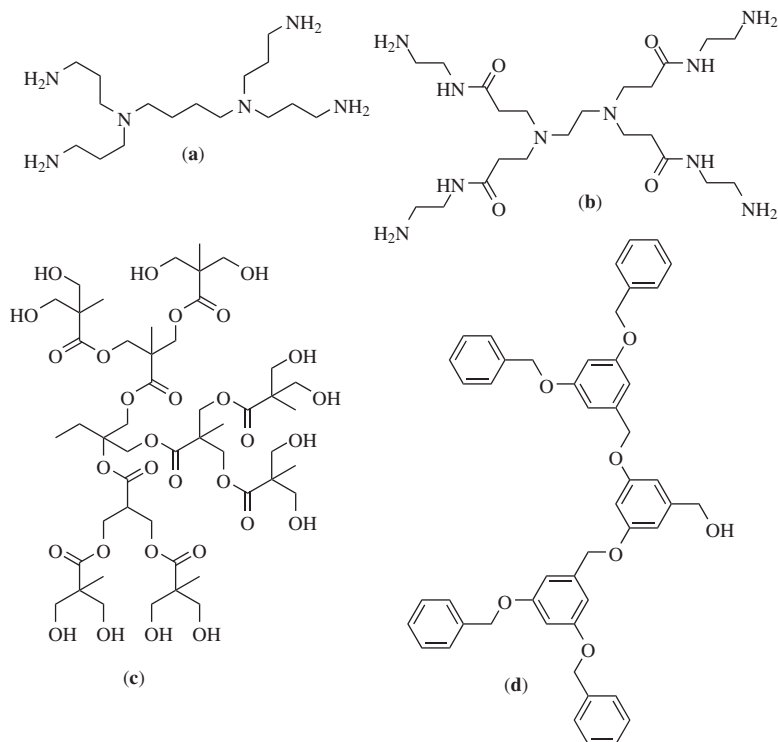


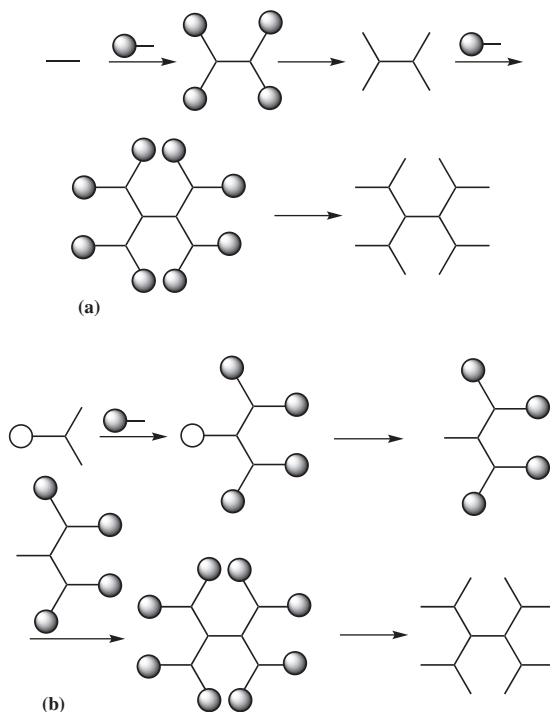
Figure 13.3. (a) PPI dendrimer, (b) PAMAM dendrimer, (c) TMP dendrimer, and (d) Fréchet dendron.

Liposomes do of course also have the ability to carry a drug load, but they suffer from the laws of thermodynamics, making them unstable below a certain concentration called the critical micellar concentration (CMC). Only relatively few dendrimer families have been investigated in connection with biology and nanomedicine (Figure 13.3), and of these are the polyamidoamine (PAMAM) dendrimers, by far the best investigated family of dendrimers.

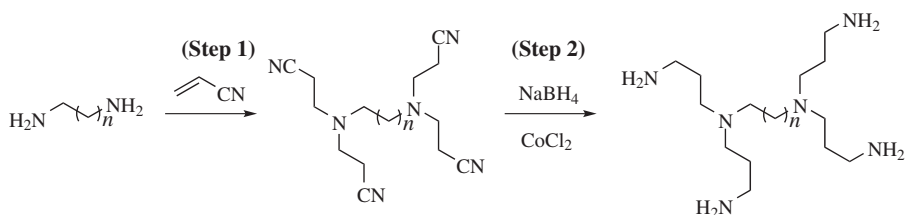
13.3 SYNTHESIS OF DENDRIMERS

Dendrimer synthesis can be divided according to two main strategies: divergent or convergent synthesis. In the divergent approach, the dendrimer is essentially synthesized beginning at the core and building outward, whereas in the convergent approach the dendrimer is built starting from the periphery and going toward the core. The two principles are illustrated in Scheme 13.1.

The early synthetic work on dendrimers was reported by Vögtle and coworkers [11] and was based on controlled divergent growth, as shown in Scheme 13.2, where a growth sequence based on Michael addition of acrylonitrile to a diamine followed by reduction of the nitrile was used.

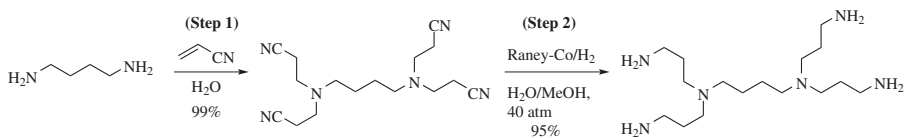


Scheme 13.1. The principles of divergent (a) and convergent (b) dendrimer syntheses. \circ and \bullet are orthogonal protective groups.

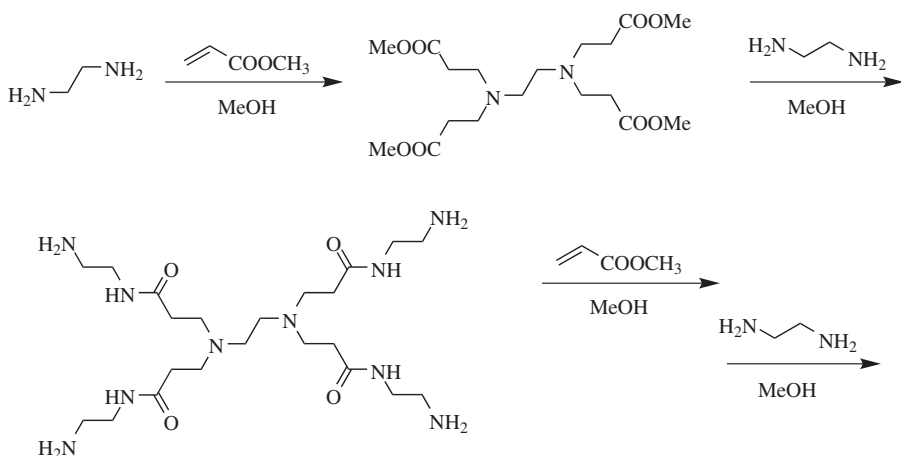


Scheme 13.2. Vögtle's dendrimer synthesis: Steps 1 and 2 are repeated for each generation.

They were not able to synthesize larger generations of dendrimers due to low yields and incomplete reactions in the reduction step. This problem was addressed and solved independently by Wörner and Mülhaupt [12] and De Brabander van den Berg and Meijer [13], who studied the reaction conditions carefully and found that performing the Michael addition in methanol and using catalytic hydrogenation for the reduction of the nitriles enabled the preparation of large generation poly(propyleneimine) (PPI) dendrimers in large quantities (Scheme 13.3). The synthetic sequence relies on the Michael addition of acrylonitrile to an amine, which proceeds in close to quantitative yields in water and the subsequent reduction of the nitrile.



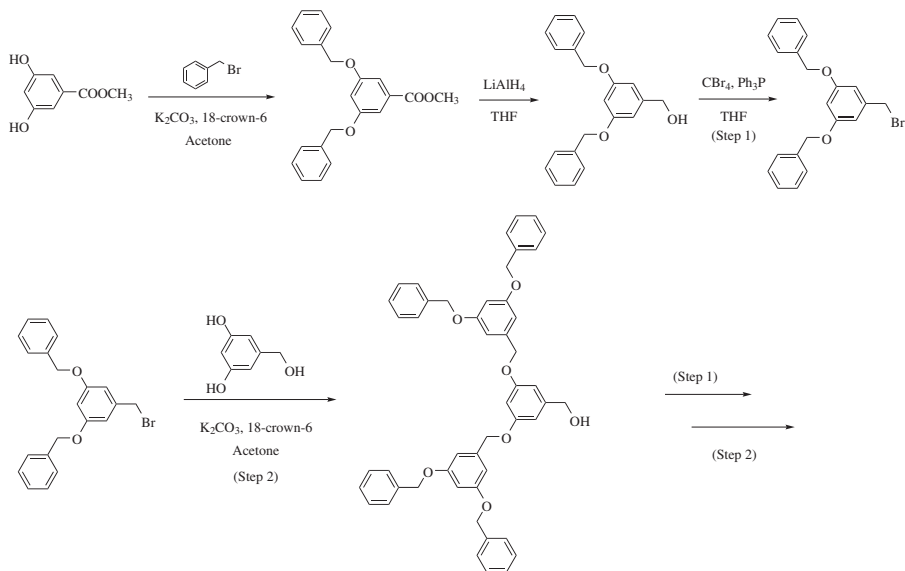
Scheme 13.3. Synthesis of PPI dendrimers with a 1,4-butanedi-amine core. Steps 1 and 2 are repeated for each building cycle.



Scheme 13.4. The divergent synthesis of PAMAM dendrimers.

The high-pressure hydrogenation step makes this procedure less suitable for laboratory-scale production of PPI dendrimers. A divergent synthetic approach is, in general, better than a convergent approach due to fewer steps; however, the situation is not as clear-cut when it comes to dendrimers. Introducing a purification step, where the desired product is isolated in the required purity, commonly solves the problem of incomplete reactions in traditional organic synthesis. This is very difficult in dendrimer synthesis because the desired products and the impurities are often very closely related with respect to physical properties and chemical reactivity. The problems are thus similar to the problems encountered in solid-phase synthesis of peptides [14] and oligonucleotides [15], and the solutions are similar: use only reactions that proceed in yields as close to quantitative as possible and accept that there is an upper limit, with respect to the size of dendrimers, that can be synthesized by divergent synthesis. Still, the divergent synthetic approach is very useful and a number of important dendrimer families are synthesized in this manner. For a comprehensive review of divergent dendrimer synthesis, see the recent excellent review by Newkome and Shreiner [5].

The PAMAM dendrimers that were discovered by Tomalia and coworkers [16, 17] are by far the most used dendrimer family, which is because they became commercially available relatively early and because the synthetic scheme is deceptively simple on paper [18]. They are synthesized by Michael addition of methylacrylate to polyamines followed by amidation by treatment with an excess of 1,2-ethanediamine (Scheme 13.4). This approach gives PAMAM dendrimers of high purity if the reaction conditions are carefully controlled.



Scheme 13.5. Convergent synthesis of benzylether dendrimers (Fréchet wedges).

The first example of convergent dendrimer synthesis was due to Fréchet and Tomalia, who described the synthesis of the family of benzylether dendrimers, which are now commonly known as Fréchet wedges [18] (Scheme 13.5).

13.4 WHAT MAKES DENDRIMERS AND DENDRONS INTERESTING IN BIOLOGY AND NANOMEDICINE?

Size matters: the way a molecule is handled by an organism depends of course not only on the chemical properties of the molecule but also on its shape and size. Small molecules that are not substrates for specific transporters can diffuse freely in and out of cells depending on their physical chemical properties (alcohol being an example), whereas macromolecules have to use the machinery of the cell to gain entry. The overwhelming majority of our drugs are small molecules, which adhere to the Lipinski rule of five:

- Not more than 5 hydrogen-bond donors.
- Not more than 10 hydrogen-bond acceptors (2×5).
- A molecular weight less than 500 Da.
- An octanol–water partition coefficient $\log P$ not greater than 5.

These rules reflect that unless there is a compound-specific mechanism for uptake of the drug, it needs to be not too polar or too unpolar because solubility in water as well as the ability to cross biological barriers such as membranes is needed. It is thus not surprising that amino groups are very popular functional groups in drugs, which make

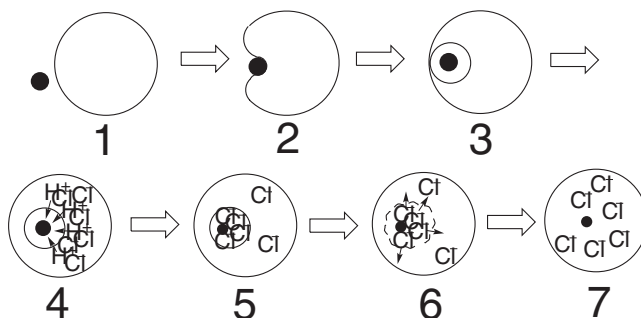


Figure 13.4. Cartoon of endocytosis.

the compound exist as both protonated (water soluble) and free amine under physiological conditions.

Cellular uptake of macromolecules (polystyrene, dendrimers, gold nanoparticles, etc.) takes place via endocytosis, which is a general mechanism for cellular uptake. Endocytosis covers at least four different subtypes of uptake mechanism—clathrin mediated, caveolas, macropinocytosis, and phagocytosis—and will often involve a binding event, where the molecule binds to a receptor leading to uptake of the compound. A primitive cartoon of the mechanism is illustrated in Figure 13.4.

Cellular uptake by simple or receptor-mediated endocytosis opens the possibility of targeted drug delivery, where the amount of drug necessary can be considerably lowered. In this way it is possible to reduce problems associated with toxicity or undesired side effects, and a prime example is the anticancer drug Doxil®, which is a formulation of the highly cardiotoxic tetracycline chemotherapeutic doxorubicin in liposomes.

13.5 TOXICITY OF DENDRIMERS

It is necessary to realize, when discussing the toxicity of dendrimers, that the term “toxicity” in reality covers two subtypes: toxicity as in toxic chemicals, such as cyanide, and immunotoxicity. The first type of toxicity is fairly straightforward because it can readily be tested in different types of cell assays. Immunotoxicity is more diffuse; it is a property that requires the presence of an immune system, and the same compound may not be toxic in all test subjects. When molecules approach the size of proteins, they can trigger a response from the immune system. The most primitive part of our immune system (the innate immune system) can react spontaneously to everything from macromolecules to liposomes, giving rise to a complement activation related pseudoallergy (CARPA) reaction, which can be as deadly as a “normal” allergic reaction. The only difference is that there might not be a reaction upon re-exposure to the same compound.

Investigating CARPA reactions is done in animal models such as pigs and is done at a late stage of drug development. So the following discussion of the toxicity of dendrimers is solely about “classic toxicity.”

The potential toxicity of dendrimers has been the topic of much discussion, and the main problem has basically been that “dendrimers” are not one family of chemical

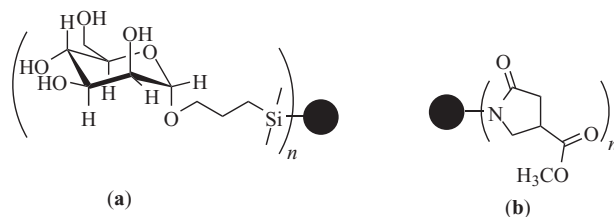


Figure 13.5. Silicon dendrimer with mannose surface groups (a) and a PAMAM dendrimer with a pyrrolidone surface (b).

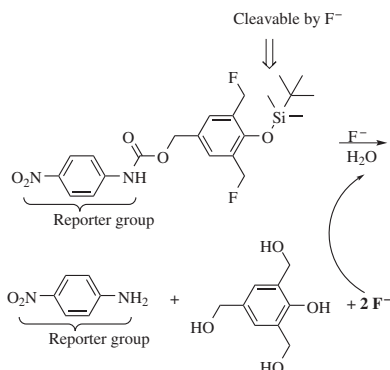
compounds, but it is the name for molecules having a certain topology in common. Thus it can be very difficult to perform comparative studies because people use different methods for testing the toxicity that differ in sensitivity. There are some guidelines at present, however, that seem to hold. The properties of a dendrimer such as solubility and toxicity depend only on the size of the dendrimer and on the surface groups. The surface charge (zeta potential) is important and has consequences for polyamine-based dendrimer families such as PAMAM and PPI dendrimers. So it is hardly surprising that simple PAMAM dendrimers are toxic behaving essentially as cationic detergents in solution. Reducing the net charge and the toxicity can be achieved by converting some of the amino groups into amides, which reduces the toxicity as shown by D'Emanuelle and coworkers [19–22] and Shi and coworkers [23]. Decorating the surface of dendrimers with carbohydrates such as mannose has also been shown to reduce the toxicity [24, 25], and recently it has been shown that PAMAM dendrimers having pyrrolidone surfaces have very low toxicity [26] (Figure 13.5).

13.6 DENDRIMERS IN DIAGNOSTICS

In the detection of a compound, the analyte relies on generation of a signal that can be used for identification, but if the amount of the analyte is small the corresponding signal can be hampered by noise or interference from other compounds present. The solution to this problem is either to have an extremely sensitive method of detection such as fluorescence and/or to amplify the signal from the analyte. The multivalent surface of dendrimers can be used for amplification of the signal either by having multivalent binding sites for the analyte or by having multiple signaling units.

One of the first examples of the potential of dendrimers in diagnostics was the DNA dendrimers described by Nilsen and coworkers [27], who showed that it was possible to detect DNA in the zeptomolar range (10^{-21} M) simply by combining the molecular recognition built in to DNA with boosting binding constants by having a dendritic structure displaying multiple binding sites. This has subsequently been used by Orentas and coworkers [28] to detect the presence of RNA from Epstein–Barr virus in post-transplant lymphoma patients.

Another and rather interesting approach to signal amplification using dendrimers has been reported by Avital-Shmilovici and Shabat [29] [127] based on their concept of self-immolative dendrimers. The principle, which is illustrated in Scheme 13.6, is based on a cascade reaction triggered by a single reaction, which has to be specific.



Scheme 13.6. The schematics of a self-amplifying system for detection of fluoride based on cleavage of a silylether.

Upon cleavage of this critical bond, the dendron or dendrimer simply falls apart, releasing the large number of molecules previously bound to the surface and thereby generating an exponentially amplified signal. It will be interesting to follow the future development of this concept into real sensors.

In spite of the growing number of papers describing dendrimer-based methods for diagnostics (for a recent overview of these, see the review by Tomalia and coworkers [30]), only a few dendrimer-based systems are on the market, and they are all intended for the detection of biological markers associated with acute myocardial infarction. Cardiovascular disease is a major cause of death in the Western world, and the ability to predict upcoming problems by monitoring critical markers saves lives.

The Dimension VISTA[®] 1500 Intelligent Lab System and the Stratus[®] system both from Dade Behring and Elecsys[®] from Roche [31] are all based on dendrimers. The principles behind the Stratus[®] system have been published by Singh and coworkers [32, 33].

It is interesting from a molecular-engineering point of view that the reactions used to modify the surface of the dendrimer are completely unspecific, giving a mixture of compounds, where the number of groups attached to the surface as well as their spatial position on the dendrimer is completely random. This is commonly seen and reflects the fact that while chemists have been extremely successful in synthesizing small molecules, the tools for synthesizing well-defined synthetic macromolecules are basically underdeveloped.

13.7 DENDRIMER-BASED REAGENTS FOR IMAGING

Dendrimers offer several advantages in connection with imaging agents. Encapsulation of imaging agents inside a dendrimer can prevent unwanted interactions with components present in tissue. The hydrodynamic ratio of the dendrimer provides a means of controlling the penetration of imaging agent into the tissue, and the multivalent surface of the dendrimer can be used for attachment of targeting ligands as well as imaging agents, allowing imaging of specific types of cells.

13.7.1 CT Scanning

Contrast agents for X-ray computed tomography (CT) scanning need to contain heavy elements for contrast, and iodine-containing compounds are commonly used. A very interesting concept that has been demonstrated recently is to use dendrimer-encapsulated metal nanoparticles (DENs), such as gold or silver. Zhang and coworkers [34] prepared Au-nanoparticles encapsulated in a G5 amino-terminated PAMAM dendrimer giving particles with the approximate composition $(\text{Au}^0)_{200}@\text{dendr}(\text{NH}_2)_{128}$. The particles had an average diameter of 4 nm and were tested in mice.

Gold nanoparticles also act as a small antenna and can be used for very specifically heating the surrounding tissue by irradiation, causing killing of the cells by overheating. This has recently been demonstrated *in vitro* with Au-DENs using HeLa cells by Kojima and coworkers [35]. They synthesized two different types of Au-DENs and found that, surprisingly, Au-DENs grown by a seeding process, where tiny clusters are formed first and allowed to grow by subsequent addition of more Au(III) and reducing agent, were much less lethal than Au-DENs grown in one step, which is the standard procedure. For more literature on Au-nanoparticles and imaging, see References 36–38.

13.7.2 Imaging Using Radioactive Isotopes (PET and SPECT)

Positron emission tomography (PET) and single photon emission computed tomography (SPECT) are based on the use of positron emitting nuclides, which are injected into the patient in the form of metal complexes or suitably labeled compounds. Fukase and coworkers [39] described recently the use of ^{68}Ga bound as DOTA-chelate for imaging the binding and uptake of different glycoclusters bound to a poly(lysine) dendron. The outline of the construct is shown in Figure 13.6.

The dendrons were also labeled with two different fluorescent labels (Cy5 and nitrobenzoxadiazole [NBD]), fluorescing red and green, respectively. Wickstrom and coworkers [40, 41] have described a system consisting of a monofunctionalized DOTA linked to dendrons built from 2,3-diaminopropanoic acid in order to amplify the amount of signal available from the system, as shown in Figure 13.7.

The dendrons were linked to a targeting moiety and ended in a cyclic analog of insulin-like growth factor 1 (IGF1) (Figure 13.8). The terminal peptide secures receptor-mediated endocytosis, allowing the construct to get into the cell, where the targeting moiety directs the imaging agent to the desired target. In this way, using a peptide nucleic acid (PNA) sequence, they targeted mutant KRAS2 mRNA, which is present in 95% of cases of pancreatic cancer [40]. The metal in the DOTA ligand was in this case ^{111}In , but DOTA is capable of binding a number of other interesting metals for imaging (^{64}Cu , $^{99\text{m}}\text{Tc}$, Gd).

13.7.3 MRI

Compounds that induce rapid relaxation of the ^1H -nuclei (affecting either the T_1 or T_2 lifetimes) enhance the contrast in magnetic resonance imaging (MRI), and the most commonly used metal for that purpose is Gd^{3+} , which needs to be fixated in a suitable ligand. DOTA and DOTA-type ligands have proven to be very useful for this purpose. There are a large number of studies of MRI-contrast agents conjugated to dendrimers

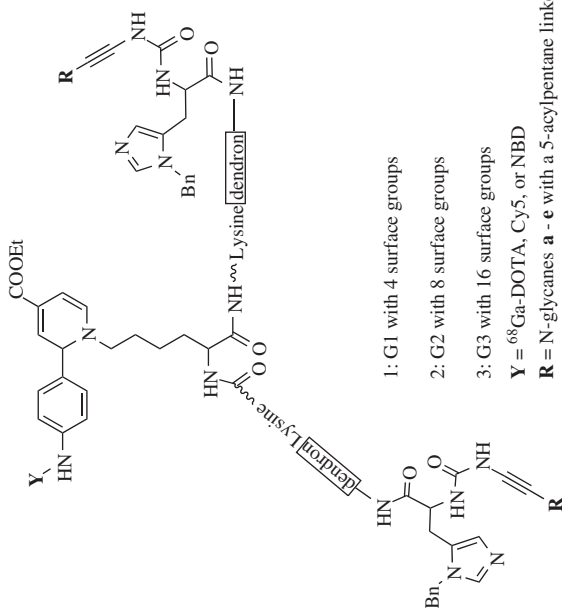
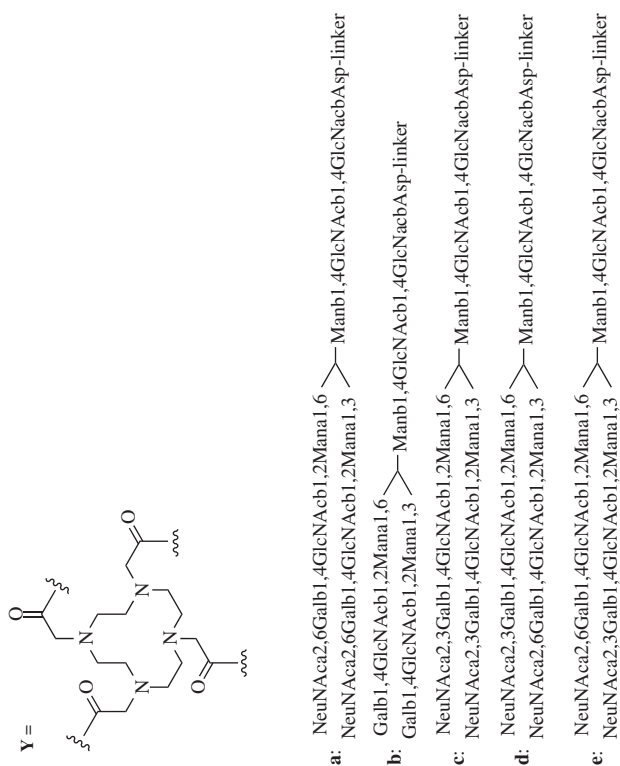


Figure 13.6. Generations and structures of glycoclusters [39]. NBD, nitrobenzoxadiazole.

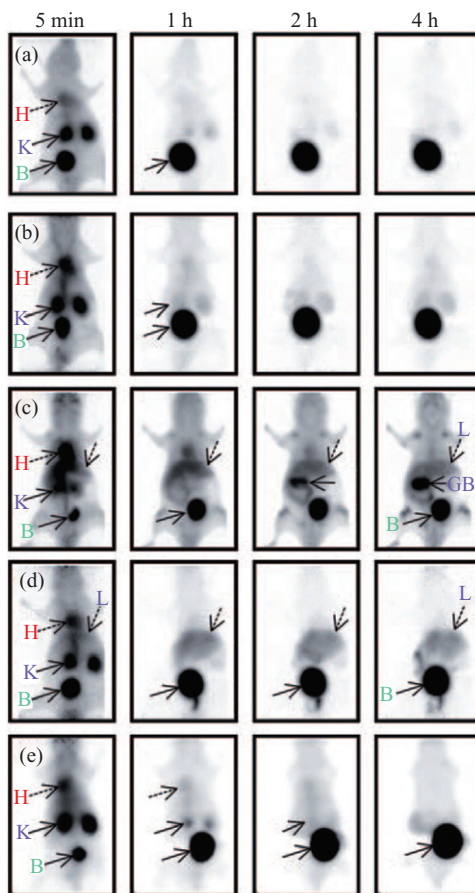


Figure 13.7. Dynamic PET imaging of glycoclusters **1a**, **2a**, and **3a–c** (a–e, respectively) in normal BALB/c nude mice. ^{68}Ga -DOTA-labeled glycoclusters (10 MBq) were administered into the tail vein of the mice ($n = 3500$ pmol, 100 mL/mouse) and the whole body was scanned by a small-animal PET scanner over 0–4 h after injection; H: heart; K: kidney; L: liver; B: urinary bladder. Source: [39]. Reproduced with permission of Wiley-VCH Verlag GmbH & Co. KGaA.

(for some recent reviews, see References 38 and 42–44), and Gadomer®-system originally developed by Schering in Berlin (now part of Bayer) has been under commercial development for a number of years. Small molecular contrast agents will disappear from the blood vessels by diffusion into the surrounding tissue; increasing the size of the systems to 3–6 nm leads to renal excretion, making them useful for imaging of the kidneys. Dendrimers of the size of 7–12 nm will stay in the blood pool, which is good for cardiovascular imaging. The polarity of the surface groups is important for the fate of the dendrimers; those having unipolar surface groups end up in the liver.

Brechbiel and coworkers looked into the synthesis of conjugates between PAMAM dendrimer and Gd-chelates by examining the different products obtained by measuring the relaxivity and found that the highest degree of “metallation” was seen by coupling

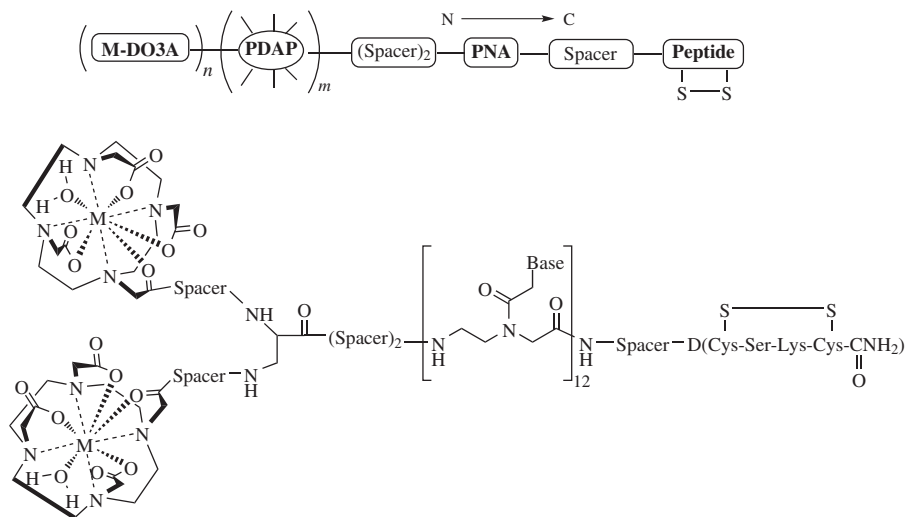


Figure 13.8. Dendron construct used for targeted imaging of pancreatic cancer. PNA = 12-mer N-GCC ATC AGC TCC-C complementary to codon 10–13 of KRAS mRNA. Peptide = 4mer short cyclic peptide analog of IGF1 (IGF1-receptor binding ligand). PDAP = polydiamidopropanoyl dendrimer. Generations 1, 3, and 4 with 2, 8, and 16 amino groups. DO3a = 1,4,7,10-tetraazacyclododecane-1,4,7-triacetate-10-acetyl macrocyclic metal chelator. M = $^{111}\text{In(III)}$ or Gd(III). Gd: MRI contrast metal; Gd-DO3a: MRI contrast complex.

the preformed chelates to the dendrimer instead of trying to saturate the dendrimer–ligand conjugate with Gd^{3+} . This was unexpected because the rare earth metal ions are otherwise known to form highly kinetically labile complexes, but the local structure on the surface of the dendrimer apparently plays an important role [45].

13.7.4 Optical Probes

Optical probes are common for *in vitro* experiments, but the lack of transparency to light below 800 nm (but opening below 10 nm in the X-ray region) of humans makes such systems less useful. However, an example from Tsien and coworkers [46] shows that such systems might be useful in connection with surgical removal of tumors, where there is a delicate balance between removing all of the tumor tissue without causing excessive damage. They functionalized the surface of an amino-terminated G5 PAMAM dendrimer with a cell-penetrating peptide, which was masked by an additional peptide strand specifically cleavable by the enzymes MMP-2 and MMP-9, which are expressed by a number of cancer cell lines. Next the dendrimer surface was labeled for MRI with the fluorescent dye Cy5 and the Gd-complex DOTA. When the masked peptide tail is cleaved it releases the dendrimer functionalized with the cell-penetrating peptide, a fluorophore and a MRI probe, which is internalized by the cancer cell. Studies in a mouse model showed that MRI could establish the position of the tumor; upon surgery the tumor was easily identified via its red fluorescence, allowing clean surgical removal of the cancer tissue.

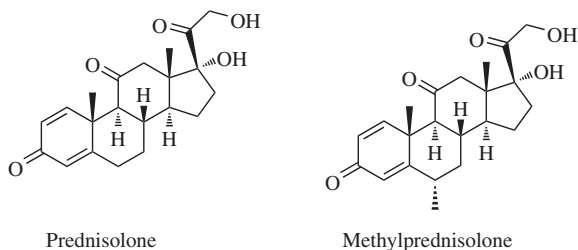


Figure 13.9. Glucocorticoids.

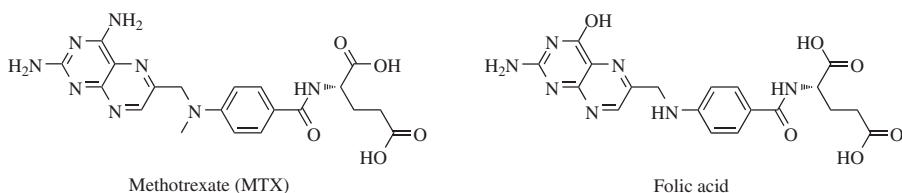


Figure 13.10. The structures of Methotrexate and folic acid.

13.8 ANTI-INFLAMMATORY ACTIVITY OF DENDRIMERS

There are a number of diseases such as arthritis that are caused by autoimmune reactions of the immune system toward parts of the organism; with increasing life span more and more people are suffering from these diseases. One of the early applications of dendrimers was as drug-delivery systems for glucocorticoids such as prednisolone [47–50] (Figure 13.9). In 2009 Tomalia and coworkers [51] serendipitously discovered that PAMAM dendrimers terminated with 2-hydroxyethyl amides had anti-inflammatory properties in themselves.

There have since been reports by Kannan and coworkers [52] on activity of PAMAM dendrimer against cerebral palsy, from Haag and coworkers [53] on surface-sulfated polyglycerol dendrimers, and from Davignon and coworkers [54–56] on PPI- and Majoral–Caminade-type dendrimers having bisphosphonic acid surface groups, all showing activity against different types of arthritic diseases. The work by Davignon and coworkers [54] even suggests that the dendrimers are better than the currently used antibodies and small molecule drugs; given the high costs of the currently used biological drugs, this is extremely interesting (for a review of dendrimers for treatment of arthritis, see Reference 57).

Baker and coworkers [58] found that PAMAM dendrimers displaying methotrexate (which is a folic acid antagonist; Figure 13.10) on the surface also had an effect on arthritis. The methotrexate was bound to the surface of the amino-terminated dendrimer through one of the carboxylic acids as an amide. Muñoz-Fernández and coworkers [59] showed that a carbosilane-based dendrimer had an effect on the Th17 cell immune response (Figure 13.11), which is involved both in the immune response to extracellular bacterial and fungal infections and also in some autoimmune diseases.

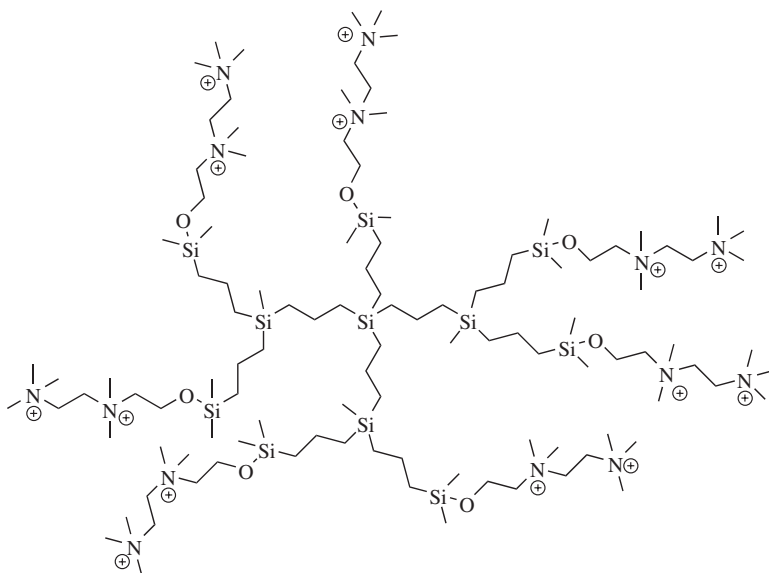


Figure 13.11. The silicon dendrimer of Muñoz-Fernández and coworkers.

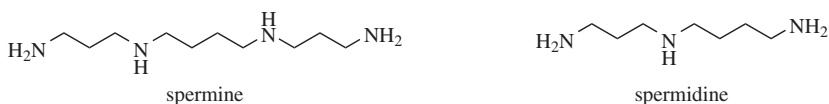


Figure 13.12. Spermine and spermidine.

13.9 DNA TRANSFECTION

Dendrimers having amino groups at the surface are polycations and form salts with polyanions such as DNA. Complexes between polyamines such as hyperbranched poly(ethyleneimine) (which is the product formed upon polymerization of ethyleneimine) have long been known to be able to transfect cells *in vitro* bringing foreign DNA into the nucleus of the cell, where it is incorporated, allowing reprogramming of the cell to perform other activities. Poly(ethyleneimine) is, unfortunately, also highly toxic, but small polyamines such as spermine and spermidine (Figure 13.12) naturally occur together with DNA.

Szoka and coworkers [60–62] discovered originally that PAMAM dendrimer–DNA complexes were capable of transfecting eukaryotic cells, thus allowing incorporation of foreign DNA into the cells. It soon became apparent that the efficiency of the process depended on the origin and quality of the PAMAM dendrimers, and it was discovered that the best results were obtained with PAMAM dendrimers containing many defects. This was since explained by the so-called umbrella model: The DNA-dendrimer complex is taken into the cell by endocytosis and is internalized in the endosome, which contains proton and chloride pumps (from the outer membrane) in the endosomal

membrane. Endosomal uptake of protons and chloride anions lead to an increased osmotic pressure inside the endosome, which at some point causes it to burst and release its contents in the cytosol. This mechanism was shown *in vitro* by a series of fluorescence labeling experiments using proton- and chloride-sensitive fluorescent labels. Upon protonation of the DNA-dendrimer complex, the DNA is released. The observed differences between imperfect and perfect PAMAM dendrimers led Szoka and coworkers to propose the so-called umbrella model. Efficient release of the DNA from the DNA-dendrimer complex requires large structural changes, which have to be induced by the Coulombic repulsion between the protonated amino groups in the dendrimer. A perfect PAMAM dendrimer has spherical symmetry and can change conformation only to a limited degree upon protonation, while the highly defective PAMAM dendrimer can behave like an umbrella, that is, unfolded, leading to a large conformational change.

13.10 siRNA DELIVERY

Small interfering RNA (siRNA) has been a hot topic since the discovery in the late 1990s. It is double-stranded RNA consisting of 20–25 base pairs that can interfere with gene expression and protein synthesis, giving an alternative to gene therapy in closing down unwanted processes in the cell. However, free RNA does not last long in a biological environment and is rapidly digested by nucleases. The first example of using a dendrimer in combination with RNA was shown by Bettinger and coworkers [63], who investigated RNA delivery using a number of different systems including poly(lysine) and Polyfect^(R), which is the trade name for PAMAM dendrimers for transfection. Since then a number of different carriers have been suggested, and the situation has recently been reviewed by Uludağ and coworkers [64]. Peng and coworkers [65–67] were among the first to investigate types of dendrimers other than PAMAM, PPI, or poly(lysine) for siRNA delivery, and they have synthesized a family of dendrimers based on a triethanol amine core having a combination of amide and amine linkages, as shown in Figure 13.13.

This design is much more flexible than the other types of dendrimers, and the distance between the amino groups in the structure can be controlled by using different types of ω -aminoalcohols as building blocks in the synthesis. These types of dendrimers have been shown to work both *in vivo* and *in vitro* for treatment of prostate cancer [68] as well as HIV [69] in a mouse model. Given that siRNAs are small compared with DNA, this has led to some interesting studies on the influence of the size and structure of the dendrimer carrier on the properties of the complexes. Pavan and coworkers [70] have used molecular simulations to study the interactions between different generations of PAMAM dendrimers and RNA and were able to reproduce the experimental findings concerning the effect of size, shape, and charge. They also suggested a new parameter to describe the balance between enthalpy and entropy, which was coined the energetic flexibility index EF given by

$$EF = \frac{\Delta H}{T\Delta S}.$$

High EF values indicate flexibility in the binding of the RNA (or DNA), and low values indicate high entropic cost.

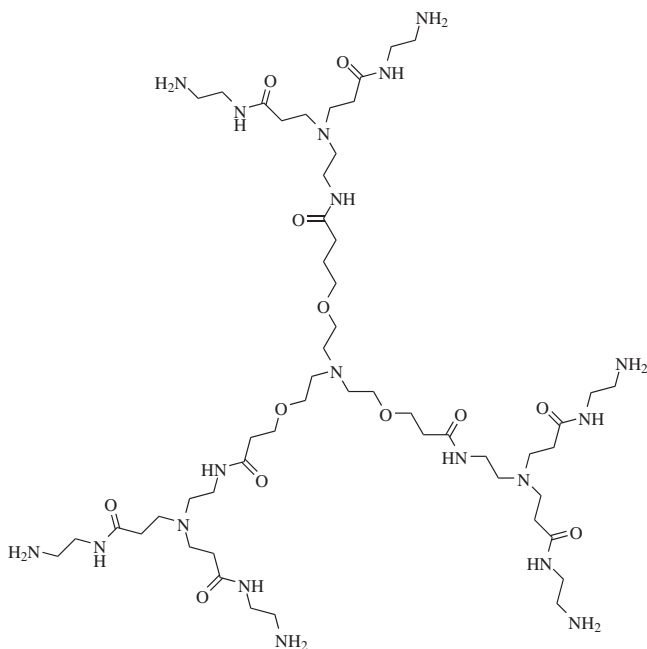


Figure 13.13. G3 triethanolamine-cored dendrimer by Peng and coworkers.

13.11 VACCINES

The immune system consists of two parts: the innate immune system and the adaptive immune system. The innate immune system reacts to immediate threats and has no memory, while the adaptive immune system takes some time before the maximum response is reached, but once a response has been established it is “memorized,” leading to a fast response on future exposure. Vaccination can provide long-term protection against a specific infectious disease by stimulating the adaptive immune system to recognize and destroy the foreign antigen. In a successful vaccination, the antigens are remembered by the immune system, which has a long-lasting effect. An example is the measles–mumps–rubella (MMR) vaccine, which is given to children and provides lifelong immunity against measles, mumps, and rubella.

Cells and microorganisms all have surfaces that display different types of compounds such as peptides or carbohydrates. These also serve as identification tags for the immune system, identifying potential threats, and it is the combination of size and surface groups that triggers an immune response from the adaptive immune system. Some microorganisms are not very immunogenic or change surface chemistry too often to be effectively recognized, so development of classical vaccines for such organisms is difficult.

Singh *et al.* [33] and Tam and coworkers [71–76] were the first to suggest dendrimers for vaccines in the form of multiple antigen peptide (MAP) dendrimers, where a multivalent presentation of a peptide antigen leads to increased immune response due to

higher binding constants. Shao and Tam [75] developed a number of conjugation methods such as thiazoline, oxime, and hydrazone ligations that are highly useful for assembly of macromolecules under mild conditions. Although many biological recognition processes involve recognition of carbohydrate motifs, the individual interactions are weak and rather nonimmunogenic. This is a problem for the development of vaccines against HIV, for example, but recent work by Wong and coworkers [77] has shown that oligomannose dendrons, which mimic the surface of the virus, are recognized by proteins involved in the immune response, opening up possibilities of developing either a vaccine or new anti-HIV drugs.

Vaccines against different types of cancer are also an area of much activity both in order to prevent specific types of cancer such as cervical cancer and because certain forms of cancer respond poorly to chemotherapy [75, 78]. The whole area of dendrimer-based vaccines and the associated problems with developing vaccines has recently been reviewed by Heegaard and coworkers [79].

13.12 CANCER

Medical treatment of cancer involves the use of cytotoxic compounds, and the cure is really a balance between killing the cancer cells without killing the patient. Many of the commonly found side effects of chemotherapy are, in fact, due to the general poisoning of the patient. Thus much effort is being devoted to developing drug-delivery systems that allow precise targeting of the cancer cells, which in turn leads to administration of lower amounts of drug and fewer side effects. Cancer cells and tissue display the so-called enhanced permeation retention (EPR) effect. The result of this effect is that large molecules such as macromolecules can enter cancer cells, but they are retained, providing a very simple mechanism for targeting cancer cells. This has been utilized for drug delivery of chemotherapeutics with macromolecules, polymers, and dendrimers.

Dendrimer-based delivery systems for chemotherapy can be based on covalent linking of the drug to the dendrimer or by using the dendrimer as a host for noncovalent binding of the drug. Both types of systems are known, and one example of such systems is covalent binding of methotrexate to the surface of a PAMAM dendrimer, which also carries folic acid units as targeting ligands [80–82]. Cancer cells overexpress folic acid receptors on their surface and this can be used for targeted drug delivery; however, the kidney cells are also rich in folic acid receptors.

Ghandehari and coworkers [83, 84] synthesized a conjugate between camptothecin and a PAMAM dendrimer, which showed *in vitro* activity against the human colorectal carcinoma cell line HCT-116. They concluded that the observed effect was not only due to release of camptothecine from the conjugate by hydrolysis but also due to the conjugate itself acting cytotoxic, which is interesting for further development in this area.

Camptothecin, like a number of other compounds used in chemotherapy, is highly insoluble in water, so conjugation to the dendrimer solubilizes the drug as well as making a drug delivery. Ghandehari and coworkers [85] showed that an analog to camptothecin SN-38 (the active metabolite of irinotecan) conjugated to a PAMAM dendrimer is capable of crossing epithelial cells (caco-2 cell culture), which is necessary to have uptake via the gastrointestinal system. Szoka and coworkers [86] reported *in vivo* results in a mouse model on camptothecin conjugates based on a PEGylated lysine

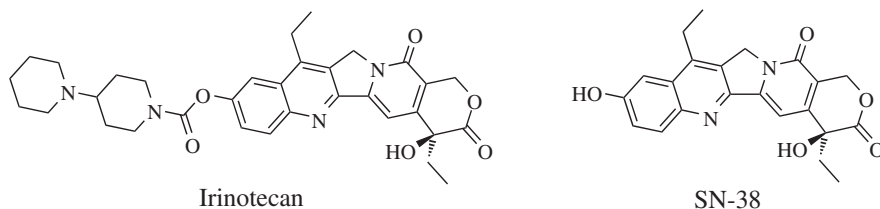


Figure 13.14. The structures of methotrexate and folic acid.

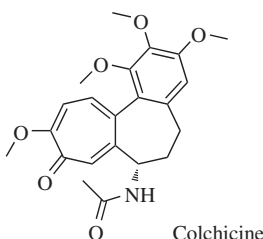


Figure 13.15. The structure of colchicine.

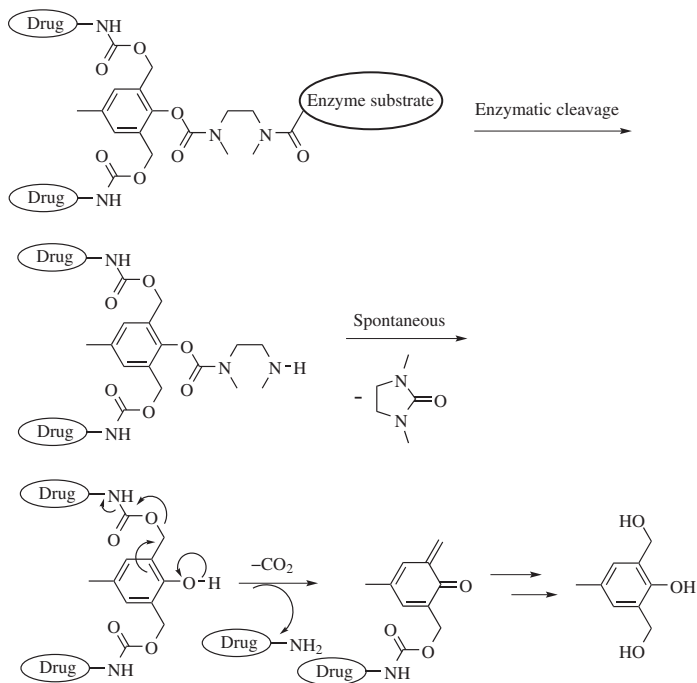
dendrimer with a molecular weight of 40 kDa. The conjugates had a half-life of 8.8 h in the blood pool and were shown to be superior to irinotecan (Figure 13.14) in murine (C26) and human colon carcinoma (HT-29) tumor models.

Shen and coworkers [87] (PAMAM conjugate) and Lim and Simanek [88] (triazine-dendrimer conjugate) have also reported on the synthesis and properties of camptothecin-dendrimer conjugates. Reymond and coworkers [89] described a system consisting of colchicines (Figure 13.15) conjugated to a glycopeptides, which was developed by screening a combinatorial library of 65,536 peptide dendrimers. They showed that the conjugate had biological activity, but the effect was due to enzymatic degradation of the peptide releasing the colchicine.

A number of other chemotherapeutical agents have also been conjugated to dendrimers; see References 2, 90, and 91. An interesting concept was introduced independently by the groups of Shabat [92], de Groot [93], and McGrath [94], who coined the principle self-immolative dendrimers or dendrimer disassembly (Scheme 13.7). The idea is to have a dendrimer that will undergo spontaneous self-degradation upon cleavage of a strategic bond. In this way a single event can release a large number of drug molecules from a dendrimer–drug conjugate or amplification of a signal can be achieved. The main problem is to find structures that can undergo this type of spontaneous disassembly and design the critical bond in a way that makes it cleavable by the desired stimuli (temperature, pH, enzymatic reaction, etc.).

This concept has been used for delivery of Camptothecin and Doxorubicin (Figure 13.16) in model systems. Very recently, Papot and coworkers described a trigger mechanism based on β -glucuronidase-induced cleavage, which is overexpressed in some types of tumors [95]. For more references on the self-immolative dendrimer concept, see References 96 and 97.

Noncovalent binding of the drug to a dendrimer has also been demonstrated. Bahadur and coworkers [98] showed that a low-generation PAMAM-type dendrimer



Scheme 13.7. Release of drug from a self-immolative dendrimer [92].

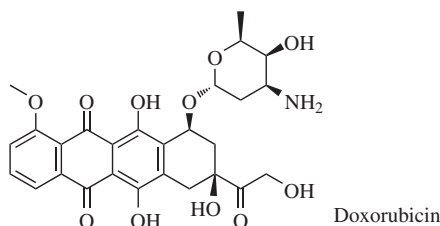


Figure 13.16. The structure of doxorubicin.

(Figure 13.17) formed complexes with doxorubicin that was taken up *in vitro* by HeLa cells and had higher activity than doxorubicin itself.

Palakurthi and coworkers [99] derivatized a generation 4-PAMAM dendrimer (64 amino groups) and a generation 3.5-PAMAM dendrimer (64 carboxylic acids) with biotin (Figure 13.18) and used the dendrimers as hosts for cisplatin. Biotin mediates cellular uptake in ovarian cancer cells, and the compounds were tested *in vitro* in the four different cell lines SKOV, OVCAR-3, A2780, and A2780/CP70. The generation 4 dendrimer constructs were better than cisplatin.

8-Methoxypsoralene (Figure 13.18) is used in the treatment of various skin diseases, including cutaneous T-cell lymphoma by photodynamic therapy. It is highly unpolar, but Wołowiec and coworkers [100] found that PAMAM dendrimers (G2.5, G3, G3.5,

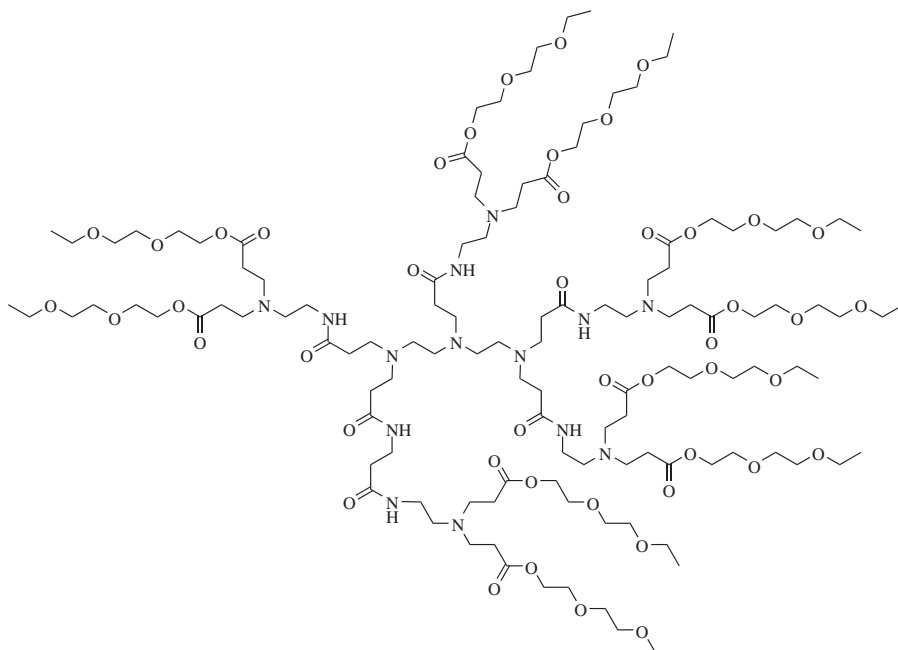


Figure 13.17. PAMAM-type dendrimer used by Bahadur and coworkers [98].

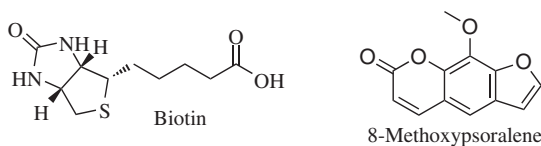


Figure 13.18. The structures of Biotin and 8-methoxypsoralene.

and G4) formed host–guest complexes with 8-methoxypsoralene capable of transdermal diffusion, enabling topical application of the compound.

A main problem with drug delivery of chemotherapeutics is to get the right release profile as well as securing delivery to the desired target. This is particularly a problem with drugs such as doxorubicin, which is irreversibly cardiotoxic. A recent review by Boyd and coworkers [101] gives an excellent comparison of the pros and cons of covalent versus noncovalent conjugation of chemotherapeutic drugs to dendrimers.

13.13 ANTIMICROBIAL AND ANTIVIRAL AGENTS

Antimicrobial and antiviral agents are the common name for compounds that either kill or inhibit bacteria, fungi, protozoans, or viruses, and they cover a large area of chemical structures and mechanisms of action. Detergents such as soaps can cause lysis of microbial membranes and subsequent death of the microorganism. Dendrimers with

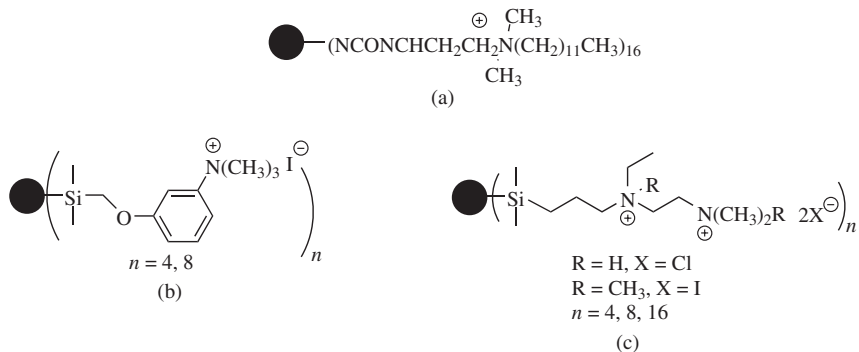


Figure 13.19. (a) PPI dendrimer with dimethyldodecylammonium as surface group [102, 125, 126]. (b) Silicon dendrimer with trimethylphenylammonium surface [103]. (c) Silicon dendrimer with a dicationic surface [104].

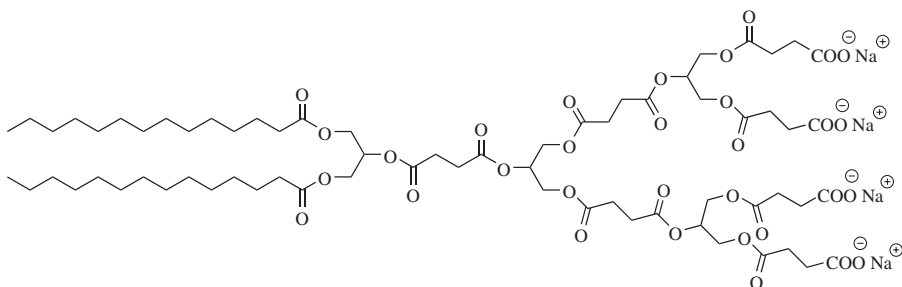


Figure 13.20. Janus dendrimer based on succinic acid and glycerol.

either a high-positive or high-negative surface charge behave essentially like covalently bound micelles of soap molecules and have antimicrobial and antiviral activity. A selection of dendrimers with cationic surface groups showing antimicrobial activity is shown in Figure 13.19.

Dendrimers with cationic surface groups seem, in general, to be more efficient than other types of cationic surfactants [102], but there is no clear relationship between the size of dendrimer and the activity, as seen in the silicon dendrimers [103, 104]. The most famous family of anionic dendrimers is also known as Vivagel[®] and is a family of lysine-based dendrimers with naphthalensulfonate groups on the surface. They have been developed by Starpharma in Australia for topical use primarily to prevent infections with HIV and herpes simplex. The first step prior to an infection with viruses such as HIV and herpes simplex is binding of the virus to receptors on the surface of the cell; the anionic dendrimers work by blocking the binding sites on the virus, which have a positive charge. Although it is a simple electrostatic interaction, it is sufficient to reduce the risk for infection. Vivagel[®] is currently in phase 3 clinical testing and is close to becoming the first commercial dendrimer-based drug.

Grinstaff and coworkers [105] reported antibacterial activity of an amphiphilic Janus dendrimer against *Bacillus subtilis*. The dendrimer is fully biodegradable and based on glycerol and succinic acid (Figure 13.20).

Glycodendrimers are interesting as antimicrobials because they can interfere with adhesion phenomena between the bacteria and the cells, but they can bind and neutralize bacterial toxins. Bacteria such as some strains of *Escherichia coli* and *Vibrio cholera* secrete toxins that cause diarrhea, and the effect of these toxins can be neutralized with suitably substituted glycodendrimers, which effectively compete with the natural binding sites in the intestinal epithelium [106–109]. Roy and coworkers [110] as well as Lindhorst and coworkers [111–113] have developed glycodendrimers that inhibit the adhesion of *Escherichia coli* through the protein FimH and inhibitors for lectins from *Pseudomonas aeruginosa* [114]. Antimicrobial peptides are a large and well-known class of peptides [115–120], and combining them with dendrimers provides a multivalent presentation. As an example, Pieters and coworkers [121] have showed that the activity of magainin-2 (Figure 13.21) boosted its hole-forming properties in an artificial membrane.

Antibiotics such as Penicillin are the classical drugs used against infections, but the golden age of antibiotics might very well be over due to the emergence of more and more resistant infections. Dendrimers have been combined with antibiotics in the form of covalently bound conjugates, which can hydrolyze *in situ*, releasing the active compound, or they can be noncovalent guest–host complexes. Hancock and Chapple [119] and Kannan and coworkers [122] have conjugated azithromycin (Figure 13.22) to a hydroxyterminated G4 PAMAM dendrimer and investigated the effect on *Chlamydia trachomatis in vitro* and found that the conjugate was more efficient than the free azithromycin. Erythromycin has also been conjugated to a dendrimer for enhancing delivery to macrophages involved in periprosthetic inflammation [123].

Pieters and coworkers [121] and Xu and coworkers [124] found that noncovalent quinolone (Figure 13.23) PAMAM-dendrimer complexes were more efficient than the quinolones alone in a series of *in vitro* results, where they determined the minimal inhibitory concentration (MIC) values. It will be interesting to see whether these results hold in a suitable *in vivo* model.

13.14 MOLECULAR ENGINEERING OF DENDRIMERS: OUTLOOK

The area of dendrimer research has changed focus during the last decade from mainly being concerned with synthesis and studies of fundamental properties to becoming mainly interested in the applications of dendrimers; in particular, the field of biomedical applications of dendrimers has exploded in interest. Much of this development has been due to the commercial availability of a few dendrimer families—PAMAM, PPI, and polyester dendrimers—and it could seem an obvious statement that the chemist has finished his or her role in this area. In this chapter a number of biomedical applications of dendrimers have been presented, and many offer great promise for the future. There is a catch, however: the vast majority of the dendrimer-based systems that have been proposed for different uses are either homogeneously substituted dendrimers or heterogeneously substituted mixtures of closely related but different compounds. In the case of the heterogeneously substituted dendrimers, the best we can say is that one or more compounds in this or that mixture have the desired activity. We can even suspect that other components in the mixture can have opposite and unwanted effects. Being able to have full control over the structure of dendrimers and being able to control the spatial arrangement of the surface groups is still lacking, and this is an area where the synthetic chemist will have plenty of work to do for the years to come.

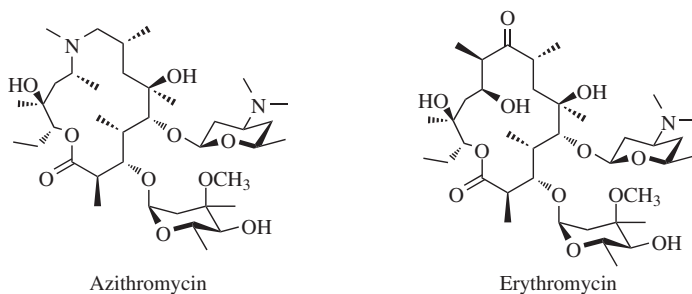


Figure 13.22. The structures of azithromycin and erythromycin.

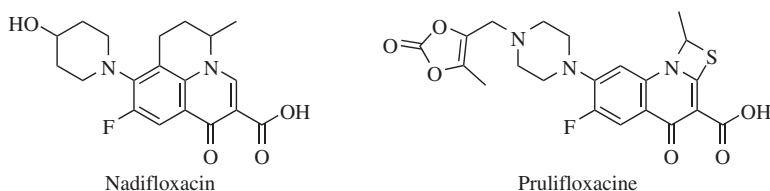


Figure 13.23. The structures of nadifloxacin and prulifloxacin.

REFERENCES

- [1] Tomalia, D. A. (2005). Birth of a new macromolecular architecture: Dendrimers as quantized building blocks for nanoscale synthetic polymer chemistry. *Progress in Polymer Science*, *30*, 294–324.
- [2] Lee, C. C., MacKay, J. A., Frechet, J. M. J., Szoka, F. C. (2005). Designing dendrimers for biological applications. *Nature Biotechnology*, *23*, 1517–1526.
- [3] Tomalia, D. A., Fréchet, J. M. J. (2002). Discovery of dendrimers and dendritic polymers: A brief historical perspective. *Journal of Polymer Science Part A—Polymer Chemistry*, *40*, 2719–2728.
- [4] Newkome, G. R., Moorefield, C. N., Baker, G. R., Saunders, M. J., Grossman, S. H. (1991). Unimolecular micelles. *Angewandte Chemie—International Edition*, *30*, 1178–1180.
- [5] Newkome, G. R., Shreiner, C. D. (2008). Poly(amidoamine), polypropylenimine, and related dendrimers and dendrons possessing different 1 → 2 branching motifs: An overview of the divergent procedures. *Polymer*, *49*, 1–173.
- [6] Newkome, G. R., Shreiner, C. (2010). Dendrimers derived from 1 → 3 branching motifs. *Chemical Reviews*, *110*, 6338–6442.
- [7] Aulenta, F., Hayes, W., Rannard, S. (2003). Dendrimers: A new class of nanoscopic containers and delivery devices. *European Polymer Journal*, *39*, 1741–1771.
- [8] Zimmerman, S. C., Lawless, L. J. (2001). Supramolecular chemistry of dendrimers. *Topics in Current Chemistry*, *217*, 95–120.
- [9] Baars, M. W. P. L., Meijer, E. W. (2000). Host-guest chemistry of dendritic molecules. *Topics in Current Chemistry*, *210*, 131–182.
- [10] Narayanan, V. V., Newkome, G. R. (1998). Supramolecular chemistry within dendritic structures. *Topics in Current Chemistry*, *197*, 19–77.

- [11] Buhleier, E., Wehner, W., Vogtle, F. (1978). Cascade-chain-like and nonskid-chain-like syntheses of molecular cavity topologies. *Synthesis*, 155–158.
- [12] Wörner, C., Mülhaupt, R. (1993). Polynitrile- and polyamine-functional poly(trimethylene imine) dendrimers. *Angewandte Chemie—International Edition*, 32, 1306–1308.
- [13] De Brabander van den Berg, E. M. M., Meijer, E. W. (1993). Poly(propylene imine) dendrimers—Large-scale synthesis by heterogeneously catalyzed hydrogenations. *Angewandte Chemie—International Edition*, 32, 1308–1311.
- [14] Bodanszky, M. *Principles of Peptide Synthesis*, Springer-Verlag, Berlin, 1983.
- [15] Herdewijn, P. E.. *Oligonucleotide Synthesis: Methods and Applications*. Methods in Molecular Biology, Humana Press, Totowa, NJ, 2005.
- [16] Tomalia, D. A., Baker, H., Dewald, J., Hall, M., Kallos, G., Martin, S., Roeck, J., Ryder, J., Smith, P. (1985). A new class of polymers: Starburst-dendritic macromolecules. *Polymer Journal (Tokyo, Japan)*, 17, 117–132.
- [17] Tomalia, D. A., Baker, H., Dewald, J., Hall, M., Kallos, G., Martin, S., Roeck, J., Ryder, J., Smith, P. (1986). Dendritic macromolecules: Synthesis of starburst dendrimers. *Macromolecules*, 19, 2466–2468.
- [18] Fréchet, J. M. J., Tomalia, D. A. *Dendrimers and Other Dendritic Compounds*, John Wiley & Sons, Chichester, 2001.
- [19] Saovapakhiran, A., D’Emanuele, A., Attwood, D., Penny, J. (2009). Surface modification of PAMAM dendrimers modulates the mechanism of cellular internalization. *Bioconjugate Chemistry*, 20, 693–701.
- [20] Jevprasesphant, R., Penny, J., Jalal, R., Attwood, D., McKeown, N. B., D’Emanuele, A. (2003). The influence of surface modification on the cytotoxicity of PAMAM dendrimers. *International Journal of Pharmaceutics*, 252, 263–266.
- [21] Jevprasesphant, R., Penny, J., Attwood, D., McKeown, N. B., D’Emanuele, A. (2003). Engineering of dendrimer surfaces to enhance transepithelial transport and reduce cytotoxicity. *Pharmaceutical Research*, 20, 1543–1550.
- [22] Jevprasesphant, R., Penny, J., Attwood, D., D’Emanuele, A. (2004). Transport of dendrimer nanocarriers through epithelial cells via the transcellular route. *Journal of Controlled Release*, 97, 259–267.
- [23] Shi, X., Lee, I., Baker, J. R., Jr. (2008). Acetylation of dendrimer-entrapped gold and silver nanoparticles. *Journal of Materials Chemistry*, 18, 586–593.
- [24] Ortega, P., Serramia, M. J., Munoz-Fernandez, M. A., de la Mata, F. J., Gomez, R. (2010). Globular carbosilane dendrimers with mannose groups at the periphery: Synthesis, characterization and toxicity in dendritic cells. *Tetrahedron*, 66, 3326–3331.
- [25] Jain, K., Kesharwani, P., Gupta, U., Jain, N. K. (2012). A review of glycosylated carriers for drug delivery. *Biomaterials*, 33, 4166–4186.
- [26] Ciolkowski, M., Petersen, J. F., Ficker, M., Janaszewska, A., Christensen, J. B., Klajnert, B., Bryszewska, M. (2012). Surface modification of PAMAM dendrimer improves its biocompatibility. *Nanomedicine: Nanotechnology, Biology, and Medicine*, 8, 815–817.
- [27] Nilsen, T. W., Grayzel, J., Prenskey, W. (1997). Dendritic nucleic acid structures. *Journal of Theoretical Biology*, 187, 273–284.
- [28] Orentas, R. J., Rospkopf, S. J., Casper, J. T., Getts, R. C., Nilsen, T. W. (1999). Detection of Epstein-Barr virus EBER sequence in post-transplant lymphoma patients with DNA dendrimers. *Journal of Virological Methods*, 77, 153–163.
- [29] Avital-Shmilovici, M., Shabat, D. (2010). Self-immolative dendrimers: A distinctive approach to molecular amplification. *Soft Matter*, 6, 1073–1080.
- [30] Tomalia, D. A., Boas, U., Christensen, J. B. *Dendrimers, Dendrons and Dendritic Polymers: From Discovery to Applications*, Chapter 5, Cambridge University Press, Cambridge, UK, 2012.

- [31] Singh, P. (2007). Dendrimers and their applications in immunoassays and clinical diagnostics. *Biotechnology and Applied Biochemistry*, 48, 1–9.
- [32] Singh, P. (1998). Terminal groups in starburst dendrimers: Activation and reactions with proteins. *Bioconjugate Chemistry*, 9, 54–63.
- [33] Singh, P., Moll, F., Lin, S. H., Ferzli, C., Yu, K. S., Koski, R. K., Saul, R. G., Cronin, P. (1994). Starburst(Tm) dendrimers—Enhanced performance and flexibility for immunoassays. *Clinical Chemistry*, 40, 1845–1849.
- [34] Liu, H., Wang, H., Guo, R., Cao, X. Y., Zhao, J. L., Luo, Y., Shen, M. W., Zhang, G. X., Shi, X. Y. (2010). Size-controlled synthesis of dendrimer-stabilized silver nanoparticles for X-ray computed tomography imaging applications. *Polymer Chemistry*, 1, 1677–1683.
- [35] Kojima, C., Cho, S. H., Higuchi, E. (2012). Gold nanoparticle-loaded PEGylated dendrimers for theragnosis. *Research on Chemical Intermediates*, 38, 1279–1289.
- [36] Huang, X., Neretina, S., El-Sayed, M. A. (2009). Gold nanorods: From synthesis and properties to biological and biomedical applications. *Advanced Materials*, 21, 4880–4910.
- [37] Murphy, C. J., Gole, A. M., Stone, J. W., Sisco, P. N., Alkilany, A. M., Goldsmith, E. C., Baxter, S. C. (2008). Gold nanoparticles in biology: Beyond toxicity to cellular imaging. *Accounts of Chemical Research*, 41, 1721–1730.
- [38] De, M., Ghosh, P. S., Rotello, V. M. (2008). Applications of nanoparticles in biology. *Advanced Materials*, 20, 4225–4241.
- [39] Tanaka, K., Siwu, E. R. O., Minami, K., Hasegawa, K., Nozaki, S., Kanayama, Y., Koyama, K., Chen, W. C., Paulson, J. C., Watanabe, Y., Fukase, K. (2010). Noninvasive imaging of dendrimer-type N-glycan clusters: In vivo dynamics dependence on oligosaccharide structure. *Angewandte Chemie—International Edition*, 49, 8195–8200.
- [40] Amirkhanov, N. V., Zhang, K. J., Aruva, M. R., Thakur, M. L., Wickstrom, E. (2010). Imaging human pancreatic cancer xenografts by targeting mutant KRAS2 mRNA with [In-111] DOTA(n)-poly(diamidopropanoyl)(m)-KRAS2 PNA-D(Cys-Ser-Lys-Cys) nanoparticles. *Bioconjugate Chemistry*, 21, 731–740.
- [41] Nariman, V., Amirkhanov, N. V., Dimitrov, I., Opitz, A. W., Zhang, K., Lackey, J. P., Cardi, C. A., Lai, S., Wagner, N. J., Thakur, M. L., Wickstrom, E. (2008). Design of (Gd-DO3A) n-polydiamidopropanoyl-peptide nucleic acid-D(Cys-Ser-Lys-Cys) magnetic resonance contrast agents. *Biopolymers*, 89, 1061–1076.
- [42] Bumb, A., Brechbiel, M. W., Choyke, P. (2011). Macromolecular and dendrimer-based magnetic resonance contrast agents. *Acta Radiologica*, 51, 751–767.
- [43] Kobayashi, H., Brechbiel, M. W. (2005). Nano-sized MRI contrast agents with dendrimer cores. *Advanced Drug Delivery Reviews*, 57, 2271–2286.
- [44] Kaminskas, L. M., Porter, C. J. H. (2011). Targeting the lymphatics using dendritic polymers (dendrimers). *Advanced Drug Delivery Reviews*, 63, 890–900.
- [45] Nwe, K., Bryant, L. H., Brechbiel, M. W. (2010). Poly(amidoamine) dendrimer based MRI contrast agents exhibiting enhanced relaxivities derived via metal preligation techniques. *Bioconjugate Chemistry*, 21, 1014–1017.
- [46] Olson, E. S., Jiang, T., Aguilera, T. A., Nguyen, Q. T., Ellies, L. G., Scadeng, M., Tsien, R. Y. (2010). Activatable cell penetrating peptides linked to nanoparticles as dual probes for in vivo fluorescence and MR imaging of proteases. *Proceedings of the National Academy of Sciences of the United States of America*, 107, 4311–4316.
- [47] Khandare, J., Kolhe, P., Pillai, O., Kannan, S., Lieh-Lai, M., Kannan, R. M. (2005). Synthesis, cellular transport, and activity of polyamidoamine dendrimer-methylprednisolone conjugates. *Bioconjugate Chemistry*, 16, 330–337.
- [48] Bilkova, E., Imramovsky, A., Sedlak, M. (2011). Recent advances in the design and synthesis of prednisolone and methylprednisolone conjugates. *Current Pharmaceutical Design*, 17, 3577–3595.

- [49] Inapagolla, R., Guru, B. R., Kurtoglu, Y. E., Gao, X., Lieh-Lai, M., Bassett, D. J. P., Kannan, R. M. (2010). In vivo efficacy of dendrimer-methylprednisolone conjugate formulation for the treatment of lung inflammation. *International Journal of Pharmaceutics*, 399, 140–147.
- [50] Elhissi, A. M. A., Martin, G., Najlah, M., Zhou, Z., D'Emanuele, A. (2010). Enhanced solubility of beclometasone dipropionate using G4 PAMAM dendrimers. *Journal of Pharmacy and Pharmacology*, 62, 1267–1268.
- [51] Chauhan, A. S., Diwan, P. V., Jain, N. K., Tomalia, D. A. (2009). Unexpected in vivo anti-inflammatory activity observed for simple, surface functionalized poly(amidoamine) dendrimers. *Biomacromolecules*, 10, 1195–1202.
- [52] Kannan, S., Dai, H., Navath, R. S., Balakrishnan, B., Jyoti, A., Janisse, J., Romero, R., Kannan, R. M. (2012). Dendrimer-based postnatal therapy for neuroinflammation and cerebral palsy in a rabbit model. *Science Translational Medicine*, 4, 130ra46.
- [53] Dervede, J., Rauschb, A., Weinhart, M., Endersa, S., Taubera, R., Lichad, K., Schirnerd, M., Zügelb, U., von Bonin, A., Haag, R. (2010). Dendritic polyglycerol sulfates as multivalent inhibitors of inflammation. *Proceedings of the National Academy of Sciences of the United States of America*, 107, 19679–19684.
- [54] Hayder, M., Poupot, M., Baron, M., Nigon, D., Turrin, C. O., Caminade, A. M., Majoral, J. P., Eisenberg, R. A., Fournie, J. J., Cantagrel, A., Poupot, R., Davignon, J. L. (2011). A phosphorus-based dendrimer targets inflammation and osteoclastogenesis in experimental arthritis. *Science Translational Medicine*, 3, 81ra35.
- [55] Hayder, M., Poupot, M., Baron, M., Nigon, D., Turrin, C. O., Caminade, A. M., Majoral, J. P., Fournie, J. J., Cantagrel, A., Poupot, R., Davignon, J. L. (2011). Phosphorus-based dendrimer as nanotherapeutics targeting both inflammation and osteoclastogenesis in experimental arthritis. *Clinical and Experimental Rheumatology*, 29, 201–202.
- [56] Hayder, M., Poupot, M., Baron, M., Turrin, C. O., Caminade, A. M., Majoral, J. P., Eisenberg, R. A., Fournie, J. J., Cantagrel, A., Poupot, R., Davignon, J. L. (2012). Frequency and route of administration in the treatment of experimental arthritis by phosphorus-based dendrimer. *Annals of the Rheumatic Diseases*, 71, A8.
- [57] Bosch, X. (2011). Dendrimers to treat rheumatoid arthritis. *ACS Nano*, 5, 6779–6785.
- [58] Thomas, T. P., Goonewardena, S. N., Majoros, I. J., Kotlyar, A., Cao, Z., Leroueil, P. R., Baker, J. R. (2011). Folate-targeted nanoparticles show efficacy in the treatment of inflammatory arthritis. *Arthritis and Rheumatism*, 63, 2671–2680.
- [59] Gras, R., Relloso, M., Garcia, M. I., de la Mata, F. J., Gomez, R., Lopez-Fernandez, L. A., Munoz-Fernandez, M. A. (2012). The inhibition of Th17 immune response in vitro and in vivo by the carbosilane dendrimer 2G-NN16. *Biomaterials*, 33, 4002–4009.
- [60] Tang, M. X., Szoka, F. C. (1997). The influence of polymer structure on the interactions of cationic polymers with DNA and morphology of the resulting complexes. *Gene Therapy*, 4, 823–832.
- [61] Tang, M. X., Redemann, C. T., Szoka, F. C. (1996). In vitro gene delivery by degraded poly-amidoamine dendrimers. *Bioconjugate Chemistry*, 7, 703–714.
- [62] Tang, M., Redemann, C. T., Szoka, F. C. (1995). Biophysical and chemical determinants of efficient gene delivery by polyamidoamine dendrimers. *Journal of Cellular Biochemistry*, 21A, 400–400.
- [63] Bettinger, T., Carlisle, R. C., Read, M. L., Ogris, M., Seymour, L. W. (2001). Peptide-mediated RNA delivery: A novel approach for enhanced transfection of primary and post-mitotic cells. *Nucleic Acids Research*, 29, 3882–3891.
- [64] Aliabadi, H. M., Landry, B., Sun, C., Tang, T., Uludağ, H. (2011). Supramolecular assemblies in functional siRNA delivery: Where do we stand? *Biomaterials*, 33, 2546–2569.
- [65] Zhou, J., Wu, J., Hafdi, N., Behr, J.-P., Erbacher, P., Peng, L. (2006). PAMAM dendrimers for efficient siRNA delivery and potent gene silencing. *Chemical Communications*, 2362–2364.

- [66] Shen, X.-C., Zhou, J., Liu, X., Wu, J., Qu, F., Zhang, Z.-L., Pang, D.-W., Quelever, G., Zhang, C.-C., Peng, L. (2007). Importance of size-to-charge ratio in construction of stable and uniform nanoscale RNA/dendrimer complexes. *Organic and Biomolecular Chemistry*, 5, 3674–3681.
- [67] Liu, X., Rocchi, P., Peng, L. (2012). Dendrimers as non-viral vectors for siRNA delivery. *New Journal of Chemistry*, 36, 256–263.
- [68] Liu, X., Liu, C., Laurini, E., Posocco, P., Pricl, S., Qu, F., Rocchi, P., Peng, L. (2012). Efficient delivery of sticky siRNA and potent gene silencing in a prostate cancer model using a generation 5 triethanolamine-core PAMAM dendrimer. *Molecular Pharmaceutics*, 9, 470–481.
- [69] Zhou, J. H., Neff, C. P., Liu, X. X., Zhang, J., Li, H. T., Smith, D. D., Swiderski, P., Aboellail, T., Huang, Y. Y., Du, Q., Liang, Z. C., Peng, L., Akkina, R., Rossi, J. J. (2011). Systemic administration of combinatorial dsRNAs via nanoparticles efficiently suppresses HIV-1 infection in humanized mice. *Molecular Therapy*, 19, 2228–2238.
- [70] Pavan, G. M., Albertazzi, L., Danani, A. (2010). Ability to adapt: Different generations of PAMAM dendrimers show different behaviors in binding siRNA. *Journal of Physical Chemistry B*, 114, 2667–2675.
- [71] Tam, J. P., Spetzler, J. C. (1997). Multiple antigen peptide system. *Methods in Enzymology*, 289, 612–637.
- [72] Tam, J. P. (1996). Recent advances in multiple antigen peptides. *Journal of Immunological Methods*, 196, 17–32.
- [73] Spetzler, J. C., Tam, J. P. (1995). Unprotected peptides as building-blocks for branched peptides and peptide dendrimers. *International Journal of Peptide and Protein Research*, 45, 78–85.
- [74] Spetzler, J. C., Tam, J. P. (1996). Self-assembly of cyclic peptides on a dendrimer: Multiple cyclic antigen peptides. *Peptide Research*, 9, 290–296.
- [75] Shao, J., Tam, J. P. (1995). Unprotected peptides as building-blocks for the synthesis of peptide dendrimers with oxime, hydrazone, and thiazolidine linkages. *Journal of the American Chemical Society*, 117, 3893–3899.
- [76] Rao, C., Tam, J. P. (1994). Synthesis of peptide dendrimer. *Journal of the American Chemical Society*, 116, 6975–6976.
- [77] Wang, S. K., Liang, P. H., Astronomo, R. D., Hsu, T. L., Hsieh, S. L., Burton, D. R., Wong, C. H. (2008). Targeting the carbohydrates on HIV-1: Interaction of oligomannose dendrons with human monoclonal antibody 2G12 and DC-SIGN. *Proceedings of the National Academy of Sciences of the United States of America*, 105, 3690–3695.
- [78] Shiao, T. C., Roy, R. (2012). Glycodendrimers as functional antigens and antitumor vaccines. *New Journal of Chemistry*, 36, 324–339.
- [79] Heegaard, P. M. H., Boas, U., Sørensen, N. S. (2010). Dendrimers for vaccine and immunostimulatory uses. A review. *Bioconjugate Chemistry*, 21, 405–418.
- [80] Zhang, Y., Thomas, T. P., Desai, A., Zong, H., Leroueil, P. R., Majoros, I. J., Baker, J. R., Jr. (2010). Targeted dendrimeric anticancer prodrug: A methotrexate-folic acid-poly (amidoamine) conjugate and a novel, rapid, “one pot” synthetic approach. *Bioconjugate Chemistry*, 21, 489–495.
- [81] Zong, H., Thomas, T. P., Lee, K.-H., Desai, A. M., Li, M.-H., Kotlyar, A., Zhang, Y., Leroueil, P. R., Gam, J. J., Holl, M. M. B., Baker, J. R., Jr. (2012). Bifunctional PAMAM dendrimer conjugates of folic acid and methotrexate with defined ratio. *Biomacromolecules*, 13, 982–991.
- [82] Majoros, I. J., Williams, C. R., Becker, A., Baker, J. R., Jr. (2009). Methotrexate delivery via folate targeted dendrimer-based nanotherapeutic platform. *Wiley Interdisciplinary Reviews. Nanomedicine and Nanobiotechnology*, 1, 502–510.

- [83] Thiagarajan, G., Ray, A., Malugin, A., Ghandehari, H. (2010). PAMAM-camptothecin conjugate inhibits proliferation and induces nuclear fragmentation in colorectal carcinoma cells. *Pharmaceutical Research*, 27, 2307–2316.
- [84] Vijayalakshmi, N., Ray, A., Malugin, A., Ghandehari, H. (2010). Carboxyl-terminated PAMAM-SN38 conjugates: Synthesis, characterization, and in vitro evaluation. *Bioconjugate Chemistry*, 21, 1804–1810.
- [85] Goldberg, D. S., Vijayalakshmi, N., Swaan, P. W., Ghandehari, H. (2011). G3.5 PAMAM dendrimers enhance transepithelial transport of SN38 while minimizing gastrointestinal toxicity. *Journal of Controlled Release*, 150, 318–325.
- [86] Fox, M. E., Guillaudeau, S., Frechet, J. M. J., Jerger, K., Macaraeg, N., Szoka, F. C. (2009). Synthesis and in vivo antitumor efficacy of PEGylated poly(l-lysine) dendrimer-camptothecin conjugates. *Molecular Pharmaceutics*, 6, 1562–1572.
- [87] Shen, Y. Q., Zhuo, Z. X., Sui, M. H., Tang, J. B., Xu, P. S., Van Kirk, E. A., Murdoch, W. J., Fan, M. H., Radosz, M. (2009). Charge-reversal polyamidoamine dendrimer for cascade nuclear drug delivery. *Nanomedicine: Nanotechnology, Biology, and Medicine*, 5, 1205–1217.
- [88] Lim, J., Simanek, E. E. (2012). Triazine dendrimers as drug delivery systems: From synthesis to therapy. *Advanced Drug Delivery Reviews*, 64, 826–835.
- [89] Johansson, E. M. V., Dubois, J., Darbre, T., Reymond, J. L. (2008). Glycopeptide dendrimer colchicine conjugates targeting cancer cells. *Bioorganic and Medicinal Chemistry*, 18, 6589–6597.
- [90] Bawarski, W. E., Chidlow, E., Bharali, D. J., Mousa, S. A. (2008). Emerging nanopharmaceuticals. *Nanomedicine: Nanotechnology, Biology, and Medicine*, 4, 273–282.
- [91] Wolinsky, J. B., Grinstaff, M. W. (2008). Therapeutic and diagnostic applications of dendrimers for cancer treatment. *Advanced Drug Delivery Reviews*, 60, 1037–1055.
- [92] Amir, R. J., Pessah, N., Shamis, M., Shabat, D. (2003). Self-immolative dendrimers. *Angewandte Chemie—International Edition*, 42, 4494–4499.
- [93] de Groot, F. M. H., Albrecht, C., Koekkoek, R., Beusker, P. H., Scheeren, H. W. (2003). “Cascade-release dendrimers” liberate all end groups upon a single triggering event in the dendritic core. *Angewandte Chemie—International Edition*, 42, 4490–4494.
- [94] Li, S., Szalai, M. L., Kevitch, R. M., McGrath, D. V. (2003). Dendrimer disassembly by benzyl ether depolymerization. *Journal of the American Chemical Society*, 125, 10516–10517.
- [95] Grinda, M., Clarhaut, J., Renoux, B., Tranoy-Opalinski, I., Papot, S. (2012). A self-immolative dendritic glucuronide prodrug of doxorubicin. *MedChemComm*, 3, 68–70.
- [96] Amir, R. J., Shabat, D. *Polymer Therapeutics I: Polymers as Drugs, Conjugates and Gene Delivery Systems*, Springer-Verlag, Berlin, 2006.
- [97] McGrath, D. V. (2005). Dendrimer disassembly as a new paradigm for the application of dendritic structures. *Molecular Pharmaceutics*, 2, 253–263.
- [98] Chandra, S., Dietrich, S., Lang, H., Bahadur, D. (2011). Dendrimer-doxorubicin conjugate for enhanced therapeutic effects for cancer. *Journal of Materials Chemistry*, 21, 5729–5737.
- [99] Yellepeddi, V. K., Kumar, A., Maher, D. M., Chauhan, S. C., Vangara, K. K., Palakurthi, S. (2011). Biotinylated PAMAM dendrimers for intracellular delivery of cisplatin to ovarian cancer: Role of SMVT. *Anticancer Research*, 31, 897–906.
- [100] Borowska, K., Laskowska, B., Magon, A., Mysliwiec, B., Pyda, M., Wołowicz, S. (2010). PAMAM dendrimers as solubilizers and hosts for 8-methoxypsoralene enabling transdermal diffusion of the guest. *International Journal of Pharmaceutics*, 398, 185–189.
- [101] Kaminskas, L. M., McLeod, V. M., Porter, C. J. H., Boyd, B. J. (2012). Association of chemotherapeutic drugs with dendrimer nanocarriers: An assessment of the merits of covalent

- conjugation compared to noncovalent encapsulation. *Molecular Pharmaceutics*, 9, 355–373.
- [102] Chen, C. Z. S., Beck-Tan, N. C., Dhurjati, P., van Dyk, T. K., LaRossa, R. A., Cooper, S. L. (2000). Quaternary ammonium functionalized poly(propylene imine) dendrimers as effective antimicrobials: Structure-activity studies. *Biomacromolecules*, 1, 473–480.
- [103] Ortega, P., Copa-Patino, J. L., Munoz-Fernandez, M. A., Soliveri, J., Gomez, R., de la Mata, F. J. (2008). Amine and ammonium functionalization of chloromethylsilane-ended dendrimers. Antimicrobial activity studies. *Organic and Biomolecular Chemistry*, 6, 3264–3269.
- [104] Rasines, B., Hernandez-Ros, J. M., de las Cuevas, N., Copa-Patino, J. L., Soliveri, J., Munoz-Fernandez, M. A., Gomez, R., de la Mata, F. J. (2009). Water-stable ammonium-terminated carbosilane dendrimers as efficient antibacterial agents. *Dalton Transactions*, 8704–8713.
- [105] Meyers, S. R., Juhn, F. S., Griset, A. P., Luman, N. R., Grinstaff, M. W. (2008). Anionic amphiphilic dendrimers as antibacterial agents. *Journal of the American Chemical Society*, 130, 14444–14445.
- [106] Thompson, J. P., Schengrund, C. L. (1998). Inhibition of the adherence of cholera toxin and the heat-labile enterotoxin of *Escherichia coli* to cell-surface GM1 by oligosaccharide-derivatized dendrimers. *Biochemical Pharmacology*, 56, 591–597.
- [107] Thompson, J. P., Schengrund, C. L. (1997). Oligosaccharide-derivatized dendrimers: Defined multivalent inhibitors of the adherence of the cholera toxin B subunit and the heat labile enterotoxin of *E. coli* GM1. *Glycoconjugate Journal*, 14, 837–845.
- [108] Thompson, J. P., Schengrund, C. L. (1996). Oligo-dendrimer inhibition of cholera toxin binding to GM1. *FASEB Journal*, 10, 1319–1319.
- [109] Schengrund, C. L., DasGupta, B. R., Thompson, J. P. (1997). Inhibition of the adherence of botulinum toxin serotype A to immobilized GT1b by multivalent oligosaccharide GT1b-derivatized dendrimers. *Journal of Neurochemistry*, 69, S17–S17.
- [110] Papadopoulos, A., Shiao, T. C., Roy, R. (2012). Diazo transfer and click chemistry in the solid phase syntheses of lysine-based glycodendrimers as antagonists against *Escherichia coli* FimH. *Molecular Pharmaceutics*, 9, 394–403.
- [111] Lindhorst, T. K., Kieburg, C., Krallmann-Wenzel, U. (1998). Inhibition of the type 1 fimbriae-mediated adhesion of *Escherichia coli* to erythrocytes by multiantennary alpha-mannosyl clusters: The effect of multivalency. *Glycoconjugate Journal*, 15, 605–613.
- [112] Lindhorst, T. K., Dubber, M., Krallmann-Wenzel, U., Ehlers, S. (2000). Cluster mannosides as inhibitors of type 1 fimbriae-mediated adhesion of *Escherichia coli*: Pentaerythritol derivatives as scaffolds. *European Journal of Organic Chemistry*, 2027–2034.
- [113] Dubber, M., Sperling, O., Lindhorst, T. K. (2006). Oligomannoside mimetics by glycosylation of “octopus glycosides” and their investigation as inhibitors of type 1 fimbriae-mediated adhesion of *Escherichia coli*. *Organic and Biomolecular Chemistry*, 4, 3901–3912.
- [114] Deguise, I., Lagnoux, D., Roy, R. (2007). Synthesis of glycodendrimers containing both fucoside and galactoside residues and their binding properties to Pa-IL and PA-III lectins from *Pseudomonas aeruginosa*. *New Journal of Chemistry*, 31, 1321–1331.
- [115] Zasloff, M. (2002). Antimicrobial peptides of multicellular organisms. *Nature*, 415, 389–395.
- [116] Tam, J. P., Lu, Y. A., Yang, J. L. (2002). Antimicrobial dendrimeric peptides. *European Journal of Biochemistry*, 269, 923–932.
- [117] Giuliani, A., Pirri, G., Nicoletto, S. F. (2007). Antimicrobial peptides: An overview of a promising class of therapeutics. *Central European Journal of Biology*, 2, 1–33.
- [118] Shai, Y. (1999). Mechanism of the binding, insertion and destabilization of phospholipid bilayer membranes by alpha-helical antimicrobial and cell non-selective membrane-lytic peptides. *Biochimica et Biophysica Acta-Biomembranes*, 1462, 55–70.

- [119] Hancock, R. E. W., Chapple, D. S. (1999). Peptide antibiotics. *Antimicrobial Agents and Chemotherapy*, 43, 1317–1323.
- [120] Yeaman, M. R., Yount, N. Y. (2003). Mechanisms of antimicrobial peptide action and resistance. *Pharmacological Reviews*, 55, 27–55.
- [121] Arnusch, C. J., Branderhorst, H., De Kruijff, B., Liskamp, R. M. J., Breukink, E., Pieters, R. J. (2007). Enhanced membrane pore formation by multimeric/oligomeric antimicrobial peptides. *Biochemistry*, 46, 13437–13442.
- [122] Mishra, M. K., Kotta, K., Hali, M., Wykes, S., Gerard, H. C., Hudson, A. P., Whittum-Hudson, J. A., Kannan, R. M. (2011). PAMAM dendrimer-azithromycin conjugate nanodevices for the treatment of Chlamydia trachomatis infections. *Nanomedicine: Nanotechnology, Biology, and Medicine*, 7, 935–944.
- [123] Bosnjakovic, A., Mishra, M. K., Ren, W. P., Kurtoglu, Y. E., Shi, T., Fan, D. N., Kannan, R. M. (2011). Poly(amidoamine) dendrimer-erythromycin conjugates for drug delivery to macrophages involved in periprosthetic inflammation. *Nanomedicine: Nanotechnology, Biology, and Medicine*, 7, 284–294.
- [124] Cheng, Y., Qu, H., Ma, M., Xu, Z., Xu, P., Fang, Y., Xu, T. (2007). Polyamidoamine (PAMAM) dendrimers as biocompatible carriers of quinolone antimicrobials: An in vitro study. *European Journal of Medicinal Chemistry*, 42, 1032–1038.
- [125] Chen, C. Z. S., Cooper, S. L. (2000). Recent advances in antimicrobial dendrimers. *Advanced Materials*, 12, 843–846.
- [126] Chen, C. Z. S., Cooper, S. L. (2002). Interactions between dendrimer biocides and bacterial membranes. *Biomaterials*, 23, 3359–3368.
- [127] Perry-Feigenbaum, R., Sella, E., Shabat, D. (2011). Autoinductive exponential signal amplification: A diagnostic probe for direct detection of fluoride. *Chemistry—A European Journal*, 17, 12123–12128.

CHAPTER 14

DYNAMIC COMBINATORIAL CHEMISTRY

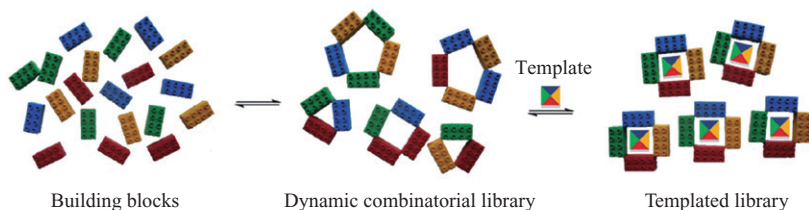
BRIAN RASMUSSEN, ANNE SØRENSEN, SOPHIE R. BEEREN, and
MICHAEL PITTELKOW

14.1 INTRODUCTION TO DYNAMIC COMBINATORIAL CHEMISTRY

Molecular recognition is difficult! The design of artificial receptors, especially biomimetic receptors that work in water, has proved challenging. Dynamic combinatorial chemistry seeks to meet this challenge by combining aspects of design (molecular engineering) with the selection approach inherent in self-assembly. In dynamic combinatorial chemistry, building blocks are allowed to react with one another using reversible chemical reactions to give mixtures of oligomers—dynamic combinatorial libraries (DCLs) [1]. Because the connections between the building blocks are reversible, the mixture is dynamic, and library members are constantly interconverting. Once the DCL reaches equilibrium, its composition is determined by the relative stabilities of the different library members. Dynamic combinatorial chemistry, therefore, is combinatorial chemistry that works under thermodynamic control (Scheme 14.1) [1–3].

DCLs respond to external stimuli. If a target molecule is added to a DCL, it will act as a template for the self-assembly of library members that recognize it. Library members that interact favorably with the template will be stabilized, and their abundance in the library will therefore increase, at the expense of other library members [4]. By analyzing these template-induced changes, the binding properties of all library members are screened simultaneously without having to isolate each species. Through this amplification process, the effective receptors are not just identified but preferentially synthesized (Scheme 14.1), which makes dynamic combinatorial chemistry an efficient discovery strategy for new receptors.

The compositions of DCLs are often analyzed using high-performance liquid chromatography (HPLC). By comparing the chromatograms for the templated and untemplated libraries, amplified species can be identified. The ratio between the concentration of the amplified species in the templated and untemplated libraries is termed the *amplification factor*. In Figure 14.1 a DCL of peptide-based acylhydrazone macrocycles



Scheme 14.1. Schematic representation of the template effect in a dynamic combinatorial library (DCL) of macrocycles. See color insert.

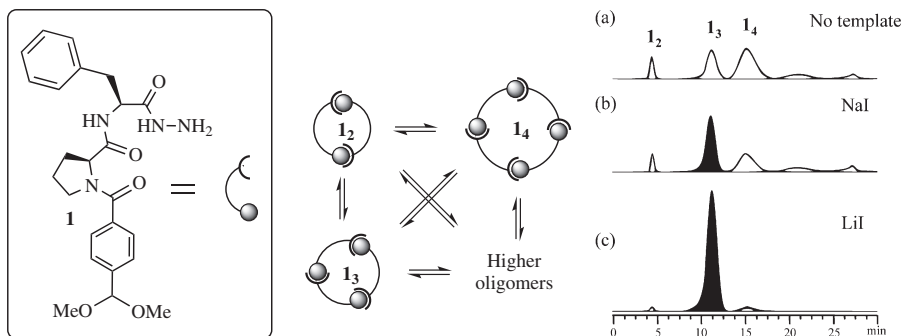
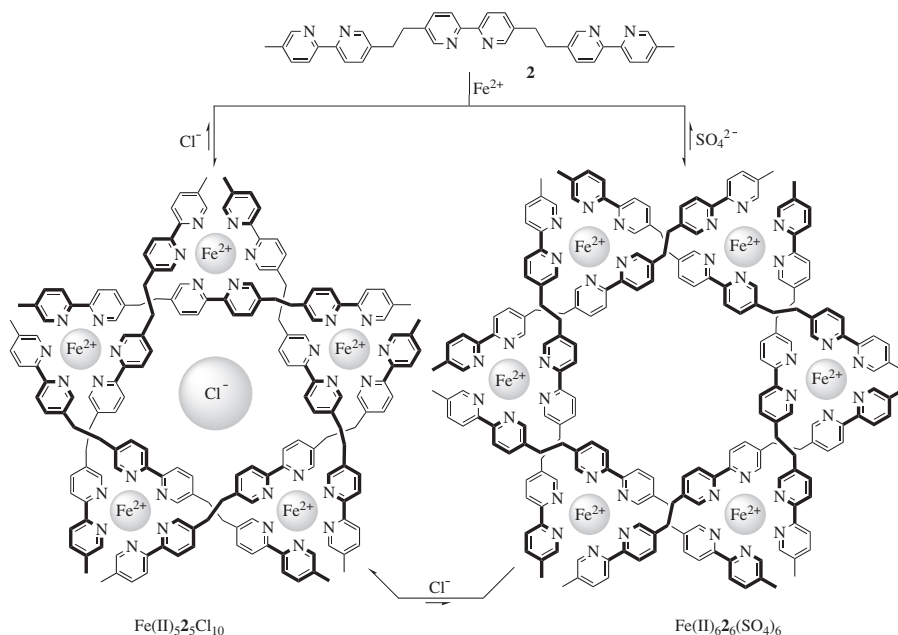


Figure 14.1. Left: A building block for acylhydrazone dynamic combinatorial chemistry. Middle: Schematic illustration of a DCL of acylhydrazone macrocycles. Right: HPLC analyses of the untemplated (a) and templated (b and c) libraries showing the amplification of macrocycle I_3 in the presence of alkali-metal ions [5]. Source of HPLC chromatograms: [5]. Reproduced with permission of the American Chemical Society.

is shown to exemplify this concept [5]. The DCL was generated from the aldehyde/hydrazide dipeptide building block, **1**, and the recognition of cations by the macrocycles formed was investigated by adding NaI and LiI to the library as templates. The cyclic trimer was identified as a receptor for Na^+ and Li^+ , as it was amplified at the expense of the cyclic dimer, tetramer, and higher macrocycles in both cases.

In dynamic combinatorial chemistry, the template selects its host from among all the possible combinations of building blocks in the DCL, and the library amplifies this host at the expense of other library members. This *survival-of-the-fittest* approach has invoked some authors to make comparisons between the dynamic combinatorial idea and Darwinian evolution [6, 7]. A strong motivation for the development of dynamic combinatorial chemistry stems from the difficulties associated with the design and preparation of strong and selective receptors, especially ones that function in aqueous solution. It has been realized that most designed receptors bind their guests much less efficiently than naturally occurring hosts [8]. Receptor design is challenging because it is hard to predict (i) the spatial structure of the designed molecule, (ii) the influence of the solvent, (iii) the strengths of the supramolecular interactions that hold the complexes together, and (iv) the superposition of multiple mutually reinforcing or

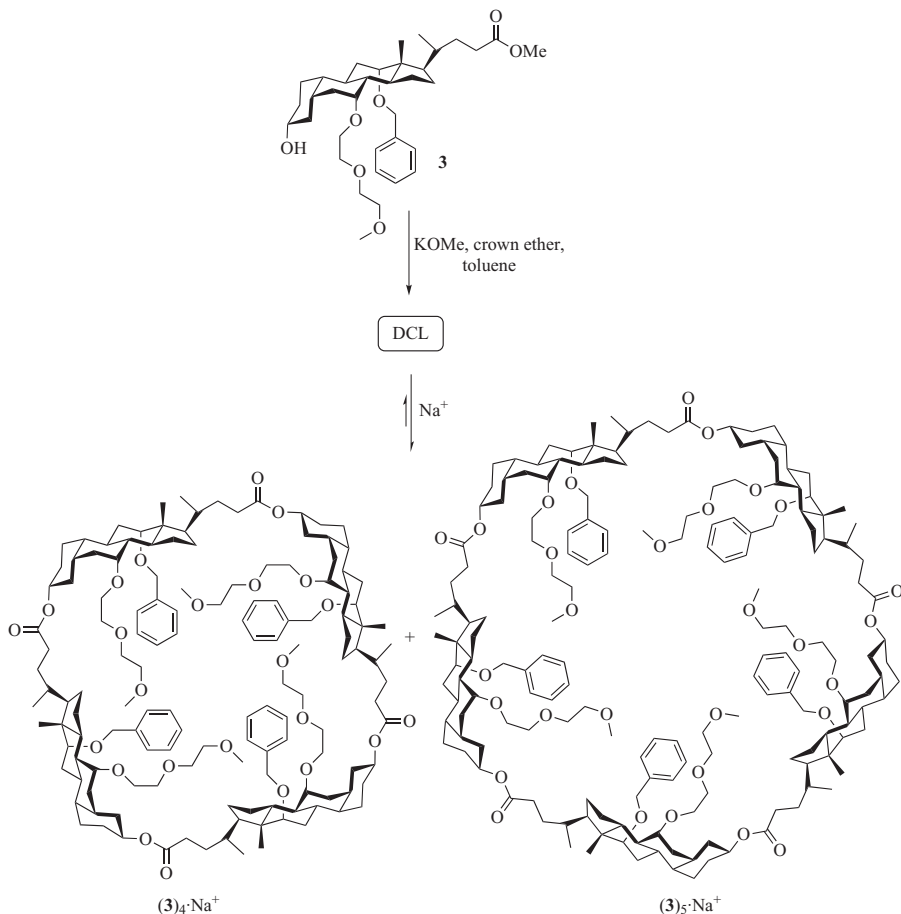


Scheme 14.2. Lehn's template adjustable DCL containing different-sized circular helicates. On the right, a sulphate-induced hexamer ($\text{Fe(II)}_6(\text{SO}_4)_6$) and on the left a chloride-binding pentamer ($\text{Fe(II)}_5\text{Cl}_{10}$). The location of the chloride anion in the cavity of the pentamer was verified using single crystal X-ray crystallography [10, 11].

competing interactions. Dynamic combinatorial chemistry can be seen as a strategy where the focus is on designing an experiment to find receptors, rather than designing the receptor. In the last decade, this approach to molecular engineering has led to the identification of high-affinity receptors with complex topologies and unexpected recognition motifs [9].

The fundamental ideas of dynamic combinatorial chemistry were conceived independently by Lehn and coworkers [10, 11] and Sanders and coworkers [12–14], and implemented in *proof-of-principle* experiments published in 1996. Meanwhile, Benner had suggested some of the concepts in a patent in 1995, but did not report any experimental results [15]. Lehn described a dynamic mixture of circular double helicates formed from the coordination of Fe(II) with *tris*-2,2'-bipyridine ligands (**2**) (Scheme 14.2). It was observed that the mixture could be biased toward a cyclic hexamer or pentamer by varying the counterion.

Sanders and coworkers explored reversible transesterification to generate libraries of cyclic oligoesters starting from a cholate-based building block (**3**) equipped with an alcohol and a methylester moiety [12, 13]. Some of the macrocycles were found to interact with alkali-metal salts (Scheme 14.3) [14, 16]. In order to facilitate exchange and ensure thermodynamic control over the library, harsh reaction conditions were required; KOMe and di-*cyclo*-hexyl-[18]-crown-6 were combined with the building blocks in boiling toluene. Where harsh conditions are required for reversibility, the stability of the building blocks, the template, and the oligomers formed in the DCL can



Scheme 14.3. Sanders' transesterification library used to identify cyclic oligocholates receptors for sodium ions [14, 16].

become an issue. Such harsh conditions may limit the types of functionalities that can be incorporated into the building blocks, as well as the types of supramolecular interactions that may be involved in recognition of a template.

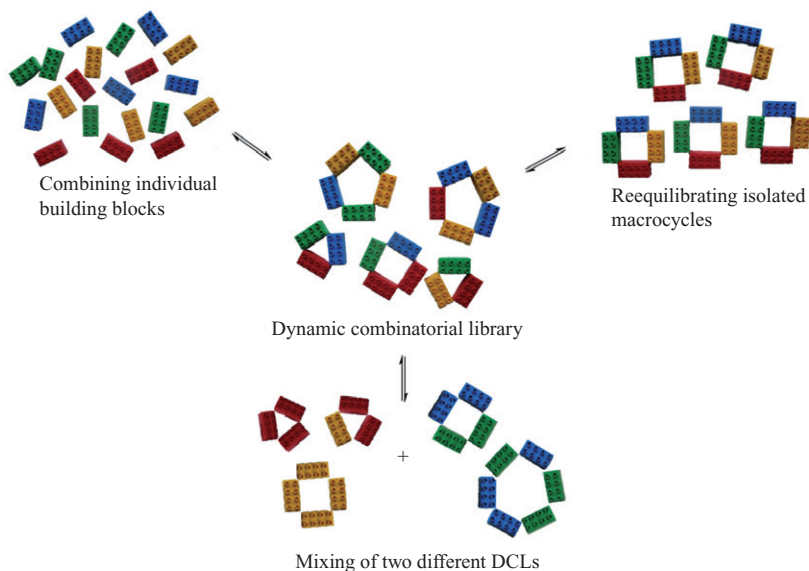
The search for suitable reversible covalent reactions that operate under mild conditions has led to the exploration of many different reactions for dynamic combinatorial chemistry [1, 17]. These include various C=N exchange reactions (e.g., imines, hydrazones, and oximes) [18], C–C bond forming reactions (e.g., the Diels–Alder reaction [19], the Henry reaction [20], and olefin metathesis [21]), various acyl-transfer reactions (e.g., transesterification and transthioesterification) [16, 22], and disulfide exchange [23]. Noncovalent interactions (e.g., metal–ligand coordination and hydrogen-bonding motifs) have also been explored but will not be discussed herein [1]. Due to their mild exchange conditions and fast reaction times, imine, hydrazone, and disulfide exchanges have become the most widely used reactions in dynamic combinatorial chemistry [24, 25].

When a new receptor has been identified in a DCL, it is often desirable to isolate the receptor so that its recognition properties may be studied. At this point, the lability of the reversible bond is no longer beneficial, as the isolated receptor might start equilibrating again, reforming the DCL. Therefore, an additional requirement for a suitable exchange reaction is that the reversibility of the process must be tamable. What is required is that the reaction is reversible under one set of condition and static (non-equilibrating) under another set of conditions. This is nicely illustrated with the disulfide exchange process. Studies on thiol oxidation and thiol–disulfide exchange have shown that (i) thiols oxidize spontaneously at 25°C in the presence of O₂ under weakly alkaline conditions [26]; (ii) thiol–disulfide interchange takes place under mild conditions at weakly basic pH [27, 28]; (iii) thiol–disulfide interchange is negligible under acidic conditions [29]; (iv) disulfide exchange does not happen when the all thiols are oxidized to disulfides; and (v) disulfide and thiol functionalities are compatible with a wide variety of other functionalities [27]. This means that disulfide DCLs may be initiated by dissolving building blocks containing thiol functionalities in water at slightly alkaline pH, and after equilibration, the reversible reaction can either be stopped by complete oxidation to disulfides or by making the solution acidic.

It is important always to check that a DCL has reached thermodynamic equilibrium so that the relative abundances of library members may be correctly interpreted as a reflection of their relative stabilities, and so that addition of a template will successfully alter the library distribution to lower the free energy of the system by amplifying effective receptors. The approach to equilibrium can sometimes, however, be hampered by precipitation or by the occurrence of kinetic traps. Kinetic traps may occur when certain library members are overly stabilized by favorable inter- or intramolecular interactions (e.g., aggregation). Once formed, these stabilized library members can be very slow to exchange their building blocks with other library members and so the library becomes trapped in a kinetically controlled, rather than thermodynamically controlled, regime.

Due to the reversibility of the reactions that link the building blocks in DCLs, thermodynamic equilibrium in a DCL can be approached from different starting points (Scheme 14.4). It is therefore possible to test if equilibrium has, in fact, been reached by combining building blocks or library members in different orders at different time points and observing whether they ultimately achieve the same distribution. If a DCL is set up using only one building block, it is most convenient to simply isolate a library member and allow this to reequilibrate. If two or more building blocks are being used, there are more possible ways to test for thermodynamic control. For example, two DCLs could be set up: one in which all the building blocks are combined together and one in which the building blocks are first equilibrated alone and then mixed together. Once equilibrium has been reached, the two libraries will be identical. If one is studying a DCL that is affected by the addition of a template, then it is also possible to test for thermodynamic control by adding the template at different times and checking that the same library composition results.

This introduction has focused on how the equilibrium composition in a DCL can be affected by the addition of templates. There are other external stimuli, such as pH, pressure, temperature, light, and electric field that can alter library compositions, and the interpretation of these changes can lead to other types of information about the studied system [24, 30]. In the following sections, we will focus on how dynamic combinatorial chemistry is used to study molecular recognition and, in particular, to discover new receptors.



Scheme 14.4. Three different starting points to test for thermodynamic equilibrium. Left: The DCL is formed by mixing four different building blocks. Right: The DCL is formed from an isolated macrocycle that is composed of the same four building blocks. Bottom: The DCL is formed by mixing two preformed DCLs. In all three starting points, the combined building block composition is the same. The three starting points give the same distribution of macrocycles at thermodynamic equilibrium. See color insert.

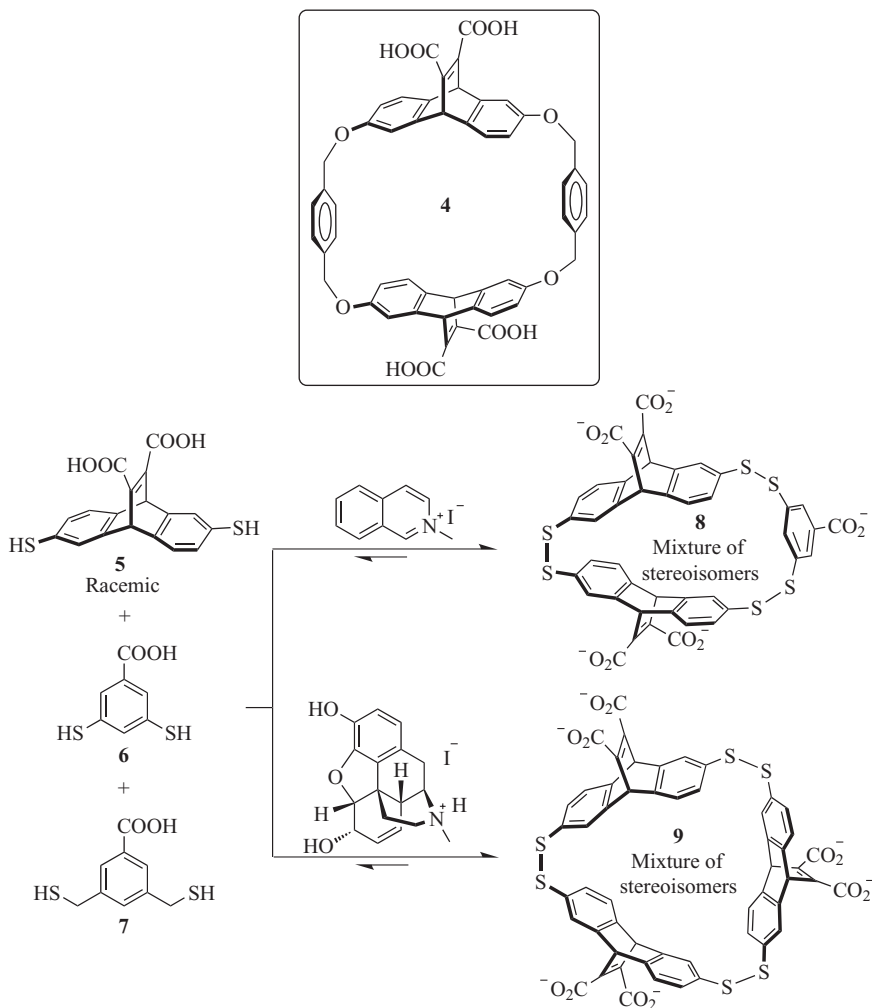
In this chapter, we will describe selected examples from the recent literature on dynamic combinatorial chemistry. We will illustrate how the use of a small number of dithiol building blocks can create large diversity in disulfide-DCLs (Section 14.2); this approach has given some of the strongest known receptors for ammonium ions. We will show how DCLs can be used to optimize the binding properties of already known receptors for anions (Section 14.3) and how the exploration of DCLs has led to new knowledge about mechanically interlocked molecules (Section 14.4). We will describe pseudopeptide DCLs that have been used to identify receptors for both anions and cations using hydrazone exchange chemistry (Section 14.5), and how boronate transesterification can be applied in dynamic combinatorial chemistry (Section 14.6). Section 14.7 describes how DCLs can target biologically interesting molecules such as proteins, DNA, and carbohydrates. Section 14.8 describes how modeling studies using computational methods have been used to aid in library design and how the determination of binding constants between DCL members and templates can be achieved by means of modeling studies without actually isolating the receptors.

14.2 CREATING DIVERSITY WITH FEW DISULFIDE BUILDING BLOCKS

One of the most attractive features of combinatorial chemistry is the ability to quickly and easily generate very large libraries of molecules with diverse structures

and properties by mixing together only a few building blocks. This section describes how a small number of dithiol building blocks have been used to generate receptors [31] that bind ammonium ions in water with some of the highest binding affinities observed for synthetic receptors.

Sanders and coworkers have explored DCLs [32] formed from dithiol building blocks (**5**, **6**, and **7**) that resemble the aromatic components of an ammonium ion receptor (**4**) reported by Dougherty and coworkers (Scheme 14.5) [33–35]. Air oxidation of the three building blocks in water at pH 9 gave rise to a DCL, and analysis using mass

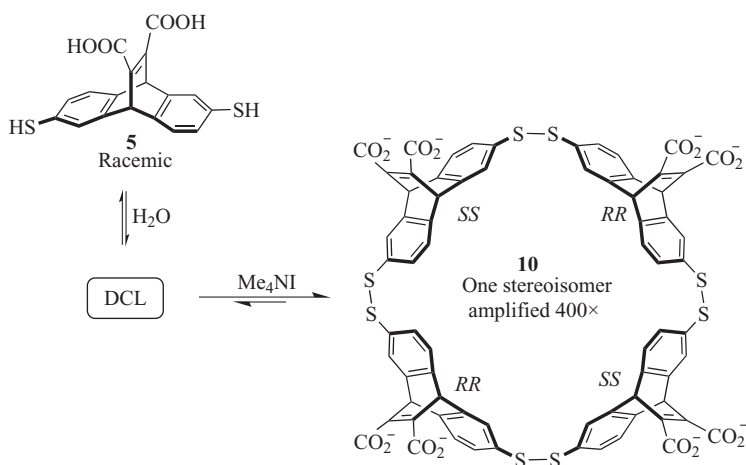


Scheme 14.5. Structure of ammonium receptor **4** [35] together with dithiol building blocks **5**, **6**, and **7**, and the two macrocycles, **8** and **9**, that are amplified in the dynamic combinatorial library upon addition of two different guests (2-methylisoquinolinium iodide and *N*-methylated morphine) [32].

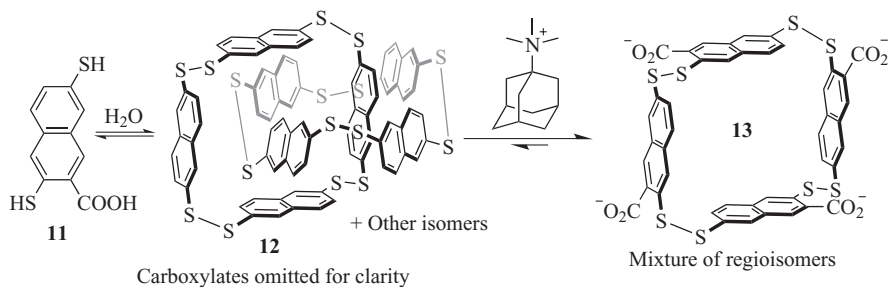
spectrometry revealed that the DCL contained more than 45 different macrocyclic oligodisulfides [32]. The library was exposed to 2-methylisoquinolinium iodide and a change in library composition was observed; macrocycle **8** was significantly amplified at the expense of most of the other library members. The amplified macrocycle was not the tetradisulfide analog of receptor **4** but rather contained one phenyl linker fewer. A high binding constant of $2.5 \times 10^5 \text{ M}^{-1}$ was measured for the interaction between receptor **8** and the 2-methylisoquinolinium iodide guest, which was similar to the affinity reported for the known receptor [32, 35].

When the same library was templated instead with *N*-methylated morphine, macrocyclic trimer **9** was amplified. Trimer **9** was isolated, and binding studies with the guest confirmed a strong binding interaction ($K_a = 7.1 \times 10^5 \text{ M}^{-1}$) [32]. Biased libraries that contained, in the appropriate ratios, only those building blocks that made up macrocycles **8** and **9**, respectively, were prepared. When templated with their respective guests, macrocycles **8** and **9** were efficiently amplified in the libraries to constitute 60% and 95% of the total library material [32].

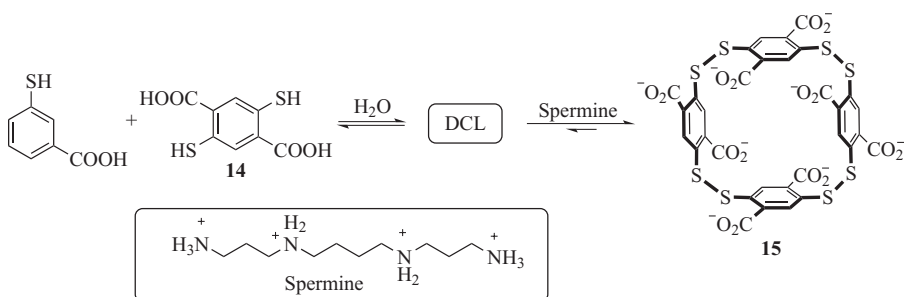
The possibility of uncovering unexpected receptors in DCLs is illustrated by the identification of tetrameric receptor **10**, which was amplified in a DCL formed from building block **5** upon templating with Me_4NI (Scheme 14.6) [36]. Building block **5** was used as a racemic mixture and was therefore capable of generating four different diastereomeric cyclic tetramers. However, it was stereoisomer **10**, with alternating *RR* and *SS* building blocks, that was amplified with an amplification factor of 400 while the other three possible diastereomers were only slightly amplified. This result shows how it is possible to obtain diastereoselective amplification in DCLs. The amplification of tetramer **10** was rather surprising, given that Me_4NI is much smaller than the morphine derivative that amplifies trimer **9**. It was speculated that **10** folds into a four-stave barrel shape so as to create a suitably small cavity to bind Me_4NI . The binding constant between tetramer **10** and Me_4NI was found to be $4.0 \times 10^6 \text{ M}^{-1}$, while trimer **9** binds Me_4NI with a binding constant of only $8.0 \times 10^2 \text{ M}^{-1}$ [36].



Scheme 14.6. Building block **5** formed a DCL of oligomers from which tetrameric receptor **10** was amplified upon addition of Me_4NI [36].



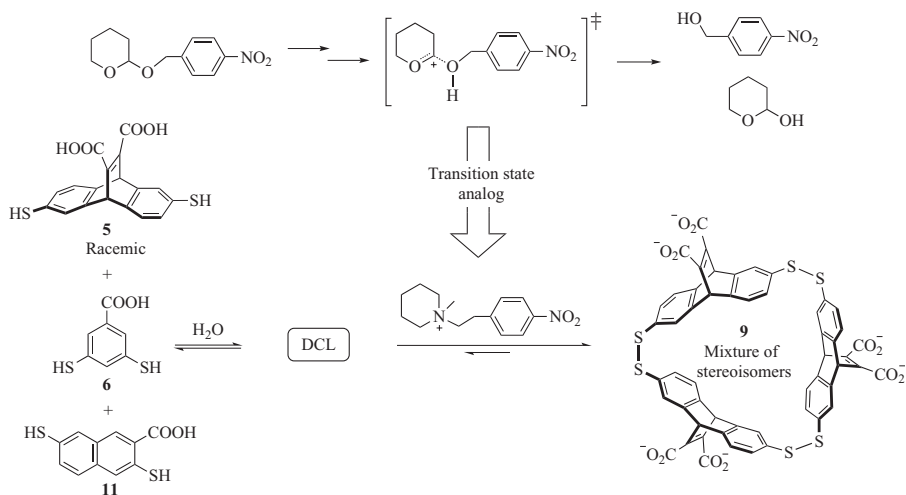
Scheme 14.7. Building block **11** forms [2]catenane **12**, which is transformed into tetrameric receptor **13** upon binding to the adamantane ammonium ion guest [37].



Scheme 14.8. A DCL from which the cyclic tetramer (**15**) was amplified by templating with spermine [38].

Dynamic combinatorial chemistry can also reveal interesting structures even when no guest is present. An example of this behavior was the discovery of octameric [2]catenane **12**, which forms quantitatively (as a mixture of isomers) from naphthalenedithiol building block **11** (Scheme 14.7) [37]. It was proposed that **12** assembles as a result of the hydrophobic effect; unfavorable exposure of the hydrophobic interior of the macrocycles to water is minimized by catenane formation. It was shown to be possible to separate the rings of the catenane and transform **12** into tetrameric macrocycle **13** by introducing an adamantane-derived ammonium ion guest that binds tightly inside the cavity of **13**.

Dynamic combinatorial chemistry has produced some of the strongest synthetic receptors known that are selective in a highly competitive aqueous environment. The high binding affinities shown by many of the disulfide-based macrocycles discovered are close to those seen for recognition events in biological systems. Tetrameric receptor **15**, for example, formed from the terephthalic acid-derived building block **14**, was identified from a DCL templated with the polyamine spermine, which it was found to bind with an association constant of $(4.5 \pm 0.3) \times 10^7 \text{ M}^{-1}$ (Scheme 14.8) [38]. It has been shown that receptor **15** can compete with the interaction between spermine and DNA [38]. The addition of spermine to solutions of certain DNA sequences can cause their helicity to change from right handed to left handed. By addition of **15** to the spermine–DNA complex, the helicity of the DNA was reverted to its original right-handed helicity, as monitored by circular dichroism (CD) spectroscopy.

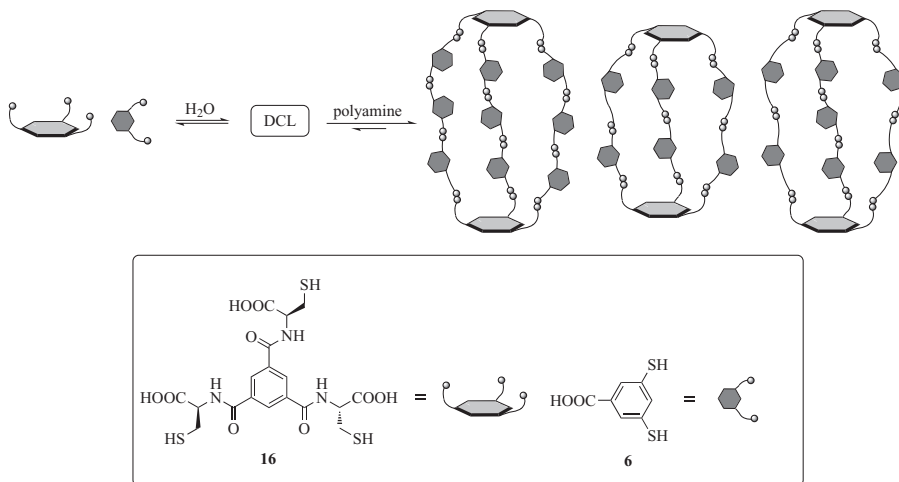


Scheme 14.9. Identification of a receptor (**9**) that recognizes a transition-state analog for acetal hydrolysis [41].

If dynamic combinatorial chemistry is used to seek receptors for guest molecules that closely resemble the transition states of given reactions—also known as transition-state analogs—it may be possible to thereby identify supramolecular catalysts from DCLs [39]. This approach has been explored for the Diels–Alders reaction [40] and for acetal hydrolysis [41]. It is most appropriate for reactions where the transition states for the rate-determining steps are markedly different from both the starting material and the product, as this minimizes the risk of product or substrate inhibition. This is the case for the acetal hydrolysis reaction shown in Scheme 14.9; a neutral reactant is converted to neutral products via a positively charged transition state, which resembles an ammonium salt that can be used as the transition-state analog. To find a receptor for the transition-state analog, a DCL was established from dithiol building blocks **5**, **6**, and **11**. Upon addition of the transition-state analog, cyclic trimer **9** was amplified. It was subsequently isolated, and kinetic studies showed that the rate of hydrolysis of the acetal was accelerated by a factor of 2 in the presence of **9**.

In the above-mentioned examples, the obtained catenanes and macrocyclic receptors are based on dithiol building blocks. However, in a study by West et al., it was shown possible to expand this array of structures to include organic cages by combining di- and trithiol building blocks [42]. Stefankiewicz et al. later described the template-induced amplification of large cages in a DCL [43]. Dithiol **6** and trithiol **16** were combined to generate a self-sorted mixture containing macrocycles of **6** (trimer and tetramer) and a dimeric cage of **16**. When templated with protonated polyamine guests (e.g., spermine), disulfide-linked cages containing up to 11 components were amplified (Scheme 14.10).

From the examples presented, it can be seen that by using only a few different building blocks (**5**, **6**, **7**, **11**, **14**, and **16**), it has been possible to prepare synthetic receptors with diverse structures for a wide range of guests, which in many cases display very high affinities. Using optimized conditions, DCLs can produce receptors in high yields while avoiding long and complicated syntheses.



Scheme 14.10. Dynamic combinatorial cages for polyamines formed from building blocks **6** and **16** [43].

14.3 OPTIMIZATION OF KNOWN RECEPTORS USING DYNAMIC COMBINATORIAL CHEMISTRY

Dynamic combinatorial chemistry can be used not only to discover new hosts but also to optimize the structures of known receptors. This is exemplified in the development of high-affinity *cyclo*-peptide-based receptors for anions in aqueous environment.

Kubik and coworkers have studied *cyclo*-peptide receptors for molecular recognition of anions [44], cations [45], and ion pairs [46]. They described a cyclic hexapeptide **17** (Figure 14.2) with alternating L-proline and 6-aminopicolinic acid subunits which was shown to form sandwich-type 2:1 complexes with anions such as halides and sulfates [47].

In subsequent work, it was found that these complexes could be stabilized by covalently linking the two *cyclo*-peptide units together via 1,6-hexanedioic acid to give receptor **18a**. The binding affinity for SO_4^{2-} was found to be $K_a = 3.5 \times 10^5 \text{ M}^{-1}$ in 50% $\text{CD}_3\text{OD}/\text{D}_2\text{O}$ [48]. Minor improvements in binding affinities were achieved by replacing the flexible linker with, for example, a more rigid aromatic linker to give receptor **18b** [49]. It was reasoned that increased rigidity would decrease the entropically unfavorable loss of conformational flexibility upon complexation of the anion.

While variation of the linker by a designed approach led to small improvements, it was found that dynamic combinatorial chemistry was an alternative and effective method to optimize the linker. The *cyclo*-peptide scaffold was functionalized with a thiol to enable the use of disulfide exchange to explore linker possibilities. *cyclo*-peptide dimer **19** was equilibrated with six different dithiol linkers (**a-f**) in 67% $\text{MeCN}/\text{H}_2\text{O}$ to generate a DCL containing *cyclo*-peptide rings separated by one or more different dithiol linkers (Figure 14.3). The library was exposed to different anions and a series of amplifications were observed. Binding studies showed that receptors **20b** and **20c** bound SO_4^{2-} an order of magnitude more efficiently than receptor **18a** [50].

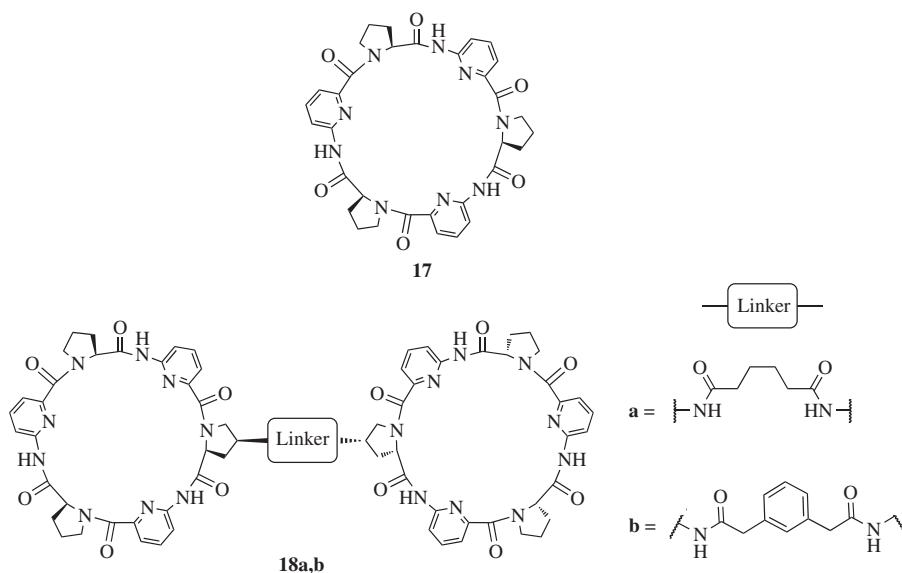


Figure 14.2. Top: Structure of *cyclo*-peptide macrocycle **17** which is capable of binding a variety of anions in 1:2 stoichiometries [47]. Bottom: Dimers of the *cyclo*-peptide macrocycles (**18**) which bind anions with high affinity in sandwich geometries [49].

Rodriguez-Docampo et al. extended these studies to receptors in which the two *cyclo*-peptide rings were connected via two linkers [51]. A DCL was prepared by mixing bis-*cyclo*-peptide **21a** with two dithiol spacers (1,2-ethanedithiol and 1,3-benzenedithiol) in 67% MeCN/H₂O at pH 9 with various anions as templates (Figure 14.4). After equilibration, significant amplifications of the doubly linked dimer of macrocycles **21b** and **21c** were observed with all added anions but most notably with the SO₄²⁻ anion. The new anion receptors possessed extraordinary binding affinities for the SO₄²⁻ anion of 4.7×10^8 and 3.9×10^7 M⁻¹, respectively [51].

These examples illustrate how elements of design and selection may work together to discover highly effective receptors. The building blocks are carefully designed, but in the DCL, self-selection of the most suitable linker enables efficient synthesis of improved receptors.

14.4 DONOR-ACCEPTOR MECHANICALLY INTERLOCKED MOLECULES FROM DYNAMIC COMBINATORIAL LIBRARIES

Mechanically interlocked molecules may be synthesized either by means of a kinetically controlled or a thermodynamically controlled approach. When self-assembled under thermodynamic control, as in a DCL, the components of the interlocked molecule are allowed to react reversibly with one another until an equilibrium mixture is reached. Ideally, the desired interlocked structure will be stabilized by intramolecular interactions (e.g., donor-acceptor interactions and hydrophobic interactions) between the interlocked components such that minimization of the total free energy of the DCL

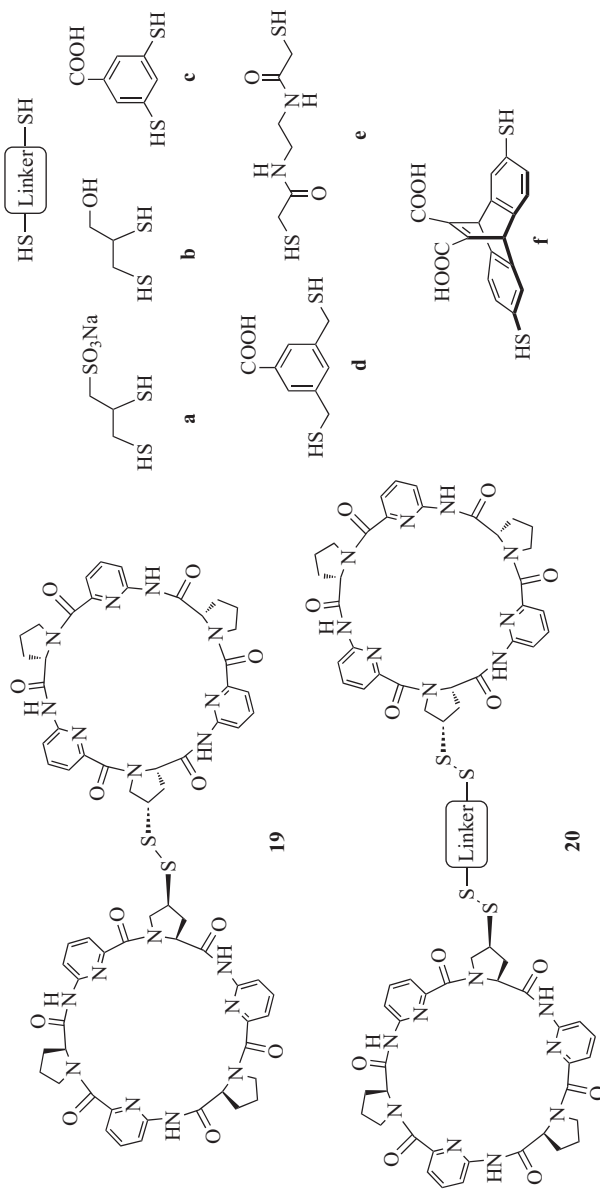


Figure 14.3. Dynamic combinatorial optimization of bis-cyclo-peptide anion receptors using disulfide DCLs [50].

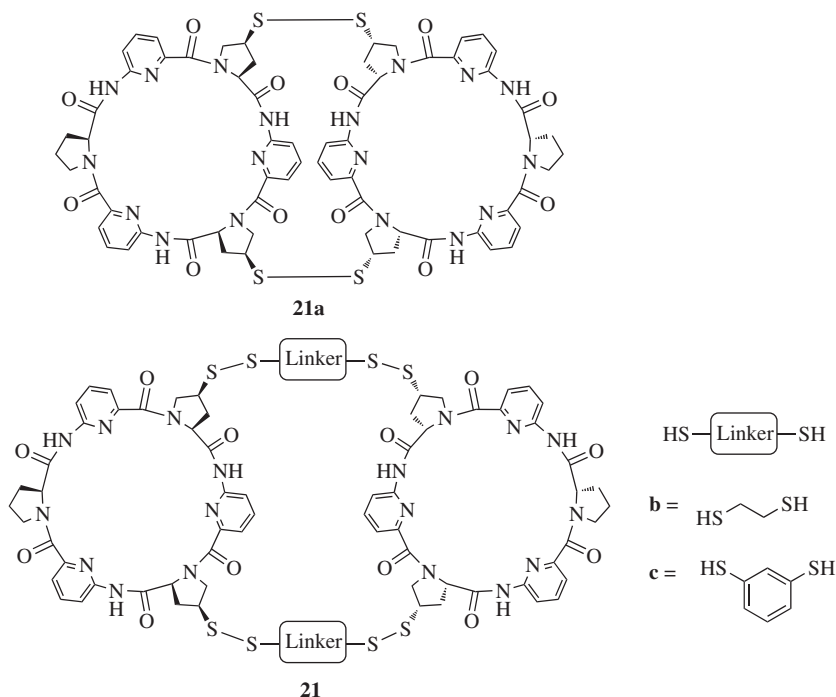


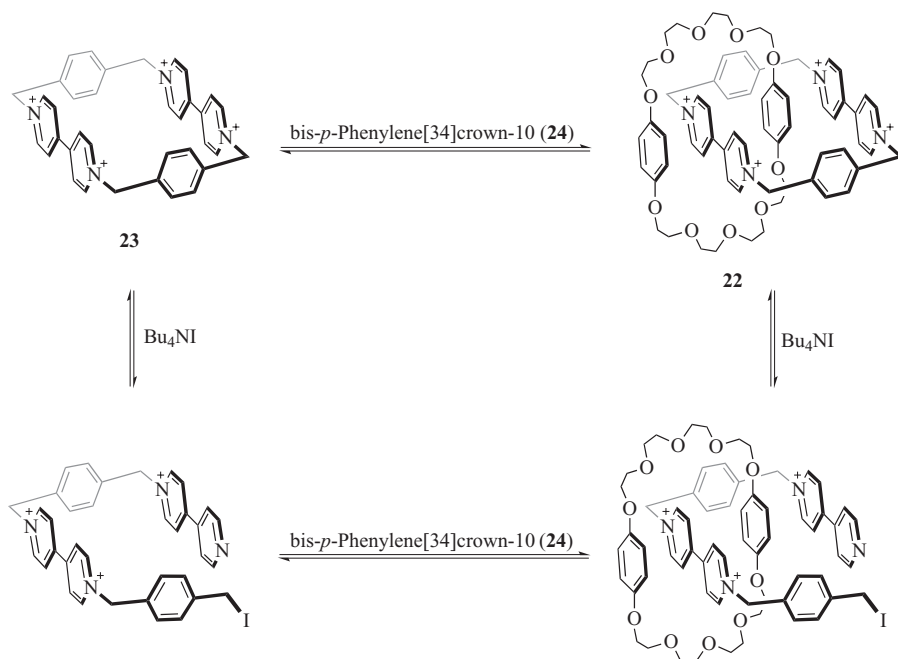
Figure 14.4. Optimization of doubly linked bis-*cyclo*-peptide (**21**) using dynamic combinatorial chemistry [51].

will lead to the amplification of this structure. If well designed, such self-assembled interlocked molecules may be obtained in high yields that are not easily achieved using kinetically controlled synthesis.

One example of the use of dynamic combinatorial chemistry in the synthesis of [2]catenanes was provided by Miljanić and Stoddart [52]. They described the thermodynamically controlled synthesis of a donor-acceptor [2]catenane (**22**) in MeCN from two isolated macrocycles: π -acceptor *cyclo*-bis(paraquat-*p*-phenylene) (**23**) and π -donor bis-*p*-phenylene[34]crown-10 (**24**) (Scheme 14.11). The assembly was achieved using a Bu₄Ni-catalyzed reversible benzylic nucleophilic substitution and was initiated by the nucleophilic opening of the *cyclo*-bis(paraquat-*p*-phenylene) ring (**23**) by the iodide ion. Thermodynamic control of the system was demonstrated by the exchange of the donor ring, bis-*p*-phenylene[34]crown-10 (**24**) for 1,5-dinaphthol[38]crown-10.

Using dynamic nucleophilic substitution, Stoddart and coworkers have also synthesized a [3]catenane [53], bis[2]catenanes [54], and a side-chain donor-acceptor polycatenane [54]. The high yields obtained for these complex structures highlight the efficiency of a thermodynamic rather than kinetic approach to catenane synthesis.

Au-Yeung et al. have described a series of donor-acceptor catenanes assembled via disulfide exchange from π -electron-rich dialkoxynaphthalene donor units (D) and π -electron-deficient naphthalenediimide acceptor units (A) (Figure 14.5a). The building blocks consist of aromatic scaffolds that are functionalized with cysteine units at



Scheme 14.11. Reaction scheme for the formation of [2]catenane **22** from **23** and **24** via reversible benzylic nucleophilic substitution with Bu_4NI acting as a catalyst [52].

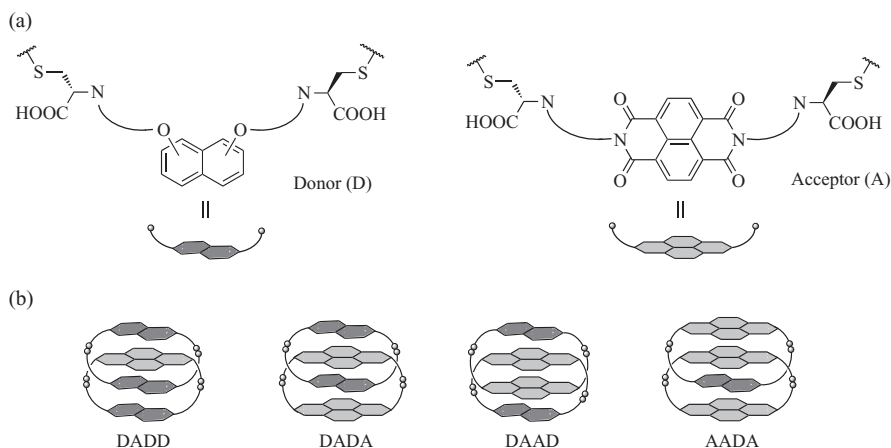
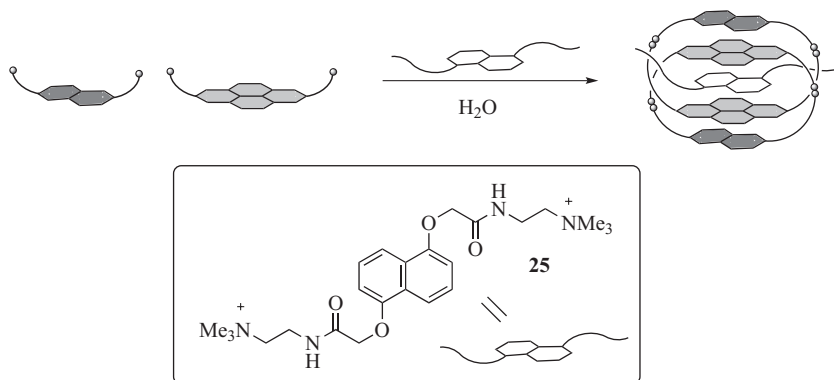


Figure 14.5. (a) Structures of the two building blocks: π -donor dialoxynaphthalene (D) and π -acceptor naphthalenediimide (A), together with their cartoon representations. (b) Arrangements of the π -units in the donor-acceptor [2]catenanes discovered using dynamic combinatorial chemistry [61].



Scheme 14.12. Structure of a dialkoxynaphthalene template (**25**) used to amplify the DAAD [2]catenane [56].

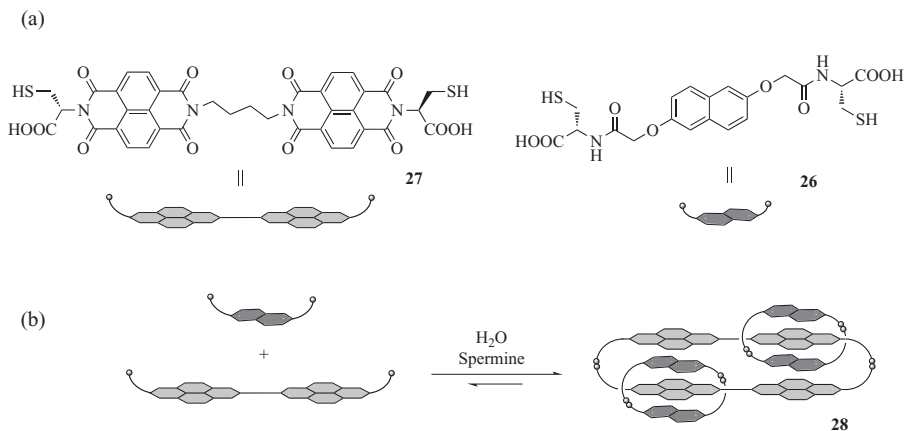
the end of a linker to give both water solubility in weakly alkaline solution and access to reversible covalent chemistry through disulfide exchange [55–61].

DCLs were prepared from these building blocks in water and in aqueous NaNO_3 solutions. By increasing the salt concentration, and therefore the ionic strength of the aqueous solution, it was found possible to amplify the formation of catenanes at the expense of macrocycles. It was reasoned that increasing the polarity of the solution would increase the role of the hydrophobic effect in dictating which library members were formed. Catenane formation would be favored as this leads to a decrease in the amount of solvent-exposed hydrophobic surfaces. In the DCLs, catenanes with previously unobserved stacking arrangements were formed. Not only was the conventional alternating DADA catenane identified but also catenanes with AADA, DAAD, and DADD arrangements of the π -donor and π -acceptors were discovered (Figure 14.5b) [61].

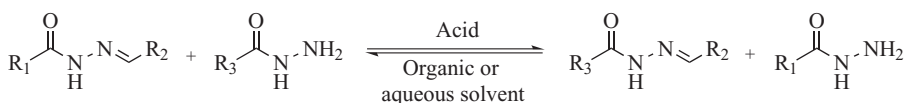
It was also found possible to increase the yield of the DAAD [2]catenane by the presence of a template [56, 60]. Considering that the DAAD [2]catenane is anionic (due to the carboxylic functionalities) and contains a π -electron-deficient interior cavity, the cationic π -electron-rich compound **25** was chosen as template for the system. The addition of dialkoxynaphthalene-based template **25** led to amplification of the DAAD [2]catenane at the expense of all other macrocycles and catenanes, and by means of nuclear magnetic resonance (NMR) studies, it was determined that the template was located inside the cavity of the [2]catenane, as shown in Scheme 14.12 [56].

Lessons learned from the discovery and exploration of this family of [2]catenanes have been exploited to synthesize higher order interlocked structures. Cougnon et al. reported that by combining a π -donor (**26**) with an extended version of the π -acceptor (**27**), it was possible to obtain a donor–acceptor [3]catenane (**28**) in a highly polar solvent (1 M aqueous NaNO_3) or in the presence of spermine acting as a template (Scheme 14.13) [62].

In DCLs formed via disulfide exchange, the exchange reaction will stop once all the thiol building blocks have been completely oxidized to disulfides. It is therefore possible that exchange will be halted and the library composition will be fixed before the libraries have reached thermodynamic equilibrium. This was the case for many of



Scheme 14.13. (a) Structure of the two building blocks (**26** and **27**). (b) The spermine template amplification of a donor–acceptor [3]catenane (**28**) [62].



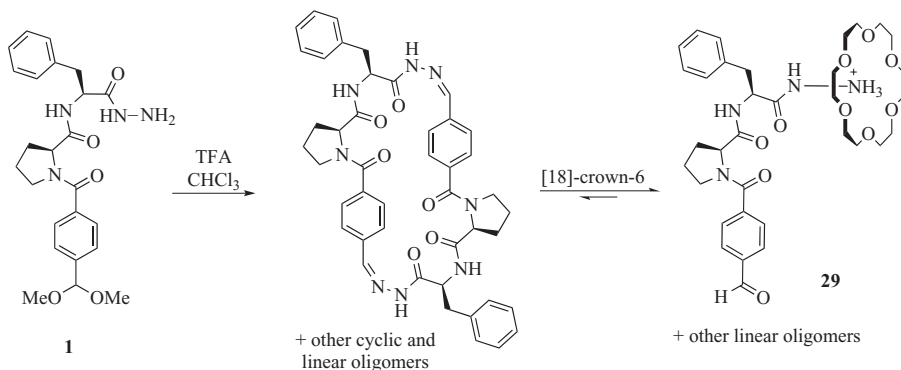
Scheme 14.14. The acylhydrazone exchange reaction.

the disulfide-linked donor–acceptor catenanes just described. While it is important to be aware of this phenomenon, such kinetically trapped molecules discovered in DCL may nevertheless exhibit fascinating structures. Furthermore, dithiothreitol (a dithiol) may be added to the library as a reducing agent to reinitiate exchange in a fully oxidized library and promote equilibration toward the thermodynamic minimum of the system [61].

The examples highlighted in this section demonstrate how dynamic combinatorial chemistry can be used to generate complex and delicate interlocked structures. Knowledge about donor–acceptor interactions, gleaned from years of molecular engineering work, has been exploited to design sophisticated DCLs from which unexpected architectures and molecular recognition motifs have been revealed.

14.5 HYDRAZONE-BASED DYNAMIC COMBINATORIAL LIBRARIES

Dynamic combinatorial chemistry using acylhydrazone exchange as the reversible reaction has gained significant popularity since it was introduced in 1999 [63]. Acylhydrazones are formed from a hydrazide and an aldehyde, and they equilibrate under acidic conditions in aqueous solution and in a variety of organic solvents (Scheme 14.14). Libraries of oligomers may be formed from building blocks containing both a hydrazide and an aldehyde or from dialdehydes and dihydrazides. When using building blocks that contain both aldehyde and hydrazide functionalities, it has proven convenient to protect the aldehyde with an acid-labile acetal that allows stable



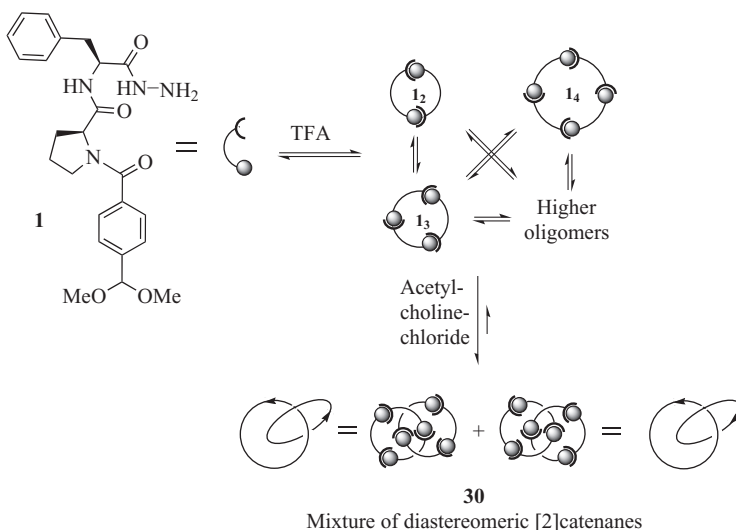
Scheme 14.15. The first reported DCL using acylhydrazone exchange [63]. The composition of a hydrazone DCL can be shifted toward the linear hydrazides by addition of [18]-crown-6 [130].

building blocks to be synthesized. By adding acid to the isolated building block, the acetal deprotects to the aldehyde and acylhydrazone formation and exchange begin immediately.

The lability of the hydrazone linkage coupled with the high dependency of the rates of formation, hydrolysis, and exchange upon pH—therefore the ability to switch on the reaction in acid and off in base—makes hydrazone exchange a good reaction for use in DCLs. The acylhydrazones are less prone to hydrolysis than imines, which make it possible to isolate library members from DCLs.

In the first publication describing acylhydrazone-based DCLs, the building block used was a dipeptide with the *C*-terminus equipped with a hydrazide and the *N*-terminus elongated via an amide linkage to an aromatic aldehyde (**1**) (Scheme 14.15) [63]. The use of an aromatic aldehyde ensured that the equilibration proceeded smoothly at room temperature and side reactions such as aldol condensations were avoided. The acylhydrazone DCL was formed by dissolving **1** in CHCl_3 and adding a small amount of trifluoroacetic acid (TFA). Analysis by HPLC and electrospray ionization–mass spectrometry (ESI-MS) showed a mixture of acylhydrazone macrocycles. The ability of the library to adapt in the presence of a template was demonstrated by addition of [18]-crown-6. By binding to the protonated hydrazides on the monomer building block (**1**) and other linear oligomers, addition of [18]-crown-6 caused a shift in the constitution of the DCL to amplify these species. The constitution of the DCL could then be shifted back to the original mixture of macrocycles by addition of K^+ -ions to complex the crown ether and release the hydrazides.

A series of pseudopeptide building blocks for acylhydrazone DCLs has since been explored. The most noteworthy example of receptor amplification in these libraries was the discovery of a hexameric catenated high-affinity receptor (**30**) for acetylcholine by Lam et al. (Scheme 14.16) [64]. The [2]catenane (**30**) was amplified and isolated in 67% yield from a DCL formed from building block **1**, which contained mainly cyclic dimer, trimer, and tetramer in the absence of a template. The [2]catenane had an exceptionally high binding affinity for acetylcholine chloride of $K_a = 1.4 \times 10^7 \text{ M}^{-1}$ in a 95:5 CHCl_3 :DMSO mixture, while the cyclic trimer and the cyclic tetramer had binding affinities of 1.5×10^3 and $5.7 \times 10^3 \text{ M}^{-1}$, respectively. The $^1\text{H-NMR}$ spectrum of the [2]catenane alone exhibited very broad features indicative of a mixture of



Scheme 14.16. Top: An acylhydrazone DCL of macrocycles from building block **1**. Bottom: The amplified hexameric [2]catenane host (**30**) for acetylcholine chloride [64].

conformations in solution. Upon addition of one equivalent of acetylcholine, however, the spectrum simplified to show sharp signals, which suggested that the acetylcholine was bound tightly by a single conformation of the catenane. The [2]catenane (**30**) has the same molecular weight as the cyclic hexamer, but the two different species were convincingly differentiated using MS-MS. The cyclic hexamer gives the pentamer, tetramer, and smaller oligomers as daughter ions, while the [2]catenane fragments directly to the trimer. The identification of this completely unexpected receptor illustrates the power of dynamic combinatorial chemistry to reveal instances of molecular recognition that would perhaps not have been uncovered using a purely designed approach to receptor synthesis.

From DCLs of acylhydrazones generated in CHCl_3 or CH_2Cl_2 (often containing small amounts of MeOH or dimethyl sulfoxide [DMSO]) in the presence of TFA [65–67], macrocyclic receptors for alkali-metal ions [5], tetraalkylammonium ions [68], and cationic alkaloids have been identified. The chirality of the amino acids has been varied and diastereoselective and enantioselective recognition have been achieved [69]. Additional catenanes have been isolated and characterized by the group headed by Gagné and Waters using dipeptide-based building blocks. They described [2]catenanes of tetrameric macrocycles that form in the absence of a template [69–71], and in similar libraries, they found strong receptors for nucleic acids and derivatives such as adenosine [72].

Most of the studies described earlier were performed in an organic solvent using a strong acid (typically 1–5% TFA) to facilitate the hydrazone exchange reaction. These rather harsh reaction conditions preclude the use of building blocks containing delicate functional groups. The use of a large excess of TFA in libraries may also interfere with molecular recognition events guided by hydrogen bonding. If milder acids are used, there is a risk that the exchange reaction will be slowed down such that the time frame of the DCL experiment becomes too long and the risk of problematic kinetic traps

increases. In the case of hydrazone-based DCLs, some practical solutions to prevent kinetic traps and to speed up the equilibrium process have been introduced. It has been shown that addition of a large excess of aniline to hydrazone DCLs accelerates the rate of exchange significantly in aqueous solutions [73]. By addition of aniline it has also been possible to reach equilibrium at the relatively high pH 6 [74]. Addition of a smaller excess of monohydrazide has been shown to facilitate exchange and avoid the occurrence of kinetic traps in acylhydrazone DCLs [75]. Furthermore, when 10 equiv. of monohydrazide is added to the library, a milder acid (e.g., 1-naphthoic acid or acetic acid) may be used to promote the exchange reaction.

Using this last approach, it has been shown that peptide-based building blocks may also be utilized to form anion receptors [76, 77]. DCLs were prepared from a ferrocene containing dihydrazide building block (**31**, unstable to prolonged exposure to TFA), an aromatic dialdehyde, excess of 4-toluic-hydrazide (10 equiv.), and 1-naphthoic acid. This gave a DCL containing a mixture of linear and cyclic library oligomers. Upon addition of dihydrogenphosphate anions to the library, a series of linear oligomers were amplified. The five-component linear receptor (**32**) adopts a helical conformation and binds two anions in a cooperative manner (Figure 14.6).

Hydrazone exchange has been used in many interesting conceptual studies in dynamic combinatorial chemistry; acylhydrazones have been used in the recognition of proteins [74], in the dynamic self-assembly of hydrogels based on G-quadruplex DNA structures [78], in the dynamic synthesis of cages, and in self-replicating systems [78]. In a series of papers, Lehn and coworkers have used hydrazone exchange to produce dynamic polymers, the so-called dynamers [79, 80]. This section is by no means a comprehensive review. Hydrazone exchange has, together with disulfide exchange, become the reversible reaction of choice in dynamic combinatorial chemistry.

14.6 BORONATE ESTER EXCHANGE IN DYNAMIC COMBINATORIAL CHEMISTRY

Boronate esters have found use in numerous applications in contemporary synthetic and supramolecular chemistry [81–83]. The preparation of dynamic polymers [84–86] and self-assembling covalent organic frameworks [87–90] are two areas in which the reversibility of boronate transesterification defines the adaptive properties of the materials. Boronic acids react with 1,2-diols and 1,3-diols to give boronate esters, and this property has been exploited extensively in sensors for carbohydrates [81, 83].

The lability of B–O bonds causes a number of processes involving boronic acids to be reversible, including boroxoaromatic transesterification [91] and boroxine exchange [92] as well as boronate transesterification (Scheme 14.17) [93, 94]. Herein we discuss the use of boronate transesterification to generate DCLs of adaptive macrocycles and capsules [95, 96] and to seek enzyme inhibitors [97].

Boronate transesterification has been used to prepare libraries of oligoboronate esters by reacting bis-boronic acids with tetraols [98–101]. When, for example, 1,4-benzene-bis-boronic acid and tetraol **33** were reacted together in a methanol solution containing either toluene or benzene, the macrocyclic 2:2-tetramer (**34**) or 3:3-hexamer (**35**), respectively, were precipitated and subsequently isolated in high yield (Scheme 14.18) [100]. Analysis by NMR spectroscopy and single crystal X-ray crystallography showed that the macrocycles were isolated as inclusion complexes with one toluene molecule and two benzene molecules, respectively, bound in the center.

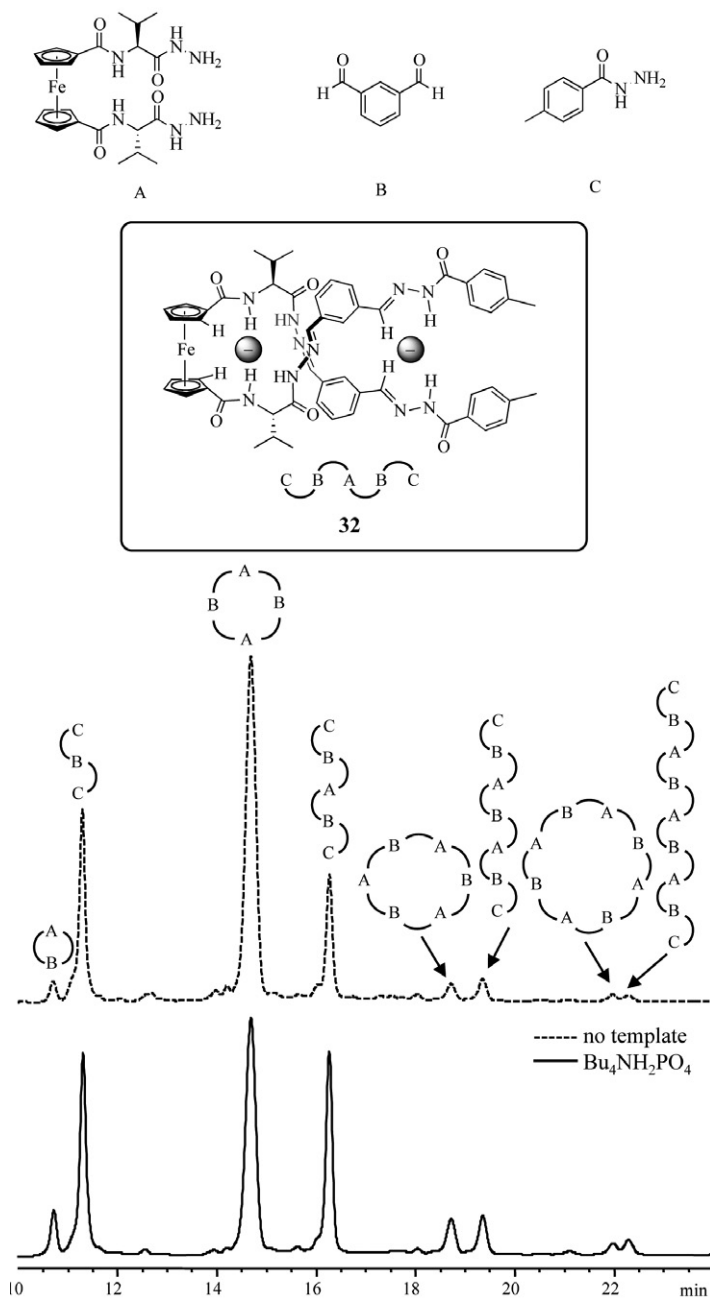
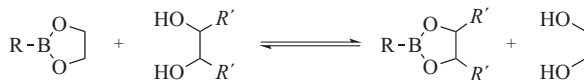
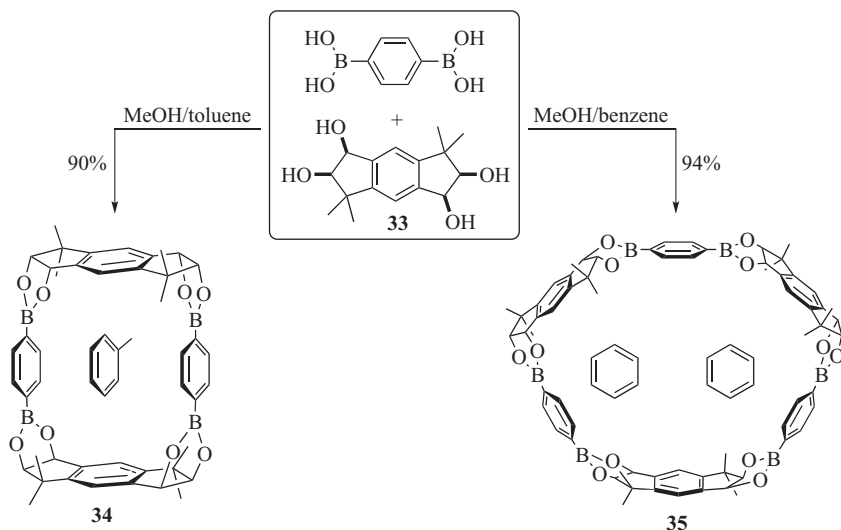


Figure 14.6. A hydrazone DCL that amplifies a linear tetrahydrazone (**32**) at the expense of cyclic structures in the presence of dihydrogenphosphate. The receptor binds two H_2PO_4^- ions in a cooperative manner and adopts a helical conformation upon binding. Source of HPLC chromatograms: [77]. Reproduced with permission of the American Chemical Society.



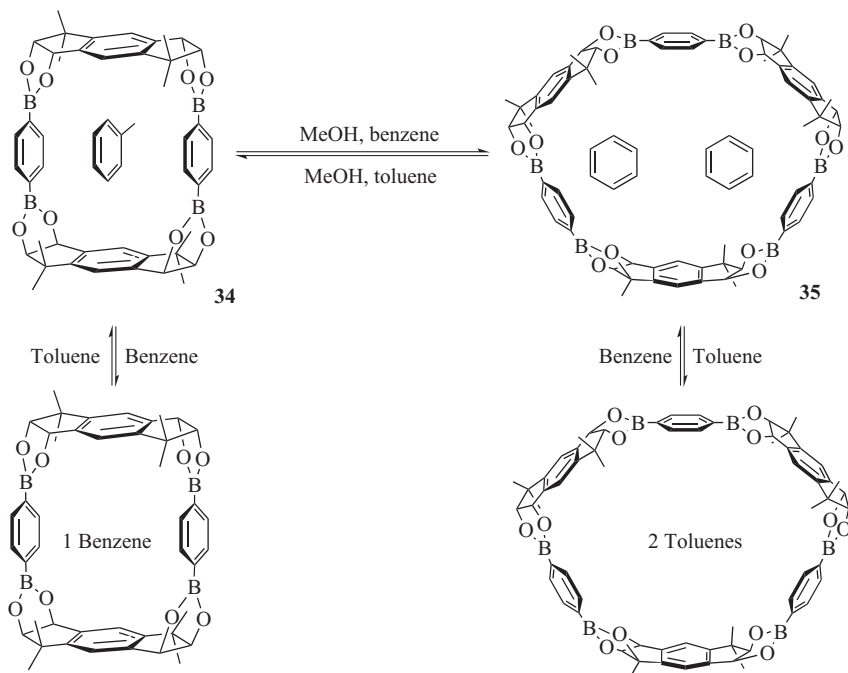
Scheme 14.17. An example of boronate transesterification: exchange of 1,2-diols.



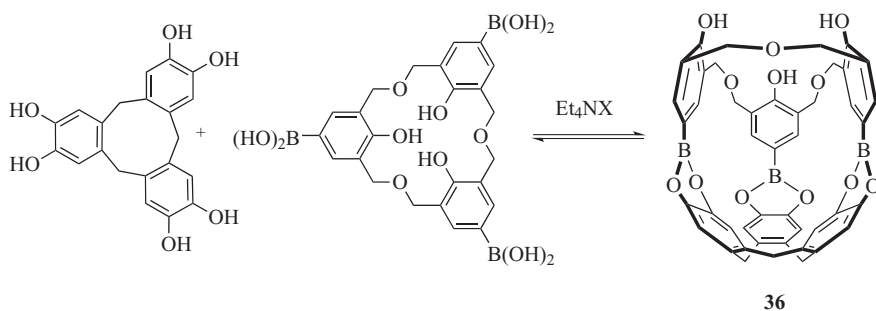
Scheme 14.18. Template-assisted macrocyclization of oligoboronate esters; the nature of the template determines the size of the macrocycle [100].

In this example, the products precipitated from the mixture, which means that the library was no longer operating under thermodynamic control. In such situations, the library composition will not necessarily reflect the receptors' respective binding abilities [102]. It will be dependent on the relative solubility of the macrocycles in the particular solvents, as well as on the binding interactions and crystal packing forces. While not strictly a DCL, the authors showed here how the reversibility of boronate transesterification may be exploited for the template-assisted self-assembly of oligoboronate esters. They also showed how to halt the equilibration of boronate esters by changing the solvent composition. It was found that if a suspension of tetrameric macrocycle **34** was stirred in a mixture of methanol and benzene, the nature of the suspended material changed, and hexameric macrocycle **35** was isolated (Scheme 14.19) [102]. Without methanol, no boronate ester interconversion was observed despite changing the nature of the template.

Kubo and coworkers described the reversible formation of boronate-ester-based capsule **36** from *cyclo*-tricatechylene and a boronic-acid-appended hexahomotrioxacalix[3]arene in the presence of Et_4NOAc (Scheme 14.20) [103]. When the two building blocks were mixed in a combination of methanol and acetonitrile, no boronate ester formation was observed, whereas when Et_4NOAc was added as a template, the 1:1 dimer was generated quantitatively. NMR analysis of the templated mixture showed several pieces of evidence that the Et_4N^+ ion was bound in the cavity of the capsule: (i) new signals for the bound guest's ethyl groups appeared that were shifted upfield



Scheme 14.19. Transesterification takes place in the presence of methanol (top) but is switched off in its absence (bottom). In the absence of MeOH, the bound guests exchange upon changing the solvent, but only with MeOH as a cosolvent does the interconversion of tetramer **34** and hexamer **35** take place [102].



Scheme 14.20. Dynamic formation of a boronate-ester-based capsule (**36**) [103].

by ~ 1.5 ppm, indicative of an aromatic shielding effect; (ii) nuclear Overhauser effect cross peaks were observed between these new ethyl group signals and selected protons on the capsule; and (iii) almost identical diffusion coefficients for the capsule and the ethyl group signals were obtained by diffusion-ordered spectroscopy (DOSY) [103].

When different Et_4N^+ salts were tested, more modest capsule formation was observed compared with Et_4NOAc , which indicated that capsule formation was not just cation,

but ion-pair driven. Titrations using UV/Vis spectroscopy of the capsule mixture with different templates showed that the equilibrium values increased in the order $\text{Et}_4\text{N}^+ > \text{Me}_4\text{N}^+ > \text{K}^+$ with AcO^- salts and in the order $\text{AcO}^- > \text{F}^- \gg \text{I}^-$ with Et_4N^+ salts [103]. From these results, the authors concluded that capsule formation was dictated mainly by size of the cation and basicity of the anion. Kubo also demonstrated that the capsule assembly could be turned on and off simply by switching the pH of the solution. An NMR study showed that when HCl was added to a solution of the Et_4NOAc -bound capsule, it collapsed but was reformed when the pH was readjusted by addition of NaHCO_3 to the solution [103].

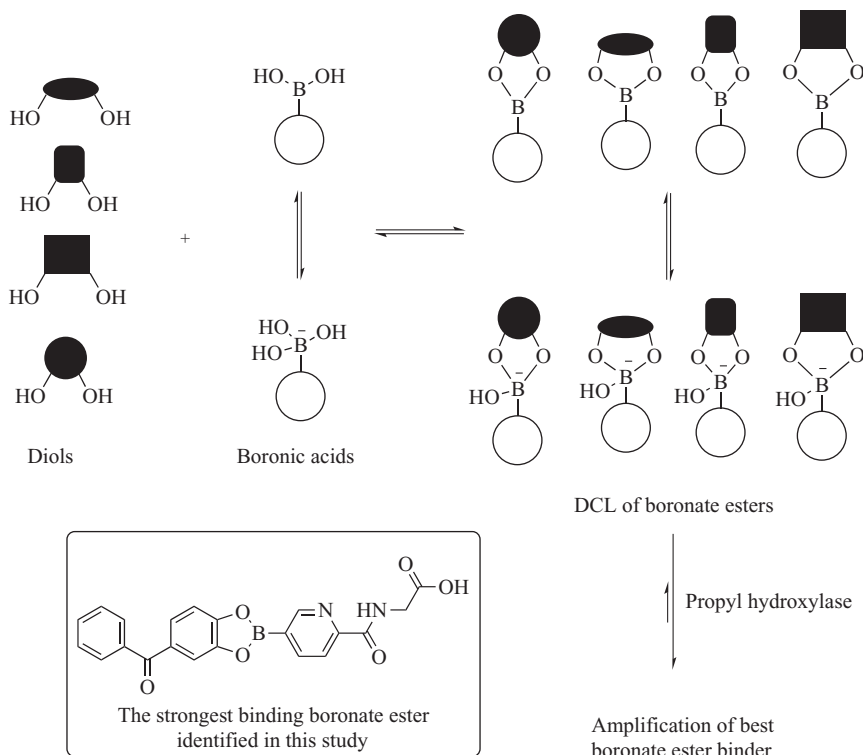
In a subsequent study, Kubo and coworkers showed that formation of the same capsule (**36**) could also be triggered by addition of Et_3N , which was encapsulated in the host as its conjugate acid, Et_3NH^+ [104]. Furthermore, addition of Bu_3N also led to capsule formation; but in this case, no guest was bound in the capsule. The molecular recognition behavior of the now empty capsule was then investigated. Using competitive binding assays, it was found that the relative affinity of the capsule for certain organic cations was $\text{Et}_4\text{N}^+ > \text{Me}_4\text{N}^+ > \text{Me}_4\text{P}^+$, and additionally, that Cs^+ could be encapsulated [104].

Schofield and coworkers recently described the use of boronate transesterification in DCLs aimed at discovering new enzyme inhibitors [97, 105]. In their latest study [97], an aromatic boronic acid was appended to a known binder of an oxygenase enzyme (propyl hydroxylase) and then combined in aqueous buffer at pH 7.5 with a range of diols. The DCL was then incubated with the enzyme, and the best binder was identified using mass spectrometry (Scheme 14.21). Binding studies with the selected boronate ester revealed high-affinity binding to the enzyme in a micromolar binding regime. A covalent analog of the identified boronate ester was then prepared, and it too displayed strong binding to the enzyme.

The use of boronate transesterification as the exchange reaction in dynamic combinatorial chemistry has the advantage that it is reversible both in organic solvents and in water at physiological pH. It can also be used in combination with other exchange processes such as metal–ligand exchange [106] and imine exchange [107]. Boronate esters, however, are often unstable, and it is not trivial to identify condition under which they do not exchange or hydrolyze. The analysis of DCLs of boronate esters and the isolation of library members can therefore be challenging. As a relatively new reaction in dynamic combinatorial chemistry, the development of exchange conditions for boronate transesterification and the exploration of template effects and selection approaches are ongoing.

14.7 TARGETING BIOLOGICAL MOLECULES USING DYNAMIC COMBINATORIAL CHEMISTRY

The recognition of biomacromolecules is an area of particular importance as it has close ties to medicinal chemistry, molecular biology, and other biological chemistry disciplines. The use of dynamic combinatorial chemistry is ideal to address the goal of recognizing complex biomacromolecules and other natural products in a strong and selective manner in their natural surroundings. It is perhaps not surprising that some of the first studies using dynamic combinatorial chemistry had the aim of recognizing biomacromolecules. These early studies have been followed by a number of reports targeting proteins and DNA, and the progress of these studies has been extensively

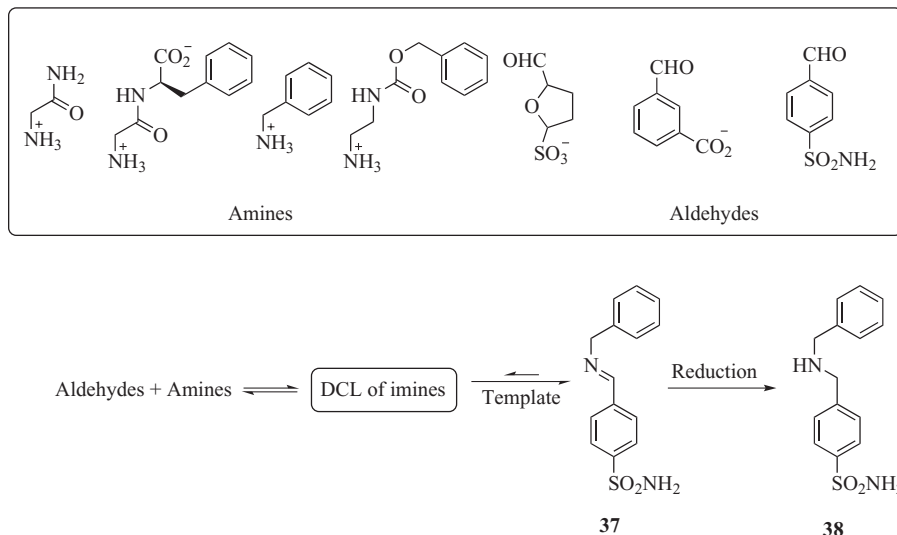


Scheme 14.21. The use of a boronate-transesterification-based DCLs for the identification of an enzyme inhibitor [97].

reviewed recently [1, 108]. In this section, we will highlight the power of DCLs by describing a few examples where the targets are proteins, duplex DNA, G-quadruplex DNA, and carbohydrates.

When searching for molecules that recognize proteins, or more specifically, for enzyme inhibitors, it is perhaps appropriate to use Fisher's classical metaphor, the *lock-and-key principle*. In a DCL designed to discover enzyme inhibitors, the library generates a series of possible keys for the lock that is the enzyme. The DCL may not necessarily contain library members corresponding to all possible combinations of the building blocks. There may be *virtual* keys in the DCL—keys (or library members) that are not present in amounts that can be detected in the DCL in the absence of the enzyme, but which may still be amplified after the addition of the enzyme. The role of the DCL is then to pick the correct key, amplify it, and synthesize it at the expense of the wrong keys.

The first efforts to recognize a protein using a DCL were described by Huc and Lehn in 1997 [109]. They used libraries of imines to target carbonic anhydrase, which is a Zn(II)-containing enzyme that is involved in the interconversion of CO_2 and HCO_3^- . They used a series of amines and aldehydes to generate small libraries of imines (Scheme 14.22). To halt the exchange, and to enable the analysis of the DCLs, the



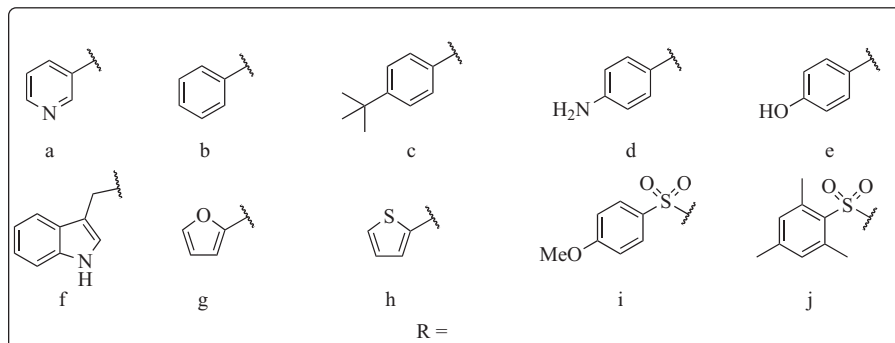
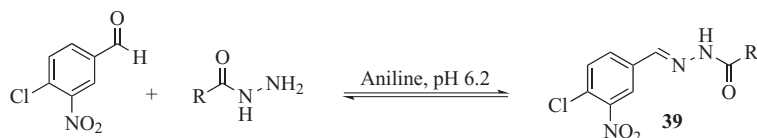
Scheme 14.22. Identification of an amine-based inhibitor (**38**) for carbonic anhydrase using an imine-based DCL [109].

imines were reduced to the corresponding amines using NaBH_3CN . The most amplified imine in Huc and Lehn's DCL was the structure shown in Scheme 14.22 (**37** and **38**) that had a similar structure to a known carbonic anhydrase inhibitor.

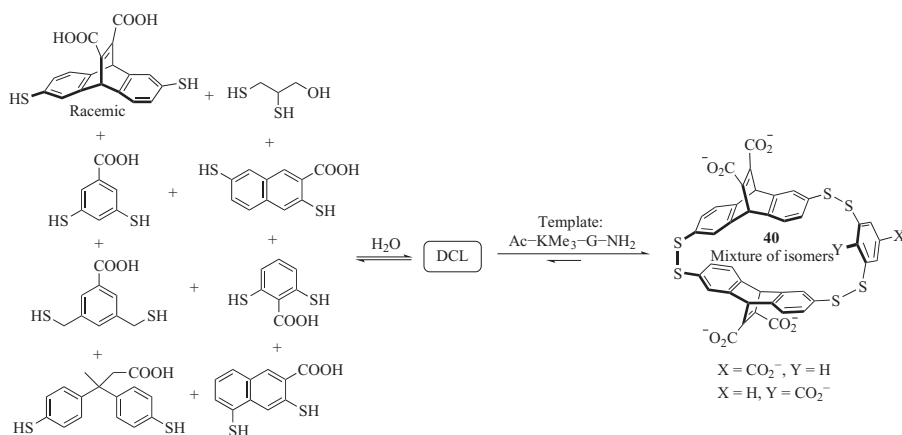
When using dynamic combinatorial chemistry for the recognition of biologically interesting molecules, it is desirable to use reversible reactions that equilibrate at or close to physiological pH. The use of imine exchange chemistry enables the reversible chemistry and templating to be performed at pH 6 [109]. Ramström et al. have described the use of acylhydrazones for the identification of enzyme inhibitors [110]. However, in their study, the DCLs were equilibrated at pH 4, and the inhibition studies were performed on the static library mixtures at physiological pH.

Greaney and coworkers recently established biocompatible conditions for hydrazone exchange by adding a large excess of aniline to a DCL of a mixture of an electron-deficient aromatic aldehyde and a series of hydrazides at pH 6.2 (Scheme 14.23) [74]. The aniline equilibrators allowed thermodynamic equilibrium to be reached within a few hours, which is fast compared to the 2 weeks used in Huc and Lehn's imine DCLs [109]. Greaney and coworkers used two different isozymes of the glutathione *S*-transferase (GST) class of enzymes as their templates and found that two different acylhydrazones (**39**) were amplified by the enzymes.

In a conceptually different approach for the recognition of proteins, Waters and coworkers used disulfide exchange chemistry to prepare DCLs to target the trimethyllysine moiety in a histone peptide [111]. It has been shown that significant protein-protein interactions that can result in gene silencing may be induced by methylation of the side-chain amines of lysine residues. Building blocks with similar structures to those described earlier in the chapter (Section 14.3) were used to generate DCLs of oligodisulfide macrocycles (Scheme 14.24). These were template with a series of dipeptides: Ac-K-G-NH_2 , Ac-KMe-G-NH_2 , $\text{Ac-KMe}_2\text{-G-NH}_2$, and $\text{Ac-KMe}_3\text{-G-NH}_2$



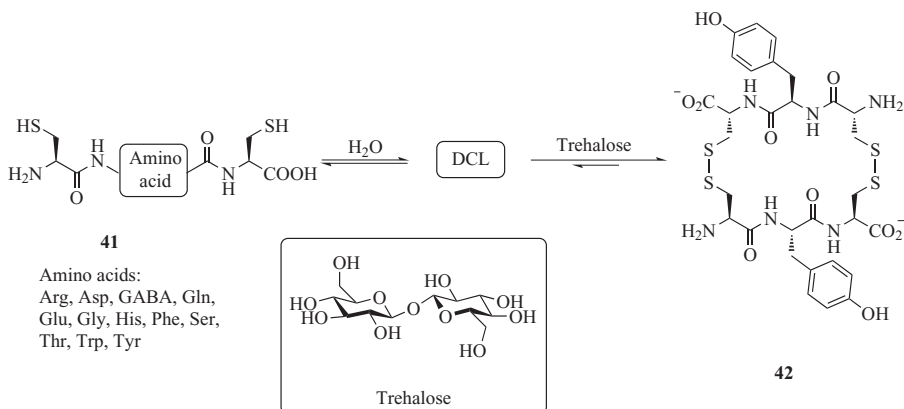
Scheme 14.23. Structure of the electron-deficient aldehyde and the 10 hydrazides used for acylhydrazone-based DCLs to target glutathione *S*-transferase [74].



Scheme 14.24. Left: The eight dithiol monomers used to prepare the DCL. Right: The amplified receptor (**40**) that is selective for the trimethyllysine moiety [111].

(K = lysine, G = glycine), and it was observed that the use of Ac-KMe₃-G-NH₂ gave rise to a large amplification of a cyclic trimer (**40**). The cyclic trimer (**40**) was isolated as a mixture of stereoisomers and found to exhibit almost native protein-like affinity. The trimethyl derivative Ac-KMe₃-G-NH₂ was bound more than twice as strongly as the dimethyl derivative Ac-KMe₂-G-NH₂ ($K_d = 25 \mu\text{M}$ vs. $58 \mu\text{M}$), and the monomethyl derivative and the nonmethylated lysine were bound only weakly.

It is important to emphasize that in this example, a small motif of a protein rather than the actual protein was targeted. This approach could, in principle, be important in the study of biological systems using supramolecular chemistry.



Scheme 14.25. A DCL of *cyclo*-peptides generated using disulfide exchange chemistry in which a cyclic dimer was amplified in the presence of trehalose [112].

The biomimetic recognition of carbohydrates is a topic of great current interest, and the complexity of carbohydrate structures makes a dynamic combinatorial approach attractive to explore. Ravoo and coworkers studied a DCL of disulfide macrocycles assembled from different tripeptide building blocks (**41**) of the general form Cys-(amino acid)-Cys [112]. It was found possible to amplify the cyclic homodimers of the tripeptides Cys-Thr-Cys and Cys-His-Cys in the presence of the monosaccharide α -D-methylfucopyranoside (MFP) and the neurotransmitter *N*-acetyl neuraminic acid (NANA), respectively. Furthermore, a cyclic homo-dimer of the tripeptide Cys-Tyr-Cys (**42**) was formed preferentially in the library in the presence of the disaccharide trehalose (Scheme 14.25). A binding constant of $2.2 \times 10^3 \text{ M}^{-1}$ was determined for this complex, which makes the receptor among the strongest biomimetic carbohydrate receptors to have been reported at this time. The selection of synthetic lectins (carbohydrate-binding proteins) from DCLs could prove valuable in further studies and manipulations of the biological functions of carbohydrates.

The recognition of specific DNA and RNA strands in their various folded and unfolded forms has attracted attention in medicinal and bioorganic chemistry. Molecular recognition of double-stranded DNA has been especially thoroughly studied, and reliable guidelines for the design of major- and minor-groove binders have been established. The past decade has also experienced an increased interest in the study of DNA-based three-dimensional structures that fold in different ways other than the well-known double helix structure. Among these, the so-called G-quadruplex DNA (Figure 14.7) has played a prominent role. G-quadruplexes are present in G-rich regions of DNA, and they form in a templated fashion around a metal ion as a consequence of a combination of π -stacking between several G-tetrads, Watson-Crick base pairing, and Hoogsteen base pairing. The G-quadruplex DNA structures are overrepresented in gene promoter regions, which has made G-quadruplexes attractive targets to recognize and stabilize using supramolecular chemistry approaches.

The first example of the use of a dynamic combinatorial mind-set for the recognition of DNA structures was carried out by Miller and coworkers [113]. They prepared a DCL of coordination complexes based on salicylaldimines and Zn^{2+} and used a resin-immobilized DNA target (Scheme 14.26). Binding of a specific component from the

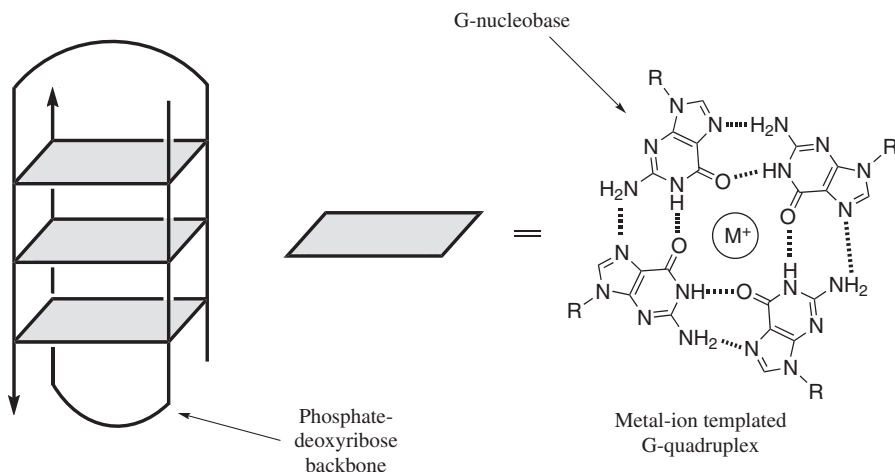
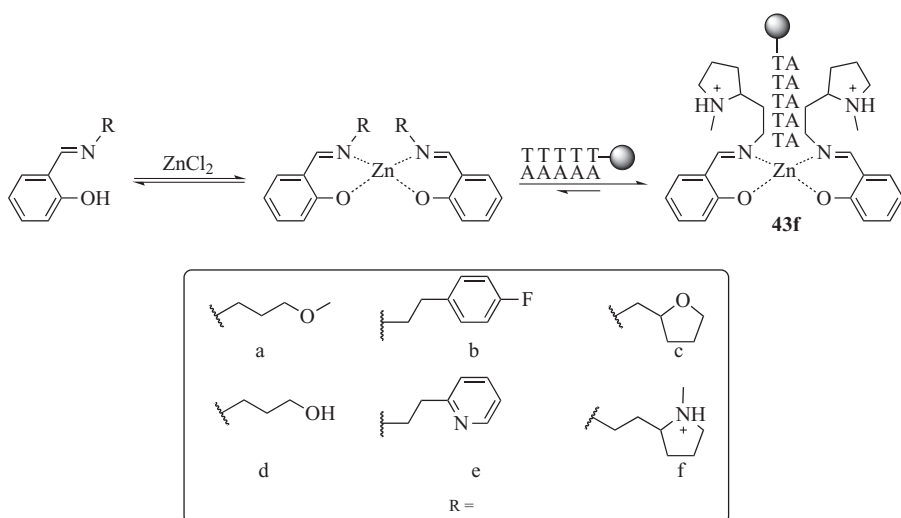


Figure 14.7. Left: Schematic illustration of a bimolecular G-quadruplex DNA structure. Right: Chemical structure of a DNA G-tetrad structure.



Scheme 14.26. A small DCL for the identification of a duplex DNA binder (**43**) [113].

DCL resulted in its removal from the solution since the DNA was immobilized on cellulose beads, which is different from most other DCL experiments where the amplification of a binding species is what is observed. Using this elegant approach, the micromolar DNA binder **43f** was identified.

Balasubramanian and coworkers have targeted DNA in a DCL approach using disulfide exchange chemistry [114]. In most of the work using disulfide exchange chemistry in DCLs, the pH of the aqueous mixtures has been slightly alkaline (pH 8–9).

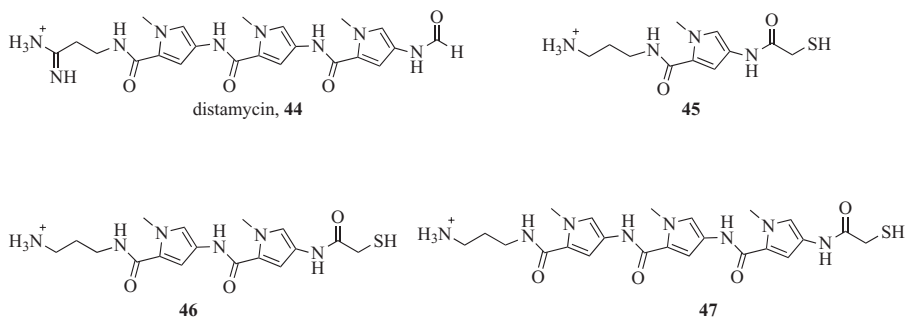


Figure 14.8. Structures of pyrrole-polyamide monothiol building blocks (**45–47**) used for the identification of duplex DNA binders [114].

Here a glutathione buffer (a thiol–disulfide buffer) was used to promote and enable equilibration within 24 h while using very dilute solutions of the disulfide building blocks at physiological pH. Inspired by a known duplex DNA minor-groove binder containing *N*-methylpyrroles and *N*-methylimidazoles, monothiol building blocks were designed that contained amide-linked *N*-methylpyrroles and closely resembled the minor-groove binder distamycin (**44**, Figure 14.8). It was found that upon equilibrating DCLs containing building blocks **45**, **46**, and **47** in the presence of either a duplex or a G-quadruplex DNA target, the conjugates **46·47** and **47·47** were amplified. The amplification factors were five to six times larger for the duplex DNA compared with the G-quadruplex DNA.

When disulfide DCLs are generated using a large excess of glutathione redox buffer, most of the thiol building blocks will be present in the DCLs as disulfide conjugates with glutathione. In this example, however, this did not pose a problem as both the DNA and the glutathione are negatively charged, so a bias toward the amplification of disulfides containing only the desired positively charged building blocks was expected in the presence of the DNA template. The relative affinities of the isolated disulfides toward the DNA templates correlated well to the relative sizes of the observed amplifications of the disulfide conjugates in the DCL. This was shown using a number of techniques, including measuring the DNA melting temperatures in the presence of the disulfides [114].

In another study, Bugaut et al. targeted G-quadruplex DNA in a similar fashion to that described earlier [115]. In this case, they explored an oxazole-peptide macrocycle—a type of quadruplex-binding ligand they had previously described [116]. A monothiol version of the quadruplex-binding ligand (**48**) was prepared and used as a scaffold upon which different monothiols could be appended (Figure 14.9). In one part of the study, they chose to explore different side chains (amines and guanidiniums) that would be positively charged at physiological pH (Figure 14.9, **A–E**). The largest amplifications were observed for the guanidinium-appended macrocycle in the presence of the c-kit G-quadruplex DNA sequence (a naturally occurring G-quadruplex DNA sequence). They isolated the various disulfides and studied their binding properties toward duplex DNA and G-quadruplex DNA. They found that there was a correlation between the amplification factors observed in the DCLs and the relative binding affinities of the isolated ligands. Furthermore, the disulfides that were amplified in the

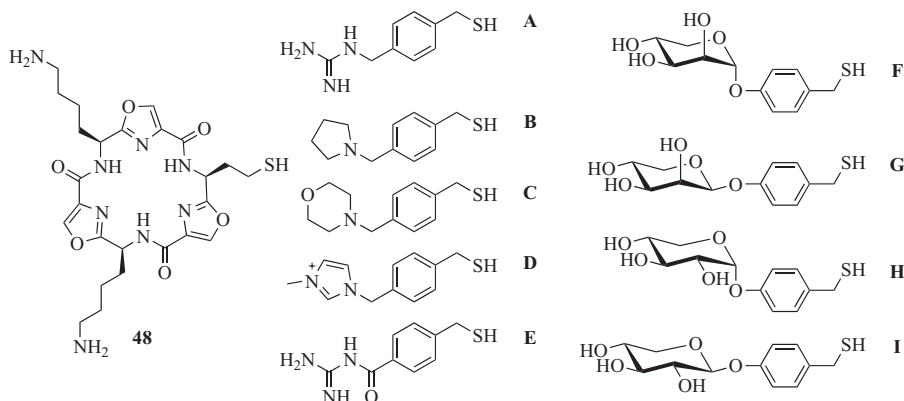


Figure 14.9. Structures of the oxazole monothiol building block (**48**) used for the identification of G-quadruplex DNA binders together with the monothiols with positively charged (**A–E**) and neutral side chains (**F–I**) [115].

presence of the G-quadruplex DNA were highly selective for the G-quadruplex DNA over the duplex DNA.

A small series of carbohydrate containing monothiols (**F–I**) were also explored in combination with the oxazole-peptide macrocycle using the same G-quadruplex DNA sequence as the template (Figure 14.9). While the binding affinities and the amplification factors for the carbohydrate conjugates were smaller than those conjugates containing the positively charged amine and guanidinium side chains, there were subtle differences between the various carbohydrates. The most strongly amplified conjugate contained carbohydrate **F**, and this was shown to have $K_d = 9.1 \mu\text{M}$, while the least amplified carbohydrate **G** had $K_d = 23.6 \mu\text{M}$.

The examples given earlier using proteins and DNA as templates in dynamic combinatorial chemistry serve to illustrate that DCLs may be used in complex systems. Several other studies using dynamic combinatorial chemistry to target biomacromolecules have been described using a variety of exchange reactions [1]. Most of these studies focus on relatively simple libraries so there is a lot of opportunity for exploration of more complex DCLs in the context of biomacromolecule recognition. While most of the studies using DCL to recognize biomacromolecules are at the proof-of-principle stage, the concept has the potential to be a valuable tool in drug discovery.

14.8 MODELING OF DYNAMIC COMBINATORIAL LIBRARIES

14.8.1 DCL Simulations to Optimize Library Design

The distribution of library members in a DCL is governed by a complex network of equilibria that describe the exchange of building blocks, the intermolecular interactions between library members, and the intermolecular interactions between library members and added templates. As a consequence, the behavior of libraries in response to certain stimuli is complex and can sometimes appear counterintuitive; addition of a template, for example, will lead to the amplification of receptors, but not necessarily the best

possible receptor [4]. The library, as a whole, responds to the template to minimize the free energy of the entire DCL, and the response will be dependent on the relative stability of all library members and complexes formed, the template concentration, the building block concentrations, and the building block composition of the various library members. The development of computational methods to study DCLs has facilitated an investigation of the parameters that affect library distributions in order to gain a better understanding of how to optimize the design of DCLs.

In an ideal situation, when a template is added to a DCL, the best host that can be formed from the building blocks would be amplified above all other possible hosts. Unfortunately, this is not always the case. Severin and coworkers first highlighted two important situations where the correlation between amplification factor and the binding affinity of the host can break down [117]. In the first study, computational models of simple DCLs containing trimeric macrocycles formed from up to three different building blocks were generated using the computer program, Gepasi [118]. The effects on the DCLs' distributions of addition of a template were investigated and revealed that there is an intrinsic tendency to amplify mixed macrocycles in preference to those containing only one type of building block. In a second study, DCLs containing only one building block, but that were capable of generating macrocycles with different sizes, were investigated [119]. Here it was observed that there is a tendency to amplify smaller macrocycles in preference to larger macrocycles.

These tendencies were first predicted on the basis of computer-simulated DCLs but have subsequently been confirmed experimentally [4, 120]. Saur and Severin demonstrated the effect of template concentration on the amplification of homo- and hetero-oligomers in a simple DCL of self-assembled trinuclear metallamacrocycles (Figure 14.10) [120]. Homotrimers AAA and BBB were mixed together to generate,

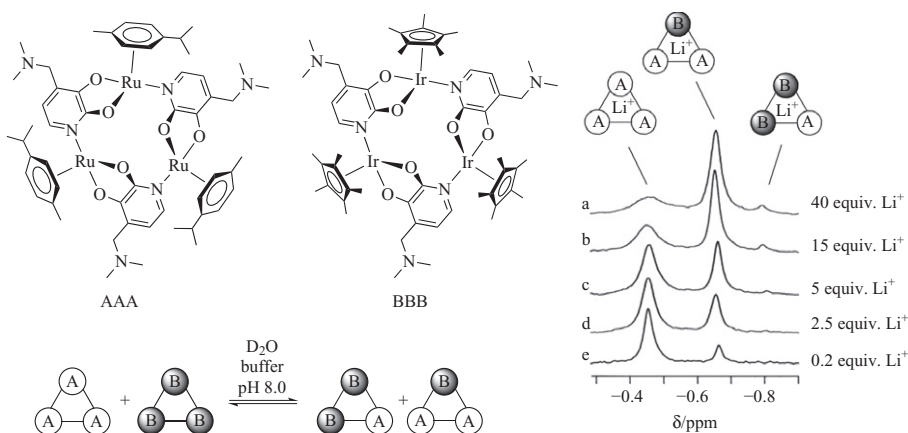


Figure 14.10. Left: A DCL of trinuclear metallamacrocycles AAA, AAB, ABB, and BBB formed via the self-assembly of $[(p\text{-cymene})\text{RuCl}_2]_2$ and $[\text{Cp}^*\text{IrCl}_2]_2$ together with the ligand 3-hydroxy-4-dimethylaminomethyl-2-(1*H*)-pyridone in phosphate buffer at pH 8. Right: ^7Li NMR spectra in D_2O of the DCL after equilibration with (a) 40, (b) 15, (c) 5, (d) 2.5, and (e) 0.2 equiv. of Li^+ [120]. Source of NMR spectra: [120]. Reproduced with permission of The Royal Society of Chemistry.

at equilibrium, an approximately 1:3:3:1 statistical mixture of AAA, AAB, ABB, and BBB. AAA had been found to exhibit a strong affinity for Li^+ ($K_{\text{AAA}} \sim 10^3 \text{ M}^{-1}$), while BBB was a very poor receptor ($K_{\text{BBB}} \sim 0.1 \text{ M}^{-1}$). Library distributions upon addition of different amounts of Li^+ were analyzed by means of ^7Li -NMR spectroscopy. Addition of 0.2 equiv. of Li^+ resulted in an amplification of AAA (the best binder), but as the Li^+ concentration was increased up to 40 equiv., the concentration of AAA decreased, and a mixed dimer AAB (a moderate binder) was amplified to the greatest extent.

These counterintuitive observations may be explained by the fact that the effect of adding a template to a DCL is determined by the additive effects of the interactions of each library member with the template. When there is a choice between producing a large number of moderately good hosts rather than a small number of stronger binders, the first of these options will sometimes be preferred. For example, the formation of two moderately binding heteromacrocycles may be preferable to the formation of only one strongly binding homomacrocycle. In the same way, a DCL may *choose* to amplify moderately binding dimers instead of stronger-binding larger oligomers because it can thereby increase the total number of available hosts. Ultimately, these effects are minimized when the different hosts have to compete for a limited number of templates, and therefore, the use of low template concentrations is advised [119].

In order to explore these trends in more complex systems and learn how to best design DCLs so that there is a good correlation between amplification factor and binding affinity, Corbett et al. developed a program called DCLsim that is capable of rapidly simulating thousands of DCLs containing more than 200 components with a wide variety of building block and template concentrations [4, 121, 122]. DCLs were generated computationally from combinations of up to seven different building blocks that were capable of forming dimers, trimers, and tetramers. The building block and template concentrations were systematically varied, and for each of 289 different sets of experimental conditions, 50 libraries were generated, with different randomly assigned binding affinities for each library member. The simulated amplification factors were then compared with the assigned binding affinities, and the probability that the best binder was among the most amplified species in the library was mapped against building block concentration and template concentration. It was concluded that the template concentration should be restricted to one-tenth of the total building block concentration to obtain an approximately 90% chance that the best host is one of the three most amplified [122]. It should be noted, however, that as the template concentration is decreased, there is an increase in the probability that good hosts are not detected because their concentrations are too low. It is therefore advisable to do preliminary screens of DCLs using a higher template concentration in order to increase the chance of seeing some kind of templating effect and then to repeat the setup of the DCLs with low template concentration to better ascertain the identity of the best hosts.

Additional computational studies have resulted in further suggestions for library design. Ludlow and Otto noted that increasing the size of the library (i.e., the number of building blocks) not only increases the probability of generating a strong binder, but it also increases the probability that a strong binder will be identified as a result of amplification [123, 124]. Orrillo and Furlan showed that the use of low template concentrations is also useful to promote the amplification of the best binder in DCLs in which library members have a tendency to interact with each other and form aggregates [125]. Severin also recommended that where possible, DCLs should be designed under reaction conditions such that the equilibria lie toward the building blocks rather than

the oligomers because when the library is mainly composed of free building blocks, there is an increased probability that the best host will be the most amplified [119].

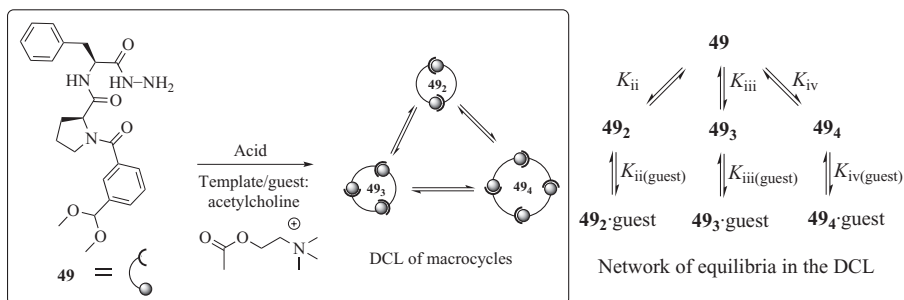
14.8.2 Estimating Association Constants Directly from the DCL

The analysis of DCL composition is most frequently achieved by means of LC-MS and occasionally NMR spectroscopy. A qualitative assessment of the influence of a template on the library distribution may be obtained by visually comparing the HPLC chromatograms of templated and untemplated libraries. Quantification of binding affinity has then traditionally required the isolation of selected receptors followed by complexation studies using techniques such as NMR, UV/Vis, fluorescence, or CD spectroscopy, isothermal titration calorimetry (ITC), or a combination of these. The development of computational methods to model DCLs has recently enabled the direct estimation of association constants from the DCLs, circumventing the need for individual binding studies on isolated receptors.

In 2007, Ludlow et al. developed a program called DCLfit, which was built upon the aforementioned simulation program, DCLsim, and may be used to calculate binding constants between the hosts and templates in a DCL directly from the changes in library distributions observed in the presence of varying amounts of template [126]. The use of DCLfit requires first setting up a series of libraries in which the concentration of the guest is varied while keeping the building block concentrations and all other experimental condition constant. After equilibration of the libraries is complete, the concentrations of all the library members in each library are measured, typically using HPLC. A guess of the various association constants for each library member with the template, and also for the equilibrium constants between the library members, is entered into the program. The program then simulates a set of DCLs and calculates the expected concentrations of the library members in the presence of varying concentrations of template. It compares these to the experimentally determined concentrations and, thus informed, makes a new guess of the equilibrium and association constants. Through an iterative approach, association and equilibrium constants that fit the concentration data are determined.

DCLfit was first applied to a DCL of peptide-based hydrazone macrocycles formed from building block **49** (Scheme 14.27) [126]. It had been observed that addition of acetylcholine chloride to the library resulted in a significant amplification of the cyclic trimer. A series of DCLs with different concentrations of acetylcholine were set up, and the concentration of cyclic dimer, trimer, and tetramer were measured by means of HPLC. Using DCLfit, the data were fitted to the model equilibrium network shown in Scheme 14.27, and binding energies of 14.1, 22.1, and 20.3 kJ/mol were determined for complexation of the guest with the dimer, trimer, and tetramer, respectively. In order to reconcile the calculated binding energies with experimentally determined values, the cyclic trimer was isolated, and its complexation with acetylcholine chloride was studied using ITC. A binding energy of 22.2 kJ/mol was determined, confirming the viability of the computational approach [126].

The possibility to assess binding constants directly from DCLs has been particularly advantageous in situations where either the amplified library member is not isolable; it is unstable or fails to interact with the template under conditions where it is stable [69], it is not soluble at concentrations required for the binding studies [126], or it gives complex spectra and multiple isomers that complicate or frustrate binding studies [55]. It may also be used to study aggregation phenomena in DCLs [127].



Scheme 14.27. Left: A DCL of hydrazone-based macrocycles was formed from tripeptide building block **49** (2 mM) in $\text{CHCl}_3/\text{MeOH}$ in the presence of trifluoroacetic acid. Right: The network of equilibria that describe the templated DCL [126].

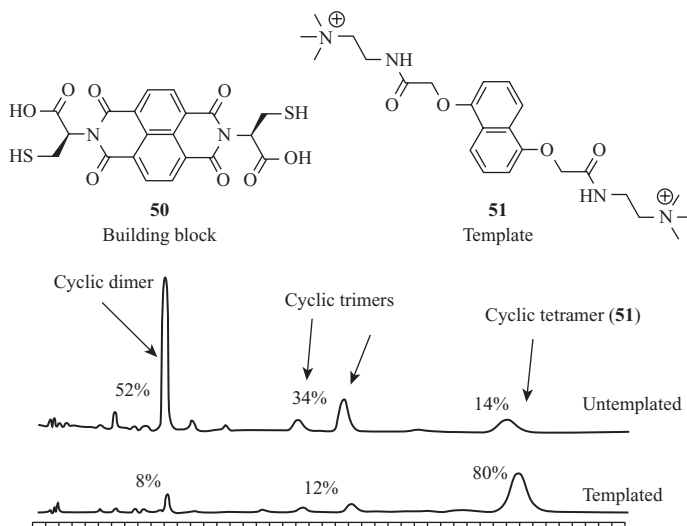


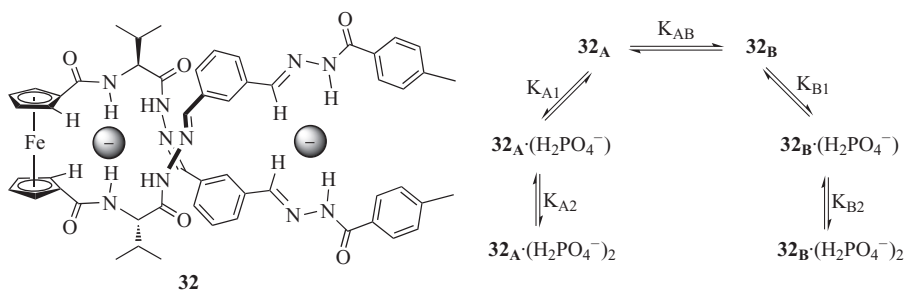
Figure 14.11. Top: Electron-deficient naphthalenediimide building block **50** and electron-rich dialkoxynaphthalene template **51**. Bottom: HPLC analysis of the DCL in the presence and absence of template **51** [55]. Source of HPLC chromatograms: [55]. Reproduced with permission of The Royal Society of Chemistry.

Au-Yeung et al. described the amplification of a naphthalenediimide-based tetramer from a DCL of dithiol building block **50** in the presence of an electronically complementary dialkoxynaphthalene guest **51** (Figure 14.11) [55]. The tetrameric receptor was isolated with the intention of conducting binding studies. However, the signals in the $^1\text{H-NMR}$ spectrum of the receptor were broad and complex over a wide temperature range presumably due to the presence of multiple conformations in solution. The $^1\text{H-NMR}$ spectrum of the host–guest complex was also broad, and binding studies by

UV/Vis spectroscopy, while suggesting a 2:1 binding mode, were inconclusive, possibly due to the complexity of the electronic transitions involving the host and guest. The authors turned to DCLfit to estimate association constants. By fitting the equilibrium concentrations of the library members to a model of the DCL, $K_1 = 10^6 \text{ M}^{-1}$ and $K_2 = 10^4 \text{ M}^{-1}$ were determined for the 2:1 interaction between **51** and the cyclic tetramer. From these values, it was concluded that each electron-rich guest **51** interacts with two electron-deficient naphthalenediimide moieties in the tetramer.

The wider application of DCLfit to systems of equilibria not usually classified as DCLs was recently demonstrated by Beeren and Sanders [77]. Having isolated a ferrocene-hydrazone-based ditopic receptor (**32**) for H_2PO_4^- , which was identified from a DCL (Section 14.5), an association constant for the 2:1 binding interaction was sought (Scheme 14.28). The $^1\text{H-NMR}$ spectrum of the receptor was complicated by the existence of two conformational isomers (one with C_2 symmetry, **32_A**, and the other with C_1 symmetry, **32_B**) in slow exchange with each other on an NMR chemical shift timescale. Titration with H_2PO_4^- resulted not only in the downfield shifting of electro-positive protons involved in binding the anion, but in the conversion of **32_B** into **32_A**, thus indicating the superior binding of the symmetrical isomer **32_A**. The mixture was considered as a dynamic *conformational* library. The $^1\text{H-NMR}$ titration was thus viewed as a series of DCLs with different template concentrations and the composition of each *library* was determined by integrating the relevant peaks in the NMR spectrum. DCLfit was used to fit the data to the network of equilibria shown in Scheme 14.28. Association constants for the interaction were thus determined ($K_{A1}K_{A2} = 800,000 \text{ M}^{-1}$, $K_{A1} \ll K_{A2}$, and $K_{B1}K_{B2} = 100,000 \text{ M}^{-1}$), and the cooperative nature of the binding—first noted in UV/Vis studies—was confirmed.

DCLs are complex, and their behavior under the influence of a template is difficult to predict. Through theoretical modeling and the computational generation of simulated libraries, a clearer understanding of DCL behavior has been achieved. Experimental guidelines have been established to help design successful DCLs, and elegant methods have been developed to obtain a quantitative assessment of association constants directly from the equilibrium library composition. DCLs do not always behave in the simple way that was hoped for when the concept was conceived, but by acknowledging their complexity and the interconnectivity of their networks of equilibria, they can be powerful tools for the study of molecular recognition and systems behavior [128, 129].



Scheme 14.28. Left: Ferrocene hydrazone-based ditopic receptor for H_2PO_4^- (**32**). Right: Network of equilibria that describe the template-induced isomerization of **32** [77].

14.9 CONCLUDING REMARKS

In this chapter we have described the use of dynamic combinatorial chemistry in the search for new receptors through a selection of state-of-the-art examples. In the coming years, we foresee the discovery of new, unexpected, strong, selective, and exciting receptors with unforeseen geometries and binding motifs. We expect the concept will influence medicinal chemistry with more biologically significant molecules being targeted and larger DCLs being explored. As new, reversible chemical reactions are introduced, the possibilities in dynamic combinatorial chemistry will expand. Dynamic combinatorial chemistry has inspired the exploration of adaptive chemical networks, with the field of *systems chemistry* emerging from this [129]. In dynamic combinatorial chemistry, the chemist can design the experiments, but ultimately, the molecules engineer themselves.

REFERENCES

- [1] Corbett, P. T., Leclaire, J., Vial, L., West, K. R., Wietor, J.-L., Sanders, J. K. M., Otto, S. (2006). Dynamic combinatorial chemistry. *Chemical Reviews*, 106, 3652–3711.
- [2] Miller, B. L. *Dynamic Combinatorial Chemistry: In Drug Discovery, Bioorganic Chemistry, and Materials Science*, John Wiley & Sons, Hoboken, NJ, 2009.
- [3] Reek, J. N. H., Otto, S. *Dynamic Combinatorial Chemistry*, John Wiley & Sons, Hoboken, NJ, 2010.
- [4] Corbett, P. T., Sanders, J. K. M., Otto, S. (2005). Competition between receptors in dynamic combinatorial libraries: Amplification of the fittest? *Journal of the American Chemical Society*, 127, 9390–9392.
- [5] Furlan, R. L. E., Ng, Y.-F., Otto, S., Sanders, J. K. M. (2001). A new cyclic pseudopeptide receptor for Li⁺ from a dynamic combinatorial library. *Journal of the American Chemical Society*, 123, 8876–8877.
- [6] Eliseev, A. V., Nelen, M. I. (1997). Use of molecular recognition to drive chemical evolution. 1. Controlling the composition of an equilibrating mixture of simple arginine receptors. *Journal of the American Chemical Society*, 119, 1147–1148.
- [7] Cousins, G. R. L., Poulsen, S.-A., Sanders, J. K. M. (2000). Molecular evolution: Dynamic combinatorial libraries, autocatalytic networks and the quest for molecular function. *Current Opinion in Chemical Biology*, 4, 270–279.
- [8] Houk, K. N., Leach, A. G., Kim, S. P., Zhang, X. (2003). Binding affinities of host-guest, protein-ligand, and protein-transition-state complexes. *Angewandte Chemie—International Edition*, 42, 4872–4897.
- [9] Hunt, R. A. R., Otto, S. (2011). Dynamic combinatorial libraries: New opportunities in systems chemistry. *Chemical Communications*, 47, 847–858.
- [10] Hasenknopf, B., Lehn, J.-M., Kneisel, B. O., Baum, G., Fenske, D. (1996). Self-assembly of a circular double helicate. *Angewandte Chemie—International Edition*, 35, 1838–1840.
- [11] Hasenknopf, B., Lehn, J.-M., Boumediene, N., Dupont-Gervais, A., van Dorsseleer, A., Kneisel, B., Fenske, D. (1997). Self-assembly of tetra- and hexanuclear circular helicates. *Journal of the American Chemical Society*, 119, 10956–10962.
- [12] Brady, P. A., Bonar-Law, R. P., Rowan, S. J., Suckling, C. J., Sanders, J. K. M. (1996). “Living” macrolactonisation: Thermodynamically controlled cyclisation and interconversion of oligocholates. *Chemical Communications*, 319–320.

- [13] Rowan, S. J., Brady, P. A., Sanders, J. K. M. (1996). Structure-directed synthesis under thermodynamic control: Macrocyclic trimers from cinchona alkaloids. *Angewandte Chemie—International Edition*, 35, 2143–2145.
- [14] Rowan, S. J., Brady, P. A., Sanders, J. K. M. (1996). Synthesis and kinetic cyclisation of quinine-derived oligomers. *Tetrahedron Letters*, 37, 6013–6016.
- [15] Benner, S. A. (1995). Receptor-assisted combinatorial chemistry. U.S. Patent 5.958.702.
- [16] Brady, P. A., Sanders, J. K. M. (1997). Thermodynamically-controlled cyclisation and interconversion of oligocholates: Metal ion templated “living” macrolactonisation. *Journal of the Chemical Society, Perkin Transactions 1*, 3237–3254.
- [17] Meguellati, K., Ladame, S. (2012). Reversible covalent chemistries compatible with the principles of constitutional dynamic chemistry: New reactions to create more diversity constitutional dynamic chemistry. *Topics in Current Chemistry*, 322, 291–314.
- [18] Belowich, M. E., Stoddart, J. F. (2012). Dynamic imine chemistry. *Chemical Society Reviews*, 41, 2003–2024.
- [19] Boul, P. J., Reutenauer, P., Lehn, J.-M. (2005). Reversible Diels–Alder reactions for the generation of dynamic combinatorial libraries. *Organic Letters*, 7, 15–18.
- [20] Vongvilai, P., Angelin, M., Larsson, R., Ramström, O. (2007). Dynamic combinatorial resolution: Direct asymmetric lipase-mediated screening of a dynamic nitroaldol library. *Angewandte Chemie—International Edition*, 46, 948–950.
- [21] Giger, T., Wigger, M., Audétat, S., Benner, S. A. (1998). Libraries for receptor-assisted combinatorial synthesis (RACS). The olefin metathesis reaction. *Synlett*, 1998, 688–691.
- [22] Leclair, J., Vial, L., Otto, S., Sanders, J. K. M. (2005). Expanding diversity in dynamic combinatorial libraries: Simultaneous exchange of disulfide and thioester linkages. *Chemical Communications*, 1959–1961.
- [23] Bang, E.-K., Lista, M., Sforazzini, G., Sakai, N., Matile, S. (2012). Poly(disulfide)s. *Chemical Science*, 3, 1752–1763.
- [24] Lehn, J.-M. (2007). From supramolecular chemistry towards constitutional dynamic chemistry and adaptive chemistry. *Chemical Society Reviews*, 36, 151–160.
- [25] Cougnon, F. B. L., Sanders, J. K. M. (2012). Evolution of dynamic combinatorial chemistry. *Accounts of Chemical Research*, 45, 2211–2221.
- [26] Wallace, T. J., Schriesheim, A., Bartok, W. (1963). The base-catalyzed oxidation of mercaptans. III. Role of the solvent and effect of mercaptan structure on the rate determining step. *The Journal of Organic Chemistry*, 28, 1311–1314.
- [27] Lees, W. J., Whitesides, G. M. (1993). Equilibrium constants for thiol-disulfide interchange reactions: A coherent, corrected set. *The Journal of Organic Chemistry*, 58, 642–647.
- [28] Fernandes, P. A., Ramos, M. J. (2004). Theoretical insights into the mechanism for thiol/disulfide exchange. *Chemistry—A European Journal*, 10, 257–266.
- [29] Gilbert, H. F. Thiol/disulfide exchange equilibria and disulfide bond stability. In *Methods in Enzymology*, Lester, P. (Ed.), Academic Press, New York, 1995; pp. 8–28.
- [30] Moulin, E., Cormos, G., Giuseppone, N. (2012). Dynamic combinatorial chemistry as a tool for the design of functional materials and devices. *Chemical Society Reviews*, 41, 1031–1049.
- [31] Otto, S., Furlan, R. L. E., Sanders, J. K. M. (2000). Dynamic combinatorial libraries of macrocyclic disulfides in water. *Journal of the American Chemical Society*, 122, 12063–12064.
- [32] Otto, S., Furlan, R. L. E., Sanders, J. K. M. (2002). Selection and amplification of hosts from dynamic combinatorial libraries of macrocyclic disulfides. *Science*, 297, 590–593.
- [33] Stauffer, D. A., Barrans, R. E., Dougherty, D. A. (1990). Concerning the thermodynamics of molecular recognition in aqueous and organic media. Evidence for significant heat capacity effects. *The Journal of Organic Chemistry*, 55, 2762–2767.

- [34] Kearney, P. C., Mizoue, L. S., Kumpf, R. A., Forman, J. E., McCurdy, A., Dougherty, D. A. (1993). Molecular recognition in aqueous media. New binding studies provide further insights into the cation- π interaction and related phenomena. *Journal of the American Chemical Society*, *115*, 9907–9919.
- [35] Ngola, S. M., Kearney, P. C., Mecozzi, S., Russell, K., Dougherty, D. A. (1999). A selective receptor for arginine derivatives in aqueous media. Energetic consequences of salt bridges that are highly exposed to water. *Journal of the American Chemical Society*, *121*, 1192–1201.
- [36] Corbett, P. T., Tong, L. H., Sanders, J. K. M., Otto, S. (2005). Diastereoselective amplification of an induced-fit receptor from a dynamic combinatorial library. *Journal of the American Chemical Society*, *127*, 8902–8903.
- [37] West, K. R., Ludlow, R. F., Corbett, P. T., Besenius, P., Mansfeld, F. M., Cormack, P. A. G., Sherrington, D. C., Goodman, J. M., Stuart, M. C. A., Otto, S. (2008). Dynamic combinatorial discovery of a [2]-catenane and its guest-induced conversion into a molecular square host. *Journal of the American Chemical Society*, *130*, 10834–10835.
- [38] Vial, L., Ludlow, R. F., Leclaire, J., Pérez-Fernández, R., Otto, S. (2006). Controlling the biological effects of spermine using a synthetic receptor. *Journal of the American Chemical Society*, *128*, 10253–10257.
- [39] Breuil, P.-A. R., Reek, J. N. H. Dynamic combinatorial chemistry for catalytic applications. In *Dynamic Combinatorial Chemistry*, Reek, J. N. H., Otto, S. (Eds.), Wiley-VCH Verlag GmbH & Co. KGaA, Weinheim, 2010; pp. 91–108.
- [40] Brisig, B., Sanders, J. K. M., Otto, S. (2003). Selection and amplification of a catalyst from a dynamic combinatorial library. *Angewandte Chemie—International Edition*, *42*, 1270–1273.
- [41] Vial, L., Sanders, J. K. M., Otto, S. (2005). A catalyst for an acetal hydrolysis reaction from a dynamic combinatorial library. *New Journal of Chemistry*, *29*, 1001–1003.
- [42] West, K. R., Bake, K. D., Otto, S. (2005). Dynamic combinatorial libraries of disulfide cages in water. *Organic Letters*, *7*, 2615–2618.
- [43] Stefankiewicz, A. R., Sambrook, M. R., Sanders, J. K. M. (2012). Template-directed synthesis of multi-component organic cages in water. *Chemical Science*, *3*, 2326–2329.
- [44] Kubik, S., Goddard, R., Kirchner, R., Nolting, D., Seidel, J. (2001). A cyclic hexapeptide containing L-proline and 6-aminopicolinic acid subunits binds anions in water. *Angewandte Chemie—International Edition*, *40*, 2648–2651.
- [45] Kubik, S., Goddard, R. (2001). Fine tuning of the cation affinity of artificial receptors based on cyclic peptides by intramolecular conformational control. *European Journal of Organic Chemistry*, *2001*, 311–322.
- [46] Kubik, S., Goddard, R. (1999). A new cyclic pseudopeptide composed of (L)-proline and 3-aminobenzoic acid subunits as a ditopic receptor for the simultaneous complexation of cations and anions. *The Journal of Organic Chemistry*, *64*, 9475–9486.
- [47] Kubik, S., Goddard, R. (2002). Conformation and anion binding properties of cyclic hexapeptides containing L-4-hydroxyproline and 6-aminopicolinic acid subunits. *Proceedings of the National Academy of Sciences of the United States of America*, *99*, 5127–5132.
- [48] Kubik, S., Kirchner, R., Nolting, D., Seidel, J. (2002). A molecular oyster: A neutral anion receptor containing two cyclopeptide subunits with a remarkable sulfate affinity in aqueous solution. *Journal of the American Chemical Society*, *124*, 12752–12760.
- [49] Reyheller, C., Hay, B. P., Kubik, S. (2007). Influence of linker structure on the anion binding affinity of bicyclopeptides. *New Journal of Chemistry*, *31*, 2095–2102.
- [50] Otto, S., Kubik, S. (2003). Dynamic combinatorial optimization of a neutral receptor that binds inorganic anions in aqueous solution. *Journal of the American Chemical Society*, *125*, 7804–7805.
- [51] Rodriguez-Docampo, Z., Eugenieva-Ilieva, E., Reyheller, C., Belenguer, A. M., Kubik, S., Otto, S. (2011). Dynamic combinatorial development of a neutral synthetic receptor that

- binds sulfate with nanomolar affinity in aqueous solution. *Chemical Communications*, 47, 9798–9800.
- [52] Miljanić, O. Š., Stoddart, J. F. (2007). Dynamic donor-acceptor [2]catenanes. *Proceedings of the National Academy of Sciences of the United States of America*, 104, 12966–12970.
- [53] Patel, K., Miljanić, O. Š., Stoddart, J. F. (2008). Iodide-catalysed self-assembly of donor-acceptor [3]catenanes. *Chemical Communications*, 1853–1855.
- [54] Olson, M. A., Coskun, A., Fang, L., Basuray, A. N., Stoddart, J. F. (2010). Polycatenation under thermodynamic control. *Angewandte Chemie—International Edition*, 49, 3151–3156.
- [55] Au-Yeung, H. Y., Pengo, P., Pantoş, G. D., Otto, S., Sanders, J. K. M. (2009). Templated amplification of a naphthalenediimide-based receptor from a donor-acceptor dynamic combinatorial library in water. *Chemical Communications*, 419–421.
- [56] Au-Yeung, H. Y., Pantoş, G. D., Sanders, J. K. M. (2009). Dynamic combinatorial synthesis of a catenane based on donor-acceptor interactions in water. *Proceedings of the National Academy of Sciences of the United States of America*, 106, 10466–10470.
- [57] Au-Yeung, H. Y., Pantoş, G. D., Sanders, J. K. M. (2009). Amplifying different [2]catenanes in an aqueous donor-acceptor dynamic combinatorial library. *Journal of the American Chemical Society*, 131, 16030–16032.
- [58] Au-Yeung, H. Y., Pantoş, G. D., Sanders, J. K. M. (2010). A water soluble donor-acceptor [2]catenane that can switch between a coplanar and a gemini-sign conformation. *Angewandte Chemie—International Edition*, 49, 5331–5334.
- [59] Au-Yeung, H. Y., Cougnon, F. B. L., Otto, S., Pantoş, G. D., Sanders, J. K. M. (2010). Exploiting donor-acceptor interactions in aqueous dynamic combinatorial libraries: Exploratory studies of simple systems. *Chemical Science*, 1, 567–574.
- [60] Au-Yeung, H. Y., Pantoş, G. D., Sanders, J. K. M. (2011). Dynamic combinatorial donor-acceptor catenanes in water: Access to unconventional and unexpected structures. *The Journal of Organic Chemistry*, 76, 1257–1268.
- [61] Cougnon, F. B. L., Au-Yeung, H. Y., Pantoş, G. D., Sanders, J. K. M. (2011). Exploring the formation pathways of donor-acceptor catenanes in aqueous dynamic combinatorial libraries. *Journal of the American Chemical Society*, 133, 3198–3207.
- [62] Cougnon, F. B. L., Jenkins, N. A., Pantoş, G. D., Sanders, J. K. M. (2012). Templated dynamic synthesis of a [3]catenane. *Angewandte Chemie—International Edition*, 51, 1443–1447.
- [63] Cousins, G. R. L., Poulsen, S. A., Sanders, J. K. M. (1999). Dynamic combinatorial libraries of pseudo-peptide hydrazone libraries. *Chemical Communications*, 1575–1576.
- [64] Lam, R. T. S., Belenguer, A. M., Roberts, S. L., Naumann, C., Jarrosson, T., Otto, S., Sanders, J. K. M. (2005). Amplification of acetylcholine-binding catenanes from dynamic combinatorial libraries. *Science*, 308, 667–669.
- [65] Furlan, R. L. E., Otto, S., Sanders, J. K. M. (2002). Supramolecular templating in thermodynamically controlled synthesis. *Proceedings of the National Academy of Sciences of the United States of America*, 99, 4801–4804.
- [66] Liu, J., West, K. R., Bondy, C. R., Sanders, J. K. M. (2007). Dynamic combinatorial libraries of hydrazone-linked pseudo-peptides: Dependence of diversity on building block structure and chirality. *Organic and Biomolecular Chemistry*, 5, 778–786.
- [67] Poulsen, S.-A., Gates, P. J., Cousins, G. R. L., Sanders, J. K. M. (2000). Electrospray ionisation Fourier-transform ion cyclotron resonance mass spectrometry of dynamic combinatorial libraries. *Rapid Communications in Mass Spectrometry*, 14, 44–48.
- [68] Cousins, G. R. L., Furlan, R. L. E., Ng, Y.-F., Redman, J. E., Sanders, J. K. M. (2001). Identification and isolation of a receptor for *N*-methyl alkylammonium salts: Molecular amplification in a pseudo-peptide dynamic combinatorial library. *Angewandte Chemie—International Edition*, 40, 423–428.

- [69] Chung, M.-K., Hebling, C. M., Jorgenson, J. W., Severin, K., Lee, S. J., Gagné, M. R. (2008). Deracemization of a dynamic combinatorial library induced by (–)-cytidine and (–)-2-thiocytidine. *Journal of the American Chemical Society*, *130*, 11819–11827.
- [70] Chung, M.-K., Lee, S. J., Waters, M. L., Gagné, M. R. (2012). Self-assembled multi-component catenanes: The effect of multivalency and cooperativity on structure and stability. *Journal of the American Chemical Society*, *134*, 11430–11443.
- [71] Chung, M.-K., White, P. S., Lee, S. J., Waters, M. L., Gagné, M. R. (2012). Self-assembled multi-component catenanes: Structural insights into an adaptable class of molecular receptors and [2]-catenanes. *Journal of the American Chemical Society*, *134*, 11415–11429.
- [72] Voshell, S. M., Lee, S. J., Gagné, M. R. (2006). The discovery of an enantioselective receptor for (–)-adenosine from a racemic dynamic combinatorial library. *Journal of the American Chemical Society*, *128*, 12422–12423.
- [73] Dirksen, A., Yegneswaran, S., Dawson, P. E. (2010). Bisaryl hydrazones as exchangeable biocompatible linkers. *Angewandte Chemie—International Edition*, *49*, 2023–2027.
- [74] Bhat, V. T., Caniard, A. M., Luksch, T., Brenk, R., Campopiano, D. J., Greaney, M. F. (2010). Nucleophilic catalysis of acylhydrazone equilibration for protein-directed dynamic covalent chemistry. *Nature Chemistry*, *2*, 490–497.
- [75] Beeren, S. R., Pittelkow, M., Sanders, J. K. M. (2011). From static to dynamic: Escaping kinetic traps in hydrazone-based dynamic combinatorial libraries. *Chemical Communications*, *47*, 7359–7361.
- [76] Beeren, S. R., Sanders, J. K. M. (2011). Ferrocene-amino acid macrocycles as hydrazone-based receptors for anions. *Chemical Science*, *2*, 1560–1567.
- [77] Beeren, S. R., Sanders, J. K. M. (2011). Discovery of linear receptors for multiple dihydrogen phosphate ions using dynamic combinatorial chemistry. *Journal of the American Chemical Society*, *133*, 3804–3807.
- [78] Sreenivasachary, N., Lehn, J.-M. (2005). Gelation-driven component selection in the generation of constitutional dynamic hydrogels based on guanine-quartet formation. *Proceedings of the National Academy of Sciences of the United States of America*, *102*, 5938–5943.
- [79] Skene, W. G., Lehn, J.-M. (2004). Dynamers: Polyacylhydrazone reversible covalent polymers, component exchange, and constitutional diversity. *Proceedings of the National Academy of Sciences of the United States of America*, *101*, 8270–8275.
- [80] Folmer-Andersen, J. F., Lehn, J.-M. (2009). Constitutional adaptation of dynamic polymers: Hydrophobically driven sequence selection in dynamic covalent polyacylhydrazones. *Angewandte Chemie—International Edition*, *48*, 7664–7667.
- [81] Nishiyabu, R., Kubo, Y., James, T. D., Fossey, J. S. (2011). Boronic acid building blocks: Tools for self assembly. *Chemical Communications*, *47*, 1124–1150.
- [82] Suzuki, A. (2011). Cross-coupling reactions of organoboranes: An easy way to construct C-C bonds (Nobel lecture). *Angewandte Chemie—International Edition*, *50*, 6722–6737.
- [83] Nishiyabu, R., Kubo, Y., James, T. D., Fossey, J. S. (2012). Boronic acid building blocks: Tools for sensing and separation. *Chemical Communications*, *47*, 1106–1123.
- [84] Niu, W., Smith, M. D., Lavigne, J. J. (2006). Self-assembling poly(dioxaborole)s as blue-emissive materials. *Journal of the American Chemical Society*, *128*, 16466–16467.
- [85] Niu, W., O’Sullivan, C., Rambo, B. M., Smith, M. D., Lavigne, J. J. (2005). Self-repairing polymers: Poly(dioxaborolane)s containing trigonal planar boron. *Chemical Communications*, 4342–4344.
- [86] Niu, W., Rambo, B., Smith, M. D., Lavigne, J. J. (2005). Substituent effects on the structure and supramolecular assembly of bis(dioxaborole)s. *Chemical Communications*, 5166–5168.
- [87] Fujita, N., Shinkai, S., James, T. D. (2008). Boronic acids in molecular self-assembly. *Chemistry—An Asian Journal*, *3*, 1076–1091.

- [88] Colson, J. W., Woll, A. R., Mukherjee, A., Levendorf, M. P., Spitzler, E. L., Shields, V. B., Spencer, M. G., Park, J., Dichtel, W. R. (2011). Oriented 2D covalent organic framework thin films on single-layer graphene. *Science*, 332, 228–231.
- [89] Spitzler, E. L., Dichtel, W. R. (2010). Lewis acid-catalysed formation of two-dimensional phthalocyanine covalent organic frameworks. *Nature Chemistry*, 2, 672–677.
- [90] Spitzler, E. L., Giovino, M. R., White, S. L., Dichtel, W. R. (2011). A mechanistic study of Lewis acid-catalyzed covalent organic framework formation. *Chemical Science*, 2, 1588–1593.
- [91] Greig, L. M., Slawin, A. M. Z., Smith, M. H., Philp, D. (2007). The dynamic covalent chemistry of mono- and bifunctional boroxoaromatics. *Tetrahedron*, 63, 2391–2403.
- [92] Tokunaga, Y., Ueno, H., Shimomura, Y., Seo, T. (2002). Formation of boroxine: Its stability and thermodynamic parameters in solution. *Heterocycles*, 57, 787–790.
- [93] Tokunaga, Y., Ueno, H., Shimomura, Y. (2007). Formation of hetero-boroxines: Dynamic combinatorial libraries generated through trimerization of pairs of arylboronic acids. *Heterocycles*, 74, 219–223.
- [94] Tokunaga, Y., Ito, T., Sugawara, H., Nakata, R. (2008). Dynamic covalent chemistry of a boronylammonium ion and a crown ether: Formation of a C₃-symmetric [4]rotaxane. *Tetrahedron Letters*, 49, 3449–3452.
- [95] Severin, K. (2009). Boronic acids as building blocks for molecular nanostructures and polymeric materials. *Dalton Transactions*, 5254–264.
- [96] Nishimura, N., Kobayashi, K. (2008). Self-assembly of a cavitand-based capsule by dynamic boronic ester formation. *Angewandte Chemie—International Edition*, 47, 6255–6258.
- [97] Demetriades, M., Leung, I. K. H., Chowdhury, R., Chan, M. C., McDonough, M. A., Yeoh, K. K., Tian, Y.-M., Claridge, T. D. W., Ratcliffe, P. J., Woon, E. C. Y., Schofield, C. J. (2012). Dynamic combinatorial chemistry employing boronic acids/boronate esters leads to potent oxygenase inhibitors. *Angewandte Chemie—International Edition*, 51, 6672–6675.
- [98] Sakurai, H., Iwasawa, N., Narasaka, K. (1996). Synthesis of a bis(boronate) compound having *s*-indacene framework and its property as a host molecule for dimethylaminopyridine. *Bulletin of the Chemical Society of Japan*, 69, 2585–2594.
- [99] Takahagi, H., Fujibe, S., Iwasawa, N. (2009). Guest-induced dynamic self-assembly of two diastereomeric cage-like boronic esters. *Chemistry—A European Journal*, 15, 13327–13330.
- [100] Iwasawa, N., Takahagi, H. (2007). Boronic esters as a system for crystallization-induced dynamic self-assembly equipped with an “on–off” switch for equilibration. *Journal of the American Chemical Society*, 129, 7754–7755.
- [101] Iwasawa, N., Takahagi, H., Ono, K., Fujii, K., Uekusa, H. (2012). Guest-induced self-assembly of a macrocyclic boronic ester containing diarylethene units: Enhancement of photoresponsivity. *Chemical Communications*, 48, 7477–7479.
- [102] Takahagi, H., Iwasawa, N. (2010). Crystallization-controlled dynamic self-assembly and an on/off switch for equilibration using boronic ester formation. *Chemistry—A European Journal*, 16, 13680–13688.
- [103] Kataoka, K., James, T. D., Kubo, Y. (2007). Ion pair-driven heterodimeric capsule based on boronate esterification: Construction and the dynamic behavior. *Journal of the American Chemical Society*, 129, 15126–15127.
- [104] Kataoka, K., Okuyama, S., Minami, T., James, T. D., Kubo, Y. (2009). Amine-triggered molecular capsules using dynamic boronate esterification. *Chemical Communications*, 1682–1684.
- [105] Leung, I. K. H., Brown, T., Jr., Schofield, C. J., Claridge, T. D. W. (2011). An approach to enzyme inhibition employing reversible boronate ester formation. *MedChemComm*, 2, 390–395.

- [106] Dreos, R., Randaccio, L., Siega, P., Tavagnacco, C., Zangrando, E. (2010). Guest driven self-assembly of a rectangular box from methylaquacobaloxime and 4,4'-biphenyldiboronic acid. *Inorganica Chimica Acta*, 363, 2113–2124.
- [107] Hutin, M., Bernardinelli, G., Nitschke, J. R. (2008). An iminoboronate construction set for subcomponent self-assembly. *Chemistry—A European Journal*, 14, 4585–4593.
- [108] Ladame, S. (2008). Dynamic combinatorial chemistry: On the road to fulfilling the promise. *Organic and Biomolecular Chemistry*, 6, 219–226.
- [109] Huc, I., Lehn, J.-M. (1997). Virtual combinatorial libraries: Dynamic generation of molecular and supramolecular diversity by self-assembly. *Proceedings of the National Academy of Sciences of the United States of America*, 94, 2106–2110.
- [110] Bunyapaiboonsri, T., Ramström, O., Lohmann, S., Lehn, J.-M., Peng, L., Goeldner, M. (2001). Dynamic deconvolution of a pre-equilibrated dynamic combinatorial library of acetylcholinesterase inhibitors. *ChemBioChem*, 2, 438–444.
- [111] Ingerman, L. A., Cuellar, M. E., Waters, M. L. (2010). A small molecule receptor that selectively recognizes trimethyl lysine in a histone peptide with native protein-like affinity. *Chemical Communications*, 46, 1839–1841.
- [112] Rauschenberg, M., Bomke, S., Karst, U., Ravoo, B. J. (2010). Dynamic peptides as biomimetic carbohydrate receptors. *Angewandte Chemie—International Edition*, 49, 7340–7345.
- [113] Klekota, B., Hammond, M. H., Miller, B. L. (1997). Generation of novel DNA-binding compounds by selection and amplification from self-assembled combinatorial libraries. *Tetrahedron Letters*, 38, 8639–8642.
- [114] Ladame, S., Whitney, A. M., Balasubramanian, S. (2005). Targeting nucleic acid secondary structures with polyamides using an optimized dynamic combinatorial approach. *Angewandte Chemie—International Edition*, 44, 5736–5739.
- [115] Bugaut, A., Jantos, K., Wietor, J.-L., Rodriguez, R., Sanders, J. K. M., Balasubramanian, S. (2008). Exploring the differential recognition of DNA G-quadruplex targets by small molecules using dynamic combinatorial chemistry. *Angewandte Chemie—International Edition*, 47, 2677–2680.
- [116] Jantos, K., Rodriguez, R., Ladame, S., Shirude, P. S., Balasubramanian, S. (2006). Oxazole-based peptide macrocycles: A new class of G-quadruplex binding ligands. *Journal of the American Chemical Society*, 128, 13662–13663.
- [117] Grote, Z., Scopelliti, R., Severin, K. (2003). Adaptive behavior of dynamic combinatorial libraries generated by assembly of different building blocks. *Angewandte Chemie—International Edition*, 42, 3821–3825.
- [118] Mendes, P. (1997). Biochemistry by numbers: Simulation of biochemical pathways with Gepasi 3. *Trends in Biochemical Sciences*, 22, 361–363.
- [119] Severin, K. (2004). The advantage of being virtual-target-induced adaptation and selection in dynamic combinatorial libraries. *Chemistry—A European Journal*, 10, 2565–2580.
- [120] Saur, I., Severin, K. (2005). Selection experiments with dynamic combinatorial libraries: The importance of the target concentration. *Chemical Communications*, 1471–1473.
- [121] Corbett, P. T., Otto, S., Sanders, J. K. M. (2004). What are the limits to the size of effective dynamic combinatorial libraries? *Organic Letters*, 6, 1825–1827.
- [122] Corbett, P. T., Otto, S., Sanders, J. K. M. (2004). Correlation between host-guest binding and host amplification in simulated dynamic combinatorial libraries. *Chemistry—A European Journal*, 10, 3139–3143.
- [123] Ludlow, R. F., Otto, S. (2008). Two-vial, LC-MS identification of ephedrine receptors from a solution-phase dynamic combinatorial library of over 9000 components. *Journal of the American Chemical Society*, 130, 12218–12219.
- [124] Ludlow, R. F., Otto, S. (2010). The impact of the size of dynamic combinatorial libraries on the detectability of molecular recognition induced amplification. *Journal of the American Chemical Society*, 132, 5984–5986.

- [125] Orrillo, A. G., Furlan, R. L. E. (2009). Supramolecular interactions between library members modulate the behavior of dynamic combinatorial libraries. *The Journal of Organic Chemistry*, *75*, 211–214.
- [126] Ludlow, R. F., Liu, J., Li, H., Roberts, S. L., Sanders, J. K. M., Otto, S. (2007). Host-guest binding constants can be estimated directly from the product distributions of dynamic combinatorial libraries. *Angewandte Chemie—International Edition*, *46*, 5762–5764.
- [127] Hunt, R. A. R., Ludlow, R. F., Otto, S. (2009). Estimating equilibrium constants for aggregation from the product distribution of a dynamic combinatorial library. *Organic Letters*, *11*, 5110–5113.
- [128] Corbett, P. T., Sanders, J. K. M., Otto, S. (2007). Systems chemistry: Pattern formation in random dynamic combinatorial libraries. *Angewandte Chemie—International Edition*, *46*, 8858–8861.
- [129] Ludlow, R. F., Otto, S. (2008). Systems chemistry. *Chemical Society Reviews*, *37*, 101–108.
- [130] Furlan, R. L. E., Cousins, G. R. L., Sanders, J. K. M. (2000). Molecular amplification in a dynamic combinatorial library using non-covalent interactions. *Chemical Communications*, 1761–1762.

INDEX

- AA-BB supramolecular polymer, 143
AADA catenane, 408
AADD array, 132
ABCD isomer, 310
ABCE isomer, 310
ABC isomer, 310
ABDE isomer, 310
ABDE tetraprotected cyclodextrin, 310
A,B-diiodide, 307
AB-di-6-*O*-tosylates, 307
ABD isomer, 310
A,B-disulfide, 307
A-B ditosylate, 309
Abe-Inouye receptor, 297
ABE isomer, 310
Absorption tuning, 4
Acceptor-acceptor-acceptor unit, 296
Ac-D-Val-Pps-Oic-Pps-Gly-D-Leu-NH
resin, 349
ACE isomer, 310
Acetal hydrolysis, 402
Acetonitrile, 206, 217, 221
mannosides in, 300
Acetylcholine, 410, 411
Acetylcholine chloride, 426
N-Acetyl-D-galactosamine, 286
N-Acetyl-D-glucosamine, 286
N-Acetyl-D-mannosamine, 286
Acetylene, 187
Acetylene-linked pyridone/pyridine
macrocycles, 296
Acetylenic scaffolds, 7
 β -D-*N*-Acetylglucosamine, 290
S-Acetyl-4-iodothiophenole 1, 49–50
N-Acetyl neuraminic acid (NANA), 286, 297,
420
A–C functionalization of cyclodextrins, 314,
317
Acoustic cavitation, 87
Acrylates, 338
Acrylonitrile, 363
Acyclic cucurbiturils, 28–29
Acyclic tripodal receptors, 291, 292, 293
Acylation, 104
of alcohols, 337–338
of carbohydrates, 338, 340
of cyclodextrins, 310
Acylhydrazone-based DCLs, targeting
glutathione-*S*-transferase using, 418,
419
Acylhydrazone dynamic combinatorial
chemistry, 393–394
Acylhydrazone exchange reaction, 409–412
N-Acyl imine, 340
8-Acyloxyppyrene-1,3,6-trisulfonate, 337
Acyl-transfer reactions, 396
Adamantane-derived ammonium ion
guest, 401
Adamantyl-substituted ferrocene, 235
Adaptive immune system, 377
A-D-A units, 297
A-D- β -cyclodextrin diol, 314
A-D-dideoxy perbenzylated
 α -cyclodextrin, 313–314
1,2-Addition, 335
Adenine, 29
Adenosine diphosphate (ADP), 16, 18
Adenosine triphosphate (ATP), 16, 18

- Adiabatic temperature change, 183
Alanine methyl ester hydrochloride, 220–221
Alcohols
 acylation of, 337–338
 oxidation of, 325–326
Aldehydes
 allenoate addition to, 338
 cyclodextrin, 325, 326
Aldehyde tosylamide cross couplings, 338
1,4-Aldol addition, 334, 335
Aldol reaction, 335
Alkali-metal ions, 411
Alkaloids, 411
Alkane, 36
Alkylation, 95, 97, 98, 99
(E)-Alkyl 2-diazo-4-phenylbut-3-enoate, 344
N-Alkyl histidines, 337–338, 343
Allene, 36
Allenoate addition, 338
Allenoate, 342
Alligator clip principle, 47–50
2A,3A-Alloepoxy- β -cyclodextrin, 319
2,3-Alloepoxy- β -cyclodextrin derivatives, 319
Allyl palladium dichloride, 346, 348
 α -helical homo-oligo-peptides, 336
 α -helical peptide, 344
 α -helix, 33
 α -peptide, 34
Amidation, 95
Amides, 25, 217
Amidopyridol, 217
Amine-based inhibitor, identification
 of, 417–418
Amines, 307
 phosphinylation of, 349–350
Amino acids, 32–36
 α -Amino acids, 32, 355
 β -Amino acids, 34, 338, 355
D-Amino acids, 32, 34, 355
 γ -Amino acids, 355
L-Amino acids, 32, 34
 ω -Aminoalcohols, 376
Amino alcohols, synthesis from
 β -cyclodextrins, 314, 315
4-Aminodurene moiety, 186
Aminomethyl anthracene, 337
Aminomethylbenzene, 295
Aminomethylpyridine, 295
Aminomethylpyrrole units, 294–295
2-Aminophenol, 325
2-Aminophenoxazin-3-one, 325
2-Amino-2-phenylethanol, 220, 221
6-Aminopicolinic acid, 403
Aminopyrrole units, 292
Aminopyrrolic artificial receptors, 293–295
Amino-terminated G5 PAMAM
 dendrimer, 373
Amphiphilic copolymers, 205–206
Amplification factors, 393–394, 424
Anchoring groups, 47–49
AND logic gate, 16
3A,2B-Anhydro-3B-deoxy-3B-thio- β -
 cyclodextrin, 319
2,3-Anhydrocyclodextrins, 319, 320
Aniline, 418
Aniline purple, 15
Aniline yellow, 15
Anion complexation, 19–25
Anionic dendrimers, 382
Anion receptors, 412
Anion recognition, 403
 calixpyrrole-type receptors and, 266–267
Anisotropy, 247
Annulenes, 8
Anthracene, 14, 15–16, 16, 94
Anthracene-based temple, 300
Anthraquinone core, redox-active switch
 based on, 62–63
Anthraquinone guests, 231
Anthraquinones, 181
Antiaromaticity, 95
Antibiotics, dendrimers and, 383, 385
Anti-inflammatory activity of
 dendrimers, 374–375
Antimicrobial agents, dendrimers
 and, 381–385
Antimicrobial peptides, 383
Antiparallel β -sheet, 33
Antiviral agents, dendrimers and, 381–385
Antracene, 78
Applications
 of fluorescent molecules, 13
 of molecularly engineered carbon
 nanotubes and graphenes, 107–110
 of photoswitches, 9, 11
Arguengo condensation, 346
Armchair orientation, 77, 78
Aromatic hexa-acid, 135
Aromaticity, 95
Aromatic molecular fragments,
 supramolecular polymers and, 129
Aromatics, electron-deficient and
 electron-rich, 25
Arthritic diseases, dendrimers and, 374
Artificial enzymes, 28
Artificial esterase, 336
Artificial graphite, 85
Arylation, 95, 97, 98, 99

- Aryl azides, 104
 Aryl diazonium, 104
 Aryl diazonium salts, 97
 Aryl glycoside hydrolysis, 325
 Arylsulfonylation, of cyclodextrins, 306
 Arylsulfonyl chlorides, bulky, 307
 Aspartate urea, 295
 Aspartic acid, 338
 Association constants
 between blue box and TTF derivatives, 27
 carbohydrate recognition, 290–291
 estimating from DCL, 426–428
 Asymmetric tetra-TTF-calix[4]
 pyrroles, 266–270
 Atomic force microscopy (AFM), 82
 Atomic layer deposition (ALD), 105
 ATP²⁻, 219
 ATP synthase transmembrane protein, 17, 18
 Atropisomerism, 36
 Au-DENs, 370
 Autocatalytic peptide ligation, 337
 Axial chirality, 36, 37
 Azacrown ethers, 24–25
 Azidation, of substituted allylic
 carbamates, 338
 Azide, 307
 2-Azido iodides, 346
 Aziridination, 104, 105
 Azithromycin, 383, 385
cis-Azobenzene, 12, 13
trans-Azobenzene, 12, 13
 Azobenzene photoswitch, 67
 Azobenzenes, 11, 12, 13
 Azo compounds, 15
 Azomethine, 104
 Azomethine ylides, 97–98, 99
 Azo violet, 15

Bacillus subtilis, 382
 2B-3A-diol, 313
 Barbituric derivatives, 165, 168
 Base pairing, 29, 30
 Bathochromic shift, 202, 204
 Bead sorting, 337
 BEMP. *See* 2-*tert*-Butylimino-2-diethylamino-
 1,3-dimethylperhydro-1,3,2-
 diazaphosphorine (BEMP)
N-Benzyl histidine, 339
 Benzene, 8, 24, 78, 414
 Benzene-based tripodal receptors, 291, 292
 1,4-Benzene-bis-boronic acid, 412
 1,3-Benzenedithiol, 404
 Benzene-extended TTF, 63–64
 1,3,5-Benzene trisamide (BTA), 140–141, 143

 Benzo-2*H*,3*H*-oxazine ring, 199
 Benzoquinone, 7, 8
p-Benzoquinone, 263
 Benzoyl esters, 312
 Benzopyrenes, 94
 2-O-Benzylated, 319
 Benzylolation-/DIBAL-promoted debenzylolation
 methodology, 323
O-Benzyl butadienoate, 340, 342
 Benzylether dendrimers, 366
 Benzylidene formation, 321
 Benzynes, 28
 β -elimination, 309
 β -methylation, 337–338
 β -sheets, 33–34
 β -substituted *N*⁵-benzyl histidine, 338
 Biaryl atropisomers, 339–340, 341–342
 Bicomponent porous networks, 149
 Bicyclic radiannulene, 8, 9
 BINAP, 37
 Binding affinity, 424
 Binding constants, 426
 (*R*)-Binol, 221–222, 223
 (*S*)-Binol, 221–222
 Biological molecules, targeting using dynamic
 combinatorial chemistry, 416–423
 Biology, relevance of dendrimers and
 dendrons for, 366–367
 Biomedical applications, of carbon nanotubes
 and graphene, 107
 Biomimetic reactions, 152, 155, 158. *See also*
 Organozymes
 Biotin, 381
 Biphenyl, 36
 Biphenylenes, 51
 2,2'-Bipyridine (bpy), 14
tris-2,2'-Bipyridine ligands, coordination with
 Fe(II), 395
 Birch reduction conditions, 97
 2,6-Bis(acetylamino)-pyridyl moieties, 161,
 163
 Bisbenzylammonium (DBA) cation, 143
 Bis-carbene catalyst, 351, 352, 353
 Bis[2]catenanes, 406
 Bis-*cyclo*-peptide, optimization of, 404, 405,
 406
 Bis-de-O-methylation, 314
 2,5-Bis(1-hydroxymethylethyl)
 thiopheno-TTF, 268
 Bis-isoquinoline ring, 226
 Bis(*m*-phenylene)-32-crown-10-based
 cryptands (BMP32C10), 143
 Bisparaphenylene[34]crown-10
 (BPP34C10), 25

- Bisphenol, 338, 339
- Bis-phosphinyl peptide palladium, 349–350
- Bis-*p*-phenylene[34]crown-10, 406, 407
- Bis-PYBOX derivatives, 158
- Bispyrrolo-TTF BP-TTF, 25
- Bistritylation, 311
- Bis-trityl reagent, 310
- Bis-TTF-calix[2]thiophene[2]pyrrole, 268–270
- Bis-TTF-calix[2]pyrrole[2]thiophene derivatives, 266–268
- Bis-uracil modules, 151, 154
- Bixrotaxane, 227, 228
- Blood glucose monitoring, 285–286, 300
- Blue box, 25–26, 222–224
 - association constants between TTF derivatives and, 27
 - synthesis of, 26
- BMP32C10. *See* Bis(*m*-phenylene)-32-crown-10-based cryptands (BMP32C10)
- BOC. *See* *tert*-Butoxycarbonyl (BOC)-protected uracil derivative
- Boc-D-Phe-Xps-Pro-D-Val-Pps-D-Leu-OMe, 346, 349
- BODIPY/phenylboronic acid derivative, 15, 16
- Boronate-ester-based capsules, 414–416
- Boronate transesterification, 398, 412–416
- Boronate-transesterification-based DCLs, enzyme inhibitor identification and, 416, 417
- Boronic acids, 412
- Boroxine exchange, 412
- Boroxoaromatic transesterification, 412
- BPP34C10, 25
- BP-TTF, 27
- Brodie method, 85
- Bromination, peptide-catalyzed
 - asymmetric, 339–340, 341–342
 - 1-Bromoallylbromide, 321
- BTA. *See* 1,3,5-Benzene trisamide (BTA)
- Buckminsterfullerene, 7, 26, 27, 48, 54–56
- 1,4-Butanediamine, 365
- tert*-Butoxycarbonyl (BOC)-protected uracil derivative, 164–165, 166
- 2,6-di-*O-tert*-Butyldimethylsilylated cyclodextrins, 318
- tert*-Butyldimethylsilylation, 310, 318
- 2-*O-tert*-Butyldimethylsilylether, 318
- tert*-Butyldimethyl silyl ethers, 317
- 2-*tert*-Butylimino-2-diethylamino-1,3-dimethylperhydro-1,3,2-diazaphosphorine (BEMP), 351
- CA. *See* Cyanuric acid (CA)
- Calixarenes, 22, 23–24, 29
- Calix[4]arenes, 26, 215
- Calixpyrroles, 22, 24
- Calix[4]pyrroles, 26, 258–259
 - conformations, 263–264
- C-allylation, 350, 351
 - chiral, 346
- Camphorsulphonic acid, 321
- Camptothecin SN-38, 378–379
- Camptothecin, 378–379
- Camptothecin-dendrimer conjugates, 379
- Cancer, dendrimer-based delivery systems for
 - chemotherapy, 378–381
- Cancer vaccines, 378
- Cantilever-based sensors, 277–279, 280
- Capping reagents, 307–308
- Carbamates, azidation of, 338
- Carbene formation, 350–351
- Carbenes, 353, 355
- Carbohydrates
 - biomimetic recognition of, 420
 - fluorescent probe for, 15, 16
 - regioselective acylation of, 338, 340
 - sensors for, 412
- Carbohydrates, molecular recognition
 - of, 284–300
 - importance of, 284–287
 - methods, 288–299
 - circular dichroism, 296
 - isothermal calorimetry, 296–298
 - MS and liquid-liquid and liquid-solid extractions, 298–299
 - nuclear magnetic resonance, 288–295
 - UV-Vis spectroscopy, 295–296
 - noncovalent interactions, 287–288
 - research goals, 299–300
- Carbon allotropes, 2
- Carbonic anhydrase, 417–418
- Carbon nanoelectronics, 107–108
- Carbon nanoforms, 79
- Carbon nanotubes (CNTs), 76–84
 - applications, 107–110
 - characterization methods, 79–82
 - fractionation of, 84
 - functionalization of, 93–100, 96–100, 106–107
 - by metal nanoparticles, 106–107
 - multiple-wall, 77, 78, 80–81, 91
 - orientations, 77, 78
 - overview, 77–79
 - photovoltaic applications, 110
 - primary purification of, 82–84
 - reactivity of, 94–95

- sensor applications, 108–110
 single-wall, 77, 78, 80, 83, 84
 solubility of, 93–94
 synthesis of, 82
 terms and nomenclature, 77–79
- Carboxylate anions, 216–217
 Carboxylic acid, 217
 Carcerands, 28, 214
 Carciplexes, 28
 Carotene, 16–18
 CARPA. *See* Complement activation related pseudoallergy (CARPA) reaction
- Catalysis, glycosidase model for, 322–323
 Catalyst libraries, 337–338, 349, 355–356
 Catalyst recycling, 355
 Catalysts. *See also* Organozymes
 for synthesis, 333–334
 Catechol derivatives, 232
 Catecholic groups, 292
 Catenand, 25
 [2]Catenane, 401, 406, 407, 410–411
 [3]Catenane, 406, 409
 Catenanes, 25, 26, 222, 223, 224, 226, 402
 synthesis of, 406–409
 Catenate, 25
 Cation complexation, 19–25
 Cationic surfactants, 382
 Cation- π -interaction, 23–24
 Cation recognition, 403
 Caveolas, 367
 Cavitands, 214, 234–235
 CBPQT⁴⁺. *See* Cyclobis(paraquat-*p*-phenylene) (CBPQT⁴⁺)
 CBPQTP⁴⁺. *See* Cyclobis(paraquat-4,4'-biphenylene) (CBPQTP⁴⁺)
 CBPQT⁴⁺ system (blue box), 25–26, 27, 222–224
 CBs. *See* Cucurbiturils
 C-C bond formation, 351, 352, 396
 CD. *See* Circular dichroism (CD)
 CDs. *See* Cyclodextrins (CDs)
 CD spectroscopy, 426
 Cellobiose, 286
 D-Cellobiose, 287, 290, 291, 299
 Cell-surface-carbohydrate interactions, 284, 285
 Centrifugation-assisted fractionation, 84
 Cerebral palsy, PAMAM dendrimer and, 374
 Chemical vapor deposition (CVD), 82, 85, 88–90
 Chemosensors, 2, 257–258. *See also*
 Nitroaromatic explosives, detection of using tetrathiafulvalene-calix[4]pyrroles
- Chemotherapy, dendrimer-based delivery systems for, 378–381
 Chemzymes, 321–326
 glycosidases, 322–325
 oxidases, 325–326
 Chiral catalyst analogs, 349
 Chiral electrochemical recognition, 247
 Chiral induction with peptidic catalysts, 338
 Chirality, 36–37
 of carbon nanotubes, 77
 types of, 36
 Chiral recognition, electrochemical, 219–222, 223
Chlamydia trachomatis, 383
 Chlorobenzene, 216
 2-Chloromethyl-4-nitrophenol, 200
 Chromophores, 4–5, 6, 158–159, 160
 combined with redox-active units, 16–18, 21
 Chromophoric conjugate molecules, 158
 CID, molecular recognition of carbohydrates and, 298
 Circular dichroism (CD), molecular recognition of carbohydrates and, 296
 Cisplatin, 380
cis-trans isomerization, 11, 13
 Clathrin-mediated uptake, 367
 Click chemistry, 19
 Clipping method, 66
 CMC. *See* Critical micellar concentration (CMC)
 C=N exchange reactions, 396
 CNT transistors, 107
 Cobalt(3), 344–345
 Colchicine, 379
 Combinatorial evolution, 2
 Complement activation related pseudoallergy (CARPA) reaction, 367
 Complementary DNA, 237, 238
 Complexation
 cation and anion, 19–25
 π -donor-acceptor, 25–27
 Cone conformation, 263, 264
 Conformational library, 428
 Conformational rearrangement, 160, 161
 Conjugated oligomers and polymers, 37–39
 Convergent synthesis, of dendrimers, 363, 364, 366
 Cooperative binding, 26
 Cooperative supramolecular polymerization, 130

- Copper-catalyzed Huisgen 1,3-dipolar cycloadditions, 307
- Copper phthalocyanine catalyst, 190, 191
- Cotton effect, 158, 296
- Coumarin derivative, 208
- Coumarin glycosides, 324
- Coupling reactions, metal-catalyzed carbon-carbon, 10–11
- Covalent secondary functionalization, 100–103
- C-P-Q (carotene, porphyrin, and quinone), 16–18
- Crater, nano-objects with morphologies resembling, 165, 166
- Critical micellar concentration (CMC), 363
- Cross conjugation, 38–39
- [18]-Crown-6, 410
- Crown ether[18]crown-6 (18C6), 22
- Crown ether moiety, 217
- Crown ethers
 - cation and anion complexation and, 19, 22
 - pseudotaxane structures and, 143, 144
 - as receptors for π -electron-deficient guests, 25
- Crown-O6S2, 23, 24
- Crown-O6S2-DBA, 23
- Crowns, 355
- Cryptands, 22, 23, 143
- Cryptophanes, 214
- Crystal-engineering approach, 133
- CT scanning, dendrimer-based reagents for, 370
- CuAAC reaction, 19, 20, 21
- Cucurbit[7]uril (CB7), 227–230, 231, 232
- Cucurbit[8]uril (CB8), 227–228, 229, 230, 232
- Cucurbiturils, 28, 29, 214, 232, 233
- Cu(I)-catalyzed azide-alkyne cycloaddition, 19
- Cu(II) oxidation, 226–227
- Cu(I) oxidation, 227
- Cutaneous T-cell lymphoma, 380–381
- Cy5, 370
- Cyanoethyl group, 49
- Cyanoethyl-protected TTF thiolates, 9
- Cyanohydrin, 324
- Cyanurates, 165, 167
- Cyanuric acid (CA), 146–148
- Cyanuric derivative, 133
- Cyclic oligocholates receptors, 395–396
- Cyclic peptides, 34, 35, 299
- Cyclic pyranose, 285
- Cyclic voltammetry, 217, 219, 220, 221, 228, 229, 230, 233, 234, 235, 248
- Cycloaddition, 20
 - Diels-Alder [4+2], 187, 188
 - functionalization of carbon nanotubes and, 95, 97–100
 - functionalization of graphene and, 95
 - photoinduced [2+2], 186, 187
 - photoinduced [4+4], 184–185
- Cyclobis(paraquat-4,4'-biphenylene) (CBPQTP⁴⁺), 224
- Cyclobis(paraquat-*p*-phenylene) (CBPQT⁴⁺), 26, 66, 246, 406
 - molecular receptors based on, 218–219
- Cyclobutadiene, 8, 28
- Cyclodehydrogenation, 90–92
- Cyclodextrin, synthesis of bridged, 325
- Cyclodextrin acids, synthesis of, 323
- Cyclodextrin aldehydes, 325, 326
- Cyclodextrin-based artificial enzymes, 305–326
 - chemzymes, 321–326
 - functionalization on the primary rim, 305–317
 - synthesis with protected cyclodextrins, 312–317
 - unprotected cyclodextrins, 305–312
 - functionalization on the secondary rim, 317–321
 - unprotected cyclodextrins, 317–321
- Cyclodextrin cyanohydrins, synthesis of, 324
- α -Cyclodextrin-dodeca(2,3)benzoate, 312
- α -Cyclodextrin-3-His derivative, 319
- α -Cyclodextrin-6-His derivative, 319
- Cyclodextrin ketones, 325
- Cyclodextrin monoaldehydes, 309
- Cyclodextrin mono-2-*O*-tosylates, 318
- 2-*O*- α -Cyclodextrin monotosylate, 318
- Cyclodextrin monotosylates, 306–307
- β -Cyclodextrin-6-*O*-tosylate, 306
- α -Cyclodextrins, 28
 - monotosylation of, 306, 307
 - per-protected, 312
 - selective deprotection of, 312–317
 - synthesis of, 307–308
 - tritylated, 310–311
- β -Cyclodextrins, 28, 233, 234, 236, 240
 - amino alcohols synthesized from, 314, 315
 - monofunctionalization of, 318, 319–321
 - monotosylation of, 306–307
 - selective deprotection of, 312–317
 - sulfonation of hydroxyl group of, 317–318
 - synthesis of, 308, 309
 - tritylated, 310–311

- γ -Cyclodextrins, 28, 307
 selective deprotection of, 312–317
 synthesis of, 308–309
 tritylated, 310–311
 Cyclodextrins (CDs), 2, 28–29, 214, 215, 232–233
 acylations of, 310
 capping, 307–308
 commercially available, 305
 functionalization on primary rim, 305–317
 functionalization on secondary rim, 317–321
 oxidation of, 309
 per-protection of, 311–312
 synthesis with protected cyclodextrins, 312–317
 tritylated, 310
 Cyclohexane, 140
 Cyclooctatetraene, 8
 Cyclopentadienes, 187, 188
 Cyclopentenones, 100
Cyclo-peptide receptors, 403–404
Cyclo-peptides, 420
 Cyclophane
 cyclobis(paraquat-*p*-phenylene), 25
 Cyclophanes, 24, 36, 260
Cyclo-tricatechylene, 414
 Cyclotrimeratrylene, 217
 D-Cysteine, 308
 L-Cysteine, 308
 Cys-Tyr-Cys, 420
 Cytosine, 29

 DAAD array, 132
 DAAD[2]catenane, 408
 DADA array, 132
 DADA catenane, 408
 DAD-ADA array, 131
 DADD catenane, 408
 DAN. *See* Dialkyl naphthalene (DAN) derivative
 Darwinian evolution, dynamic combinatorial chemistry and, 394
 DAT. *See* Diaminotriazine (DAT)
 Davis temple architecture, 289–291, 300
 DBA. *See* Bisbenzylammonium (DBA) cation
 D-band, 79, 80
 DB24C8. *See* Dibenzo[24]crown-8 (DB24C8)
 DCC. *See* *N,N'*-Dicyclohexylcarbodiimide (DCC)
 DCLfit (software), 426, 428
 DCLs. *See* Dynamic combinatorial libraries (DCLs)
 DCLsim (software), 425, 426

 3D cuboctahedral redox-system, 244
 DDA-AAD array, 131
 Debenzylation, 312–313, 314, 316
 Defect-group generalization and functionalization, 96–97
 Demethylation of cyclodextrins, 313, 314–315, 317
 Dendralenes, 38
 Dendrimer disassembly, 379, 380
 Dendrimer-encapsulated metal nanoparticles (DENs), 370
 Dendrimer esterases, 337
 Dendrimers, 2, 39, 361–385
 anti-inflammatory activity, 374–375
 antimicrobial and antiviral agents, 381–385
 cancer and, 378–381
 dendrimer-based reagents for imaging, 369–373
 in diagnostics, 368–369
 DNA transfection, 375–376
 molecular engineering of, 383
 properties of, 361–363
 relevance to biology and nanomedicine, 366–367
 siRNA-delivery, 376–377
 synthesis of, 363–366
 toxicity of, 367–368
 vaccines and, 377–378
 Dendritic box, 362
 Dendritic polyphenylenes, 91, 92
 Dendrons, 361
 Fréchet, 363
 relevance for biology and nanomedicine, 366–367
 DENs. *See* Dendrimer-encapsulated metal nanoparticles (DENs)
 2-Deoxy-D-glucose, 286
 2-Deoxy-D-ribose, 286
 2-Deoxyglucose, 290
 2-Deoxyribose recognition, 296
 Dess-Martin periodinane, 309, 324
 Desymmetrization of diol, 349
 Detectors, 213
 Diacetylaminopyridine derivatives, 152, 154
 2,6-Di(acetylamino)-pyridyl moieties, 163, 164
 Diacetylaminopyrimidine moieties, 135
 Diagnostics, dendrimers and, 368–369
 Dialkoxynaphthalene (DNP), 223–224, 406–408
 Dialkoxynaphthalene (DNP) template, 427
 Dialkyl naphthalene (DAN) derivative, 157–158
 Dialkyl zinc, 345

- Dialkyne, 54
 Diamidopyridine module, 133, 134
 Diamine, 363
 1,4-Diaminobenzene, 48
 (*R,R*)-*trans*-1,2-Diaminocyclohexane, 293
 (*S,S*)-*trans*-1,2-Diaminocyclohexane, 293
 4,9-Diaminoperylene-quinone-3,10-diimine (DPDI), 151, 153
 2,3-Diaminopropanoic acid, 370
 Diamino-purine derivatives, 158, 161
 Diaminotriazine (DAT), 149, 151, 152, 158, 160
 Diaminotriazine functionalized (hexaphenyl) benzene derivatives, 151, 152
 Diaminotriazine moieties, 168, 169
 Diaminotriazine OPV derivatives, 168, 169
 Diamond, 76
 Diaryl phosphine chloride, 349
 DIBAL-H. *See* Diisobutylaluminum-hydride (DIBAL-H)
 Dibenzo[24]crown-8 (DB24C8), 22, 143, 226
 1,4-Dibenzoylbenzene-3',3''-disulfonyl imidazole, 318
 Dibenzylammonium (DBA), 22–24
 Di(4-bromophenyl)ethyne, 91
 2,3-di-*O*-Dibutylstanylidene, 318
 DIC. *See* Diisopropyl carbodiimide (DIC)
 Dicarboxylate derivatives, 217, 218
 1,2-Dichloroethane, 50
 Dichloromethane, 19
 Dicyanohydrins, 324
N,N'-Dicyclohexylcarbodiimide (DCC), 35, 308
 Di-*cyclo*-hexyl-[18]-crown-6, 395
 Diels-Alder [4+2] cycloaddition, 20, 187, 188
 Diels-Alder reaction, 334–335, 396, 402
 Diffusion-ordered spectroscopy, 415
 Difluoroboron dipyrromethene (BODIPY), 14, 15
 Dihydroazulene (DHA), 12, 13
 Dihydroazulene (DHA) photoswitch, 68, 69
 Dihydroazulene (DHA)/vinylheptafulvene (VHF) system, 68
 Dihydrodithienobenzene, 12, 13
 Dihydrogenphosphate, 413
 Dihydrophenanthrene, 11, 12
 Dihydropyrene, 12
 1,5-Dihydroxynaphthalene, 25
 3,4-Dihydroxyphenylacetic acid (DOPAC), 219
 1,2-Diiodoethane, 8–9
 Diisobutylaluminum-hydride (DIBAL-H), 312–313, 314, 317
 Diisopropyl carbodiimide (DIC), 35, 342
 Dimannoside receptors, 286
 Dimension VISTA 1500 Intelligent Lab System, 369
 Dimerization
 of AB-di-6-*O*-tosylates, 307–308
 of anthracene, light-induced, 184, 186
 α,α -Dimethoxytoluene, 321
N,N-Dimethylacetamide (DMA), 50
 4-Dimethylaminopyridine (DMAP), 100
 Dimethyldiazapyrenium unit, 232
 Dimethylformamide (DMF), 87, 88, 312
N,N-Dimethylformamide (DMF), 19
 Dimethyl sulfoxide (DMSO), 309, 312, 411
N,N-Dimethylthiocarbonyl chloride, 50
 9,10-Dimethyltriptycene, 242
 Dimethylviologen (DMV), 225–226
 1,5-Dinaphthol[38]-crown-10, 406
 3,5-Dinitrobenzoylchloride, 273
 Dinitro-bipyridyl core, molecular switch synthesis based on, 62
 Dinitrogen tetroxide, 181
 2,4-Dinitrotoluene (DNT), detection of, 278
 1,2-Diols, 412, 414
 1,3-Diols, 412
 Diols, desymmetrization of, 349
 Diphenylchlorophosphate, 342, 343
 Diphenylmethane-*p,p'*-disulfonylchloride, 307–308
 2-Diphenylphosphineyl phenyl methylamine, 345
 1,3-Dipolar cycloaddition, 19, 20
 Diquat, 228–229
 Direct exfoliation, 87–88
 Directional complementary couples, 129
 Disaccharide receptors, 286
 Disaccharide recognition, 287, 298–299
 in water, 290, 298
 Disaccharides, 285
 Distamycin, 422
 2,3-Disubstituted indole derivatives, 342
 1,4-Disubstituted triazole, 19
 Disulfide DCLs, 397
 dithiol building blocks in, 398–403
 Disulfide exchange, 396, 397, 403, 408–409
 Dithienylethene, 11, 12, 13
 Dithienylethene photoswitch, 67, 68
 1,4-Dithiobenzene, 48
 Dithiol 6, 402
 Dithiol building blocks, 427
 in disulfide DCLs, 398–403
 1,3-Dithiolium rings, 6
 1,3-Dithiolylidene moieties, 215
 Dithiothreitol, 409
 Ditosylation, 307

- Divergent synthesis, of dendrimers, 363, 364, 365
- DMF. *See* Dimethylformamide (DMF)
- DMSO. *See* Dimethyl sulfoxide (DMSO)
- DMV. *See* Dimethylviologen (DMV)
- DNA
- G-quadruplex, 412, 420–423
 - hydrogen-bonded dimers and, 29–31
 - oxidative cleavage of, 344
- DNA- β -CD conjugate, 238–239
- DNA dendrimers, 368
- DNA hybrid, 158, 160
- DNA-programmed assembly of nanostructures, 69
- DNA pseudoknot, 237, 238
- DNA recognition, 420–423
- DNA transfection, dendrimers and, 375–376
- DNP. *See* Dialkoxynaphthalene (DNP)
- DNT. *See* 2,4-Dinitrotoluene (DNT)
- Dodecyl β -D-maltoside, 287
- Dodecyl- β -maltoside, 296
- Donor-acceptor catenanes, 406–408
- Donor-acceptor dyad salt synthesis, 60, 61
- Donor-acceptor mechanically interlocked molecules, 404–409
- Donor-acceptor norbornadienes, 191, 192
- DOPAC. *See* 3,4-Dihydroxyphenylacetic acid (DOPAC)
- DOTA ligands, 370
- DOTA-type ligands, 370
- Double-strand DNA, 240, 241
- Downhill polymerization, 130
- Doxil, 367
- Doxorubicin, 367, 379–380, 381
- DPDI. *See* 4,9-Diaminoperylene-quinone-3,10-diimine (DPDI)
- Drug delivery, dendrimers and dendrons and, 361, 366–367
- Drug discovery, DCLs and, 423
- Duplex DNA binder, 420–421, 422
- Dyes, 13–19
- Dye-sensitized solar cells (DSSC), 110
- Dynamers, 412
- Dynamic combinatorial chemistry, 3, 393–429
- boronate ester exchange in, 412–416
 - disulfide building blocks and, 398–403
 - donor-acceptor mechanically interlocked molecules from dynamic combinatorial libraries, 404–409
 - hydrazone-based dynamic combinatorial libraries, 409–412
 - introduction to, 393–398
 - modeling dynamic combinatorial libraries, 423–428
 - optimization of known receptors using, 403–404
 - reactions for, 396
 - targeting biological molecules using, 416–423
- Dynamic combinatorial libraries (DCLs), 393.
- See also* Disulfide DCLs
 - compositions of, 393–394
 - DCL simulations to optimize library design, 423–426
 - donor-acceptor mechanically interlocked molecules from, 404–409
 - estimating association constants directly from, 426–428
 - hydrazone-based, 409–412
 - modeling of, 423–428
 - pseudopeptide, 398
 - receptor recognition properties, 397
 - supramolecular catalysts from, 402
 - targeting biological molecules and, 416–423
 - template adjustable, 395
 - templates and, 393–395, 397, 423–425, 426–428
 - thermodynamic equilibrium in, 393, 397–398, 409
- Escherichia coli*, 383
- Effectors, 213
- 18C6, 22, 26
- Elecsys, 369
- Electrical energy, storage technologies, 179–180
- Electroactive guests, 227–236
- Electrochemical chiral recognition, 219–222, 223
- Electrochemically triggered macrocyclic systems, 222–227, 228
- interlocked assemblies based on organic compounds, 222–226
 - interlocked assemblies based on transition metals, 226–227, 228
- Electrochemical sensors, MPTTF and, 260
- Electrocyclic reactions, 13
- Electron acceptors, 7
- Electron-deficient aromatics, 25
- Electron donors, 7
- Electron-rich aromatics, 25
- Electrostatic interactions, 128
- Elongation direction, supramolecular polymers with H-bonds perpendicular to, 143–149
- Elongation phase, 130

- Encapsulation
 of instable compounds, 28
 of organic molecules in water, 28–29
- End groups, of dendrimers, 361
- Endocytosis, cellular uptake of, 367
- Energy
 renewable, 179 (*See also* Molecular solar thermal (MOST) systems)
 storage technologies, 179–180, 183
- Energy consumption, world, 179
- Energy release, in MOST systems, 190–191
- Enhanced permeation retention (EPR)
 effect, 378
- Enzyme inhibitor, identification of, 416, 417
- Enzymes, 333. *See also* Artificial enzymes;
 Cyclodextrin-based artificial enzymes;
 Organozymes
 GST, 418, 419
- Epitaxial growth from SiC, 88–89
- Epoxidation, 326, 336, 338, 342
- EPR. *See* Enhanced permeation retention (EPR) effect
- Erythromycin, 383, 385
- D-Erythrose, 335
- ESI, molecular recognition of carbohydrates
 and, 298
- Esterification, 95
- 1,2-Ethanediamine, 365
- 1,2-Ethanedithiol, 404
- Ethylene diamine, 242
- Evaporation-induced organization
 process, 148–149
- Exfoliation
 direct, 87–88
 reduced graphene oxide by
 oxidative, 85–87
- Exocomplexation, 361–362
- Expanded [6]radialene, 7
- Explosives, detecting. *See* Nitroaromatic
 explosives, detection of using
 tetrathiafulvalene-calix[4]pyrroles
- Extended Π -systems, 270–272
- Extended-tetrathiafulvalene (exTTF)
 derivatives, 215–216
- Fe-based catalysts, 355
- Ferrocene (Fc)
 modulation of electrochemical
 behavior, 237–238
 molecular receptors based on, 216–217
- Ferrocene (Fc)- β -cyclodextrin
 recognition, 238–239
- Ferrocene (Fc)-CD associations, 232–233
- Ferrocene (Fc) derivatives, 235–236
- Ferrocene (Fc)-DNA- β -cyclodextrin
 conjugate, 237–239
- Ferrocene (Fc)-hydrazone-based ditopic
 receptor, 428
- Ferrocene (Fc) redox probes, 244, 245
- α -Ferrocenylalkylurea-based chiral
 receptors, 221
- (Ferrocenylmethyl)tempammonium
 guests, 230–231
- Feynman, Richard P., 2
- Fidel-Crafts C-alkylation, 335–336
- Flow field-flow fractionation, 84
- Fluophores, 198–199
- Fluorescein, 14
- Fluorescence, activation with fluorophore-
 oxazine dyads, 200–205
- Fluorescence imaging at nanoscale, 197–198
- Fluorescence switching with photochromic
 oxazines, 11, 197–209
 design and assembly of photoswitchable
 nanoparticles, 205–207
 design and synthesis of fluorophore-oxazine
 dyads, 199–200
 fluorescence activation with fluorophore-
 oxazine dyads, 200–205
 fluorescence imaging at nanoscale, 197–198
- Fluorescent probes for carbohydrates, 15, 16
- Fluoride, detection of, 369
- Fluorophore-oxazine dyads
 design and synthesis of, 199–200, 201
 fluorescence activation with, 200–205
- Fluorophore-photochrome dyads, 202–204,
 206–207, 208
- Fluorophores, 4, 13–19
- Folic acid, 374, 379
- Förster resonance energy transfer
 (FRET), 353
- Fractionation of carbon nanotubes, 84
- Fréchet dendron, 363
- Fréchet wedges, 366
- Free energy, H-bonds and, 131
- FRET. *See* Förster resonance energy transfer
 (FRET)
- Friedel-Crafts acylation, 104
- D-Fructose, 16
- L-Fucose, 286
- Fulgide, 12
- Fullerene C60, 93
- Fullerene chemistry, 76–77
- Fullerenes, 76, 93, 244, 247
 reactivity, 94–95
 solubility, 93–94
- Fulvalene diruthenium systems, 11, 188–190
 (Fulvalene)tetracarbonyldiruthenium, 188

- Functionalization
- of carbon nanotubes, 93–96, 96–100, 101
 - cycloadditions, 97–100
 - defect-group generation and functionalization, 96–97
 - by metal nanoparticles, 106–107
 - noncovalent functionalization, 100, 102
 - sidewall alkylation and arylation, 97, 98, 99
 - of graphene, 93–96, 100–106
 - additions using nonoxidizing reagents, 104
 - by metal nanoparticles, 106–107
 - noncovalent functionalization, 104–106
 - oxidation and covalent secondary functionalization, 100–103
 - reduction, 103–104
 - primary, 95–96
 - secondary, 95, 96
- Functionalization toolbox, 95–96
- Furanose rings, 285
- Gadomer-system, 372
- D-Galactose, 16, 286
- α -D-Galactoside, 287
- β -D-Galactoside, 287
- G5 amino-terminated PAMAM dendrimers, 370
- Gas-phase oxidation, 82
- G-band, 79–80
- Gd-chelates, 372–373
- GFP. *See* Green fluorescent protein (GFP) chromophore
- Gibbs free energy of dimerization, 29–30, 31
- Glaser-Eglinton-Hay reaction, 10
- Glucocorticoids, dendrimers as drug-delivery system for, 374
- D-Glucose, 16, 286, 290, 291
- Glucose-selective receptors, 300
- Glucose sensors, 285–286
- α -D-Glucoside, 287
- β -D-Glucoside, 287
- β -Glucuronidase-induced cleavage, 379
- Glutathione, 422
- Glutathione *S*-transferase (GST) class of enzymes, 418, 419
- Glycerol, 382
- Glyoclusters, 371, 372
- Glycodendrimers, 383
- Glycoluril, 28
- Glycosidases, 322–325
- Glycoside hydroxylases, 322–325
- Gold, interaction between thiols and, 106–107
- G-quadruplex DNA, 412, 420–423
- Graphene. *See also* Reduced graphene oxide (RGO)
 - applications, 107–110
 - defined, 77
 - by direct exfoliation, 87–88
 - formation of, 103–104
 - functionalization of, 93–96, 100–106, 100–107
 - by metal nanoparticles, 106–107
 - large-area, by CVD, 88–90
 - nanographenes, 90–92
 - reactivity of, 94–95
 - on SiO₂, 103–104
 - solubility of, 93–94
 - synthesis of, 84–85
- Graphene electronics, 108–110
- Graphene nanoribbons (GNRs), 90, 91
- Graphite, 76
- Graphite oxide (GO), 77
 - photovoltaic applications, 110
 - preparation of, 85–86
- Green fluorescent protein (GFP) chromophore, 5, 6, 14
- GST. *See* Glutathione *S*-transferase (GST) class of enzymes
- G-tetrads, 420
- G3 triethanolamine-cored dendrimer, 376, 377
- Guanidiniums, 30, 31
- Guanine, 29
- Hamilton-type receptor, 133
- H-bond acidity, functionalization of carbon nanotubes and, 101
- H-bond-based nanostructuration of supramolecular organic materials, 128–170
- 1D H-bonded nanostructured materials, 133–149
 - H-bonded supramolecular main-chain polymers, 133–143
 - supramolecular polymers with H-bonds perpendicular to the elongation direction, 143–149
- 2D H-bonded networks, 149–155
- H-bond discrete nanostructures, 155–170
 - nontemplated self-organized systems, 161–170
 - templated supramolecular systems, 157–161
- principles in H-bonded soft matters, 129–133
- H-bond basicity, functionalization of carbon nanotubes and, 101

- H-bond discrete nanostructures, 155–170
 nontemplated self-organized systems, 161–170
 templated supramolecular systems, 157–161
- H-bonded nanofibers, 147
- H-bonding binding groups, 292
- H-bond recognition systems, 133–143
- H-bonds, 128–129
 defined, 131
 free-energy association and, 131
- H-bond templated chromophoric stacks, 158, 160
- Heat release, in MOST, 183
- Heck reaction, 10
- Helical chirality, 36
- Helical nanostructures, 148–149
- Helical stacked structures, 158, 160
- Helicene, 36
- Helicene derivatives, 143, 146
- p*-Helix channel, 157
- Helices, 128
- Hemicarceplexes, 28
- Hemicarcestrand, trapping of cyclobutadiene in, 28
- Henry reaction, 396
- Hepatitis C virus, mannose and, 286
- Heptakis(6-*O*-pivaloyl)- β -cyclodextrin, 321
- Heptakis(6-*O*-*tert*-butyldimethylsilyl)- β -cyclodextrin, 318, 319
- Herpes simplex, 382
- Heterocycle catalysts, 350, 351
- Heterodinuclear macrocycle, 226
- Hetero-oligomers, 424–425
- Hexa-acid, 135, 138
- Hexahomotrioxacalix[3]arene, 414–415
- Hexakis(6-*O*-acetyl-2,3-di-*O*-benzyl)cyclomaltohexaose, 312
- 1,6-Hexanedioic acid, 403
- β -Hexapeptide, 34
- Hexose recognition, 296
- Highest occupied molecular orbital (HOMO), reactivity and, 94–95
- Highest occupied molecular orbital-lowest unoccupied molecular orbital (HOMO-LUMO) gap, 38, 46, 51
- Highly ordered pyrolytic graphite (HOPG), 81, 85, 100, 103, 146
- Highly ordered pyrolytic graphite (HOPG) surface, 158
- High-performance liquid chromatography, analysis of dynamic combinatorial libraries and, 393–394
- High pressure carbon monoxide (HiPco) method, 82, 84
- Histone peptide, 418–419
- HIV. *See* Human immunodeficiency virus (HIV)
- HOBt. *See* 1-Hydroxybenzotriazole (HOBt)
- HOMO. *See* Highest occupied molecular orbital (HOMO)
- HOMO-LUMO. *See* Highest occupied molecular orbital-lowest unoccupied molecular orbital (HOMO-LUMO) gap
- Homo-oligomers, 424–425
- Honeycomb structure, 151, 152, 153
- Hoogsteen base pairing, 420
- HOPG. *See* Highly ordered pyrolytic graphite (HOPG)
- Horner-Wadsworth-Emmons olefination reaction, 53–54
- Host-guest complexation, 4
- HP β CD. *See* Hydroxypropyl- β -cyclodextrins (HP β CD)
- Huisgen reaction, 19, 97
- Human colon carcinoma (HT-29) tumor models, 379
- Human colorectal carcinoma cell line HCT-116, 378
- Human immunodeficiency virus (HIV), 286, 382
- Human immunodeficiency virus (HIV) vaccine, 378
- Hummers oxidation, 86
- Hydrazides, 418, 419
- Hydrazine, 86, 307
- Hydrazone-based dynamic combinatorial libraries, 409–412
- Hydrazone exchange chemistry, 398, 409–412, 418
- Hydrazone macrocycles, 426
- Hydrazones, 396
- Hydrogels, 412
- Hydrogen-bonded dimers, 29–31
- Hydrogen peroxide, 336
- Hydrolysis
 of glycosides, 323
 of 4-nitrophenyl acetate, 336–337
- Hydroquinone, 7, 8, 25
- 1-Hydroxybenzotriazole (HOBt), 308
- 4-Hydroxybenzylideneimidazolinone, 5
- 2-Hydroxy-cyclodextrin, 314
- 3-Hydroxy-cyclodextrin, 314
- 3-Hydroxy-4-dimethylaminomethyl-2-(1H)-pyridone, 424
- 2-Hydroxyethylamides, 374
- O-2 Hydroxyl groups, 310
- Hydroxyl groups, cyclodextrins and, 305, 306–309, 310–312, 317–321

- Hydroxyl protection, 310–312
 Hydroxymethyl diphenylphosphine, 349–350
 Hydroxypropyl- β -cyclodextrins (HP β CD), 233, 324
 Hysteresis effect, 66
- Imaging, dendrimer-based reagents
 for, 369–373
 CT scanning, 370
 imaging using radioactive isotopes (PET and SPECT), 370, 371, 372
 MRI, 370–373
 optical probes, 373
- Imidazole, 307
 Imidazolic groups, 292
 Imidic systems, 133, 134
 Imine exchange, 416
 Imines, 340, 342, 396, 417–418
 Immune system, 367, 377
 Immunotoxicity, 367
 Incident laser light, 39
 Indigo, 15
 2*H*,3*H*-Indole heterocycle, 199
 Indole oxidation, 342
 Indolic groups, 292
 3*H*-Indolium chromophore, 200, 202, 203–204
 Indolylum/phenolate, 12
 Indolyl moiety, 343
 Infrared spectroscopy (IR), 79
 Inkjet printing, 108
 Innate immune system, 367, 377
 Inositol, 340, 342
 Inouye receptor, 296
 In-plane lattice defects, 90
 Instable compounds, encapsulation of, 28
 Insulin-like growth factor 1, 370
 Interlocked assemblies
 based on organic compounds, 222–226
 based on transition metals, 226–227, 228
 Iodobenzene, 50
 Ionic guests, recognition of, 213–214
 Ion pair recognition, 403
 Irinotecan, 379
 Iron thiolate aryldiisocyanide metallo-cyclic structure, 24, 245
 Isodesmic supramolecular polymerization, 130
 Isonitrile group, 48
 Isothermal calorimetry (ITC), 291
 molecular recognition of carbohydrates and, 296–298
 Isothermal titration calorimetry, 426
 ITC. *See* Isothermal calorimetry (ITC)
- J-aggregates, 139, 140
 Janus dendrimer, 382
 Jorgensen model, 29–30, 31
- 2-Keto-3-deoxy-nononic acid, 286
 Ketone 15
 oxidation and, 325
 synthesis of, 325
 Ketones, cyclodextrin, 325
 Kinetic traps, 397, 412
- Langmuir-Blodgett films, 59, 66
 Lanthanides, 355
 Large-area graphene by chemical vapor deposition, 88–90
 LC-MS, 426
 LDA. *See* Lithium diisopropylamide (LDA)
 Lectins, 288
 Light, switch molecules and, 66–69
 Light harvesters, 13–19
 Light optical microscopy (LOM), 82
 Limonene, 181
 Linear conjugation, 38–39
 α -1,4-Linked D-glucosyl units, 305
 Linked anthracenes, 181, 184–186, 187
 1-4-Linked disaccharides, 299
 Lipinski rule of five, 366
 Liquid crystallinity, 11
 Liquid crystals, 140
 Liquid-liquid extractions, 298–299
 Liquid-phase oxidation, 82–84
 Liquid-solid extractions, 298–299
 Lithium diisopropylamide (LDA), 8, 54
 Locked nucleic acid (LNA)
 nucleotides, 31–32, 34
 Logic gates, 15–16
 Lowest unoccupied molecular orbital (LUMO), 47–48
 reactivity and, 94–95
 Lysine-based dendrimers, 382
- Macrocycles
 with hydrophobic cavities, 28–29
 monopyrrolo-TTF, 260–263
 Macrocyclic host molecules, 19–29
 cation and anion complexation, 19–25
 encapsulation of instable compounds, 28
 encapsulation of organic molecules in water, 28–29
 π -donor-acceptor complexation, 25–27
 Macrocyclic receptors, 400–402. *See also* Supramolecular redox transduction
 Macrocyclic systems, electrochemically triggered, 222–227, 228

- Macrolactone formation, 308
 Macropinocytosis, 367
 Magainin-2, 383, 384
 Majoral—Caminade-type dendrimers, 374
 Maleimide, 334–335
 Maltose, 286
 2A-3A-Mannoepithio derivative, 319
 2,3-Manno-epoxide, 319
 Mannose, 386–287
 D-Mannose, 286
 Mannose-binding systems, 300
 α -D-Mannoside, 287
 β -D-Mannoside, 287
 Mannoside recognition, 294
 Mannosides, in acetonitrile, 300
 2,3-Manoepoxy- β -cyclodextrin derivatives, 319
 Material sciences, electroactive macrocyclic receptors and, 247, 248
 Mauveines, 15
 MCH solution, 165
 Measles-mumps-rubella (MMR) vaccine, 377
 Mechanically controlled microscopy break junctions (MCBJs), 47–48
 Mechanically interlocked molecules, 398, 404–409
 Melamine, 149, 151–152, 154
 Melamine-functionalized calix[4]arene, 161, 162
 Melanocortin-concentrating hormone (MHC), 345
 Merocyanine, 12, 161, 162
 Mesitylenedisulfonyl chloride, 307
meta-anchoring, 39
meta-benzene system, 51
meta cross conjugation, 39
 Metacyclopentadiene, 12
 Metal-catalyzed carbon-carbon coupling reactions, 10–11
 Metal-ligand exchange, 416
 Metallic CNTs, 107
 “Metallic” tubes, 94–95
 Metal nanoparticles, functionalization of graphene and carbon nanotubes by, 106–107
 Metals. *See also* Transition metals
 self-assembled macrocyclic redox-active receptors and, 240, 242–245
 Methanesulfonic acid, 258
 Methanol, 414, 415
 Methotrexate, 374, 378, 379
 8-Methoxy psoralene, 380–381
 3A-O-Methyl, 314, 317
 Methyl α -D-fucoside, 287, 298
 Methyl α -D-glucoside, 290, 291
 N-Methylated morphine, 399, 400
 6-O-Methylated perbenzylated α -cyclodextrin, 313
 Methyl β -D-cellobioside, 287, 290, 291
 Methyl β -D-glucoside, 290, 291, 292
 N-Methyl-4-chloromethyl-2-nitroaniline, 319
 α -D-Methylfucopyranoside (MFP), 420
 N-Methyl histidine, 338, 340
 N-Methylimidazoles, 422
 2-Methylisoquinolinium iodide, 399, 400
 α -Methyl-Leu oligomers, 336
 Methyl orange, 15
 Methylphosphine transfer, *O*- to *N*-, 349–350
 Methylprednisolone, 374
 N-Methylpyrroles, 422
 3-(N-Methylthiazolium-4-yl)alanine, 338
 MFP. *See* α -D-Methylfucopyranoside (MFP)
 MHC. *See* Melanocortin-concentrating hormone (MHC)
 Michael addition, 345
 dendrimer synthesis and, 363–364, 365
 1,4-Michael addition, 334
 m-nitrophenyl tosylate, 318
 Molecular electronics, design and synthesis of organic molecules for, 46–69
 organic molecular rectifiers, 59–61
 organic molecular switches, 61–69
 organic molecular wires, 47–59
 Molecular engineering
 amino acids, 32–36
 chirality and, 36–37
 conjugated oligomers and polymers, 37–39
 of dendrimers, 383
 DNA and hydrogen-bonded dimers, 29–31
 dyes, 13–19
 fluorophores, 13–19
 light harvesters, 13–19
 macrocyclic host molecules, 19–29
 modified oligonucleotides, 31–32
 molecular function, 4–5
 nonlinear optical chromophores, 39–40
 overview, 1
 photo/thermoswitches, 9–13
 redox-active units, 5–9
 Molecular functions, 4–5, 6
 Molecular knots, 25
 Molecular properties, 4
 Molecular receptors incorporating redox-active subunit, 215–219
 Molecular rectifiers, organic, 59–61

- Molecular solar thermal (MOST)
 systems, 179–192
 energy profile for, 180
 energy release, 190–191
 energy storage, 183
 engineering challenges, 181–184
 heat release, 183
 molecular systems, 184–190
 fulvalene diruthenium system, 188–190
 linked anthracenes, 184–186, 187
 norbornadiene-quadracyclane
 system, 186–188, 189, 190, 191, 192
 stilbene systems, 184, 185, 186
 outlook, 191–192
 photochemistry, 181–183
 stability and availability, 184
 stability tests, 191, 192
- Molecular switches, organic, 61–68
- Molecular transistors, 61, 62
- Molecular weight, of dendrimers, 361
- Molecular wires, organic, 47–59
 synthesis and properties of, 50–59
 terminal connectivity, 47–50
- Monoalkylations, 319
- Monofunctionalization, of
 β -cyclodextrins, 319–321
- 3-O-Mono-modified cyclodextrin, 319
- Mono-6-O-tosylation, 306
- Monopivaloylation, 318
- Monopyrrolo-TTF (MPTTF), 27, 260, 264
- Monopyrrolo-TTF (MPTTF)
 macrocycles, 260–263
- Monopyrrolo-TTF (MPTTF)-PEG, 25, 27
- Monosaccharides, 285, 287. *See also individual monosaccharides*
 most common natural, 286
 recognition in water, 290
- Mono-*tert*-butyldimethylsilylation, 318
- Monothiols, 423
- Monotosylation, 306–307
 of heptakis-6-*O*-(*tert*-butyldimethylsilyl)- β -cyclodextrin, 318
- Moore's law, 2
- MPTTF. *See* Monopyrrolo-TTF (MPTTF)
- MRI, dendrimer-based reagents for,
 370–373
- MS, molecular recognition of carbohydrates
 and, 298–299
- Multiple antigen peptide (MAP)
 dendrimers, 377–378
- Multiwall carbon nanotubes (MWCNTs), 77,
 78, 80–81, 91, 101, 236, 240
 applications, 110
 functionalization of, 97
- Myocardial infarction, detection of biological
 markers of, 369
- NAc D-glucosamine, 290, 291
- Nace reaction, 309
- NADH coenzyme, 37
- Nadifloxacin, 385
- NANA. *See* N-Acetyl neuraminic acid
 (NANA)
- Nanofibers, 2, 140
- Nanographene propellers, 91
- Nanographenes
 by organic synthesis, 90–92
 ozone treatment of, 102, 103
- Nanographite discs, 91
- Nanomaterials, 128
- Nanomedicine, relevance of dendrimers and
 dendrons for, 366–367
- Nanoparticles, 128, 133
 photoswitchable, 205–207, 209
- Nanorings, 133, 165, 168
- Nanorods, 140
- Nanoscale electronics, 46
- Nanostructures, H-bond discrete, 155–170
- Nanotechnology, 1
- Nanotubes, from cyclic peptides, 34, 35
- Nanovesicles, 128, 161, 163–164
- Naphthalene, 94
- Naphthalene chromophores, 158, 160
- Naphthalenediimide (NDI), 406, 407
- Naphthalenediimide (NDI) building
 block, 427–428
- Naphthalenediimide (NDI)
 derivatives, 157–158
- Naphthalenedithiol, 401
- β -Naphthalenesulfonyl chloride, 318
- 1-Naphthoic acid, 412
- Naphthalene derivatives, 158, 160
- Naphthalensulfonate groups, 382
- NBD. *See* Nitrobenzodiazole (NBD)
- NBI. *See* N-unsubstituted naphthalene
 bisimide (NBI) derivatives
- NDI. *See* Naphthalenediimide (NDI)
- Negishi reaction, 10–11
- Neutral guests, recognition of, 213
- NHCs. *See* N-Heterocyclic carbenes (NHCs)
- N-Heterocyclic carbene (NHC)-palladium
 catalysts, 351
- N-Heterocyclic carbenes (NHCs), 346, 348
- N-H $\bullet\bullet\bullet$ X $^-$ interactions, 266
- Ni(II/III) oxidation, 226
- Ni tetraazamacrocyclic mononuclear unit, 242
- Nitrile, dendrimer synthesis and reduction
 of, 363, 364

- Nitroaromatic explosives, detection of using
 tetrathiafulvalene-calix[4]
 pyrroles, 257–280
 asymmetric tetra-TTF-calix[4]
 pyrroles, 266–270
 calix[4]pyrroles, 258–259
 extended Π -systems, 270–272
 MPTTF macrocycles, belts, and
 cages, 260–263
 potential application, 273–279, 280
 self-complexation and switching, 272–273
 symmetric tetra-TTF-calix[4]
 pyrroles, 263–266
 tetrathiafulvalene, 259–260
- Nitrobenzodiazole (NBD), 370, 371
- 2-Nitroketones, 338
- 4-Nitrophenoxy chromophore, 200, 204
- 4-Nitrophenyl acetate, hydrolysis of, 336–337
- 4-Nitrophenyl α -D-glucopyranoside, 324
- 4-Nitrophenyl β -D-glucopyranoside, 324
- Nitro-substituted oligophenylene (OP), 50–51
- Nitrosyl chloride, 181
- NMP, 87, 88
- NMR. *See* Nuclear magnetic resonance (NMR)
- Noble metal catalysts, 355–356
- Noncovalent functionalization
 of carbon nanotubes, 100, 102
 of graphene, 104–106
- Noncovalent interactions
 carbohydrate recognition and, 287–288
 use of template molecules, 157
- Nonlinear optical (NLO)
 chromophores, 39–40
- Nonpolar adsorption, functionalization of
 carbon nanotubes and, 101
- Nontemplated self-organized
 systems, 161–170
- Norbornadiene-quadracyclane system, 181,
 186–188, 189, 190, 191, 192
- N-terminal aspartic acid side chain,
 decarboxylation of, 344–345
- Nuclear magnetic resonance (NMR), 426
 molecular recognition of carbohydrates
 and, 288–295
- Nuclear Overhauser effect, 415
- Nucleic acids
 biomimetic exploitation of oligomeric, 158
 redox-recognition/transduction with, 236–
 240, 241
- Nucleophilic Michael addition, 338, 339
- Nucleotides, 31–32
- N-unsubstituted naphthalene bisimide (NBI)
 derivatives, 168, 169, 170
- Octaacid cavitand, 234
- Octameric [2]catenane, 401
- Octyl β -D-galactoside, 291
- Octyl β -D-glucopyranoside, 340
- Octyl β -D-glucoside, 292, 295, 296
- Octyl β -D-mannoside, 292, 293
- Octyl β -galactoside, 295, 296
- p*-Octyphenyl rod molecule, 157
- ODCB. *See* Orthodichlorobenzene (ODCB)
 solution
- OFETs. *See* Organic field-effect transistors
 (OFETs)
- Olefin, 336
- Olefin metathesis, 396
- Oligoadenylic eicosamer, 158
- Oligoborane esters, 414
- Oligomers, conjugated, 37–39
- Oligonucleotides, modified, 31–32
- Oligo(phenyleneethynylene) (OPE), 50–54,
 57, 58–59, 165, 167
- Oligo(phenyleneethynylene) (OPE)
 derivatives, 140, 142
- Oligo(phenyleneethynylene) (OPE)-like
 molecular rectifier, 60, 61
- Oligo(phenylenevinylene) (OPV), 50–51,
 53–54, 56, 58–59, 146–148, 150
- Oligo(phenylenevinylene) (OPV)
 derivatives, 168, 169
- Oligo(thiopheneethynylene) (OTE), 54–55
- Oligothiophenes, 54
- 1,2-alternate conformation, 263, 264
- 1,3-alternate conformation, 263, 264, 268,
 271
- 1D H-bonded nanostructured
 materials, 133–149
 H-bonded supramolecular main-chain
 polymers, 133–143
 supramolecular polymers with H-bonds
 perpendicular to the elongation
 direction, 143–149
- OPE. *See* Oligo(phenyleneethynylene)
 (OPE)
- OPE5-TTF cruciform-like molecular
 switch, 63–64, 65
- Opsin proteins, 4–5, 6
- Optical probes, 373
- Optical sensors, 15
- OPV. *See* Oligo(phenylenevinylene) (OPV)
- Organic compounds, interlocked assemblies
 based on, 222–226
- Organic field-effect transistors (OFETs), 247
- Organic guest molecules, redox-recognition/
 transduction with, 215–222, 223
- Organic light-emitting diodes (OLEDs), 38

- Organic molecules
 responsive receptors for, 214. *See also*
 Supramolecular redox transduction
 in water, encapsulation of, 28–29
- Organic synthesis, 1
 for organic molecular rectifiers, 59–61
 for organic molecular switches, 61–69
 for organic molecular wires, 47–59
- Organozymes, 2, 333–356
 outlook, 353–356
 peptide mimetic metal complexes, 344–353
 peptides in organocatalysis, 334–344
- Orientations, of carbon nanotubes, 77
- Orthodichlorobenzene (ODCB) solution, 135
- OTE. *See* Oligo(thiopheneethynylene) (OTE)
- Ouroboros, 238, 273
- Output signal, 213
- Ovarian cancer cells, 380
- Oxazine rings, 199–200, 201, 206–207, 208
- Oxazines, 11, 12
- Oxazole-peptide macrocycle, 422–423
- Oxazoline, 350
- 2,6-bis(2-Oxazolyl)pyridine (PYBOX)
 moieties, 158
- Oxidases, 325–326
- Oxidation
 of alcohols, 325–326
 of cyclodextrins, 309
 functionalization of carbon nanotubes
 and, 95–96
 functionalization of graphene and, 95–96,
 100–103
 ketone 15 and, 325
 of tetrathiafulvalene, 259
 thiol, 397
- Oxidative cyclodehydrogenation, 90–92
- Oxidative exfoliation, 85–87
- Oximes, 396
- Oxypyrrolic groups, 292
- PAF. *See* Proton-activated fluorescence (PAF)
- Palladium ligands, 345, 346
- Palladium phosphine complexes, 349
- Palmitoyl esters, 310
- PAMAM. *See* Polyamidoamine (PAMAM)
 dendrimers
- Pancreatic cancer, dendrimer construct used
 for targeted imaging of, 370, 373
- para*-anchoring, 39
- [2,2]Paracyclophane, 37
- para* linear conjugation, 39
- Parallel β -sheet, 33
- Parapyridinophane, 37
- Parapyridinophane NADH model, 37
- Paraquat, 7, 8, 25, 29, 228–229
- Paraquat-based receptors, 218–219
- Paraquat derivatives, 143
- Partial-cone conformation, 263, 264
- π -conjugated supramolecular molecular
 modules, 135
- PDI. *See* Perylene diimide (PDI)
- π -donors, 406–408
- PEGA. *See* Polyethylene glycol
 polyacrylamide (PEGA) polymer
- PELF. *See* Pro-Glu-Leu-Phe (PELF)
- Penicillin, 383
- Pentagon-heptagon Stone-Wales defects, 90
- Pentapeptide, 32, 33
- Peptide-based acylhydrazone
 macrocycles, 394–395
- Peptide-based receptors, 297–298
- Peptide building blocks, 32–36
- Peptide carbene palladium complexes, 351,
 352, 353, 354
- Peptide coupling reactions, 35
- Peptide dendrimers, 337
- Peptide engineering, 34
- Peptide ligation, autocatalytic, 337
- Peptide mimetic metal complexes, 344–353,
 344–354
- Peptide nucleic acid (PNA), 34–36
- Peptide nucleic acid (PNA) sequence, 370
- Peptide organocatalysts, 334–344, 353–356
- Peptide phosphine ligand, 345
- Peptide transition metal complexes,
 353–356
- Peracetylation, 311–312
- Perbenzoylated cyclodextrins, 312–313
- Perbenzylated cyclodextrin-monoazides,
 314
- Perbenzylation, 312
- Periprosthetic inflammation, 383
- Permethylation, 311–312
- Per-6-O-tritylated cyclodextrins, 310–311
- Per-protection of cyclodextrins, 311–312
- Perylene derivatives, 149
- Perylene diimide (PDI), 14
- Perylene diimide (PDI) compound, 61, 62
- Perylene diimide (PDI) derivatives, 135–136,
 139, 140, 148, 149, 150
- Perylene diimide (PDI) fluorophore, 19
- Perylenetetracarboxydiamide (PTCDI),
 151
- PET. *See* Positron emission tomography
 (PET)
- PG. *See* Pro-Gly (PG)
- PGSE. *See* Pulse gradient-stimulated echo
 (PGSE)

- pH. *See also* Physiological pH
 boranate-ester-based capsule assembly
 and, 416
 DNA recognition and, 421–422
- Phagocytosis, 367
- Phenanthroline, 22, 355
- Phenanthroline macrocycle, 22
- Phenylacetylenic scaffolds, 164
- meta*-Phenylene, 39
- para*-Phenylene, 39
- Phenyl iodide, 351
- Phosphine catalysts, 350, 351
- Phosphine-containing ligands, 350
- Phosphine peptides, 345–346
- Phosphines, 355
- Phosphinylation, 345–346, 347
 of amine, 349–350
- Phosphoramidites, 338
- Photochemistry, 181–183
- Photochromic oxazines, fluorescence
 switching with, 197–209
 design and assembly of photoswitchable
 nanoparticles, 205–207
 design and synthesis of fluorophore-oxazine
 dyads, 199–200
 fluorescence activation with fluorophore-
 oxazine dyads, 200–205
 fluorescence imaging at
 nanoscale, 197–198
- Photoinduced [2+2] cycloaddition
 reaction, 186, 187
- Photoinduced [4+4] cycloaddition
 reaction, 184–185
- Photoinduced isomerization, 188, 189, 190
- Photoinduced water splitting, 180
- Photoisomers, spectral overlap of, 181,
 182–183
- Photoresponsive switches, 67–69
- Photoswitchable fluorophores, 2
- Photoswitchable nanoparticles, 205–207, 209
- Photoswitches, 4, 9–13
- Photovoltaic applications, of carbon
 nanotubes and graphenes, 110
- Photovoltaic energy generation, 179–180
- Phthalocyanins, 14, 15
- Phthalhydrazide-helicene, 143, 146
- pH variation, chromophores and, 158, 161
- Physiological pH
 biologic molecule recognition and, 418
 DNA recognition and, 422–423
- Picric acid (PA)
 extended Π -systems and, 270–272
 interaction with bis-TTF-calix[2]
 thiophene[2]pyrrole, 268–270
- Pillararenes, 29
- π -acceptors, 406–408
- π -CNT stacking, 93
- π -conjugated bridge, 40
- π -conjugated molecules, 5–6, 46
- π -conjugated oligomers and polymers, 38
- π -donor-acceptor complexation, 25–27
- π -electron-donating properties, of TTF,
 259
- π - π aggregates, 163
- π - π interactions, 129, 143, 146, 149, 157
- π - π stacking, 219
- Pipsyl chloride, 50
- Pivaloyl, 310, 312
- Planar chirality, 36, 37
- Pmh-peptide catalyst, 338, 340
- PMMA. *See* Polymethyl methacrylate
 (PMMA) matrix
- PNAANI. *See* Poly(*N*-acetylaniline)
 (PNAANI)
- p-n-p* junctions, 149
- Podand, 22
- Point chirality, 36
- Polarity/polarizability, functionalization of
 carbon nanotubes and, 101
- iso*-Polyacetylene, 38
- Polyacetylenes (PAs), 38–39
- Polyamides, 38
- Polyamidoamine (PAMAM) dendrimers, 362,
 363, 365, 372–373
 chemotherapy and, 378–381
 commercial availability of, 383
 drug-delivery and, 374
 with pyrrolidone surface, 368
 siRNA delivery and, 376
 toxicity of, 368
- Polyamidoamine (PAMAM) dendrimers-
 DNA complexes, 375–376
- Polyamines, 403
- Polyammoniums, 217
- Polyanilines (PAs), 38
- Polyanion, 29
- Polyaza crown ether, 22
- Polycatenane, 406
- Polycationic oligomer, 158, 159
- Polycations, 29
- Polycyclic aromatic hydrocarbons, 94
- Poly(diacetylene) (PDA), 38
- Polydimethylsiloxane (PDMS), 89
- Polyester dendrimers, 383
- Polyethyleneglycol (PEG), 107
- Polyethylene glycol polyacrylamide (PEGA)
 polymer, 338
- Poly(ethyleneimine), 375

- Polyethyleneoxy chains, 161
 Polyfect, 376
 Polyimide cantilever, 278
 Poly(lysine), 376
 Poly(lysine) dendron, 370
 Polymers
 conjugated, 37–39
 supramolecular (*See* Supramolecular polymers)
 Polymethyl methacrylate (PMMA), 89
 Polymethyl methacrylate (PMMA)
 matrix, 204, 205
 Poly(*N*-acetylaniline) (PNAANI), 240, 241
 Polynucleotide, 30
 Poly(phenyleneethynylene) (PPE), 38
 Polyphenylene (PP), 38
 Poly(phenylenesulfide) (PPS), 38
 Poly(phenylenevinylene) (PPV), 38
 Poly(propyleneimine) (PPI) dendrimers, 363, 364–365, 374
 commercial availability of, 383
 with dimethyldodecylammonium as surface group, 382
 siRNA delivery and, 376
 toxicity of, 368
 Polypyrroles (PPys), 38
 Polystyrene, 37–38
 Polythiophenes (PTs), 38
iso-Poly(triacetylene), 39
 Poly(triacetylene) (PTA), 38
 Porphyrin, 14, 16–18, 260
 difunctionalized with PYBOX moieties, 158, 159
 Porphyrin-based boxes, 246
 Porphyrin-based carbohydrate receptor, 295
 Positron emission tomography (PET),
 dendrimer-based reagents for, 370, 371, 372
 Post-source decay mass spectroscopy (PSD-MS), 309
 PPD-NH₂. *See* Pro-Pro-Asp-NH₂ (PPD-NH₂)
p-Phenylenevinylene derivatives, 143
 PPI. *See* Poly(propyleneimine) (PPI) dendrimers
 Prato 1,3-dipolar cycloaddition reaction, 54–55, 97–98
 Prednisolone, 374
 Primary functionalization, 95–96
 Pro-Asp-Leu-Phe (PDLF), 335
 Pro-D-Pro-Aib-Trp-Trp, 336
 Pro-Glu-Leu-Phe (PELF), 335
 Pro-Gly (PG), 335
 Proline, 221, 222, 335
 L-Proline, 403
 Proline amide, 354
 Proline-based organocatalysts, 334
 Proof-of-principle experiments, 395
 Pro-Pro-Asp-NH₂ (PPD-NH₂), 334
 Propyl hydroxylase, 416
 Proteins
 opsin, 4–5, 6
 recognition of, 417–418
 Proton-activated fluorescence (PAF), 337, 338
 Prulifloxacin, 385
 PSD-MS. *See* Post-source decay mass spectroscopy (PSD-MS)
 Pseudoknot, DNA, 237, 238
Pseudomonas aeruginosa, 383
 Pseudopeptide DCLs, 398
 Pseudorotaxane complexes, 22–24
 Pseudorotaxanes, 222–223
 Pseudotaxane, 25
 Pseudotaxane structures, 143, 144
 PTCDI. *See* Perylenetetra-carboxy-diamide (PTCDI)
 Pulse gradient-stimulated echo (PGSE), 234, 235
 Purification, of carbon nanotubes, 82–84
 Purine bases, 29
 PYBOX. *See* 2,6-bis(2-Oxazolyl)pyridine (PYBOX) moieties
 PyBrop, 35
 Pyrene, 14
 Pyridone NHs, 296
 Pyridylalanine, 338
 Pyridyl alanine peptides, 340, 342
 Pyridyl residues, 350
 Pyrimidine bases, 29
 Pyromellitic diimide (PMDI), 7, 8
 2-Pyrone, 28
 Pyrrole-polyamide monothiol building blocks, 422
 Pyrrolic tripodal receptors, 292, 293
 Pyrrolidination, 104
 Pyrrolidine formation, 99
 Pyrrolidone surface of PAMAM dendrimer, 368
 Pyrrolo-annulated TTFs, 9, 260

 Quadruple H-bond system, 135, 136
 Quantum yield, 181, 182
 Quinolone, 383, 385
 Quinones, 16–18, 242

 Racemization, 36
 Radial breathing modes (RBM), 79–80

- Radialenes, 8
- Radioactive isotopes, imaging using, 370, 371, 372
- Raman spectroscopy, 79–80, 81
- Reactivity, of carbon nanotubes, graphene, and reduced graphite oxide, 94–95
- Reagent K, 35
- Receptors
dynamic combinatorial chemistry and design of, 394–395
optimization of, 398, 403–404
- Receptor unit, chemosensor, 258
- Rectifiers, organic molecular, 59–61
- Redox-active bistable [2]rotaxane, synthesis of, 66
- Redox-active cavities, 248
- Redox-active host assemblies, 213–215
- Redox-active responsive ligand, 217, 218
- Redox-active switch, based on anthraquinone core, 62–63
- Redox-active units, 5–9
combined with chromophores, 16–18, 21
- Redox activity, 4
- Redox-driven recognition process, 248
- Redox-receptors. *See also* Self-assembled macrocyclic redox-active receptors
design of, 246–247
- Redox-recognition/transduction, with organic guest molecules, 215–222, 223
- Redox-responsive systems, 2
- Redox-switchable working mode, 214, 215
- Reduced graphene oxide (RGO), 77, 84–92.
See also Graphene
by oxidative exfoliation followed by reduction, 85–87
photovoltaic applications, 110
solubility of, 93–94
- Reduction, 95
formation of graphane and, 103–104
- Regioselective reductive benzylidene, 321
- Resin encoding, 356
- Resorcinarene derivatives, 215
- Responsive mode, 213
- Retinal, 5, 6
- Retro-aldol reactions, catalysts for, 335–336
- Rhodamine, 14
- Rhodium peptide complex, 344
- D-Ribose, 286
- Ribose recognition, 296
- Ring nano-objects, 165
- Ring shape nanostructures, 147
- RNA recognition, 420
- Rosettes, 128, 133, 161, 165, 167, 168, 169
- Rotacatenane, 225–226
- Rotaxanes, 23, 25, 26, 222, 223, 225, 227, 228
electrochemically-triggered, 229–230
MPTTF and, 260
- Ru(bpy)₃²⁺, 14
- Ruthenium fulvalenes, 181
- Saccharide recognition. *See also* Carbohydrates, molecular recognition of
in water, 298
- S-acylation, 50
- Salicylaldimines, 420
- SAMs. *See* Self-assembled monolayers (SAMs)
- Scanning electron microscopy (SEM), 82
- Scanning probe microscopy (SPM), 149
- Scanning tunneling microscopy break junctions (STM-BJs), 47
- Scanning tunneling microscopy (STM), 82
- Screen-printed electrode, 240
- Secondary electrostatic interaction, 131
- Secondary functionalization, 95, 96, 100–103
- Second-generation tripodal receptors, 293
- Selective deprotection, cyclodextrin synthesis and, 312–317
- Self-assembled cyclic oligomers, 152, 154
- Self-assembled macrocyclic redox-active receptors, 240–245
- Self-assembled monolayers (SAMs), 50–51, 60, 67
- Self-complementarity, 146
- Self-complementary units, 129
- Self-complexation and switching, of tetra-TTF-calix[4]pyrroles, 272–273
- Self-immolative dendrimers, 368–369, 379, 380
- “Semiconducting” tubes, 94–95
- Sensor applications of carbon nanotubes and graphene electronics, 108–110
- Sergeant-and-soldier effect, 140
- Sidewall alkylation and arylation, 97, 98, 99
- Silicon dendrimer, 368, 375, 382
- Silver, interaction between thiols and, 106
- Silylether, 317
cleavage of, 369
- Single-cantilever-based tetra-TTF-calix[4]pyrrole technology, 277–278, 279
- Single photon emission computed tomography (SPECT), dendrimer-based reagents for, 370
- Single-point method, 23
- Single-strand DNA, 84, 240, 241
- Single-wall carbon nanotubes (SWCNTs), 77, 78, 80, 83, 84, 98, 99
applications, 107, 108–109

- siRNA-delivery, dendrimers and, 376–377
- Size-exclusion chromatography, 84
- Small interfering RNA, dendrimers and, 376–377
- SN-38, 378, 379
- S_N2 substitution reactions, 9
- Sodium sulfide, 307
- Soft nanoparticles, 161
- Solar energy, 2
- Solar spectrum match, 181–182
- Solar thermal energy storage and conversion, molecular systems for. *See* Molecular solar thermal (MOST) systems
- Solid-phase approach to monofunctionalization of cyclodextrin, 309
- Solid-state polymer matrix, 191
- Solubility, of carbon nanotubes, graphene and reduced graphene oxide, 93–94
- Solvatochromism, 4
- Solvophobic interactions, 214
- Sonication conditions, 87
- Sonogashira reactions, 9, 11, 49–50, 53, 54, 58, 60, 351, 352
- SPECT. *See* Single photon emission computed tomography (SPECT)
- Spectral overlap of photoisomers, 181, 182–183
- Spermidine, 375
- Spermine, 375, 401, 409
- Spherands, 22, 23
- Spherical nanoparticles, 161–164
- Spirane, 36
- Spiropyran, 12
- Split-mix libraries, 337, 355–356
- SPM. *See* Scanning probe microscopy (SPM)
- Stability tests, in MOST systems, 191, 192
- Starpharma, 382
- Staudenmaier method, 85
- Stereoselective catalysis of C-C bond formation, 333
- cis*-Stilbene, 12
- trans*-Stilbene, 12
- Stilbenes, 181
epoxidation of, 326
- Stilbene systems, 184, 185, 186
- Stille reaction, 11
- Stone-Wales defects, 94
- Storage enthalpy of *cis/trans* isomerization of “stilbene-like” molecules, 184–185
- Stratus system, 369
- Succinic acid, 382
- Sulfides, 350
- Sulfonamide groups, 292
- 2-*O*-Sulfonate, 318
- Sulfonate esters, 317–318
- Sulfonation, of hydroxyl group of β -cyclodextrins, 317–318
- Sulfoxide, 36
- Supercritical conditions, direct exfoliation under, 87–88
- Supertritylation, 311
- Supramolecular chemistry, development of chemosensors and, 257
- Supramolecular noncovalent functionalization, 95, 104–106
- Supramolecular polymers, 39. *See also* H-bond-based nanostructuring of supramolecular organic materials
H-bonded main-chain, 133–143
with H-bonds perpendicular to the elongation direction, 143–149
mechanisms of, 129–131
- Supramolecular pore, 157–158
- Supramolecular redox transduction, 213–249
electroactive guests, 227–236
electrochemically triggered macrocyclic systems, 222–227, 228
perspectives on, 245–249
redox-recognition/transduction with nucleic acids, 236–240, 241
with organic guest molecules, 215–222, 223
self-assembled macrocyclic redox-active receptors, 240–245, 246, 247
- Suzuki reactions, 10, 351, 352, 353
- SWCNTs. *See* Single-wall carbon nanotubes (SWCNTs)
- Switches
organic molecular, 61–68
photoresponsive, 67–69
- Symmetric tetra-TTF-calix[4]pyrroles, 263–266
- syn/anti* ratios, 334
- syn*-singlet state, 188
- Synthesis
of carbon nanotubes, 82
of dendrimers, 363–366
- Synthetic ion channel, 157–158
- Synthetic lectins, 288
- syn*-triplet state, 188
- Systems chemistry, 429
- TBACl. *See* Tetrabutylammonium chloride (TBACl)
- TCB. *See* 1,2,4-Trichlorobenzene (TCB)

- TCNQ. *See* 7,7,8,8-Tetracyano-*p*-quinodimethane (TCNQ)
- TCNQF₄. *See* Tetrafluorotetracyano-*p*-quinodimethane (TCNQF₄)
- TDB. *See* Tridodecyloxybenzyl (TDB) moiety
- TEM. *See* Transmission electron microscopy (TEM)
- Template-directed synthesis, 26
- Templated supramolecular systems, 157–161
- Templates, dynamic combinatorial libraries and, 393–395, 397, 423–425, 426–428
- Temple architecture, 289–291, 300
- TEMPO. *See* 2,2,6,6-Tetramethylpiperidin-1-yl)oxyl (TEMPO)
- Tentagel, 334
- Terephthalic acid-derived building block, 401
- Terminal connectivity, 47–50
- Tetraalkylammonium ions, 411
- Tetrabutylammonium chloride (TBACl), 266
- Tetracarboxylporphyrin derivatives, 155, 156
- Tetrachloro-*p*-benzoquinone, 263
- Tetracyanoethylene (TCNE), 7, 8
- Tetracyano-*p*-quinodimethane (TCNQ), 6–7, 59–60, 260
- Tetraethynylethenes (TEEs), 40
- Tetrafluoro-*p*-benzoquinone, 263
- Tetrafluorotetracyano-*p*-quinodimethane (TCNQF₄), 244
- Tetrahydrazone, 413
- Tetrahydrofuran (THF), 165
- Tetrakis[ethynylpyrene] derivative, 152, 154
- Tetrameric macrocycle 13, 401
- Tetrameric receptor 10, 13, 15, 400, 401
- Tetramesylation, 310
- 2,2,6,6-Tetramethylpiperidine-1-oxyl-4-amino-4-carboxylic acid (TOAC), 336
- 2,2,6,6-Tetramethylpiperidin-1-yl)oxyl (TEMPO), 336
- N,N,N',N'*-Tetramethyl-*p*-phenylenediamine (Wurster's blue), 7
- Tetramethylthio-TTF (TMT-TTF), 25
- Tetraol 33, 412
- 6-*O*-Tetra-ols, 314
- Tetrapyrrolyl-TTF derivatives, 244
- Tetrathiafulvalene (TTF), 6, 7, 25, 27, 52–53, 234, 259–260
- organic molecular rectifiers and, 59–60
- Tetrathiafulvalene (TTF) belts, 260–263
- Tetrathiafulvalene (TTF) building blocks, 8–9
- Tetrathiafulvalene (TTF) cage, 262–263
- Tetrathiafulvalene (TTF)-calixpyrrole, 26, 27
- Tetrathiafulvalene (TTF)-calix[4]pyrrole. *See* Nitroaromatic explosives, detection of using tetrathiafulvalene-calix[4]pyrroles
- Tetrathiafulvalene (TTF)-calix[4]pyrrole conjugates, 215
- Tetrathiafulvalene (TTF) derivatives
- association constants between blue box and, 27
- molecular receptors based on, 215–216
- Tetrathiafulvalene (TTF)-PDI conjugate, 19, 21
- Tetrathiafulvalene (TTF)-radiannulene (TTF-RA), 8
- Tetrathiafulvalene (TTF) redox-active unit, 19
- Tetrathiafulvalene (TTF) redox probe, 239
- Tetrathiafulvalene (TTF) units, 222–226, 242
- Tetratrylated α cyclodextrins, 310
- Tetra-TTF-calix[4]pyrroles
- applications of, 273–279, 280
- asymmetric, 266–270
- extended Π -systems, 270–272
- self-complexation and switching, 272–273
- symmetric, 263–266
- synthesis of, 264
- Tetrazol-5-ylalanine, 338
- Th17 cell immune response, 374, 375
- Thermal energy, storage
- technologies, 179–180
- Thermodynamic control, combinatorial chemistry and, 393, 394
- Thermodynamic equilibrium, in DCL, 393, 397–398, 409
- Thermodynamic parameters, in supramolecular polymerization reactions, 129
- Thermodynamic theoretical model of nanostructure formation, 165
- Thermogravimetric analysis (TGA), 79, 80–81
- Thermoswitches, 4, 9–13
- THF. *See* Tetrahydrofuran (THF)
- Thienylvinylene moiety H-bond-based supramolecular nanofibers, 143, 146
- Thin-film RGO-polyvinylidene fluoride (PVDF) loudspeaker, 108, 109
- Thin-film transistors (TFTs), 107
- Thioglycosylated Fc derivatives, 233
- Thiol anchoring group, 47
- Thiol-disulfide exchange, 397
- Thiol oxidation, 397

- Thiols, interaction with silver or gold, 106–107
- Thiol-substituted benzene, 61
- Thiophenol anchoring group, 48–49
- Thiophenol synthesis, 48
- Thiourea, 319
- 3D networks, 133
- Three-point star motif, 155
- Three-tautomer equilibrium, 132
- Thymidine-functionalized OPV molecules, 158, 160
- Thymine, 29
- TMP dendrimer, 363
- TMSOTf. *See* Trimethylsilyl trifluoromethansulphonate (TMSOTf)
- TMT-TFF, 27
- TNB. *See* 1,3,5-Trinitrobenzene (TNB)
- TNT. *See* 2,4,6-Trinitrotoluene (TNT)
- TOAC. *See* 2,2,6,6-Tetramethylpiperidine-1-oxyl-4-amino-4-carboxylic acid (TOAC)
- 4-Toluioic-hydrazide, 412
- 4-Tolyl bornic acid, 351
- Topoisomeric lactones, 309
- Toroid nano-objects, 165, 167
- Toroids, 2, 133
- Tosyl, 307
- Tosylation, 306, 318
- 6-*O*-Tosyl- β -cyclodextrin, 308
- Tosyl chloride, 306, 318
- 2-*O*-Tosyl derivatives, 319
- N*-Tosyl imidazole, 306, 318
- Toxicity, of dendrimers, 367–368
- Transducer unit, chemosensor, 258
- Transesterification, 396
- boranate, 398, 412–416
- Transesterification library, 395–396
- Transfer-print processes for graphene microsheets, 89–90
- Transistors, molecular, 61, 62
- Transition-metal catalysts. *See* Organozymes
- Transition metals
- interlocked assemblies based on, 226–227, 228
- organozymes and, 344–353
- relative abundance of, 356
- Transition-state analogs, 402
- Transmission electron microscopy (TEM), 82, 133
- Transthioesterification, 396
- Tree-shaped nanosized molecules, 39
- D-Trehalose, 287, 298
- 1,3,5-Triazine, 242
- 2,4,6-Tribenzyl inositol, 343
- 1,2,4-Trichlorobenzene (TCB), 151
- Tricosapeptide, 384
- Tridodecyloxybenzyl (TDB) moiety, 165, 168
- Trifluoroacetic acid, 200, 427
- Trimer 9, 400
- Trimerization process, 149
- Trimethylenecyclopropane, 8
- 2,3,3-Trimethyl-3*H*-indole, 200
- Trimethyllysine moiety, 418–419
- Trimethylphenylammonium surface, 382
- Trimethylsilyl trifluoromethansulphonate (TMSOTf), 312
- 1,3,5-Trinitrobenzene (TNB), 262–263
- detection of in solid state, 277
- extended Π -systems and, 270–272, 276
- interaction with bis-TTF-calix[2] thiophene[2]pyrrole, 268–269
- interaction with tetra-TTF-calix[4] pyrrole, 264–266
- tetra-TTF-calix[4]pyrroles and detection of, 277–280
- 2,4,6-Trinitrotoluene (TNT)
- extended Π -systems and, 270–272
- interaction with bis-TTF-calix[2] thiophene[2]pyrrole, 270
- Trinuclear metallamacrocycles, 424–425
- meso*-Tri-*O*-benzyl inositol derivative, 342
- 6-*O*-Triols, 314
- Triphenylphosphine, 50
- Tripodal receptors, 291, 292–293
- 2,4,6-Tripyridyl-1,3,5-triazine ligand, 246
- Tris-acetic-EDTA-Mg²⁺, 155
- Tris-macrocyclic hosts, 242
- Tris-TTF-cage molecule, 262–263
- Trithiol 16, 402
- Tritylated α cyclodextrins, 310
- Tritylation, regioselective, 310–311
- Trityl chloride, 310
- TSTU, 35
- TTF. *See* Tetrathiafulvalene (TTF)
- 2D H-bonded networks, 149–155
- Two-dimensional logic memory molecular circuit, 64–66
- 2D networks, 133
- UHV-STM. *See* Ultra-high-vacuum scanning tunneling microscopy (UHV-STM)
- Ullmann-type dimerization, 62
- Ultra-high-vacuum scanning tunneling microscopy (UHV-STM), 135

- Umbrella model, 375–376
- Unlocked nucleic acid (UNA)
nucleotides, 31–32, 34
- Unprotected cyclodextrins, 305–312,
317–321
- Uphill polymerization, 130
- Uracilic recognition sites, 135
- Urea, 30, 31, 217
- Ureidic tripodal receptor, 291, 292
- Ureidic zinc porphyrin receptor, 295
- Ureido pyrimidinone (UPy) derivatives, 135,
136
- Ureido pyrimidinone (UPy) recognition
motif, 132, 135
- Ureidotriazine, 143, 145
- UV-Vis spectroscopy, 295–296, 426
- Vaccines, dendrimers and, 377–378
- Valeryl esters, 310
- Van der Waals interactions, 128
- Vector-selective reaction, 308
- Vibrio cholera*, 383
- Vinylheptafulvene (VHF), 12, 13
- Viologens, 29
- Vivagel, 382
- V-shaped polyimide cantilever, 278, 279
- Water
encapsulation of organic molecules
in, 28–29
mono- and disaccharide recognition in, 290,
298
- Watson-Crick base pairing, 420
- Weitz-type redox system, 6, 8
- Wennemers organocatalyst, 334, 335
- Wittig reaction, 58
- Wittig-type reaction, 63
- Wurster's blue, 7
- Wurster-type redox system, 7, 8
- X-ray absorption spectroscopy (XAS), 79
- X-ray photoelectron spectroscopy (XPS), 79
- D-Xylose, 290
- Zeolites, 181
- Zero bandgap “metallic” category of carbon
nanotubes, 77–78
- Zero-bias Kondo effect, 64
- Zeta potential, 368
- Zigzag orientation, 77, 78
- Zn-based catalysts, 355
- Zwitterionic donor-acceptor dyad, 60
- Zwitterionic isomers, 203–204, 206, 207, 208